NAMRL MONOGRAPH 21 USAARL 73-1

HUMAN HEAD AND NECK RESPONSE TO IMPACT ACCELERATION

Channing L. Ewing and Daniel J. Thomas

ARMY – NAVY

Joint Report

NAVAL AEROSPACE MEDICAL RESEARCH LABORATORY

U. S. ARMY AEROMEDICAL RESEARCH LABORATORY

August 1972

ERRATA SHEET

Page 1	last paragraph, first line, change "was" to "is"
Page 2	last paragraph, second line, begin sentence with "Consider a man"
Page 3	third line from top of page, eliminate one "to" first paragraph, second line, change "juction" to "junction"
Page 6	first paragraph, add sentence: "The accelerometers were Systron Donner 4303A accelerometers with a ± 25 and ± 50 range, while the rate gyroscopes were comparable units manufactured by Fairchild Controls."
Page 7	first paragraph, second line, change "suprious" to "spurious"
Page 10	second paragraph, first line, change "of" to "at"
Page 14	last paragraph, last line, change "not a random" to "not at random"
Page 22	last paragraph, fourth line, change "(-)" to read: (references 8 and 9 of the Anthropometry Section)
Page 38	variable RHN, first line, change "ot" to "of"
Page 53	third main paragruph, fourth line, change "coordinate system is Figures 3 and 4" to "coordinate system in Figures 3 and 4"
Page 59	Table One - Change "3 = Estomorphy"to "3 = Ectomorphy"
Page 68	Fifth paragraph, fourth line, change "data would be taken" to "data should be taken"
Page 85	first paragraph, sub-paragraph 2, change "information input into the machine" to "information was provided the machine"
Page 106	fourth paragraph , third line, change "damping ration" to "damping ratio"
Page 107	Figure DP-13 should be corrected to read D= 0.90199
Page 129	equation (3) change to read:

$$\begin{bmatrix} 0 & 1 \\ -\omega_2^2 & -2\zeta_2\ \omega_2 \end{bmatrix}$$

equation (4) change to read:

$$\left(1 - \frac{\omega_2^2}{\omega_1^2}\right) x_1$$

change line under equation (4) to read "matrix" in lieu of "matirx"

Page 131	change equation (7) to read:

$$x(k + 1)T = G(T)\ x\ (kT) + H(T)\ u\ (kT)$$

Page 147	All HZ on this page should read "Hz"

Unclassified
Security Classification

DOCUMENT CONTROL DATA - R & D

(Security classification of title, body of abstract and indexing annotation must be entered when the overall report is classified)

1. ORIGINATING ACTIVITY (Corporate author)	2a. REPORT SECURITY CLASSIFICATION
Naval Aerospace Medical Research Laborarory Naval Aerospace and Regional Medical Center Pensacola, Florida 32512	Unclassified
	2b. GROUP N/A

3. REPORT TITLE

HUMAN HEAD AND NECK RESPONSE TO IMPACT ACCELERATION

4. DESCRIPTIVE NOTES (Type of report and inclusive dates)

5. AUTHOR(S) (First name, middle initial, last name)

Channing L. Ewing and Daniel J. Thomas

6. REPORT DATE	7a. TOTAL NO. OF PAGES	7b. NO. OF REFS
10 August 1972	373	17

8a. CONTRACT OR GRANT NO.	9a. ORIGINATOR'S REPORT NUMBER(S)
DOT-HS-187-2-295	
b. PROJECT NO. M4312.01-5001BE1J	NAMRL Monograph 21
c.	9b. OTHER REPORT NO(S) (Any other numbers that may be assigned this report)
d.	USAARL 73-1

10. DISTRIBUTION STATEMENT

Approved for public release; distribution unlimited

11. SUPPLEMENTARY NOTES	12. SPONSORING MILITARY ACTIVITY
Joint report with U. S. Army Aeromedical Research Laboratory, Fort Rucker, Alabama	

13. ABSTRACT

A methodical investigation and measurement of human dynamic response to impact acceleration was conducted as a Joint Army-Navy-Wayne State University investigation.

Linear accelerations were measured on the top of the head, at the mouth, and at the base of the neck. Angular velocity was also measured at the base of the neck and at the mouth. A redundant photographic system was used for validation. All data were collected in computer-compatible format and data processing was by digital computer. Selected data analysis on 41 representative human runs involving 12 subjects of the 236 human runs completed to date are presented.

Description of the experimental design, data collection and processing is given in detail. Ancillary research efforts in support of the program are also described.

Representative plots of the human kinematic response are presented, discussed, and compared. Repeatability and quality control plots are also presented. There are a total of 755 computer drawn plots illustrating a characteristic, repeatable response of human subjects to impact acceleration.

ia

DD FORM 1 NOV 65 1473 (PAGE 1)

S/N 0101-807-6801

Unclassified
Security Classification

14. KEY WORDS	LINK A		LINK B		LINK C	
	ROLE	WT	ROLE	WT	ROLE	WT
Human acceleration effects						
Dynamic response						
Differential displacements						
Differential angular and linear acceleration						
Biomechanics						
Impact acceleration						
Bioengineering						
Acceleration tolerance						
Biodynamics Model						

ih

Approved for public release; distribution unlimited

HUMAN HEAD AND NECK RESPONSE TO IMPACT ACCELERATION

Channing L. Ewing and Daniel J. Thomas

NAMRL Monograph 21

Approved by

Ashton Graybiel, M.D.
Assistant for Scientific Programs

Released by

Captain N.W. Allebach, MC USN
Officer in Charge

10 August 1972

Details of illustrations in
this document may be better
studied on microfiche

Naval Aerospace Medical Research Laboratory
Naval Aerospace Medical Institute
Naval Aerospace and Regional Medical Center
Pensacola, Florida 32512

1C

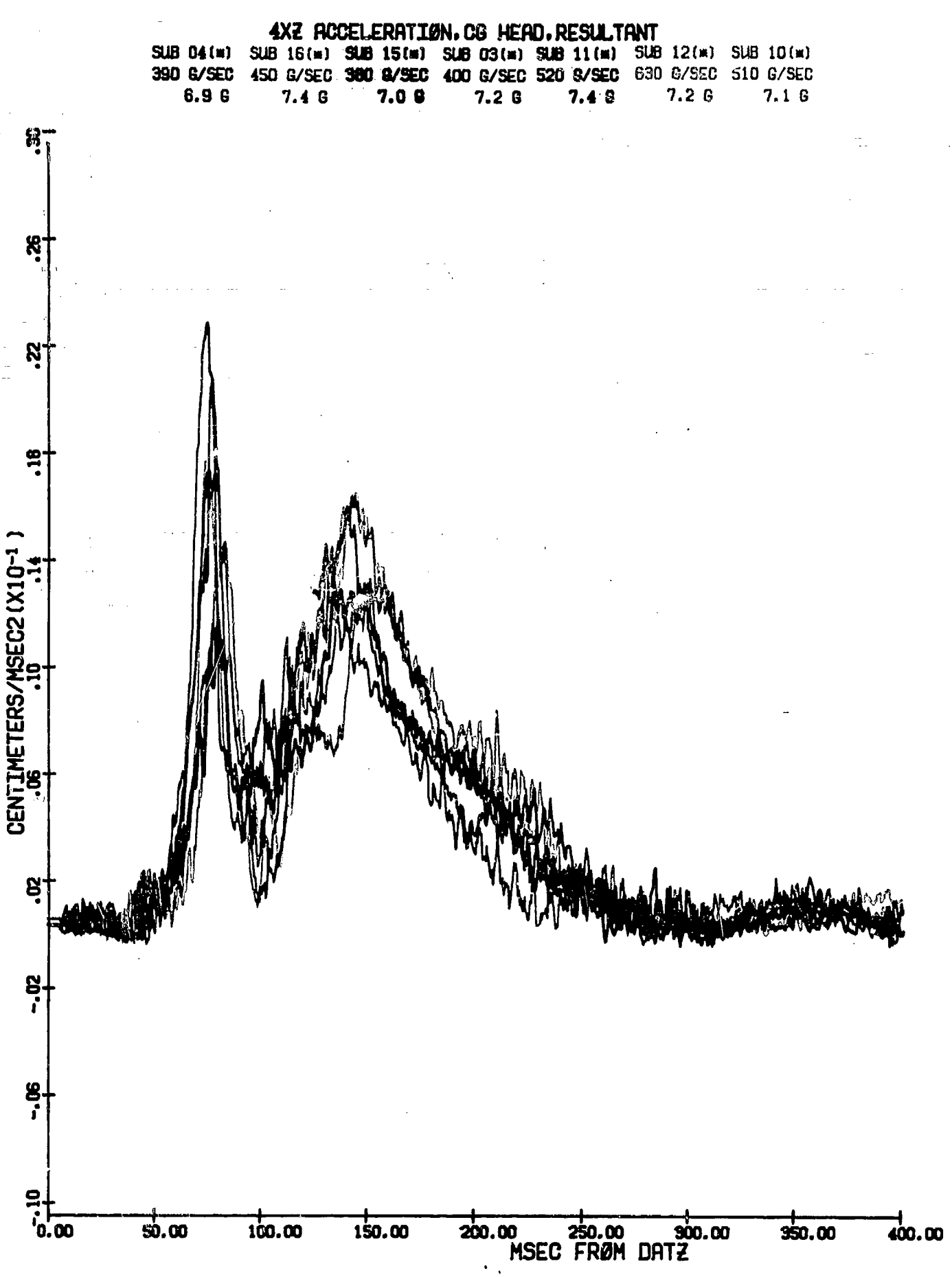
4XZ ACCELERATIØN.CG HEAD.RESULTANT
SUB 04(M) 390 G/SEC 6.9 G
SUB 16(M) 450 G/SEC 7.4 G
SUB 15(M) 380 G/SEC 7.0 G
SUB 03(M) 400 G/SEC 7.2 G
SUB 11(M) 520 G/SEC 7.4 G
SUB 12(M) 630 G/SEC 7.2 G
SUB 10(M) 510 G/SEC 7.1 G
CENTIMETERS/MSEC2(X10-1)
.30
.26
.22
.18
.14
.10
.06
.02
-.02
-.06
-.10
0.00
50.00
100.00
150.00
200.00
250.00
300.00
350.00
400.00
MSEC FRØM DATZ

ii

ACKNOWLEDGEMENTS

The research work reported herein was supported by the U. S. Army Medical Research and Development Command; the U. S. Navy, Bureau of Medicine and Surgery; and the Office of Naval Research, Medical and Dental Division. Preparation of this report was supported by the National Highway Traffic Safety Administration of the U. S. Department of Transportation.

Many individuals have given long overtime hours to this program over the past 6 years, but are too numerous to list. Certain individuals have made far greater than average contributions: CAPT George W. Beeler, Jr. MSC USA made crucial contributions to experimental design, data acquisition system and data processing design. Chief Warrant Officer Daniel T. Hartfield USN of the NAMRL Detachment wrote all the original Data Processing programs, and established Data Processing format standards. Many of his programs are still in use even though highly modified.

Mrs. Juanita Howell is due especial thanks for her devoted, selfless and expert administrative assistance. Mrs. Elizabeth White wrote several computer programs and gave generously of her own time and thoughts. LCDR David Gills MC USN contributed significantly and creatively to the program while at USAARL.

At Wayne State University, under the direction of Professor Lawrence Patrick, Frank Du Pont, Kenneth Trosien, and Jerry Glinski contributed invaluable engineering advice and support as well as reliable operation of the WHAM II device.

Numerous persons assisted from the U. S. Army Aeromedical Research Laboratory, including Mr. Hurlie Huffman, Spec. 4 James Newton USA, CAPT David Schrunck MC USAR and CAPT Barry Landfield MC USAR.

Finally, Mr. H. Gerald Williamson of NAMRL Detachment gave very long hours and expert knowledge to complete all the data processing for this report. Mr. John McNulty of QEI, Inc. wrote several significant computer programs. LCDR Paul Majewski MC USN provided critical review of the anthropometry data.

ADMINISTRATIVE INFORMATION

Trade names of materials or products of commercial or nongovernment organizations are cited only where essential to precision in describing research procedures or evaluation of results. Their use does not constitute official endorsement or approval of the use of such commercial hardware or software.

TABLE OF CONTENTS

√

4XM ACCELERATIØN.CG HEAD.X DIRECTIØN

SUB 04(M)	SUB 16(M)	SUB 15(M)	SUB 03(M)	SUB 11(M)	SUB 12(M)	SUB 10(M)
390 G/SEC	450 G/SEC	380 G/SEC	400 G/SEC	520 G/SEC	630 G/SEC	510 G/SEC
6.9 G	7.4 G	7.0 G	7.2 G	7.4 G	7.2 G	7.1 G

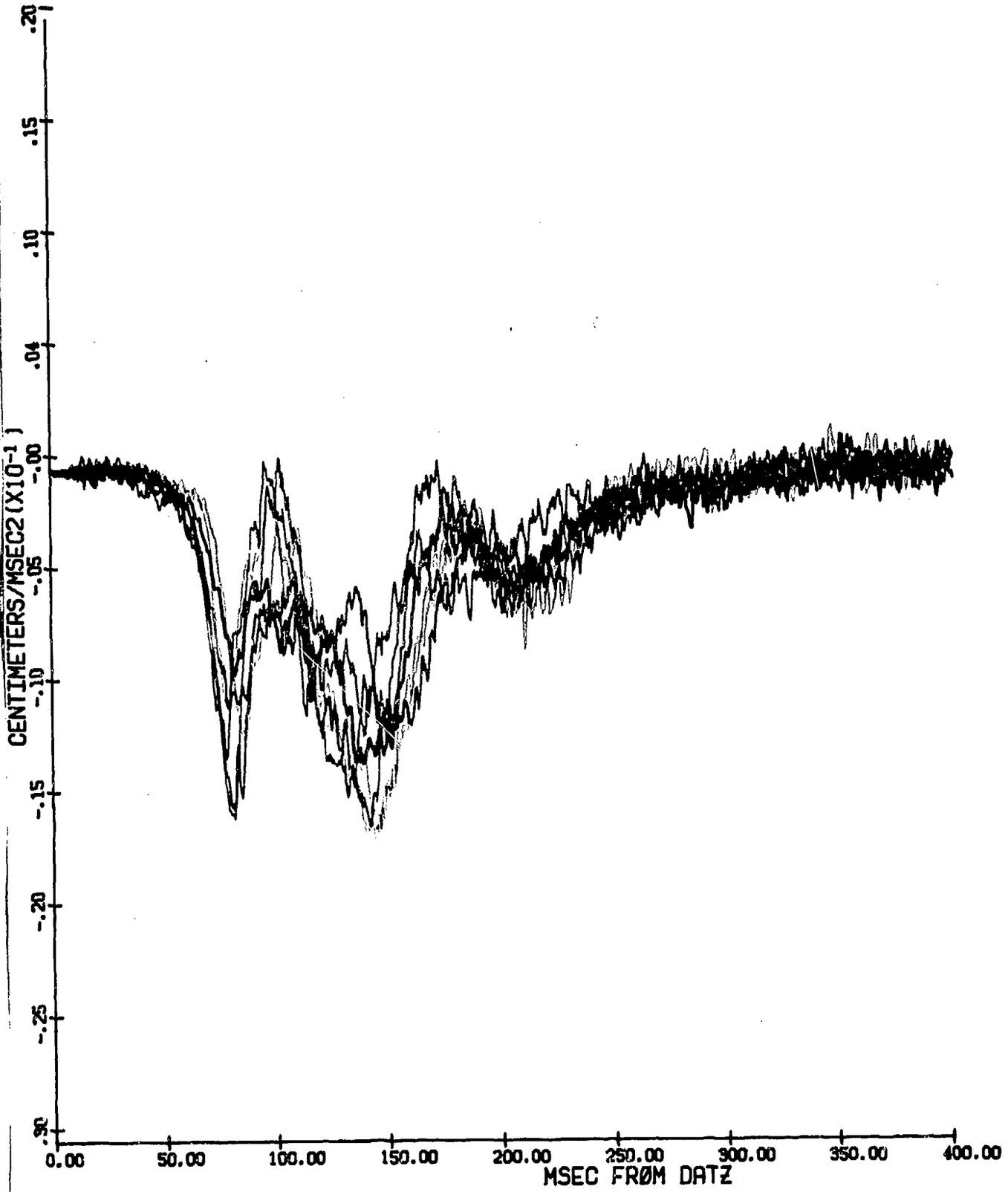

VJ

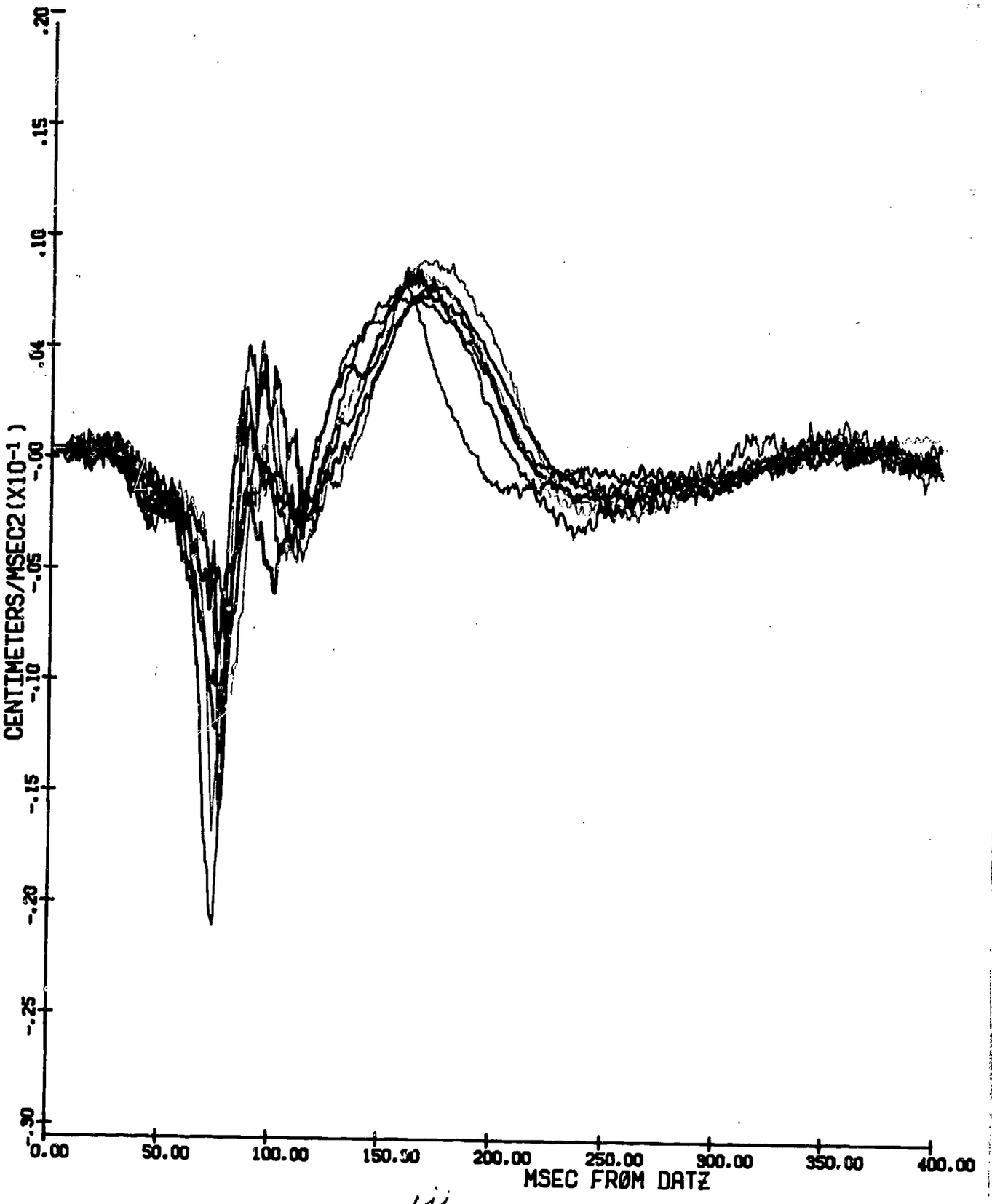
4ZM ACCELERATIØN.CG HEAD.Z DIRECTIØN
SUB 04(m) SUB 16(m) SUB 15(m) SUB 03(m) SUB 11(m) SUB 12(m) SUB 10(m)
390 G/SEC 450 G/SEC 380 G/SEC 400 G/SEC 520 G/SEC 690 G/SEC 510 G/SEC
6.9 G 7.4 G 7.0 G 7.2 G 7.4 G 7.2 G 7.1 G
CENTIMETERS/MSEC2 (X10-1)
.20
.15
.10
.04
-.00
-.05
-.10
-.15
-.20
-.25
-.30
0.00
50.00
100.00
150.00
200.00
250.00
300.00
350.00
400.00
MSEC FRØM DATZ

VII

EXPERIMENTAL AND SYSTEMS DESIGN, APPARATUS AND EXPERIMENTAL PROCEDURE CHAPTER

THEORETICAL BACKGROUND

Evaluation of candidate human protective devices against impact acceleration requires human simulation by such analogs as cadavers, dummies, mathematical models and various primates. The human analog is required because man cannot tolerate the extreme impact forces against which such systems are designed to afford protection.

All human analog testing and data derived therefrom suffers from one principal defect. Its correspondence to living man is not quantitatively demonstrable, largely because of the almost complete absence of quantitative human dynamic response data, and injury criteria pertaining thereto. As a consequence, dummies are designed to reproduce static rather than dynamic anthropometric measurements.

The use of living volunteers to test protective systems is dangerous, expensive and difficult to interpret. If a subject is not used as his own control, variance between subjects makes comparisons difficult. Adjustments of certain protective restraint systems are a very large factor in their ability to protect, but are difficult to reproduce validly for crash tests even for the same subject.

Development of a valid human analog would result in the capability to reproduce man's inertial dynamic response in a standard test object. Such an analog does not exist today. Its development requires determination of the following:

1. Mass, center of mass location and principal moments of inertia of the important body segments. (Some of these data are available)

2. Functional relationships between those body segments in the dynamic environment. The goal is to be able to predict dynamic response to a given segment, given the input accelerations to that segment.

The following logic was used to attempt to measure response data which would be useable for analog design and validation:

1. Man's dynamic response to small experimentally produced increments of sled acceleration (1) peak, (2) rate of onset, (3) duration at peak and (4) vector directions, is safely measureable up to the point of voluntary tolerance.

2. An analog which accurately reproduces man's dynamic responses to simple, experimentally produced individual input accelerations will yield a valid total dynamic response to complex input accelerations such as those of a crash.

It was believed that such responses could only be measured by instrumenting the living human being.

Successful measurement, instrumentally, of human head and neck response requires the ability to mount transducers on the man to achieve (a) reproducibility of placement between runs; (b) lack of spurious movement of the transducer relative to the man; (c) results which could be related to the human population rather than to the individual alone; (d) location of the transducers in the plane of expected motion; and (e) repeated runs on a single instrumented individual to determine the repeatability of any data collected, as well as to eliminate inter-subject variation.

The majority of pre-1967 instrumentation effort has usually been directed toward the vehicle. Instrumentation of Stapp's experiments was limited by the state-of-the-art of inertial measurement transducers, especially accelerometers and rate gyroscopes. In those experiments, Stapp noted that head-mounted transducers as mounted on a helmet or a "bite-plate" could not give useable results. (1)

If instrumentation can be firmly mounted on the man, changes in his dynamic response due to changes in any of the input as measured on the subject can be precisely determined. These changes with increasing input accelerations can be exactly measured by using each subject as his own control. Differences between instrumented subjects can be determined by comparisons of dynamic response obtained from identical input acceleration pulses applied to them.

A joint Army-Navy project was initiated in 1966 at the Naval Aerospace Medical Institute, Pensacola, Florida to make these measurements. The last run was completed on 27 April 1969.

Dynamic response of the head and neck to experimentally applied impact acceleration was the first subject of study. Previous studies (1, 2) have demonstrated the difficulties inherent in measuring accelerations and displacements of the head and neck, as referenced to the seat. One difficulty has been in the means of generating the input acceleration. Many studies have been performed on acceleration facilities in which an initial acceleration was given, followed by a "constant" velocity phase (actually a deceleration of less than 0.5 G), followed by a terminal shaped deceleration pulse.

One disadvantage of such an accelerator is the necessity for establishing a condition of zero dynamic response prior to entry into the deceleration phase. If the head and neck were responding to the initial acceleration or subsequent velocity decay at the time of initiation of the input acceleration, an artifact would be introduced into the measured response to the deceleration pulse.

Another disadvantage is that physiological data collected during an experiment cannot be related to a single pulse but instead are related to a series of pulses. It would appear easier to determine the effect of a single pulse if the experimental pulse were induced with the subject at both inertial and physiological "rest".

Another difficulty lies in the complexity of the forces acting simultaneously on the head. A man seated on a sled and restrained by pelvic and shoulder harness when subjected to a $-G_x$ acceleration transmitted to his body by an interaction of his body with the seat back and restraint harness. (2) The sled moves away from the pelvis in the direction of acceleration, but the pelvic restraint which couples the man to the seat transmits the acceleration to the pelvis and thus to the torso. The

torso then attempts to rotate around the restrained pelvis in the mid-sagittal plane but is prevented from doing so by the shoulder restraint harness. Both the pelvic and shoulder harnesses stretch in response to to the dynamic load of the subject. A reversal of torso trajectory then occurs, resulting in the torso being forced down and back. Concurrently, the torso is being moved through space with the acceleration vehicle.

The head and neck also respond by rotating through space about a center of rotation in the neck or neck-torso juction area. Schulman et al. have shown that th· neck is capable of considerable stretch. (2) Therefore, displacements of the head as measured from a seat reference point are difficult to interpret due to the complexity of motion of the entire sled-torso-head system.

The purposes of the present study were fourfold: (1) to measure precisely the complete input acceleration to the head and neck measured at the first thoracic vertebra; (2) to measure precisely the dynamic response of the head and neck to the input acceleration; (3) to develop a method of obtaining the data in such a format that automatic data processing may be used extensively; (4) to develop and validate a general method for the experimental measurement of the bioengineering characteristics of the human body with such precision, accuracy and repeatability that a mathematical model or other analog of the human dynamic response to impact acceleration can be constructed. Such a model has many important applications, but previous modeling attempts have been handicapped by a paucity of data of necessary quality, resulting in models of limited utility.

EXPERIMENTAL DESIGN

The following procedures were adopted in order to achieve the stated goals:

1. Displacement was measured by double integration with respect to time of acceleration measured on the head and T_1 spine by accelerometers and rate gyros rigidly mounted on the man in completely reproducible locations whose relationship to bony anatomy was measured by x-ray anthropometry.

2. A second and independent means of measuring displacement consisted of sled-mounted, pin-registered, high-speed, high-precision, 16 mm cine cameras. Data derived from photographic data reduction were used to validate transducer-derived data.

3. All data were collected in a format compatible with automatic data processing by digital computer.

4. All data of primary interest were collected on the acceleration end of the track.

In the design of these experiments, certain simplifying assumptions were made. The first was that all accelerations acting on the head and neck of the seated pelvic- and torso-restrained individual subjected to a $-G_x$ acceleration would be detectable at the first thoracic vertebra (T_1) or base of the neck since all accelerations acting on the head and neck must be transmitted through the vertebral column. Only those

additional accelerations transmitted by the soft tissues of the neck could be a source of error. Therefore, the acceleration measured at T_1 was presumed to serve as input information to the head and neck. The second assumption was that the head is a rigid body, and the third, that all significant head and neck motion would be coplanar with the plane of induced acceleration, i.e., the mid-sagittal plane.

In order to describe clearly the complex motion of the head and neck, all motion was considered as occurring in four two-dimensional coordinate systems, as described in the Theoretical Kinematics Chapter:

1. The laboratory coordinate system was selected as the position occupied by the sled coordinate system immediately prior to the onset of acceleration to the sled.

2. The sled coordinate system was selected as an arbitrary photographic reference system fixed to the chair back with a known orientation to gravity.

3. The T_1 coordinate system was established as a two-point photographic reference system on the T_1 mount, as shown in Figure DP-9 with axes directions further defined electronically as described under the section on Transducer System.

4. The head coordinate system was established by photographic targets on the head (bregma) mount and the mouth mount as shown in Figure DP-9 with axes directions further defined electronically as described under the section on Transducer System.

Two redundant systems tracked the coordinate systems. The first system used an inertial reference platform mounted on each coordinate system of the head and T_1 with miniature transducers to measure acceleration and angular velocity. In the second, high-precision cinematography was used to measure displacements of the coordinate systems. Velocities and accelerations also were determined from the measured displacements by differentiation with respect to time.

Precise anatomical displacement information can be obtained from the measured coordinate system displacements if several requirements are met: (1) The transducers and the photographic targets must be uniquely fixed to each individual; this was satisfied by the construction of mouth, head and spine mounts that can be placed only in one position on each man. (2) The position of each photographic target and each transducer must be recorded for each individual; this was accomplished by x-ray and photographic anthropometry of each subject's head and neck with the mounts in place. (3) The position of each transducer and target in space must be determined just prior to the onset of acceleration; this requirement was met by data from the lateral and posterior cameras and by the x-ray anthropometry. Once all anatomical displacements were determined, a comparison was made to validate the results obtained by the use of either the photographic or transducer systems.

Each system used to accomplish the entire experiment was carefully integrated with each other. The equipment and techniques will be described system by system.

SYSTEMS DESIGN AND APPARATUS

Transducer System

Transducer systems forming inertial reference platforms were established at three locations: The spine (T_1) system was positioned over the posterior spinous process of T_1 and consisted of two accelerometers mounted with their sensitive axes at right angles in the mid-sagittal plane, and a rate gyroscope with the sensitive axis perpendicular to the mid-sagittal plane of the subject. The force-balance accelerometers weighed 14.2 grams each, while the rate gyroscopes weighed approximately 94 grams. The head system was positioned over the back of the shaven head of the subject and consisted of two accelerometers mounted with their sensitive axes at right angles to one another in the mid-sagittal plane. The mouth system was positioned by a bite-block and consisted of a duplicate set of the transducers mounted at T_1. The transducer placement is illustrated in Figure 1.

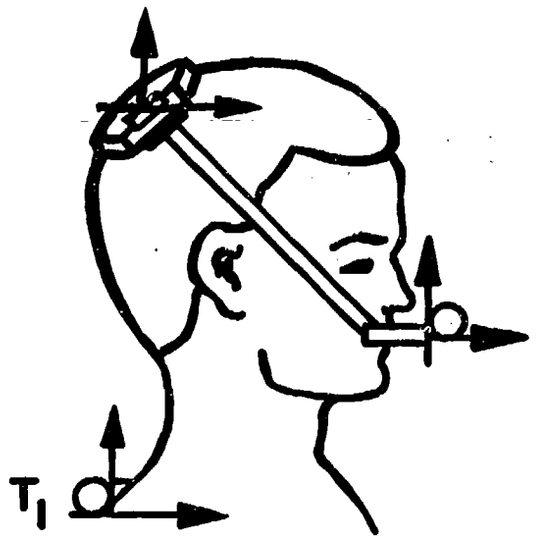

FIGURE 1

The head and mouth system outputs were combined to form a single head output as described under OUTVAR in the Data Processing Chapter. The outputs of the head system and those of the T_1 system were used for tracking, each with respect to the laboratory coordinate system. The displacements of T_1 were then subtracted from those of the head to produce differential head displacement relative to T_1.

The selection of transducers and the remainder of the electronic data system was made to limit the error of the overall system to 0.5%. This criterion dictated the choice of linear accelerometers that had a maximum nonlinearity error of 0.1% full scale and ± 5000 deg/sec rate gyros with a maximum error of 0.5% full scale within the range of expected angular rates. The accelerometers responded as a second order system with natural frequency ranging from 112 Hz to 165 Hz and damping ratios from 0.5 to 0.8. The rate gyroscopes had a natural frequency of 64 Hz ± 4 Hz with damping of 0.6 ± 0.1.

Transducer outputs were hard wired to operational amplifiers at the analogue tape recorder. Time-locking of the transducer recording with the photographic data system was accomplished by an electrical pulse (T_0 pulse), recorded on one of the tape channels, that reset the continuously-counting camera timers to zero.

The time axis of the experiment was established by the 100 kHz crystal oscillator in the tape recorder phase-lock system. All transducer outputs recorded on the analogue tape were phased to this time reference.

Transducer Mounting System

A mount consisting of three modules was required at each transducer system location. One module was required to obtain conformity to the subject's anatomy in a completely repeatable way; the second was required to maintain the transducers in a known standard configuration; and the third was required to mate the individual anatomical modules to the common transducer modules.

The mouth mount and head mount were designed to compress the skull between them, thus preventing motion relative to the head during acceleration. The connection between the head and mouth mounts was established and maintained under considerable constant pressure by a harness.

A pressure mold of the shaven bregma of the subject was used to construct the head anatomical module. The mouth anatomical module was constructed by making a metal casting of the teeth, hard palate, and upper jaw.

The T_1 anatomical module was constructed by making a pressure mold of the spinal column of the subject from C_5 through T_3 and cutting it to fit anatomically. It was secured by a harness that maintained the mount on the selected site under considerable pressure. The acceleration pulse drove the mount against its spinal anchor point, thus improving stability during the dynamic event.

The three mounts were thus installed in a precisely repeatable location for each run. After the anatomical mounts were constructed for each subject, the transducer modules were installed on the center line so that each was coplanar with the other two. Once these relationships were established, changing the mounts from one subject to another was a brief task.

Immediately prior to each run, the subject was positioned so that all transducer systems were coplanar in the mid-sagittal plane which was the plane of expected induced movement.

Motion of the mounts relative to the anatomical mounting site would produce suprious displacements and accelerations as measured both instrumentally and photographically. It was thus necessary to determine the presence or absence of such relative motion. Motions of the T_1 mount relative to the spine were determined photographically by the posterior and lateral cameras. While some motion was detected, particularly on early high-G runs, later mount improvements reduced these movements to relative insignificance. Motions of the head mount relative to the mouth mount were determined photographically on the frame of film taken at the instant of highest head acceleration.

The extent of stability of the head and mouth mount is illustrated by review of the headspan plots (HSP), plots 612 through 632. The change in dimension throughout the runs is minimal.

Photographic Data System

Pin-registered, sled-mounted 16 mm movie cameras were selected to avoid the parallax problem, as suggested by Shulman's work. (2) To prevent loss of high frequency response data, 500 frames/sec were exposed. One camera was mounted on the sled at shoulder level and to the right of the subject, with the film plane paralleling the plane of expected motion. A second camera was located directly to the rear of the subject at shoulder level. Each camera timed the center of shutter opening of each frame of film to within $\pm$ 0.1 msec. The timers produced positive time-locking of the cameras and the analogue data on the tape recorder.

Photographic lighting during acceleration was provided by sled-mounted flood lights.

Figure DP-9 is an example of the photographic information taken at the point of maximum differential head displacement during a sled run.

Data Train System

The electronic data train used to record and compute the outputs of the transducers is diagrammed in Figure 2. The train was designed to minimize the manhours required to obtain the desired measurements and to improve their accuracy. Although high-speed photography is simple and useful for data collection, analysis of the films requires an inordinate amount of time and does not lend itself to the precise determination of instantaneous acceleration.

The redundant transducer system was chosen to permit the instantaneous assessment of the differential relationships between the head and T_1 of the subject and permitted tracking the linear and angular components of the head and T_1 of the subject in inertial space.

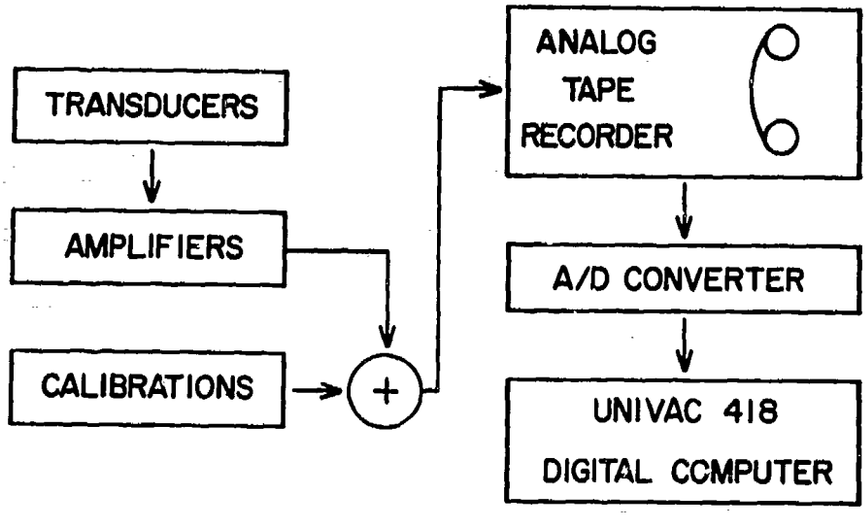

Schematic Representation of Data Acquisition and Processing System for Transducer Data

FIGURE 2

Signals leaving the transducers were amplified and scaled by integrated circuit operational amplifiers. These units were designed to permit the experimenter to expand the range of the transducer outputs so that the expected range of experimental output corresponded roughly to full range on the tape recorder. The setting was done with switchable resistor networks and the stability of the amplifiers was such that monthly calibration was sufficient to guarantee a maximum error of 0.1%.

The greatest source of error in the system was contributed by the analog magnetic tape recorder. An Ampex FR 1800L tape recorder having an overall signal-to-noise ratio of 53 dB, or about 0.5% root mean square noise, was selected. The remainder of the data train was chosen to reduce all other noise and inaccuracy to an insignificant level. The recorder was calibrated at the time of each experimental run in order to achieve the full benefit of the recorder specifications.

A phase-locked tape speed servo was used in the analogue tape recorder to provide short-term constancy and linearity, but the electronic stability was such that frequent recalibration was necessary. In addition, the Ampex FR 1800L used to reproduce the analogue signals for plotting and A/D conversion was also used by another experimenter in the laboratories, which caused frequent calibration changes. In order to minimize the time and effort required to retain system accuracy, a calibration sequencer was built into the system immediately prior to each experimental run. This sequencer recorded a series of constant voltage levels on each channel of the tape recorder. During subsequent data reduction (see Data Processing Chapter)

the output voltage levels of the calibration sequence were used to generate a first-order transformation to calibrate the incoming data.

The data transmitted to a remote site, played back through an identical recorder, were sampled at 2000 samples per second with a 10-bit accuracy, and transmitted to the core of the computer for processing. The sampling rate was selected to be at least 10 times the expected maximum frequency of the response. The mounts provided eight data channels which, along with a chair accelerometer channel, were digitized. Once the data were resident in the computer, a series of processing programs was applied to them as described in the Data Processing Chapter.

Computer Systems

The UNIVAC 1108-3G multiprocessor system installation at the NASA Slidell Computer Complex was utilized in the processing of data and calculation of derived variables. This system is a general purpose, high performance processor consisting of six tapes of subsystems:

1. Central Processor Units (CPU)
2. Input/Output Controller (IOC)
3. Main Storage Modules
4. Auxiliary Storage Subsystem
5. System Interconnection Components
6. Peripheral Subsystems

The UNIVAC 1108 multiprocessor system includes three central processors, each of which can perform all functions required for the execution of instructions, arithmetic, logic, input/output, and executive control. Each central processor unit contains control registers, arithmetic section, control section, input/output section, indexing section, and storage class control section.

This system has two input/output controllers. The IOC is an independent device that controls the operation of up to sixteen peripheral subsystems under the direction of the three central processing units. Once an I/O request has been issued to an IOC, the IOC controls the operation and transfer of data between main storage and eight high-speed data channels. Each channel can transfer data at speeds up to 250,000 words per second.

The main storage module is a magnetic core consisting of 32,768 thirty-six bit words. This storage area is expandable in pairs to a maximum of slightly more than 262 K words. The effective instruction cycle time for main storage is 750 nanoseconds.

The auxiliary storage subsystems consist of three types of magnetic drums: three high-speed FH-432 drums with a total of 786,432 words capacity, four medium-speed FH-1782 drums with a total of 8,388,608 words capacity. Each word of storage consists of 36 bits. In the worst case (Fastrand II drums) the average access time is 92 milliseconds with a word transfer rate of 25,590 words per second.

Peripheral subsystems include twenty-two Uniservo VIII - C seven track tape units having a maximum transfer rate of 96,000 six-bit characters per second, two card punches, two card readers, and five high speed printers with a printing rate of 1200 lines per minute. Also included are five UNIVAC 1004 remote batch terminals, and a number of UNIVAC Uniscope 300 CRT terminals, UNIVAC DCT 500 data terminals, and IBM 1050 data terminals.

A UNIVAC 500 DCT demand terminal is located at the NAMRL Detachment of the NASA Michoud Assembly Facility. The DCT 500 efficiently transfers data between the terminal and the centrally located UNIVAC 1108 processor. The system consists of a 132 position per line printer and an American Standard Code Character set. It can operate at speeds of up to 300 bits per second and selectable printer speeds of ten, fifteen or thirty characters per second.

The plotting of digital information as presented in this report is accomplished by the use of a Stromberg-Carlson Model S-C 4020 microfilm printer/plotter. Input to the S-C 4020 is in the form of 1/2 inch magnetic tape and is an off-line process utilizing tape created by the UNIVAC 1108 processor. A set of special software routines developed and maintained by the computer installation is used in the generation of the tapes for plotting.

The S-C 4020 utilized IBM seven track tapes in densities of 200, 556, or 800 bits per inch. It will accept data from magnetic tape at input rates up to 62,500 six-bit characters per second and print these data at speeds in excess of 17,000 alpha-numeric or symbolic characters per second. The plotting of scientific curves can be accomplished at a speed of 12,500 plotting points per second, or if being used exclusively as a printer, will print 7,000 lines per minute. Graphs or frames combining characters, vectors, and curves vary with complexity but an average annotated graph can be recorded in milliseconds.

The S-C 4020 printer/plotter is capable of translating high-speed digital data into alpha-numeric characters, symbols and lines. This is accomplished by means of the CHARACTRON® Shaped Beam Tube. This tube contains a built-in character-forming section consisting of an electron gun, character-selection plates and a character Matrix. The electron gun directs an electron beam towards the Matrix through the character-selection plates. The beam is deflected by these plates so that it passes through the desired Matrix aperature. As the beam leaves the Matrix, it has been shaped in the form of the character aperature through which it passed. The beam is then deflected to the proper position on the tube face. Images on the tube face are recorded by either a 35 mm or a 16 mm camera positioned above the tube.

The S-C 4020 displays characters on an area of 1024 horizontal and 1024 vertical spaces ("rasters") resulting in over one million addressable positions. After the desired margins have been reserved, the maximum range of the plot is scaled to the remaining rasters and the grid is drawn. Retaining the same scale factors, all data points are converted to its equivalent rasters and projected on the screen and film. The center of any available character may be projected on any of the addressable positions. The minimum area occupied by a character in the grid is three horizontal by three vertical spaces.

The following equations are used to compute the scale factors. Variables A and B represent the X axis scale factors and C and D represent the Y axis scale factor.

$$A = \frac{(1023. - FMR) - RML}{XR - XL}$$

$$B = FML - A \times XL$$

$$C = \frac{(1023. - FMT) - FMB}{YT - YB}$$

$$D = FMB - C + YB$$

where:

FMR = spaces reserved for right margin

FML = spaces reserved for left margin

XR = right limit of the scaled plotting area

XL = left limit of the scaled plotting area

FMT = spaces reserved for top margin

FMB = spaces reserved for bottom margin

YT = top limit of the scaled plotting area

YB = bottom limit of the scaled plotting area

These equations are used to convert data coordinates X and Y into raster coordinates for plotting.

$$IX = A \times X + B$$

$$IY = C \times Y + D$$

A Xerox Copyflo II-3 printer is available to produce single copies continuously from either 16 mm or 35 mm roll microfilm. These hard copies are produced at the rate of 28 frames (copies) per minute.

Accelerator System

The WHAM II, an acceleration device designed, constructed and operated by Wayne State University Biomechanics Research Center was modified for use in this investigation by adding the numerous safety redundancies required for man-rating. The device permitted use of the acceleration end for producing the experimental acceleration pulse and hence the subject was at rest during his initial condition as required by the instrumentation system.

A sled was designed and constructed by WSU especially for this project. It has a steel seat which permits forward and backward tilting in the mid-sagittal plane as well as rotation in the horizontal plane. A modified A-1 aircraft lap belt and shoulder harness with an inverted V and a chest safety strap formed the restraint system. This was secured as tightly as the subject would allow for each run, with the sole exception that the chest safety strap was simply made snug, with very little tension.

Seat back and shoulder harness heights were made adjustable to the individual, thus achieving maximum subject safety and restraint during acceleration and deceleration. This also permitted unhampered photography of the T_1 mount and the rear of the head and neck.

Experimental Controls and Determinations

The following methods were used to determine the effects of different values of a single variable and to control the effects of other variables believed to influence the dynamic response:

1. To control the effect of rate of onset of acceleration it was kept constant at a nominal 250 G/sec for the initial series of runs on each subject.

2. To determine the effect of rate of onset of acceleration the first step was to repeat the entire initial profile of increments of peak sled acceleration at a rate of onset double that of the initial series; that is, at a nominal 500 G/sec.

3. To control the effects of individual variations in muscle mass, strength and other anthropometric and anthropomorphic sources of variance, each subject was used as his own control.

4. To determine the effects of the subject size, subjects were selected on the basis of their sitting height.

5. To control the effect of variations in peak sled acceleration the accelerator control settings were reproduced as nearly as possible for each run at a given peak acceleration level.

6. To determine the effect of variations in peak sled acceleration each subject was exposed to individual runs at 1-G increments from 3 G through 10 G.

7. To control the effect of sled acceleration vector direction it was kept constant for all runs.

8. To control the effect of variations in distance between accelerometers in the mount and that of spatial relationships between accelerometers and rate gyroscope, the accelerometers and rate gyroscope were locked into place on the transducer module, and the entire transducer module was shifted to the corresponding mating and anatomical module of subsequent subjects. Thus the spatial relationships of the accelerometers and rate gyroscopes relative to each other for a given mount were constant for the entire series of runs.

9. To control the effect of differing distances between subjects from anatomical landmarks on any individual to the transducer module and photographic targets, precise photographic and x-ray anthropometry was performed on all subjects with the anatomical and transducer modules in place. Distances from external and internal landmarks to transducers and to the photographic targets were precisely known and did not vary from run to run on a given subject. Therefore, transformation of the measured accelerations and velocity from the point of measurement to the center of mass of the head of a given subject or to any specified location on the head of that subject was possible within a sagittal plane.

10. To determine the effect of instrumentation weight and its distribution each subject was exposed to several runs at both rates of onset with all mounts and photographic targets but with no instrumentation mounted except in the T_1 mount. These runs were termed unencumbered runs, and photographic data derived therefrom will be compared to those derived from fully instrumented runs. These data have not yet been analyzed.

11. To determine run-to-run repeatability for a given set of run parameters on individual subjects, multiple runs were performed on selected subjects at selected sled peak acceleration and rate of onset of acceleration values. These data are presented in plots 517 through 611.

12. To determine the change in distance between the T_1 and head anatomical coordinate systems due to the dynamic event, the change which occurred during a normal head nod of the fully instrumented and restrained volunteer were measured photographically. The reduced data from the special version of TROUTP (known as TROUTH) were compared with those from the dynamic event and the true change due to the acceleration determined.

The effect of the restraint variable is assumed to be independent of the fundamental relationship between the T_1 acceleration and the head acceleration. However, as a practical matter, each individual restraint system was adjusted as tightly as possible for each run, both as a safety measure and to keep the photographic targets within the field of view of the sled-mounted cameras. Parenthetically it should be noted that the restraint adjustment procedure was determined experimentally to result in apparent excellent control of the restraint variable, as will be shown later. An analysis of the precise effects of variations in the restraint of an individual subject on the dynamic response of the head and neck must be performed, but has not yet been accomplished.

Subjects and Procedure

Volunteer subjects from the U. S. Army were initially screened carefully by medical history, examination of personnel and health records, and independent interviews with two flight surgeons.

Those prospective subjects resulting from the screening were measured anthropometrically and preliminary selection was based on the single criterion of sitting height.

Candidates surviving the second selection were then examined thoroughly by specialists in aerospace medicine, dentistry, orthodontics, radiology, otorhinolaryngology, ophthalmology, neurology and psychiatry and vestibular physiology. All candidates who qualified in these examinations became subjects in the study; only about 5% of the volunteers successfully completed the entire selection program.

Two flight surgeons of the research team, who were physically qualified by the same standards, volunteered for duty and made several experimental runs as subjects.

A careful interim medical history was obtained from each subject prior to a run, and a physical examination and urinalysis were performed.

Following each run, the subject was carefully examined and studies made of his vestibular function, cardiac and neurological status, and urine. A 24-hour post-run history was taken prior to his next run. One run per subject per day was the maximum exposure rate.

The seated individuals were subjected to a $-G_x$ impact acceleration at the acceleration end. The end of the experimental conditions of interest occurred when dynamic response was substantially complete, which occurred in every instance prior to the end of the initial acceleration pulse. The sled achieved a peak velocity which remained relatively constant until the sled brakes were activated. Sled breaking produced a smooth 2-G deceleration until zero sled velocity was attained. Acceleration pulse shape for each run was triangular with a long decay.

A complete experimental run profile of nominal values for each subject included:

1. 3G through 10G at 250 G/sec in 1-G increments.

2. 3G through 8G at 500 G/sec in 1-G increments.

3. 6G, 250 G/sec; 10G, 250 G/sec; and 6 G, 500 G/sec unencumbered runs.

This involved a design goal of 17 runs for each subject.

Of the 236 human exposures to $-G_x$ impact acceleration in this program, 30 runs were incompletely instrumented and 7 were conducted on subjects wearing helmets; therefore, 199 human runs fulfilled the requirements for data analysis.

Six subjects completed the stated 17-run profile. An additional two subjects completed runs through 6 G, 500 G/sec, omitting only the 7 G and 8 G, 500 G/sec runs, for a total of 15 runs per subject. Of these eight subjects, two also completed 9 G, 500 G/sec runs. Additional runs were made, ranging in number from 1 through 11 by various other subjects.

Due to the extensive instrumentation, data retrieval, and data processing arrangements made for each experimental exposure, large masses of data are available. It was necessary to select for the present report data that were available in nine categories established by peak sled acceleration and rate of onset from 12 subjects. The selection was not a random, but was made on the basis of data available to meet

the requirements of this report. A listing of the runs selected is presented in the Results Chapter.

The effort has resulted in the formulation of an extensive body of experimental data. This report is a limited selection from the data base. Data presented consists of kinematic, and anthropometric variables requested by the Department of Transportation along with a detailed discussion of the methods of acquiring, processing, and analyzing the variables. Validation procedures and variables specifically selected to demonstrate validation are also presented.

REFERENCES

(1) Stapp, J. P, Human Exposure to Linear Acceleration. Part 2. The Forward Facing Position and the Development of a Crash Harness. WADC TR-5915. Part 2. Wright-Patterson Air Force Base, Ohio, Wright Air Development Center. 1951.

(2) Schulman, M., Critz, G. T., Highly, F. M. and Hendler, E., Determination of Human Tolerance to Negative Impact Acceleration. NAEC-ACEL 510. Philadelphia, Pa., Naval Air Engineering Center, Aerospace Crew Equipment Laboratory, 1963.

(3) Patrick, L. M., Von Kirk, D. J., and Nyquist, G. W., Vehicle Acceleration Crash Simulator. Proceedings of the Twelfth Stapp Car Crash Conference. New York, Society of Automotive Engineers, Inc., 1968, pp. 402 - 423.

THEORETICAL KINEMATICS OF THE EXPERIMENTS CHAPTER

Daniel J. Thomas

GENERAL

Within the context of the experimental program the effort to measure the exact kinematics of the human head and neck is of paramount importance. The results of the effort constitutes the major portion of this report. A detailed description of the theoretical kinematics to understand and describe the measurements, derived variables, and validation procedures is required.

The study of the mechanics of human subjects can be organized according to classical mechanics. The size and shape of the human beings constitute geometry. The mass distribution parameters associated with the size and shape constitute the statics of human subjects. The motions of anatomical segments constitute the kinematics. The forces and torques underlying these motions constitute the dynamics. The classification of the mechanics of human subjects into geometry, statics, kinematics, and dynamics is completely sufficient provided the analysis is restricted to the consideration of rigid body mechanics. For these experiments the rigid bodies are:

1. The head with attached mouth and head mounts, and their attached targets and transducers.

2. The first thoracic vertebra with attached spine mount, transducers and targets. The kinematic measurements of the experiment documents the motions between these two rigid bodies and is valid to the degree that each body remains rigid. This is what is meant by the measurement of the response of the head and neck. In order to systematically provide for these measurements and to make the coordinate system transformations necessary to analyze the data a standard procedure for defining coordinate systems and kinematic variables and a minimal set of defined coordinate systems is required.

DEFINITIONS OF COORDINATE SYSTEMS

Although the experiments to date were confined to two dimensions, the approach to the description of the coordinate systems and variables is applicable in three dimensions. This was achieved by first defining a set of basic orthogonal three dimensional coordinate systems. The variables are all expressed in terms of these coordinate systems. Although a standard procedure for defining coordinate systems has been adopted by the laboratory, this system was not in effect at the time of collection and initial processing of the two dimensional data from the human runs conducted at Wayne State University (1). Therefore, the current program and variables which were measured or used in intermediate calculations do not conform to the laboratory standard. However, all variables which are plotted for this report have been expressed within the laboratory standard as a final step prior to plotting.

The minimum rules for coordinate system definition which were identified and selected are:

1. Select an origin.

2. Select the first and second axes of the system, which must be at right angles to each other.

3. Define the third axis and all operations, parameters and variables within the coordinate system by use of a right-hand rule.

4. +0 degrees to +90 degrees (first quadrant) will always be subtended by the positive axes in the plane in which the angle is described.

For this report the notation X, Y, Z is used to specify the 1st, 2nd, and 3rd axis of any defined coordinate system.

The units of measure for all kinematic variables will be centimeters, radians, and milliseconds, with the exception that categorization and identification of runs uses G for acceleration and G per second for rate of onset. One G is equivalent to .000980616 centimeters per millisecond squared. Also, values extracted from the plots for discussion in the text have been converted into more readily comprehended units, in which case the units are given.

The coordinate systems required for these experiments are grouped into four categories:

1. Reference - is any coordinate system in which measurements are directly taken.

2. Instrumentation - is any coordinate system established by instrumentation or photographic target location.

3. Anatomical - is any coordinate system established by the anatomical landmarks of a test subject.

4. Principal - is any coordinate system established by determination of the center of gravity and principal axes of the moment of inertia of a defined rigid segment.

The defined coordinate systems remain rigid throughout the experiment.

The individual coordinate systems required for these experiments are further defined below.

The reference coordinate systems (Figure 1) are:

1. The inertial reference coordinate system is one in which the linear and angular acceleration is zero. The origin at data analysis time zero (DATZ) is at zero velocity at the origin of the laboratory reference system defined below. The +Z axis is opposite in direction to gravity and the +X axis is opposite in direction

REFERENCE COORDINATE SYSTEMS

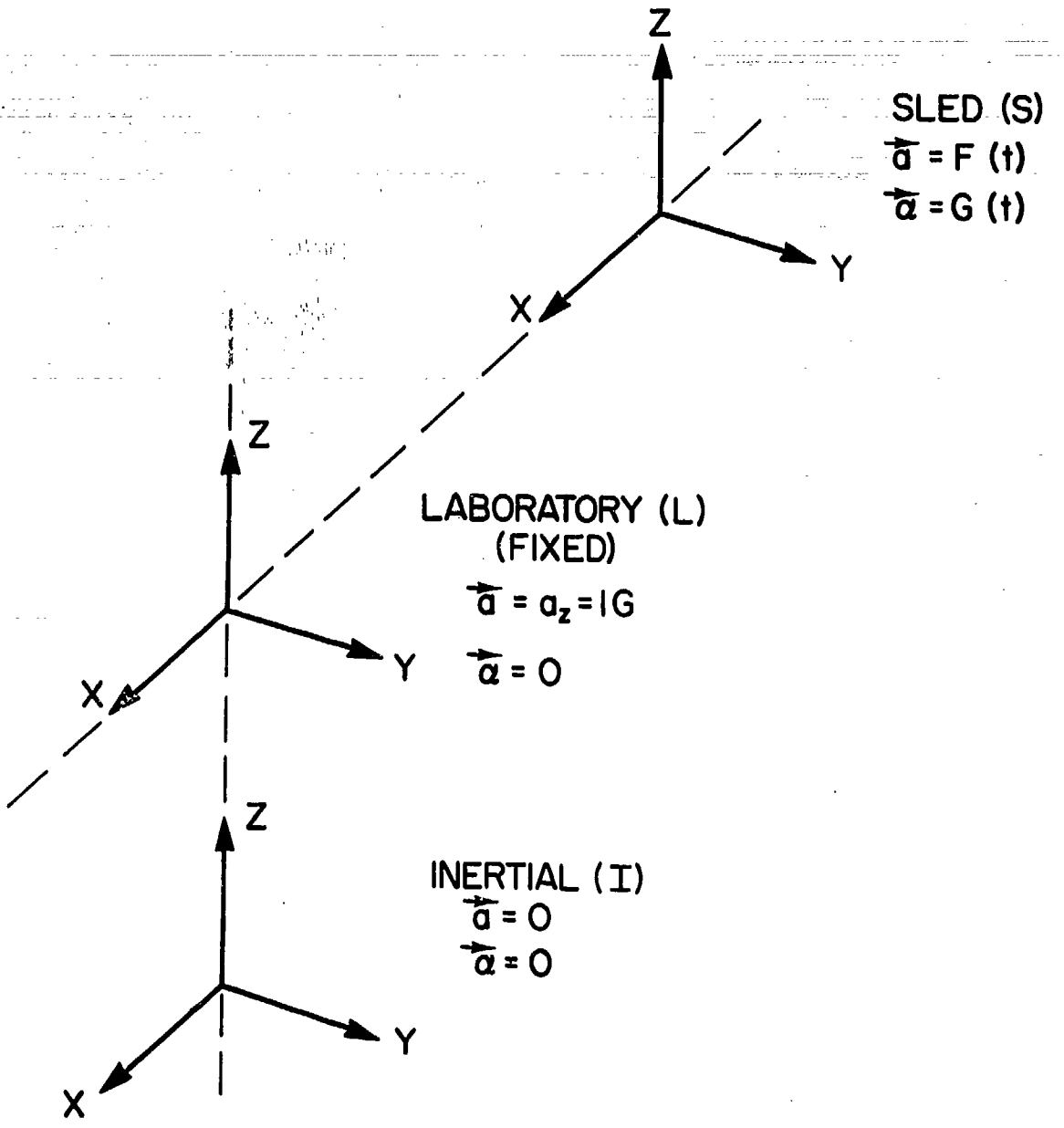

FIGURE 1

to the acceleration stroke. This coordinate system translates relative to the laboratory reference system at a velocity dependent on the acceleration of gravity.

2. The sled reference coordinate system has its origin fixed to the sled chair target center with axes parallel to the inertial reference system.

3. The laboratory reference coordinate system has its origin fixed at the point occupied by the sled chair target center prior to the onset of acceleration with axes parallel to the inertial sled reference system.

4. The Telereadex reference system is established by the film reader device at the sled chair origin with axes slightly rotated from the sled reference axes. This coordinate system is not illustrated because of its minor differences from the sled reference coordinate system.

The instrumentation coordinate systems are:

1. The photo head mount instrumentation coordinate system (Figure 2) has its origin at the midpoint between the head mount target and the mouth mount target. The +X axis is in the direction of the line between the targets from the head mount target to the mouth mount and the +Z axis is perpendicular to the line between the targets in the superior direction of the man.

2. The photo spine mount instrumentation coordinate system (Figure 3) has its origin at the midpoint between the spine mount targets. The +X axis is in the direction of the line connecting the targets in the anterior direction of the man and the +Z axis is perpendicular to this line in the superior direction of the man.

3. The transducer mouth mount instrumentation coordinate system (Figure 2) has its origin at the midpoint between the mouth accelerometers. The +X axis is parallel to the superior surface of the mouth mount in the anterior direction and the +Z axis is perpendicular to the +X axis in the superior direction.

4. The transducer head mount instrumentation coordinate system (Figure 2) has its origin at the midpoint between the top of the head accelerometers. The +X axis is parallel to the superior surface of the mount in the anterior direction and the +Z axis is perpendicular to the +X axis in the superior direction.

5. The transducer center of head instrumentation coordinate system is identical to the photo head mount instrumentation coordinate system by virtue of the fact that the mouth mount target was placed at the midpoint between the mouth mount accelerometers and the head mount target was placed at the midpoint between the head mount accelerometers.

6. The transducer spine mount coordinate system (Figure 3) has its origin at the midpoint between the spine mount accelerometers. The +X axis is parallel to the superior surface of the mount in the anterior direction and the +Z axis is perpendicular to the +X axis in the superior direction. This coordinate system has its origin identical to the photo spine mount instrumentation coordinate system with a fixed angle (0.2 radians) between respective +X axes.

INSTRUMENTATION AND ANATOMICAL COORDINATE SYSTEMS (HEAD)

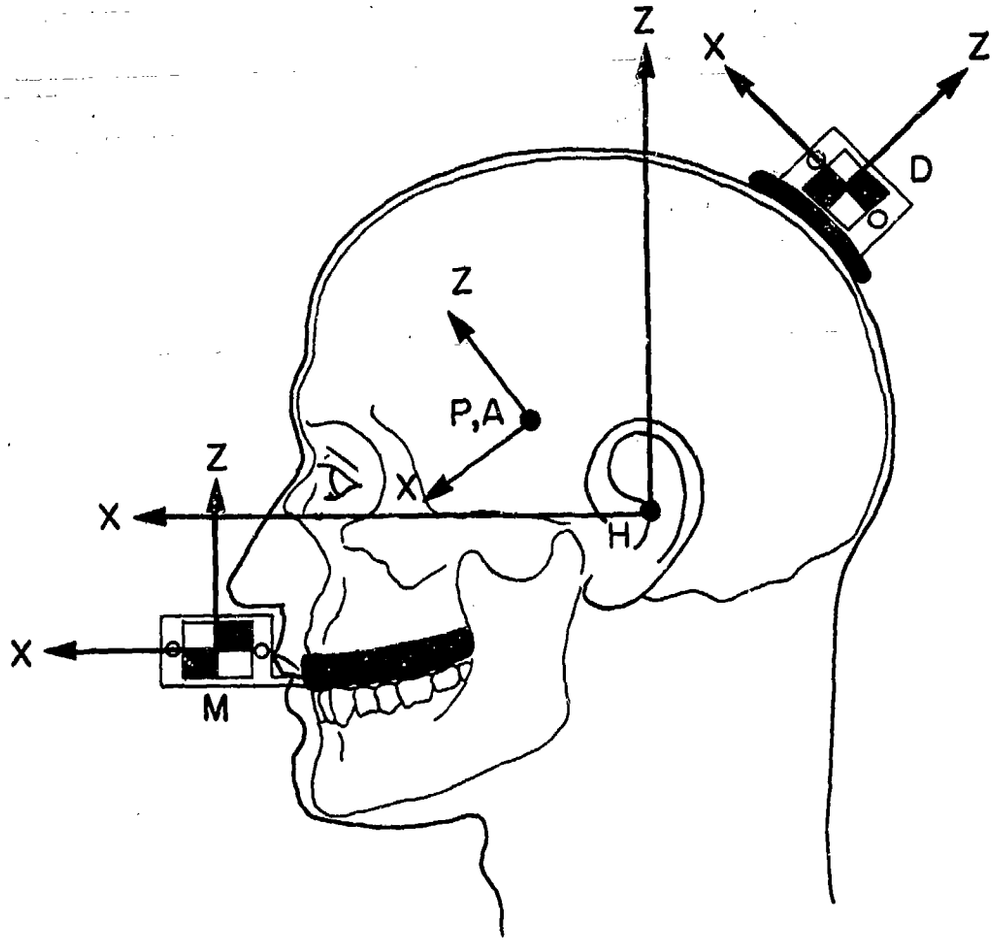

INSTRUMENTATION COORDINATE SYSTEMS

P = PHOTO HEAD MOUNT
A = TRANSDUCER CENTER OF HEAD
M = TRANSDUCER MOUTH MOUNT
D = TRANSDUCER HEAD MOUNT

ANATOMICAL COORDINATE SYSTEM

H = HEAD ANATOMICAL

FIGURE 2

INSTRUMENTATION AND ANATOMICAL COORDINATE SYSTEMS (SPINE)

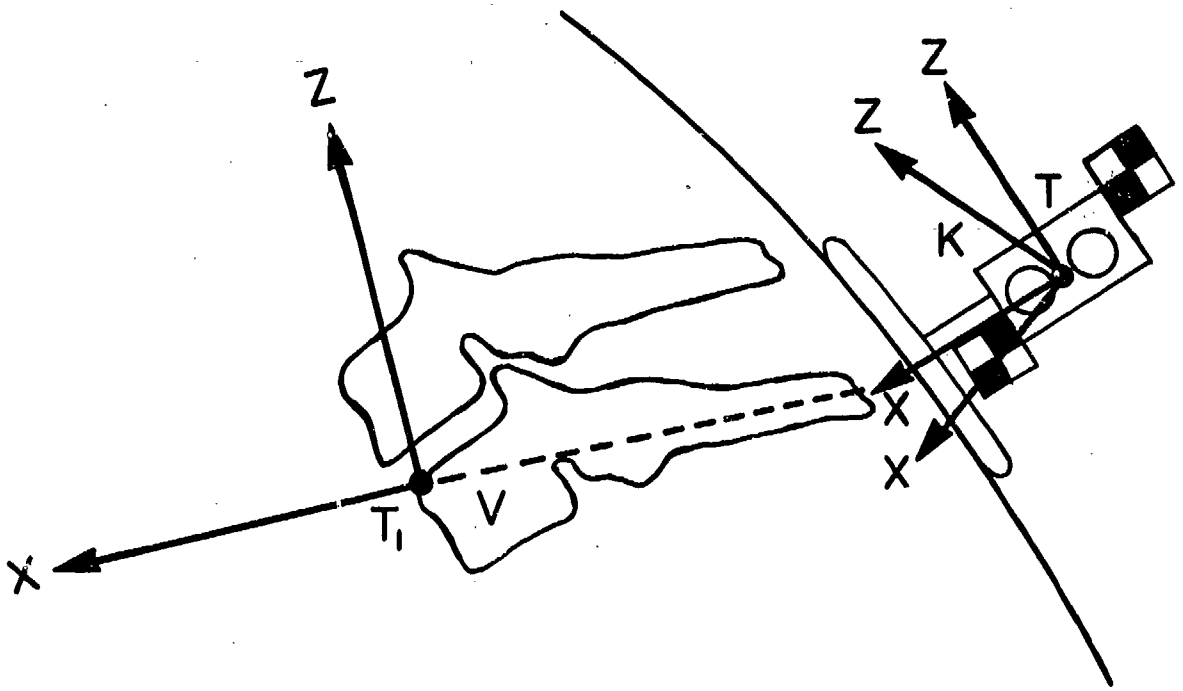

V = FIRST THORACIC VERTEBRA

INSTRUMENTATION COORDINATE SYSTEMS

K = PHOTO SPINE MOUNT

T = TRANSDUCER SPINE MOUNT

ANATOMICAL COORDINATE SYSTEM

T_1 = SPINE (T_1)

FIGURE 3

The anatomical coordinate systems are:

1. The head anatomical coordinate system (Figure 2) is derived from an anatomical plane which is specified by the superior edge of each auditory meatus and by the infraorbital notches. The origin is at the midpoint of a line connecting the superior edges of the right and left auditory meati. The +X axis is from the origin through the midpoint of a line connecting the infraorbital notches in the anatomical plane. The +Z axis is from the origin in the superior direction perpendicular to the anatomical plane. For the purpose of this work, the XZ plane thus described is considered a precise definition of the mid-sagittal plane.

2. The spine (T_1) anatomical coordinate system (Figures 3 and 4) has its origin at the anterior superior corner of the first thoracic vertebral body (T_1). The +X axis is defined by a direction connecting the midpoint of the superior corner and the inferior corner of the posterior spinous process of T_1 to the anterior superior corner of T_1. The +Z axis is perpendicular to the X axis in the plane of the above three points and in the superior direction.

All principal coordinate systems must be experimentally determined and therefore are expressed in terms of the chosen anatomical coordinate system. The principal coordinate system is:

1. The head principal coordinate system is expressed in terms of the head anatomical coordinate system and has its own origin at the center of gravity of the head as defined in the Tulane and NAMRL studies, both of which are still unpublished ( ). There is insufficient information to specify the principal axes of the moment of inertia so the axes remains undefined. The origin (C.G.) is illustrated in Figure 5.

ANATOMICAL COORDINATE SYSTEM (SPINE)

FIGURE 4

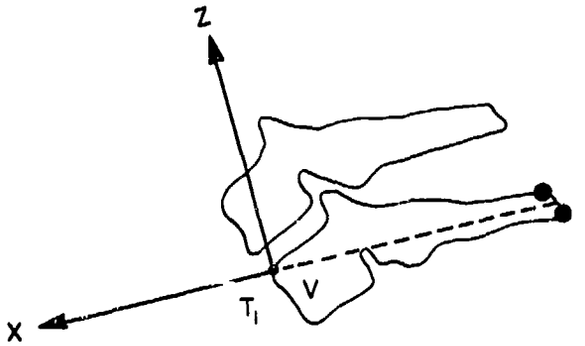

T_1 = SPINE (T_1) ANATOMICAL COORDINATE SYSTEMS
V = FIRST THORACIC VERTEBRA

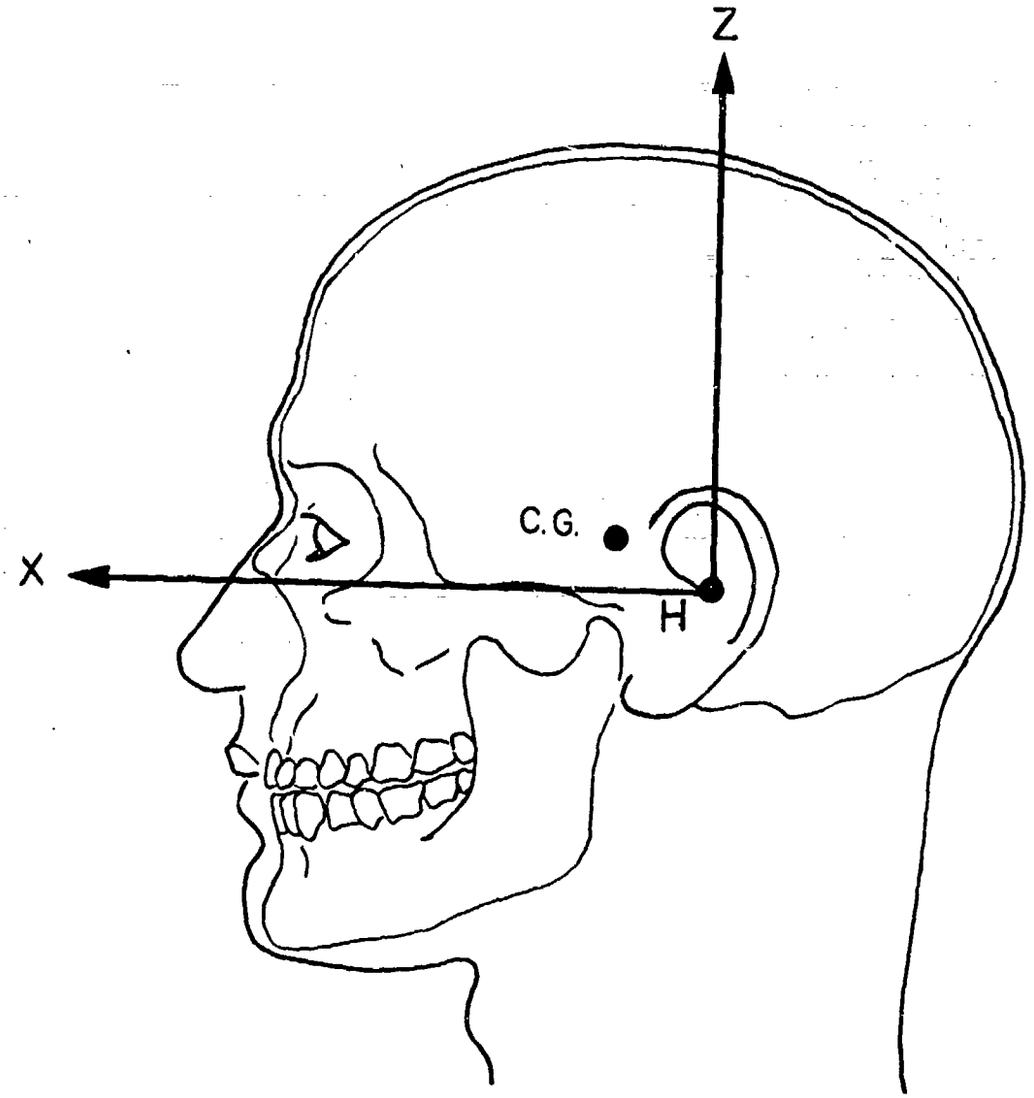

H = HEAD ANATOMICAL COORDINATE SYSTEM
C.G. = CENTER OF GRAVITY OF HEAD

FIGURE 5

DEFINITIONS OF PHYSICAL TERMS USED TO DEFINE VARIABLES

The kinematics of human subjects constitute the major portion of the data presented in this report. The anatomical segments of interest are treated as rigid bodies. Therefore, the terms used to define the variables are taken from rigid body kinematics. The definition of physical terms is as follows:

1. Displacement is a vector quantity describing the position of one point relative to another point.

2. Angular displacement is a transformation describing the orientation of one coordinate system relative to another coordinate system. For two dimensional motion where the angular displacement is restricted to a single plane, the angular displacement is identical to an angle defined by the angular position of one vector direction relative to another vector direction.

3. Velocity is a vector quantity describing the time rate of change of displacement.

4. Angular velocity is a vector quantity describing the instantaneous angular time rate of change of the angular displacement of one coordinate system relative to another coordinate system. For two dimensional motion in which angular displacement is an angle, angular velocity is the time rate of change of the angle.

5. Acceleration is a vector quantity describing the time rate of change of velocity.

6. Angular acceleration is a vector quantity describing the time rate of change of angular velocity.

For this report all points selected for displacement measurements are origins of defined coordinate systems. Since all motions discussed in this report are two dimensional and constrained to the mid-sagittal plane of the subject, description of vector directions are sufficient to define the angle identical to angular displacement.

All vector directions selected for angular displacement measurements are the directions of the axes of defined coordinate systems. In general, all terms are vector quantities except angular displacement. In particular for this report since the motions are two dimensional, the linear quantities are vectors described by two components and the angular quantities can be treated as scalers requiring only a magnitude. In most cases the magnitude of the linear quantities is also given.

DEFINITION OF VARIABLES

The kinematic variables presented in graphical form are defined. Selected variables that are needed to clarify the definitions of variables which are graphically presented are also defined. The definitions consist of vector and scaler magnitudes, vector Cartesian components and one polar angle and are arranged by computer program names or stage of processing.

A variable of the same name is fundamentally the same physical quantity with necessary processing changes introduced by each program. The definitions will reflect this. The groupings of the variables in order are:

PLOT
INTERMEDIATE
TROUTP
PHDATA
REDUCED PHOTOGRAPHIC DATA
TROUT
OUTVAR
DSCALE
BETHO2
BETHBH
ANALOGUE
ICONDS
ANXRAY

The definition of the variables includes a statement of its physical nature along with a statement of source where considered necessary for clarity. A variable once defined under a grouping will only have its changes noted within succeeding groupings.

The PLOT grouping consists only of variables appearing on the plots. The INTERMEDIATE grouping consists of two simply computed variables that are required to compute the plotted variable. The other groupings refer to the analogue data, programs or photographic data reduction which is explained in the appropriate sections. Selected important angular and linear displacement variables are illustrated by drawings. The source of all variables which are presented is illustrated in flow chart format. The charts showing the source of the plotted variables do not show PLOT blocks. These blocks are implied.

Two important constants fixed by the transducer mount design are given after the variable definitions.

PLOT Variables	Definitions
DATZ	is Data Analysis Time Zero which is 36 milliseconds prior to the statistically determined sled peak acceleration.
HSP	is the magnitude of distance of the head target center from the mouth target center, Figures 6 and 8.
MCT	is the magnitude of displacement of the head principal coordinate system origin (C.G.) relative to the spine (T1) anatomical coordinate system origin, as computed from PLOT XCN and PLOT ZCN, Figures 7 and 8.

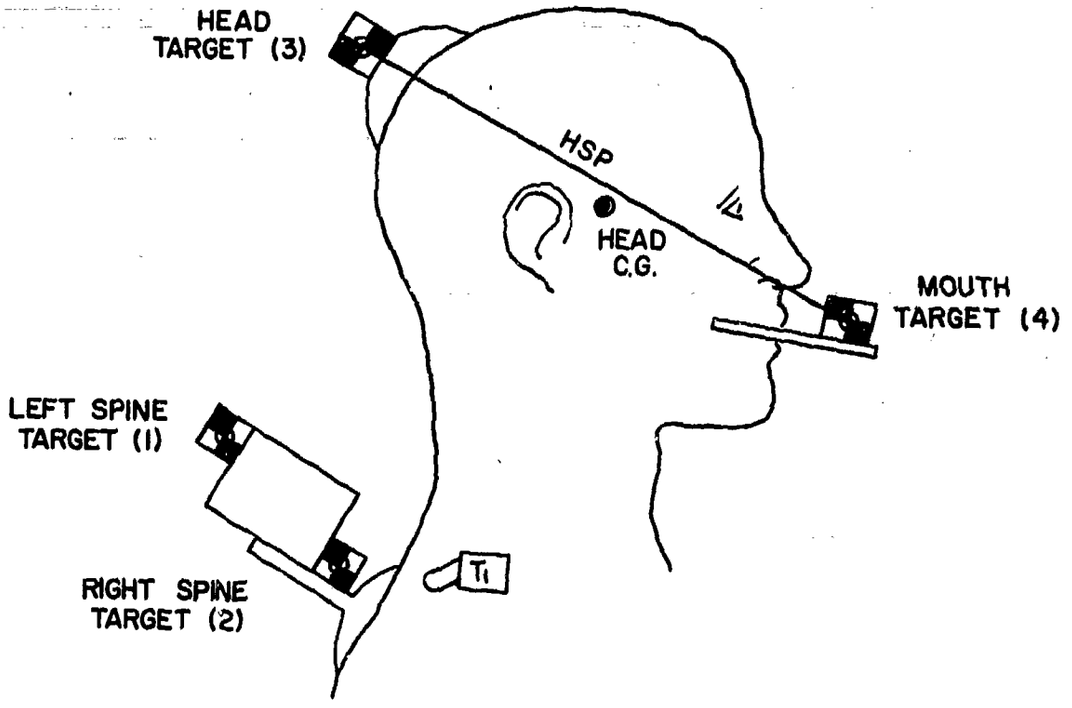

ILLUSTRATION OF HSP AND SUBJECT MOUNTED PHOTOGRAPHIC TARGETS

FIGURE 6

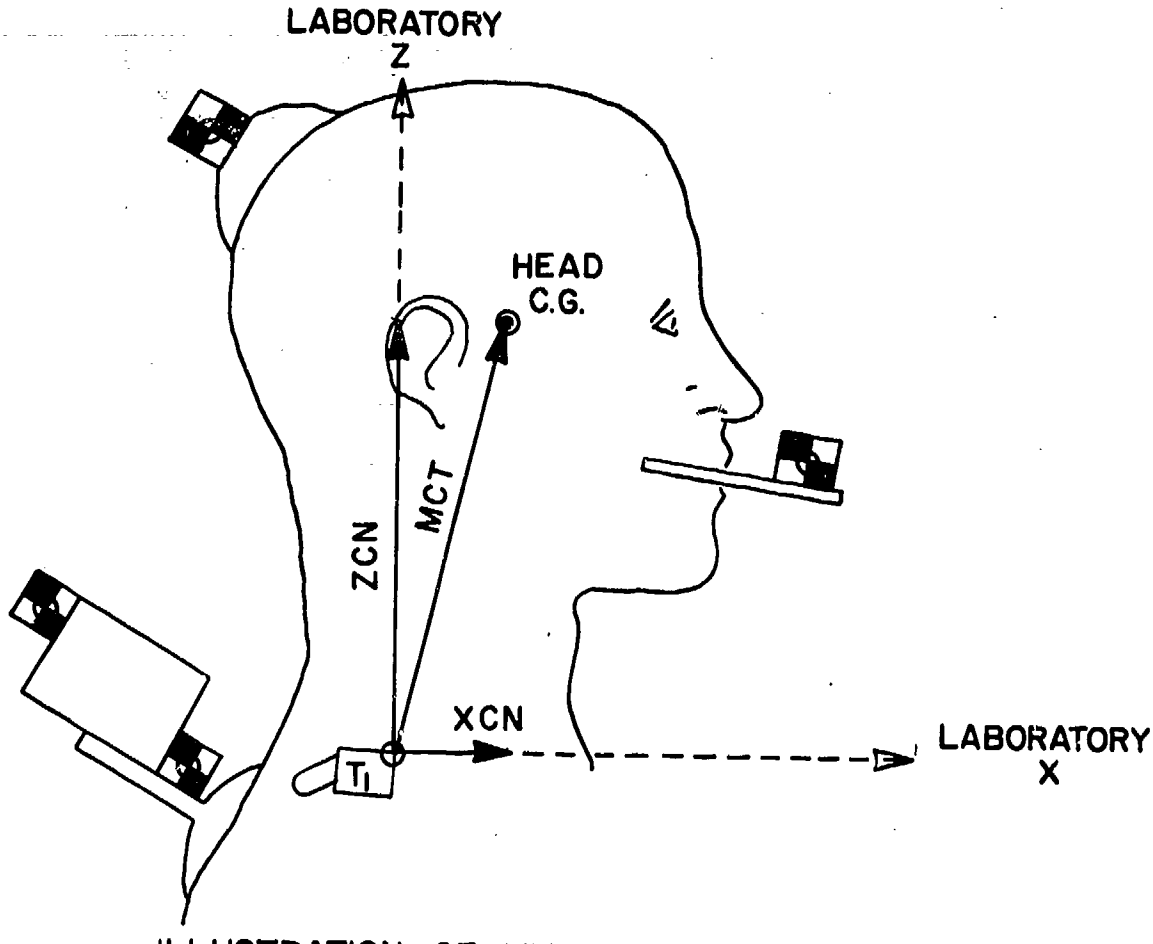

ILLUSTRATION OF VARIABLE MCT, COMPONENTS XCN AND ZCN IN LABORATORY COORDINATE SYSTEM DIRECTIONS

FIGURE 7

SOURCE OF VARIABLES XCN, ZCN, MCT, MCX, MCZ, HSP

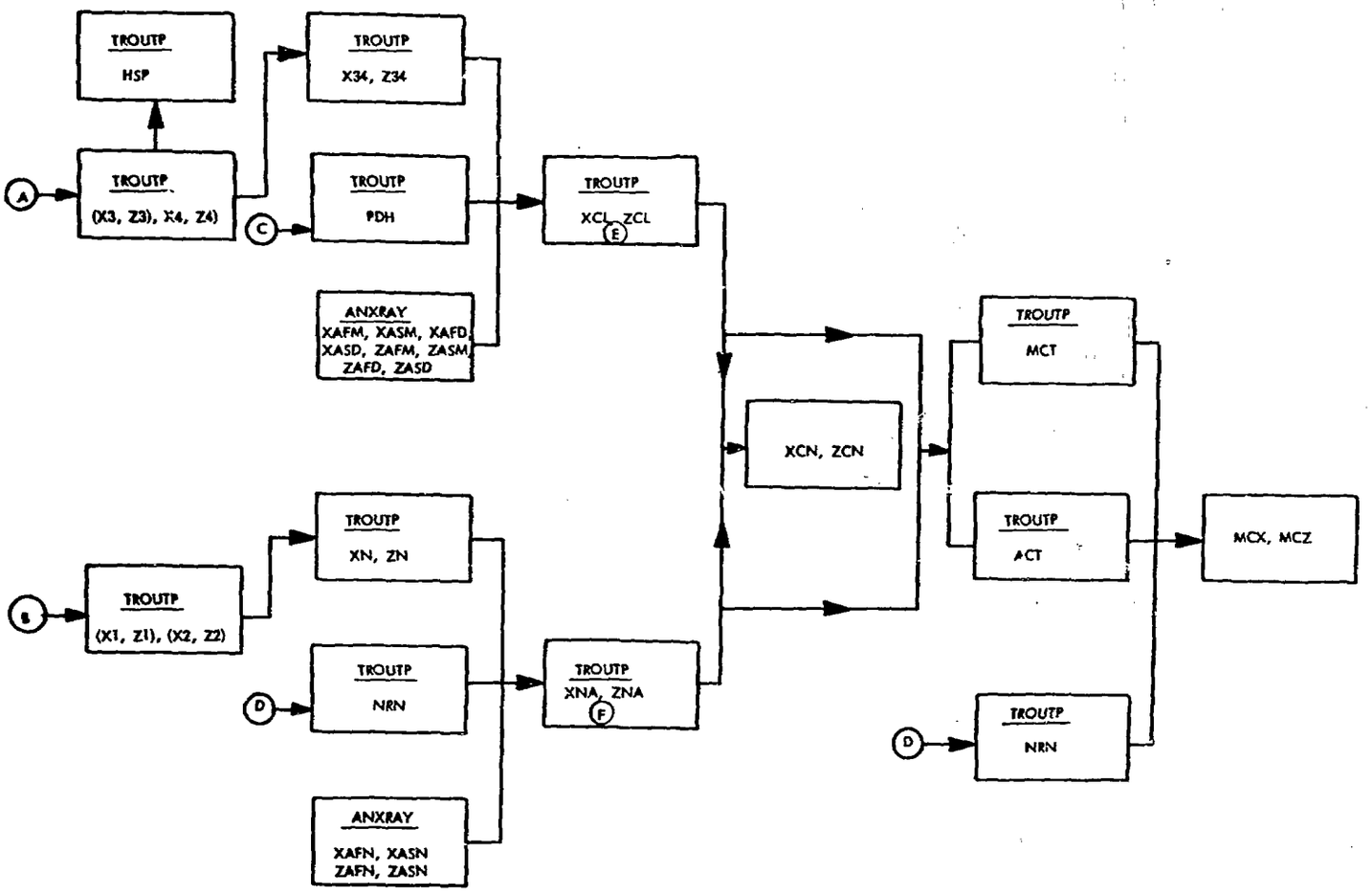

FIGURE 8

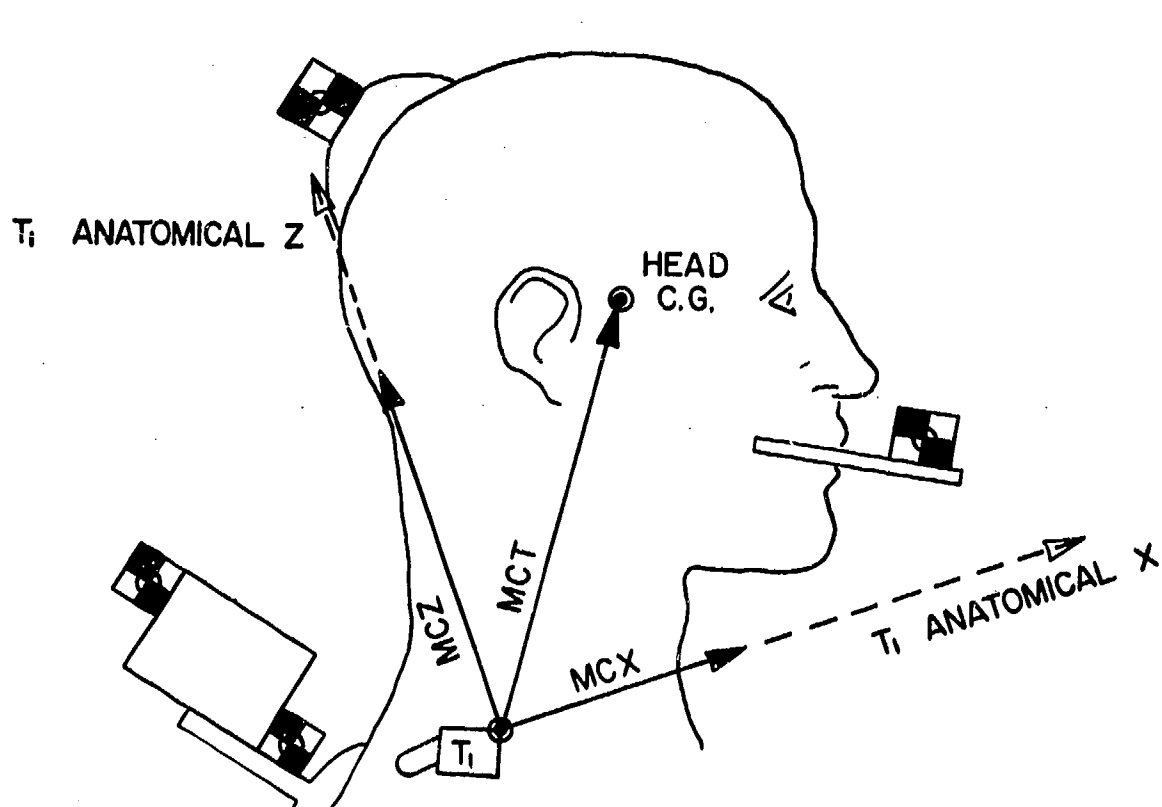

ILLUSTRATION OF VARIABLE MCT, COMPONENTS MCX, MCZ IN THE T_i ANATOMICAL COORDINATE SYSTEM DIRECTIONS

FIGURE 9

SOURCE OF VARIABLES XCV, ZCV, XNV, ZNV, XZV, NNV

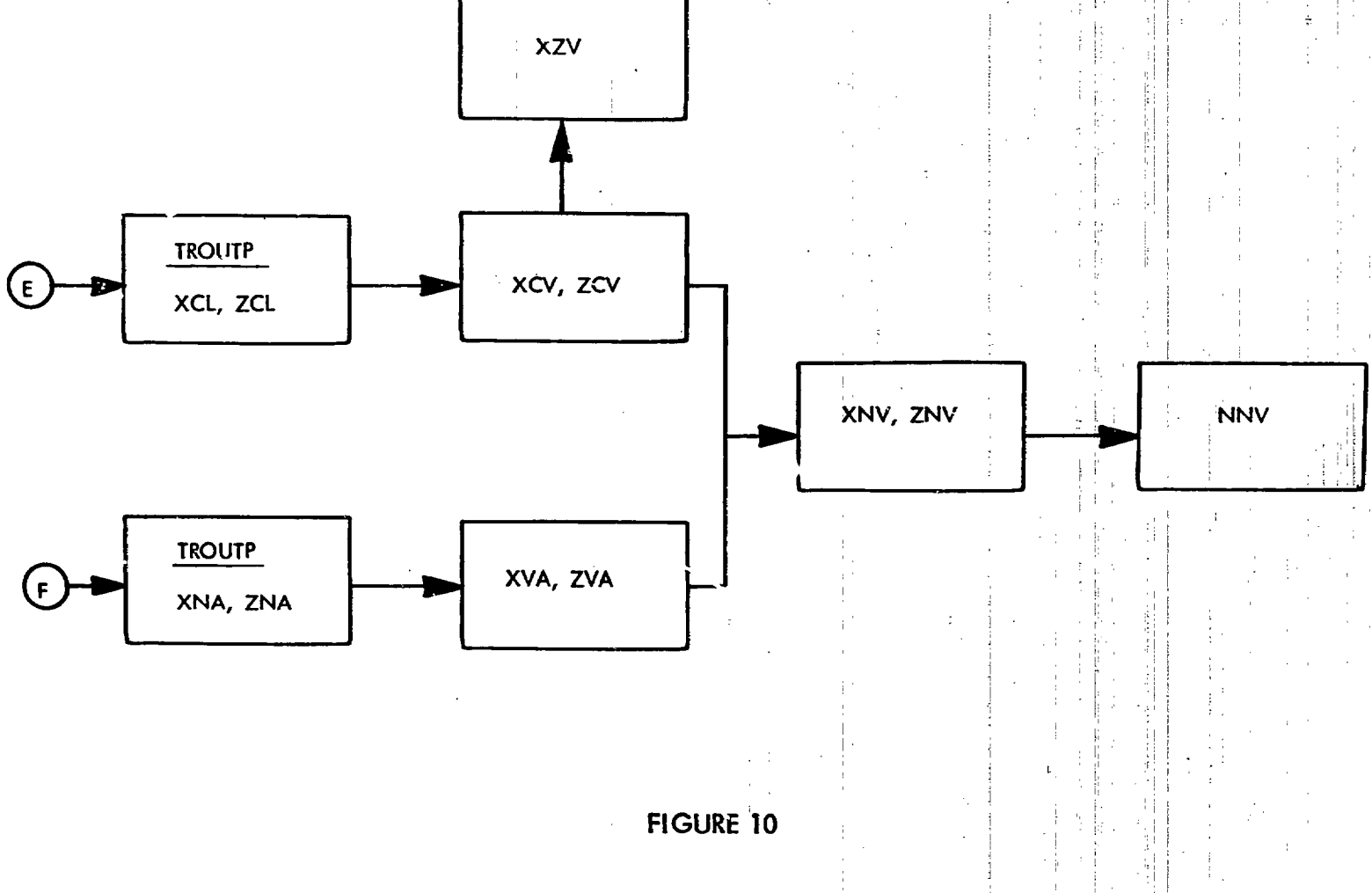

FIGURE 10

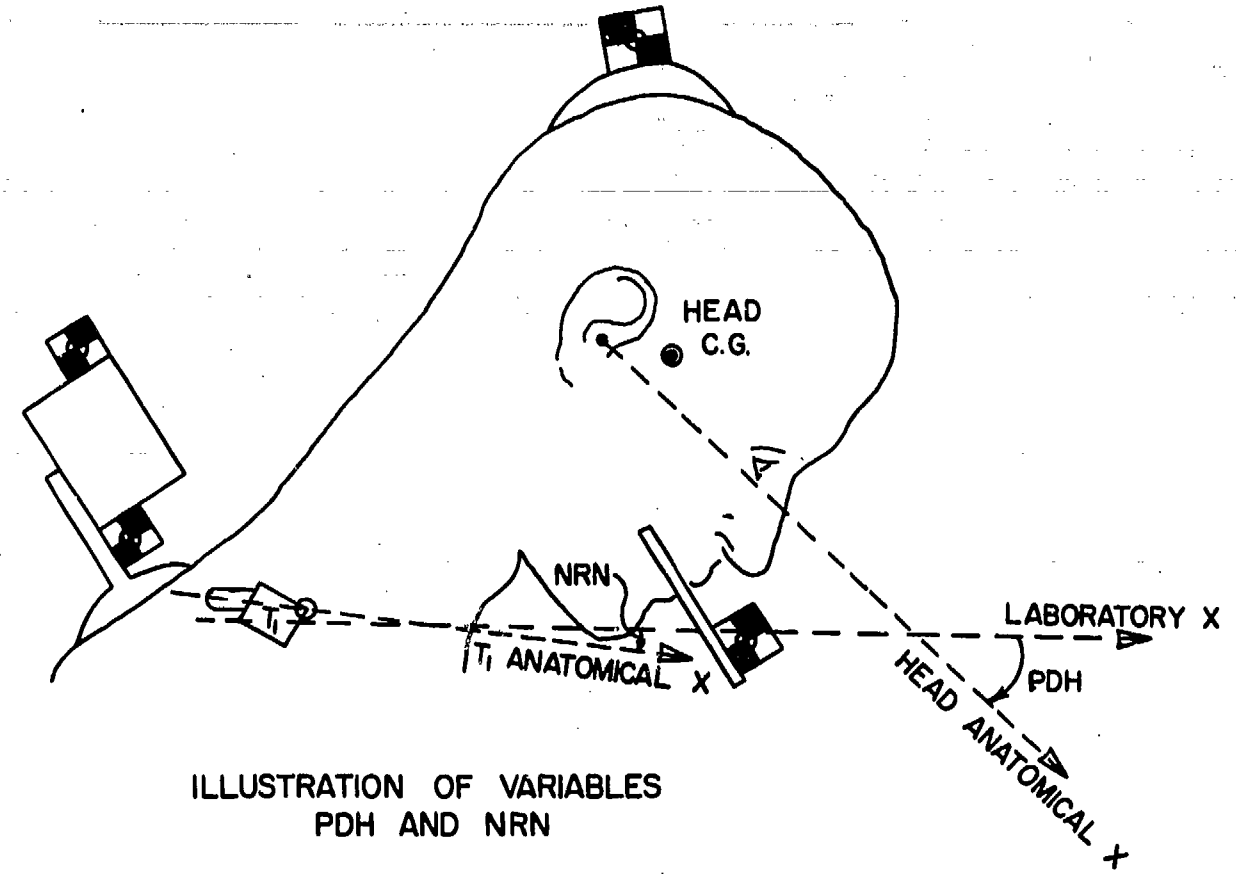

ILLUSTRATION OF VARIABLES
PDH AND NRN

FIGURE 11

SOURCE OF VARIABLES PHN, NRN

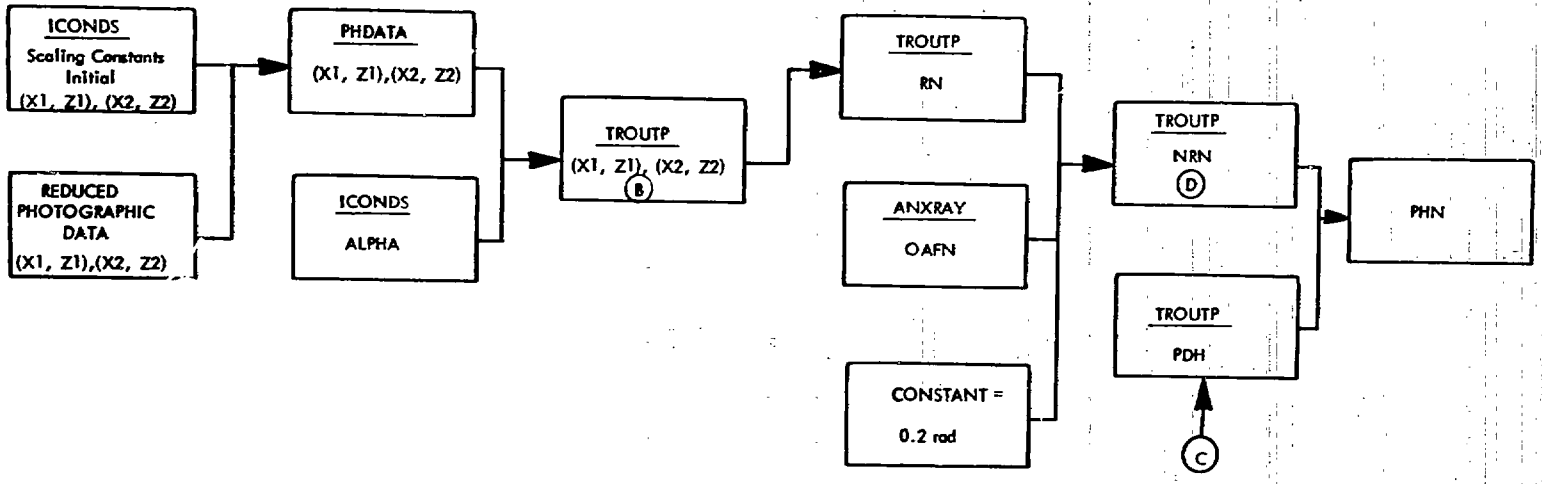

FIGURE 12

SOURCE OF VARIABLE PDH

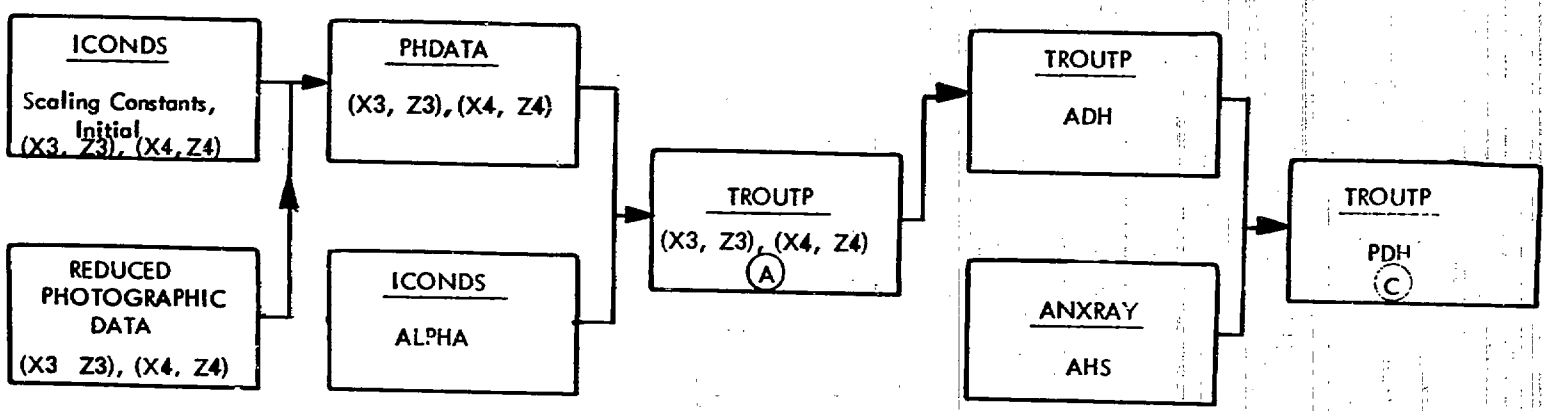

FIGURE 13

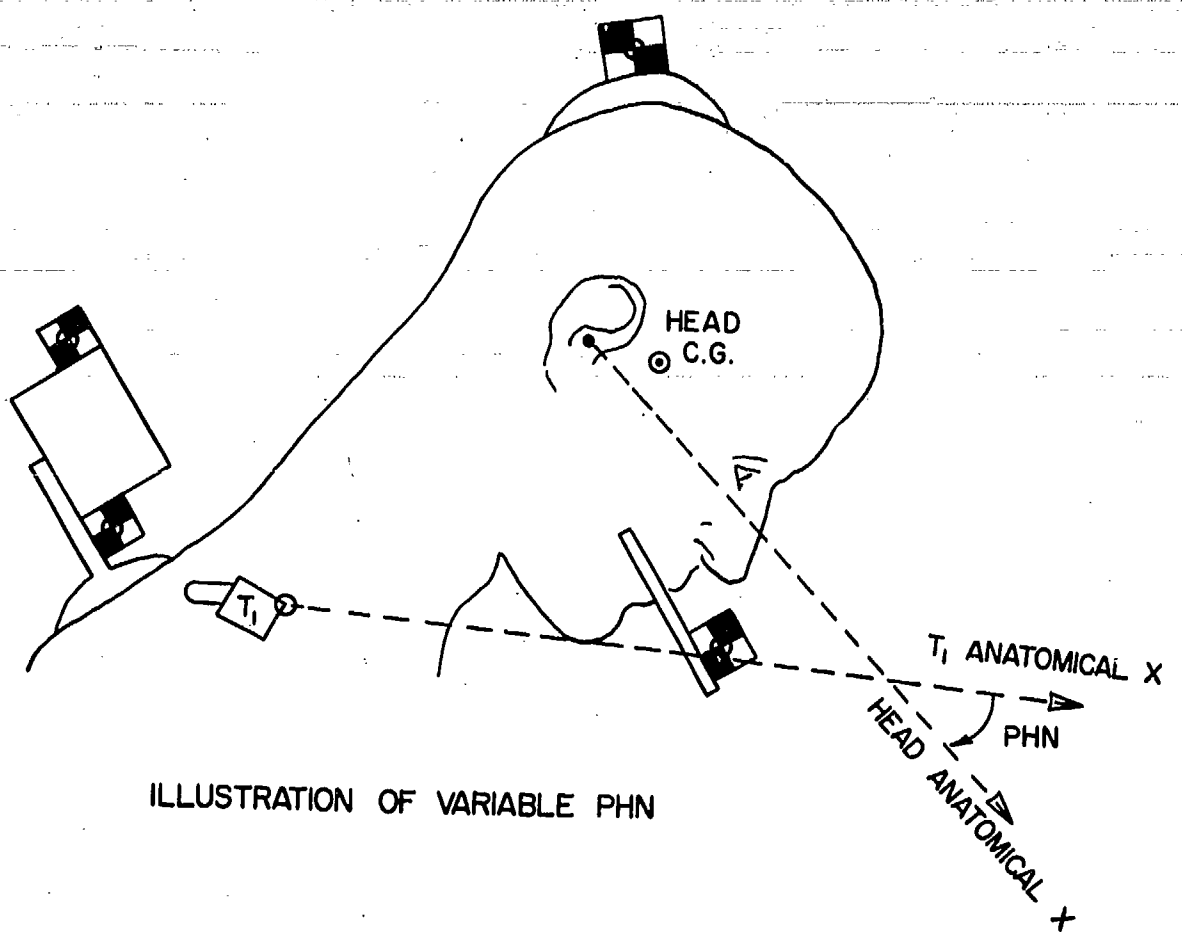

ILLUSTRATION OF VARIABLE PHN

FIGURE 14

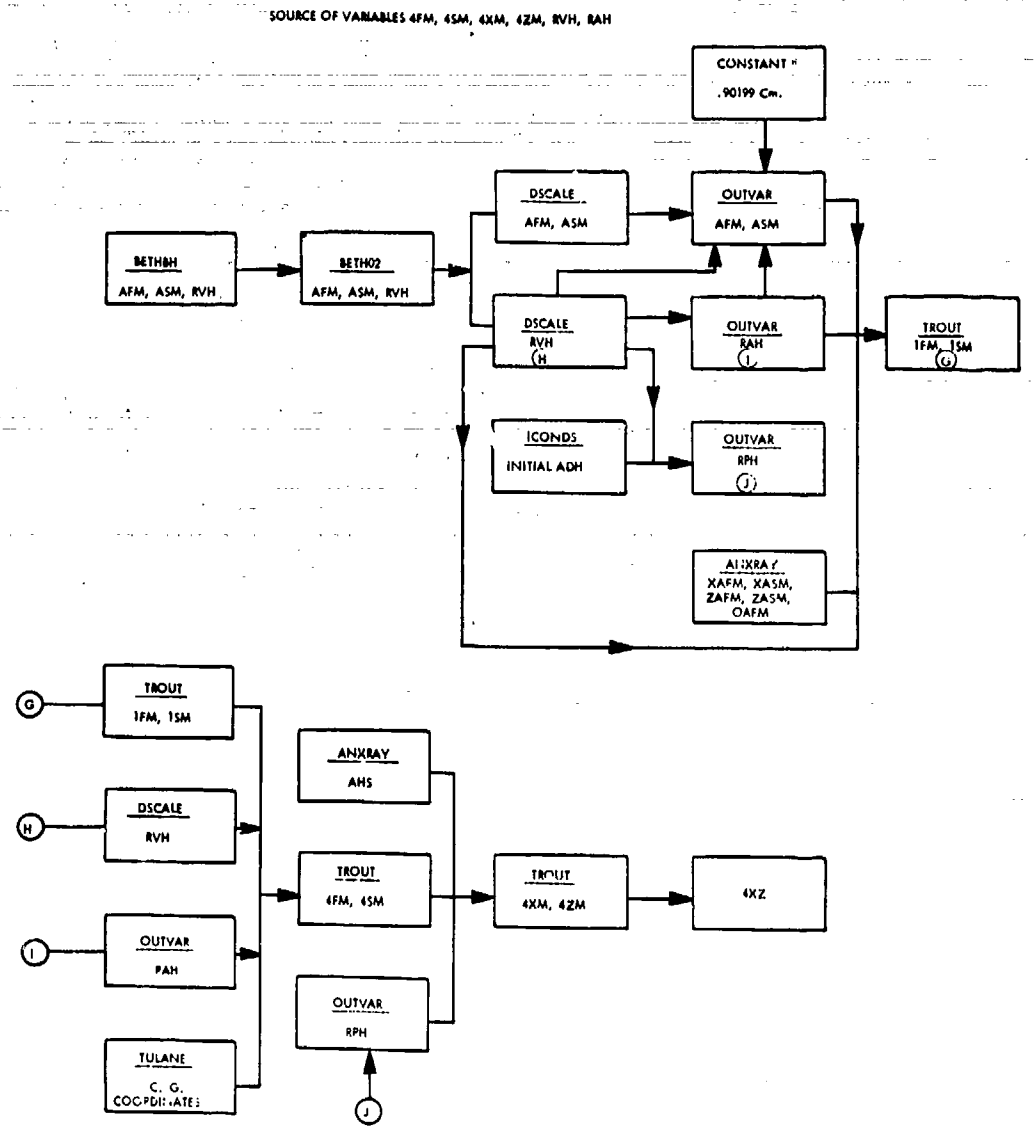
SOURCE OF VARIABLES 4FM, 4SM, 4XM, 4ZM, RVH, RAH
CONSTANT
.90199 Cm.
DSCALE
AFM, ASM
OUTVAR
AFM, ASM
BETH0H
AFM, ASM, RVH
BETH02
AFM, ASM, RVH
DSCALE
RVH
H
OUTVAR
RAH
I
TROUT
1FM, 1SM
G
ICONDS
INITIAL ADH
OUTVAR
RPH
J
AUXRAY
XAFM, XASM,
ZAFM, ZASM,
OAFM
G
TROUT
1FM, 1SM
H
DSCALE
RVH
I
OUTVAR
RAH
TULANE
C. G.
COORDINATES
ANXRAY
AHS
TROUT
4FM, 4SM
OUTVAR
RPH
J
TROUT
4XM, 4ZM
4XZ

FIGURE 15

SOURCE OF VARIABLE RDH

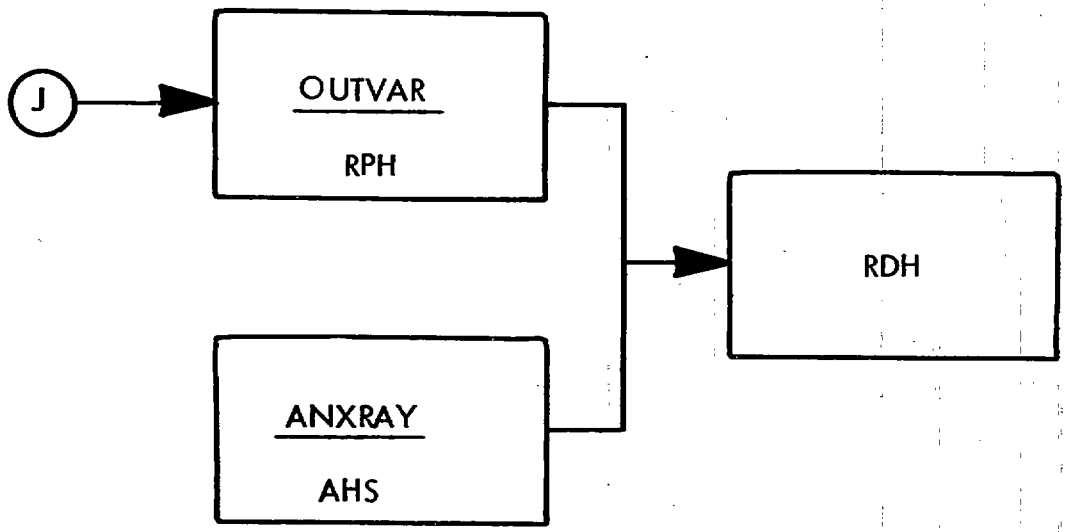

FIGURE 16

SOURCE OF VARIABLES RVN, RHN

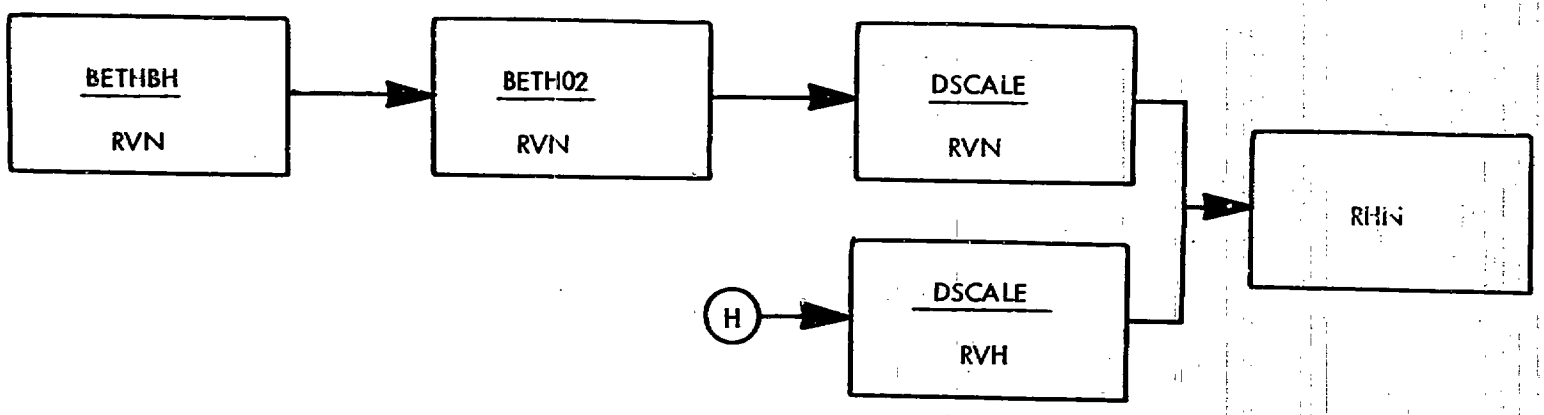

FIGURE 17

MCX	is the component of displacement of the head (C.G.) relative to the (T_1) anatomical coordinate system origin along the +X axis of the T_1 anatomical coordinate system, Figures 8 and 9.
MCZ	is the component of displacement of the head (C.G.) relative to the T_1 anatomical coordinate system origin along the +Z axis of the T_1 anatomical coordinate system, Figures 8 and 9.
NNV	is the magnitude of the velocity of the head (C.G.) relative to the T_1 anatomical coordinate system origin, Figure 10.
NRN	is the magnitude of the angular displacement of the +X axis of the T_1 anatomical coordinate system relative to the +X axis of the laboratory coordinate system, Figures 11 and 12.
PDH	is the magnitude of the angular displacement of the +X axis of the head anatomical coordinate system relative to the +X axis of the laboratory coordinate system as computed from photographic data, Figures 11 and 13.
PHN	is the magnitude of the angular displacement of the +X axis of the head anatomical coordinate system relative to the +X axis of the T_1 anatomical coordinate system as computed from photographic data. It is PLOT PDH minus PLOT NRN, Figures 12 and 14.
RAH	is the magnitude of the angular acceleration of the angle from the +X axis of the head anatomical coordinate system relative to the +X axis of the laboratory reference coordinate system as computed from the rate gyroscope. It is the time rate of change of PLOT RVH, Figure 15.
RDH	is the same as PLOT PDH except that it is computed from the rate gyroscope data, Figure 16.
RHN	is the magnitude ot the angular velocity of the angle from the +X axis of the head anatomical coordinate system relative to the +X axis of the T_1 anatomical coordinate system as computed from the rate gyroscopes, Figure 17.

RVH	is the magnitude of the angular velocity of the angle from the +X axis of the head anatomical coordinate system relative to the +X axis of the laboratory reference coordinate system as computed from the rate gyroscope, Figure 15.
XCN	is the component of displacement of the head C.G. relative to the T1 anatomical coordinate system origin along an axis parallel to the +X axis of the sled reference coordinate system, Figures 7 and 8. It is TROUTP XCL minus TROUTP XNA.
XCV	is the component of the velocity of the head C.G. relative to the sled reference coordinate system origin along an axis parallel to the +X axis of the sled reference coordinate system. It is the time rate of change of TROUTP XCL, Figure 10.
XDC	is the displacement of the sled coordinate system origin relative to the laboratory coordinate system origin. This displacement is constrained to the laboratory -X axis, Figure 18.
XNV	is the component of the velocity of the head C.G. relative to the T1 anatomical coordinate system origin along an axis parallel to the +X axis of the sled reference coordinate system. It is XCV minus INTERMEDIATE XVA, Figure 10.
XVC	is the velocity of the sled coordinate system origin relative to the laboratory coordinate system. This velocity is constrained to the laboratory -X axis, Figure 18.
XZV	is the magnitude of the velocity of the head C.G. relative to the sled reference coordinate system origin as computed from PLOT XCV and PLOT ZCV, Figure 10.
ZCN	is the component of the displacement of the head C.G. relative to the T1 anatomical coordinate system origin along an axis parallel to the +Z axis of the sled reference coordinate system data. It is TROUTP ZCL minus INTERMEDIATE ZNA, Figures 7 and 8.
ZCV	is the component of velocity of the head C.G. relative to the sled reference coordinate system origin along an axis parallel to the +X axis of the sled reference coordinate system. It is the time rate of change of TROUTP ZCL, Figure 10.

SOURCE OF VARIABLES AXC, XVC, XDC

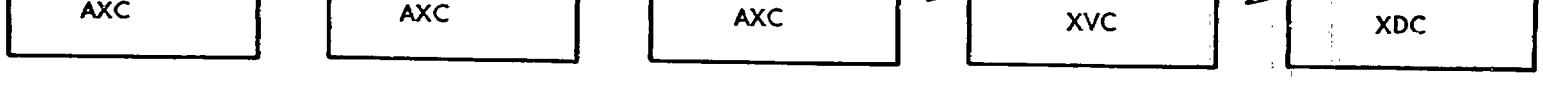

FIGURE 18

ZNV	is the component of velocity of the head C.G. relative to the T_1 principal coordinate system origin along an axis parallel to the +Z axis of the sled reference coordinate system. It is PLOT ZCV minus INTERMEDIATE ZVA, Figure 10.
4FD	is the same as PLOT 4FM except it is computed from the head accelerometers, Figure 19.
4FM	is the component of acceleration of the head C.G. relative to the inertial reference coordinate system origin along the head anatomical coordinate +X axis system as computed from mouth accelerometers, Figure 15.
4SD	is the same as PLOT 4SM except it is computed from the head accelerometers, Figure 19.
4SM	is the component of acceleration of the head C.G. relative to the inertial reference coordinate system origin along the head anatomical +Z axis as computed from the mouth accelerometers, Figure 15.
4XM	is the component of acceleration of the head C.G. relative to the inertial reference coordinate system origin along the inertial reference coordinate system +X axis as computed from the mouth accelerometers, Figure 15.
4XZ	is magnitude of the acceleration of the head C.G. relative to the inertial reference coordinate system origin as computed from 4XM and 4ZM, Figure 15.
4ZM	is the component of acceleration of the head C.G. relative to the inertial reference coordinate system origin along the inertial reference coordinate system +X axis as computed from the mouth accelerometer, Figure 15.

INTERMEDIATE Variables	Definitions
XVA	is the component of velocity of T_1 anatomical coordinate system origin relative to the sled coordinate system origin along the sled coordinate +X axis. It is the time rate of change of TROUTP XNA, Figure 10.

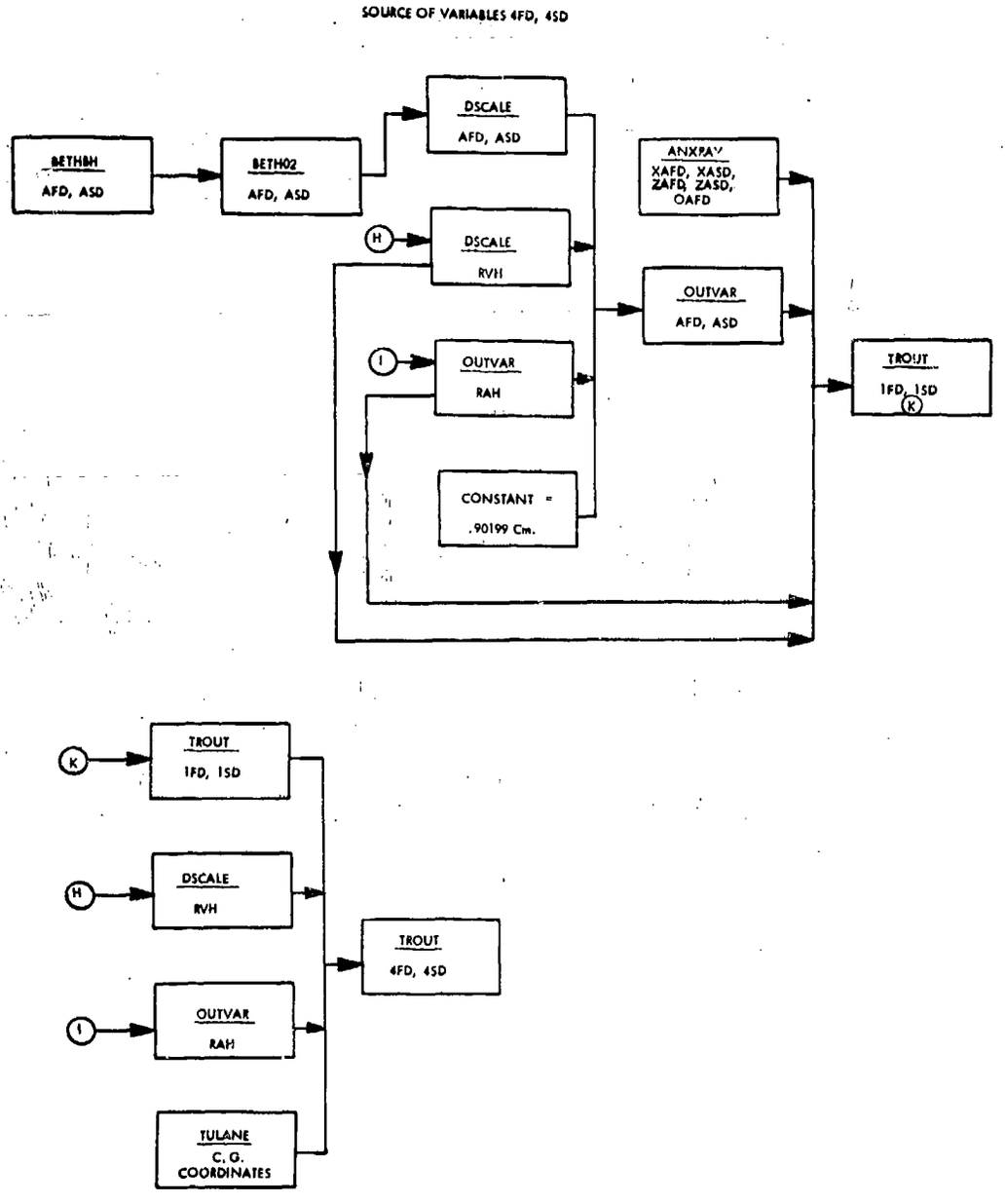
SOURCE OF VARIABLES 4FD, 4SD
BETHBH
AFD, ASD
BETH02
AFD, ASD
DSCALE
AFD, ASD
ANXPAV
XAFD, XASD,
ZAFD, ZASD,
OAFD
H
DSCALE
RVH
OUTVAR
AFD, ASD
I
OUTVAR
RAH
TROUT
1FD, 1SD
K
CONSTANT =
.90199 Cm.
K
TROUT
1FD, 1SD
H
DSCALE
RVH
TROUT
4FD, 4SD
I
OUTVAR
RAH
TULANE
C. G.
COORDINATES

FIGURE 19

ZVA	is the component of velocity of the T_1 anatomical coordinate system origin relative to the sled reference coordinate system origin along the sled reference coordinate system +Z axis. It is the time rate of change of TROUTP ZNA, Figure 10.

TROUTP Variables	Definitions
HSP	is the same as PLOT HSP, Figures 6 and 8.
X1	is the component of displacement of the posterior (left) spine target center relative to the sled reference coordinate system origin along the sled reference coordinate system X axis, Figures 6 and 8.
Z1	is the Z component associated with TROUTP, Figures 6 and 8.
X2	is the component of displacement of the anterior (right) spine target center relative to the sled reference coordinate system origin along the sled reference coordinate system X axis, Figures 6 and 8.
Z2	is the Z component associated with TROUTP X2, Figures 6 and 8.
X3	is the component of displacement of the head target center relative to the sled reference coordinate system X axis, Figures 6 and 8.
Z3	is the Z component associated with TROUTP X3, Figures 6 and 8.
X4	is the component of displacement of the mouth target center relative to the sled reference coordinate system origin along the sled reference coordinate system X axis, Figures 6 and 8.
Z4	is the Z component associated with TROUTP X4, Figures 6 and 8.
X34	is the component of displacement of the photographic head mount instrumentation coordinate system origin relative to the sled reference coordinate system origin along the sled reference coordinate system +X axis, Figures 8 and DP-11.
Z34	is the Z component associated with TROUTP X34, Figures 8 and DP-11.

XN	is the component of displacement of the photographic spine mount instrumentation coordinate system origin relative to the sled reference coordinate system origin along the sled reference coordinate system X axis, Figures 8 and DP-11.
ZN	is the Z component associated with TROUTP XN, Figures 8 and DP-11.
XCL	is the component of displacement of the head C.G. relative to the sled reference coordinate system X axis, Figure 8.
ZCL	is the Z component associated with TROUTP XCL, Figure 8.
XNA	is the component of displacement of the spine T_1 anatomical coordinate system origin relative to the sled reference coordinate system origin along the sled reference coordinate system X axis, Figure 8.
ZNA	is the Z component associated with XNA, Figure 8.
ACT	is the polar angle of TROUTP MCT displacement vector relative to the laboratory reference coordinate system +X axis, Figure 8.
MCT	is the same as PLOT MCT, Figures 6, 7 and 8.
NRN	is the same as PLOT NRN except it is negative, Figures 11 and 12.
RN	is the magnitude of the angular displacement of the photographic spine mount instrumentation coordinate system +X axis relative to the laboratory +X axis, Figures 12 and DP-11.
ADH	is the magnitude of the angular displacement of the photographic head mount instrumentation system -X axis relative to the laboratory reference coordinate system +X axis, Figures 13 and DP-11.
PDH	is the same as PLOT PDH except it is negative, Figures 11 and 13.

PHDATA Variables	Definitions
X1, Z1, X2, Z2 X3, Z3, X4, Z4	are the same as TROUTP variables of the same name except they are expressed in the Telereadex reference coordinate system, Figures 12 and 13.

REDUCED PHOTOGRAPHIC DATA	Definitions
X1, Z1, X2, Z2 X3, Z3, X4, Z4	are the same as PHDATA variables of the same name except they are unscaled and are stored on data cards and card image tapes, Figures 12 and 13.

TROUT Variables	Definitions
1FD	is the component of acceleration of the head anatomical coordinate system origin relative to the inertial reference coordinate system origin along the head anatomical coordinate system +X axis as computed from the head mount accelerometers, Figure 19.
1SD	is the Z component associated with TROUT 1FD, Figure 19.
1FM	is the same as TROUT 1FD except it is computed from the mouth mount accelerometers, Figure 15.
1SM	is the same as TROUT 1SD except it is computed from the mouth mount accelerometers, Figure 15.
4FD,4SD, 4FM 4SM,4XM,4ZM	are the same as PLOT variables of the same name, Figures 15 and 19.

OUTVAR Variables	Definitions
AFM	is the component of acceleration of the transducer mouth mount instrumentation coordinate system origin relative to the inertial reference coordinate system origin along the transducer mouth mount instrumentation coordinate system +X axis, Figure 15.
ASM	is the Z component of acceleration associated with OUTVAR AFM, Figure 15.
AFD	is the component of acceleration of the transducer head mount instrumentation coordinate system origin relative to the inertial reference coordinate system origin along the transducer head mount instrumentation coordinate system +X axis, Figure 19.
ASD	is the Z component associated with OUTVAR AFD, Figure 19.

RPH	is the magnitude of the angular displacement of the photographic head instrumentation coordinate system -X axis relative to the laboratory reference coordinate system +X axis, Figure 15.
RAH	is the negative of PLOT RAH, Figure 19.
XVC, XDC	are the same as PLOT variables of the same name except they are not in standard coordinate systems, Figure 18.

DSCALE Variables	Definitions
AFM	is the scaled digital value of the mouth mount anterior accelerometer output, Figure 15.
ASM	is the scaled digital value of the mouth mount superior accelerometer output, Figure 15.
AFD	is the scaled digital value of the head mount anterior accelerometer output, Figure 19.
ASD	is the scaled digital value of the head mount superior accelerometer output, Figure 19.
RVH	is the scaled digital value of the mouth mount rate gyroscope output. It is the negative of the plotted RVH which has been converted to standard format, Figures 15, 17 and 19.
AXC	is the scaled digital value of the sled accelerometer, Figure 18.
RVN	is the negative of the magnitude of the angular velocity of the angle of the transducer T_1 mount coordinate system +X axis relative to the laboratory reference coordinate system +X axis. It is the scaled digital value of the T_1 spine mount rate gyroscope output, Figure 17.

BETHO2 Variables	Definitions
AFM, ASM, AFD, ASD, RVH, RVN, AXC	are the same as DSCALE variables of the same name except they are unscaled, Figures 15, 17 and 18.

BETHBH Variables	Definitions
AFM, ASM, AFD ASD, RVH, RVN AXC	are variables identical to BETHO2 variables of the same name except they are in unsorted digital tape format, Figures 15, 17, 18 and 19.

ANALOGUE Variables	Definitions
AFM, ASM, AFD ASD, RVH, RVN AXC	are variables identical to the DSCALE variables of the same name except they are in analogue voltage format. These variables are not illustrated separately.

ICONDS Variables	Definitions
ADH	is the initial value of TROUTP ADH, Figure 15.
RN	is the initial value of TROUTP RN, Figure 12.
ALPHA	is the magnitude of the angular displacement of the +X axis of the Telereadex reference coordinate system relative to the +X axis of the laboratory reference coordinate system, Figures 12 and 13.
X1, Z1, X2, Z2, X3, Z3, X4, Z4	are initial values of PHDATA variables of the same name, Figures 12 and 13.

ANXRAY Variables	Definitions
XAFM	is the component of displacement of the center of the anterior mouth accelerometer relative to the head anatomical coordinate system origin along the head anatomical coordinate system +X axis, Figures 8 and 15.
XASM	is the component of displacement of the center of the superior mouth accelerometer relative to the head anatomical coordinate system origin along the head anatomical coordinate system +X axis, Figures 8 and 15.
ZAFM	is the Z component associated with XAFM, Figures 8 and 15.
ZASM	is the Z component associated with XASM, Figures 8 and 15.

OAFM	is the magnitude of the angular displacement of +X axis of the transducer mouth mount instrumentation coordinate system relative to the +X axis of the head anatomical coordinate system as computed from x-ray, Figure 15.
XAFD	is the component of displacement of the center of the anterior head accelerometer relative to the head anatomical coordinate system origin along the head anatomical coordinate system +X axis, Figures 8 and 19.
XASD	is the component of displacement of the center of the superior head accelerometer relative to the head anatomical coordinate system origin along the head anatomical coordinate system +X axis, Figures 8 and 19.
ZAFD	is the Z component associated with XAFD, Figures 8 and 19.
ZASD	is the Z component associated with XASD, Figures 8 and 19.
OAFD	is the magnitude of the angular displacement of +X axis of the transducer head mount instrumentation coordinate system relative to the +X axis of the head anatomical coordinate system as computed from x-ray data, Figure 19.
AHS	is the magnitude of the angular displacement of the +Z axis of the head anatomical coordinate system relative to the +X axis of the photographic head instrumentation coordinate system as computed from x-rays, Figures 15 and 16.
XAFN	is the component of displacement of the center of the anterior T_1 accelerometer relative to the T_1 anatomical coordinate system origin along the T_1 anatomical coordinate system +X axis, Figure 8.
XASN	is the component of displacement of the center of the superior T_1 accelerometer relative to the T_1 anatomical coordinate system origin along the T_1 anatomical coordinate system +X axis, Figure 8.
ZAFN	is the Z component associated with XAFN, Figure 8.
ZASN	is the Z component associated with XASN, Figure 8.

OAFN	is the magnitude of the angular displacement of +X axis of the transducer spine mount instrumentation coordinate system relative to the +X axis of the T_1 anatomical coordinate system as computed from x-ray data, Figure 12.

CONSTANT	Definitions
.02 radians	fixed angle between the photo spine mount instrumentation coordinate system +X axis and the transducer spine mount instrumentation coordinate system +X axis, Figure 3.
.90199 centimeters	one half the distance between the centers of adjacent accelerometers within a given mount. This constant was identical for all transducer mounts, Figure DP-13.

REFERENCES

(1) Thomas, D. J. and Ewing, C. L., Theoretical Mechanics for Expressing Impact Accelerative Response of Human Beings. AGARD Conference No. 88 on Linear Acceleration of Impact Type, Oporto, Portugal, 1971.

(2) NAMRL Detachment Standard Operating Procedure 002 - Laboratory Standard for Definition of Coordinate Systems.

ANTHROPOMETRY CHAPTER

Channing L. Ewing
CAPT MC USN

One of the questions which continually arises in human biodynamics research and development is the effect of differences in subject size or of sizes of components or organs (such as the head or the arm) or of their mass distribution.

The experimental design included consideration of this question in several ways:

1. Determination of the effects of sled peak acceleration and of rate of onset of acceleration, by subjecting each volunteer to increments of peak acceleration of 1G, while keeping the rate of onset constant. Then the sled peak acceleration was kept constant and the rate of onset of acceleration was changed. Thus the effect of the acceleration pulse could be determined completely independently of physical size for each volunteer, by each acting as his own control.

2. The subjects were especially selected originally because of their physical size in the parameters of sitting height alone. (1,2,3) Using the U.S. Navy Anthropometric Survey of 1964 as a guide, subjects were selected roughly within the fifth, fiftieth, and ninety-fifth percentiles of sitting height. (4) Comparisons between individuals and between groups could then be made to determine the effects of sitting height on run results.

3. Comparisons between individuals and between groups could be made to determine the effects of other external anthropometric variables.

4. Determination of location of each transducer and photographic target relative to an anatomical coordinate reference system. (See Data Processing chapter)

5. Determination of the location of head C.G. on each volunteer, by extrapolation from cadaveric measurement. (See X-ray Anthropometry data reduction in Data Processing chapter)

These headings will be discussed in the same order.

1. Subject acting as his own control-observation of the presented data will reveal the utility or absence thereof of this approach.

2. Grouping of volunteer data by subject size will reveal the utility of this approach also. This is facilitated by the tabular material in the Results Chapter.

3. Externcl Anthropometry - Clauser's group at the USAF Aerospace Medical Research Laboratory was requested to perform external anthropometry on all subjects in the study on completion of the run series in April 1969. (5)

The data obtained are presented in the accompanying tables. Table 1 lists all the measurements and the estimated centers of mass and the estimated weights. Table 2 lists just those measurements applicable to this report. All linear and circumferential measurements are given in centimeters. All weights are given in grams, save where noted. Those values preceded by * were calculated according to the methods in reference (6).

The anthropometric techniques used are those presented in his monograph. (6) Those procedures were described for use on cadaveric material and were modified by Clauser as stated below to measure the volunteers.

A brief description of the particular measurements given in Table 2 is in order. Head breadth is obtained by using spreading calipers to measure the maximum horizontal breadth of the head (Figure 1). Head circumference is obtained by using a flexible tape measure, passed above the brow ridges and parallel to the Frankfort plane, to measure the maximum circumference of the head. (Figure 2). The Frankfort plane is a horizontal plane passing posteriorly from the inferior most surface of the orbit to the superior most surface of the auditory meatus. (Figure 6) Head length is obtained by using spreading calipers to measure the maximum length of the head between the glabella and the occiput. (Figure 3) The height of the head is a derived dimension calculated by subtracting the chin-neck intersect height from stature. (Figures 4, 5) The chin-neck intersect is defined as the intersection of the following two planes: (1) from the menton posteriorly, parallel to the Frankfort plane and (2) vertically along the anterior neck surface upward. (Figure 6) The chin-neck intersect height is obtained by measuring the distance from the floor to the chin-neck intersect with the subject standing erect. (Figure 5)

Sitting height is obtained by measuring the height from the sitting surface to the top of the head, with the subject sitting erect. (Figure 7) Stature is obtained by measuring the height from the floor to the top of the head, with the subject standing erect. (Figure 5)

The total body weight was obtained by weighing the nude subject to the nearest gram. The weight in pounds is listed for convenience and was obtained by multiplying the kilogram weight by 2.2.

The weight of the head (from Clauser) and the weight of the head and neck (from NAMRL load cell) are estimates and should not be taken as exact measured values. The value given by Clauser has been corrected by Clauser by multiplying the value obtained from the predictive equation (7) by a correction factor in order to allow for the observation that the sum of the parts, as calculated from values obtained from the predictive equations, is slightly greater than the observed total body weight. Clauser attributes the discrepancy to the loss of body fluids when the cadaver was dismembered prior to obtaining individual segment weights. The same correction technique is applied to the live subject data. It should be emphasized that all the calculated data presented in both tables have been corrected such that the sum of the parts will be equivalent to the measured total body weight. If the regression equations given in reference (6) are used in an attempt to verify the tabular values, an error will at first be apparent unless the foregoing explanation is recalled.

4. Location of transducers relative to anatomy - Inertial sensors mounted on anatomical locations of biological specimens, including living human beings, measure the inertial events occurring at that location only. To be able to generalize to a population larger than the instrumented individual, it would appear desirable and indeed necessary to be able to specify the inertial events occurring at a site standard for all subjects. It is hereby proposed that such a procedure might reduce variance in the data, caused by anatomical variation in the population.

The standard site should be one with a known quantitative relationship to the anatomical location of the center of gravity of the instrumented body segment of interest. For purposes of the present experiments, it is also important to be able to establish a known quantitative relationship to a coordinate system fixed to the body segment of interest.

Investigations of all cadaveric anthropometric data available in the literature indicate that no head center of mass data referred to a completely defined anatomical coordinate system and satisfactory for use in this series of experiments was available. Clauser's work is the best available. (6)

A study was undertaken at the request of the principal investigator by Walker and Harris at Tulane University. (8)

As a means of reporting the data measured by the Tulane study, a series of anatomical reference coordinate systems was developed by the NAMRL research team. In order to make and represent quantitative measurements in the mid-sagittal plane, it was necessary to develop a system of x-ray anthropometry which could be used to relate two dimensional mid-sagittal plane head C. G. location data derived from cadaveric studies to similar head C.G. locations on living volunteers.

The volunteers who made the acceleration runs reported herein were subjected to x-ray anthropometry while wearing mouth and head mounts, and the spine mount. A lead bar of known length was placed in the mid-sagittal plane coplanar with the transducer mounts. An x-ray was then made of the head facing to the right and of the first thoracic vertebra. These x-rays permitted good visualization of the external auditory meati; the infraorbital ridges; the angular and linear location of the anatomical and transducer mounts relative to all observable anatomical features; and a good measure of skin thickness between anatomical mounts and the nearest body point. These features could be visualized at leisure and without injury or discomfort to the subject. Furthermore, for these experiments, a three dimensional problem was reduced to a two dimensional one.

The anatomical coordinate systems were established by selecting anatomical features which would be visible by x-ray and which would be as rigid as possible, dynamically or statically. The anatomical features also had to be easily locatable by the same means in cadavers and should not change due to death or cadaveric preservation techniques.

For the head, the Frankfort plane was selected as the basis of such a coordinate system. For T_1 the anterior superior corner of the vertebral body and the superior posterior and inferior posterior corners of the posterior spinous process, as seen on lateral x-ray were used. (See Figures 3 and 4 of Theoretical Kinematics Chapter)

The x-ray anthropometry procedure was as follows:

a. Fix the anatomical and transducer mounts to the head and the spine as done for each acceleration run. Repeatability of mount positioning was established by the use of unique individual anatomical mounts for each subject as previously explained.

b. Small spherical lead anatomical markers were placed at the superior edge of each auditory meatus and at the infraorbital notches, as shown in Figure 8.

c. A precision lead linear calibration rule was placed in the mid-sagittal plane as shown in Figure 8 and Figure 9.

d. A lateral x-ray of the skull including head mount and mouth mount screws and the lead anatomical markers was taken. Unfortunately, reproduction of these x-rays does not permit demonstration of the head and mouth screws which are very small.

e. A lateral x-ray of the cervical spine including the spine mount, screw holes and the first thoracic vertebra was taken next, as shown in Figure 9. Unfortunately, reproduction of these x-rays does not permit demonstration of the T_1 vertebral body.

The x-rays were acceptable only if: the calibration device, the anatomical markers or features and the mount screw holes or screws were clearly visible with good resolution. Occasionally this required repetition of an x-ray but every effort was made to minimize exposure for each volunteer. Acceptable x-rays were then submitted for data reduction. (See X-ray Anthropometry Data Reduction in Data Processing Chapter)

The anatomical coordinate systems which were then established using these data points are described under that heading in the Theoretical Kinematics section. The head coordinate system is illustrated in Figure 2 and the spine coordinate system is Figures 3 and 4 of that section.

Once the coordinate system was established on the x-rays, the precise location of each of the transducers within it could be determined. Furthermore, the head C.G. could also be established within the head anatomical coordinate system, thus permitting transformations of the transducer data to the C. G. using rigid body mechanics.

5. Location of the head center of gravity for each volunteer.

Head center of gravity measurements on cadavers were undertaken in 1968 by NAMRL because of the paucity of useable data available at that time. A study performed by Tulane University on sixteen cadavers determined the head C.G.

locations within the head anatomical coordinate system. (8) The measurements which are previously unpublished are presented in Figure 10. This study will be reported in detail elsewhere.

Another study performed by Becker, on five cadavers, also previously unpublished, gave comparable results which are also presented in Figure 10. (9)

One of the findings both by the Tulane group and by Becker was that no useable data exist concerning head-neck C.G. location. Therefore, all transformations in this report used the averaged head C.G. location, as determined by the Tulane measurements because of the larger population size and presented in Figure 10. While it would appear much more realistic to use head-neck C.G., quantitatively useable data, as noted, are not known to exist.

It is of some interest to note the small variance of head C.G. locations when expressed in the head anatomical coordinate system, which also is previously unpublished. It would appear that such a coordinate system may be of considerable utility in biodynamics research in view of the fortuitous location of its origin near the measured head C.G.

The averaged data from the Tulane study for sixteen head C.G. locations in the head anatomical coordinate system are:

$$\overline{X} = +0.883 \text{ cm}, \quad \overline{Z} = +2.145 \text{ cm} \qquad (8)$$

The averaged data from the NAMRL study for five head C.G. locations in the head anatomical coordinate system are:

$$\overline{X} = +1.33 \text{ cm}, \quad \overline{Z} = +2.09 \text{ cm} \qquad (9)$$

REFERENCES

(1) Ewing, C. L., Thomas, D. J., Beeler, G. W., Jr., Patrick, L. W., and Gillis, D. B., Dynamic Response of the Head and Neck of the Living Human to -G Acceleration. Proceedings of the Twelfth Stapp Car Crash Conference, New York: Society of Automotive Engineers, Inc., 1968, pp. 424-439.

(2) Ewing, C. L., Thomas, D. J., Patrick, L.M., Beeler, G. W., and Smith, M.J., Living Human Dynamic Response to -G Impact Acceleration. II Accelerations Measured on the Head and Neck. Proceedings of the Thirteenth Stapp Car Crash Conference. New York: Society of Automotive Engineers, Inc., 1969, pp. 400-415.

(3) Ewing, C. L. and Thomas, D. J., Human Dynamic Response to $-G_x$ Impact Acceleration. AGARD Conference Proceedings No. 88 (AGARD-CP-88-71) on Linear Acceleration of Impact Type. 7 Rue Ancelle 92 Nevilly - Sur-Seine, France. 1971. pp. 11-1 through 11.12.

(4) Gifford, E. C., Provost, J. R. and Lazo, J., Anthropometry of Naval Aviators - 1964. NAEC-ACEL 533. Philadelphia, Pa., Naval Air Engineering Center, Aerospace Crew Equipment Laboratory, 1965.

(5) Clauser, C.E., An Inquiry into the Ranges of Values Existing in the U. S. Navy Acceleration Study. Wright-Patterson Air Force Base, Ohio. 6570th Aerospace Medical Research Laboratory. June 1969. Unpublished data.

(6) Clauser, C.E., McConville, J. T. and Young, J. W. , Weight, Volume and Center of Mass of Segments of the Human Body. AMRL-TR-69-70. Aerospace Medical Research Laboratory, Aerospace Medical Division, Air Force Systems Command, Wright-Patterson Air Force Base, Ohio, August 1969.

(7) Ibid., p.46

(8) Walker, L., Harris, E., and Pontius, U., Letter report of data from ONR contract N00014-69-A-0248-0001, with Tulane University. The Evaluation of Some Physical Measurements of the Head and Neck of Human Cadavers. 16 November 1971 (Unpublished)

(9) Becker, E. B., Measurement of the Mass Distribution Parameters of Anatomical Segments, accepted for publication for the 16th Stapp Car Crash Conference, 11 August 1972. In press.

VARIABLE	003	004	007	009	010	011	012	013	015	016	017
Acromion-Rad Lgth	30.5	33.3	35.3	32.4	35.0	33.0	33.5	31.0	31.3	31.0	32.5
Age (Years)	24.0	23.0	21.0	21.0	25.0	22.0	21.0	24.0	21.0	19.0	20.0
Ankle Circumference	21.7	22.0	21.4	21.6	22.9	22.5	22.0	21.2	21.4	22.5	22.1
AP Dpth at Thelion	19.4	20.4	19.4	20.2	18.3	21.2	19.2	16.3	20.5	19.6	21.2
Arm Circ, Axillary	30.5	32.1	28.7	30.5	29.0	30.5	30.6	29.1	30.7	34.5	32.0
Ball Hum-Rad Lngth	28.2	31.2	33.7	30.5	33.9	30.9	31.4	29.3	29.1	29.4	29.9
Biacromial Breadth	40.7	41.0	41.5	39.9	40.7	42.4	40.8	43.1	39.7	43.6	40.4
Biceps Circ Flex, L	30.1	28.9	27.3	30.3	29.0	32.5	31.0	28.5	32.2	35.5	33.4
Biceps, Circ, Flex, R	30.7	31.6	27.5	31.5	29.9	33.8	33.4	29.5	32.9	35.9	33.8
Biceps, Circ, Rlax R	29.9	28.6	26.0	30.1	29.4	30.5	30.3	27.0	30.7	33.4	32.6
Bicristale Br (Bone)	28.0	27.4	29.9	27.2	29.5	27.1	28.8	23.1	26.7	25.8	28.4
Bispinous Breadth	24.3	23.2	26.5	23.8	24.3	24.3	24.0	17.9	23.5	20.6	25.7
Buttock, Circumf	92.5	92.7	93.5	94.4	100.0	95.2	96.4	87.3	91.7	100.2	98.8
Calf Circ, Left	35.2	36.0	34.1	36.5	36.6	38.2	36.3	33.6	36.0	39.9	37.5
Calf Circ, Right	35.1	36.6	34.1	37.1	37.5	37.9	36.6	33.2	36.1	40.0	37.6
Cervicale Height	144.9	146.3	160.5	140.9	163.1	148.2	155.7	140.3	142.4	146.1	146.8
Cervicale Ht, Sit.	65.8	68.1	71.1	62.7	70.5	67.9	68.1	61.2	64.0	66.0	66.7
Chest Breadth	31.7	35.9	32.3	37.3	33.7	33.4	34.6	33.7	34.2	33.6	36.0
Chest Circumf.	92.4	93.7	90.5	99.8	93.5	94.8	95.1	89.1	98.2	99.5	100.6
Chest Depth	22.3	23.7	22.4	25.1	22.6	24.8	24.5	20.4	24.7	25.7	26.0
Chin/Neck Height	145.3	146.4	161.5	143.7	165.9	150.4	158.5	143.9	145.4	148.0	146.2
*CM-Acromion U Arm	15.6	16.1	18.1	16.3	17.0	17.3	18.3	14.6	15.0	14.1	15.2
*CM-Heel Foot	11.3	11.6	12.2	11.1	12.2	11.6	12.1	11.0	11.1	11.3	11.0
*CM-Meta 3 Hand	1.5	1.9	1.6	1.2	1.5	1.6	1.8	1.4	1.3	1.6	1.4
*CM-Radiale Forearm	9.7	10.1	11.3	9.8	11.2	10.4	11.0	11.0	10.0	10.2	10.0
*CM-Suprastern Trnk	22.1	21.1	23.9	21.6	22.9	22.9	22.7	19.2	21.7	20.2	22.7
*CM-Tibiale Calf	14.4	13.4	15.4	14.2	16.1	14.5	15.2	14.1	13.5	14.2	15.1
*CM-Top of Head H	11.1	10.9	11.0	10.8	11.1	11.3	11.5	10.5	10.7	11.0	11.1
*CM-Top of HeadTB	71.6	72.5	76.9	69.0	80.7	73.3	76.2	69.9	69.5	73.7	73.2
*CM-Troch Thigh	15.0	15.8	18.4	15.7	19.3	15.9	18.8	15.8	15.2	15.6	15.9

TABLE ONE

VARIABLE	003	004	007	009	010	011	012	013	015	016	017
Elbow Brdth, Left	7.0	7.1	7.2	6.9	6.6	7.3	7.6	6.5	6.9	6.7	6.8
Elbow Brdth, Right	7.1	7.1	7.2	7.1	6.8	7.4	7.7	6.5	6.8	6.8	6.9
Eye Height, Sit. (cm)	81.0	81.3	84.9	79.0	85.6	83.8	84.8	77.7	79.3	80.6	79.4
Femur Brdth, Left	8.9	10.0	10.0	9.5	10.1	9.6	10.7	9.7	9.6	9.6	9.6
Femur Brdth, Right	9.0	10.1	10.0	9.4	10.1	9.5	10.7	9.7	9.7	9.6	9.6
Foot Length	25.1	26.6	28.3	26.5	28.6	25.7	27.3	27.8	26.3	24.9	26.2
Forearm Circ, Relax	27.0	27.2	25.5	27.0	26.5	27.2	28.7	26.5	27.5	28.8	29.6
Hand Breadth, Meta	8.5	8.7	9.0	9.2	8.8	9.0	9.5	9.5	8.8	9.0	8.9
Hand, Circ, Meta III	21.0	21.5	21.9	22.3	20.8	21.9	23.0	22.7	21.2	22.1	21.8
Hand Length	18.8	20.3	22.1	19.7	20.8	20.1	20.4	20.4	19.2	19.1	19.4
*Head-Trunk Length	82.9	83.3	87.5	78.7	88.9	86.5	86.6	80.7	82.8	83.1	82.1
Head Breadth	15.1	15.5	14.6	15.3	14.3	15.4	15.6	14.4	16.0	15.5	16.3
Head Circumference	56.1	55.6	56.2	56.2	56.4	57.3	58.1	54.7	55.8	56.7	56.4
Head Length	19.7	19.0	20.3	19.2	18.9	19.9	20.1	19.2	18.4	19.2	19.0
*Height of Head	25.0	24.6	24.4	23.4	25.0	24.9	24.4	23.7	23.3	23.5	24.7
Hip Breadth	33.4	33.7	35.5	36.7	36.1	35.9	35.4	31.1	33.7	34.9	35.7
Hip Depth	24.0	24.6	23.4	22.8	27.3	22.6	24.2	22.2	23.7	27.9	26.5
*H-C S'Type Comp 1	3.5	5.0	4.0	2.5	4.0	3.0	3.0	2.0	5.5	5.5	4.0
*H-C S'Type Comp 2	4.5	6.0	2.5	6.0	2.5	6.0	5.5	4.5	6.0	6.5	6.0
*H-C S'Type Comp 3	2.0	1.5	4.5	1.0	4.0	2.5	3.0	2.5	1.5	0.5	0.5
Iliac Crest Fat	11.0	22.0	12.6	7.7	13.8	8.3	9.8	6.3	15.7	19.4	10.9
Knee Circumference	35.0	37.0	36.1	36.1	37.5	37.4	38.6	34.6	38.5	38.0	37.2
Lat Malleolus Ht.	7.0	6.9	8.0	6.1	7.4	7.1	7.9	5.4	6.2	6.8	5.8
Radiale - Stylion	25.4	24.8	28.3	25.7	28.7	26.1	26.5	27.6	26.5	25.6	25.8
Shoulder Ht, Sitting	60.6	61.3	64.2	57.8	65.7	59.7	60.6	58.8	57.4	59.3	60.4
Sitting Height	92.4	92.9	97.9	89.2	97.9	95.7	95.8	88.4	90.4	91.9	90.5
Sit. Hght Percentile	53.0	60.0	96.0	17.0	96.0	87.0	88.0	12.0	30.0	47.0	30.0
SKF Iliac Crest	14.5	28.5	16.5	10.2	18.0	11.0	12.9	8.4	20.5	25.2	14.3
SKF Juxta Nipple	8.0	9.1	7.8	4.6	6.1	6.1	5.0	4.5	8.5	17.9	15.0
SKF Mal Xiphoid	10.5	10.0	10.0	6.0	10.2	5.9	6.1	5.8	10.0	9.3	11.8

TABLE ONE

VARIABLE	003	004	007	009	010	011	012	013	015	016	017
SKF Medial Calf, R	12.2	5.5	10.5	5.1	8.5	6.2	4.1	4.8	5.4	11.8	7.1
SKF Subscapular	10.0	11.3	9.0	8.4	12.0	12.0	8.1	9.1	19.8	14.0	12.9
SKF Triceps	9.5	7.7	10.5	8.1	10.7	4.5	7.7	5.1	12.3	15.0	9.9
Stature	170.3	171.0	185.9	167.1	190.9	175.3	182.9	167.6	168.7	171.5	170.9
Substernale Height	119.7	119.6	129.4	117.7	135.3	117.9	127.8	116.7	117.5	120.4	120.9
Suprasternale Height	138.8	139.2	152.4	135.3	156.7	140.3	149.5	135.5	136.3	139.8	139.4
Tenth Rib Breadth	28.4	29.6	28.3	30.3	30.4	27.6	29.6	26.3	30.3	29.6	31.4
Tenth Rib Circum.	76.6	83.8	75.9	82.0	82.0	74.5	77.2	71.0	83.5	88.5	87.5
Tenth Rib Depth	20.0	22.3	20.7	23.0	21.9	20.5	19.6	18.0	24.0	25.8	23.6
Tenth Rib Height	106.8	110.3	121.1	106.5	121.1	107.5	117.1	105.7	105.3	109.6	111.6
Tibiale Height	44.1	42.8	49.2	44.2	51.5	45.4	49.9	44.5	42.4	44.6	47.4
Top Head - Prosthion	17.1	16.2	18.4	17.1	17.8	18.9	17.6	17.2	16.3	18.6	17.5
Top Head - Tragion	13.6	12.9	13.8	12.5	13.0	13.9	13.9	13.0	12.2	13.2	13.5
Tragion Ht, Sitting	78.7	79.9	84.0	77.1	84.4	82.0	82.2	75.9	77.5	79.5	77.2
Trochanterion Ht.	87.4	87.7	98.4	88.4	102.0	88.8	96.3	86.9	85.9	88.4	88.8
*Trunk Length	57.9	58.7	63.1	55.3	63.9	61.6	62.2	57.0	59.5	59.6	57.4
Upper Thigh Circ.	55.1	55.8	52.7	54.6	61.0	55.9	55.2	50.0	54.5	60.2	59.2
Waist Breadth	30.2	30.0	30.1	29.2	31.7	29.6	30.3	25.5	31.1	30.6	32.8
Waist Depth	21.5	20.6	21.3	21.7	23.1	20.7	19.7	18.8	23.0	25.7	24.7
Wall - Prosthion	19.7	19.1	19.5	20.3	18.9	18.5	20.2	22.0	18.3	17.8	19.7
Wall - Tragion	9.6	9.1	10.5	10.3	9.2	9.8	10.4	11.4	9.5	9.4	9.0
Weight at 18	119.0	145.0	145.0	155.0	170.0	150.0	155.0	145.0	130.0	170.0	235.0
*Weight Calf	3280	3363	3344	3531	3965	3612	3683	3044	3233	3889	3837
*Weight Foot	1026	1076	1089	1080	1212	1065	1105	1048	1032	1098	1146
*Weight Forearm	1038	1098	991	1074	1069	1101	1235	1024	1077	1232	1269
*Weight Hand	390.0	471.0	443.0	423.0	418.0	458.0	531.0	453.0	389.0	478.0	444.0
*Weight Head	4538	4483	4524	4652	4758	4609	4791	4274	4463	4797	4912
Wt in Kilograms (Total Body)	67.5	71.0	69.5	71.3	80.5	71.7	75.1	60.4	69.8	81.2	81.7

TABLE ONE

VARIABLE	003	004	007	009	010	011	012	013	015	016	017
Weight in Pounds (Total Body)	148.5	156.2	152.9	156.9	177.1	157.7	165.2	132.9	153.6	178.6	179.7
*Weight Thigh	7651	8176	7462	7861	9368	7790	8076	6376	7734	9467	9425
*Weight Trunk	32866	34271	34869	35118	40015	35504	37363	29231	35004	39807	40456
*Weight Upper Arm	1658	1939	1725	1796	1832	1766	1842	1503	1702	2134	2044
Weight (Usual)	150.0	160.0	155.0	160.0	183.0	160.0	168.0	140.0	150.0	182.0	180.0
Wrist Brdth (Bone)	5.5	6.3	5.9	5.5	5.5	6.0	6.5	5.9	5.3	6.0	5.6
Wrist Circumference	16.2	17.0	16.7	16.5	16.9	17.2	17.8	16.4	16.6	17.5	17.0
Wt - Recent Change	22.0	-15.0	-	-	4.0	5.0	-	-	6.0	-	-

*Calculated Value
CM = Center of Mass
H-C = Heath - Carter Somatotype
1 = Endomorphy
2 = Mesomorphy
3 = Estomorphy

TABLE ONE

VARIABLE \ SUBJECT	003	004	007	009	010	011	012	013	015	016	017
Age (Years)	24.0	23.0	21.0	21.0	25.0	22.0	21.0	24.0	21.0	19.0	20.0
Chin/Neck Hgt.	145.3	146.4	161.5	143.7	165.9	150.4	158.5	143.9	145.4	148.0	146.2
Head Breadth	15.1	15.5	14.6	15.3	14.3	15.4	15.6	14.4	16.0	15.5	16.3
Head Circumference	56.1	55.6	56.2	56.2	56.4	57.3	58.1	54.7	55.8	56.7	56.4
Head Length	19.7	19.0	20.3	19.2	18.9	19.9	20.1	19.2	18.4	19.2	19.0
*Height of Head	25.0	24.6	24.4	23.4	25.0	24.9	24.4	23.7	23.3	23.5	24.7
Sitting Height	92.4	92.9	97.9	89.2	97.9	95.7	95.8	88.4	90.4	91.9	90.5
Sit. Hgt. Percentile	53.0	60.0	96.0	17.0	96.0	87.0	88.0	12.0	30.0	47.0	30.0
Stature	170.3	171.0	185.9	167.1	190.1	175.3	182.9	167.6	168.7	171.5	170.9
*Weight Head**	4538	4483	4524	4652	4758	4609	4791	4274	4463	4797	4912
*Weight Head&Neck***	4450	N.A.	4527	4196	4541	3874	4545	3661	4155	4463	4191
Wt in Kilograms (Total Body)	67.5	71.0	69.5	71.3	80.5	71.7	75.1	60.4	69.8	81.2	81.7
Weight in Pounds (Total Body)	148.5	156.2	152.9	156.9	177.1	157.7	165.2	132.9	153.6	178.6	179.7

(All linear measurements are given in centimeters. All weight measurements are given in grams, unless otherwise noted.)

* Calculated Value

** Clauser (Estimate)

*** NAMRL Load Cell (Estimate)

TABLE TWO

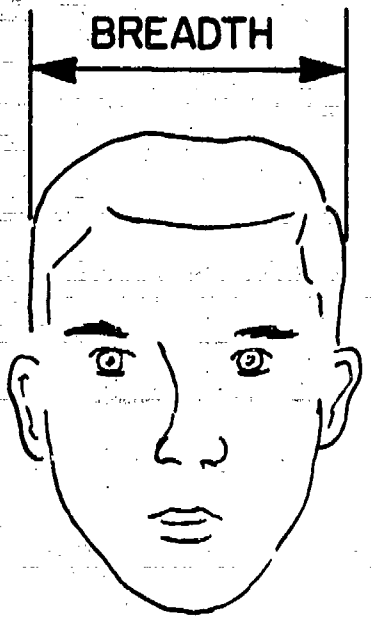

FIGURE 1

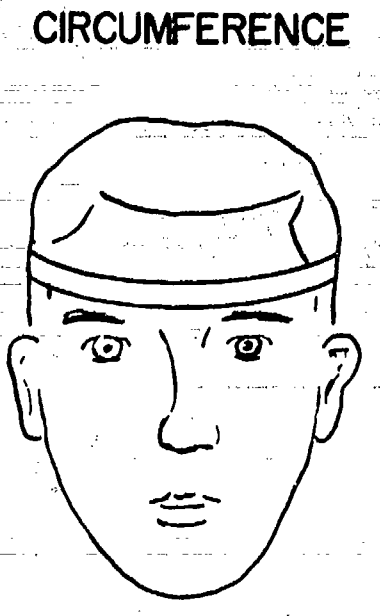

FIGURE 2

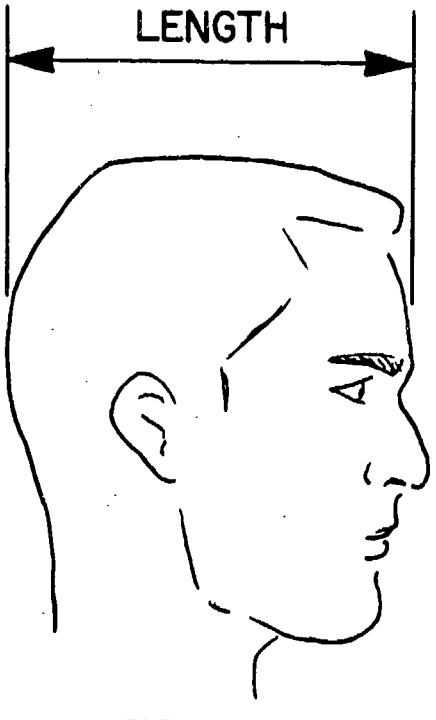

FIGURE 3

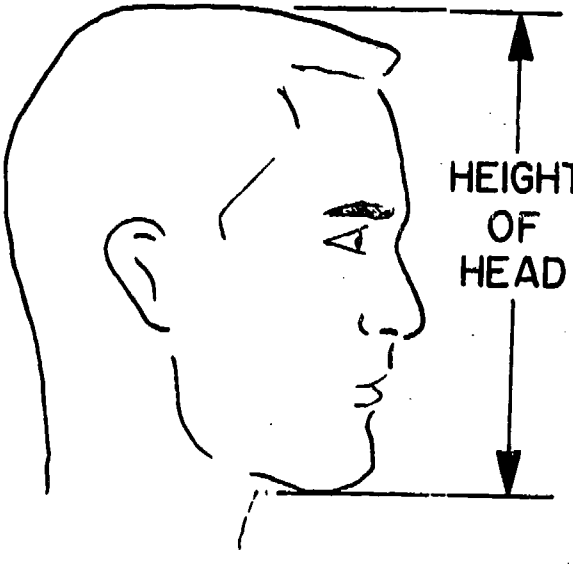

FIGURE 4

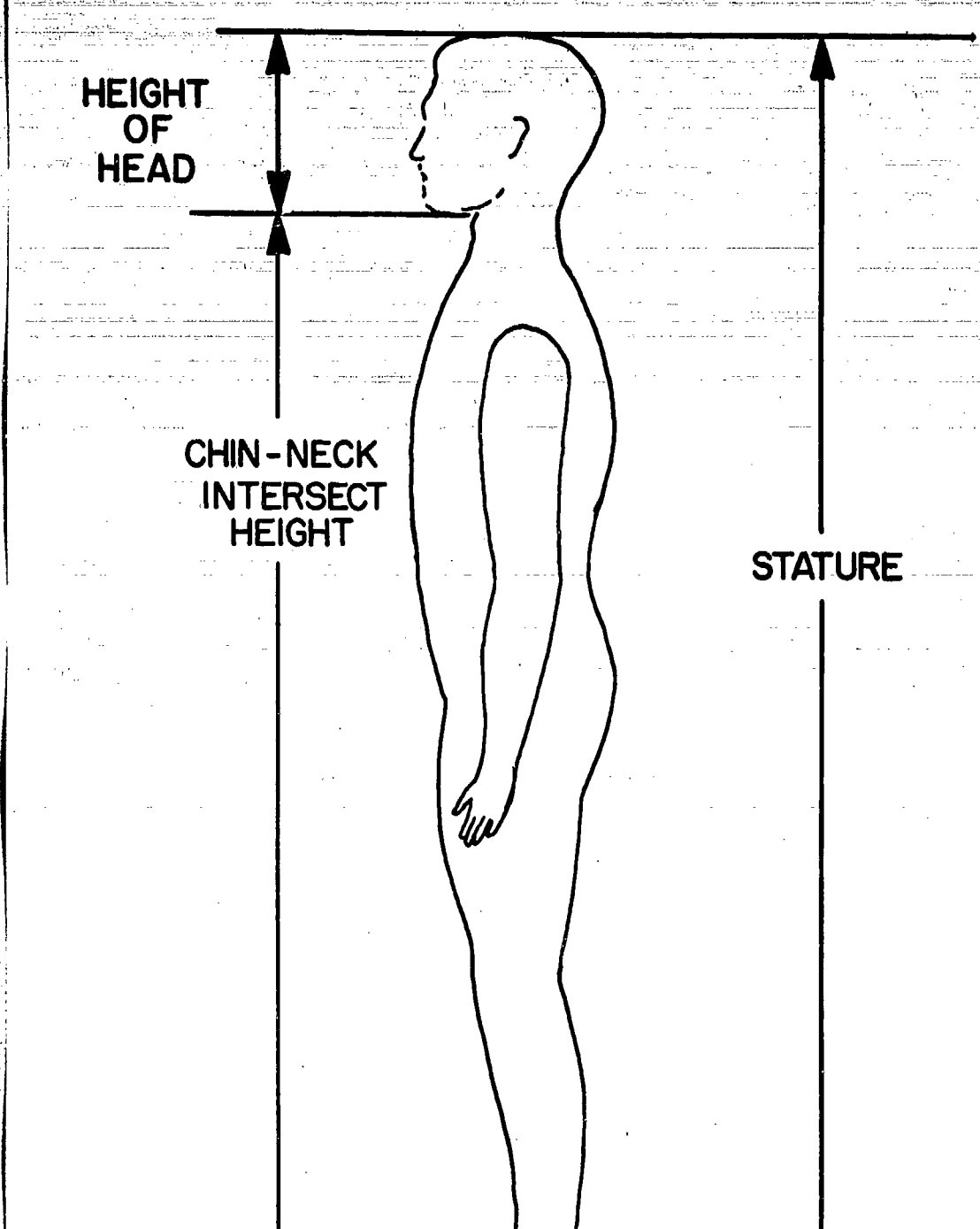

FIGURE 5

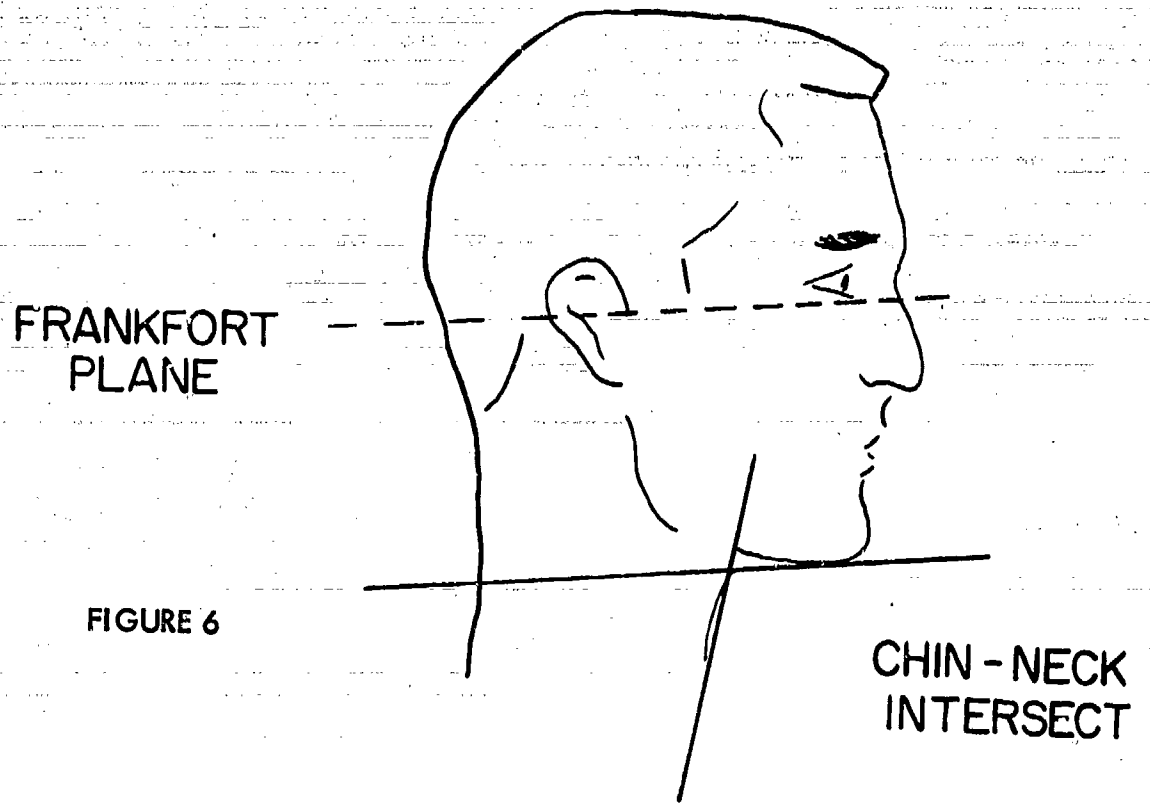

FIGURE 6

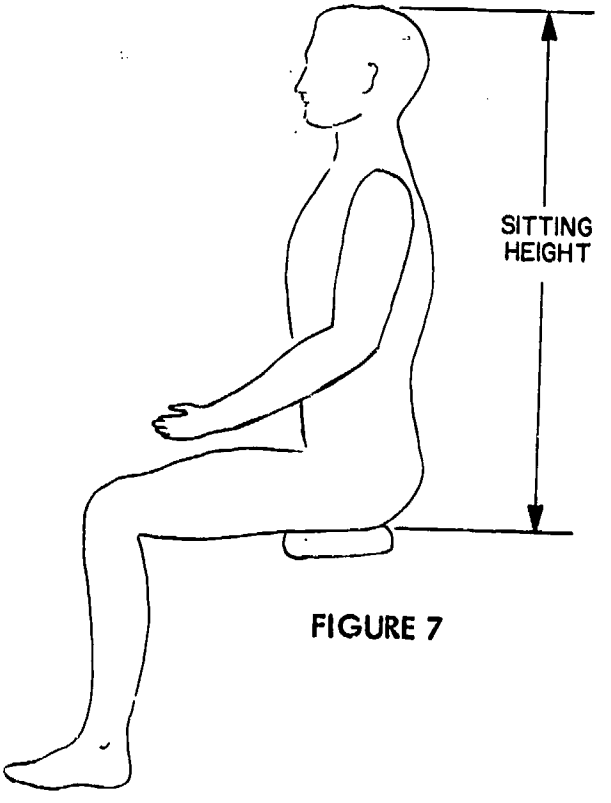

FIGURE 7

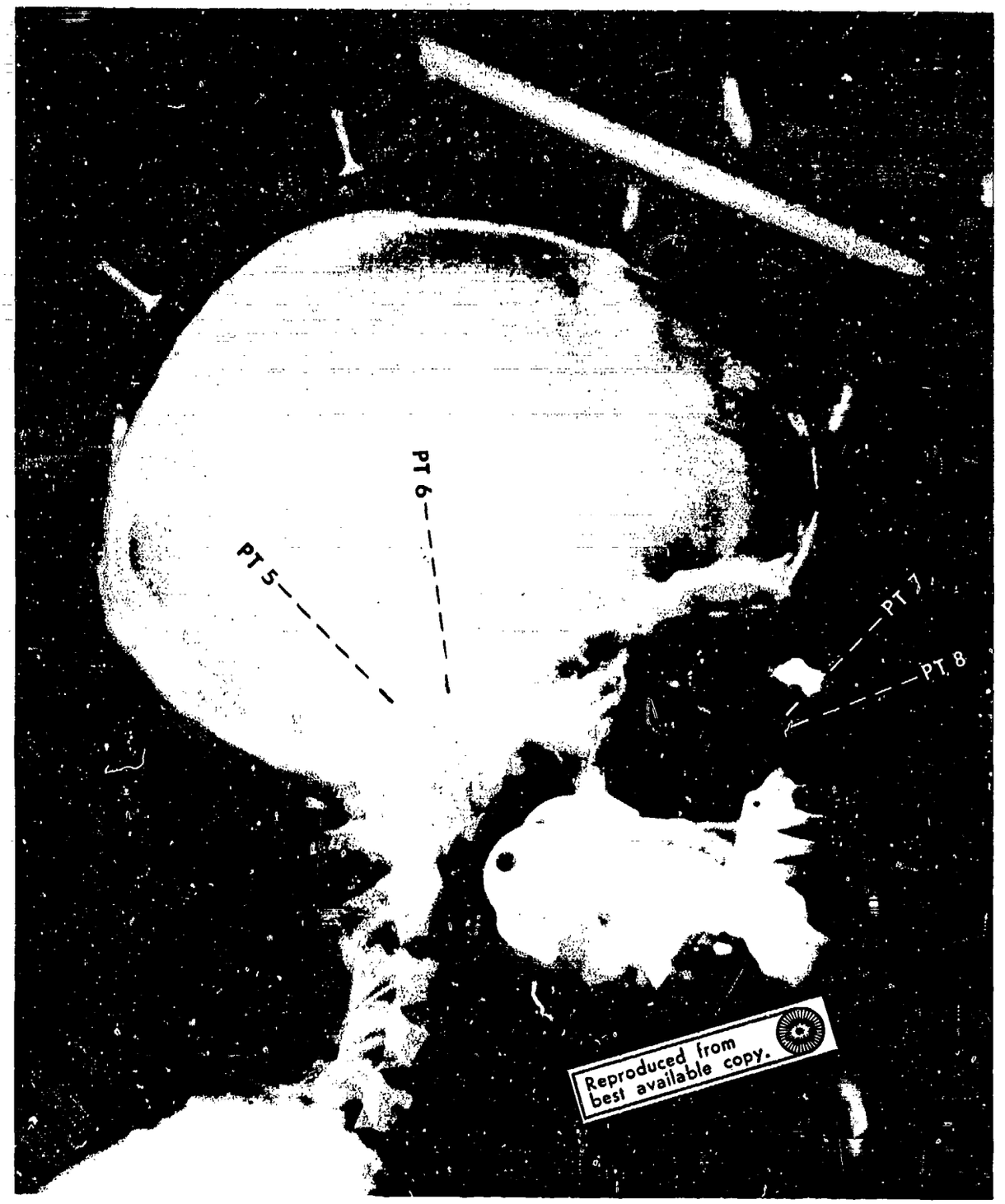

FIGURE 8 Lateral Skull Anthropometry X-ray

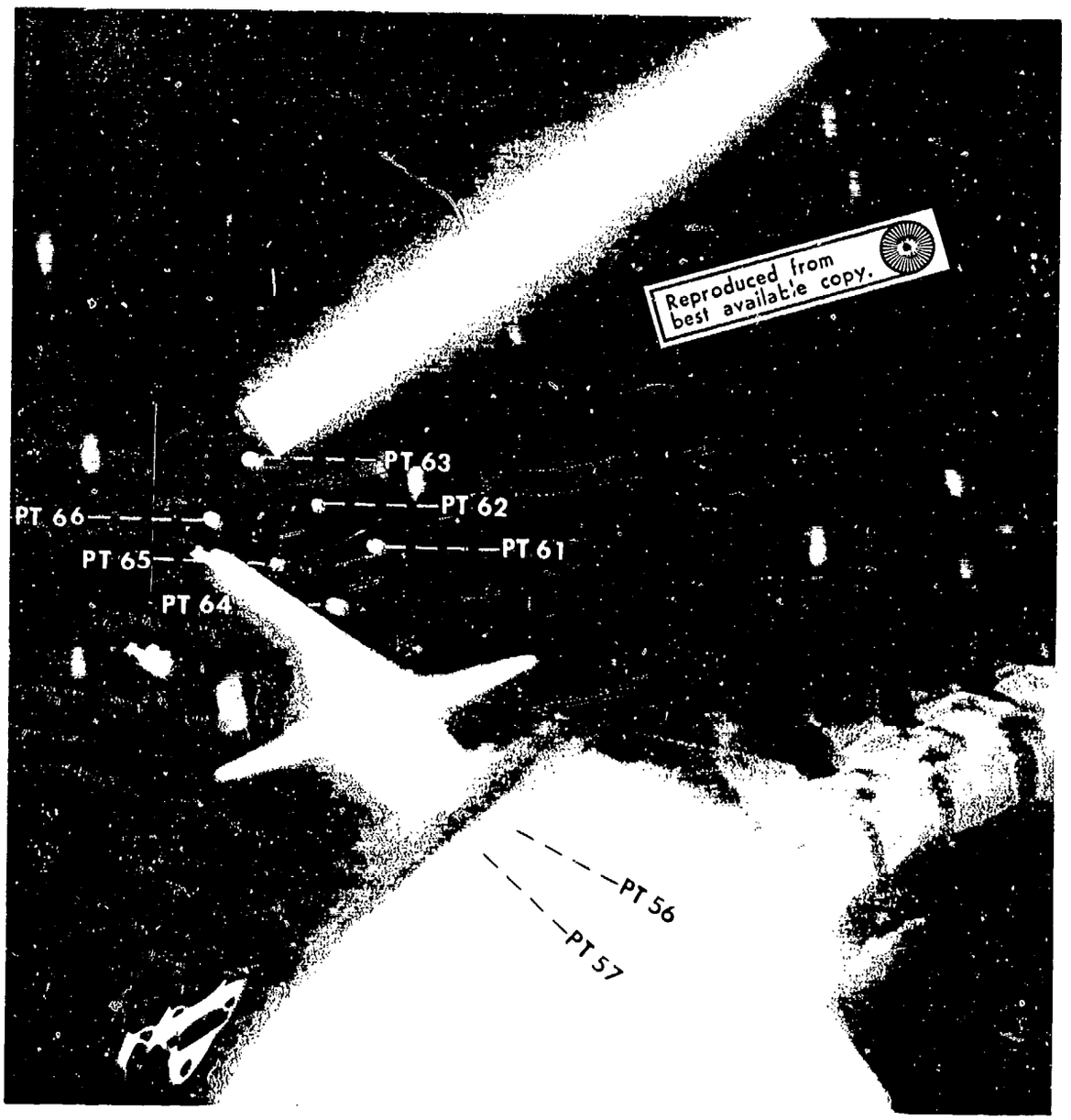

FIGURE 9 Lateral Cervical Spine Anthropometric X-ray

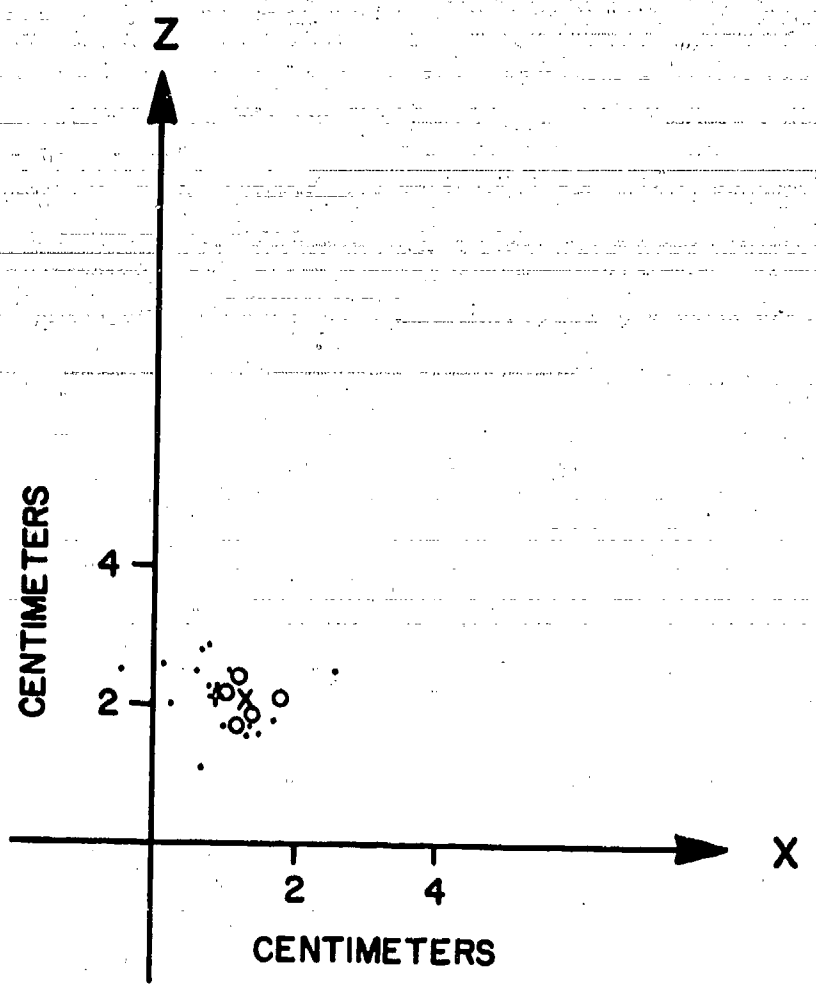

o – CENTER OF GRAVITY (NAMRL DET. # 1)

x – AVERAGED C.G. (NAMRL DET. # 1)

• – CENTER OF GRAVITY (TULANE)

+ – AVERAGED C.G. (TULANE)

FIGURE 10 Center of Gravity Expressed in the Head Anatomical Coordinate System

DATA PROCESSING CHAPTER

Sharon W. Katona

SENSOR DATA PROCESSING

Sensor data processing began with the creation of analog tapes containing, for each transducer channel, nine calibration steps of known voltage levels provided by a calibrator-amplifier, and the voltage output from the given transducer.

These tapes were recorded at the experimental site at 60 ips on an Ampex FR 1800L fourteen channel FM instrumentation recorder, which had an FM flat band-pass of DC to 20 kHz. After recording, the tapes were transported in cases shielded against magnetism to NAMRL, Pensacola, where an identical Ampex FR 1800L was utilized for playback.

Servo control of tape motion was employed in all runs to insure that the tape on the playback FR 1800L would be completely synchronized with the tape speed variations, if any, of the recording FR 1800L. Since the FR 1800L uses IRIG Standard tape speed control frequency of 100 kHz for 60 ips tape speed, it was decided to use the control track frequency as the master timing clock in A/D conversion also. Playback of the analog tape was, however, accomplished at a tape speed of 15 ips; therefore, the control track frequency (master clock) became 25 kHz. This four-fold speed reduction was employed to facilitate analog strip chart monitoring of playback and to insure remaining within the sampling rates available to the A/D converter.

At the recording (experimental) site an analog signal calibrating unit was employed to provide the steps of known precision voltage levels from -1.4 to + 1.4 volts which were applied to each sensor channel. Upon completion of the calibration steps, recorder input channels were returned to the sensor channels and their respective signal conditioning amplifiers.

For the duration of the calibration steps, a 1.4 volt control gate, DC level shift, (Figure DP-2) was applied to one track of the recording FR 1800L. Similarly, when the output from the transducers was recorded and for a short time before each run, a second control gate was applied to this same channel. The second gate was concluded at the end of the run. These two control gates provided the triggering signal for the A/D sampling periods and rates.

The playback FR 1800L was physically located remote from the A/D converter and computer facility at NAMRL, Pensacola. Fifty ohm coaxial transmission cables approximately 150 feet long were required for playback of the analog data to the A/D converter. Amplifiers for each playback channel were employed to interface

the playback FR 1800L with these transmission lines. These amplifiers had provision for adjusting the analog signal level in gain increments of 0.5, 1.0 and 2.0. This interfacing unit also provided the means of using the 25 kHz servo control signal (master clock) to direct sampling of the A/D data. Sampling rates were triggered by the gates contained on the control track. (See Figure DP-0)

The precision of the servo control track (master clock) and of the control gates was such that repeated digitizing, over a period of two years, of the same run resulted in sampling of the same portions of the analog signal. This was demonstrated by comparison plots of the sorted data.

The band-pass of these interfacing amplifiers was DC to at least 10 kHz,and the gain increments were maintained to within a few millivolts.

The A/D converter offered the option of digitizing 7 to 14 channels. Since the experimental analog tapes contained up to 10 channels of sensor data, the 14 channel option was elected.

The A/D converter digitized each channel sequentially and thus introduced a small time skew of one channel relative to another. The time required to sample an individual channel was 37.5 microseconds. This introduced a maximum time skew across 14 channels of approximately 500 microseconds. Since the playback speed was 1/4 the data acquisition speed, the maximum possible time skew introduced was 125 microseconds. Compared to the basic band-pass characteristics of the transducers, this is considered to be an insignificant source of error in the data.

The first step in the A/D procedure consisted of a visual evaluation of the data on each channel. The analog tape was played back,and strip charts were made. These strip charts were carefully examined to determine how many samples of calibration and data would be taken to insure adequate data acquisition. In addition, a check was made to determine if the signal on any channel exceeded the upper and lower limits ($\pm$ 1.414 volts) of the A/D converter. Any such channel was half-gained at the time of A/D conversion.

Sampling rates were set at least 10 times the highest anticipated data frequency: 200 samples/second for calibration and 2000 samples/second for data at the time of the experiment. With playback speed 1/4 of record speed, these rates became 50 samples/second and 500 samples/second respectively.

An assembly language program on the UNIVAC 418 digital computer was used to collect data from the A/D.

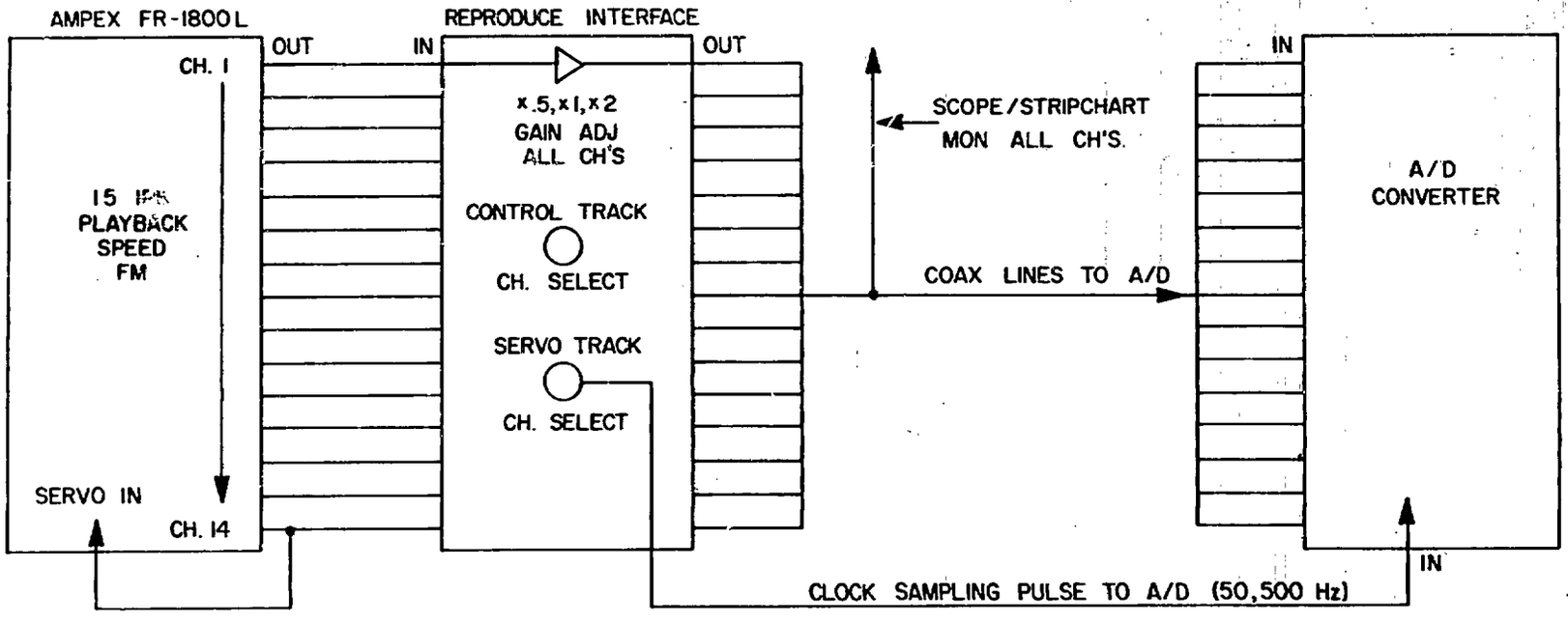

ANALOG PLAYBACK FOR A/D CONVERSION

FIGURE DP-0

BETHBH - The A/D Conversion Program

BETHBH is an assembly language program which collects digital data from an A/D converter, stores it on a FASTRAND drum and then records on digital tape a permanent file of the digitized data for the run being processed. Because a large amount of data is arriving in real time, a double buffered procedure is used to allow continuity of input and to facilitate immediate data transfer onto the drum. BETHBH does not alter the data in any way; it serves only as a data transfer operation.

Input to BETHBH is the digital output from the A/D converter and a card containing the following parameters.

1. The run number
2. Output tape name
3. Number of channels to be converted
4. Number of records of calibration data
5. Number of samples/record
6. Number of records of data
7. Number of samples/record
8. Number of seconds to wait between calibration A/D conversion and data A/D conversion.

This input is utilized in the following A/D procedure:

1. The BETHBH program is loaded on the UNIVAC 418.
2. The analog tape is loaded on the FR 1800L tape recorder.
3. A switch is set on the UNIVAC 418 which will enable the computer to accept digitized data as soon as it is available.
4. The analog tape is started and the first control gate appears. The A/D converter receives the clock signal which triggers sampling and digitizing of the calibration steps at 50 samples/second. The computer accepts from the A/D the number of samples of calibration data for each channel which were specified in the input card.
5. The computer, having satisfied its requirements for channel calibration data, stays away a prescribed number of seconds. The first control gate ends and the A/D suspends sampling.
6. The second control gate triggers sampling and digitizing at the rate of 500 samples/second. The computer accepts from the A/D the number of samples for each channel which was specified in the input card.
7. As a final step BETHBH writes an output tape containing all of the data collected on the drum.

BETHBH is a multi-run program enabling this procedure to be followed on up to 20 runs without reloading the program.

BETHBH Validation

As a validation of the A/D conversion system, two completely arbitraty test tapes were digitized at regular intervals (approximately every 10 runs) throughout a given group of runs. The first of these test tapes contained triangular waves of known amplitudes. This tape was digitized, sorted and plotted. The plotted data were then compared to analog strip charts of the test tape. A second tape contained alternating zero and full scale DC levels. It was digitized, sorted and processed by a statistical program (STATAD) which calculated the mean, variance and standard deviation of the levels. Evaluation of the output from these two test tapes gave a very precise measure of the performance of the system. If an indication of impaired performance was detected, all digitized data subsequent to the last successful run of the test tapes was discarded. The system was then checked and the hardware or software defects causing the problem were determined and corrected. The test tapes were then run again. If they were found to measure satisfactory performance of the system, the A/D process was then resumed. The test tape data after A/D conversion, sorting and plotting were retained as reference data.

The data were, at the conclusion of the operation of the program BETHBH, resident in digital form on digital magnetic tape, unsorted as to channel. A separate tape was used for each run and these tapes were and are maintained as a primary reference. Furthermore, the original analog tape for every run is presently preserved in cabinets which are protected against magnetism, dust, humidity and temperature extremes.

It was then necessary to sort the digital data by channel, which was accomplished by operation of the BETHO2 program on the data.

BETHO2 - The Data Sort Program

BETHO2 is a FORTRAN program that sorts and reorders 14 channel A/D output data as specified by the user.

Input to BETHO2 consists of the output tape from A/D conversion and parameter cards specifying which channels contain data, the desired order for the data, and the variable name to be assigned to each channel. The A/D output tape contains data ordered exactly as converted; that is, first data value for each of fourteen channels, second data value for each of fourteen channels and so on. This input is utilized in the following sort procedure:

1. Each data value on the input tape contains channel identification information in the high order six bits and digitized data in the low order twelve bits. BETHO2 drops off the channel identification information.

2. Using the channel identification information, BETHO2 sorts the data. All fourteen channels are sorted regardless of whether they contain data.

3. The sorted data are stored on the drum.

4. The sorted data for the channels which contain data are pulled from the drum in the specified order, and variable names are added.

5. An output tape is written containing the sorted data in the specified order.

BETHBH and BETHO2 Validation

As a validation of the sort procedure and further verification of the A/D procedure, all of the BETHO2 output channels were plotted. A scaling factor of 0.00069053396 was used on the data which transformed each data value from analog-to-digital units to voltage, for plotting purposes.

This conversion permitted the comparison of BETHO2 plots of the data (Figure DP-1) with the analog strip chart plots of the same data (Figure DP-2) generated from the original analog tape at the time of A/D conversion. These comparisons of each channel of each run are on file and show no degradation of the analog signal by the A/D conversion process or by the sorting process. It is considered that this is the best possible verification of the absence of artifact due to hardware and/or software to this point. If a channel was noted to have defective data for any reason, it was excluded from further processing until the cause of the defect could be determined.

Several runs suffered from sudden transducer failure midway through the run. While no such runs were used in this report, options 3 or 4 of program OUTVAR could be used to yield perfectly valid results due to the considerable redundancy of the instrumentation system design.

A single digital tape was used to record the BETHO2 output from each run and these tapes were and are maintained as a primary reference.

The data were then subjected to a scaling program, DSCALE.

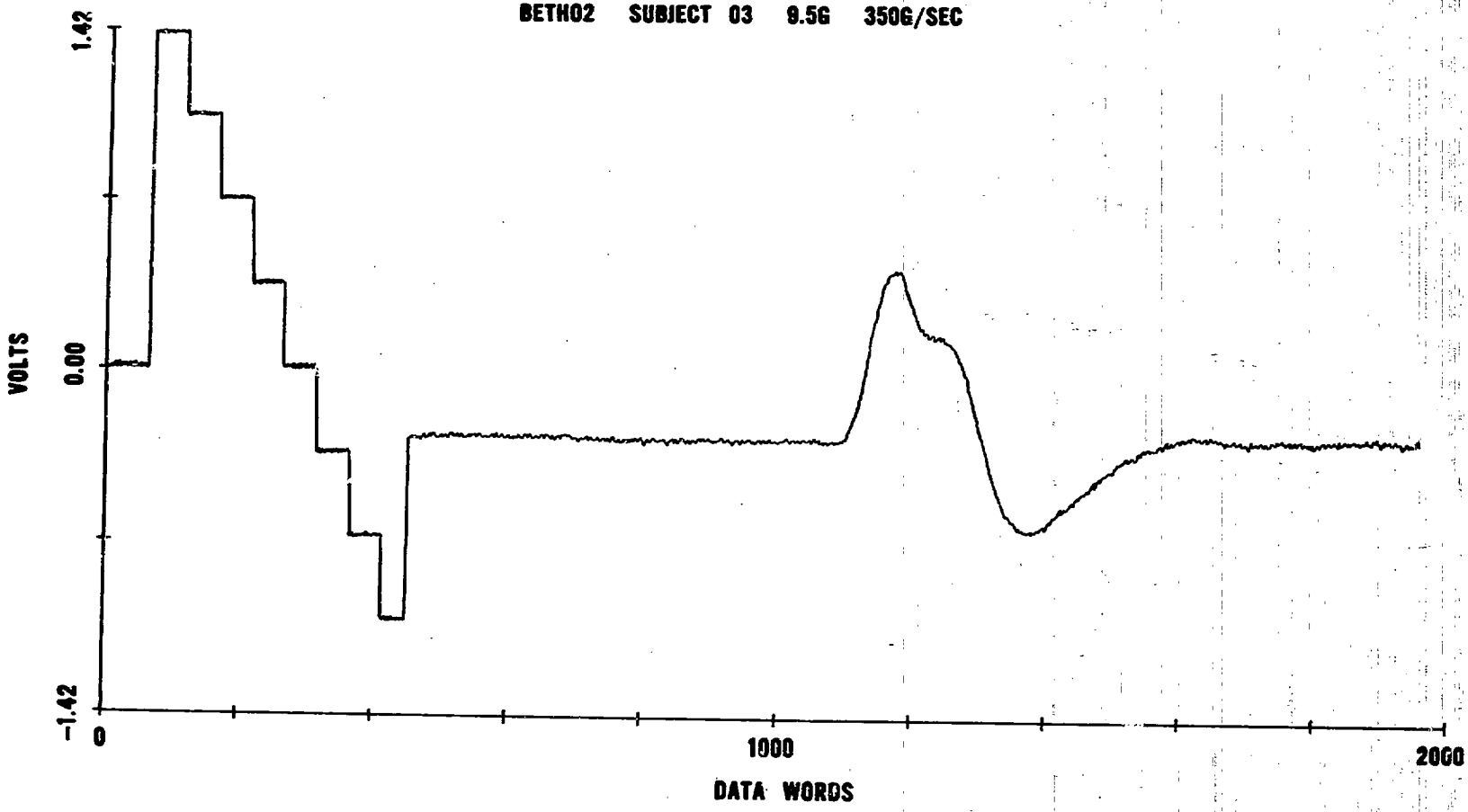

FIGURE DP-1 RVH as Plotted from Sorted Digital Data

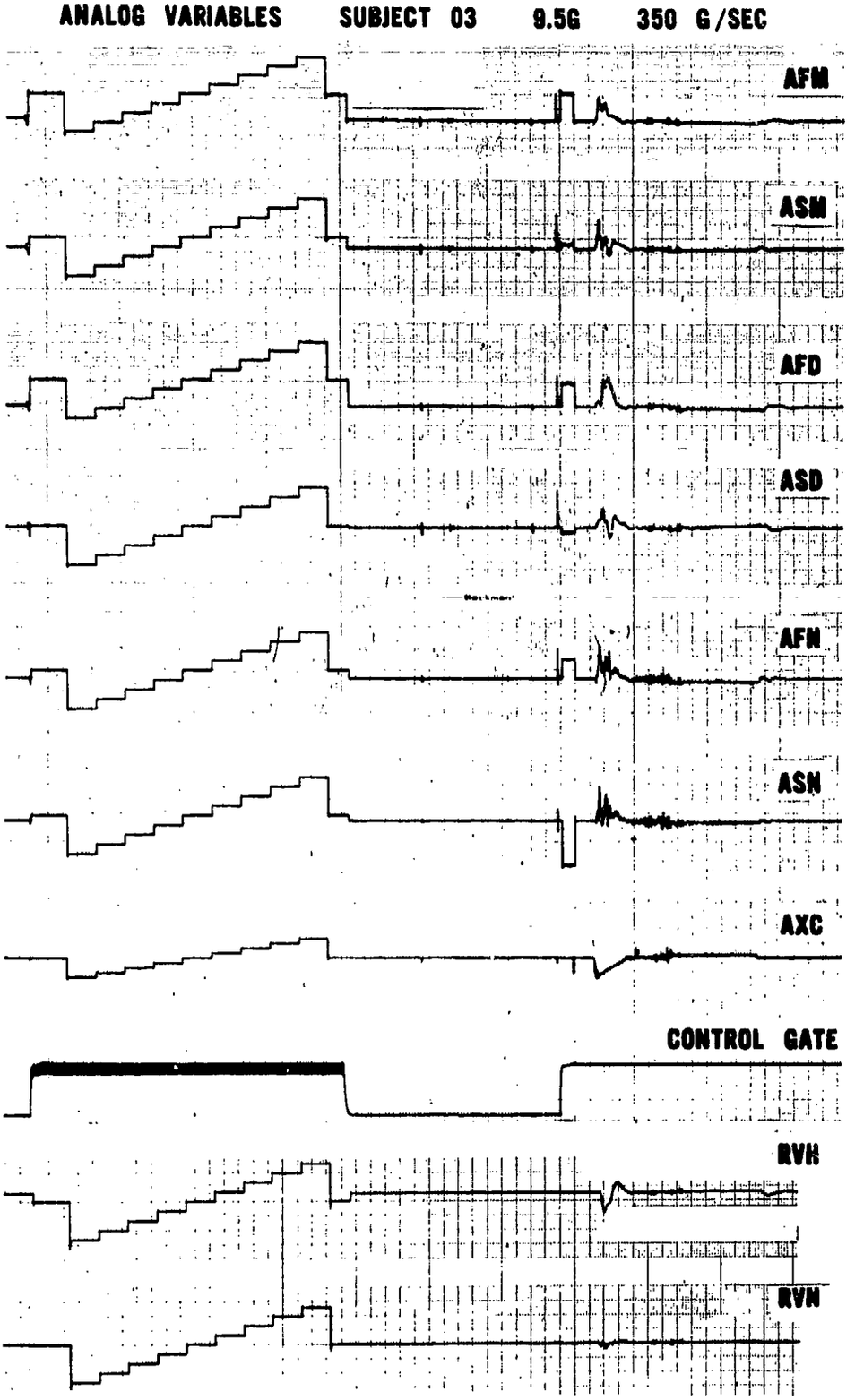

FIGURE DP-2 An Example of the Analog Strip Chart Recordings from Each Channel

DSCALE - The Transducer Scaling Program

DSCALE is a FORTRAN program which performs three major functions. The first function of DSCALE is to locate and identify points of experimental interest within the input data stream. These points of interest are:

1. T_o, the time of a specified pulse of known amplitude and duration on the sled accelerometer channel. T_o provides a means for determining the location of any frame of film relative to the time of occurrence of the sensor data. (See Photographic Data Processing)

2. The peak sled acceleration.

3. DPTZ, a computer defined time zero which represents the beginning of the data of experimental interest.

DSCALE's second function is to convert the data from the system of units which is the analog-to-digital converter's representation of voltage to physical units of acceleration and angular velocity (cm/msec^2 and radians/msec). This conversion involves linear least squares analyses of calibration data for the tape recorder - A/D system, the range amplifiers, and the accelerometers and rate gyros.

After the data are converted, the last function of DSCALE is to edit the data and to save only that portion of experimental significance.

The input to DSCALE is a digital tape containing nine calibration steps of known voltage level, and data from each of the accelerometer and rate gyro channels. This tape is the sorted output data from the analog-to-digital conversion. Transducer output is expressed in a system of units which is the A/D converter's representation of voltage. Additional input includes identification specifications which define T_o and DPTZ; the high, low and null input/output voltages for each range amplifier; and the manufacturer's calibration for each transducer. DSCALE uses this input as it does the following:

1. All of the transducer output data are multiplied by 0.00069053396. This transforms the data from analog-to-digital units to voltage.

2. The calibration steps for each analog recorder channel are examined, and step averages are computed for each channel. An examination is made to determine if each step average lies within predetermined limits. Steps which do not fall within these limits are deleted. The deletion of more than six steps for any channel aborts the run. All valid step averages are maintained for future usage.

3. The sled accelerometer data is examined and T_o is located. T_o is defined to be the first data point of a pulse that has a minimum amplitude of -0.5 volts and a duration of 3.5 msec.

4. The sled peak acceleration is located by examining a 10 point running average of all of the sled acceleration data after T_o. The point of peak acceleration is where this running average reaches its maximum.

5. A backward running average is begun from the sled peak acceleration. When this average falls below 40 percent of the peak acceleration, the averaging stops and 30 data points are stepped back. The data value reached is, by input definition, Data Processing Time Zero (DPTZ). DPTZ is thus defined to be the data point which occurs 15 msec prior to the time at which 40 percent of the averaged sled peak acceleration is reached.

6. For each channel, the 32 data points immediately before DPTZ are averaged to get a number, BASE, which is utilized in rate gyro scaling.

7. A least squares linear fit is executed for each channel using the calibration step averages previously calculated as the dependent values, and input voltages to the calibrator as independent values. The calibrator input voltages were supplied on log sheets which accompanied each analog tape and were incorporated into punch cards as input to DSCALE. The slope (B2) and intercept (B1) from the least squares fit for a given channel are used to transform each data point (D) of that channel.

$$A = (B2)(D) + B1 \tag{1}$$

where A is the corrected data point.

8. A second least squares fit for each channel is used to incorporate the range amplifier settings. The high, low and null input/output voltages for each range amplifier were supplied on log sheets which accompanied each analog tape and were incorporated into punch cards as input to DSCALE. The resulting slope (B6) and intercept (B5) are used to transform each corrected point (A) of a given channel.

$$S = (B6)(A) + B5 \tag{2}$$

where S is the corrected data point.

9. A final least squares fit is done to convert voltages to accelerations and angular velocities. This fit uses the appropriate manufacturer's calibration for a given transducer. The manufacturer's calibration was incorporated into punch cards as input to DSCALE. The slope (B8) and intercept (B7) of this final fit are applied to each corrected data point (S) of a given transducer.

$$F = (B8)(S) + B7 \tag{3}$$

where F is a completely scaled data point.

10. The above described transformation from D to F is executed in one step. It may readily be seen that given:

$$A = (B2)(D) + B1 \tag{4}$$

$$S = (B6)(A) + B5 \tag{5}$$

$$F = (B8)(S) + B7 \tag{6}$$

A final slope (B12) and intercept (B11) may be calculated.

$$B12 = (B8)(B6)(B2) \quad (7)$$

$$B11 = (B8)(B6)(B1) + (B8)(B5) + B7 \quad (8)$$

The total data transformation for any data point D of a given transducer is

$$F = B11 - BASEL + (B12)(D) \quad (9)$$

where BASEL is an offset constant.

$$BASEL = O \text{ for accelerometers}$$

$$BASEL = B11 + (B12)(BASE) \text{ for rate gyros} \quad (10)$$

where BASE was previously defined as being the average of 32 data points immediately preceding DPTZ and BASEL is the scaled BASE.

11. Each scaled accelerometer data point is multiplied by 0.000980616 to convert it from G's to cm/msec^2 and the scaled rate gyro data is multiplied by 0.00001745329 to convert it from degrees/sec to radians/msec.

12. The final action of DSCALE is to create a digital output tape containing 1,000 corrected data values for each transducer. The output for each transducer begins with data point DPTZ and consists of the data for 500 msec after DPTZ.

DSCALE Validation

As a validation of the scaling procedure and the computer program, all of the DSCALE output was plotted by a digital computer-driven Stromberg-Carlson 4020 plotter (Figures DP-3 and DP-4) and carefully compared, channel by channel, with its corresponding BETHO2 plot (Figure DP-1) and analog strip chart (Figure DP-2). Plots showing discrepancies were investigated and the cause determined and corrected. These plots were and are maintained on file.

Some of the plots presented herein were originally designed to verify transducer and photographic scaling. An examination of the PDH (derived from the head angular position as computed from photographic data) vs RDH (derived from the scaled head rate gyro) comparison plots (Plots 633 through 673) illustrate the precision and accuracy of sensor and photographic scaling.

A single digital tape was used to record the DSCALE output from each run and these tapes were and are maintained as a primary reference.

Figure DP-5 illustrates the flow of sensor data to a DSCALE output tape compatible with the UNIVAC 1108 computer system.

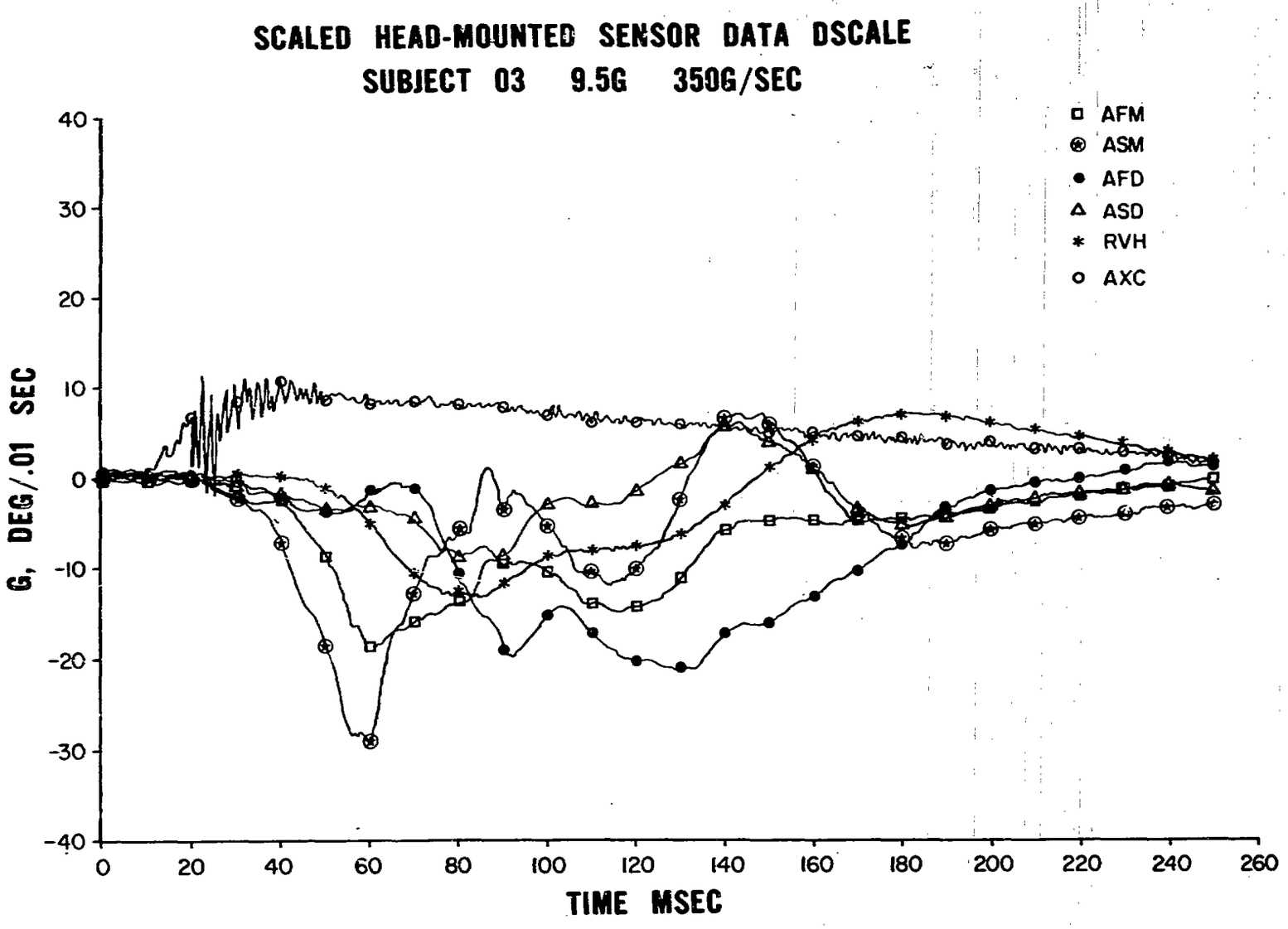
SCALED HEAD-MOUNTED SENSOR DATA DSCALE
SUBJECT 03 9.5G 350G/SEC
AFM
ASM
AFD
ASD
RVH
AXC
G, DEG/.01 SEC
TIME MSEC
40
30
20
10
0
-10
-20
-30
-40
0
20
40
60
80
100
120
140
160
180
200
220
240
260

FIGURE DP - 3

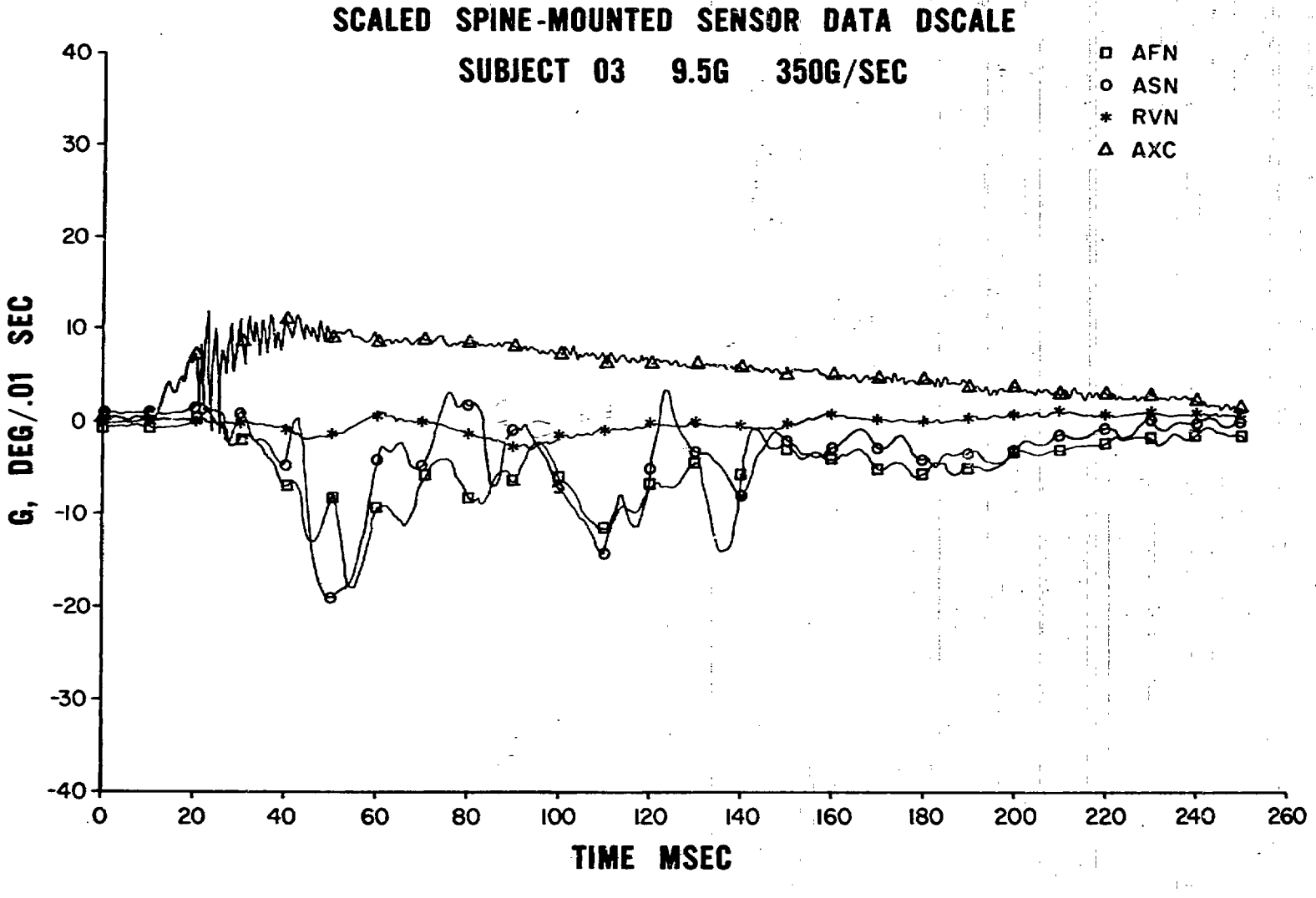
SCALED SPINE-MOUNTED SENSOR DATA DSCALE
SUBJECT 03 9.5G 350G/SEC
AFN
ASN
RVN
AXC
G, DEG/.01 SEC
TIME MSEC
40
30
20
10
0
-10
-20
-30
-40
0
20
40
60
80
100
120
140
160
180
200
220
240
260

FIGURE DP - 4

SENSOR DATA (DSCALE)

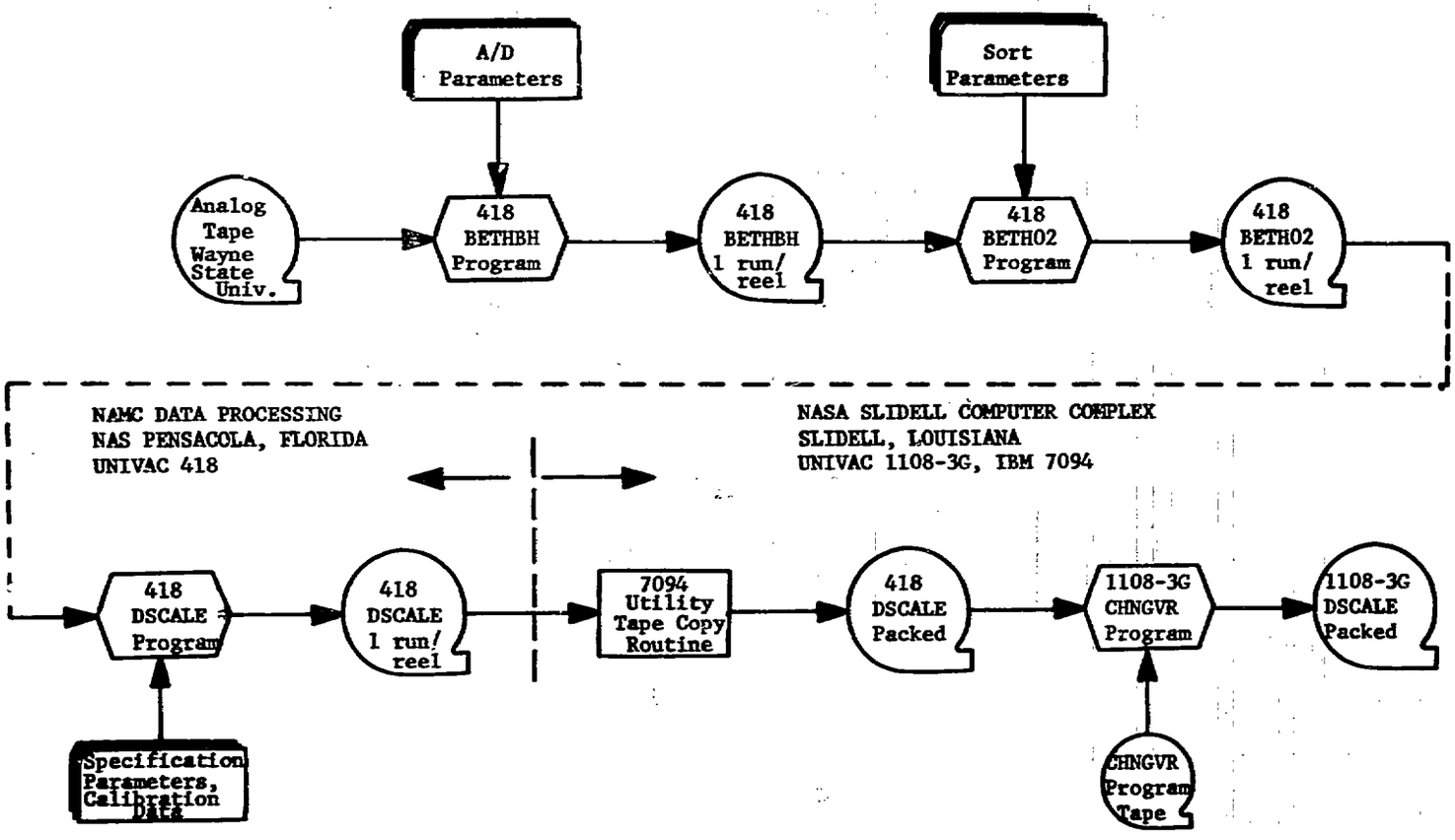

FIGURE DP-5

While the sensor data were being digitized, sorted and scaled, a simultaneous effort was underway to acquire scaled photographic data (PHDATA) and to establish the x-ray anthropometry and initial conditions necessary for subsequent processing.

PHOTOGRAPHIC DATA PROCESSING

The filming of each human exposure to impact acceleration began before the placement of the subject on the sled and continued until the end of the experiment. The sequence of events filmed may be classified in four areas:

1. An identification board was placed in the sled-mounted camera field of view. This identification board contained the sled run number, the human run number, the subject identification number, the nominal G level and rate of onset, the camera framing rate, and the Julian date, along with accumulator pressure and volume.

2. An inverse L-shaped calibration device which had a tripod mounting which fit into precisely located and machined pin holes on the sled was mounted. The design was such that, when placed, the calibration device was located in a plane corresponding to the mid-sagittal plane of the volunteer subject and had straight lines perpendicular and parallel to gravity. The centers of the targets which defined the lines were 12 inches apart. The cameras were actuated momentarily to record the board and calibration device on the beginning of each data film. Figure DP-6 illustrates such a frame of photo data calibration. The plumb line used to verify the calibration device is visible at right.

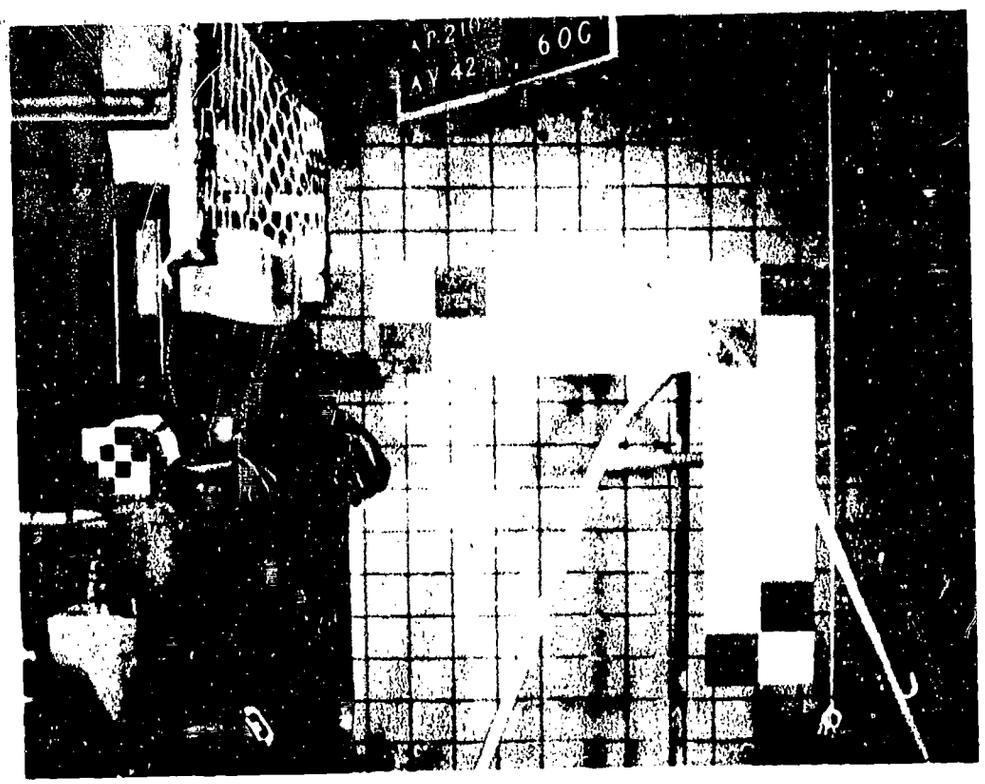

FIGURE DP-6 A Frame of Film Demonstrating the I.D. Board and Calibration Device

3. The subject was then placed on the sled and positioned prior to the onset of acceleration (Figure DP-7).

FIGURE DP-7 A Frame of Film Demonstrating the Volunteer's Position Prior to the Onset of Acceleration

4. Acceleration was initiated, and the resulting response of the volunteer's head and neck was filmed. Figure DP-8 shows the point of maximum neck extension during a run.

FIGURE DP-8 A Frame of Film Demonstrating the Resulting Response of the Volunteer's Head and Neck

The arbitrary T_o pulse on the sensor data AXC channel gave a means for determining the location of any frame of film relative to the time of occurrence of the sensor data (since the pulse could be precisely located in time in each sensor channel) and simultaneously reset the camera timers to 0. Therefore, the first non-zero camera timer reading occurred within 2 msec of the T_o pulse for frame rates of 500 F.P.S. which were standard for all runs. First motion was marked by the appearance of a light which was a flashbulb triggered by the closing of a microswitch as the ram left the resting position (See Figure DP-8 just in front of the forehead).

After the completion of each run, the exposed film was mailed to the Photographic Laboratory at Eglin AFB for precision development and printing. Film from both the posterior and lateral sled-mounted cameras was available on most runs. On some runs, a supplementary lateral camera provided color coverage of the experiment at varied frame rates.

The developed film negatives were then forwarded to the Mathematical Services Laboratory at Eglin for data reduction.

Photographic data reduction was accomplished by use of Benson Lehner Telereadex Type 29E equipment interfaced with an IBM 523 summary punch. When the horizontal and vertical cross-wires of the device were aligned so that their intersection was on a desired point, analog voltages were generated which represented the coordinates

of that point relative to any other point selected as origin. All targets were measured relative to the sled target origin on data runs. These voltages were then digitized and the digitized coordinates were punched on standard 80 column cards. Table 1 presents card format and Table 2 and Figure DP-9 present data point identification. One card was punched per point. This card contained, in addition to the coordinates, point identification and information obtained from the identification board seen at the beginning of each film. This latter information was input to the summary punch from the Telereadex key board and a set of constant input switches.

The specific procedure utilized by the Mathematical Services Laboratory was as follows:

1. The film negative was mounted and projected on the operator's screen.

2. The identification board was read and required information input into the machine via the Telereadex key board and constant switches.

3. Ten calibration frames containing the calibration device were reduced. A time code of 600000 was entered for all calibration frames. The sled target origin was the X and Z zero point.

4. The film was then advanced to the first frame with a human subject and a non-zero time reading. This frame corresponds to the first frame of film after the T_o pulse, some time prior to acceleration.

5. The film was then advanced to the first frame in which the first motion light appeared.

6. The film was then retreated 25 frames, at which point data reduction began. The sled target origin was the X and Z zero point. The six digit camera timer time was read on each data frame.

7. Data reduction of every frame was continued for 300 frames.

The above procedure described was designed to insure that sufficient precise data were reduced. The film negatives were carefully stored in individual cans for each run and were and are maintained in a controlled environment as a primary reference.

The computer analysis of photographic data began with the receipt of the reduced data cards in Pensacola. Computer programs were then utilized to select the pre-acceleration data necessary for determination of initial conditions and to determine which portion of the reduced data was of experimental interest. The ten frames of calibration data and ten frames of pre-acceleration data were used to develop horizontal and vertical scaling constants (see program ICONDS). These scaling constants and the remaining reduced photographic data were input to a photographic scaling program, PHDATA, and were used to accomplish the following:

1. The X and Z coordinates of each point from each frame and the corresponding frame time were read into digital computer storage arrays.

4XM ACCELERATION OF HEAD C.G. IN X DIRECTION

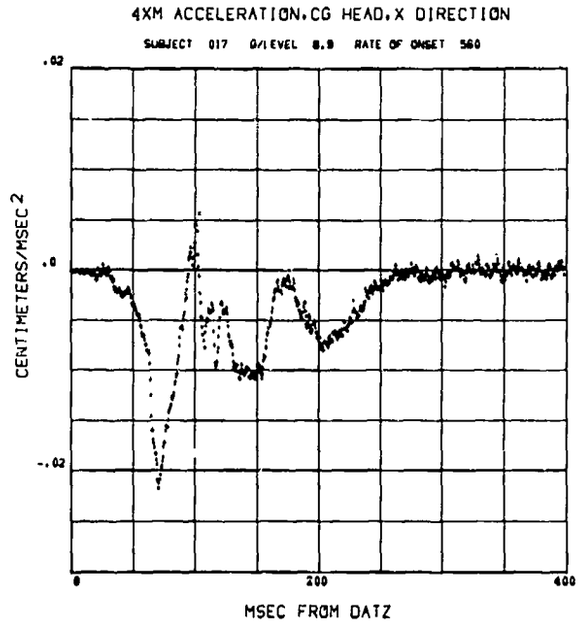

77

4ZM ACCELERATION OF HEAD C.G. IN Z DIRECTION

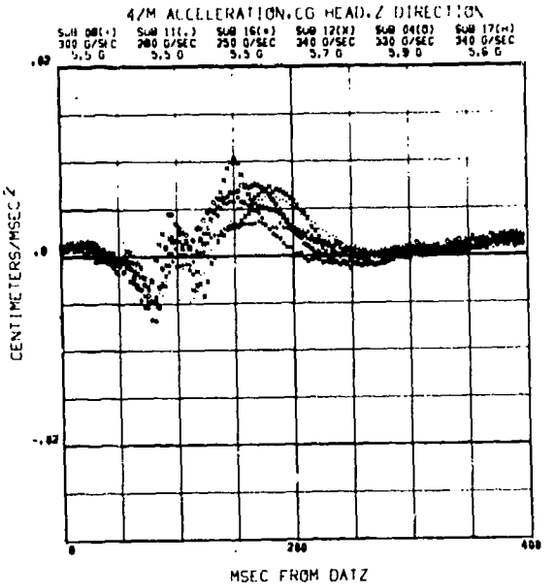

78

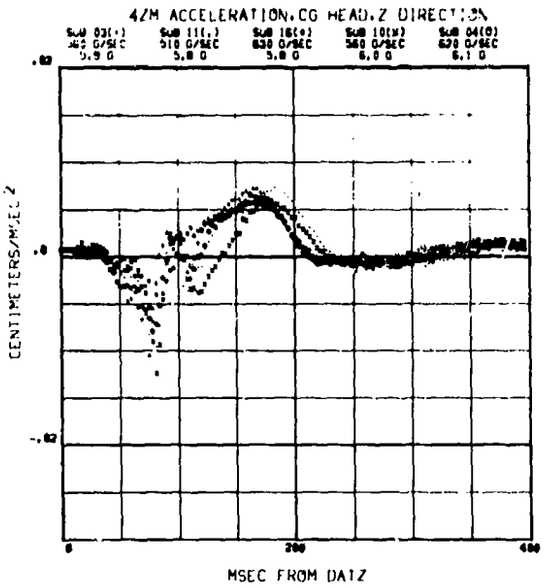

79

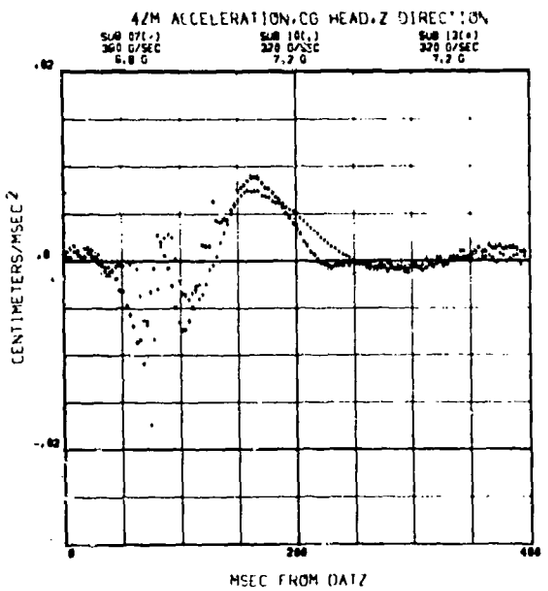

80

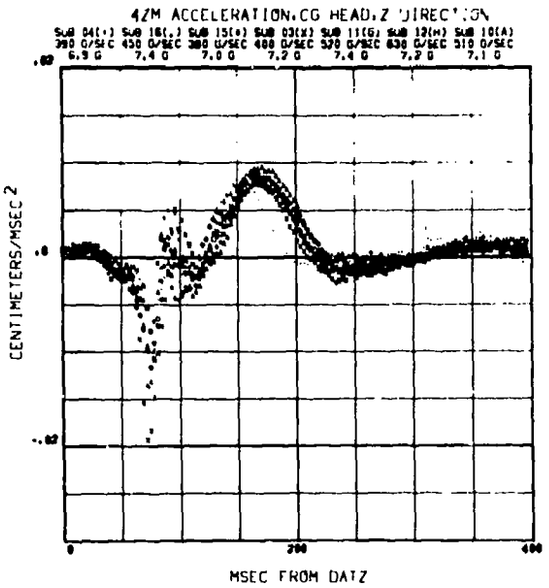

81

4ZM ACCELERATION OF HEAD C.G. IN Z DIRECTION

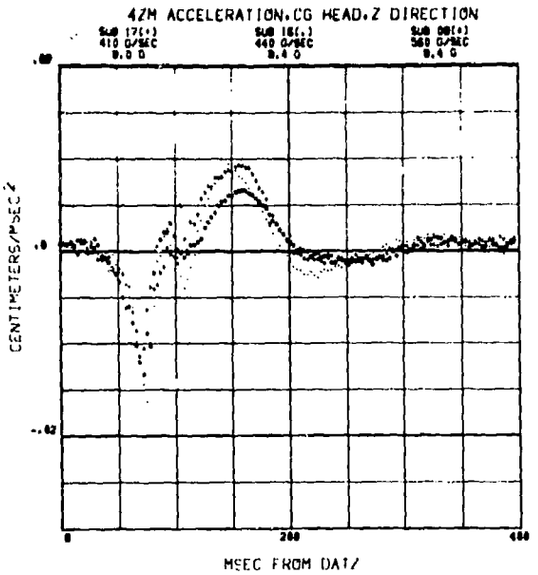

82

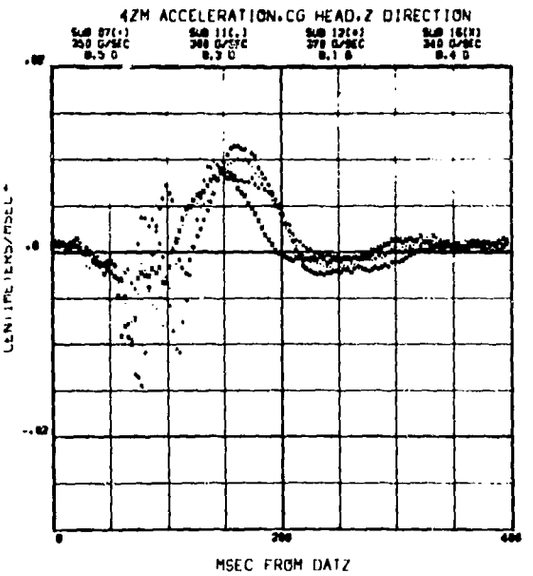

83

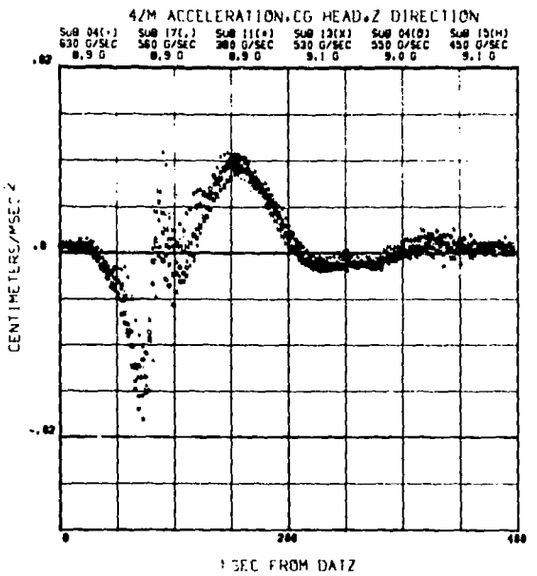

84

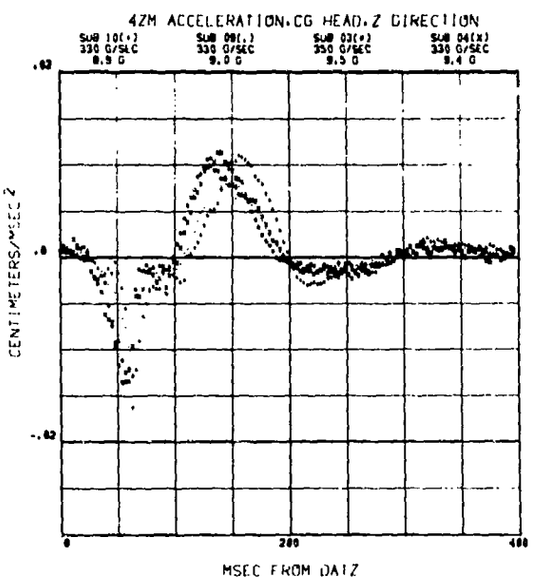

85

4ZM ACCELERATION OF HEAD C.G. IN Z DIRECTION

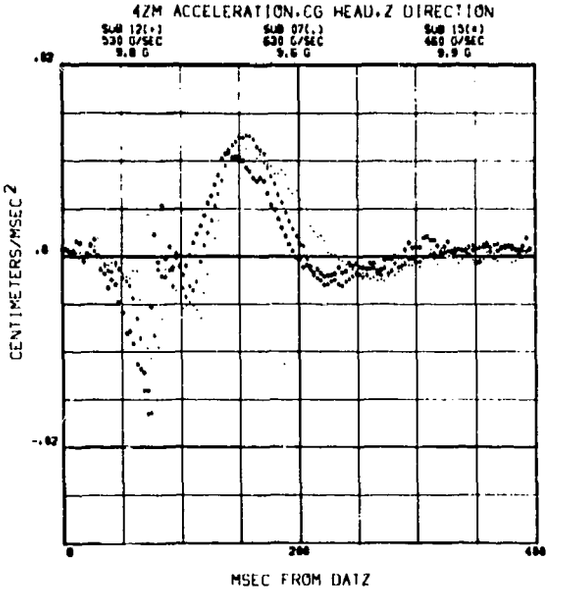

86

4ZM ACCELERATION OF HEAD C.G. IN Z DIRECTION

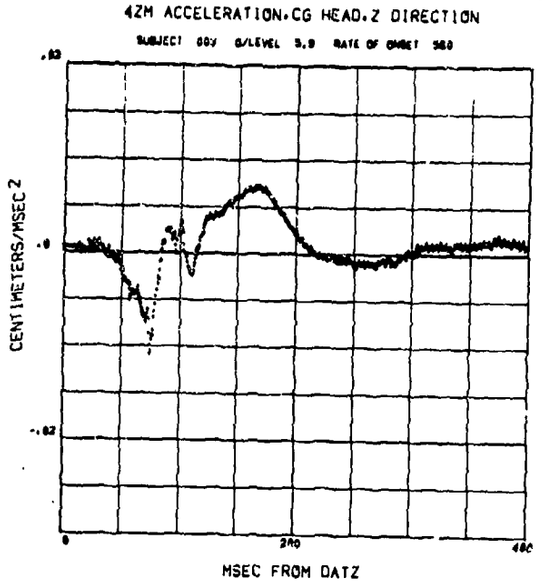

87

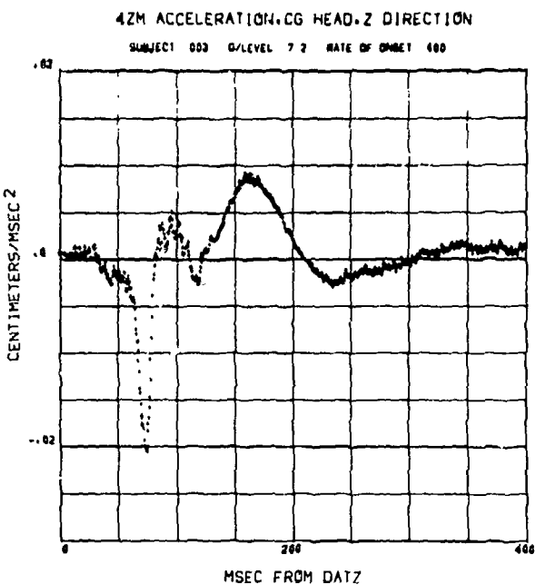

88

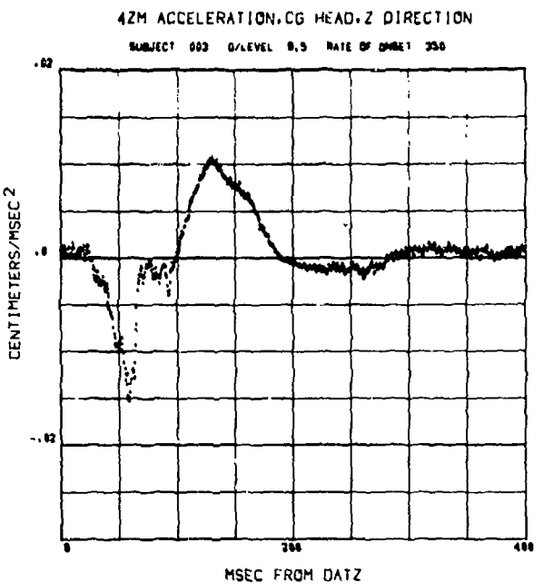

89

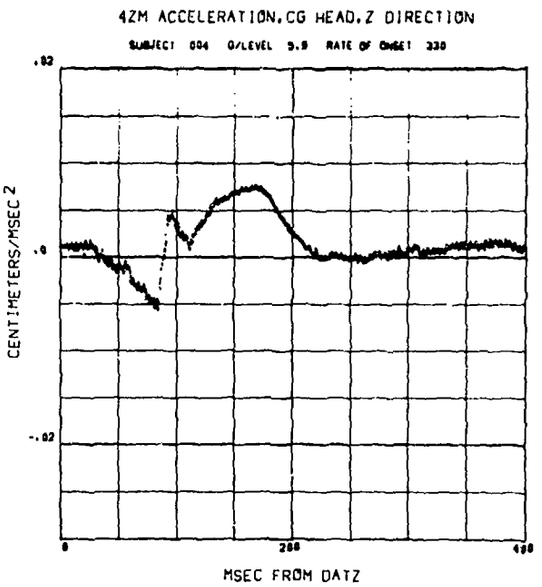

90

4ZM ACCELERATION OF HEAD C.G. IN Z DIRECTION

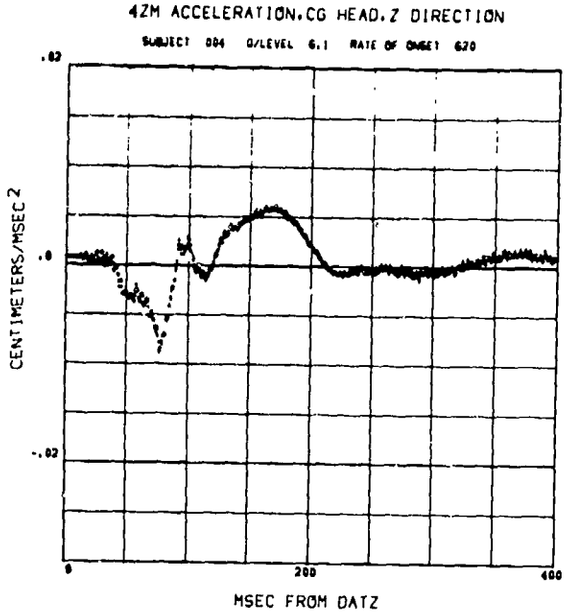

91

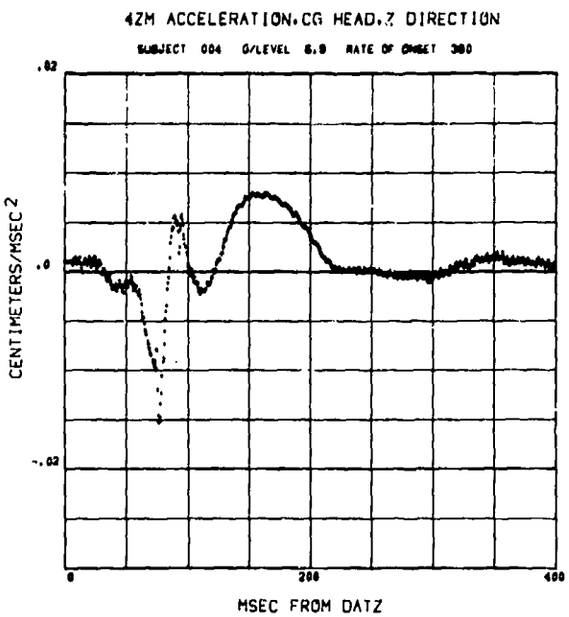

92

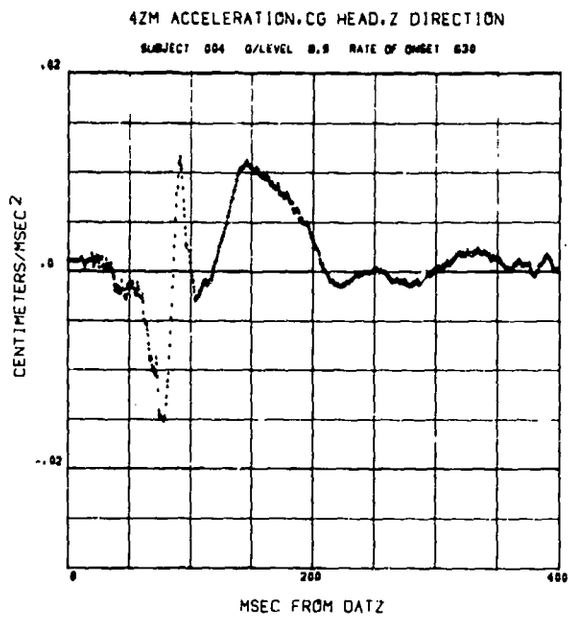

93

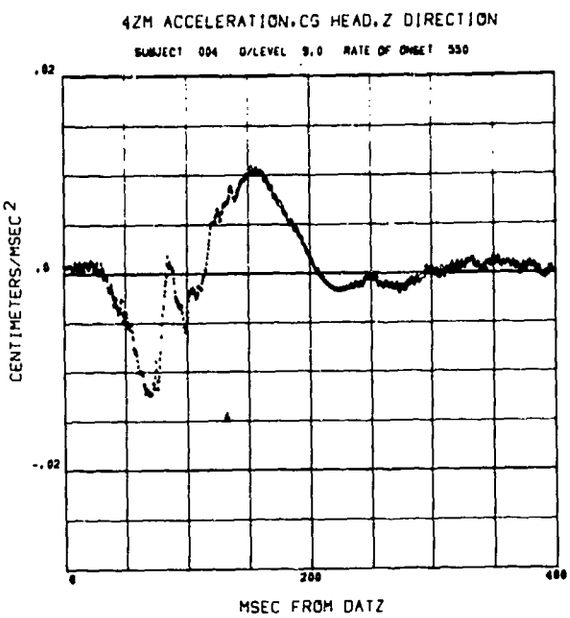

94

4ZM ACCELERATION OF HEAD C.G. IN Z DIRECTION

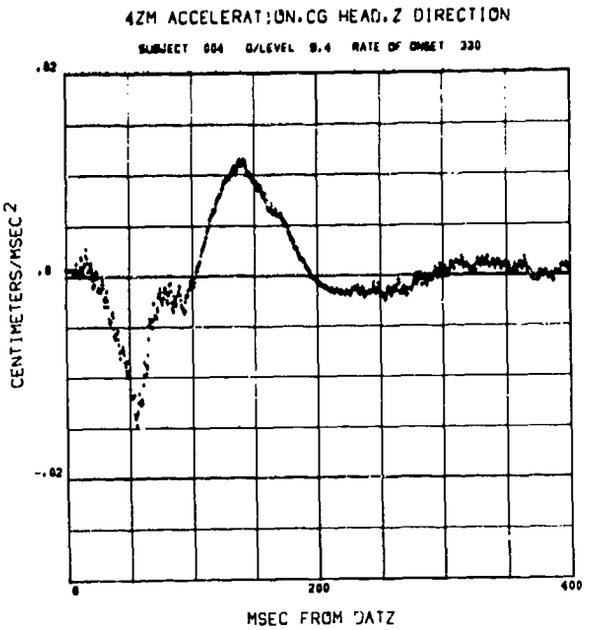

95

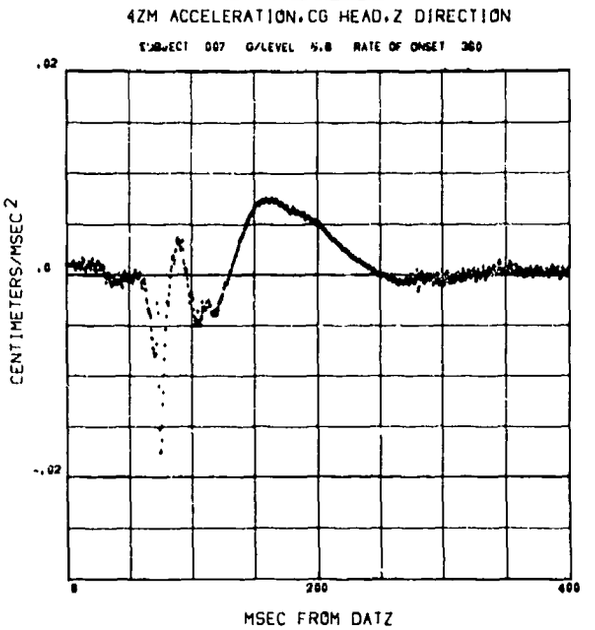

96

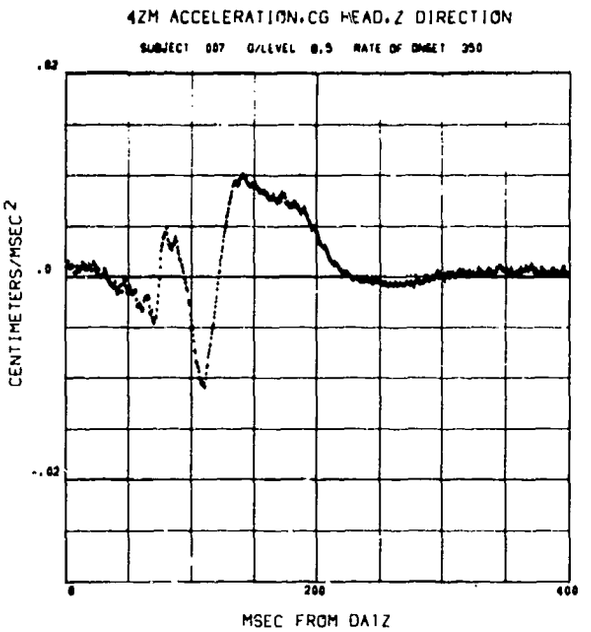

97

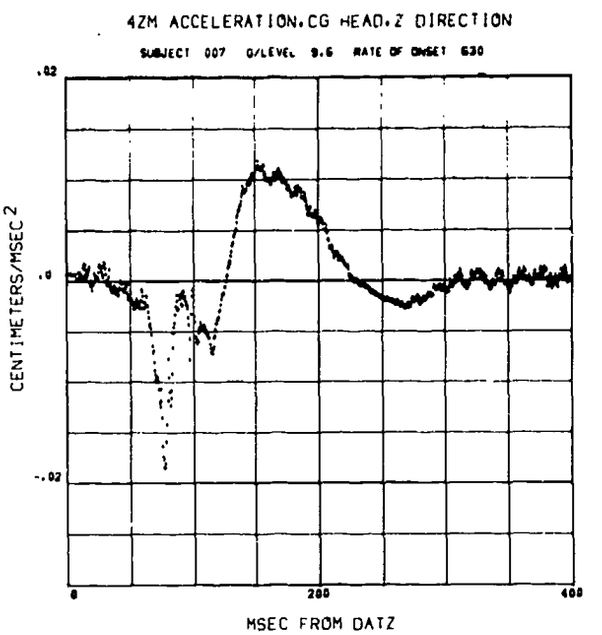

98

4ZM ACCELERATION OF HEAD C.G. IN Z DIRECTION

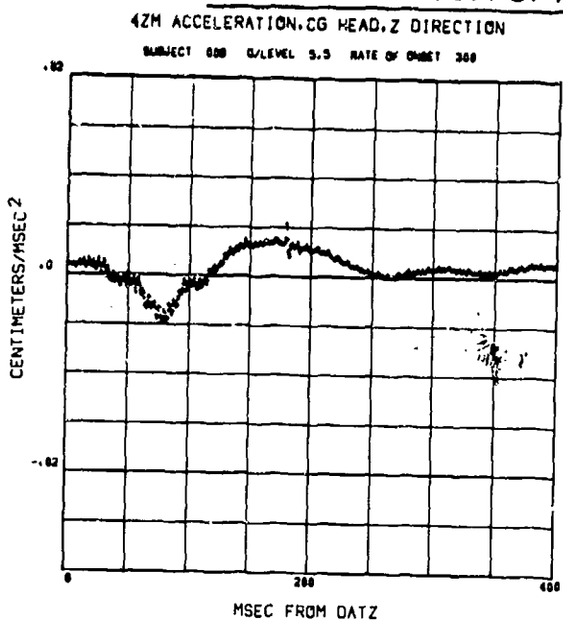

99

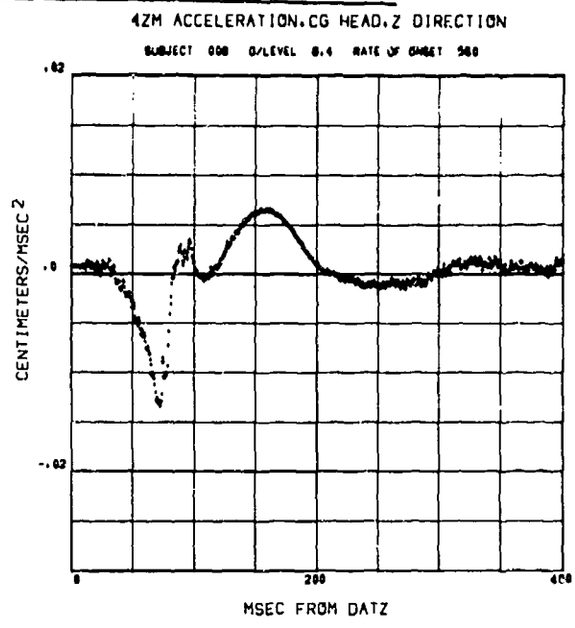

100

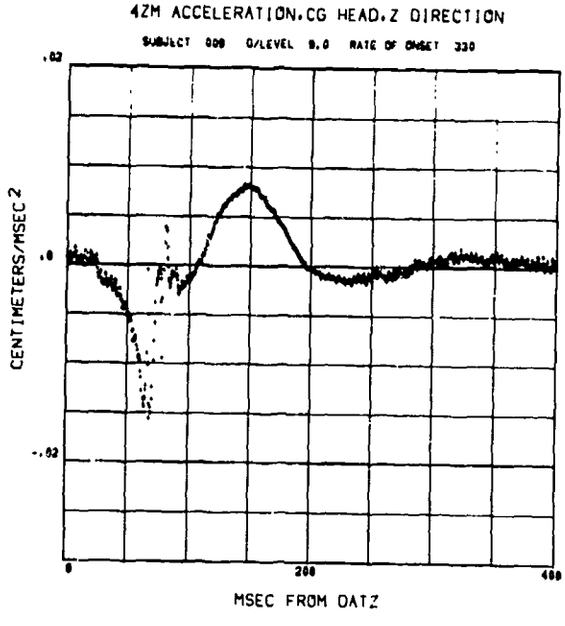

101

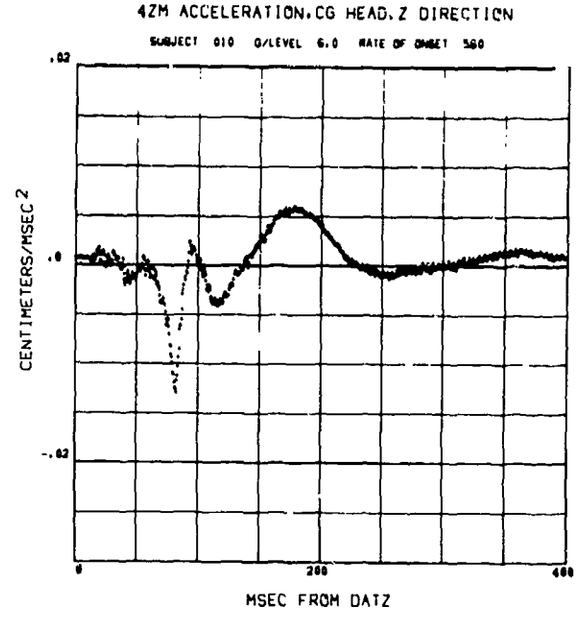

102

4ZM ACCELERATION OF HEAD C.G. IN Z DIRECTION

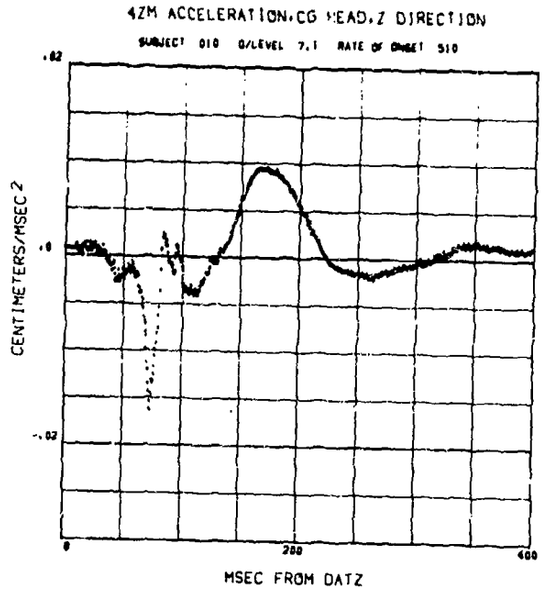

103

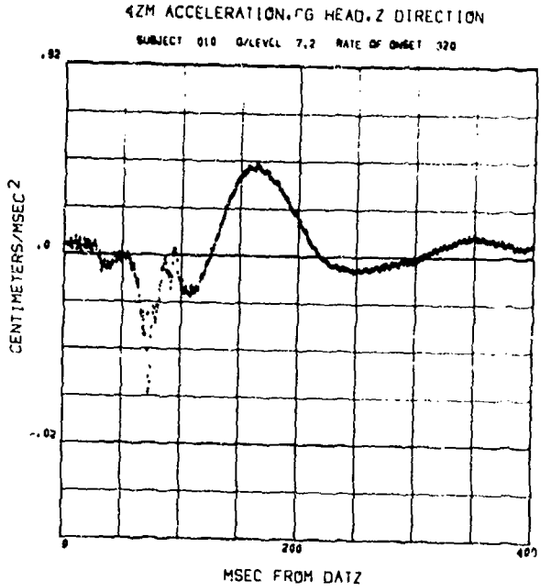

104

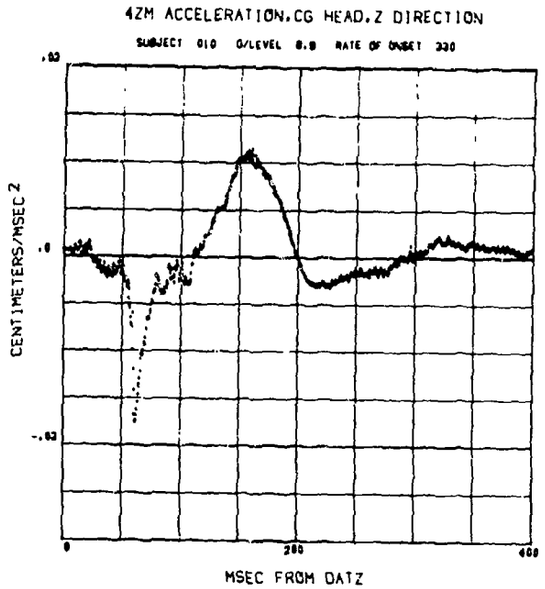

105

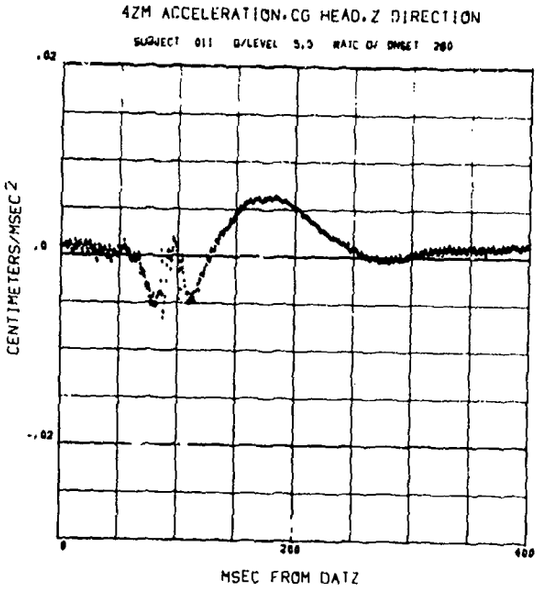

106

4ZM ACCELERATION OF HEAD C.G. IN Z DIRECTION

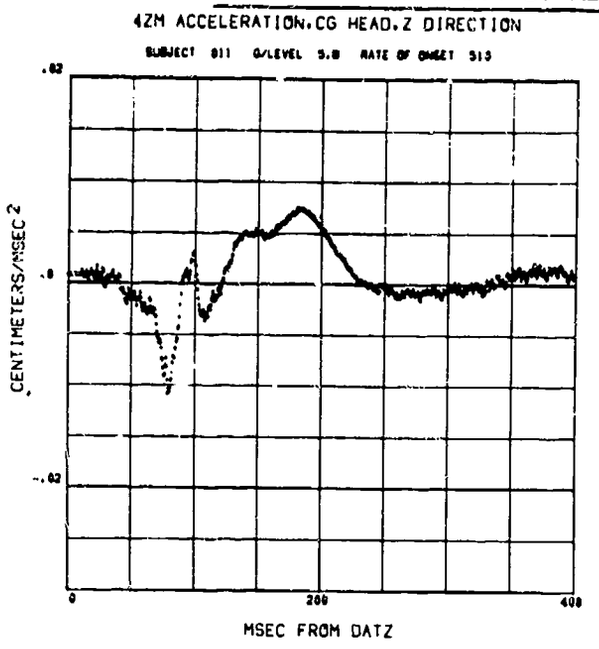

107

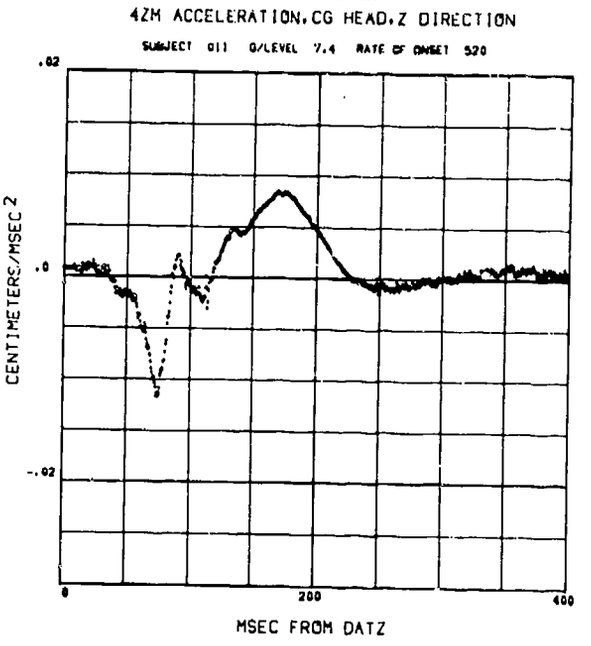

108

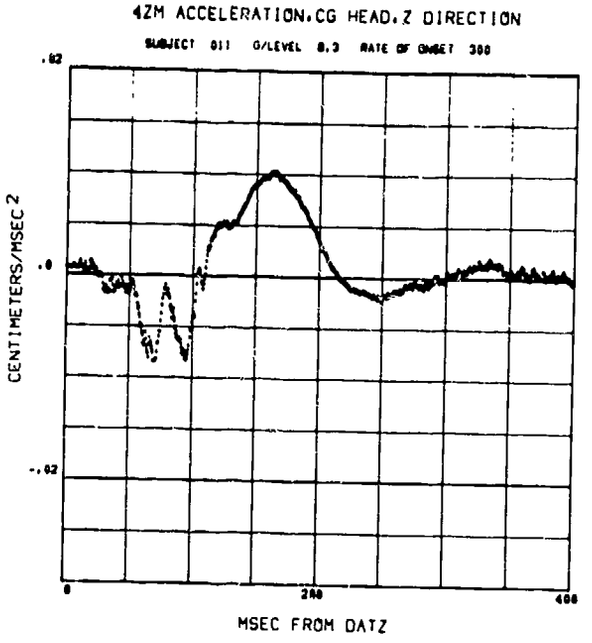

109

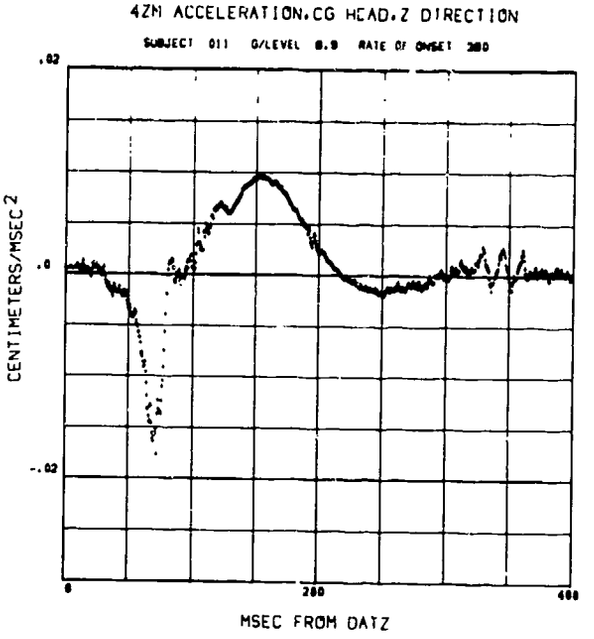

110

4ZM ACCELERATION OF HEAD C.G. IN Z DIRECTION

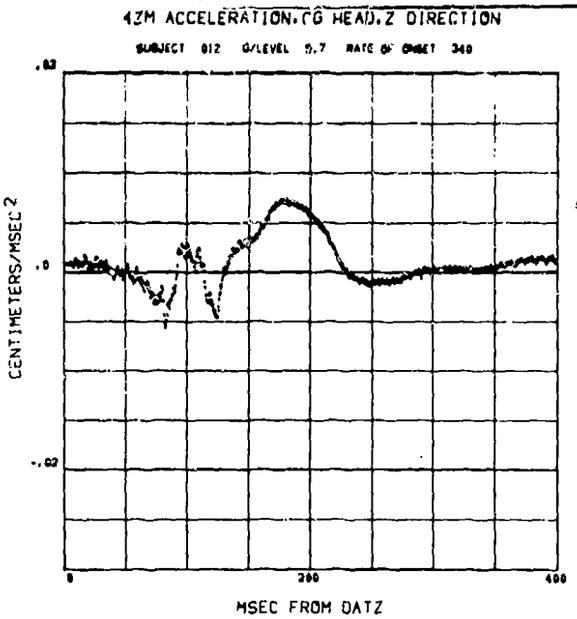

111

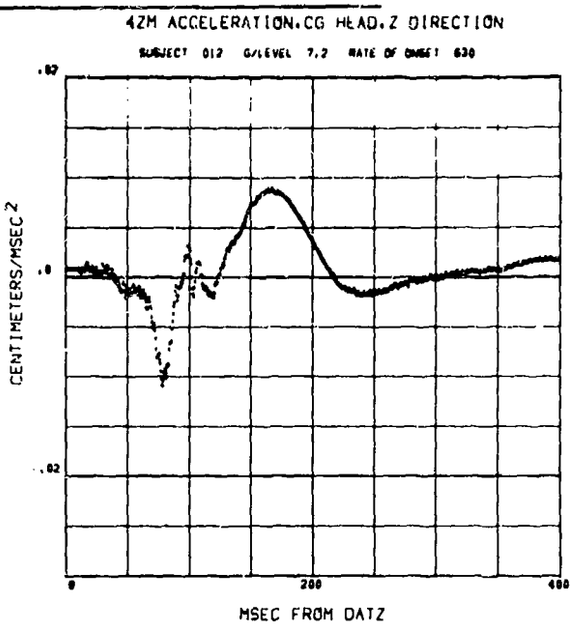

112

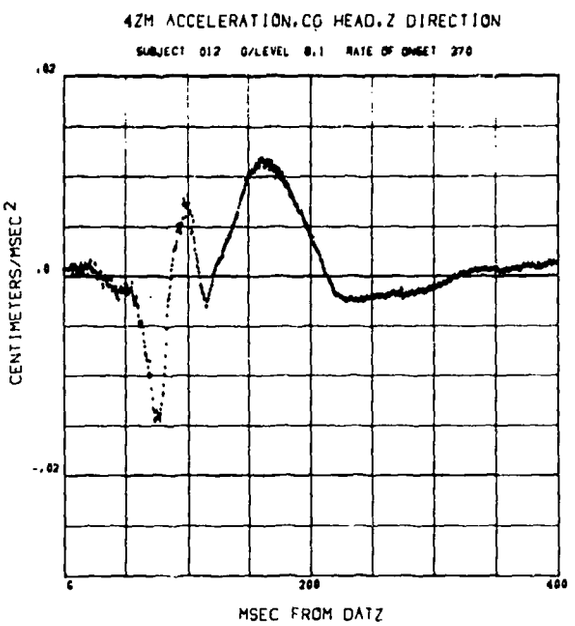

113

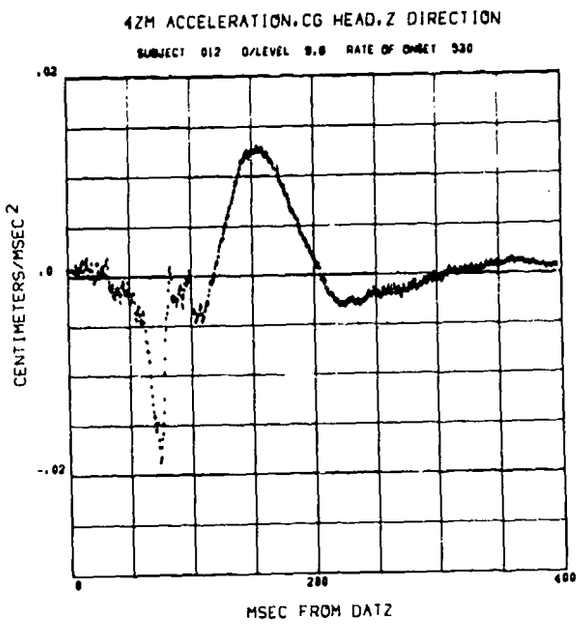

114

4ZM ACCELERATION OF HEAD C.G. IN Z DIRECTION

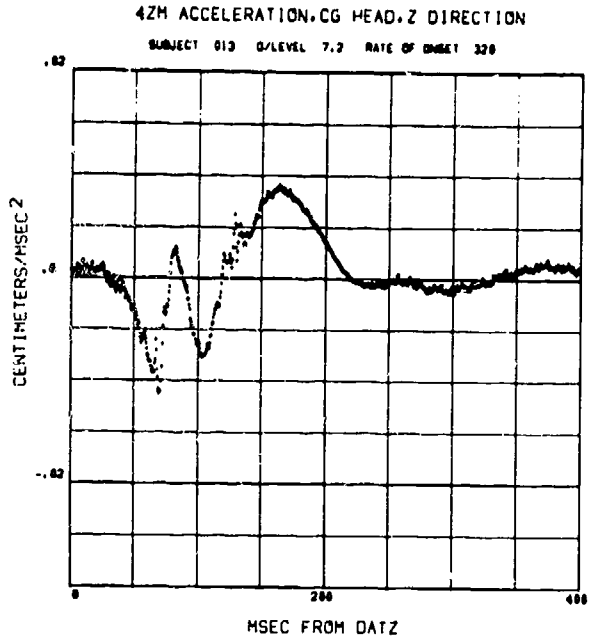

115

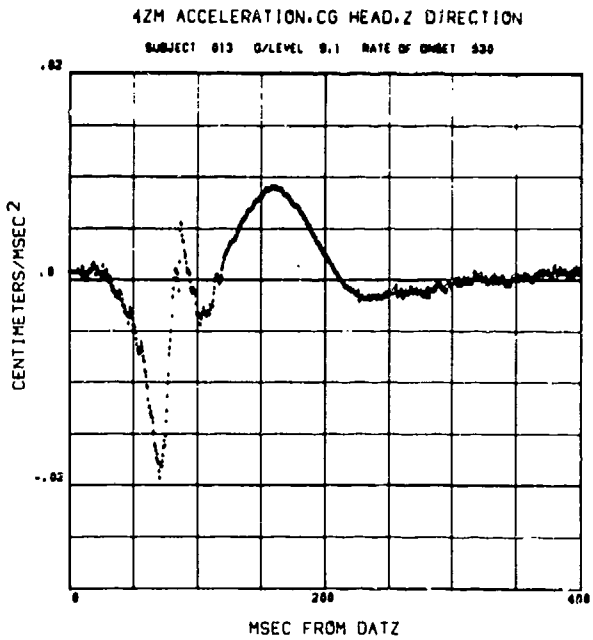

116

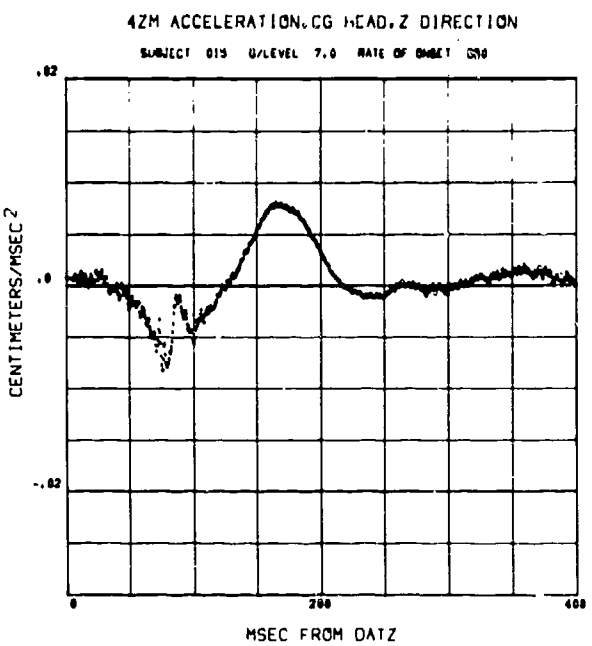

117

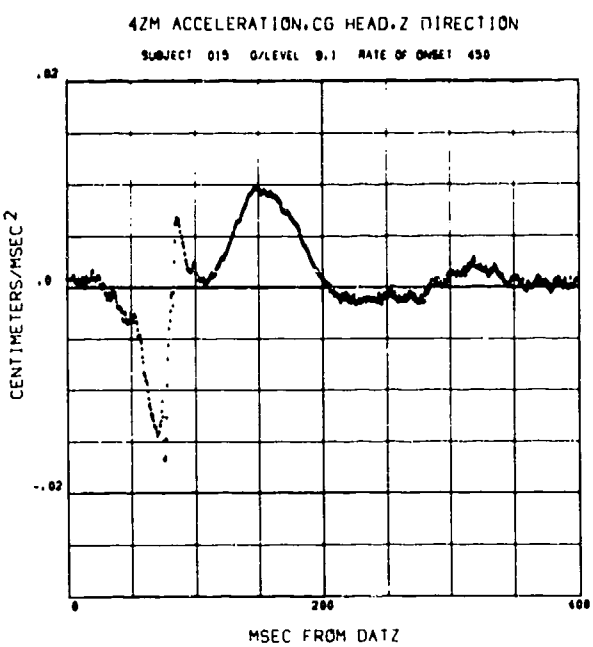

118

4ZM ACCELERATION OF HEAD C.G. IN Z DIRECTION

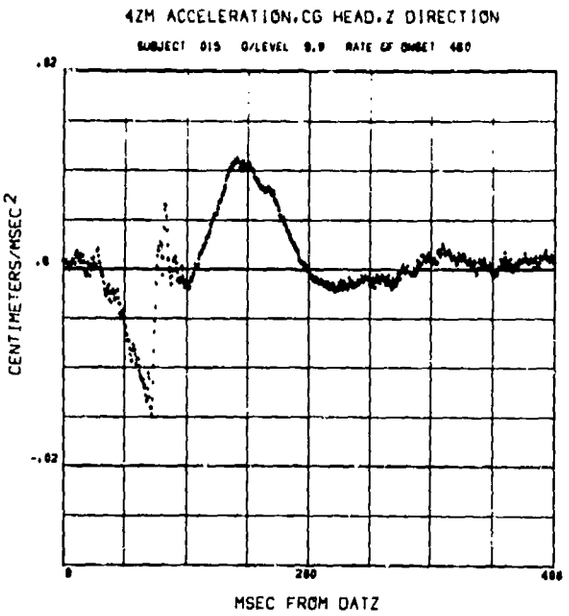

119

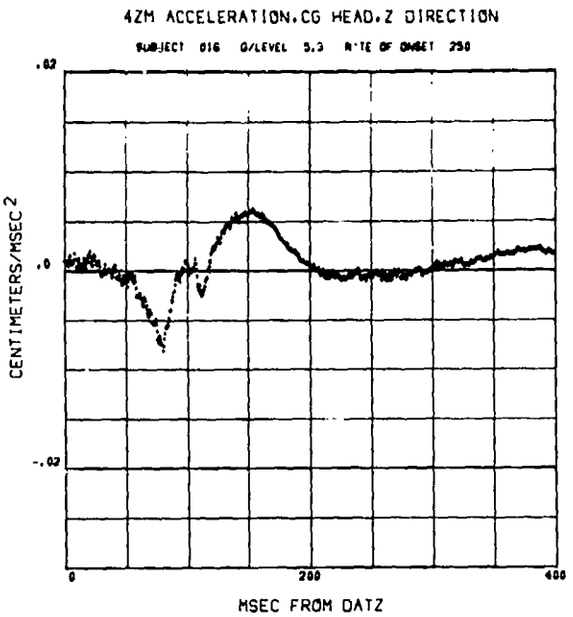

120

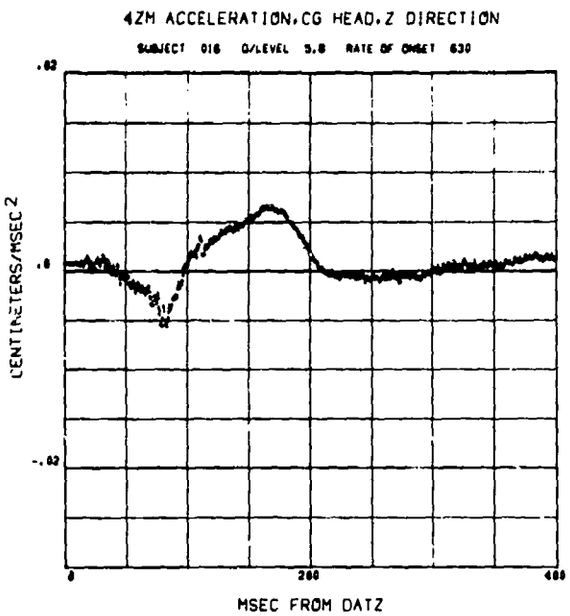

121

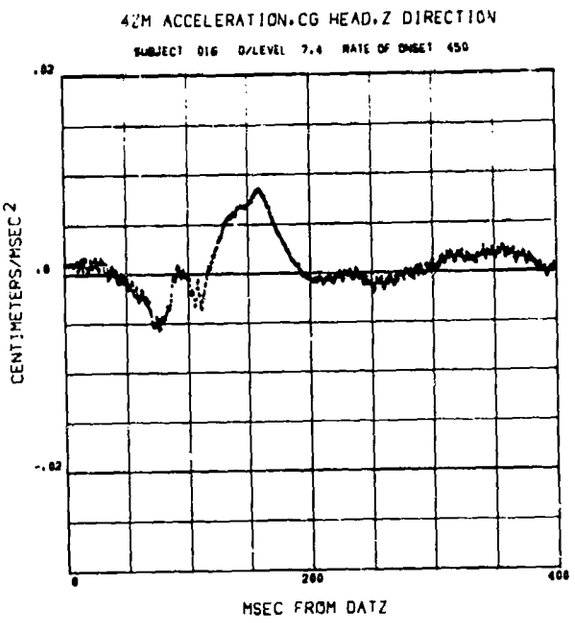

122

4ZM ACCELERATION OF HEAD C.G. IN Z DIRECTION

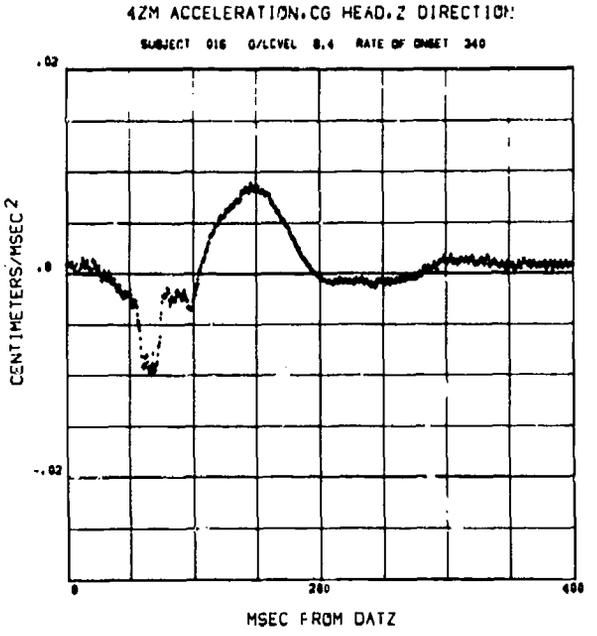

123

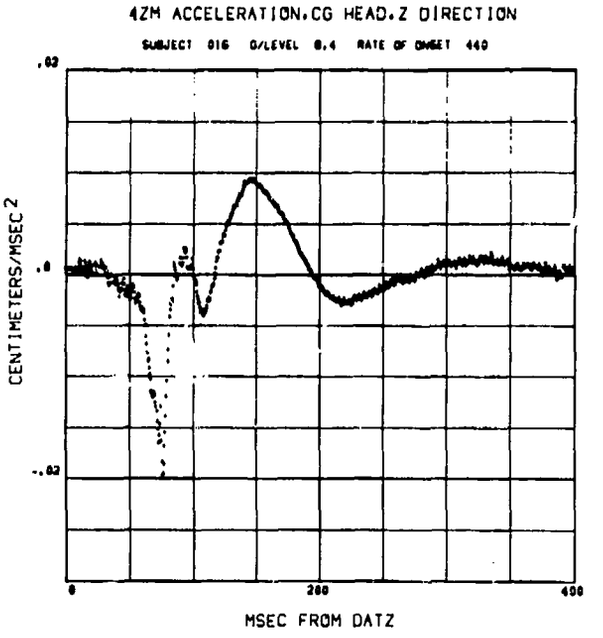

124

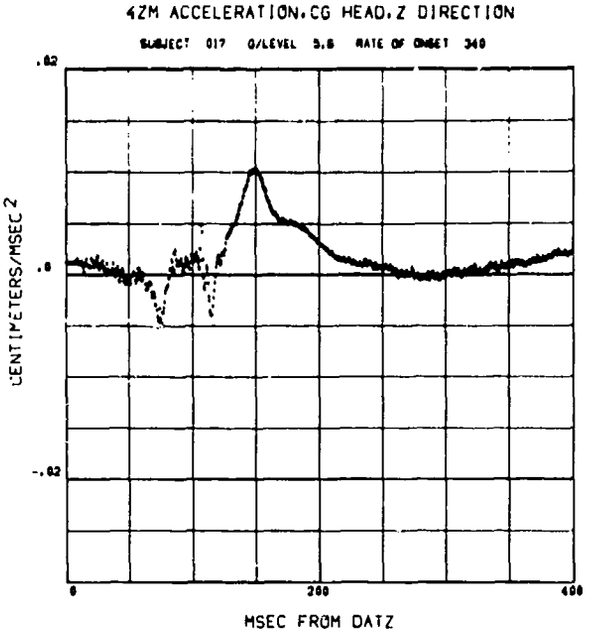

125

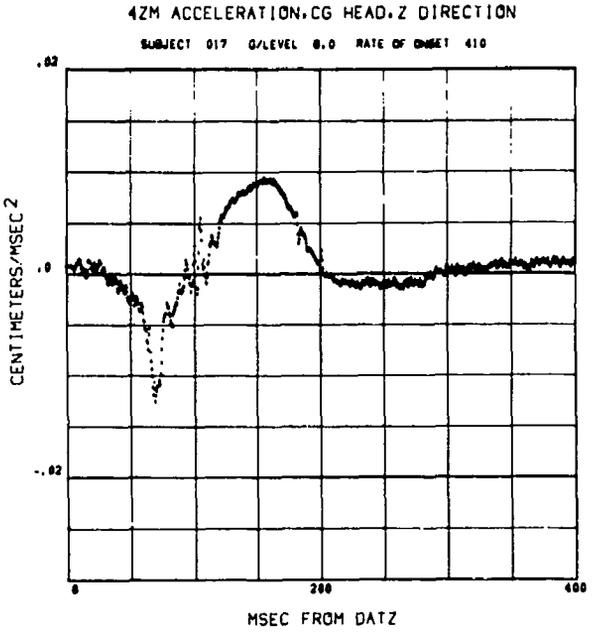

126

4ZM ACCELERATION OF HEAD C.G. IN Z DIRECTION

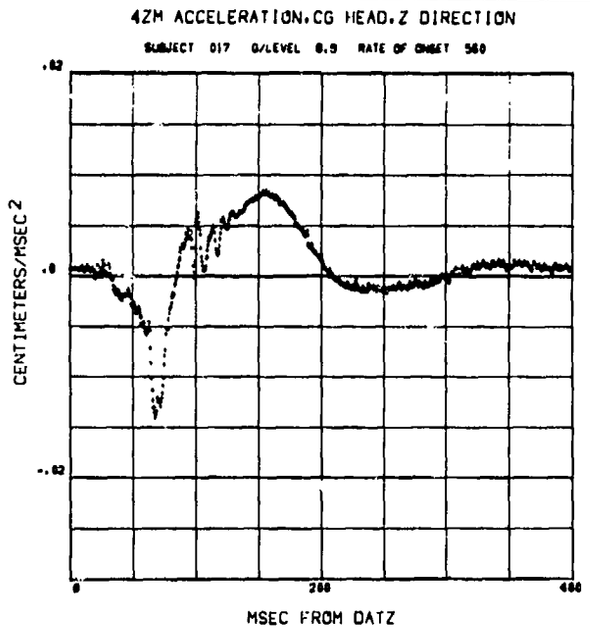

127

4XZ RESULTANT ACCELERATION OF HEAD C.G.

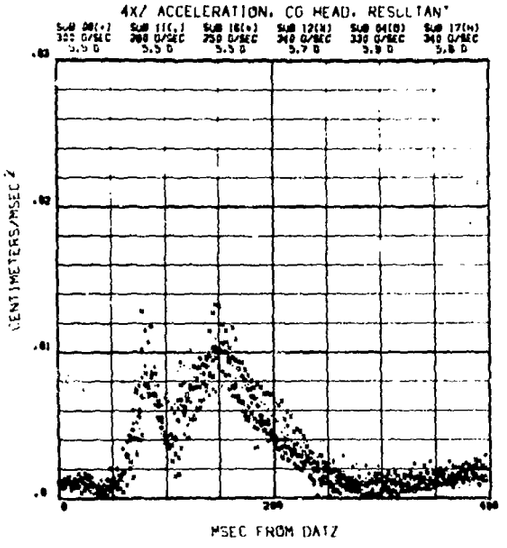

128

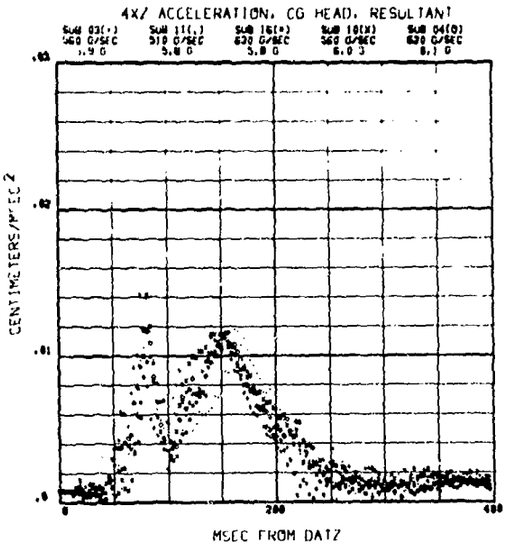

129

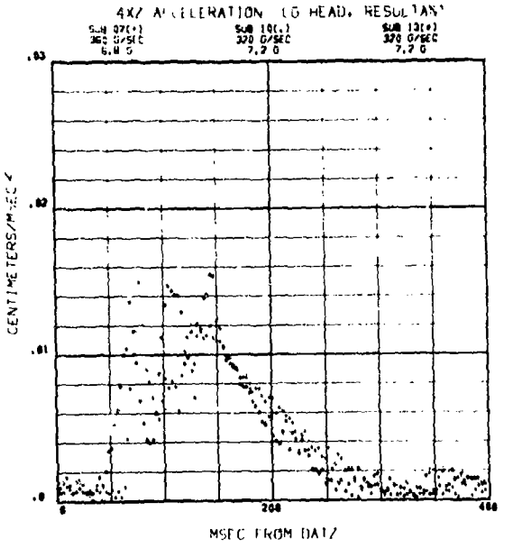

130

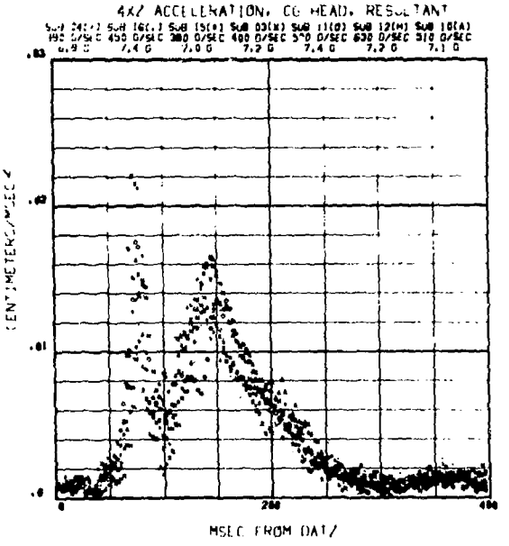

131

4XZ RESULTANT ACCELERATION OF HEAD C.G.

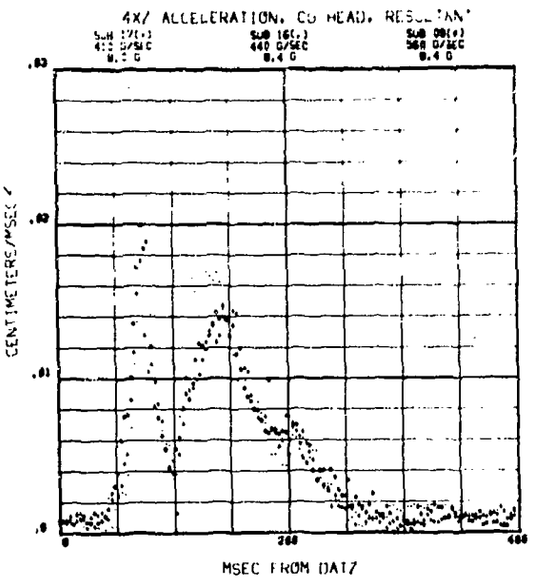

132

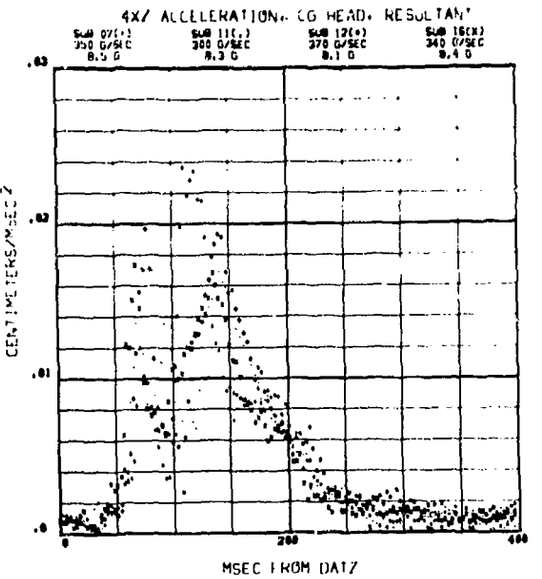

133

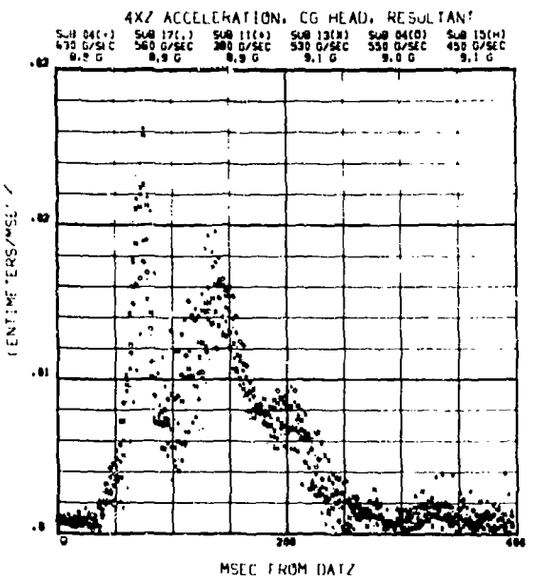

134

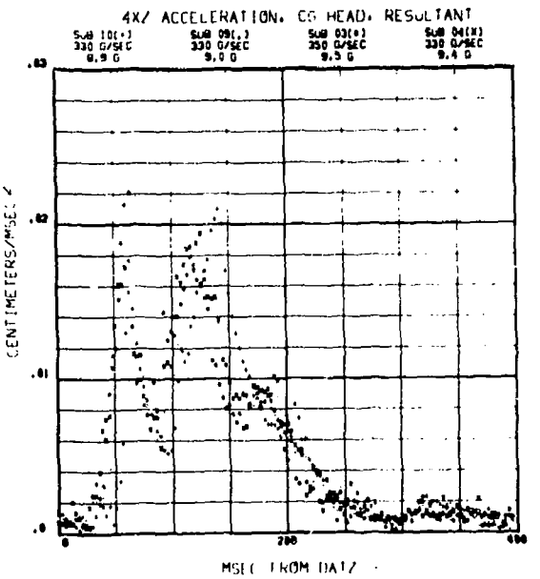

135

4XZ RESULTANT ACCELERATION OF HEAD C.G.

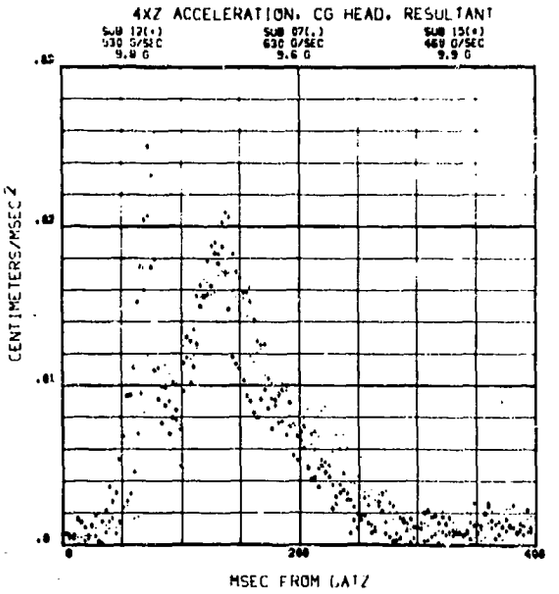

136

4XZ RESULTANT ACCELERATION OF HEAD C.G.

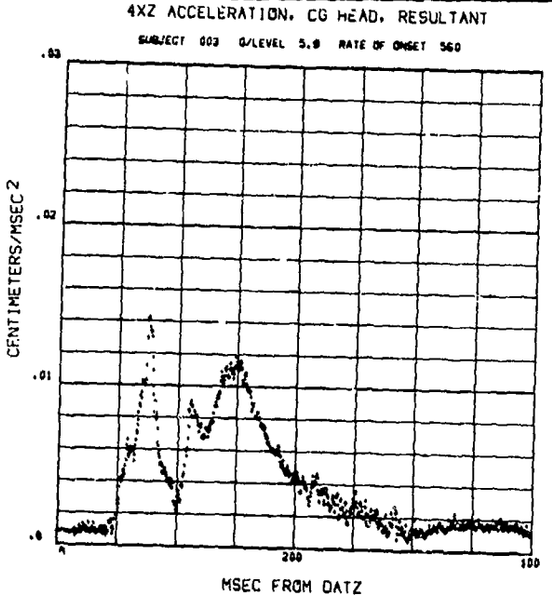

137

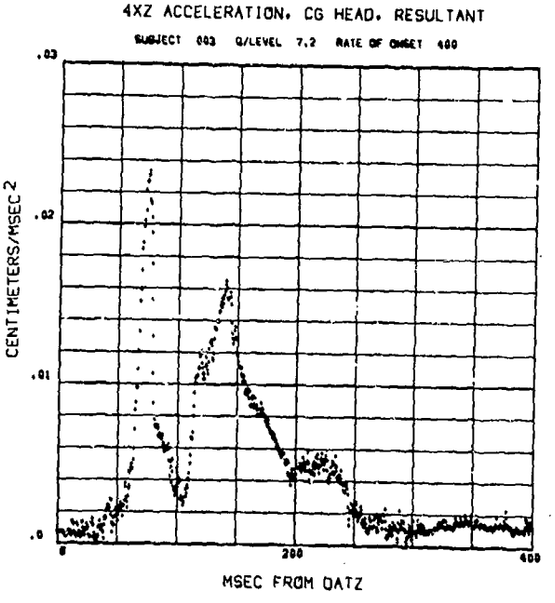

138

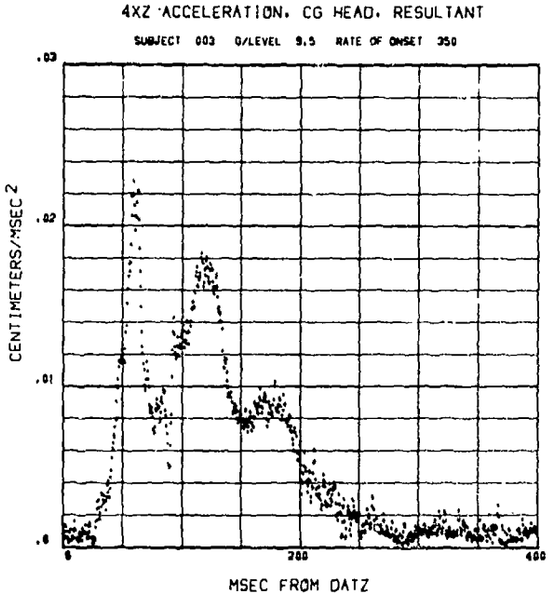

139

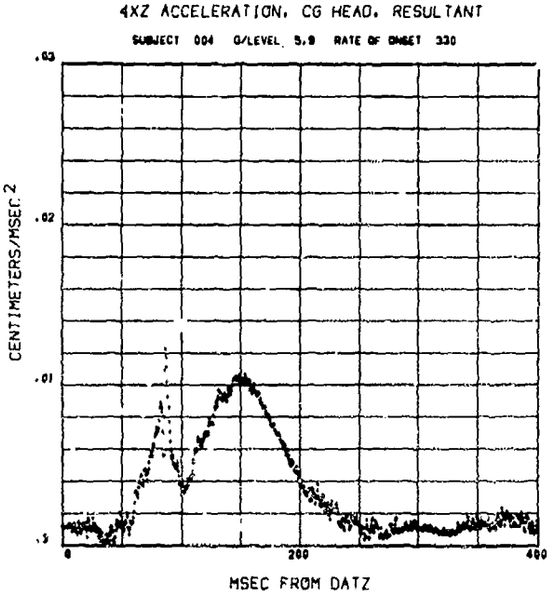

140

4XZ RESULTANT ACCELERATION OF HEAD C.G.

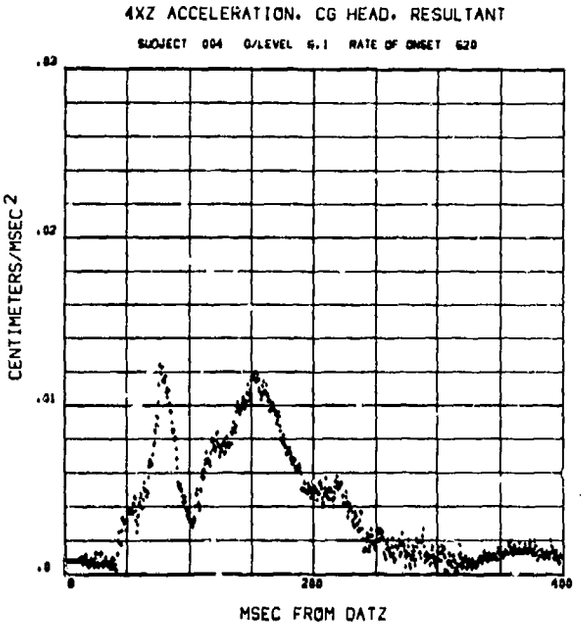

141

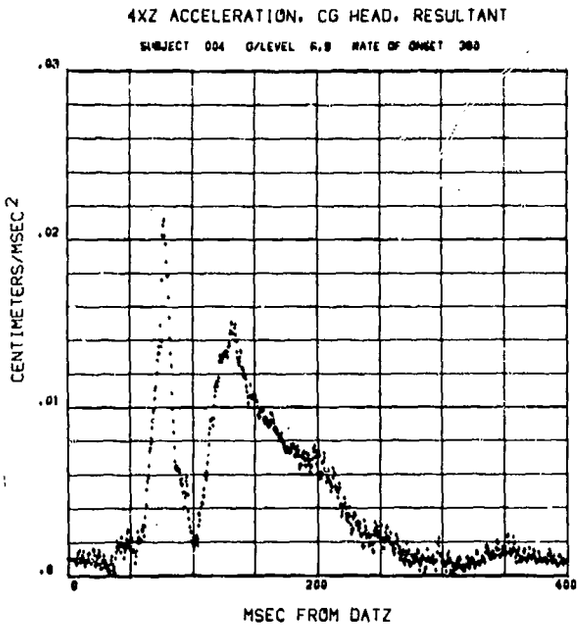

142

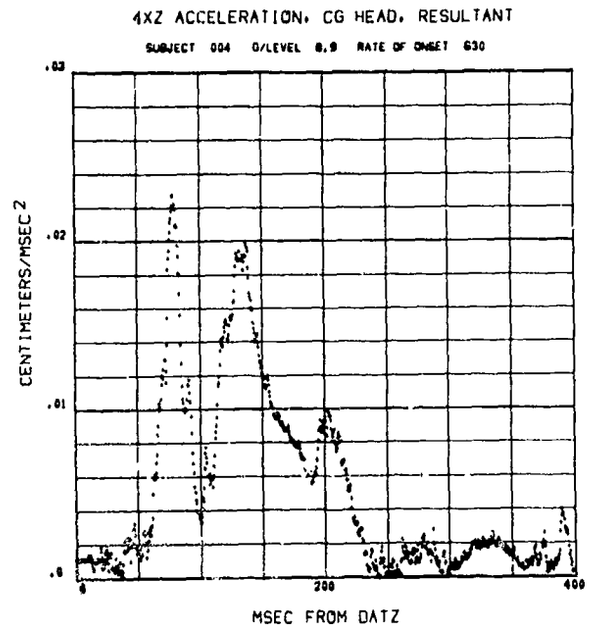

143

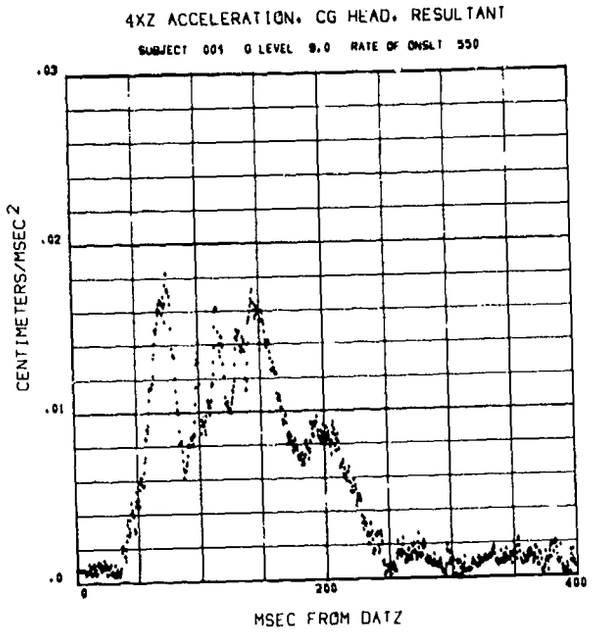

144

4XZ RESULTANT ACCELERATION OF HEAD C.G.

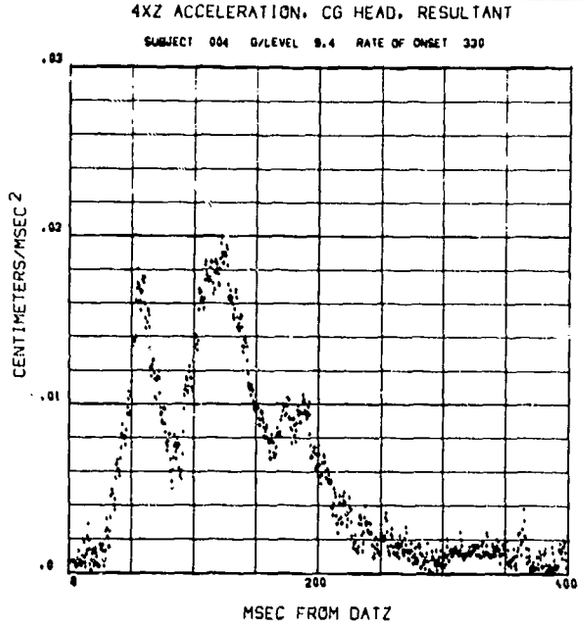

145

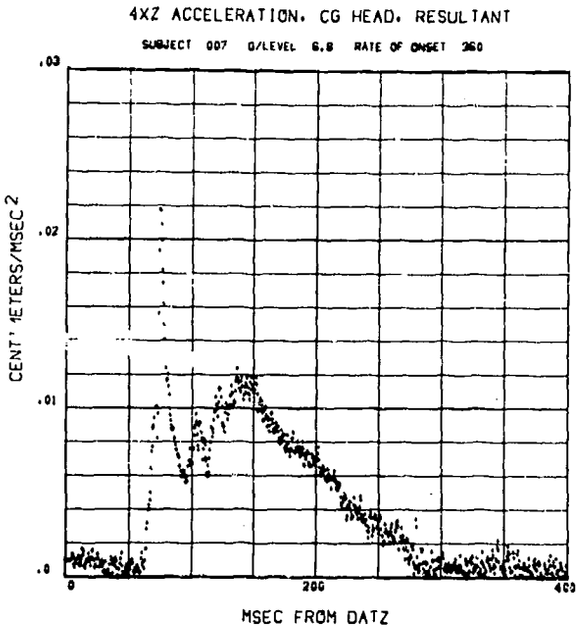

146

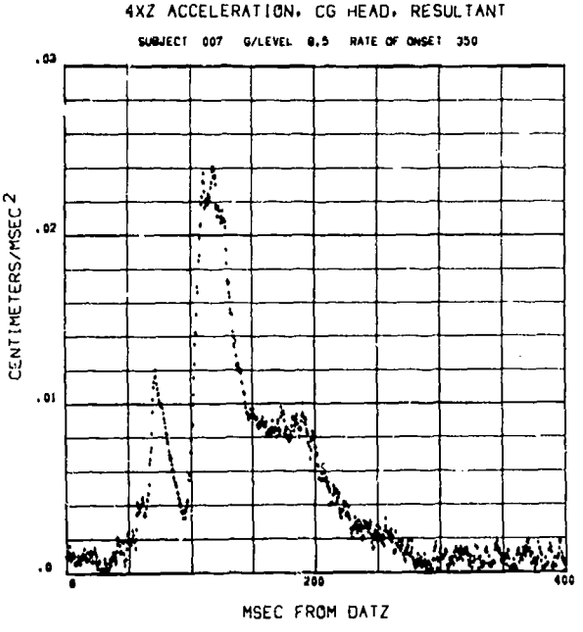

147

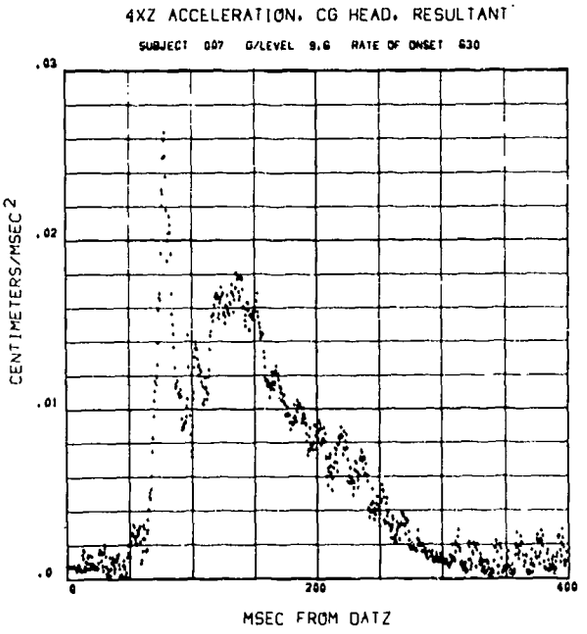

148

4XZ RESULTANT ACCELERATION OF HEAD C.G.

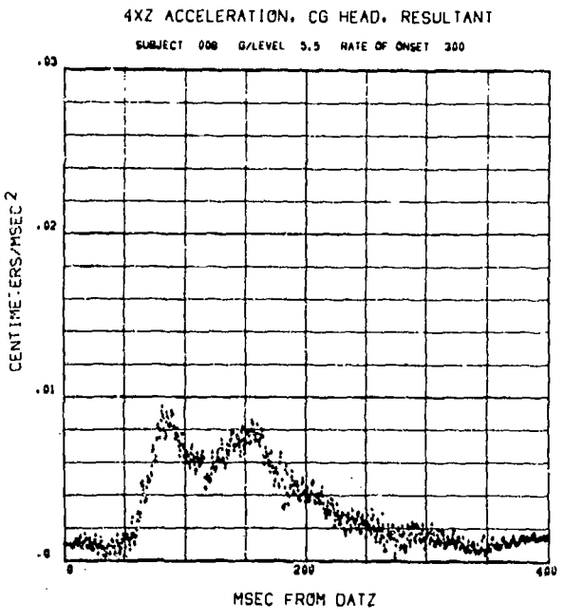

149

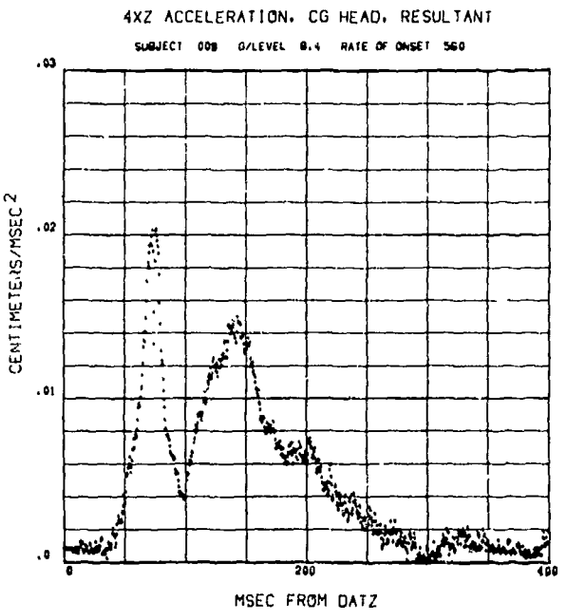

150

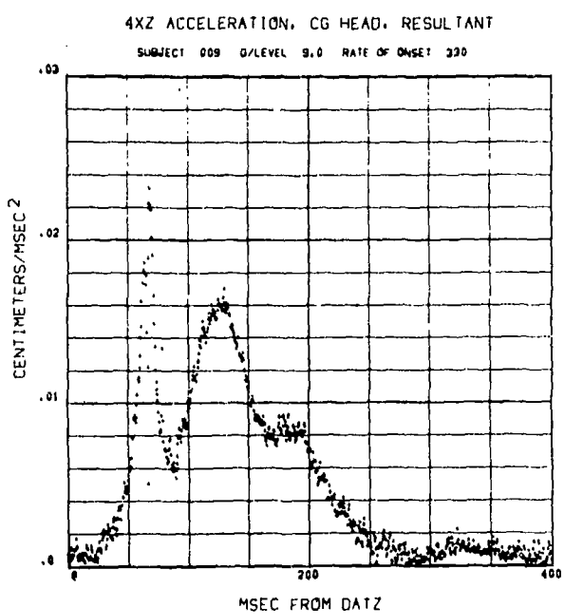

151

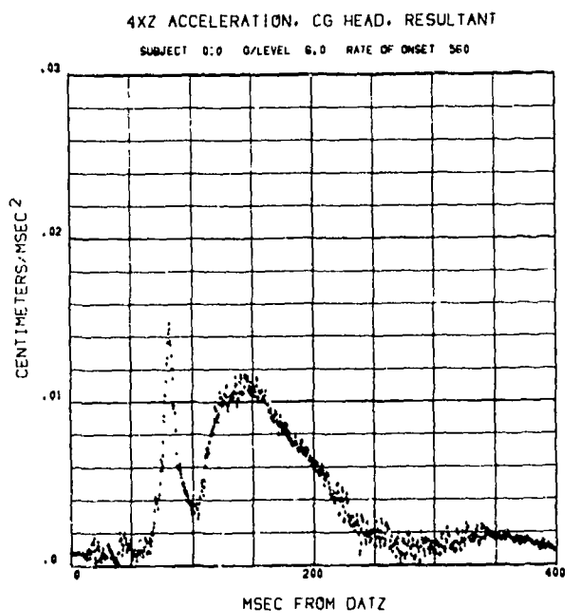

152

4XZ RESULTANT ACCELERATION OF HEAD C.G.

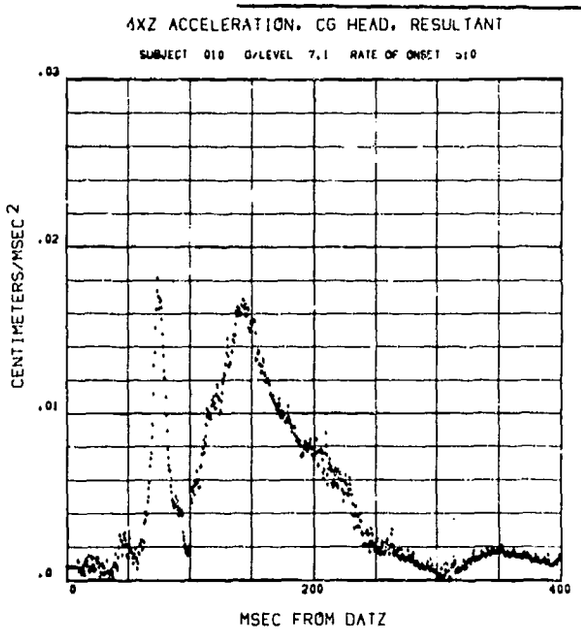

153

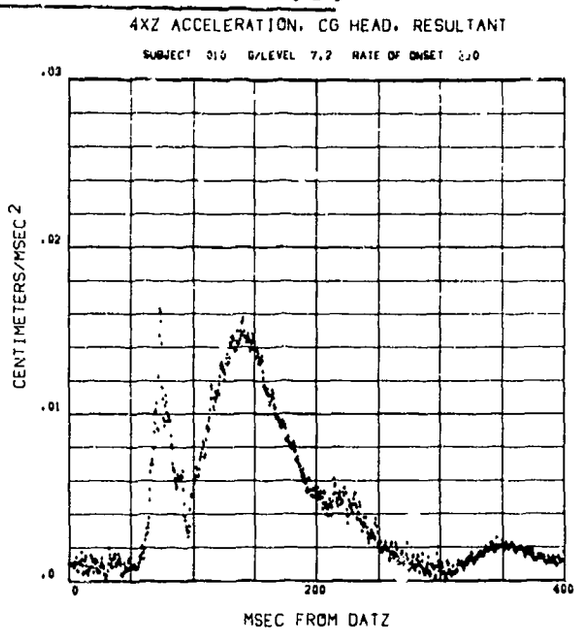

154

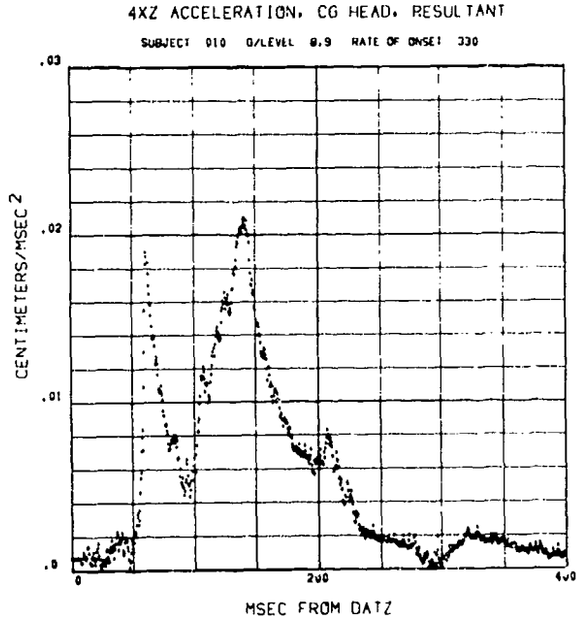

155

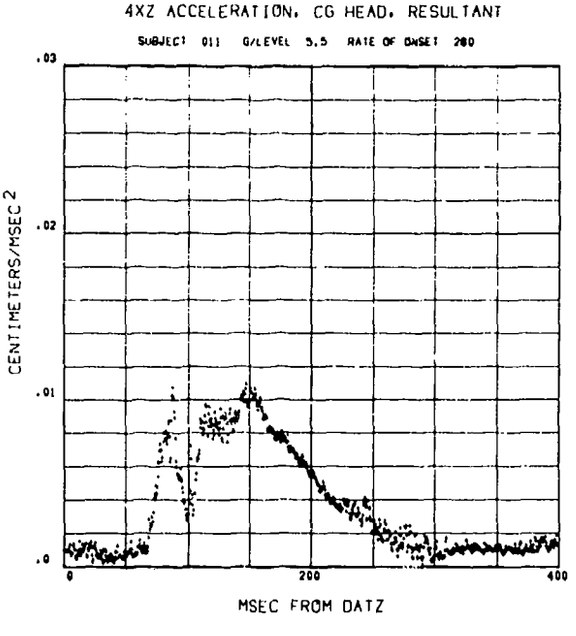

156

4XZ RESULTANT ACCELERATION OF HEAD C.G.

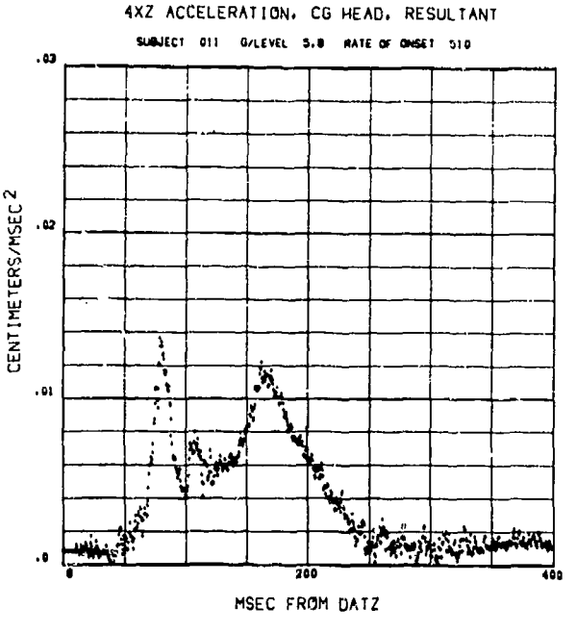

157

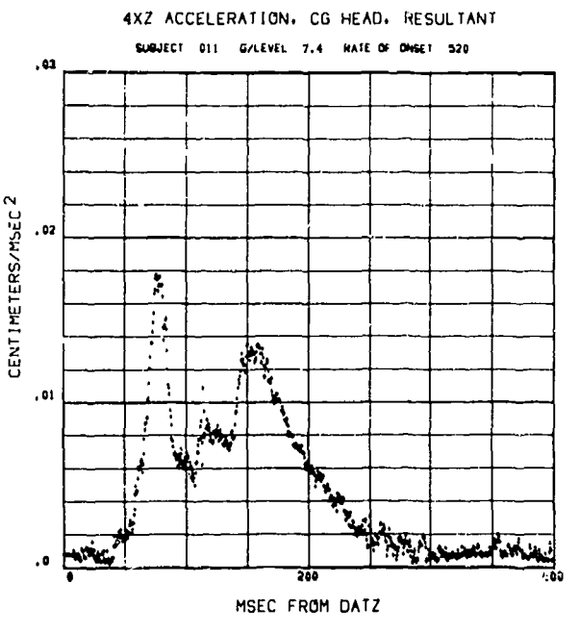

158

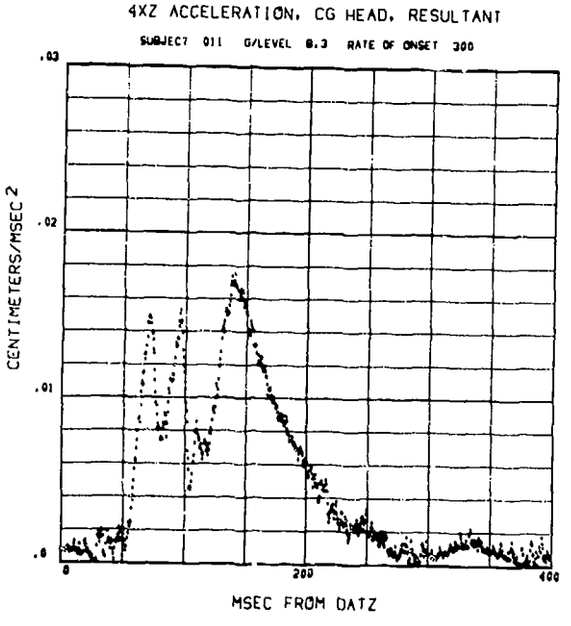

159

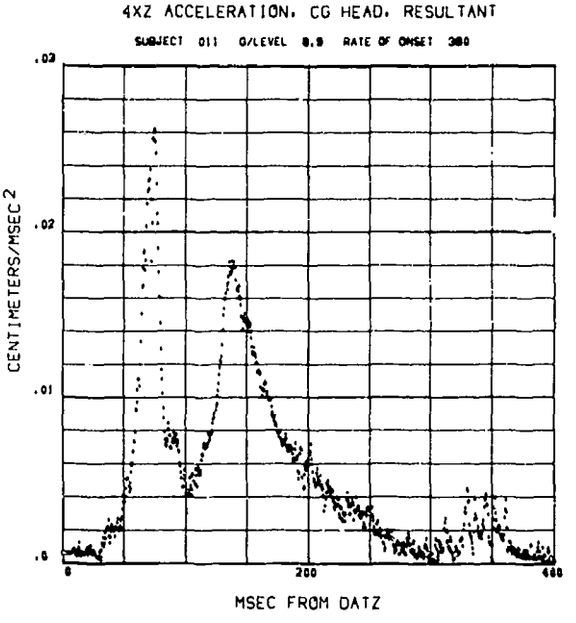

160

4XZ RESULTANT ACCELERATION OF HEAD C.G.

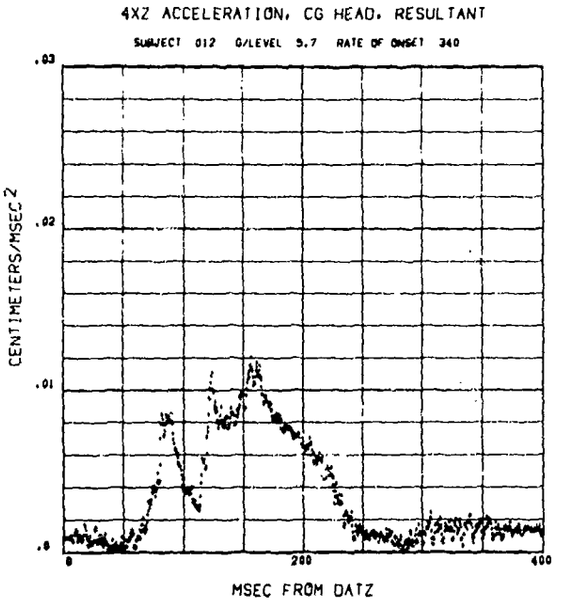

161

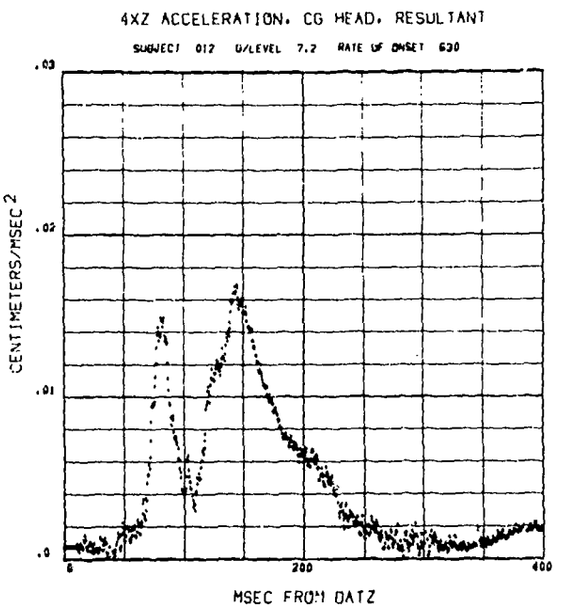

162

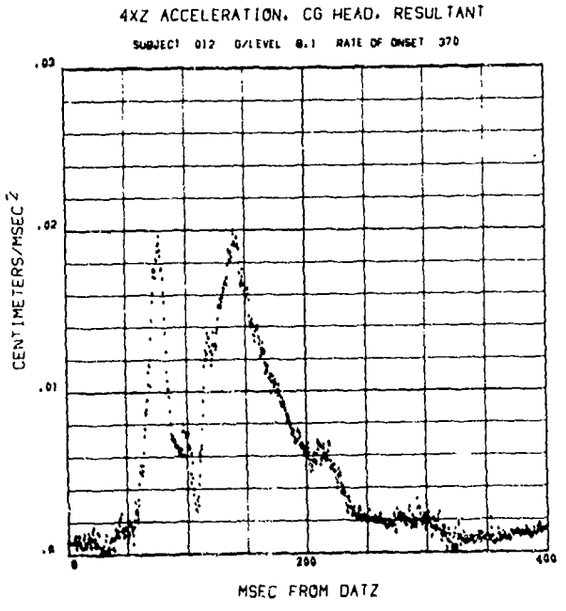

163

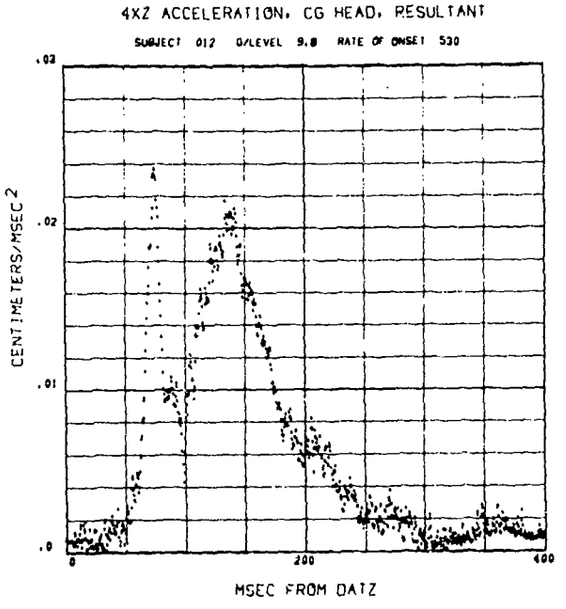

164

4XZ RESULTANT ACCELERATION OF HEAD C.G.

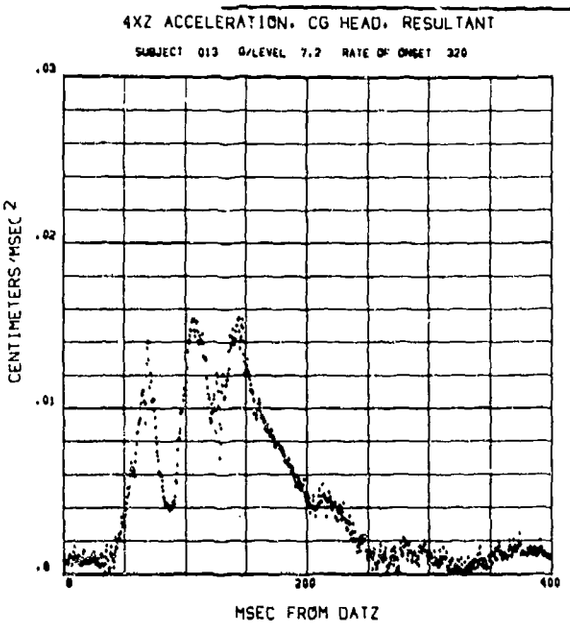

165

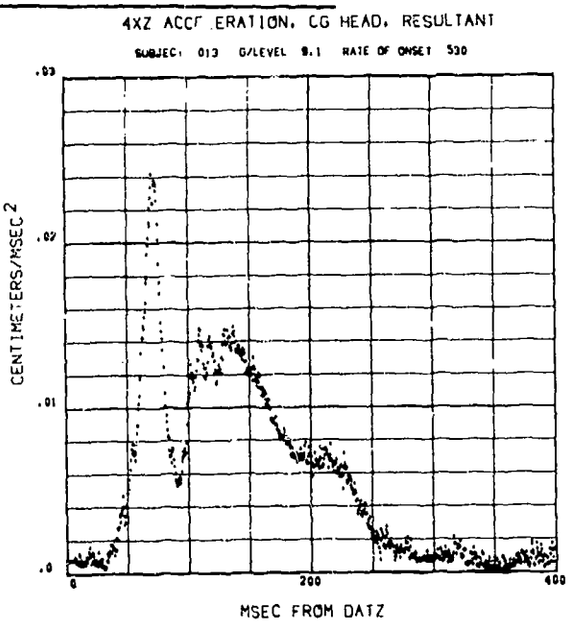

166

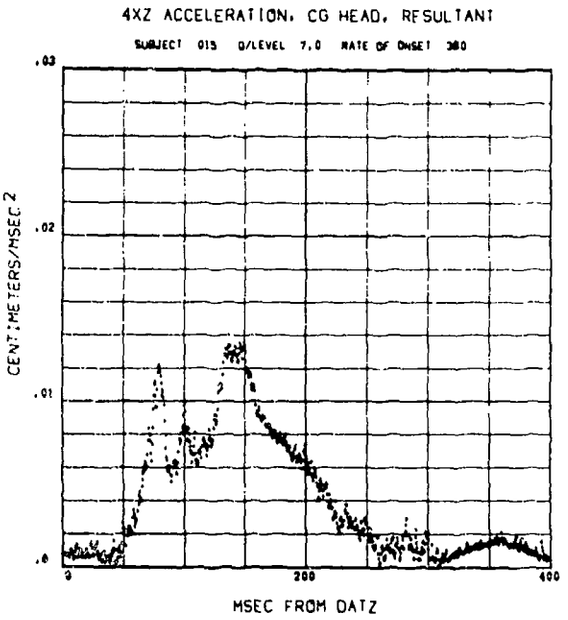

167

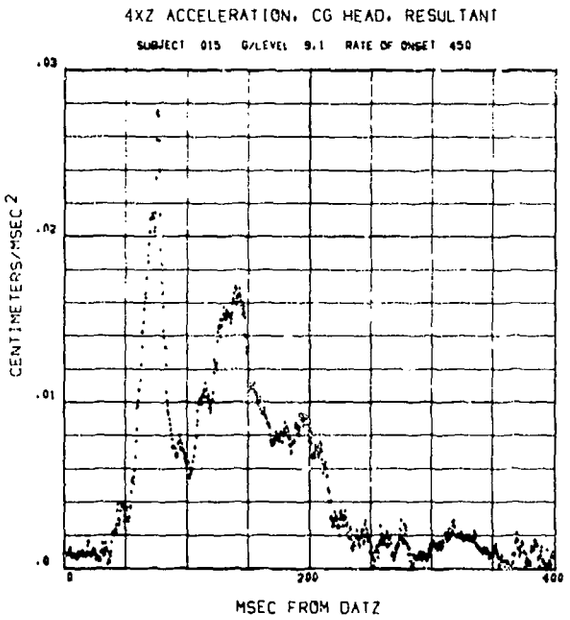

168

4XZ RESULTANT ACCELERATION OF HEAD C.G.

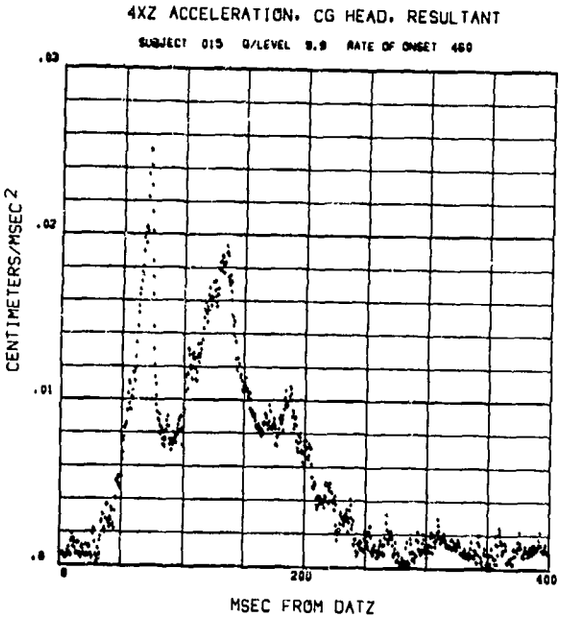

169

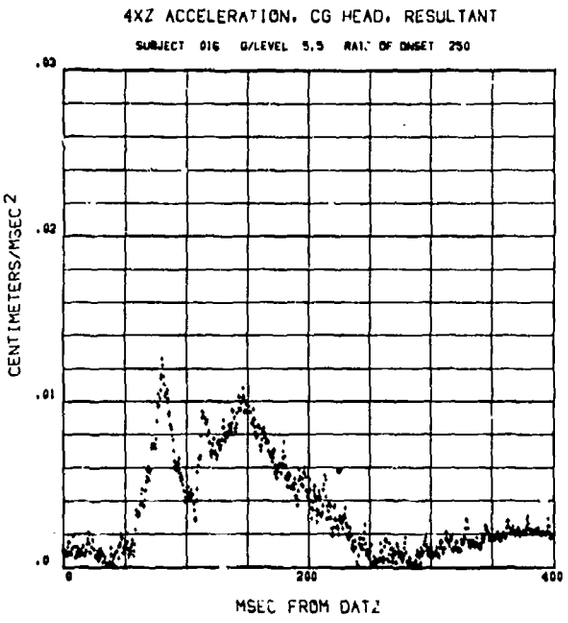

170

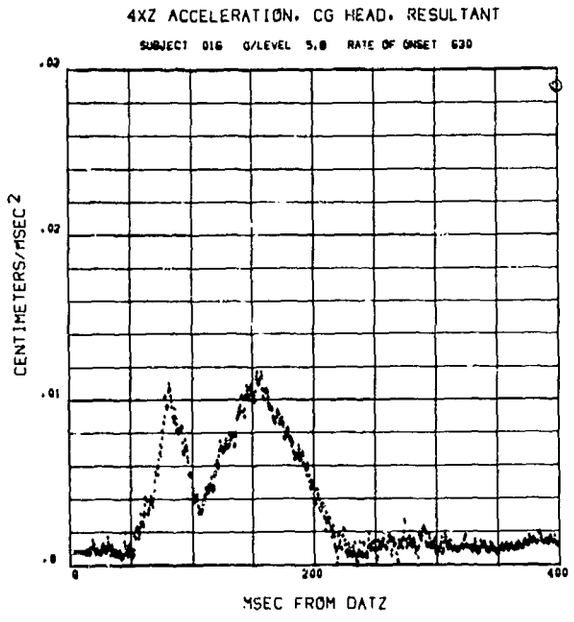

171

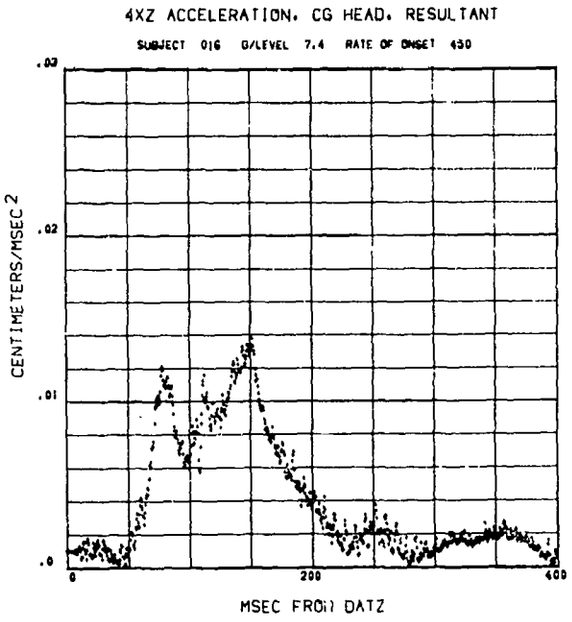

172

4XZ RESULTANT ACCELERATION OF HEAD C.G.

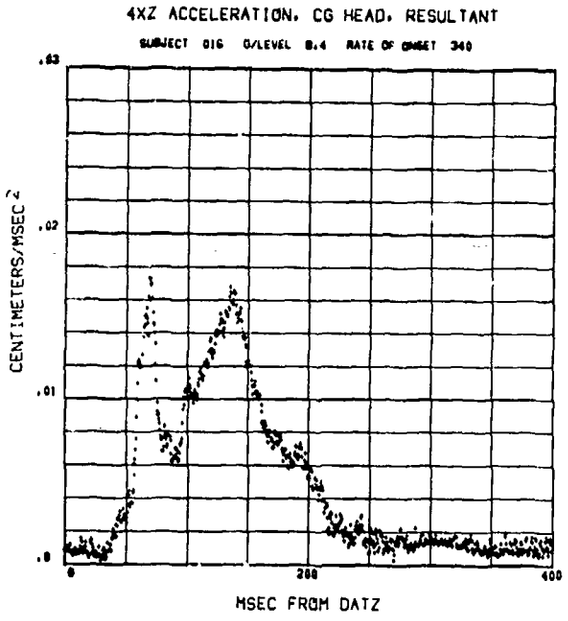

173

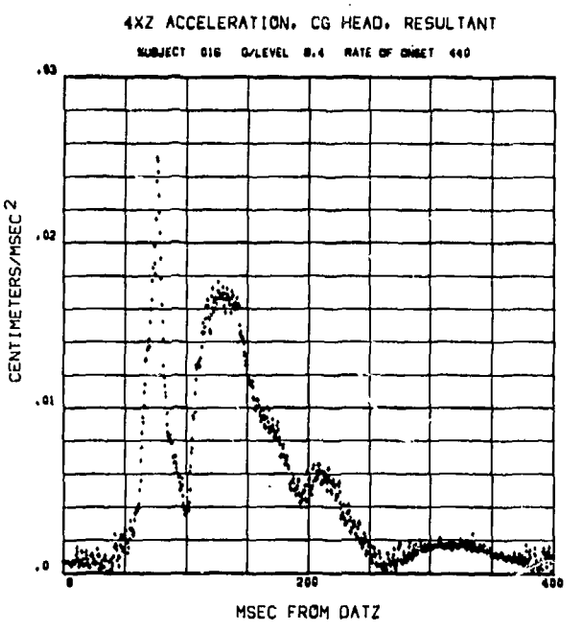

174

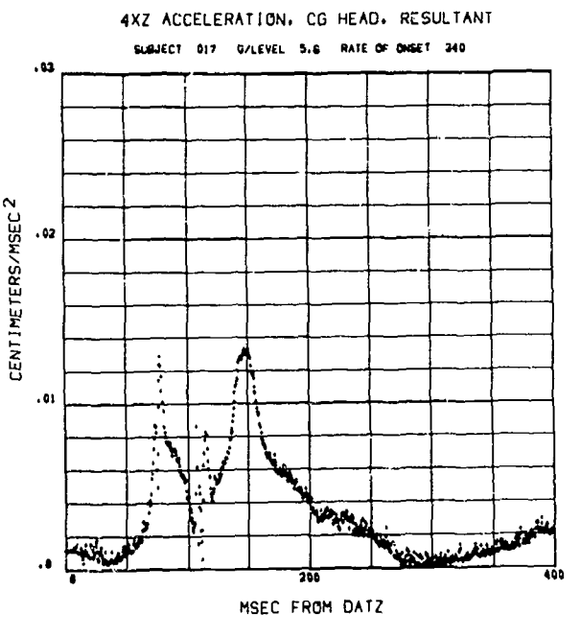

175

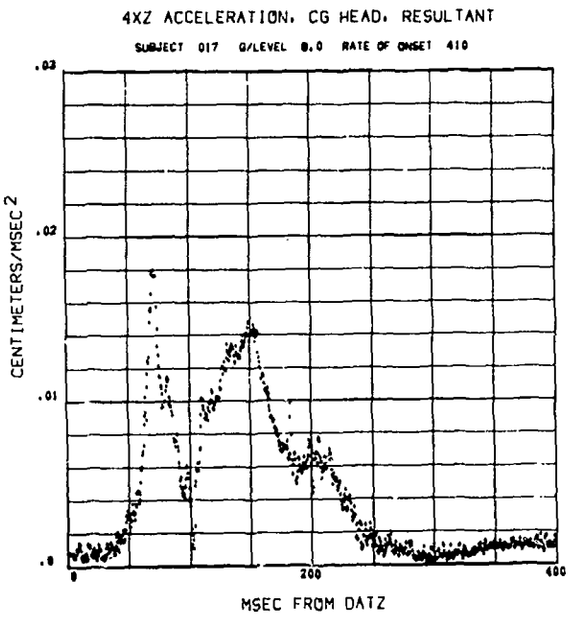

176

4XZ RESULTANT ACCELERATION OF HEAD C.G.

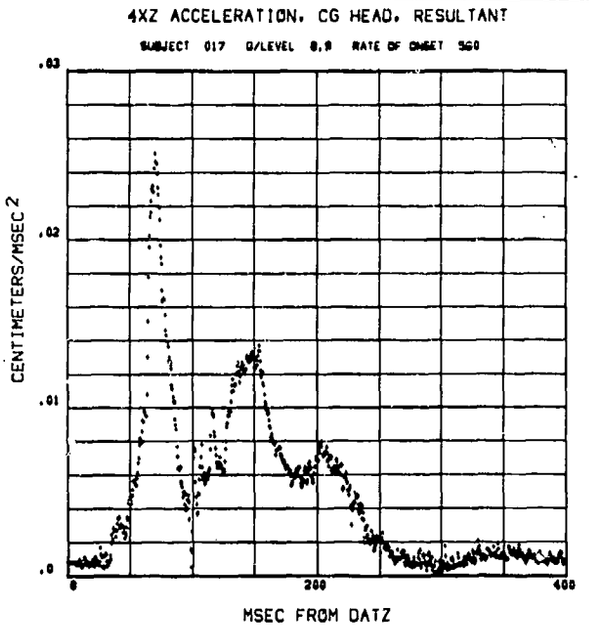

177

XCV VELOCITY OF HEAD C.G. RELATIVE TO SLED ORIGIN

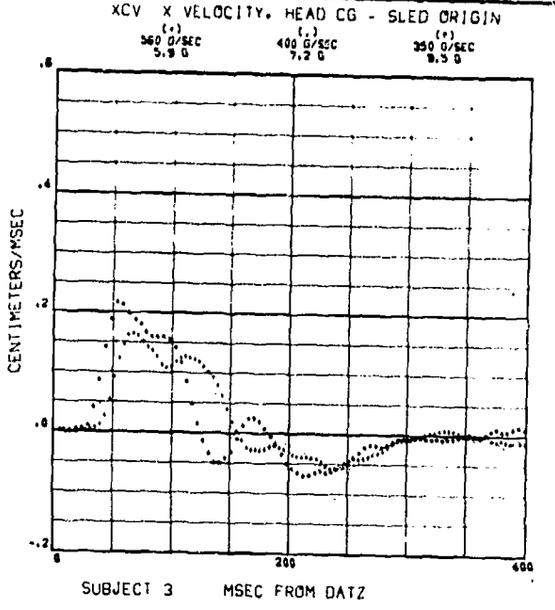

178

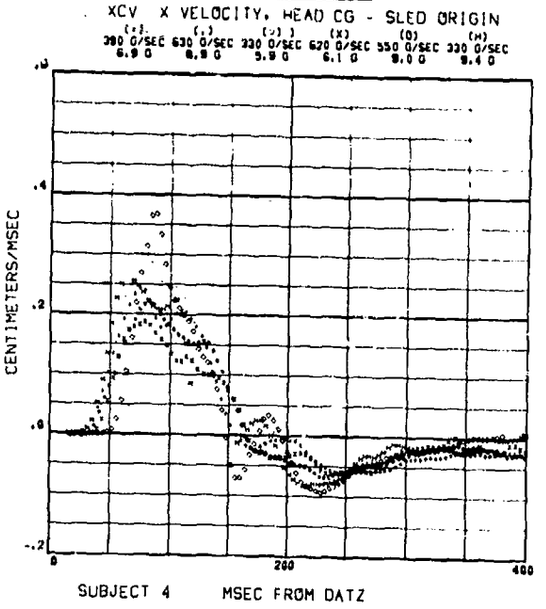

179

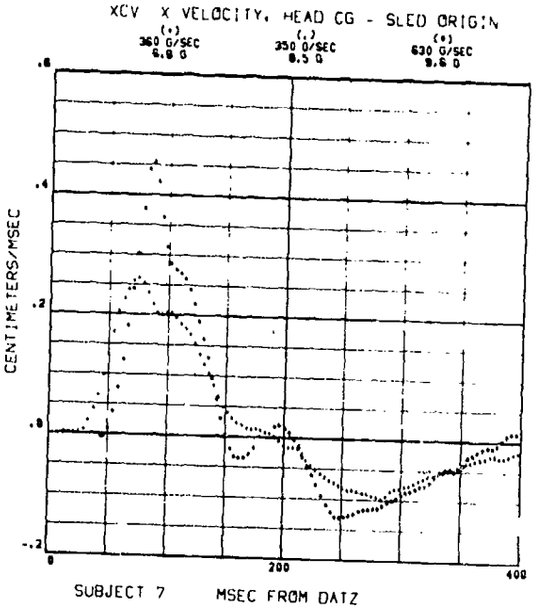

180

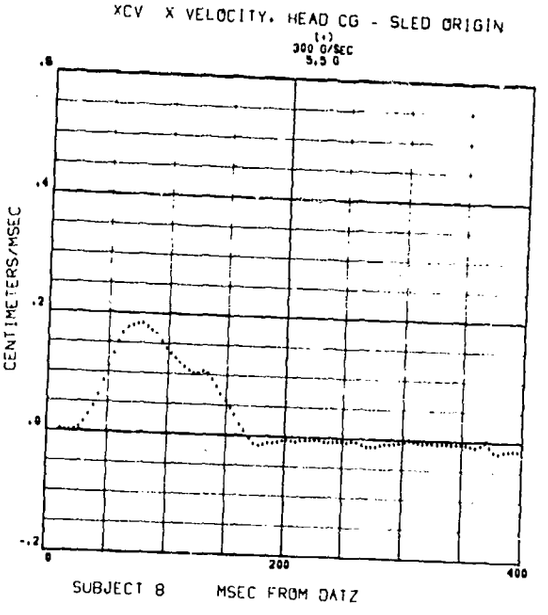

181

XCV VELOCITY OF HEAD C.G. RELATIVE TO SLED ORIGIN

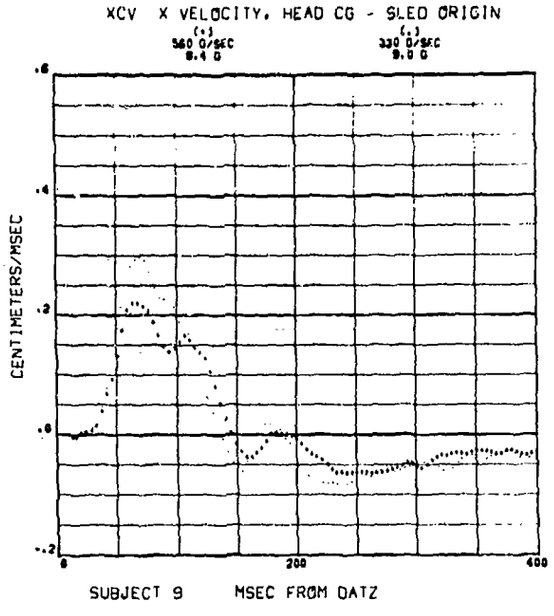

182

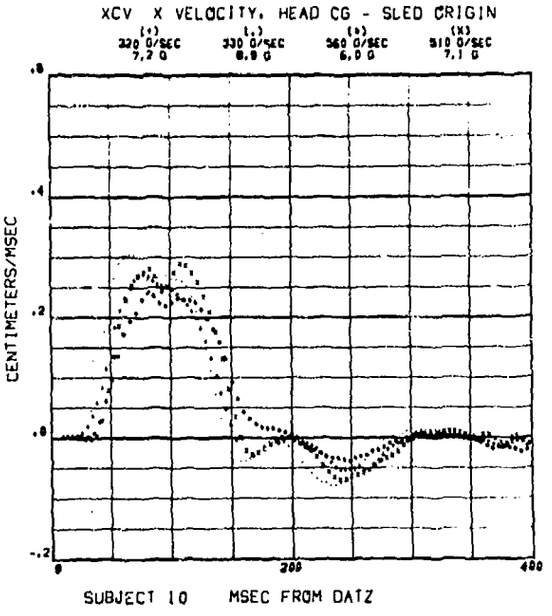

183

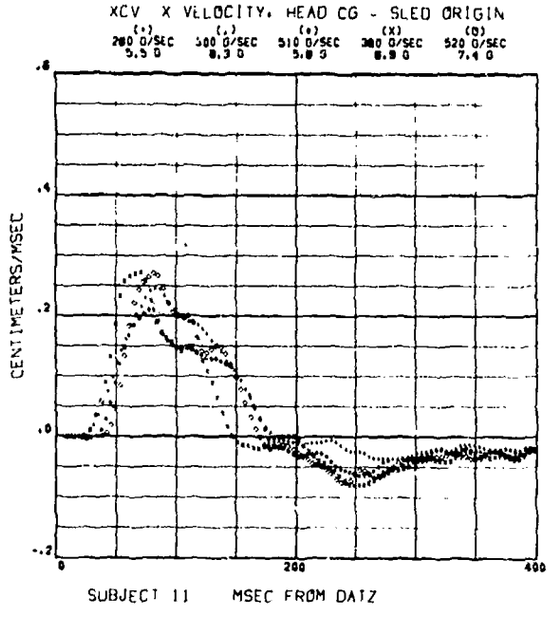

184

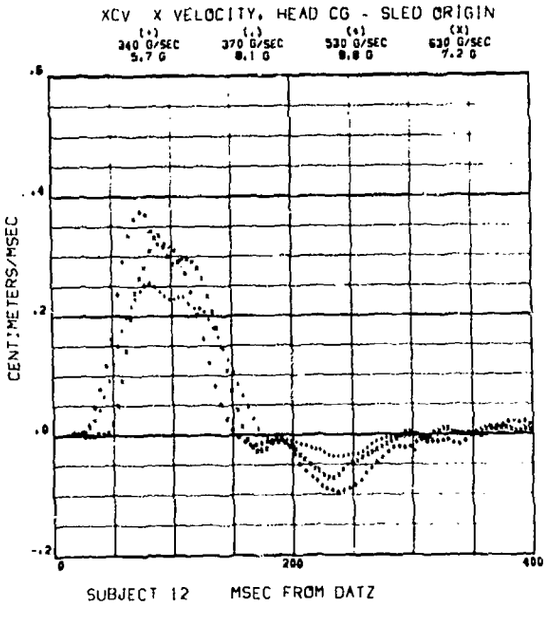

185

XCV VELOCITY OF HEAD C.G. RELATIVE TO SLED ORIGIN

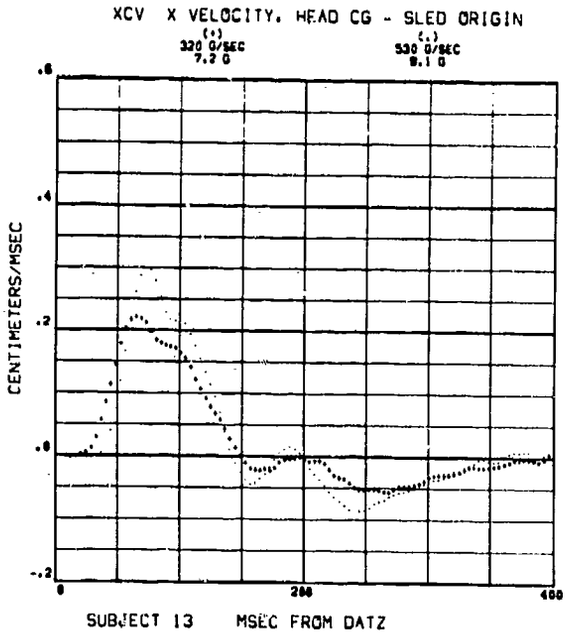

186

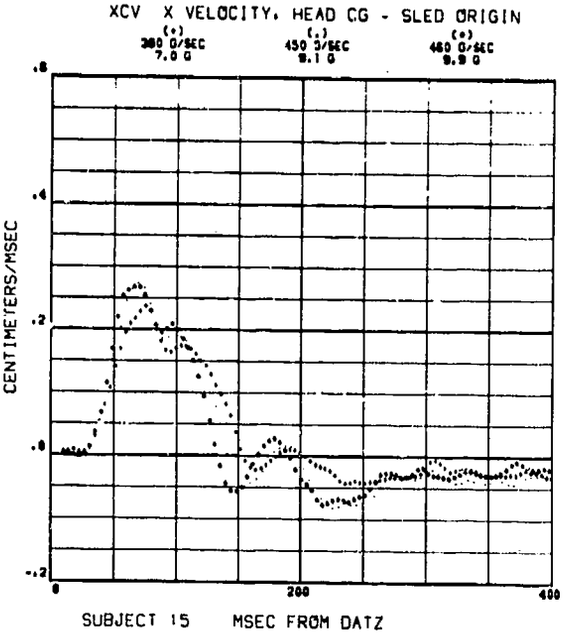

187

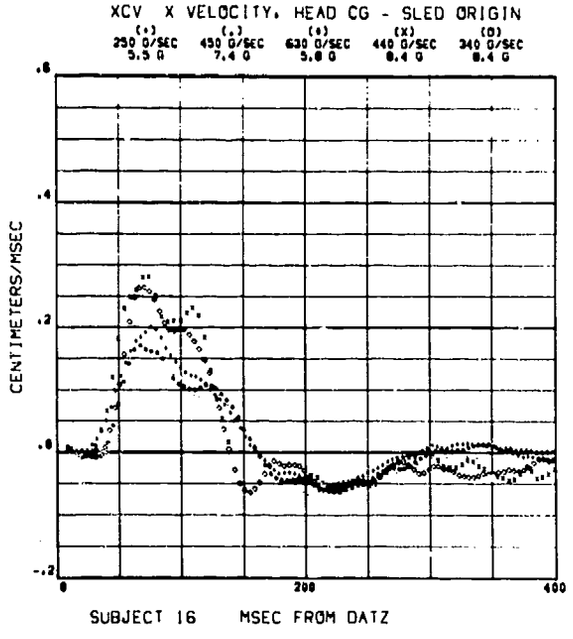

188

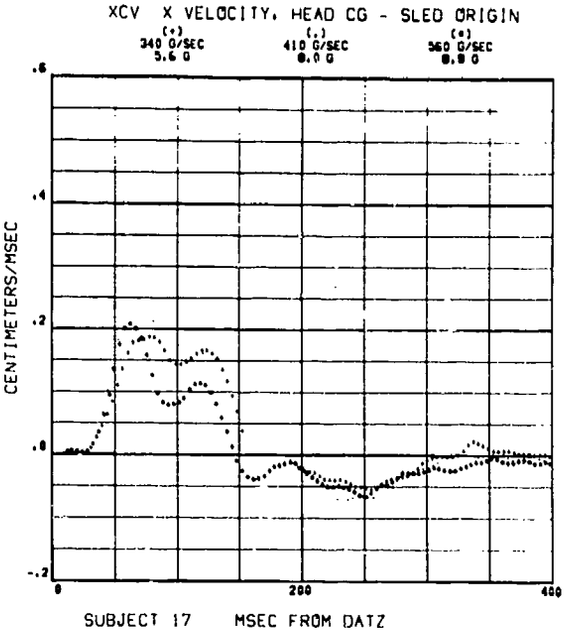

189

XCV VELOCITY OF HEAD C.G. RELATIVE TO SLED ORIGIN

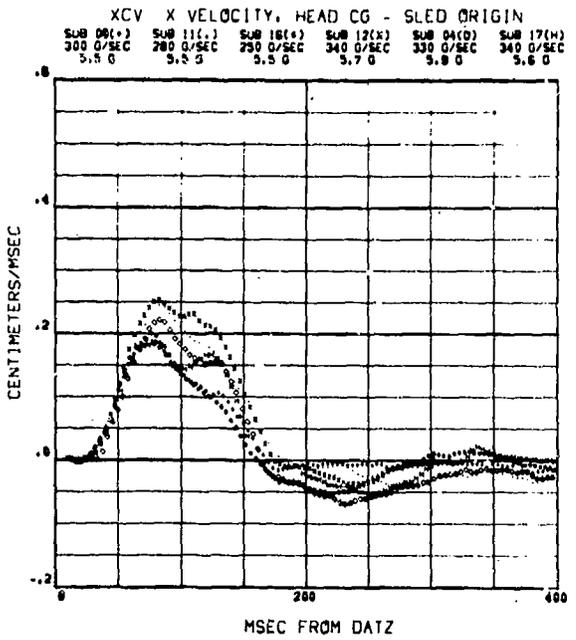

190

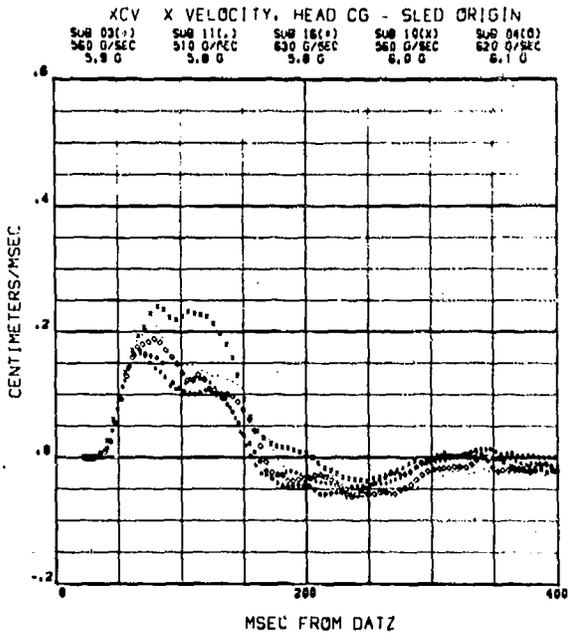

191

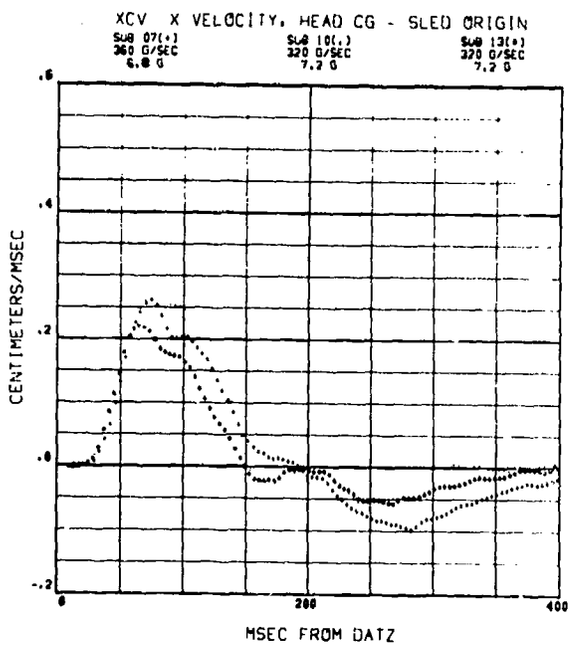

192

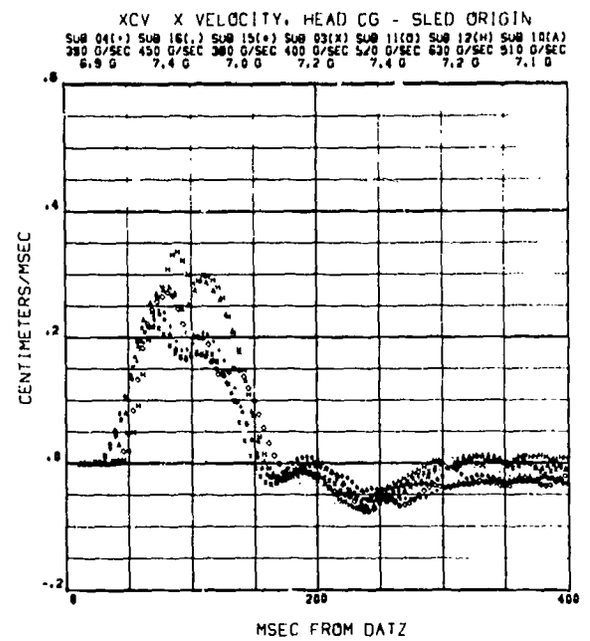

193

XCV VELOCITY OF HEAD C.G. RELATIVE TO SLED ORIGIN

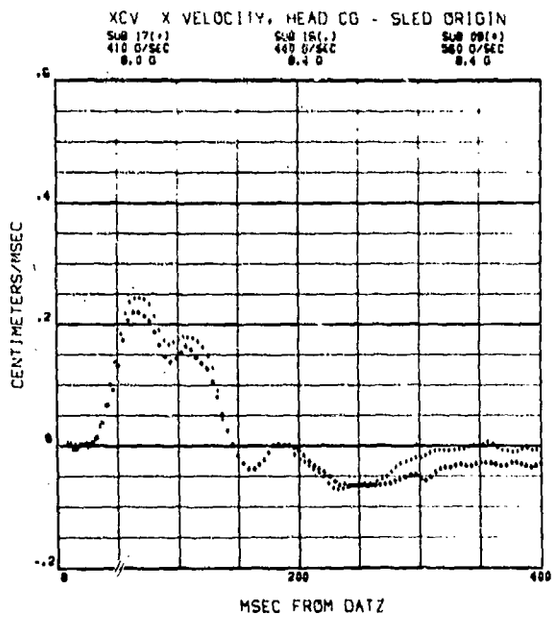

194

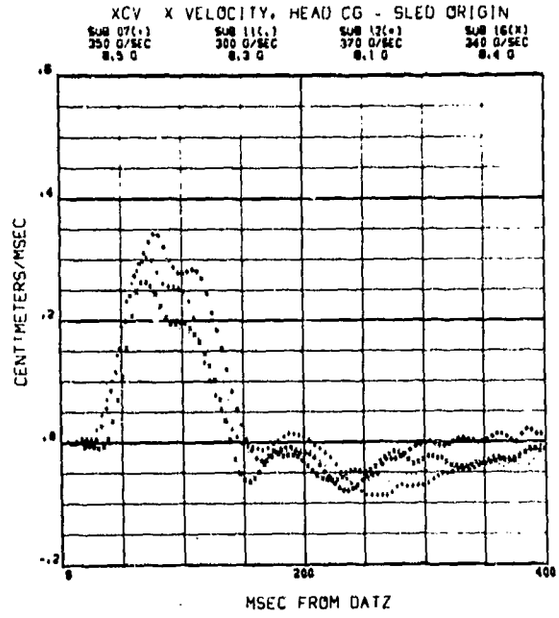

195

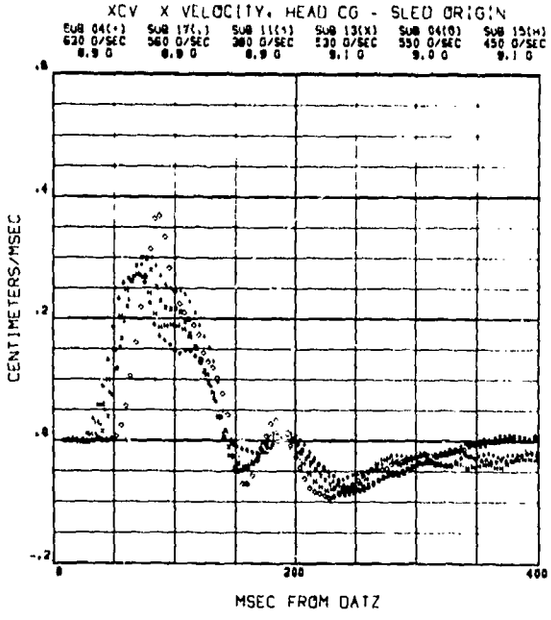

196

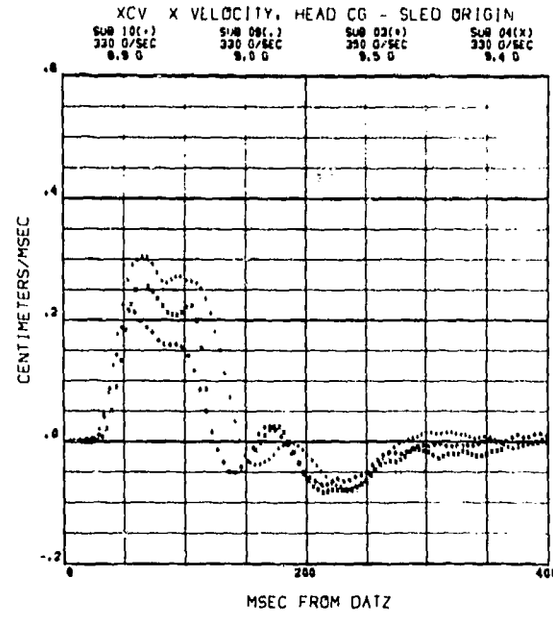

197

XCV VELOCITY OF HEAD C.G. RELATIVE TO SLED ORIGIN

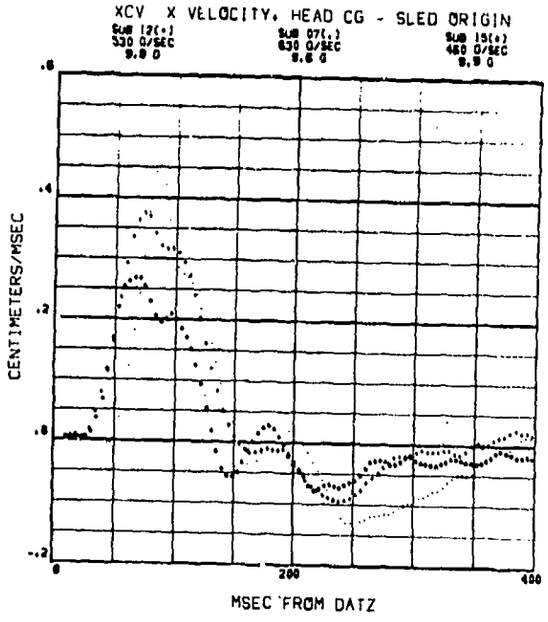

198

ZCV VELOCITY OF THE HEAD C.G. RELATIVE TO THE SLED ORIGIN IN THE Z DIRECTION

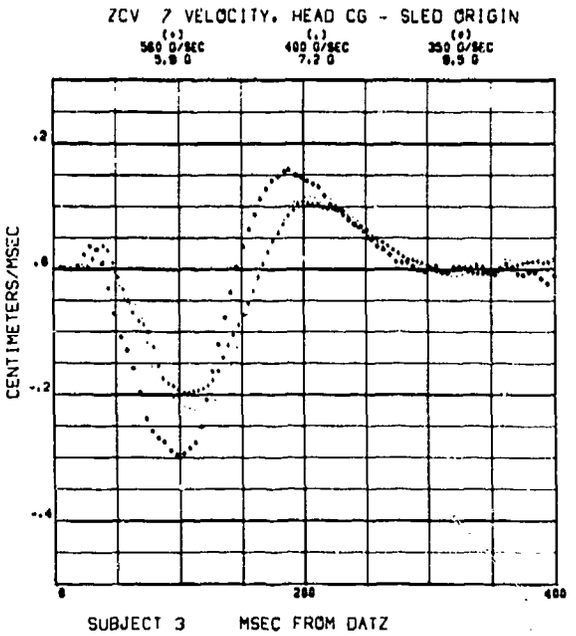

199

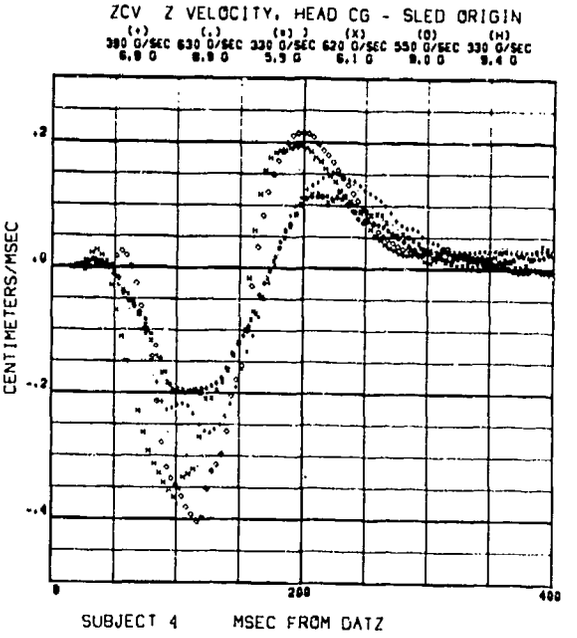

200

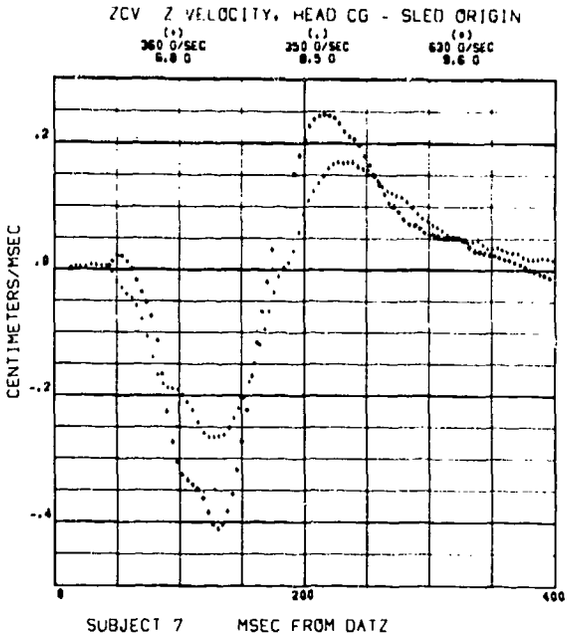

201

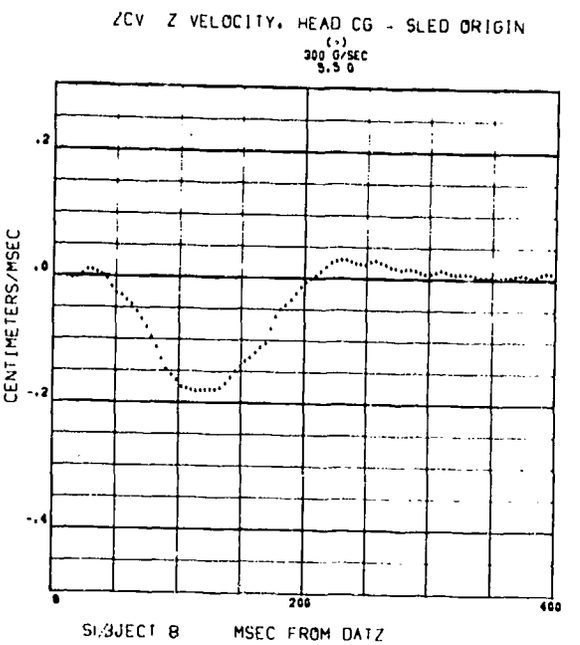

202

ZCV VELOCITY OF THE HEAD C.G. RELATIVE TO THE SLED ORIGIN IN THE Z DIRECTION

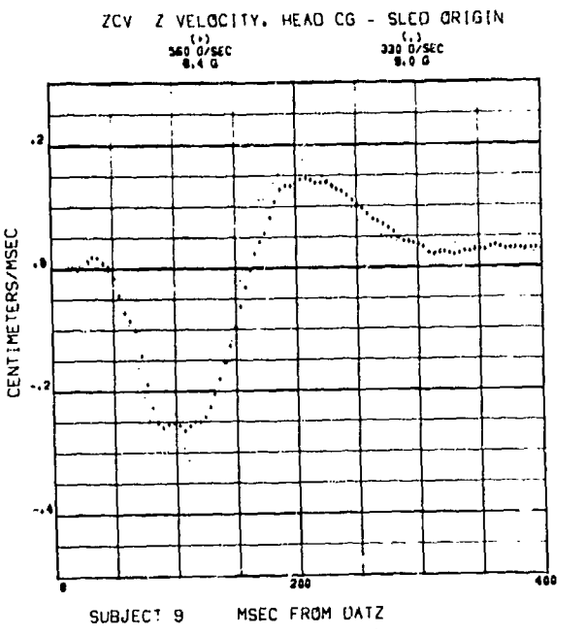

203

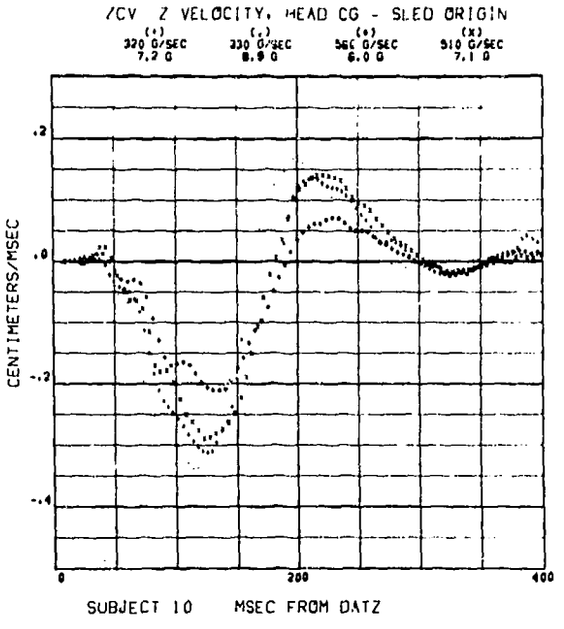

204

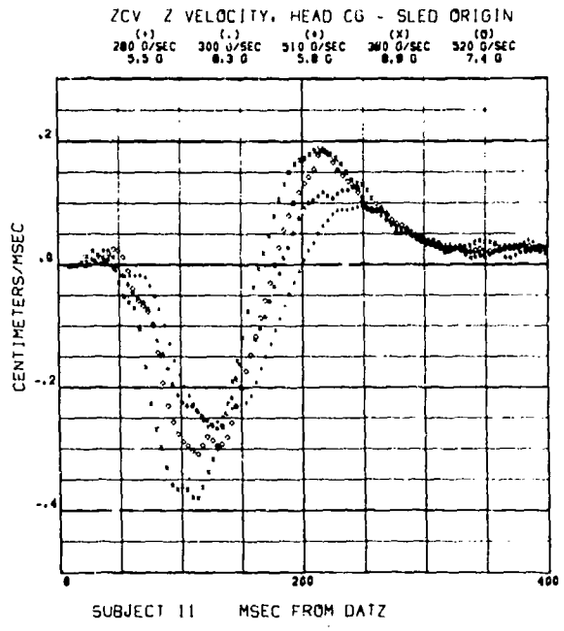

205

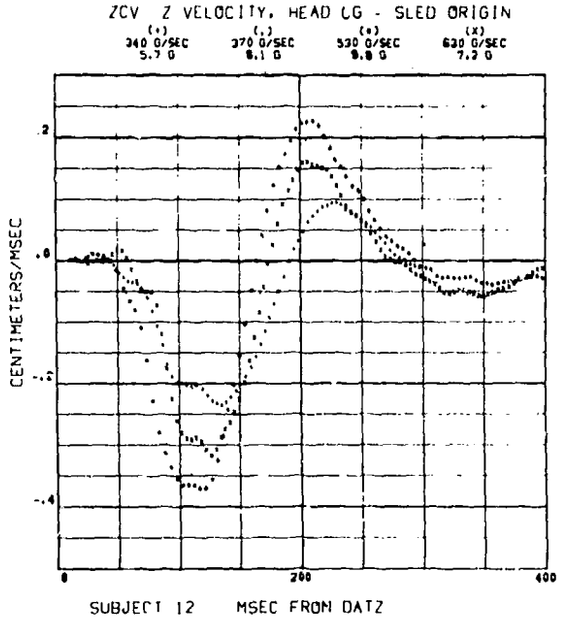

206

ZCV VELOCITY OF THE HEAD C.G. RELATIVE TO THE SLED ORIGIN IN THE Z DIRECTION

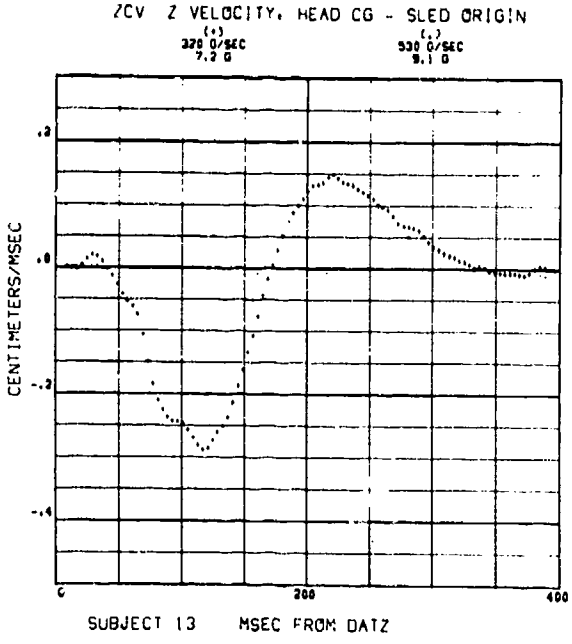

207

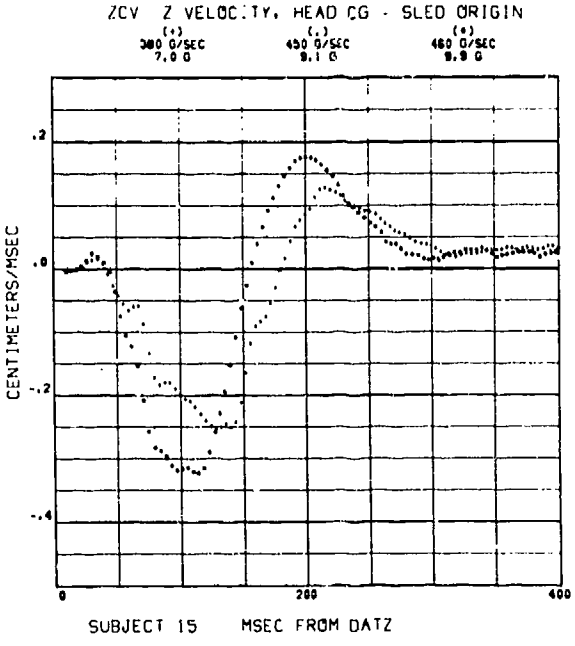

208

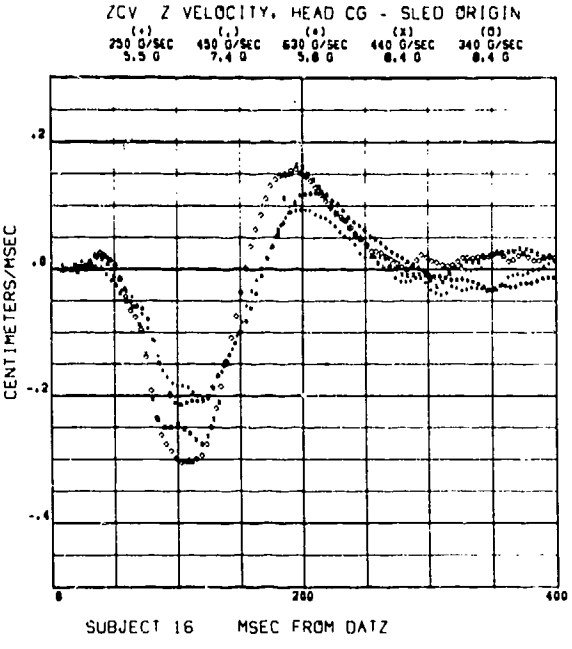

209

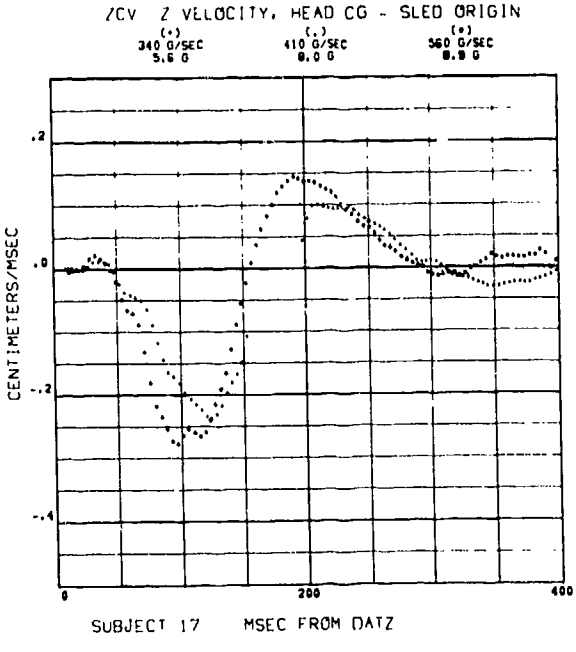

210

ZCV VELOCITY OF THE HEAD C.G. RELATIVE TO THE SLED ORIGIN IN THE Z DIRECTION

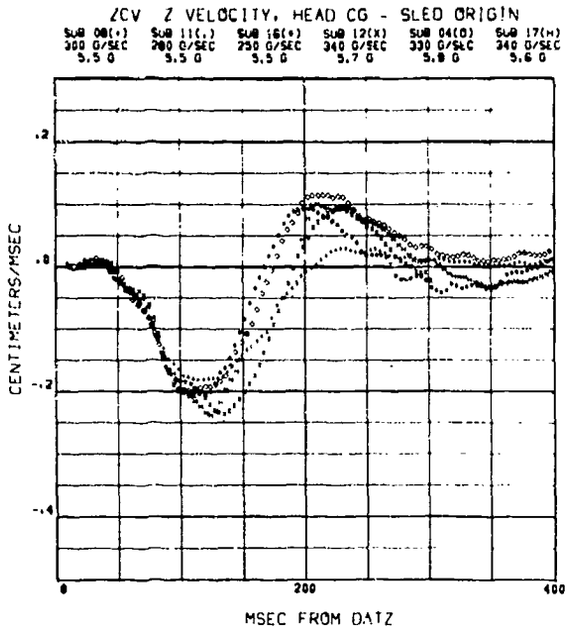

211

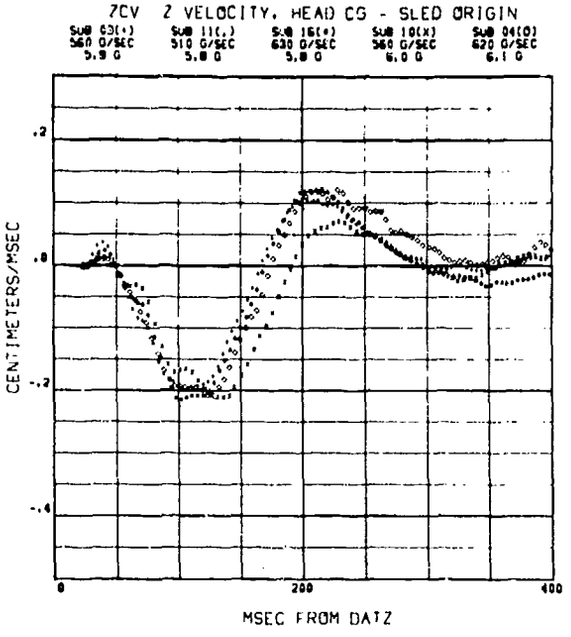

212

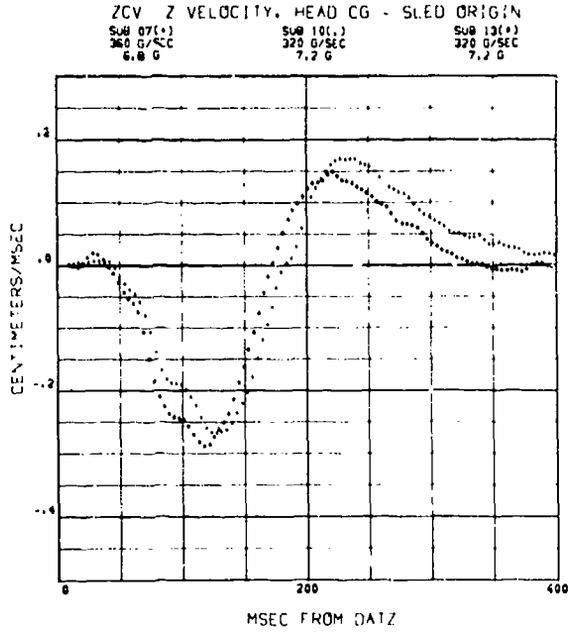

213

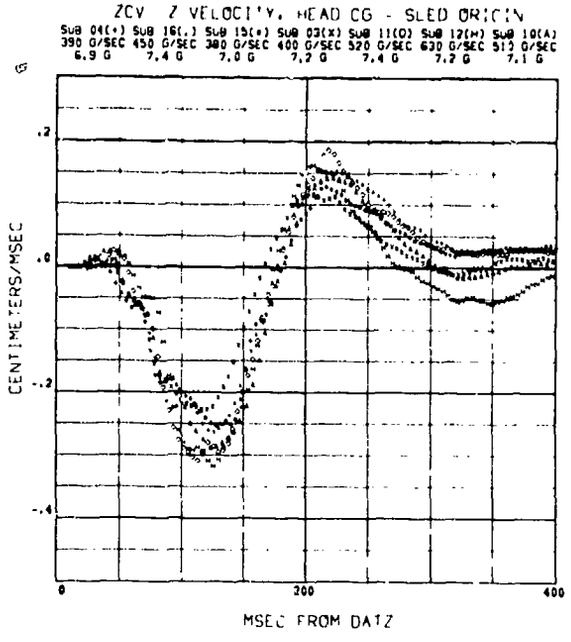

214

ZCV VELOCITY OF THE HEAD C.G. RELATIVE TO THE SLED ORIGIN IN THE Z DIRECTION

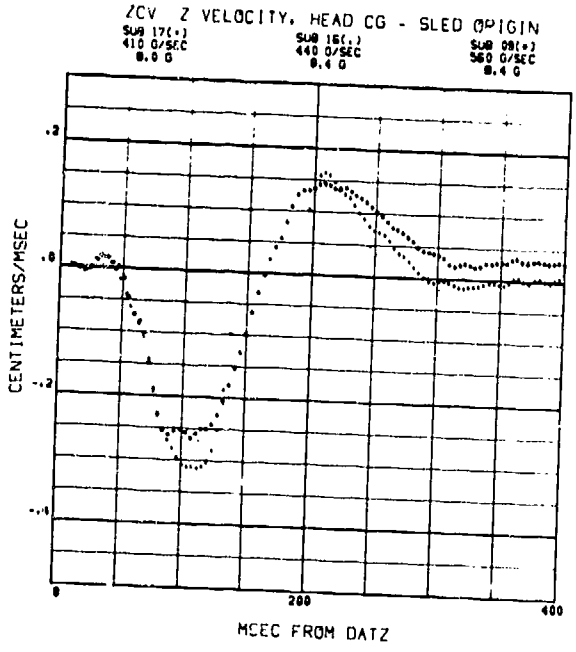

215

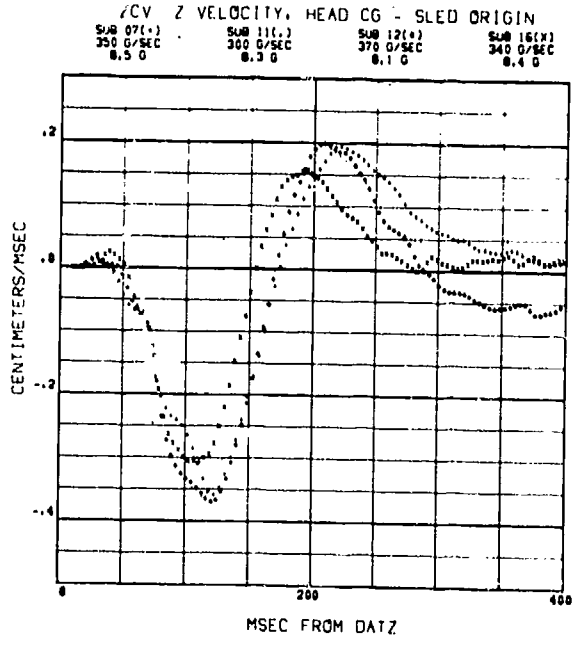

216

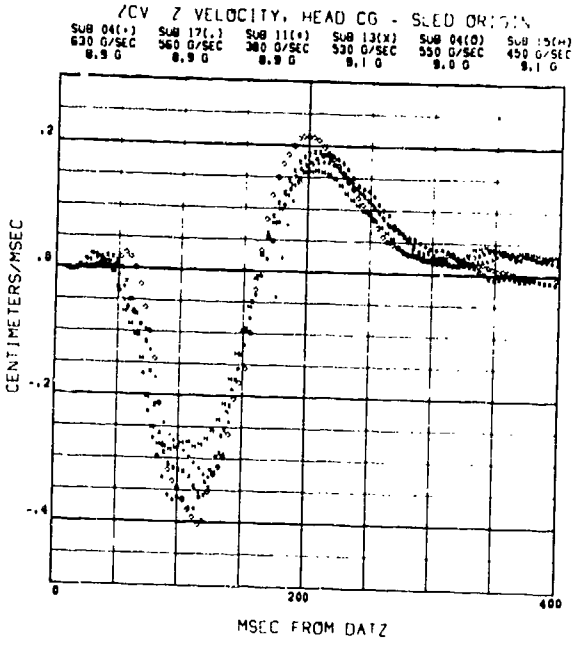

217

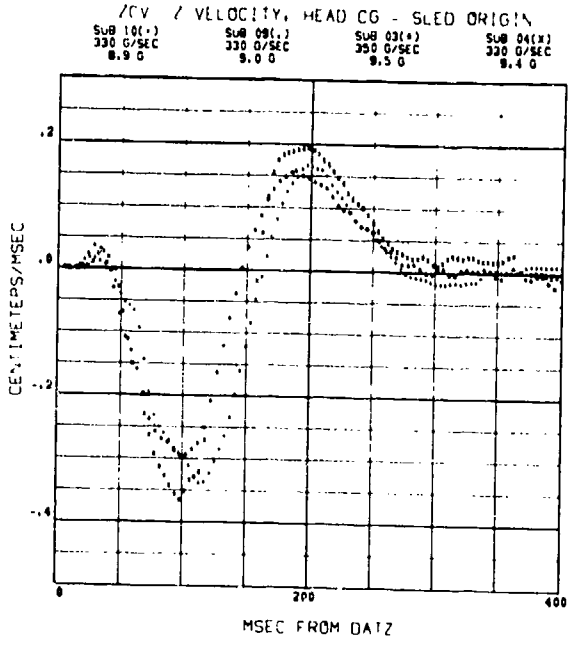

218

ZCV VELOCITY OF THE HEAD C.G. RELATIVE TO THE SLED ORIGIN IN THE Z DIRECTION

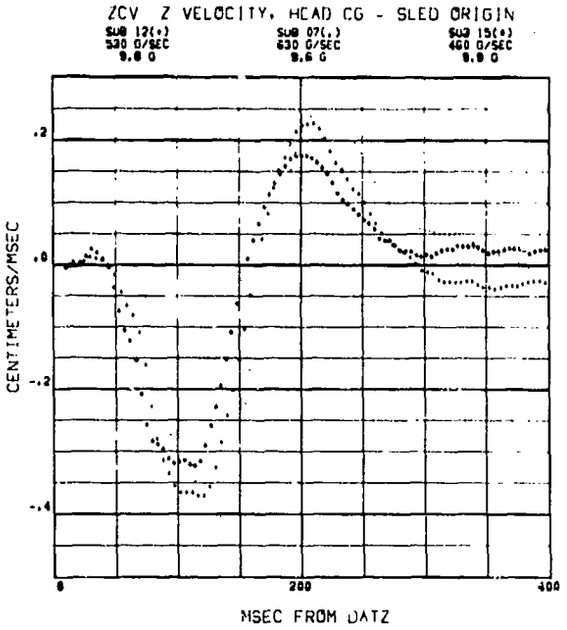

XZV MAGNITUDE OF THE VELOCITY OF THE HEAD C.G. RELATIVE TO THE SLED ORIGIN

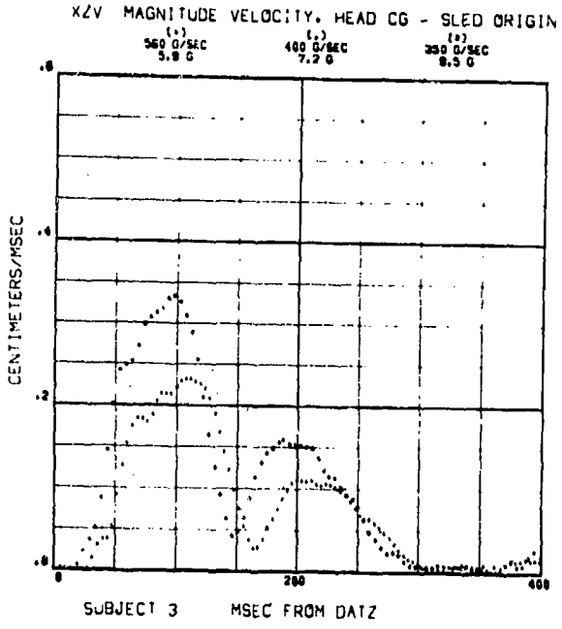

220

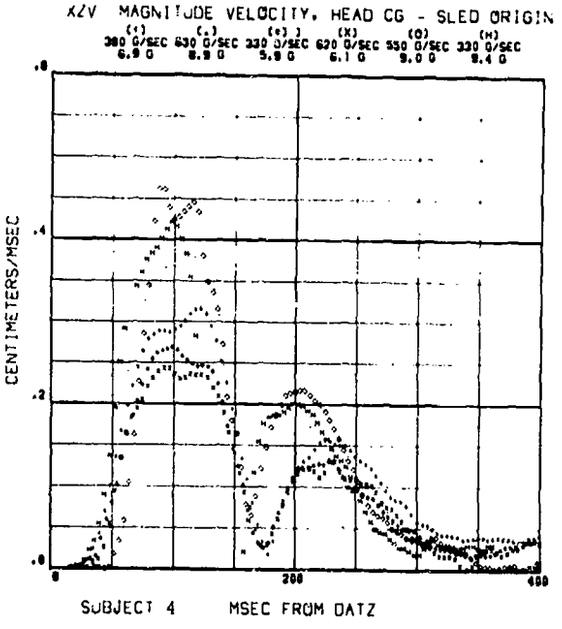

221

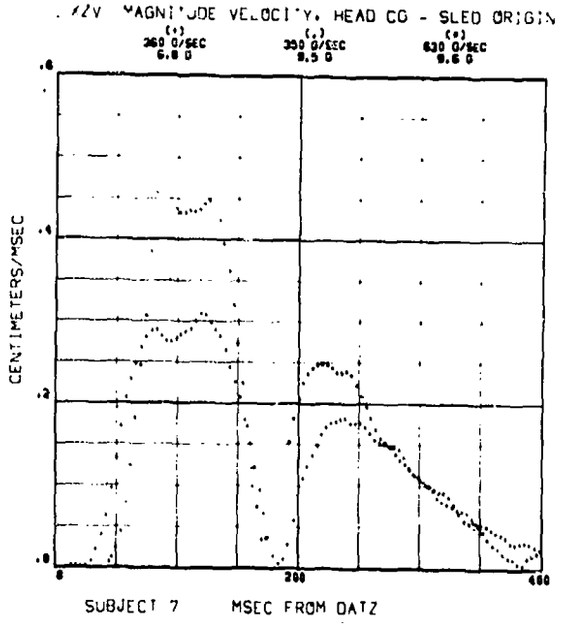

222

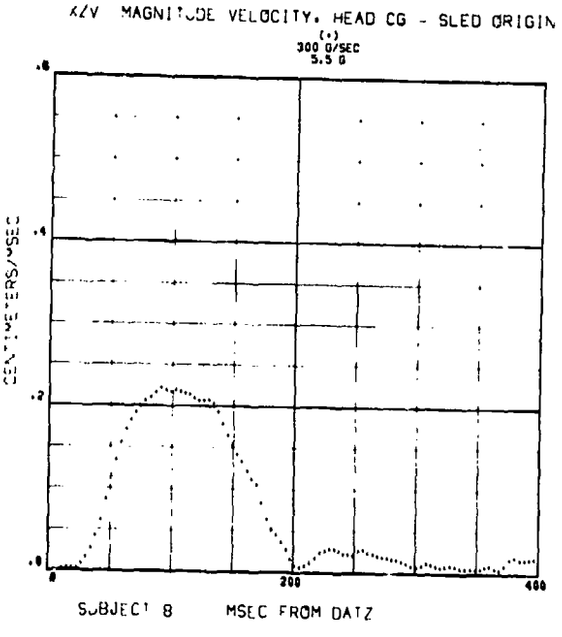

223

XZV MAGNITUDE OF THE VELOCITY OF THE HEAD C.G. RELATIVE TO THE SLED ORIGIN

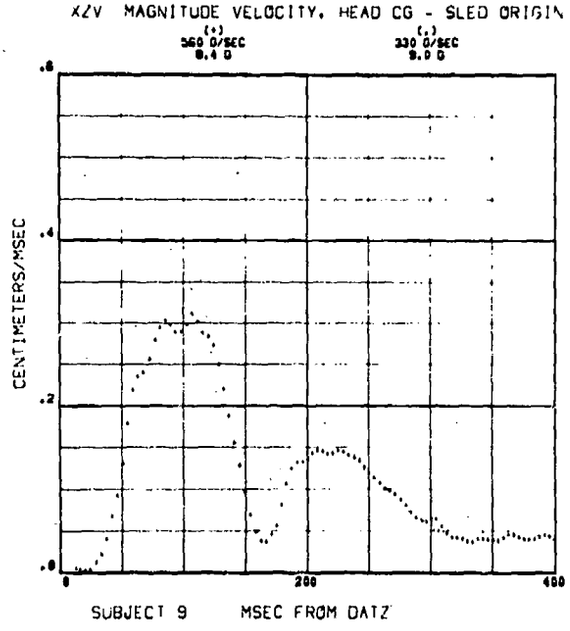

224

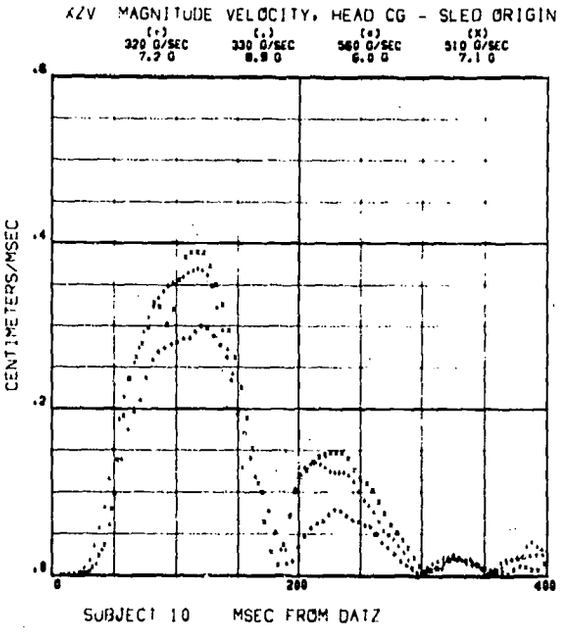

225

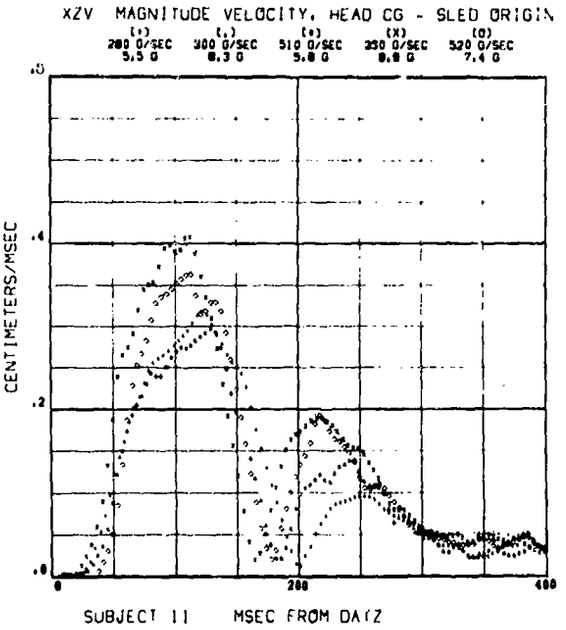

226

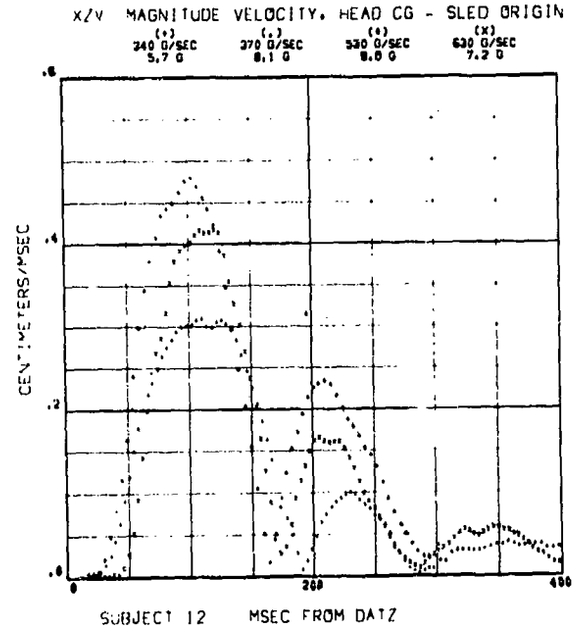

227

XZV MAGNITUDE OF THE VELOCITY OF THE HEAD C.G. RELATIVE TO THE SLED ORIGIN

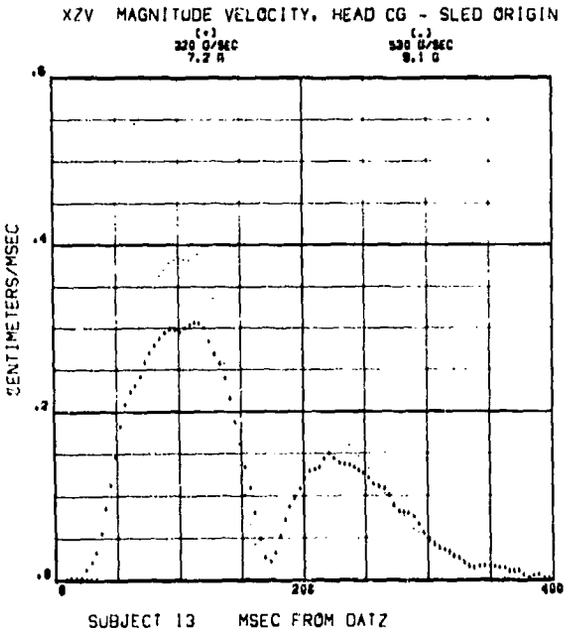

228

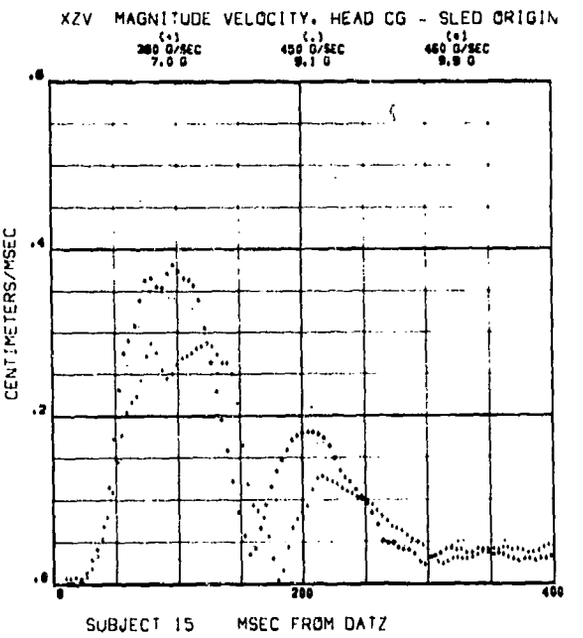

229

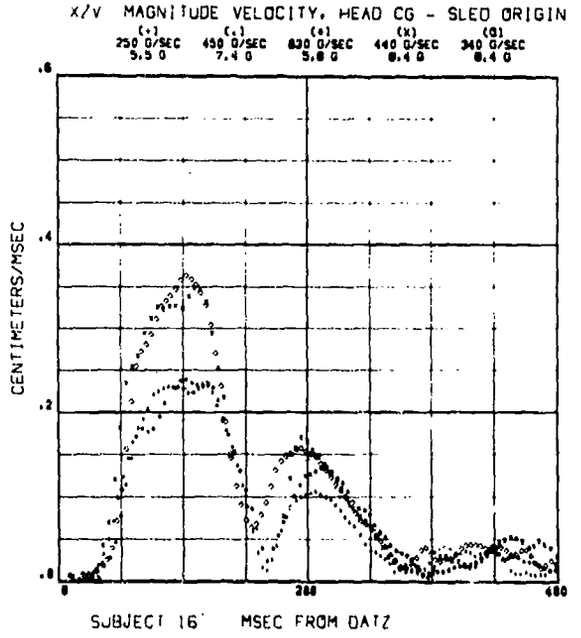

230

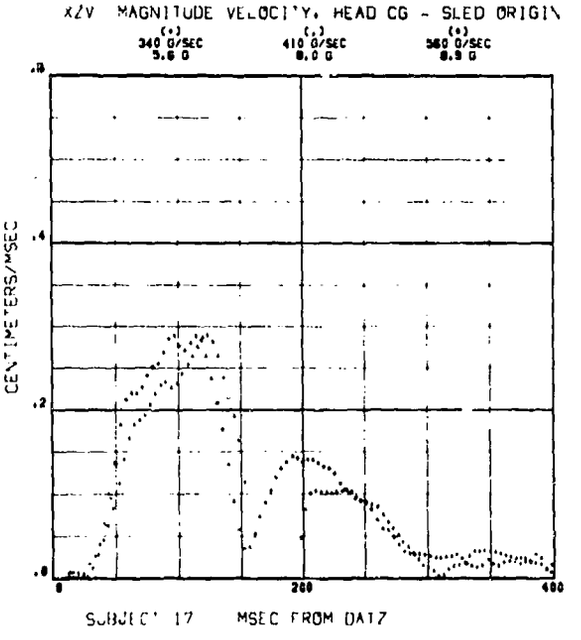

231

XZV MAGNITUDE OF THE VELOCITY OF THE HEAD C.G. RELATIVE TO THE SLED ORIGIN

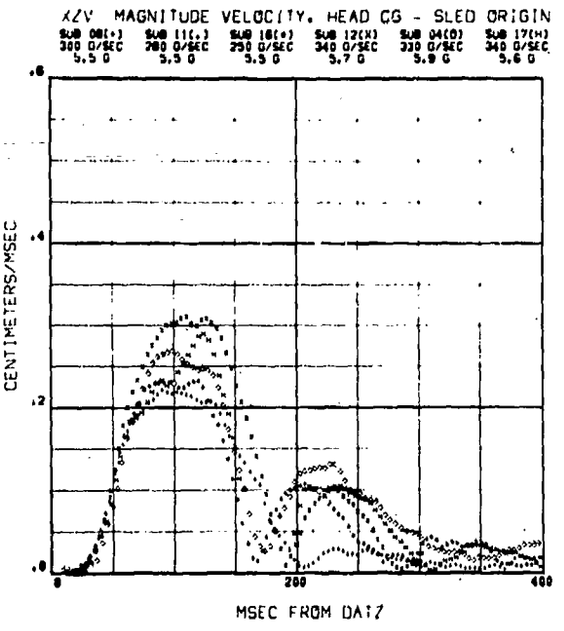

232

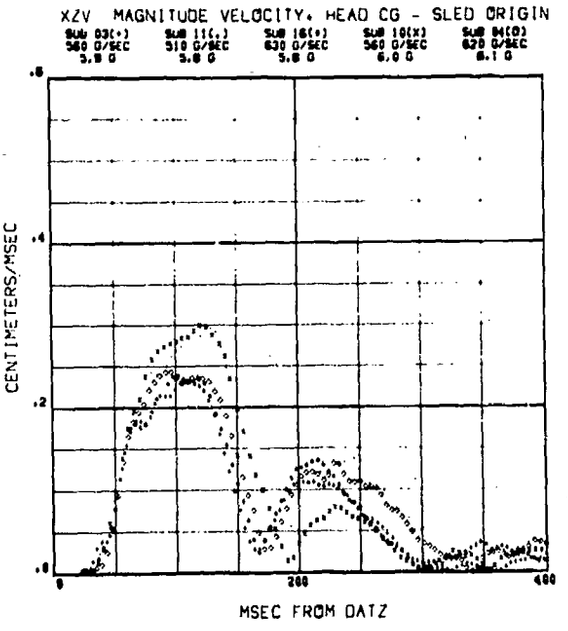

233

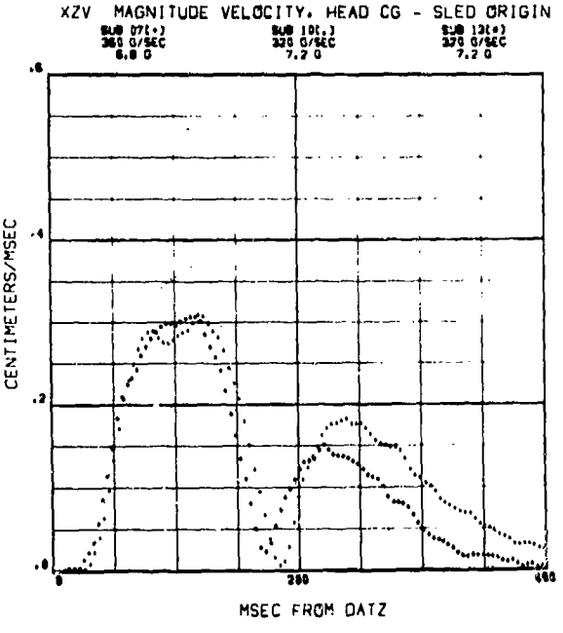

234

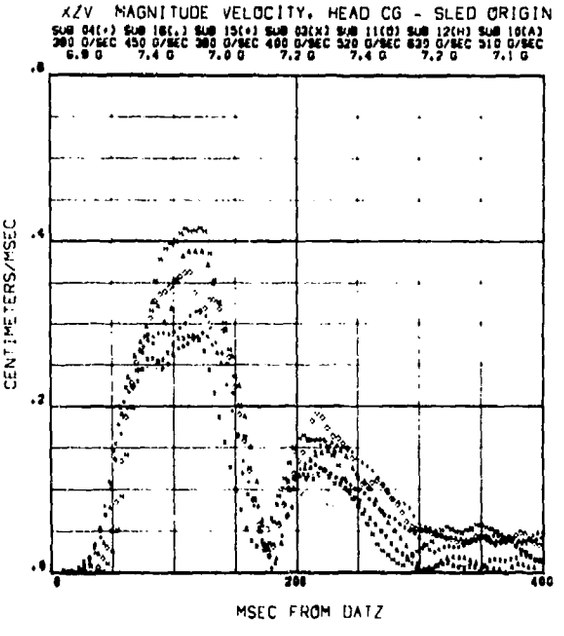

235

XZV MAGNITUDE OF THE VELOCITY OF THE HEAD C.G. RELATIVE TO THE SLED ORIGIN

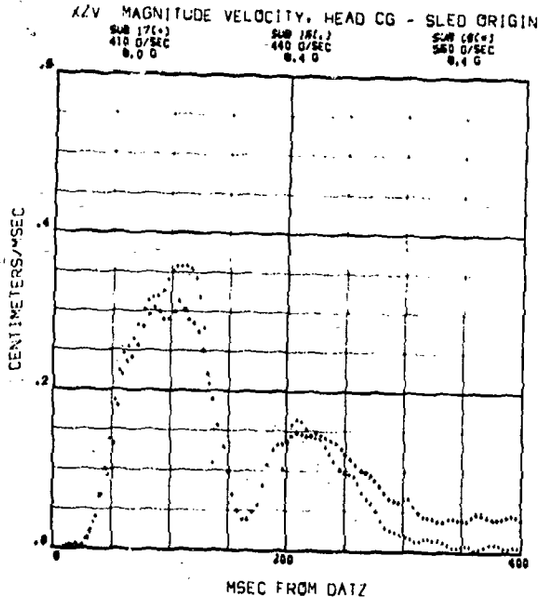

236

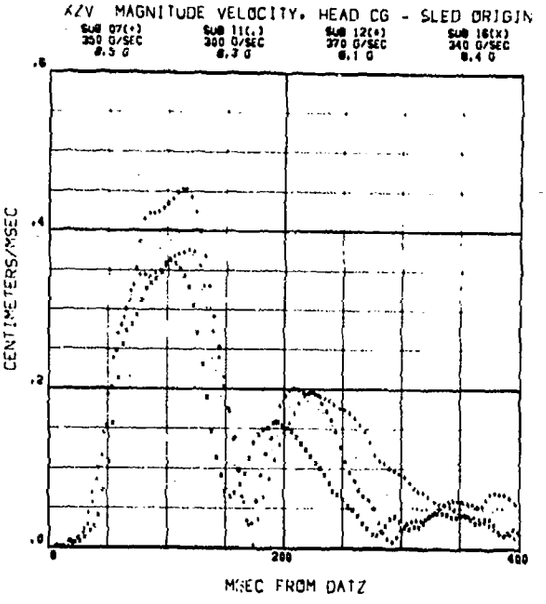

237

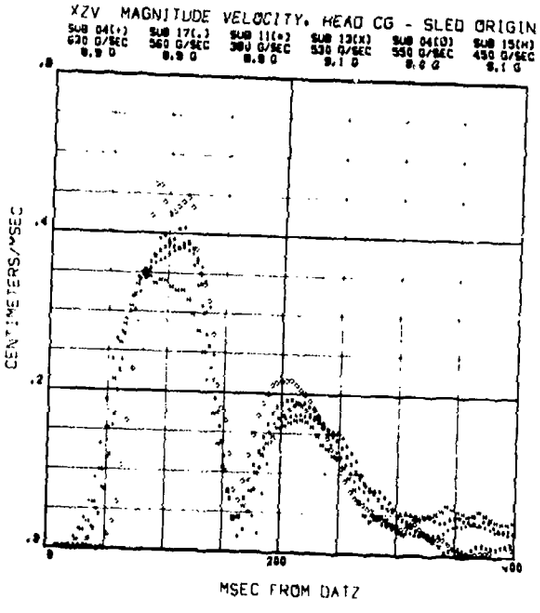

238

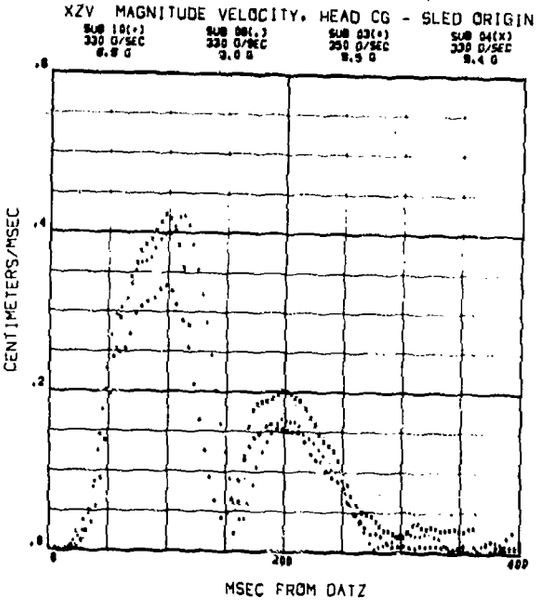

239

XZV MAGNITUDE OF THE VELOCITY OF THE HEAD C.G. RELATIVE TO THE SLED ORIGIN

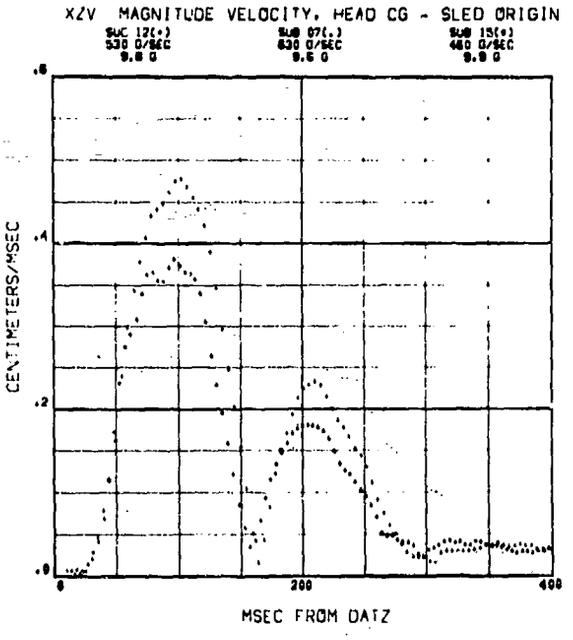

240

XNV VELOCITY OF THE HEAD C.G. RELATIVE TO THE T_1 ORIGIN IN THE X DIRECTION

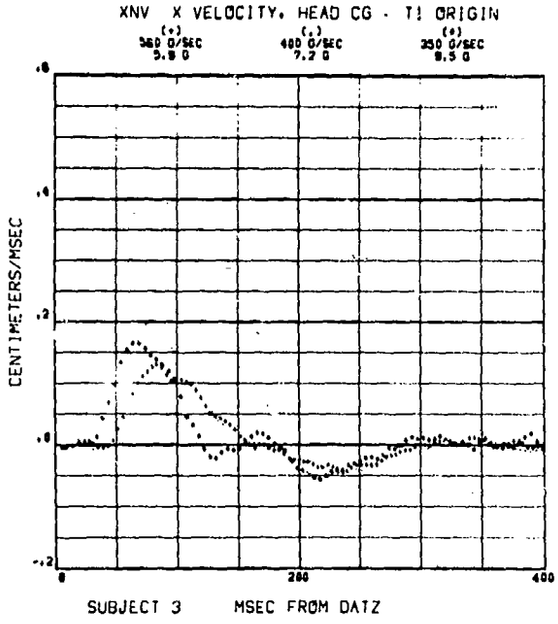

241

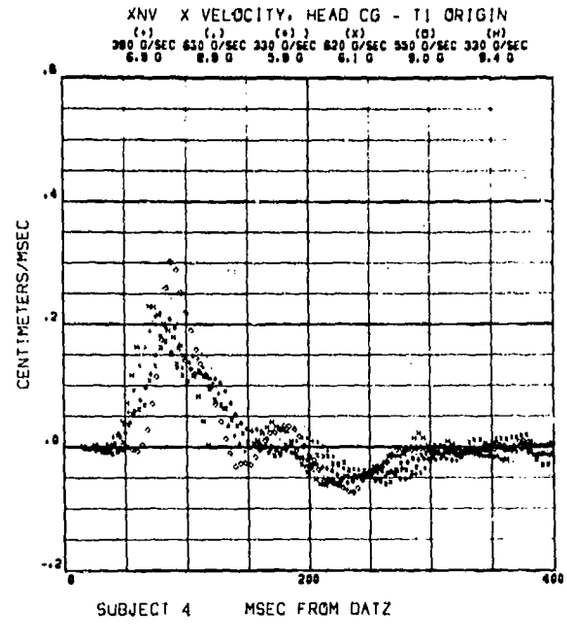

242

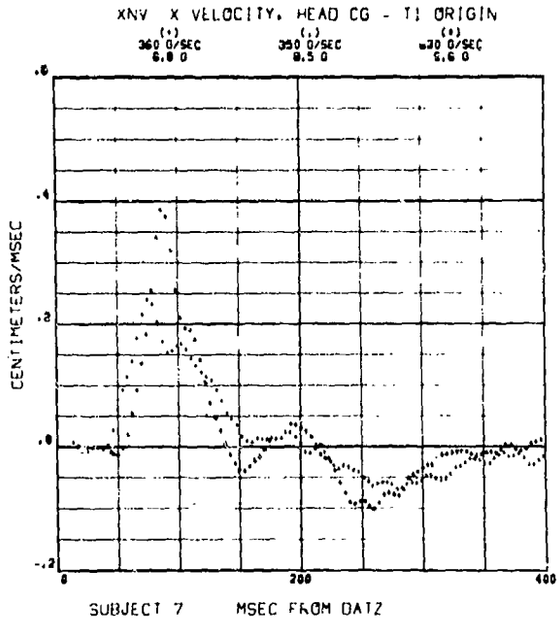

243

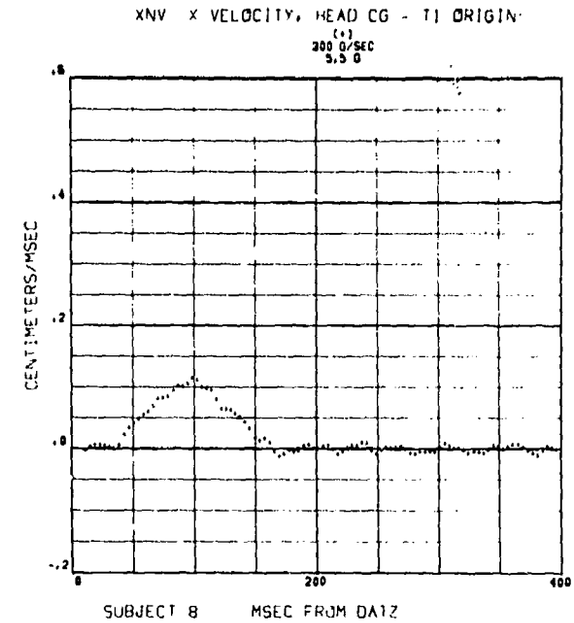

244

XNV VELOCITY OF THE HEAD C.G. RELATIVE TO THE T_1 ORIGIN IN THE X DIRECTION

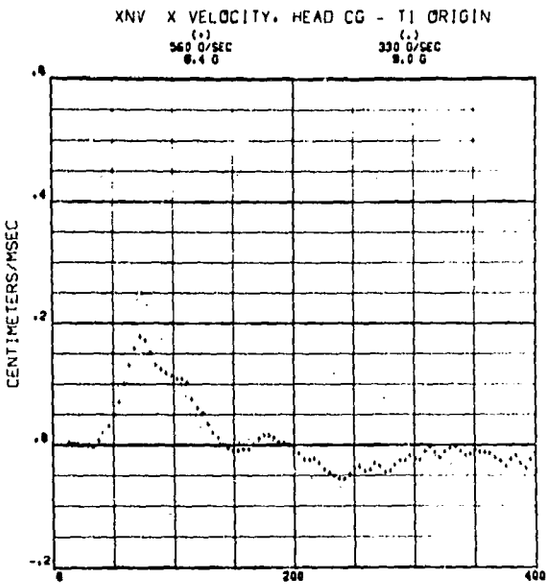

245

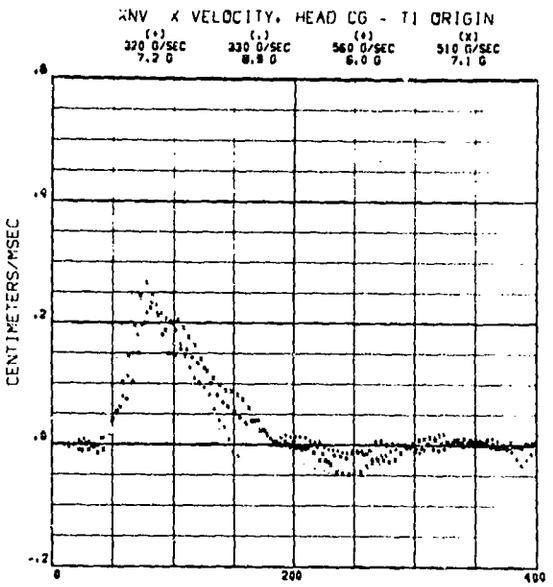

246

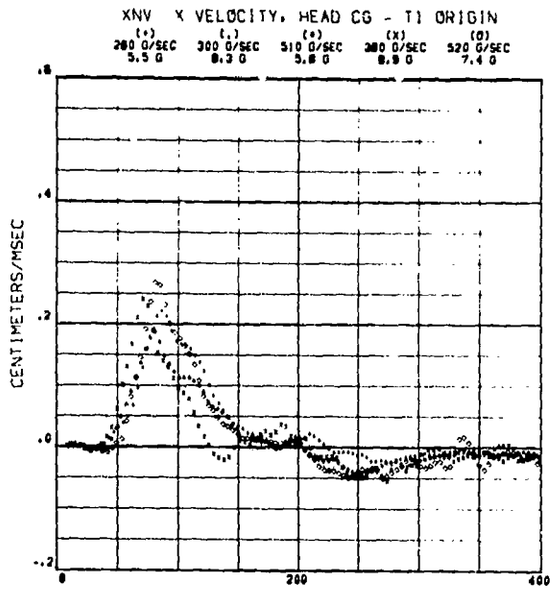

247

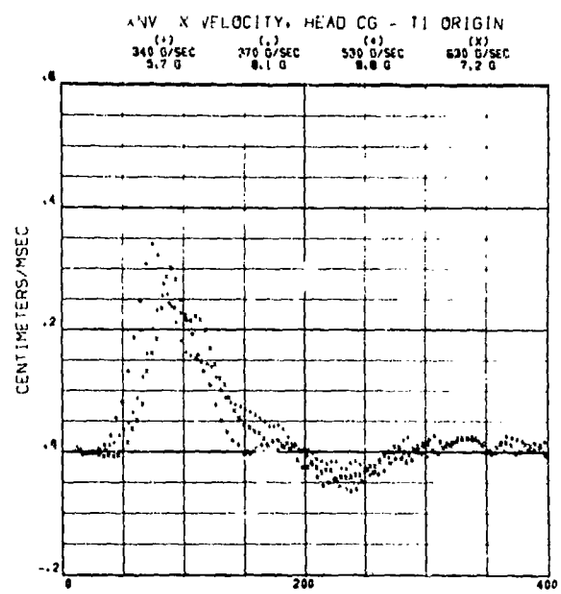

248

XNV VELOCITY OF THE HEAD C.G. RELATIVE TO THE T_1 ORIGIN IN THE X DIRECTION

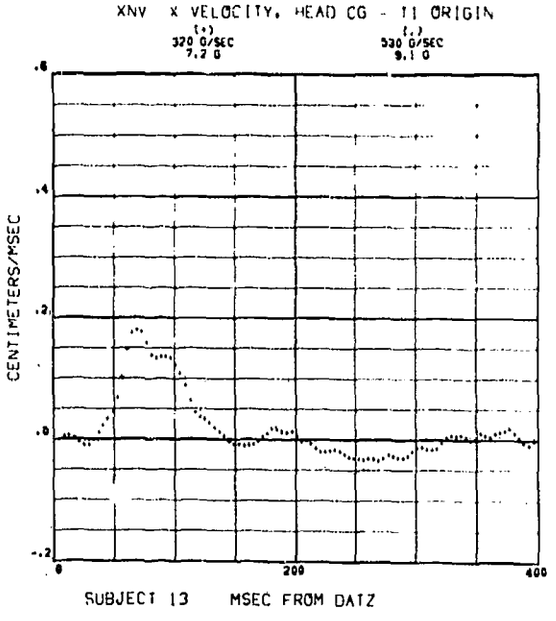

249

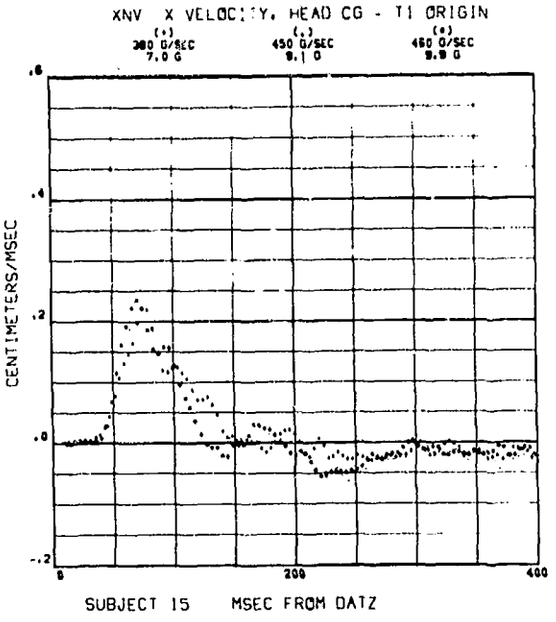

250

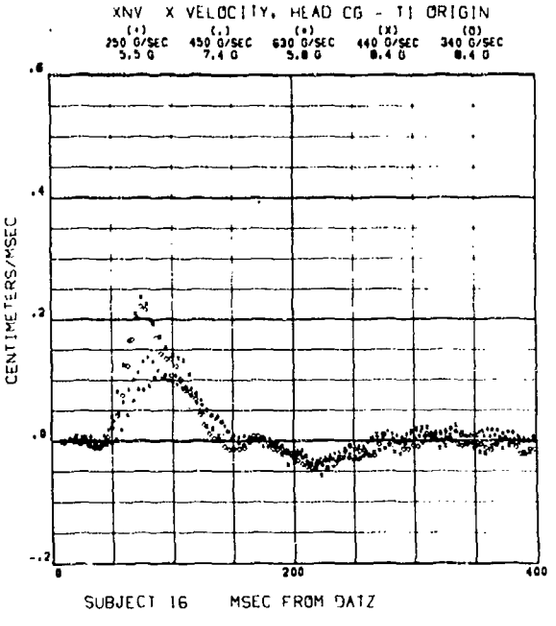

251

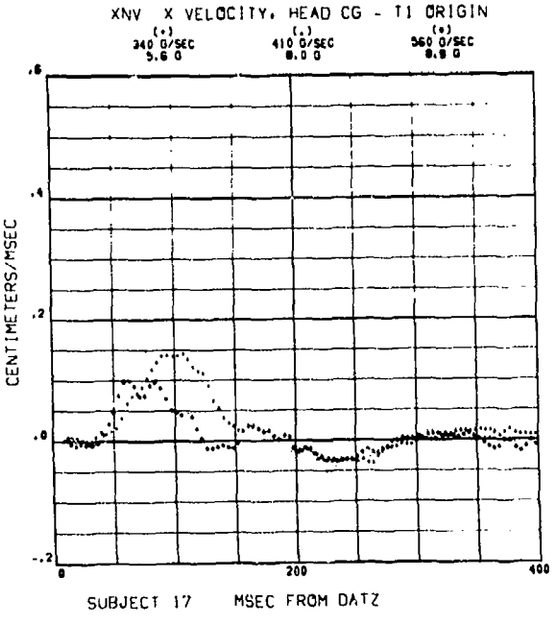

252

XNV VELOCITY OF THE HEAD C.G. RELATIVE TO THE T_1 ORIGIN IN THE X DIRECTION

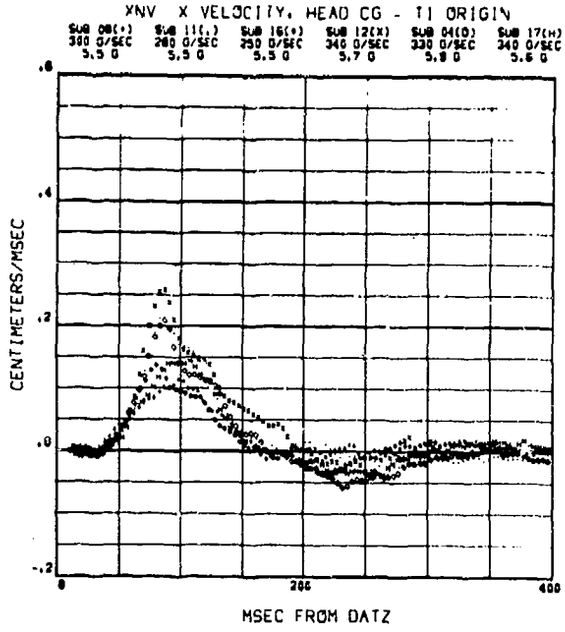

253

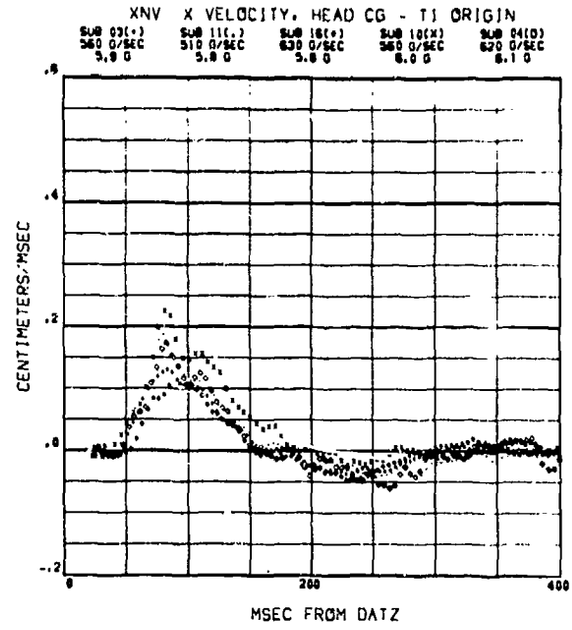

254

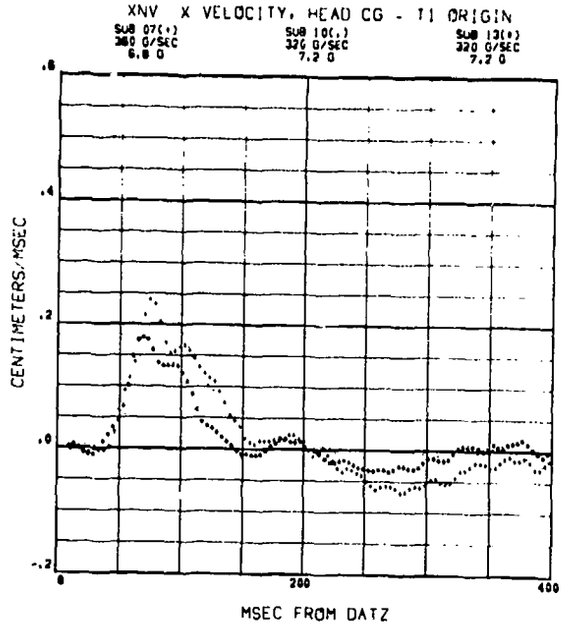

255

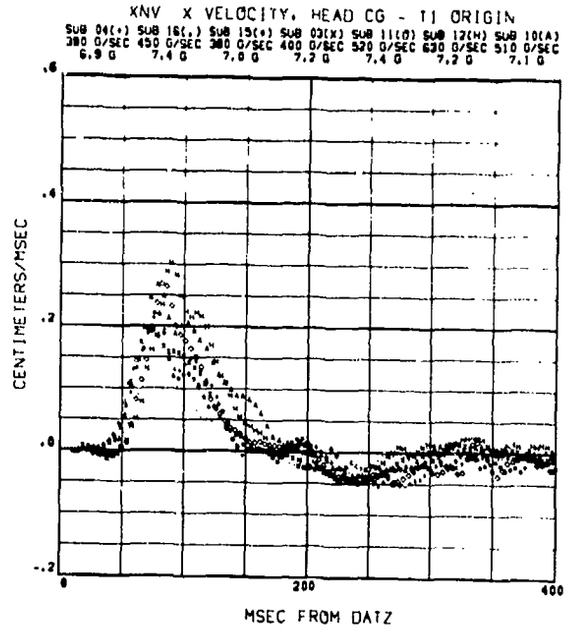

256

XNV VELOCITY OF THE HEAD C.G. RELATIVE TO THE T_1 ORIGIN IN THE X DIRECTION

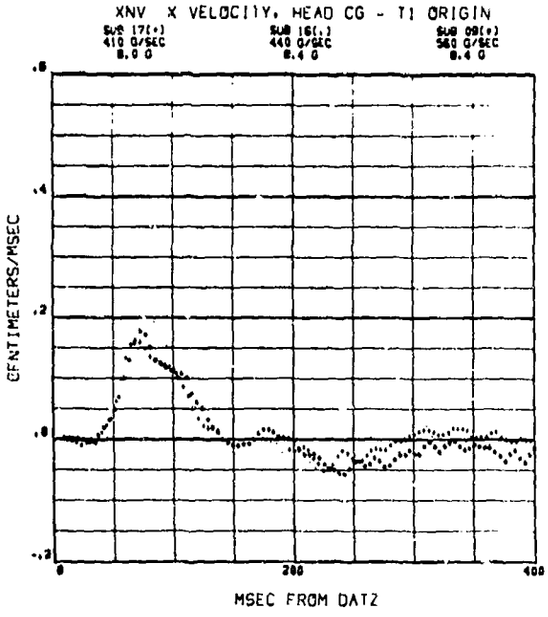

257

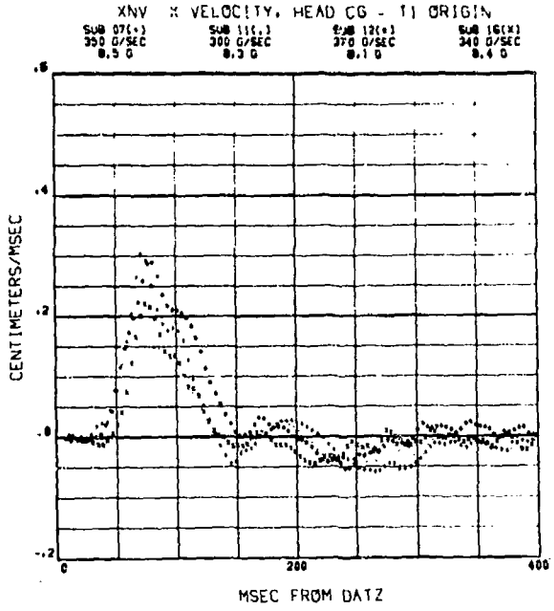

258

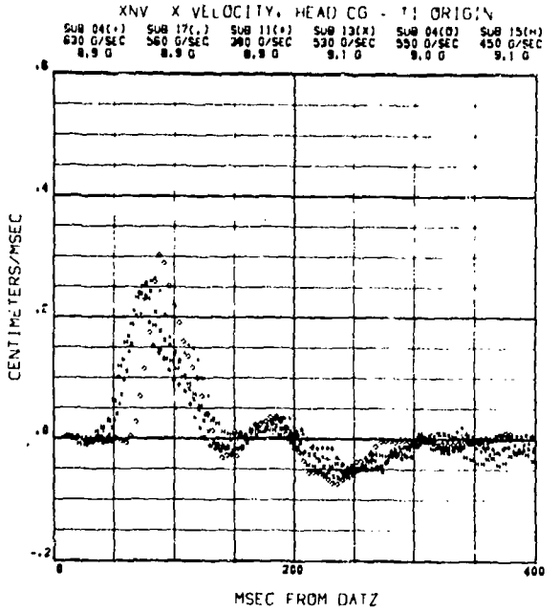

259

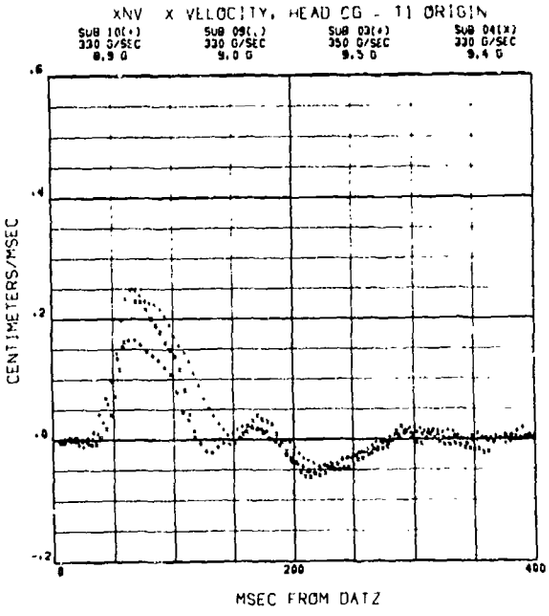

260

XNV VELOCITY OF THE HEAD C.G. RELATIVE TO THE T_1 ORIGIN IN THE X DIRECTION

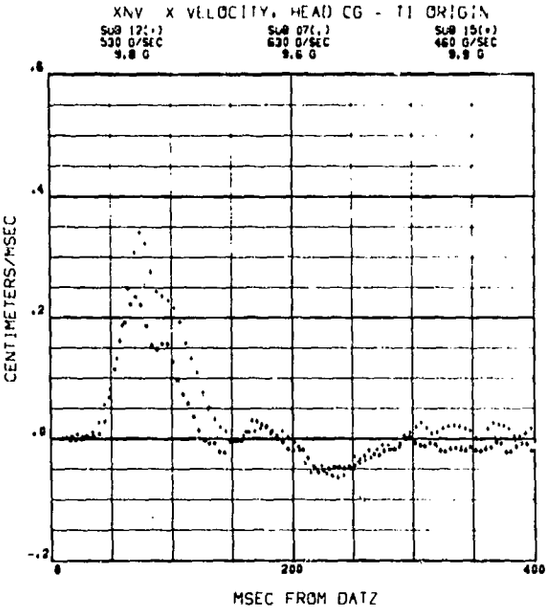

261

ZNV VELOCITY OF THE HEAD C.G. RELATIVE TO THE T_1 ORIGIN IN THE Z DIRECTION

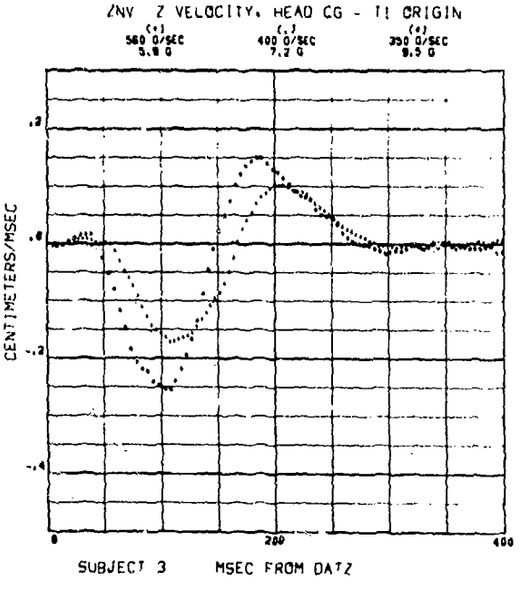

262

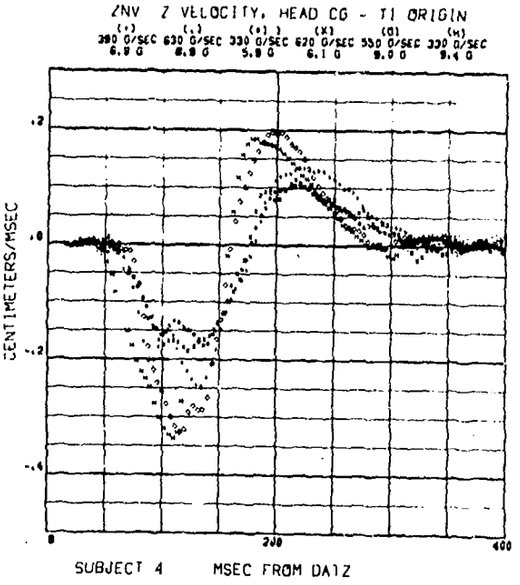

263

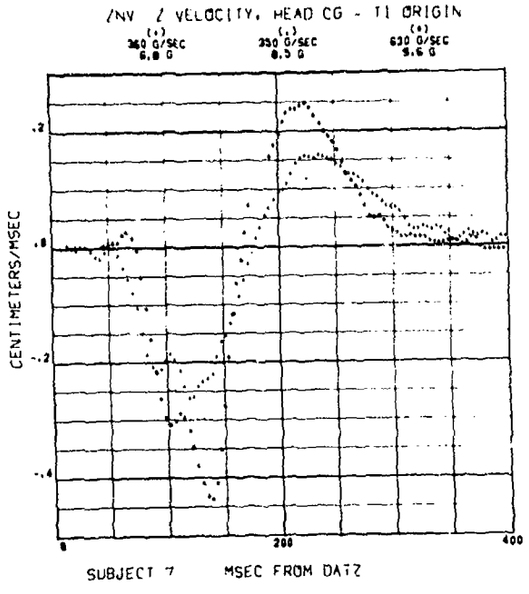

264

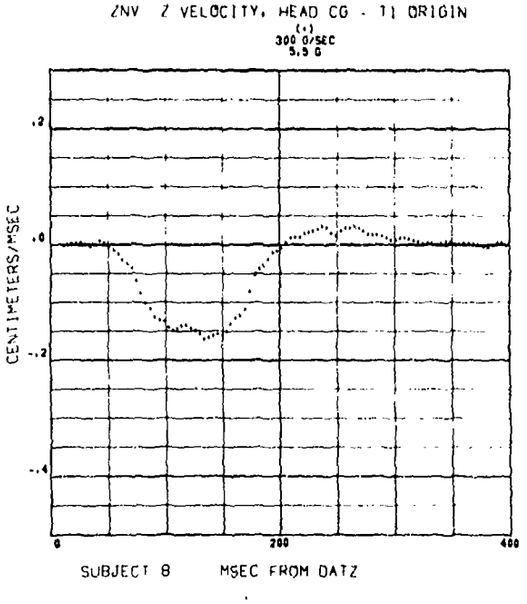

265

ZNV VELOCITY OF THE HEAD C.G. RELATIVE TO THE T_1 ORIGIN IN THE Z DIRECTION

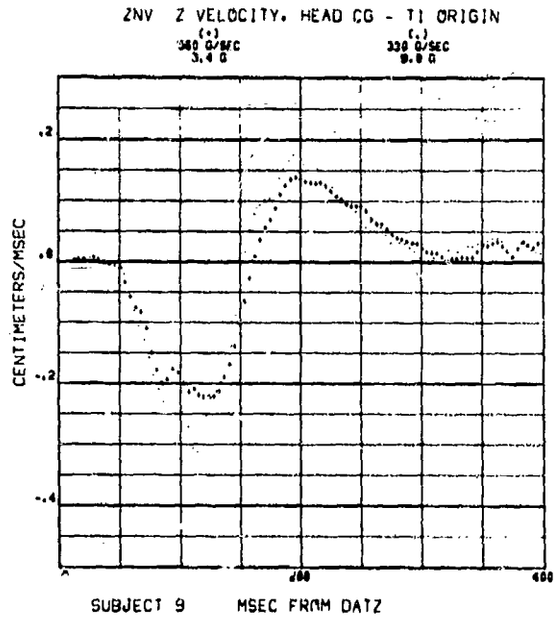

266

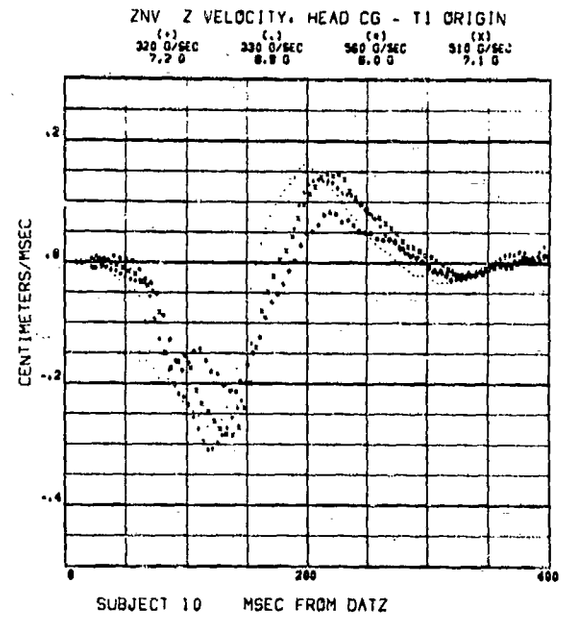

267

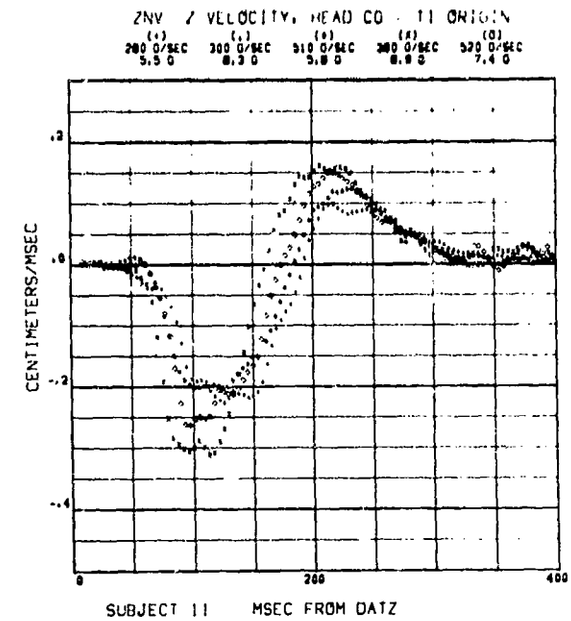

268

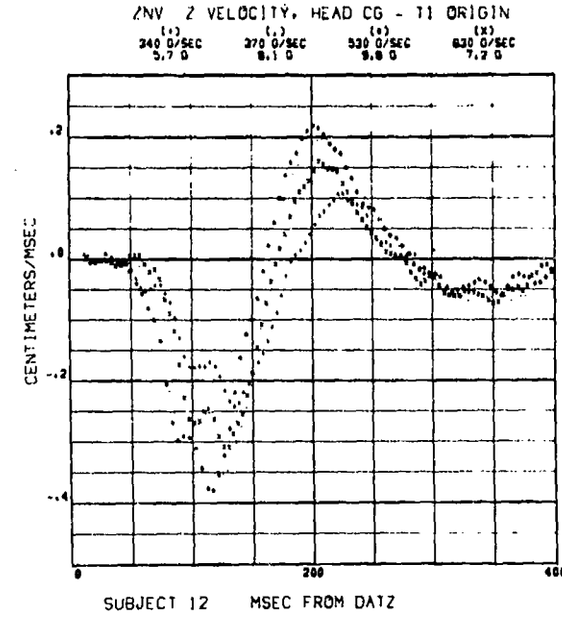

269

ZNV VELOCITY OF THE HEAD C.G. RELATIVE TO THE T_1 ORIGIN IN THE Z DIRECTION

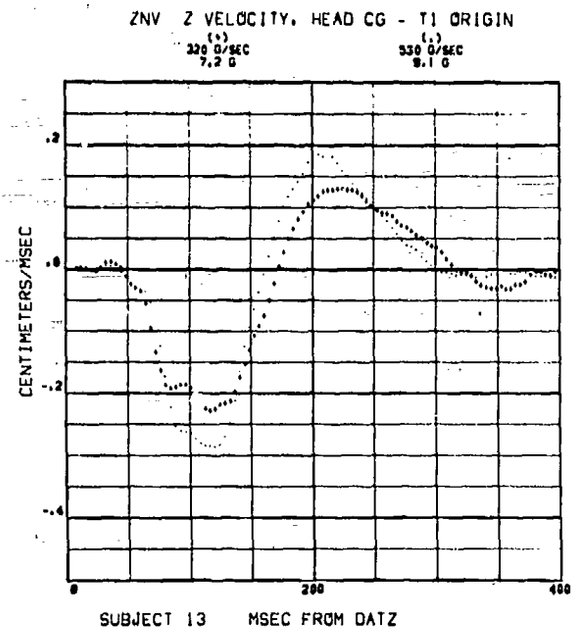

270

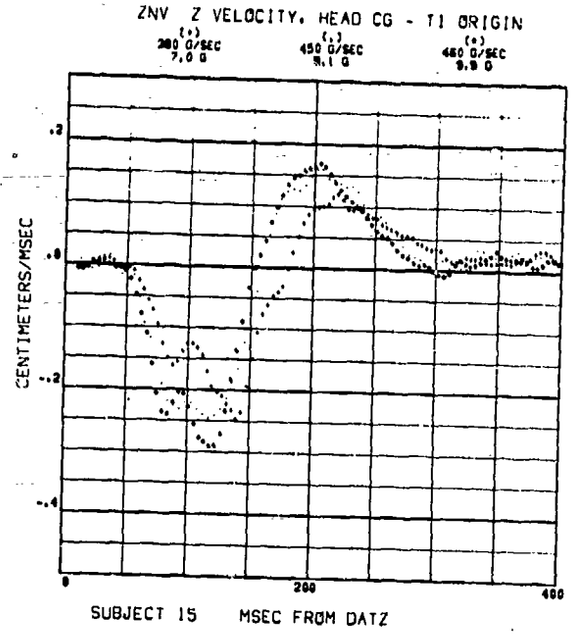

271

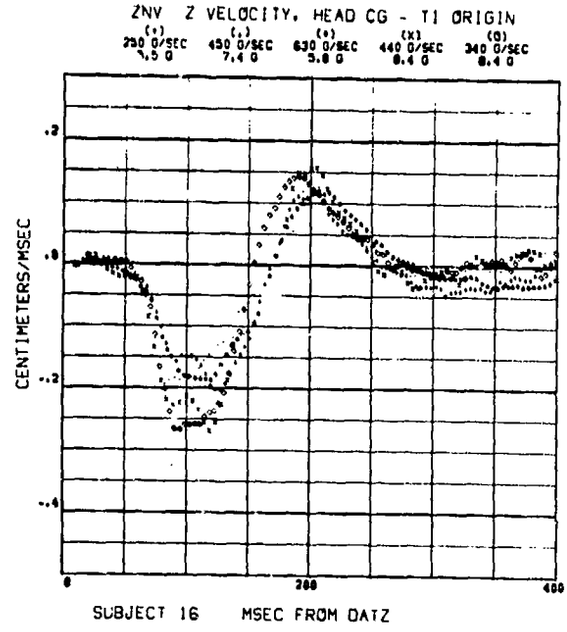

272

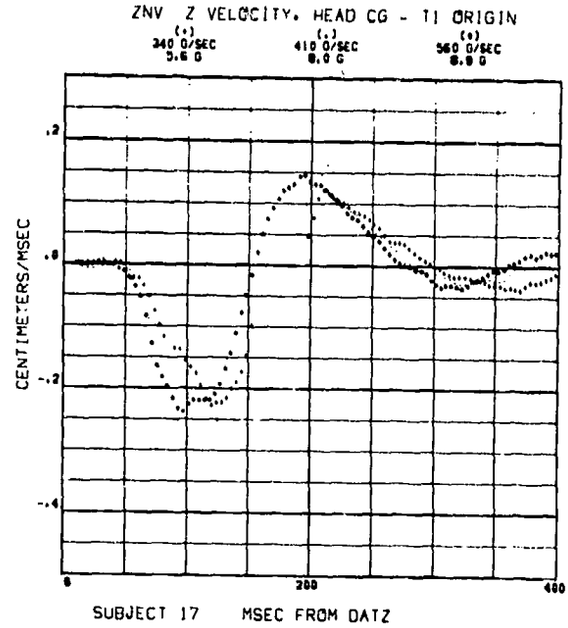

273

ZNV VELOCITY OF THE HEAD C.G. RELATIVE TO THE T_1 ORIGIN IN THE Z DIRECTION

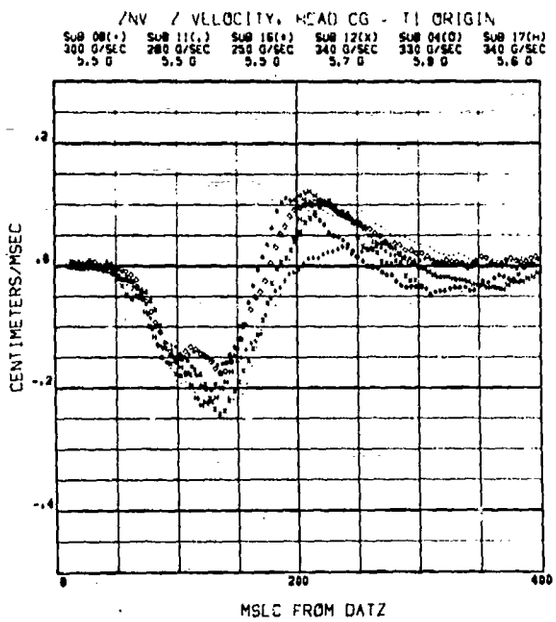

274

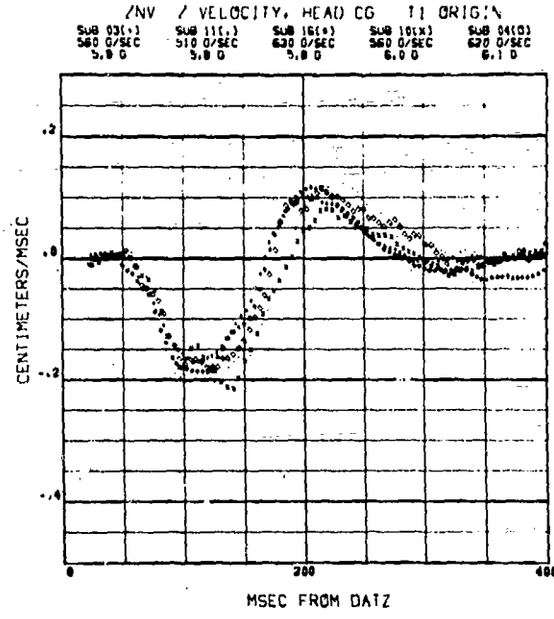

275

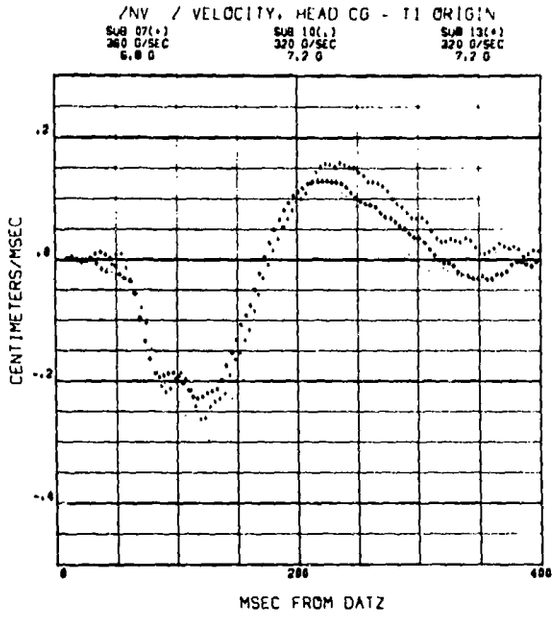

276

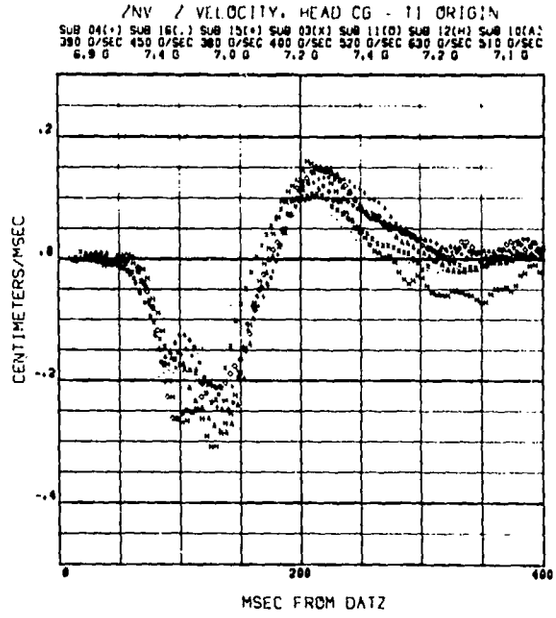

277

ZNV VELOCITY OF THE HEAD C.G. RELATIVE TO THE T_1 ORIGIN IN THE Z DIRECTION

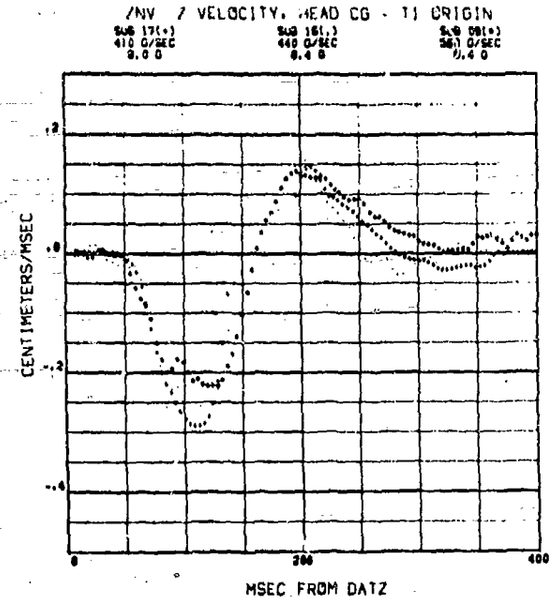

278

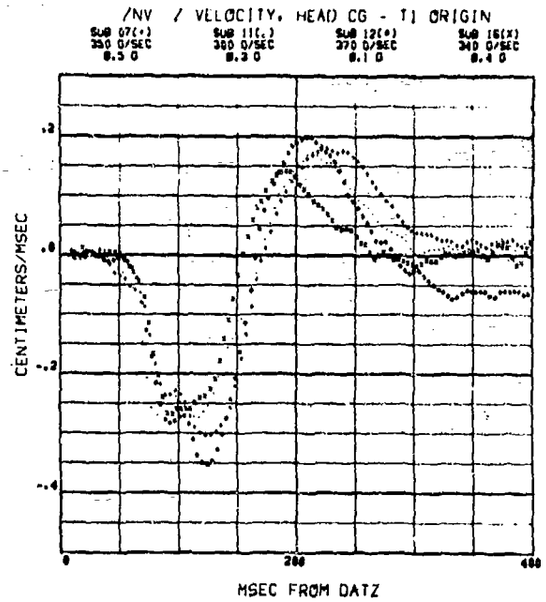

279

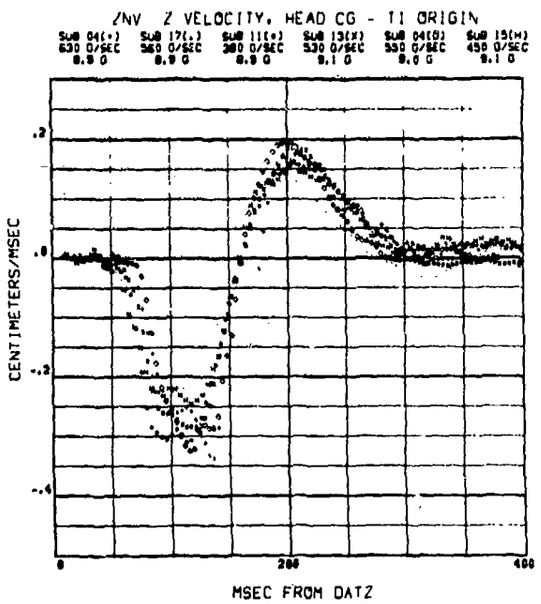

280

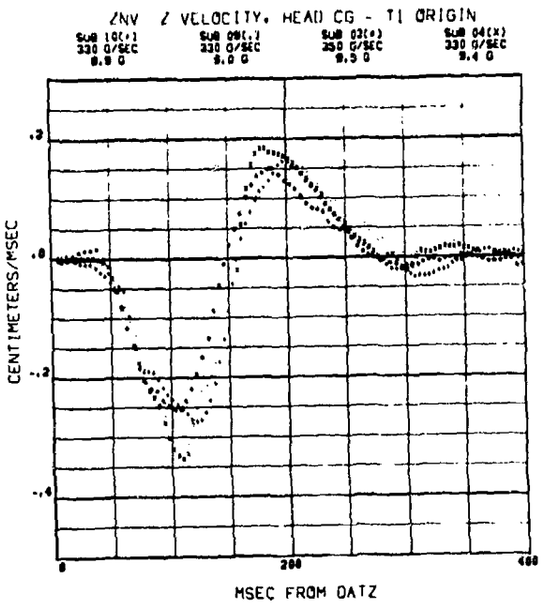

281

ZNV VELOCITY OF THE HEAD C.G. RELATIVE TO THE T_1 ORIGIN IN THE Z DIRECTION

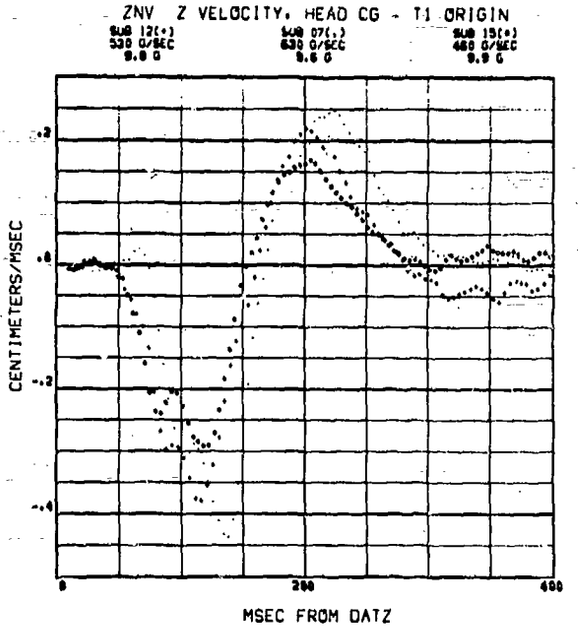

NNV MAGNITUDE OF VELOCITY OF THE HEAD C.G. RELATIVE TO THE T_1 ORIGIN

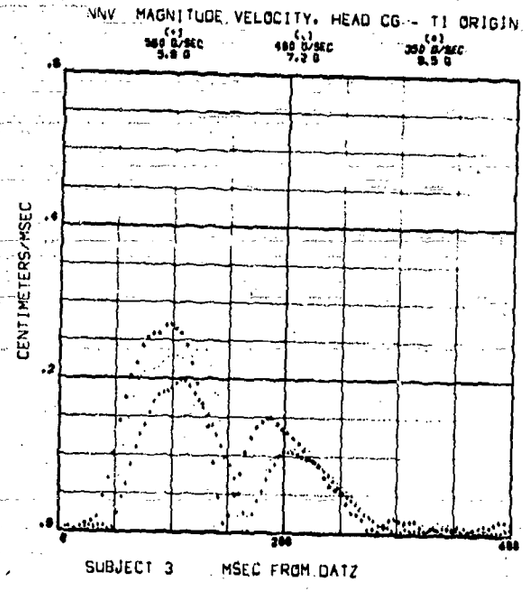

283

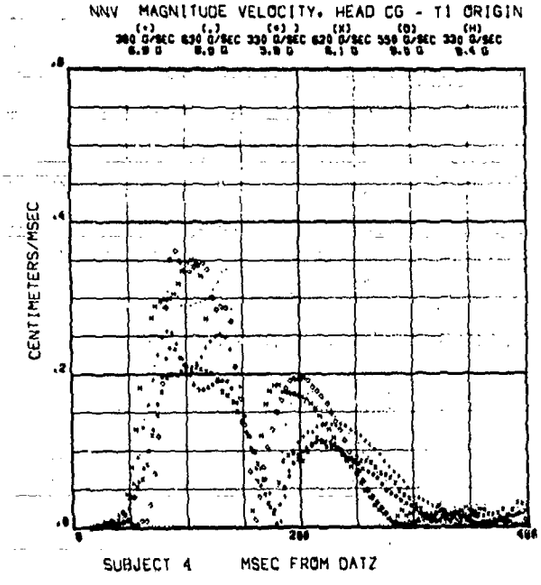

284

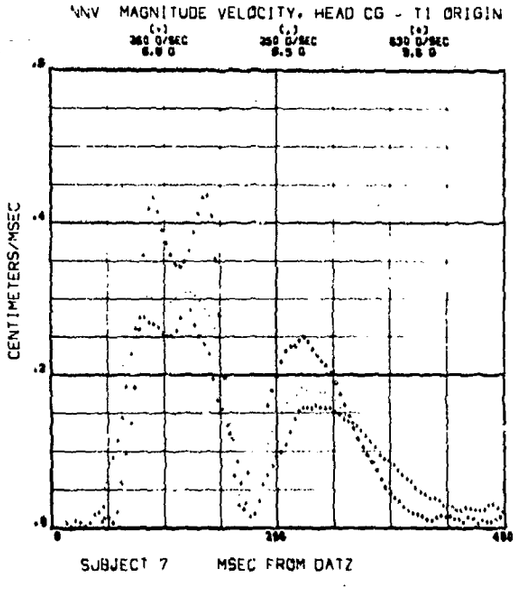

285

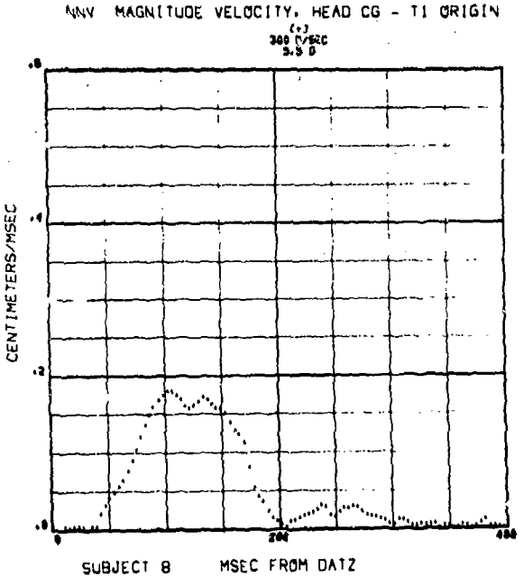

286

NNV MAGNITUDE OF VELOCITY OF THE HEAD C.G. RELATIVE TO THE T_1 ORIGIN

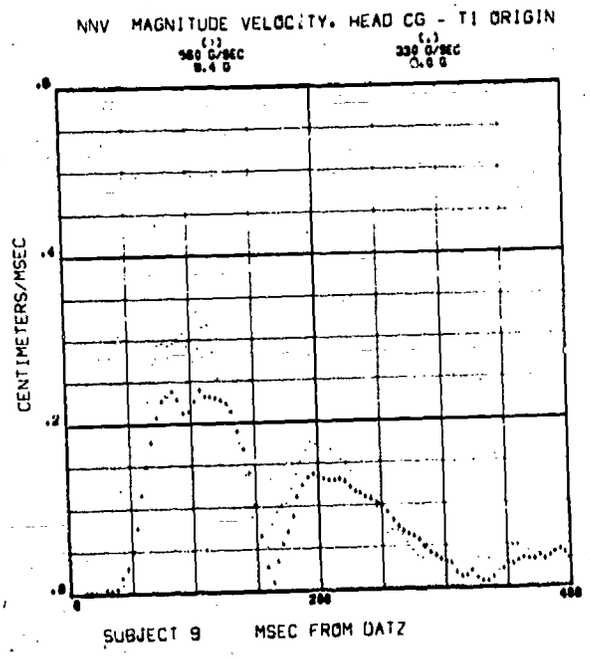

287

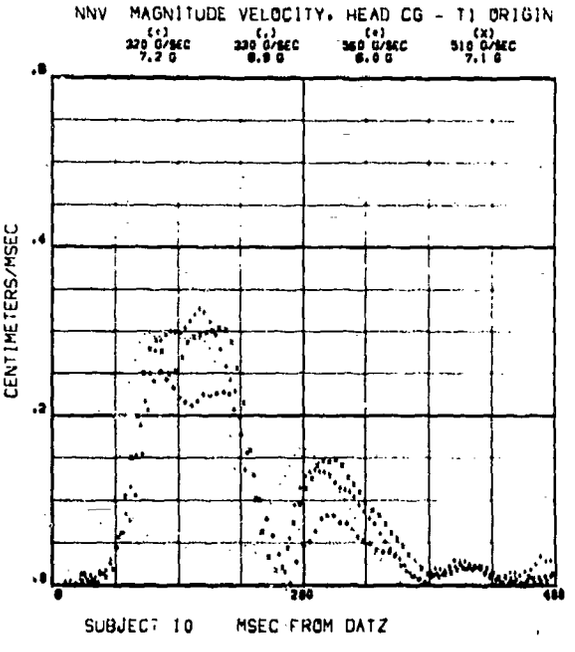

288

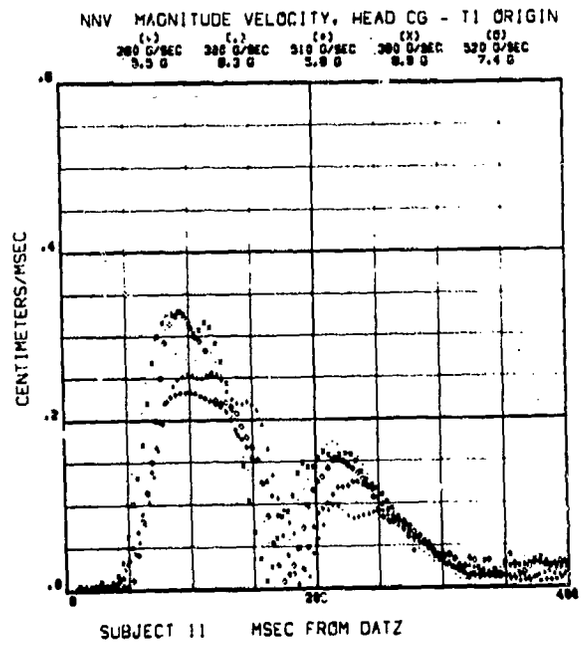

289

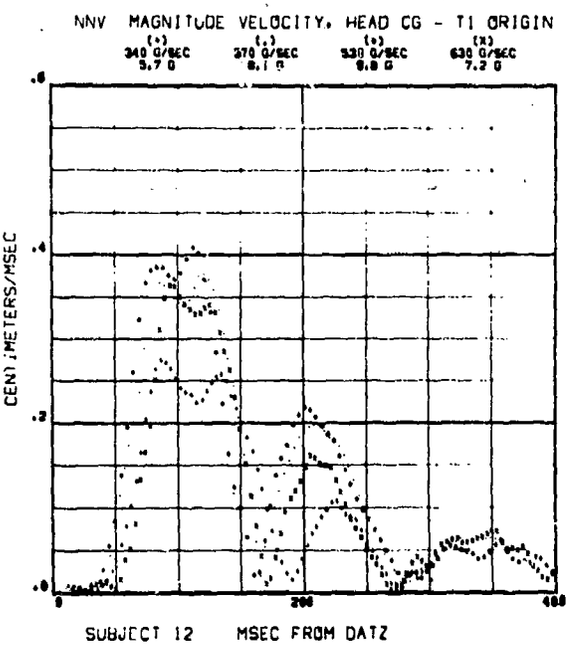

290

NNV MAGNITUDE OF VELOCITY OF THE HEAD C.G. RELATIVE TO THE T_1 ORIGIN

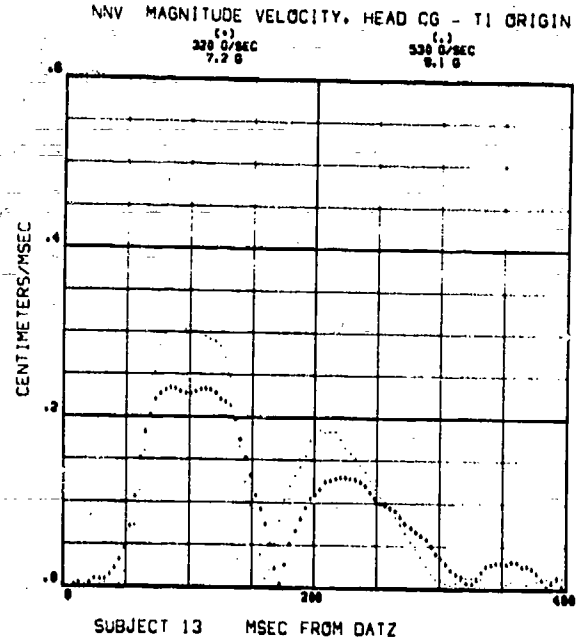

291

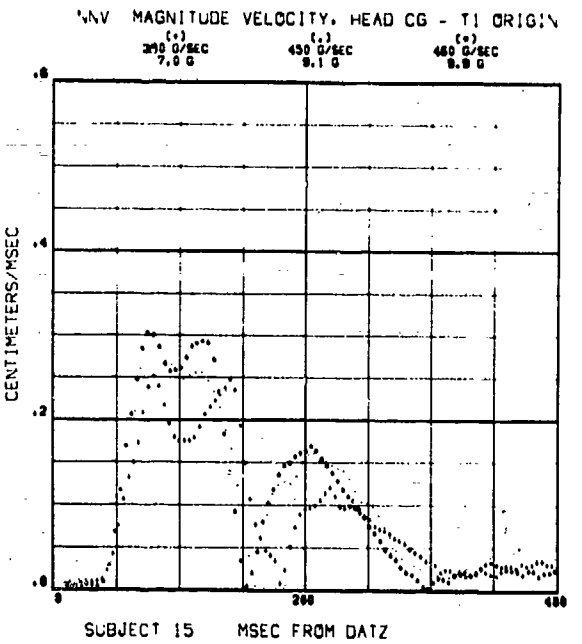

292

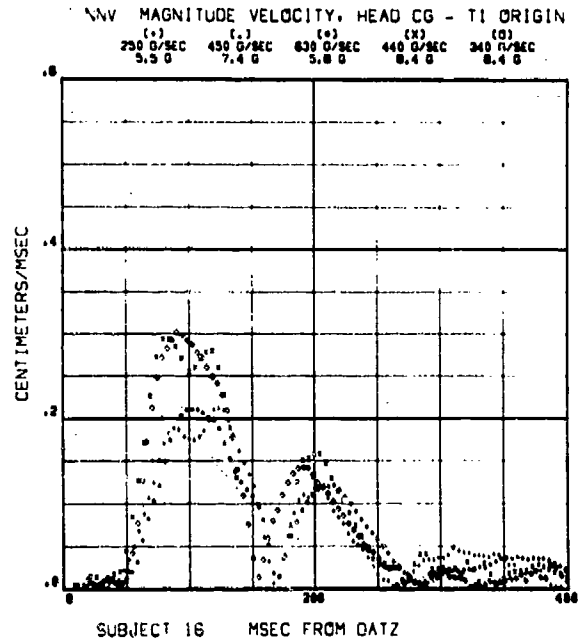

293

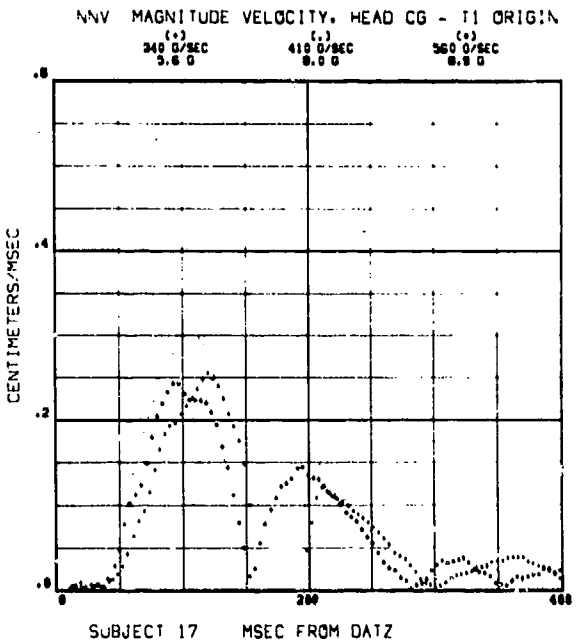

294

NNV MAGNITUDE OF VELOCITY OF THE HEAD C.G. RELATIVE TO THE T_1 ORIGIN

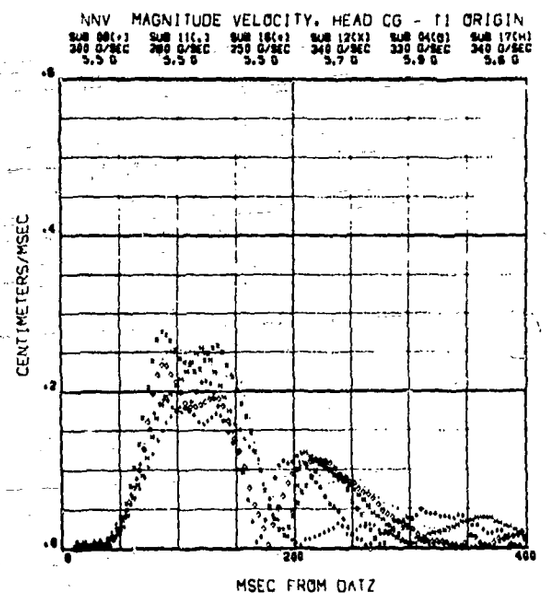

295

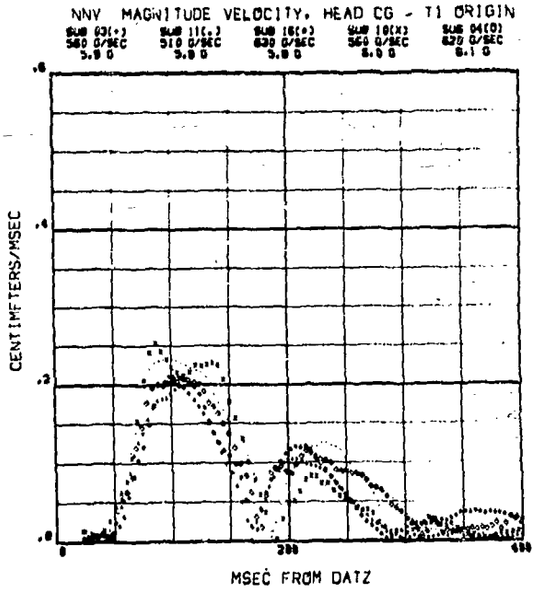

296

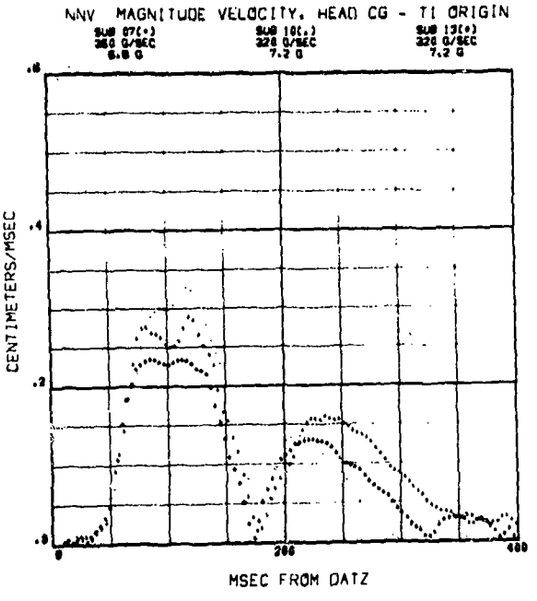

297

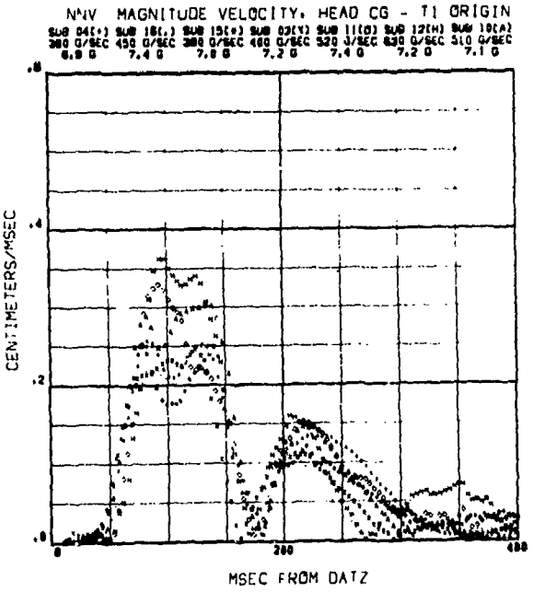

298

NNV MAGNITUDE OF VELOCITY OF THE HEAD C.G. RELATIVE TO THE T_1 ORIGIN

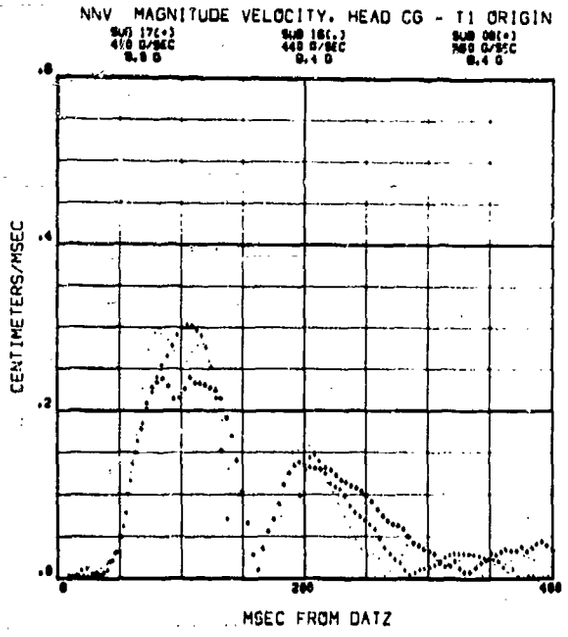

299

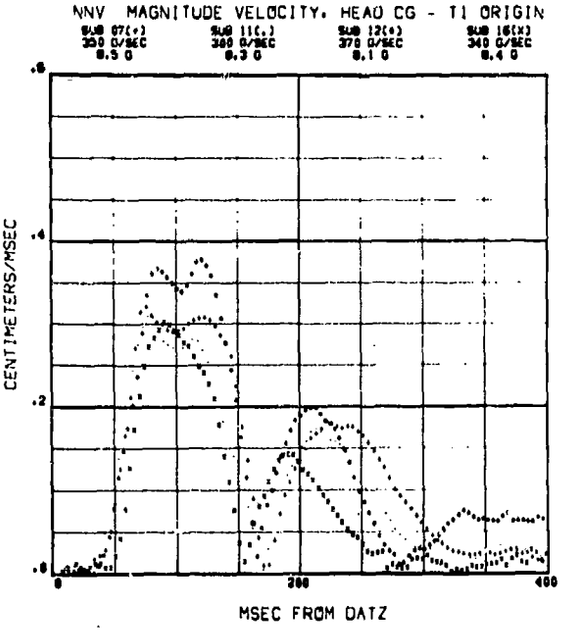

300

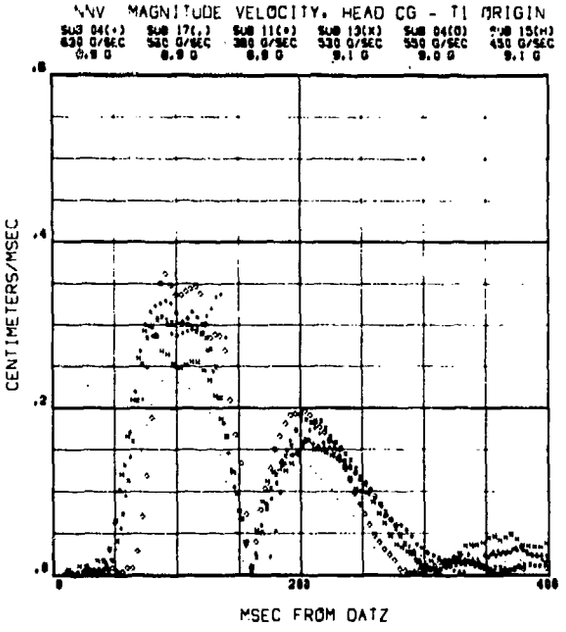

301

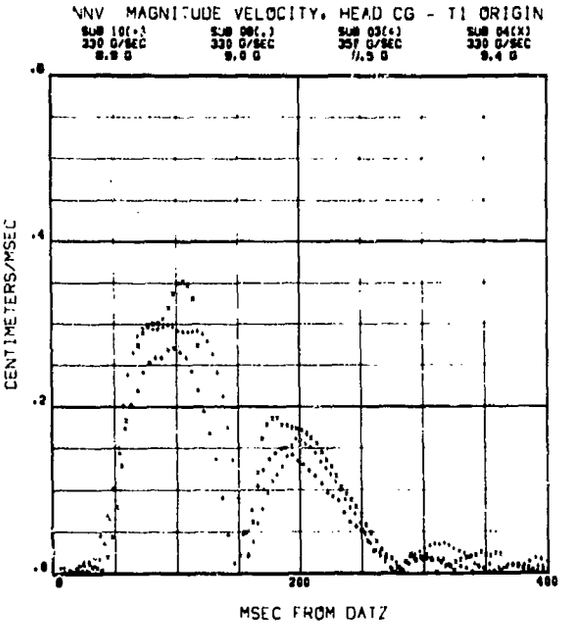

302

NNV MAGNITUDE OF VELOCITY OF THE HEAD C.G. RELATIVE TO THE T_1 ORIGIN

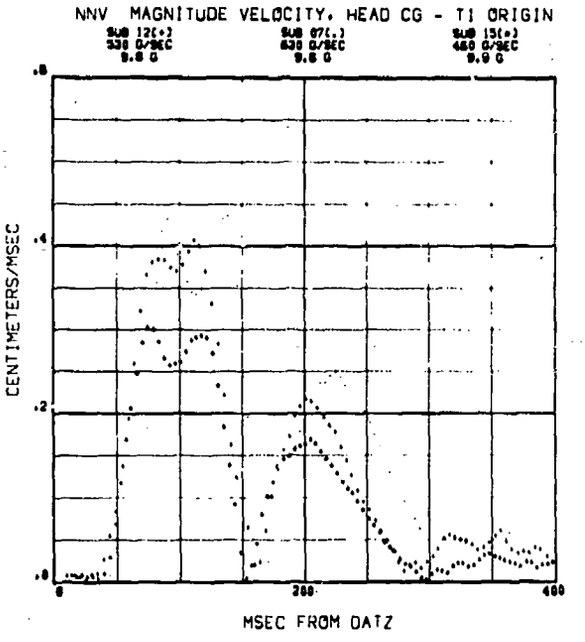

303

XCN DISPLACEMENT OF THE HEAD C.G. RELATIVE TO THE T_1 ORIGIN IN THE X DIRECTION

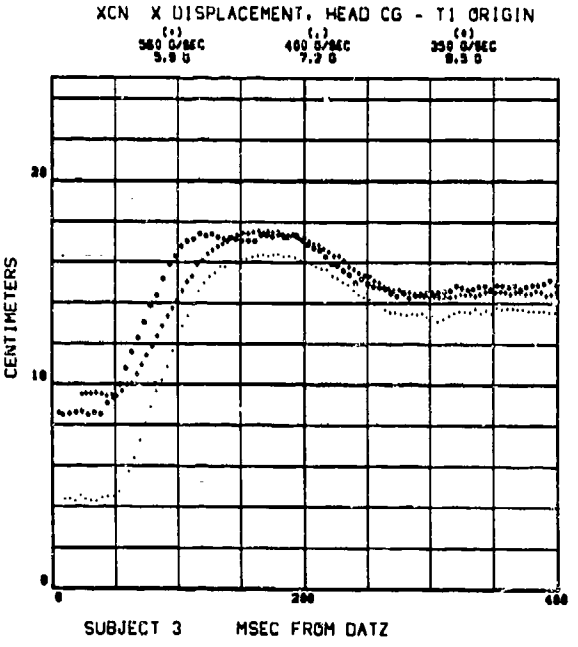

304

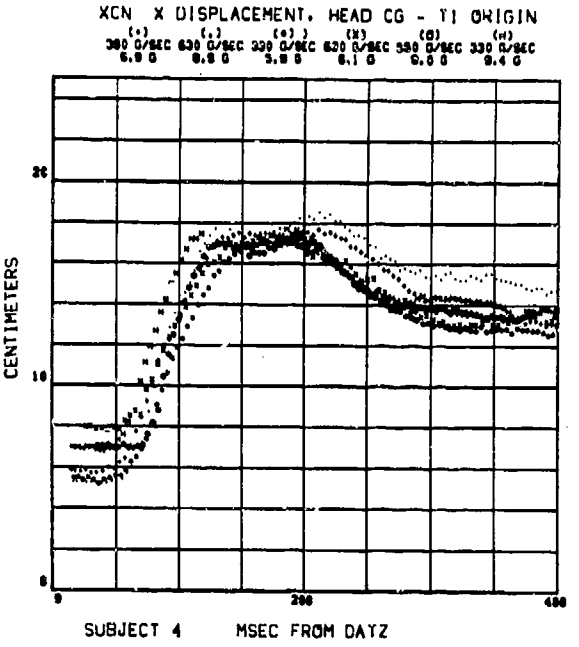

305

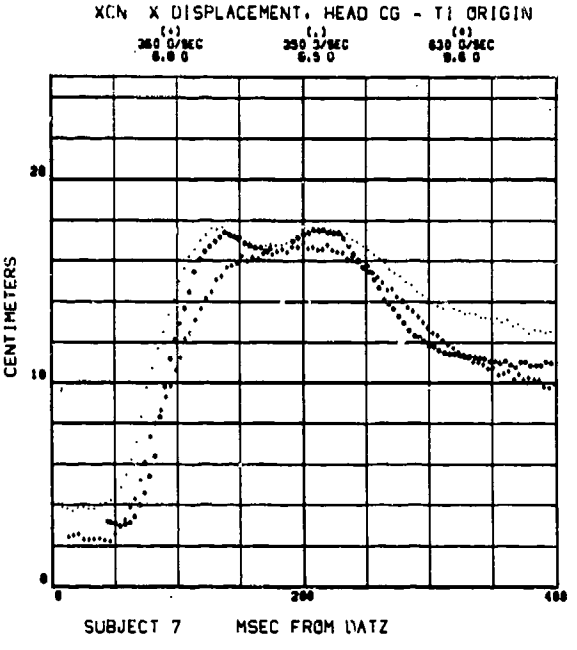

306

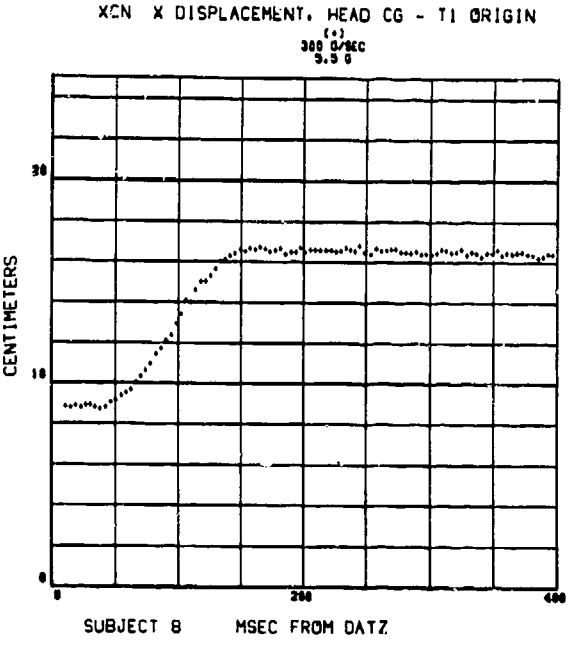

307

XCN DISPLACEMENT OF THE HEAD C.G. RELATIVE TO THE T_1 ORIGIN IN THE X DIRECTION

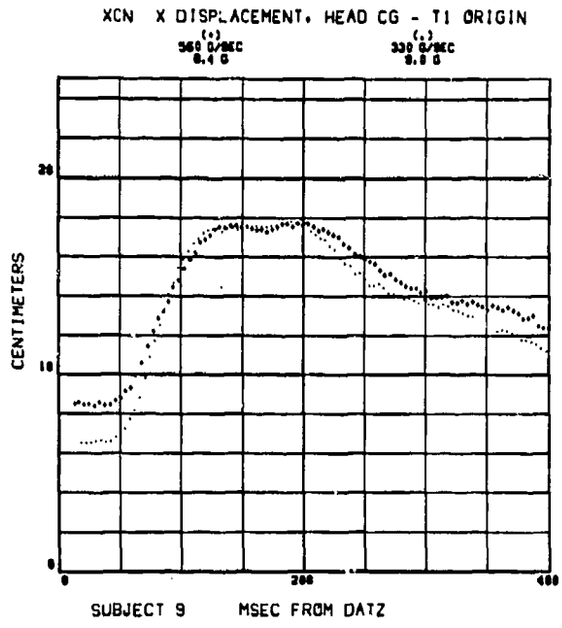

308

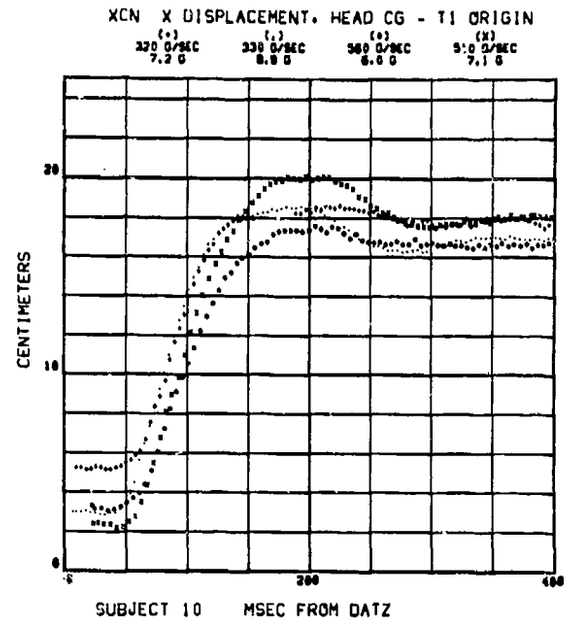

309

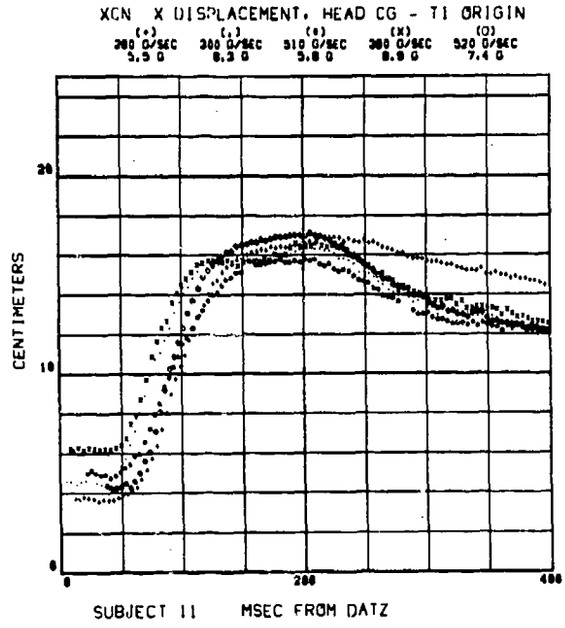

310

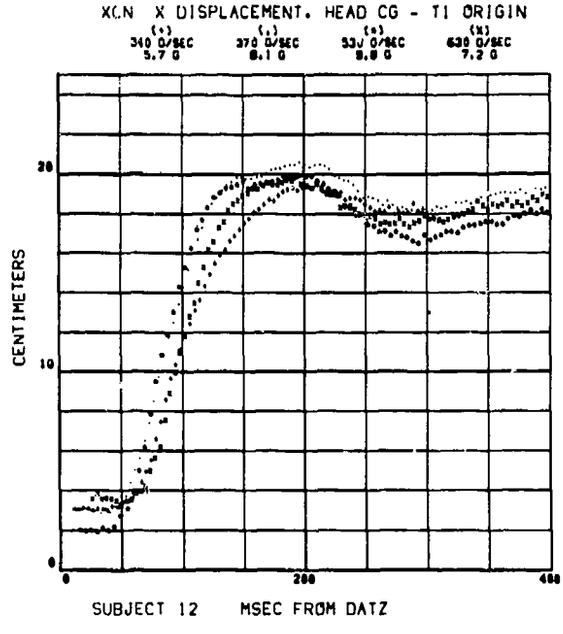

311

XCN DISPLACEMENT OF THE HEAD C.G. RELATIVE TO THE T_1 ORIGIN IN THE X DIRECTION

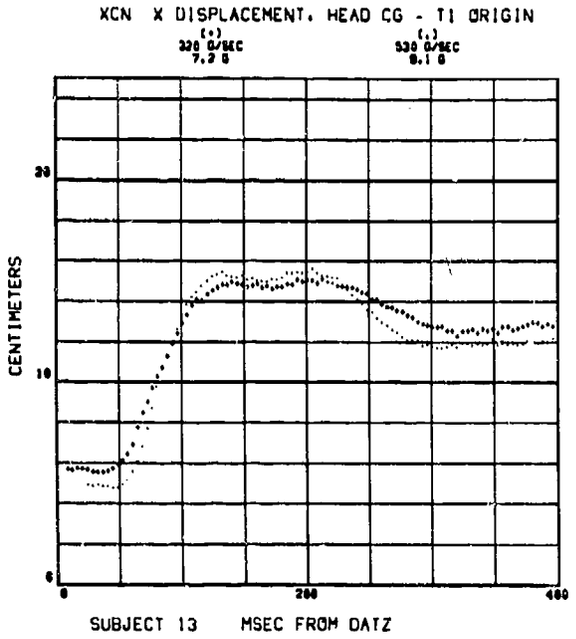

312

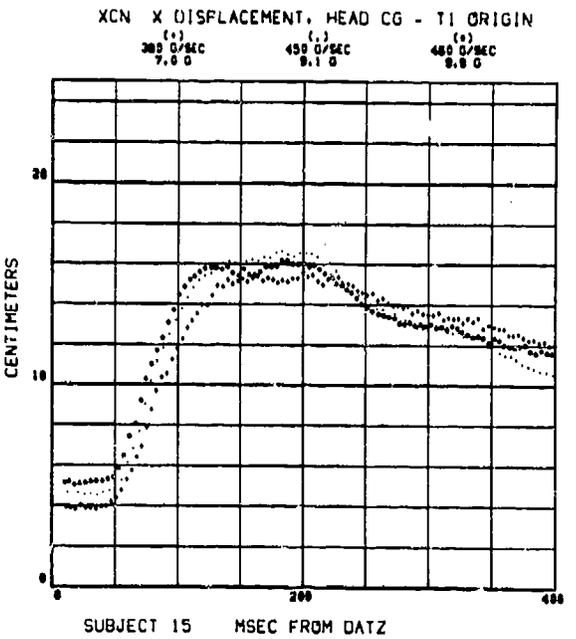

313

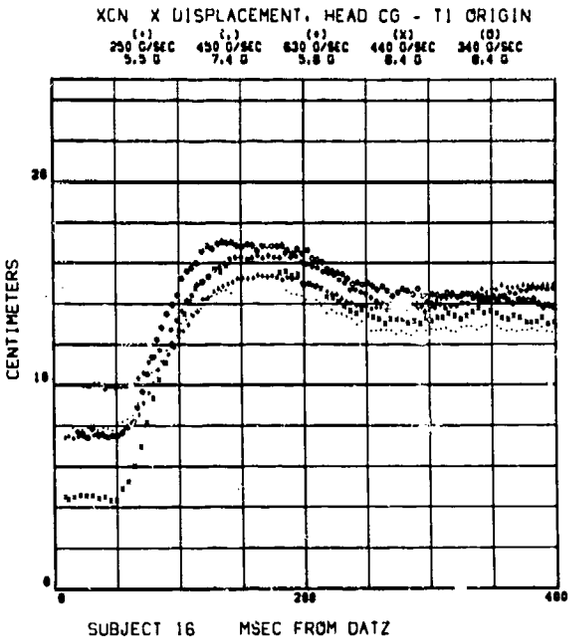

314

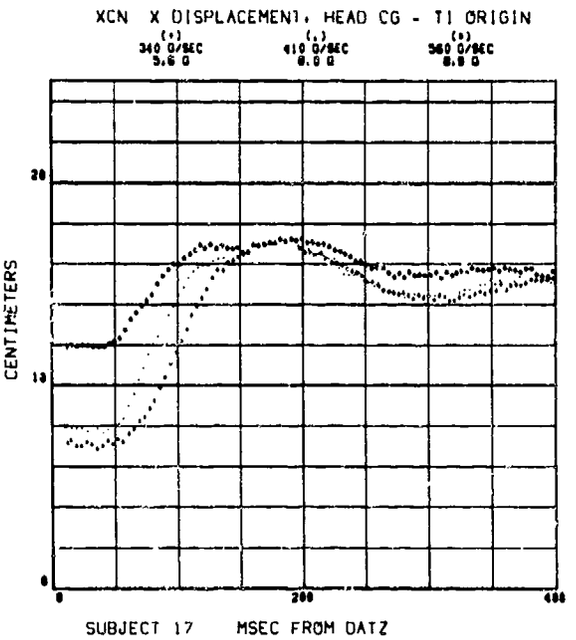

315

XCN DISPLACEMENT OF THE HEAD C.G. RELATIVE TO THE T_1 ORIGIN IN THE X DIRECTION

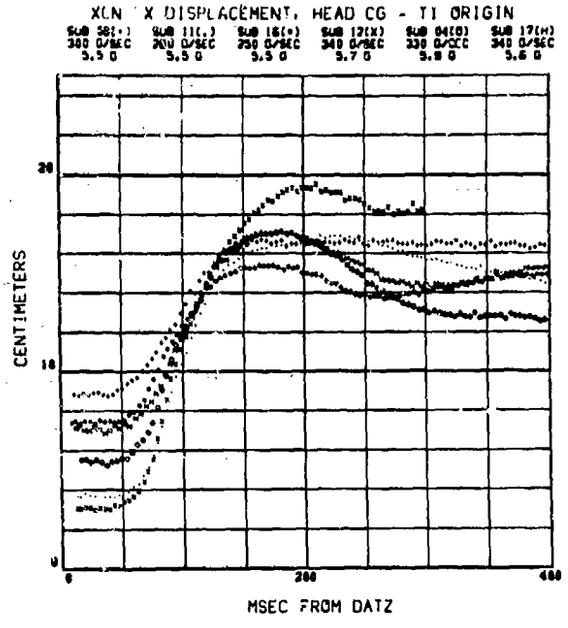

316

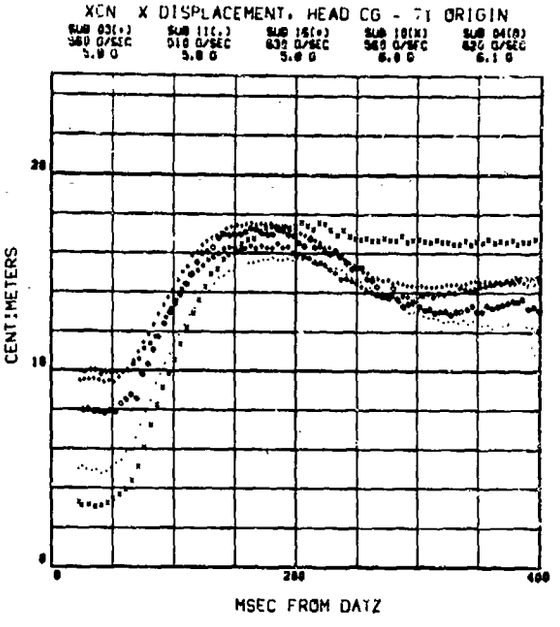

317

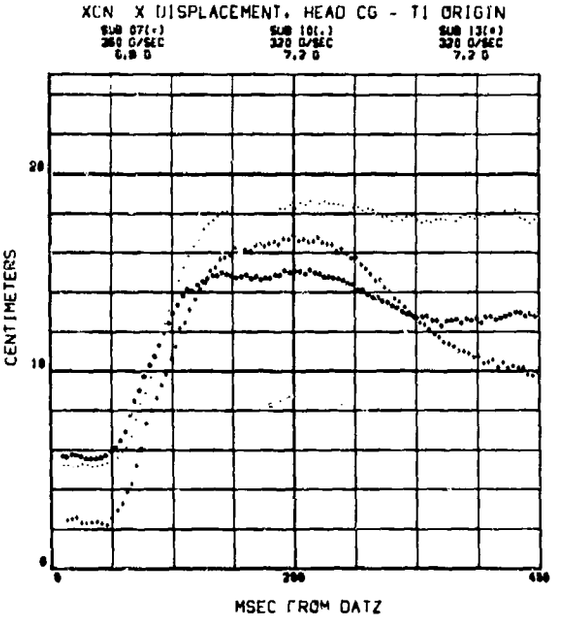

318

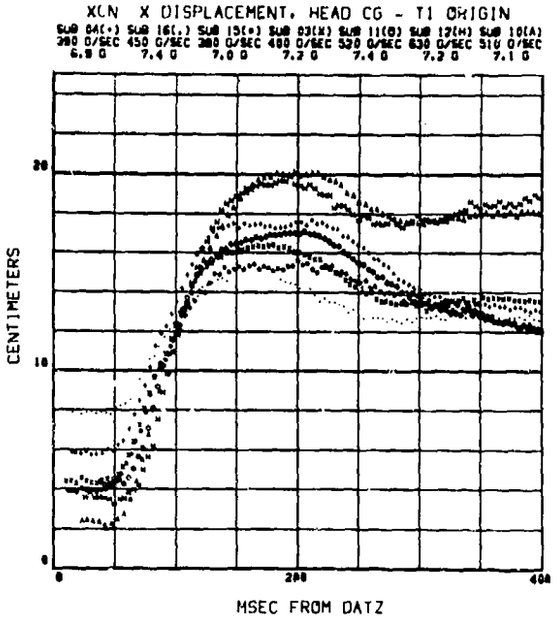

319

XCN DISPLACEMENT OF THE HEAD C.G. RELATIVE TO THE T_1 ORIGIN IN THE X DIRECTION

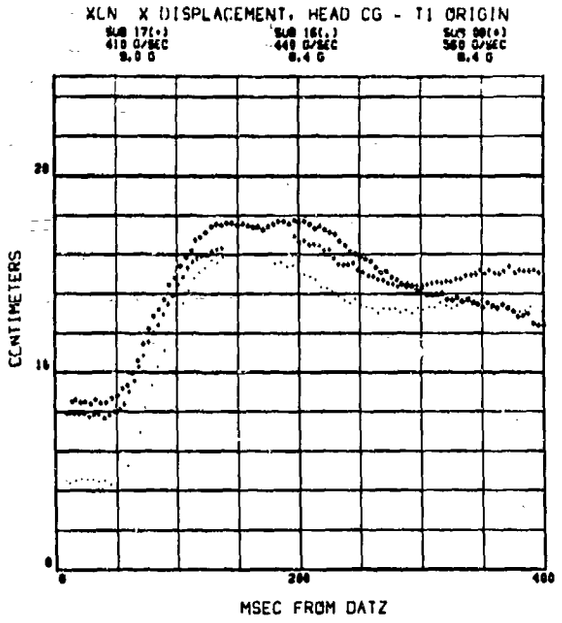

320

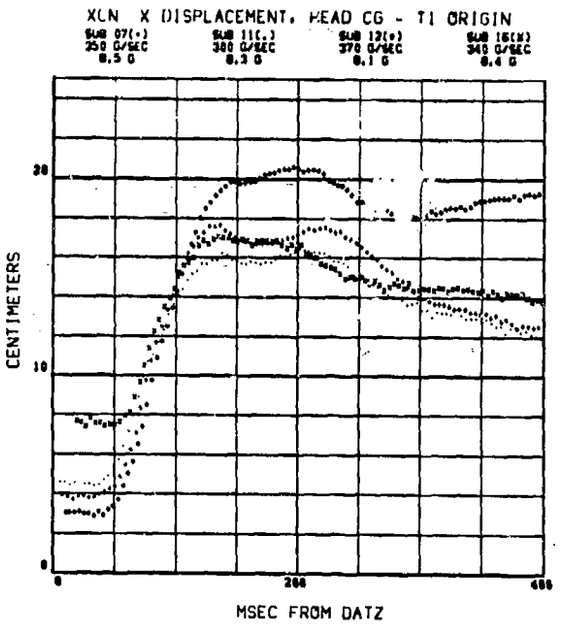

321

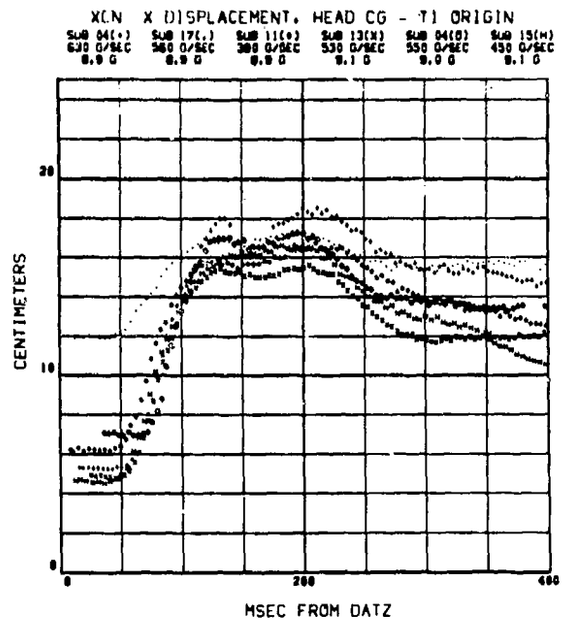

322

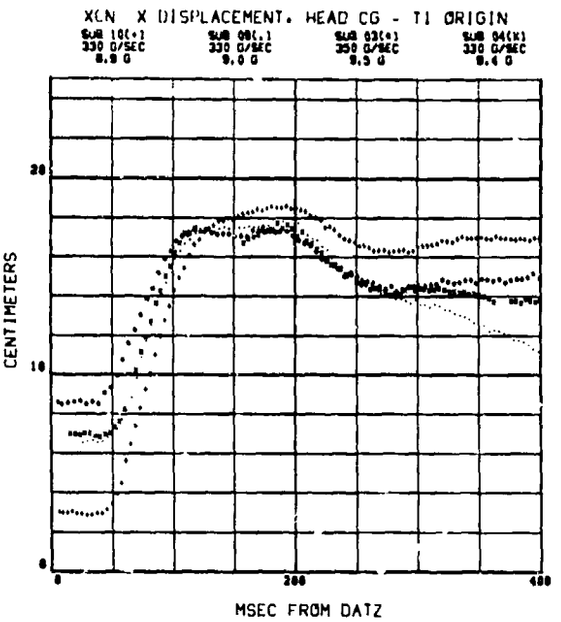

323

XCN DISPLACEMENT OF THE HEAD C.G. RELATIVE TO THE T_1 ORIGIN IN THE X DIRECTION

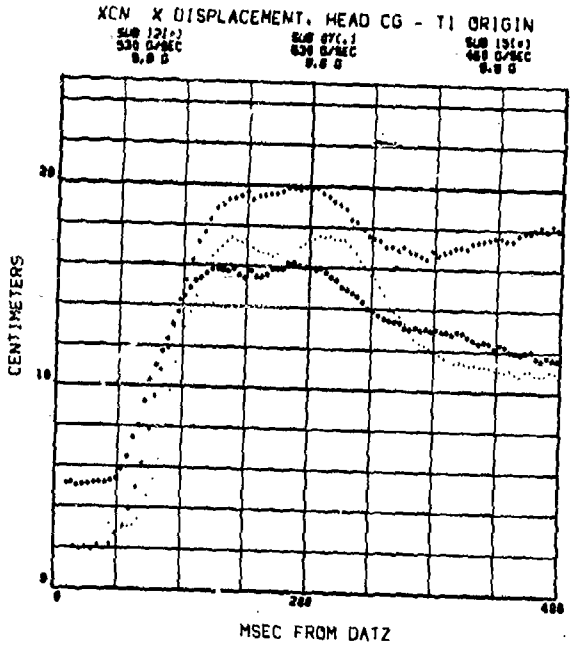

ZCN DISPLACEMENT OF THE HEAD C.G. RELATIVE TO THE T_1 ORIGIN IN THE Z DIRECTION

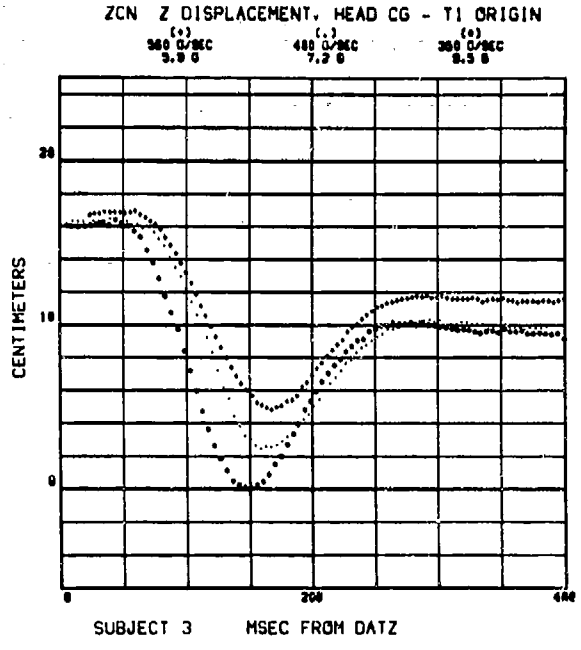

325

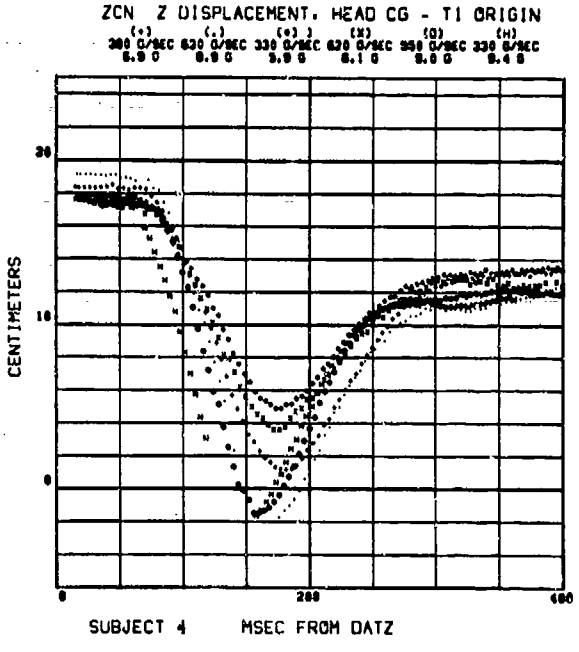

326

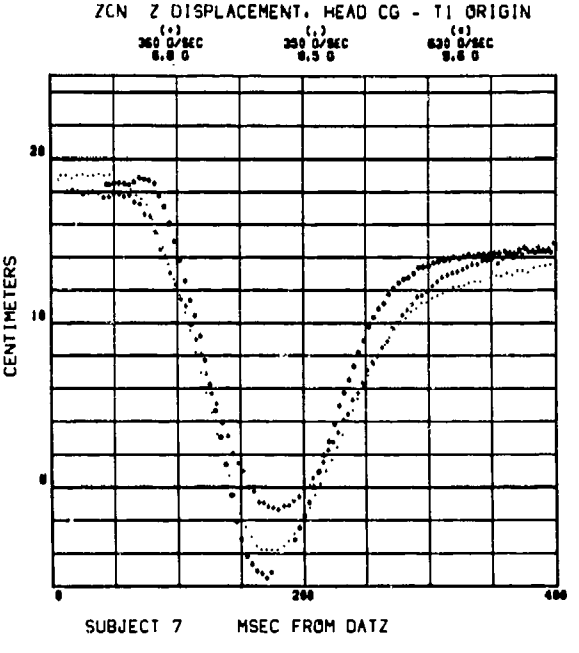

327

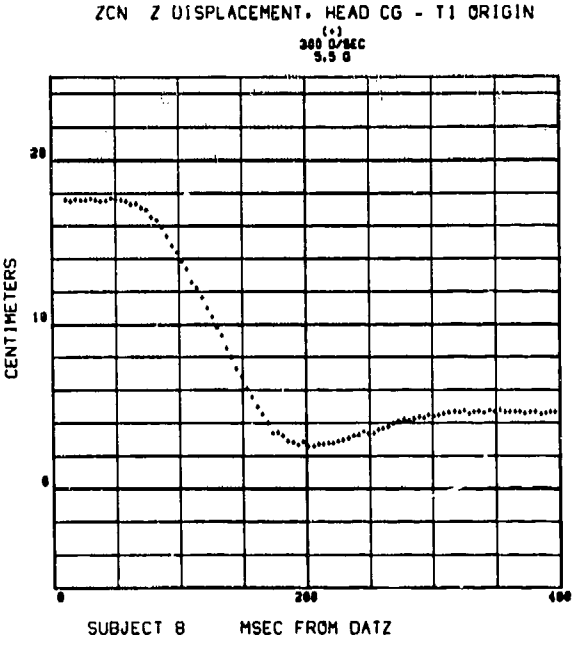

328

ZCN DISPLACEMENT OF THE HEAD C.G. RELATIVE TO THE T_1 ORIGIN IN THE Z DIRECTION

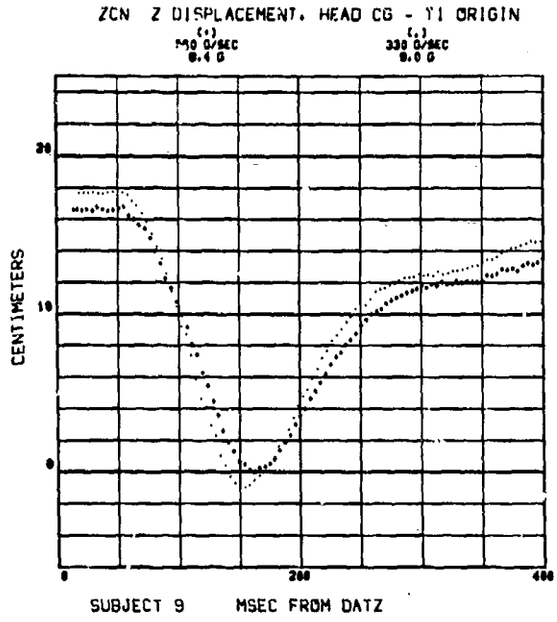

329

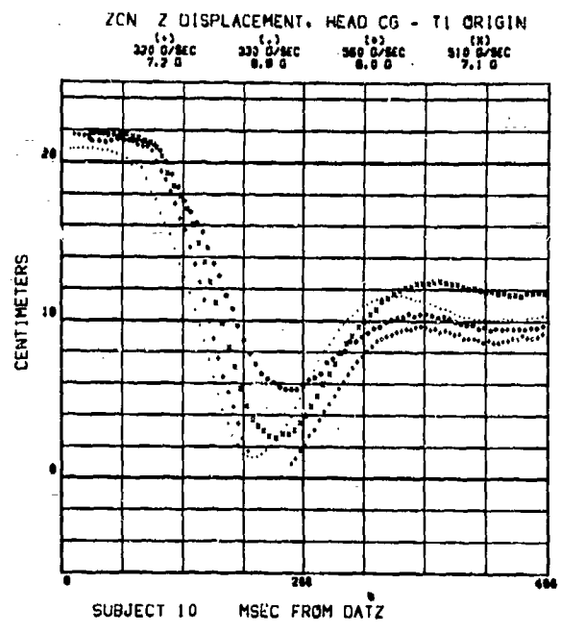

330

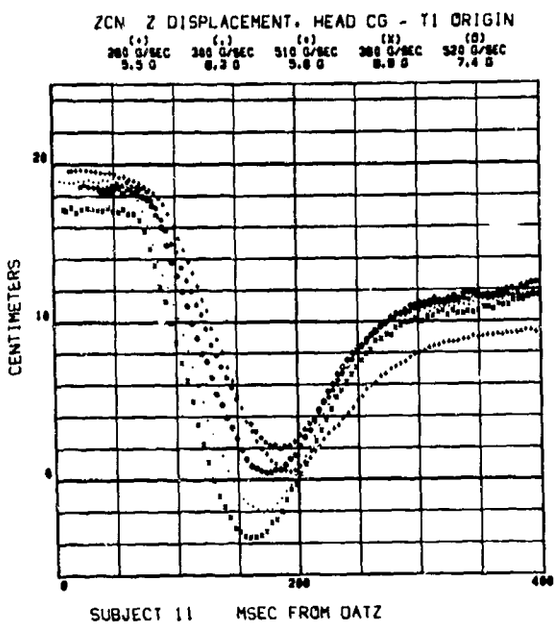

331

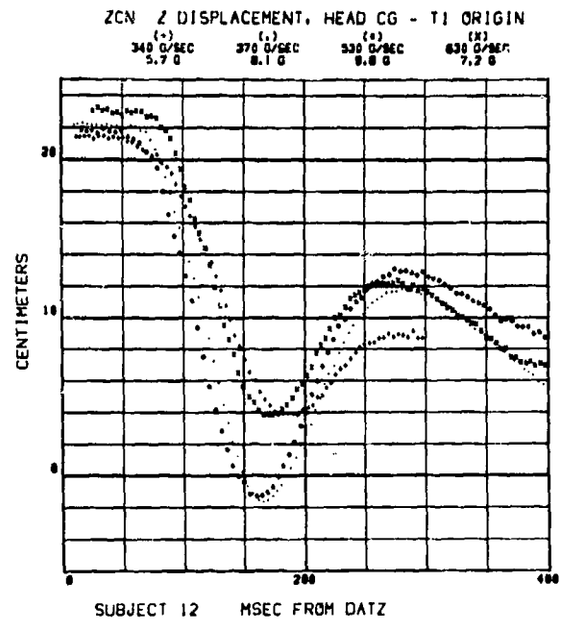

332

ZCN DISPLACEMENT OF THE HEAD C.G. RELATIVE TO THE T_1 ORIGIN IN THE Z DIRECTION

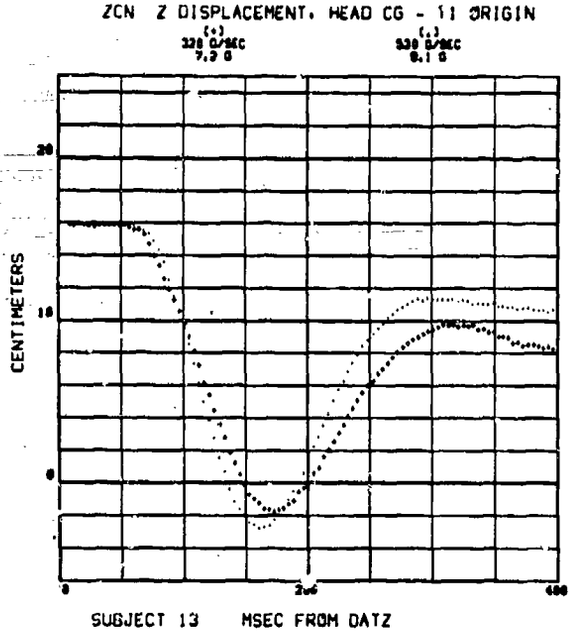

333

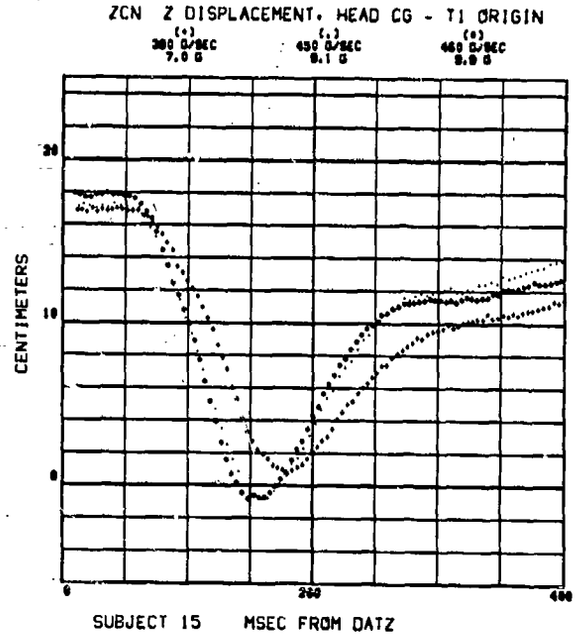

334

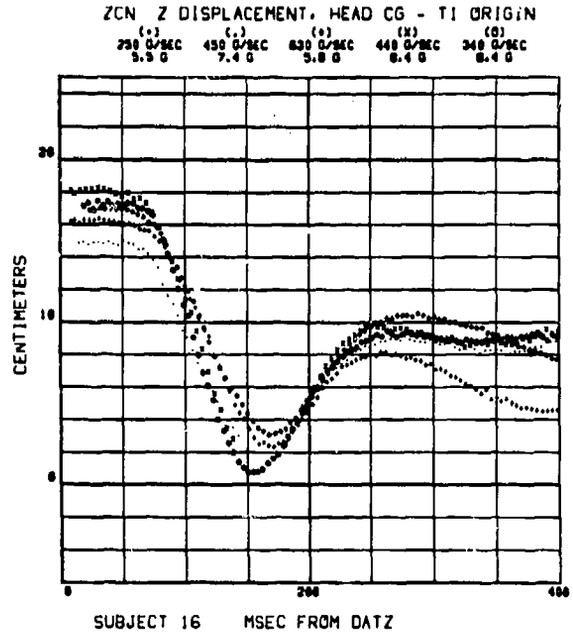

335

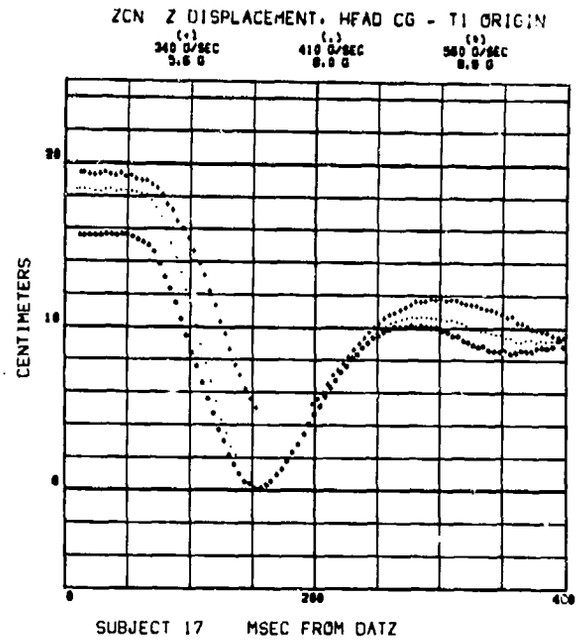

336

ZCN DISPLACEMENT OF THE HEAD C.G. RELATIVE TO THE T_1 ORIGIN IN THE Z DIRECTION

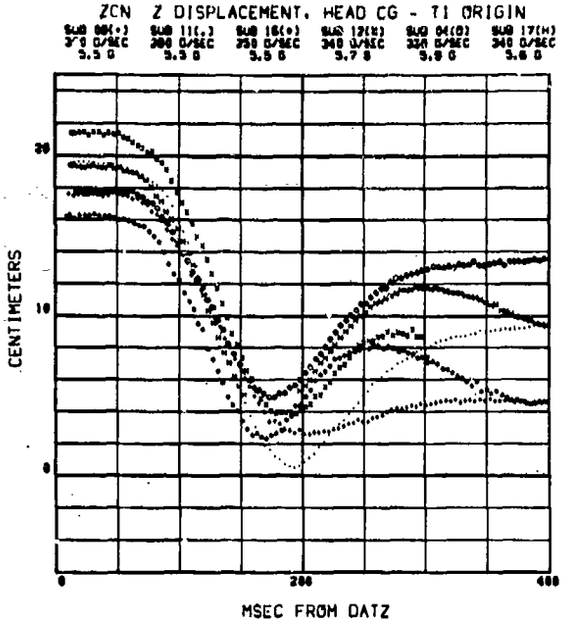

337

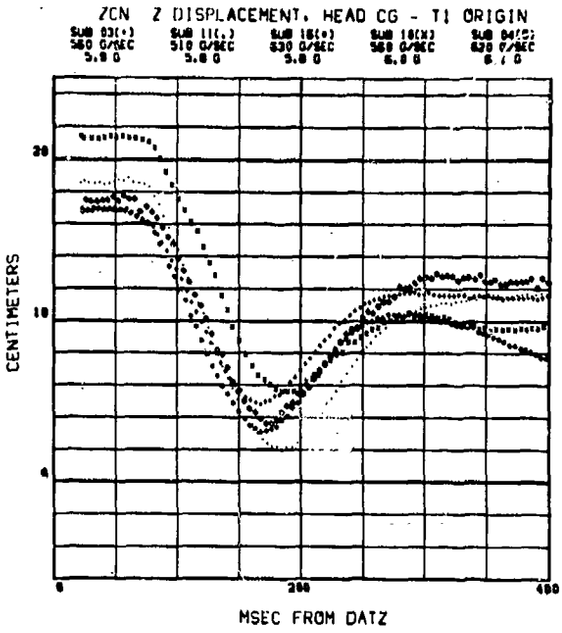

338

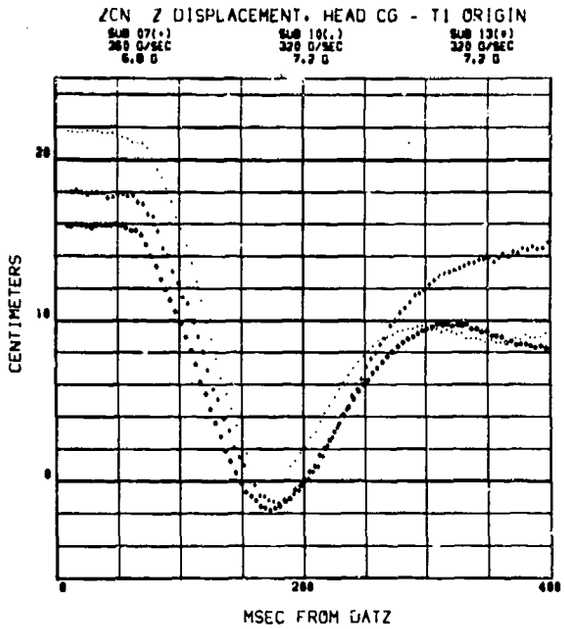

339

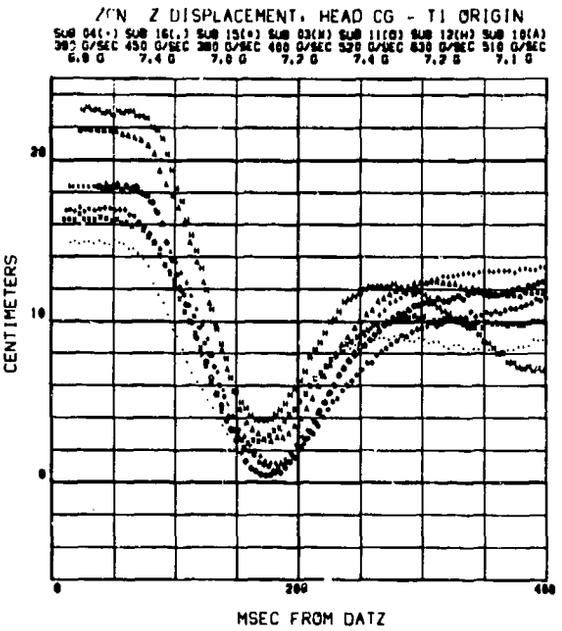

340

ZCN DISPLACEMENT OF THE HEAD C.G. RELATIVE TO THE T_1 ORIGIN IN THE Z DIRECTION

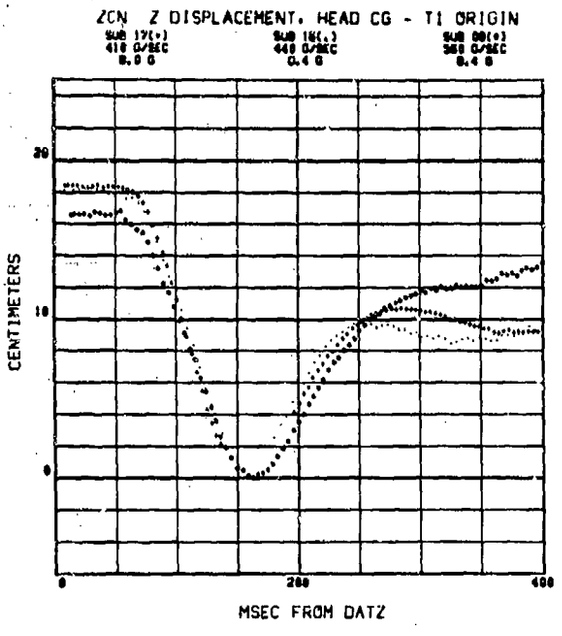

341

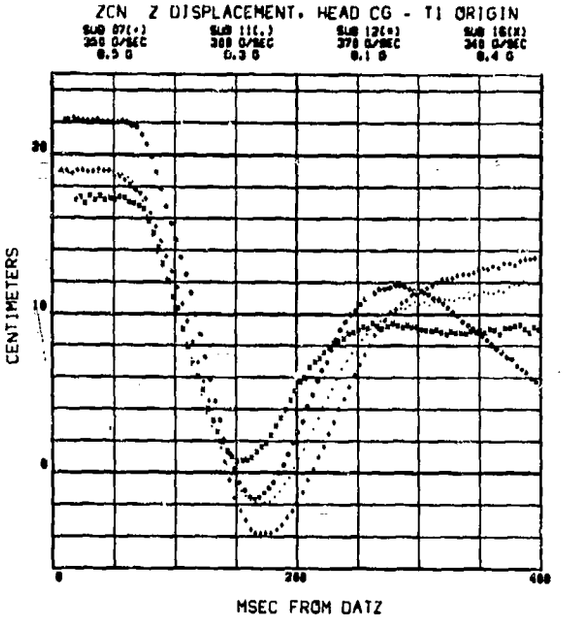

342

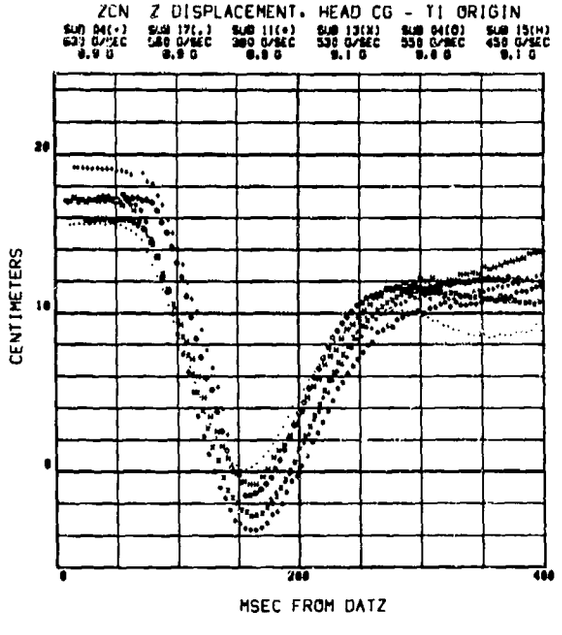

343

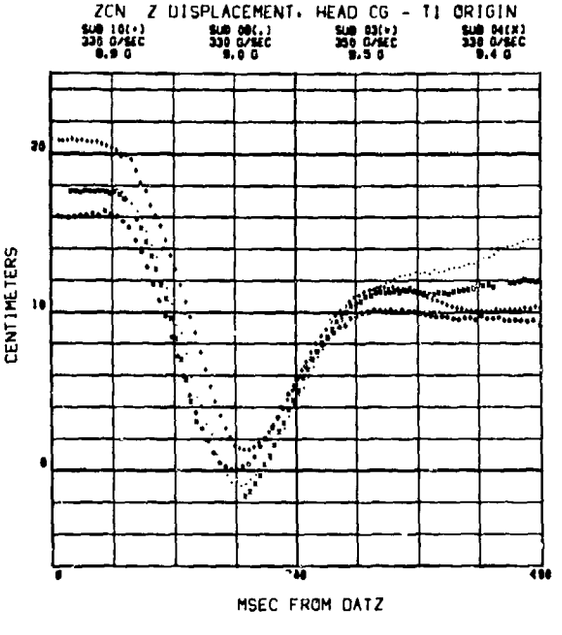

344

ZCN DISPLACEMENT OF THE HEAD C.G. RELATIVE TO THE T_1 ORIGIN IN THE Z DIRECTION

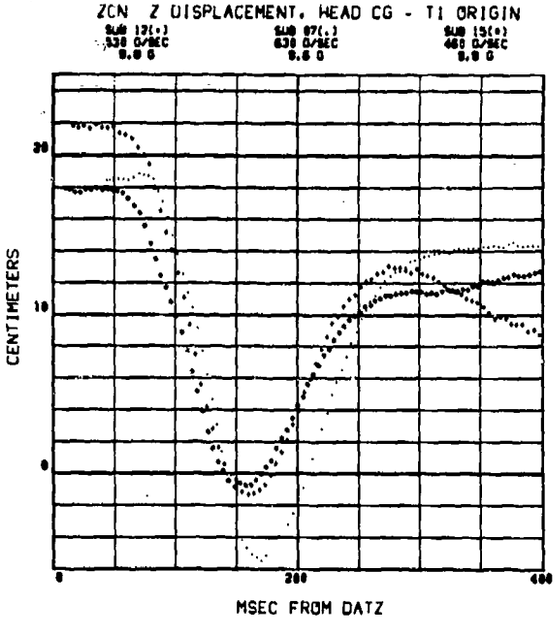

345

MCT MAGNITUDE OF THE DISPLACEMENT OF THE HEAD C.G. RELATIVE TO THE T_1 ORIGIN

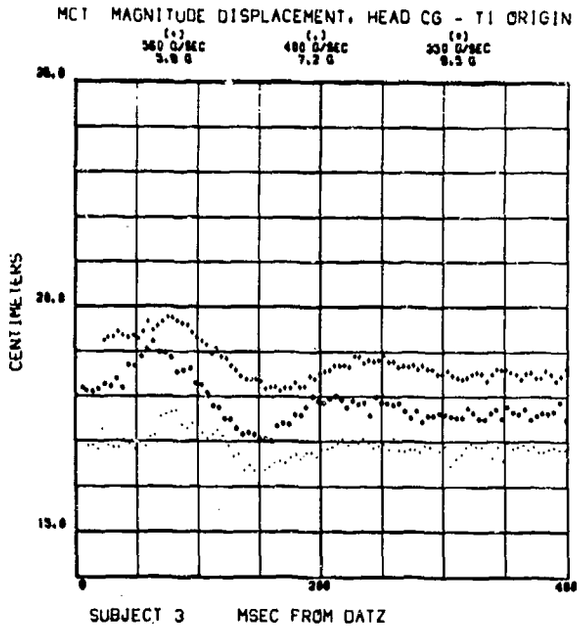

346

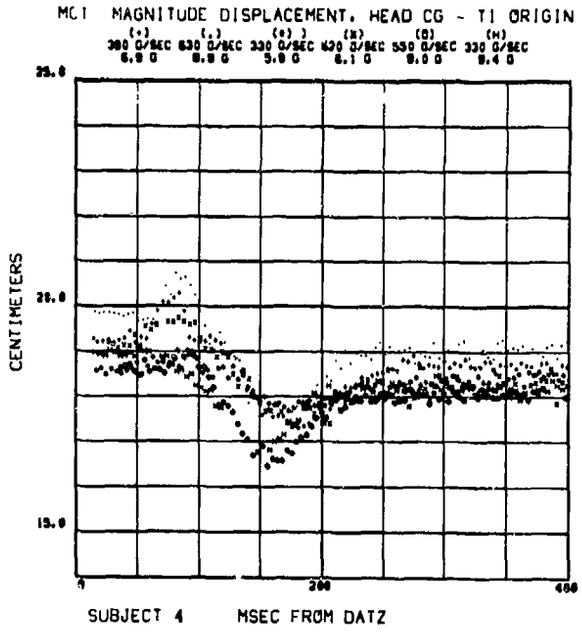

347

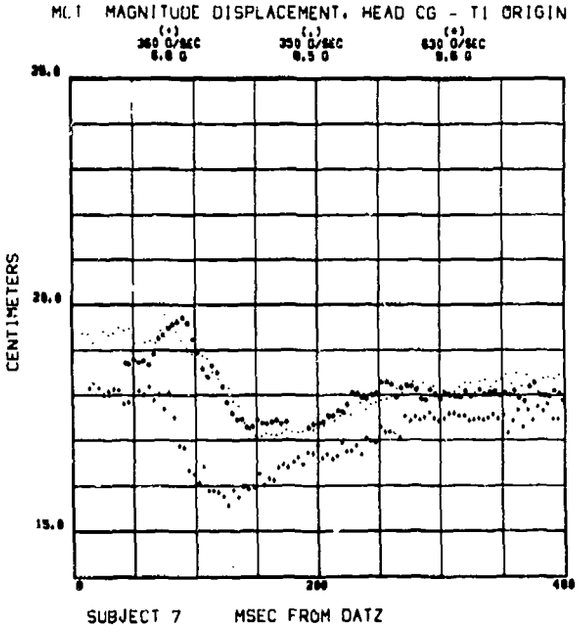

348

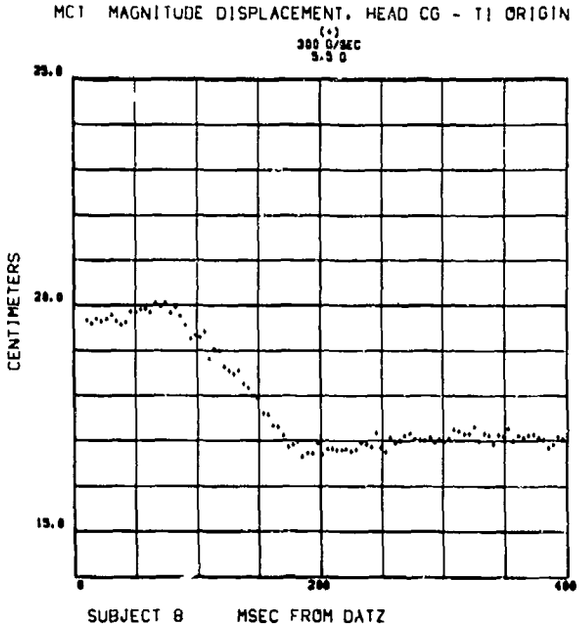

349

MCT MAGNITUDE OF THE DISPLACEMENT OF THE HEAD C.G. RELATIVE TO THE T_1 ORIGIN

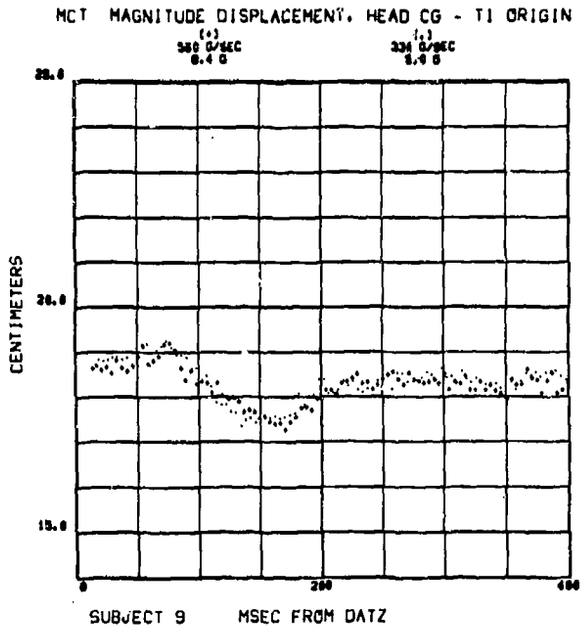

350

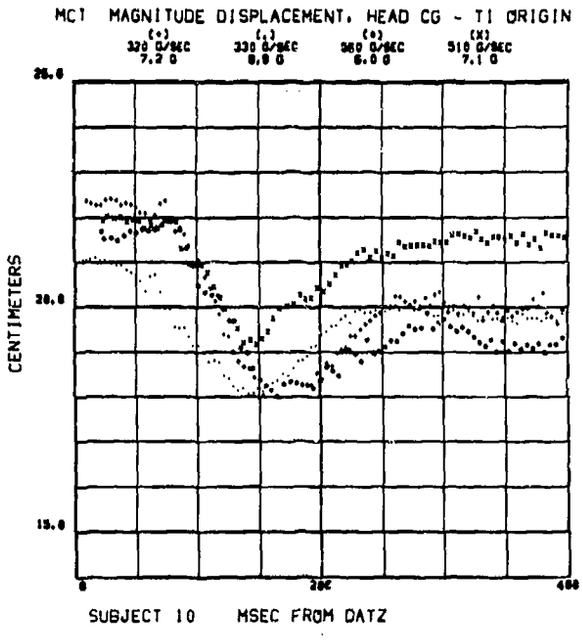

351

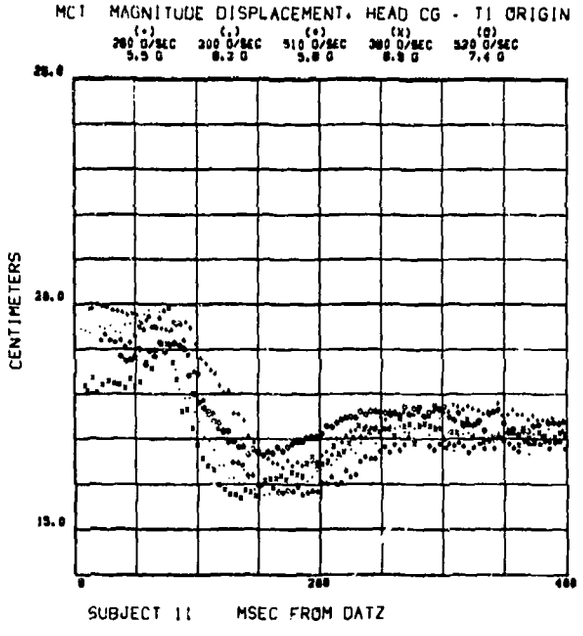

352

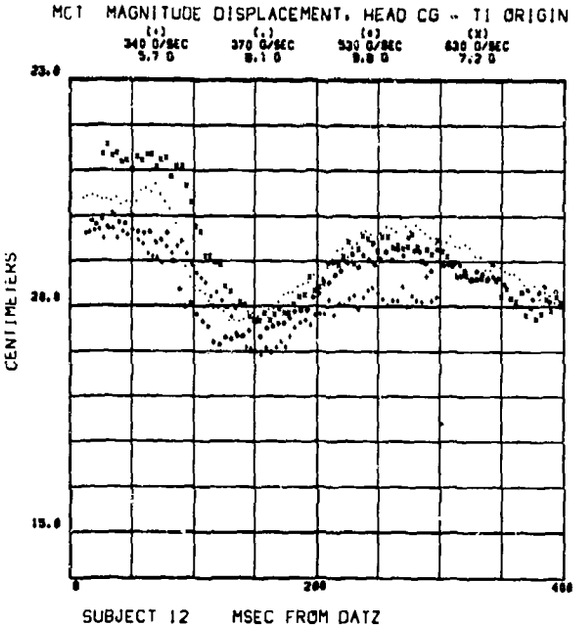

353

MCT MAGNITUDE OF THE DISPLACEMENT OF THE HEAD C.G. RELATIVE TO THE T_1 ORIGIN

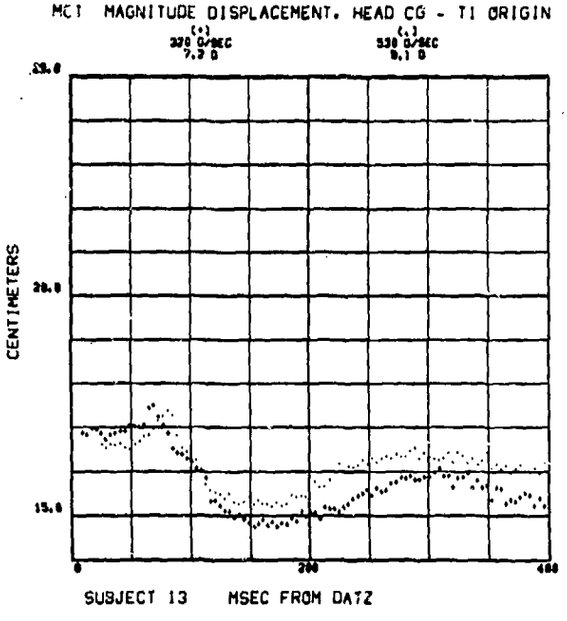

354

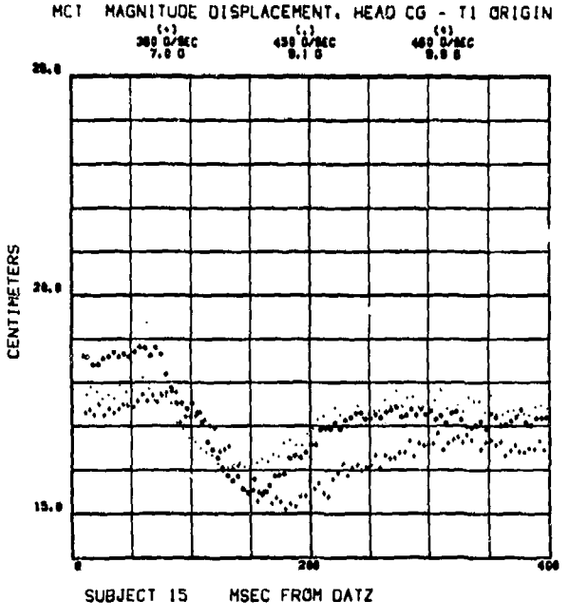

355

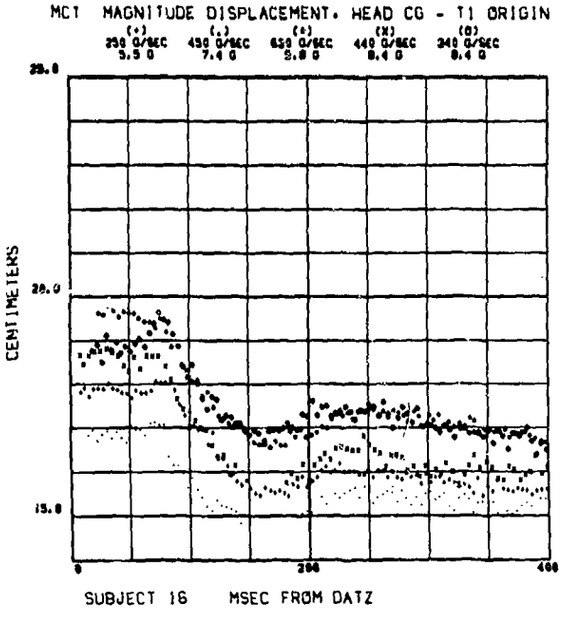

356

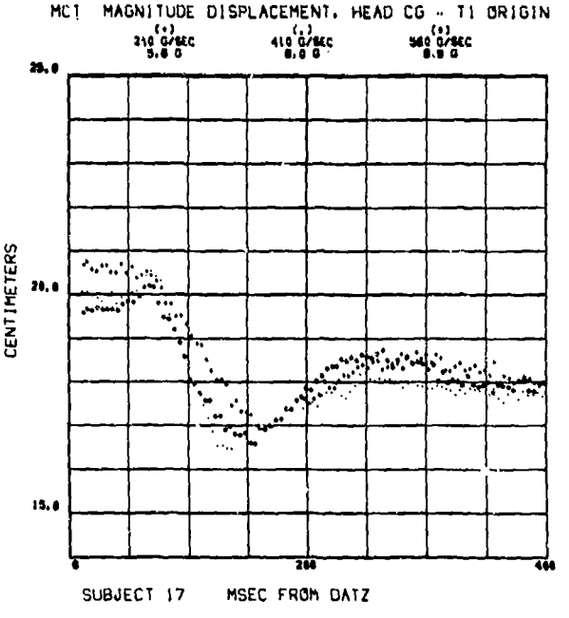

357

MCT MAGNITUDE OF THE DISPLACEMENT OF THE HEAD C.G. RELATIVE TO THE T_1 ORIGIN

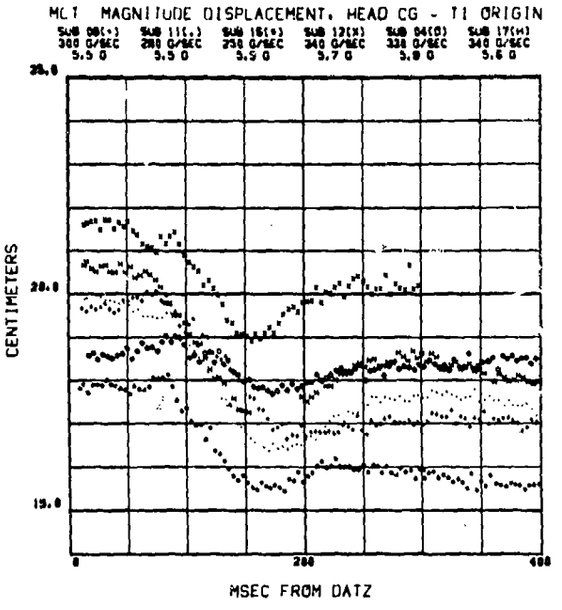

358

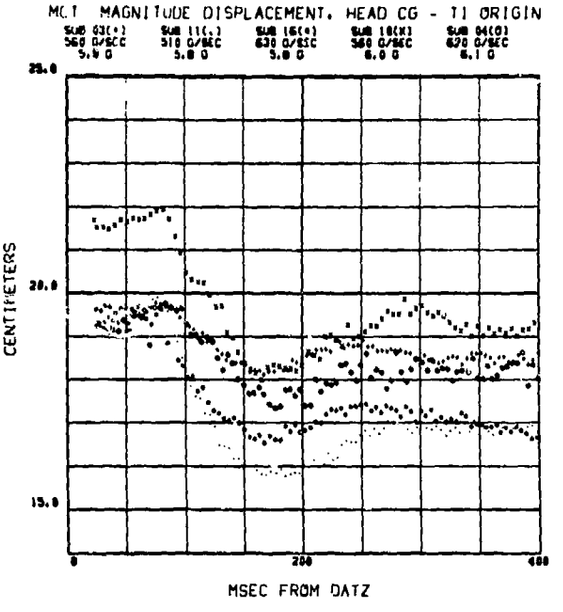

359

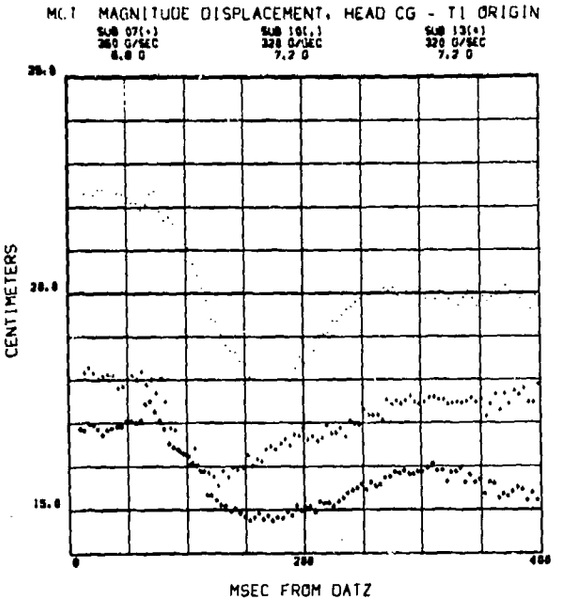

360

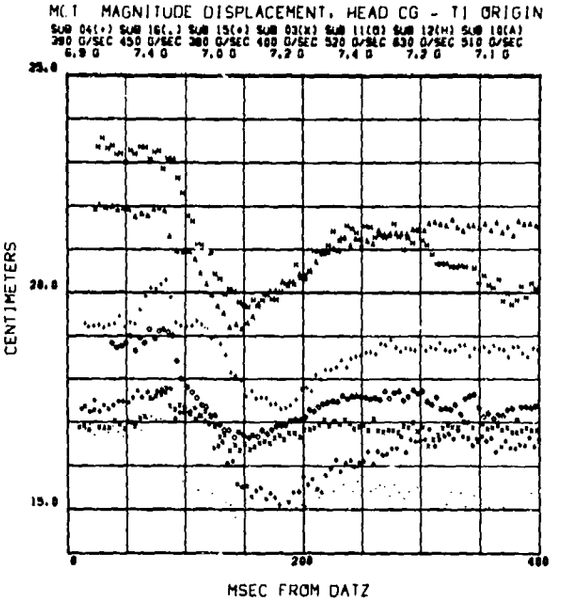

361

MCT MAGNITUDE OF THE DISPLACEMENT OF THE HEAD C.G. RELATIVE TO THE T_1 ORIGIN

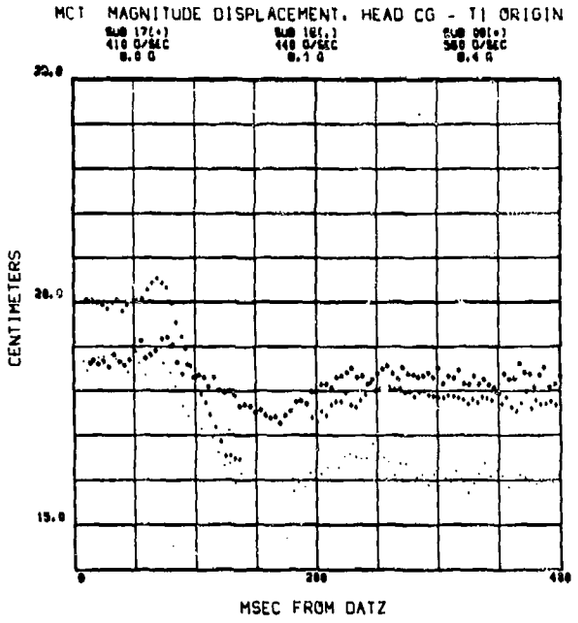

362

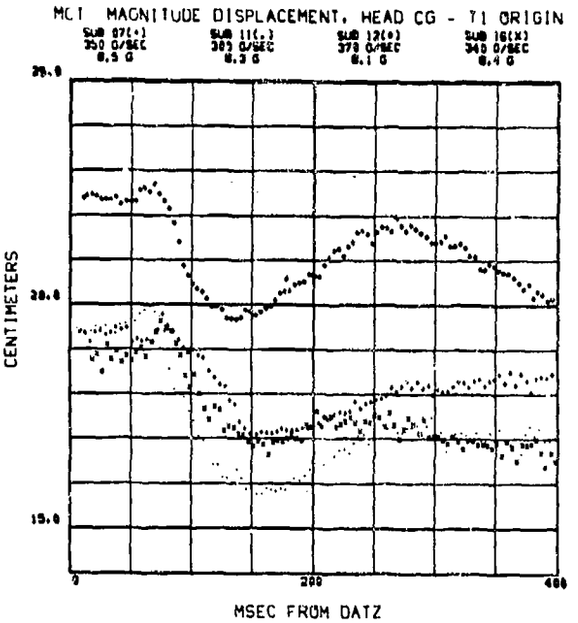

363

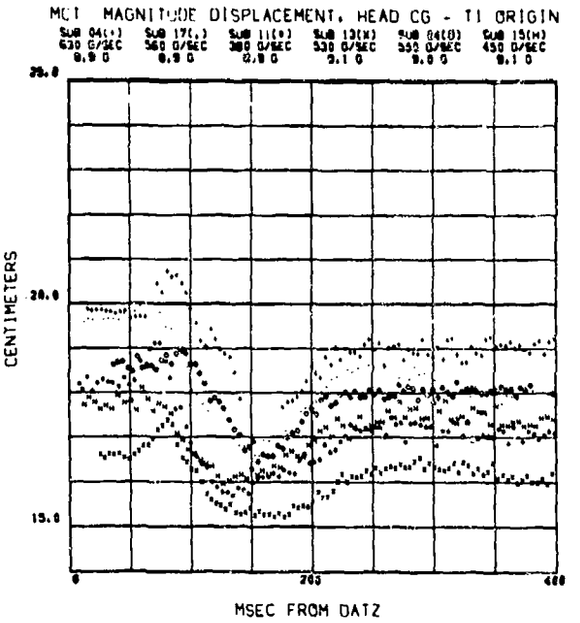

364

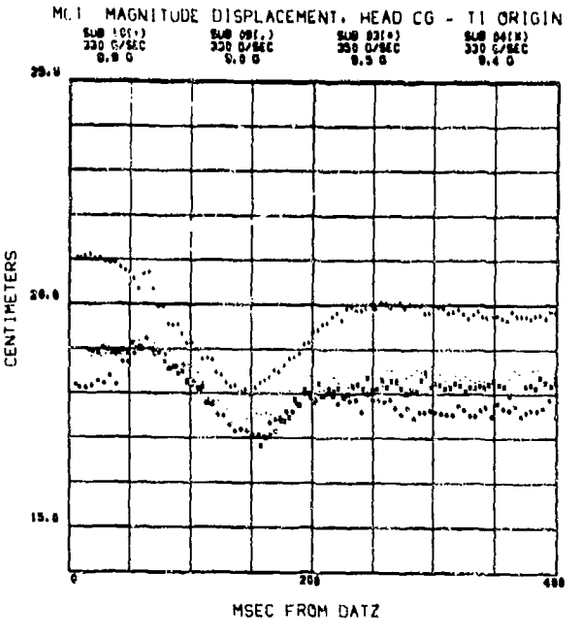

365

MCT MAGNITUDE OF THE DISPLACEMENT OF THE HEAD C.G. RELATIVE TO THE T_1 ORIGIN

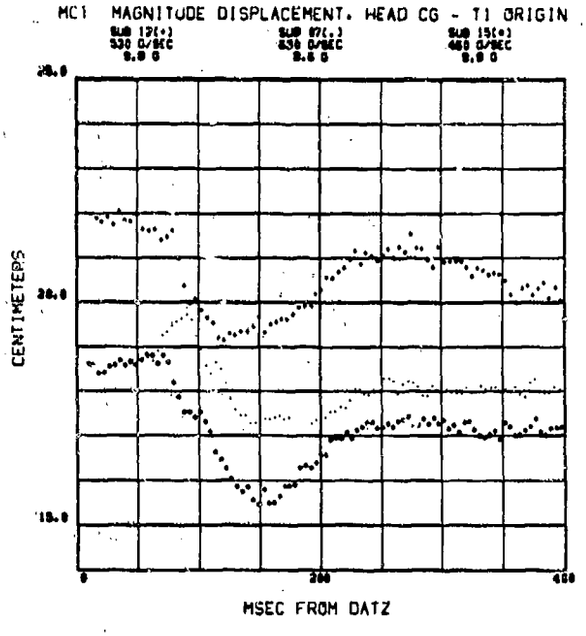

366

RAH ANGULAR ACCELERATION OF THE HEAD

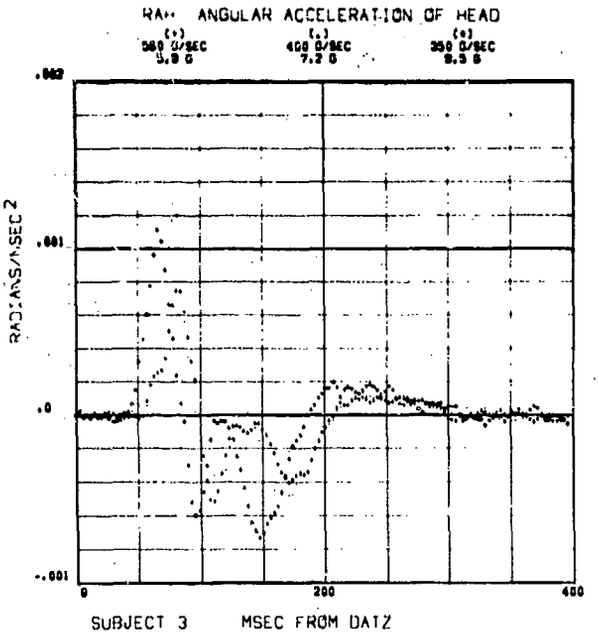

367

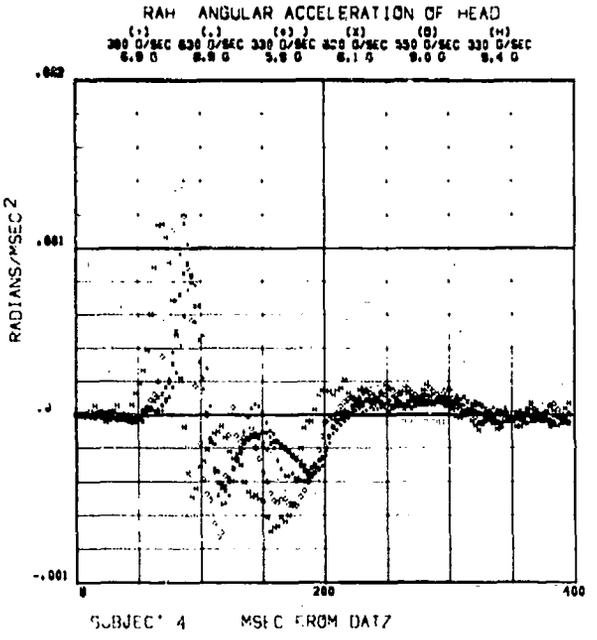

368

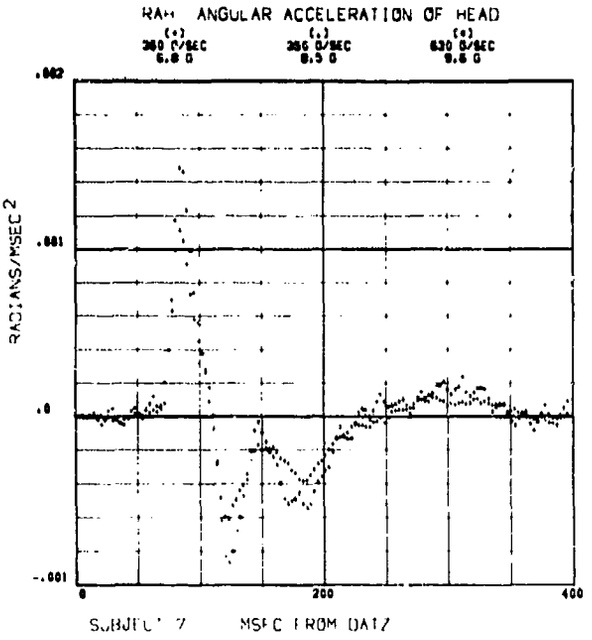

369

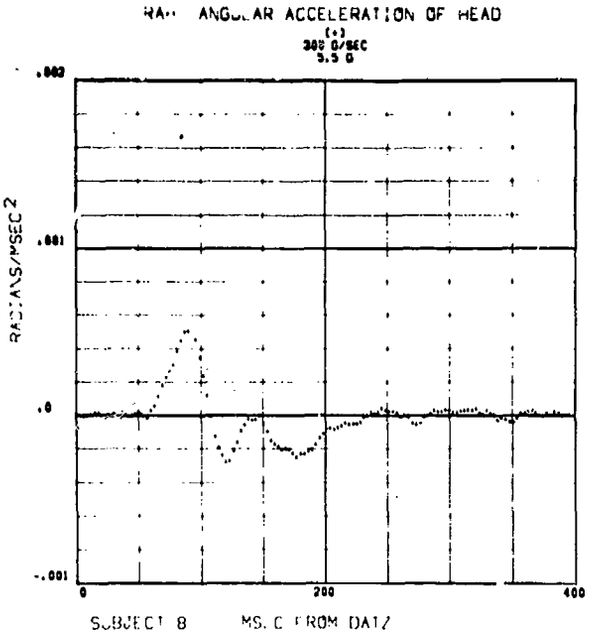

370

RAH ANGULAR ACCELERATION OF THE HEAD

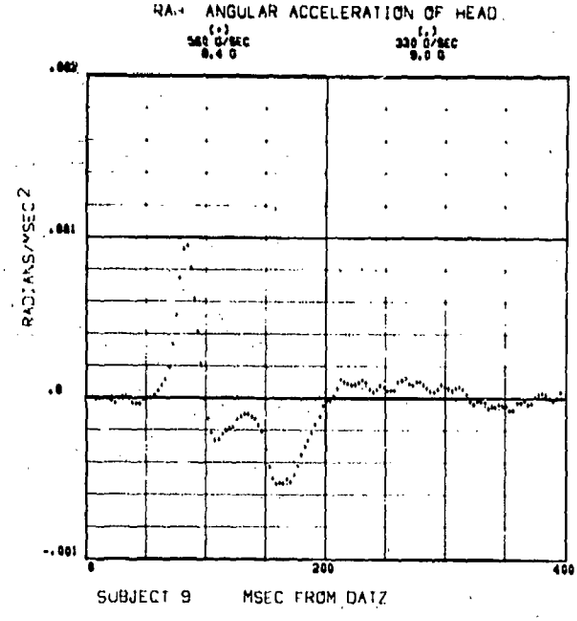

371

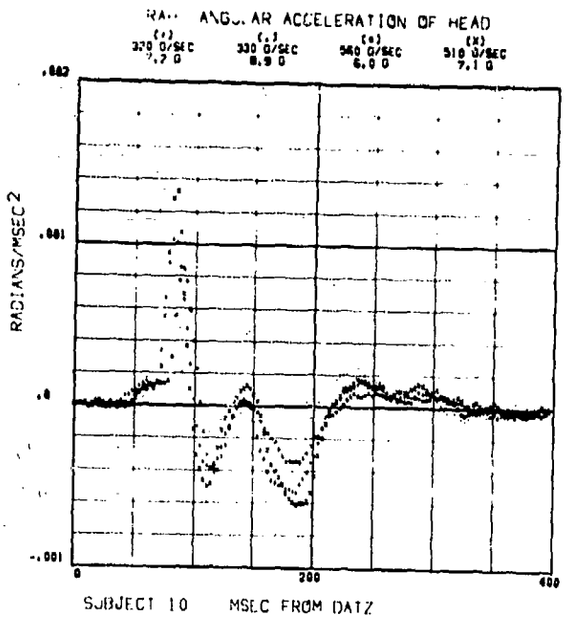

372

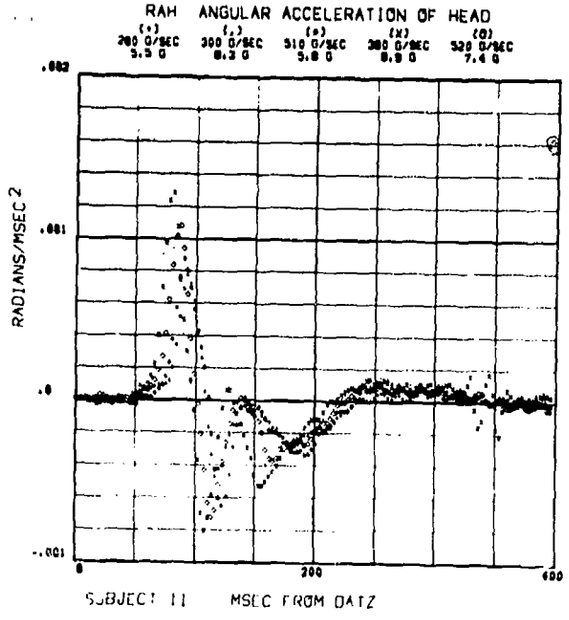

373

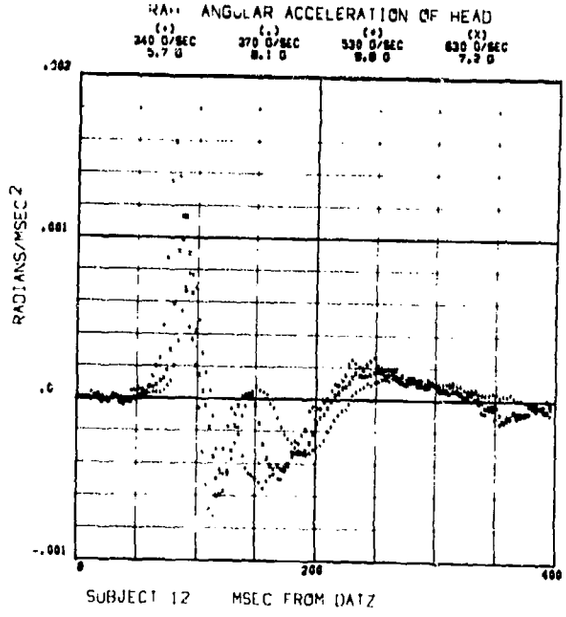

374

RAH ANGULAR ACCELERATION OF THE HEAD

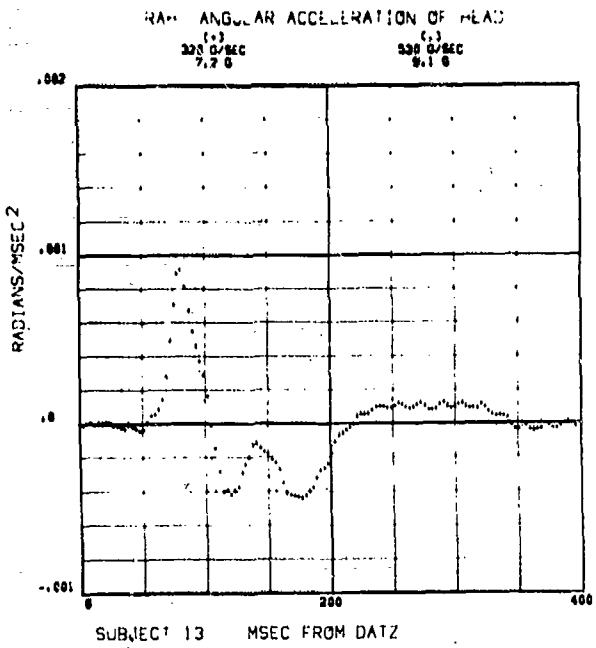

375

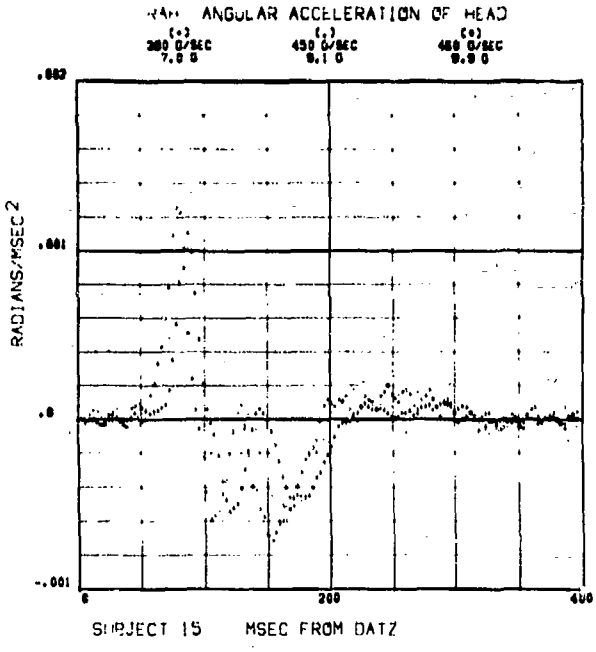

376

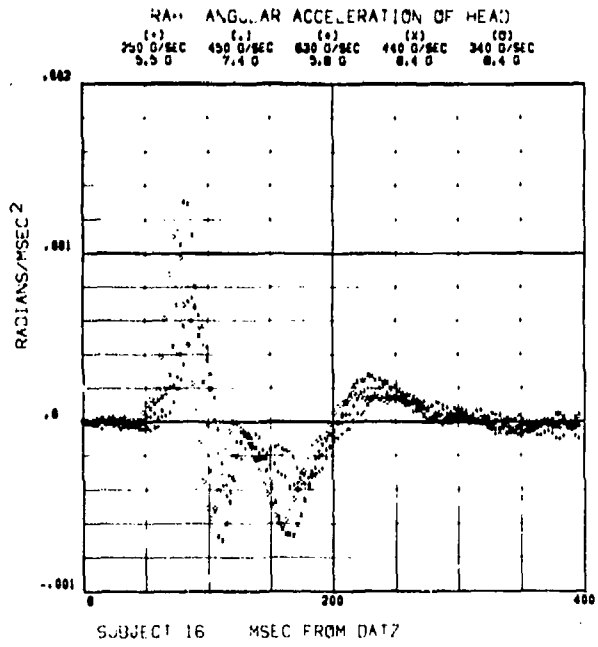

377

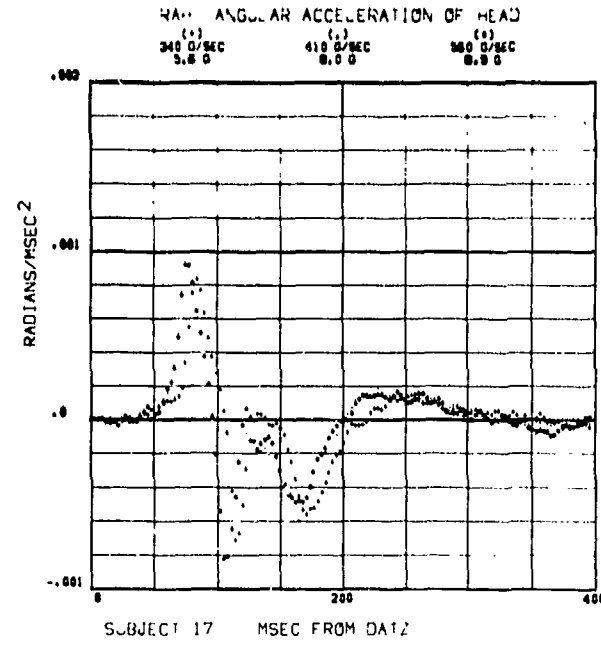

378

RAH ANGULAR ACCELERATION OF THE HEAD

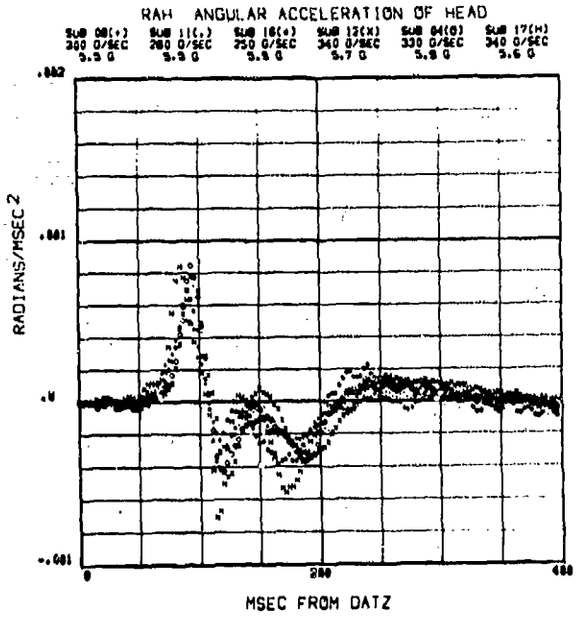

379

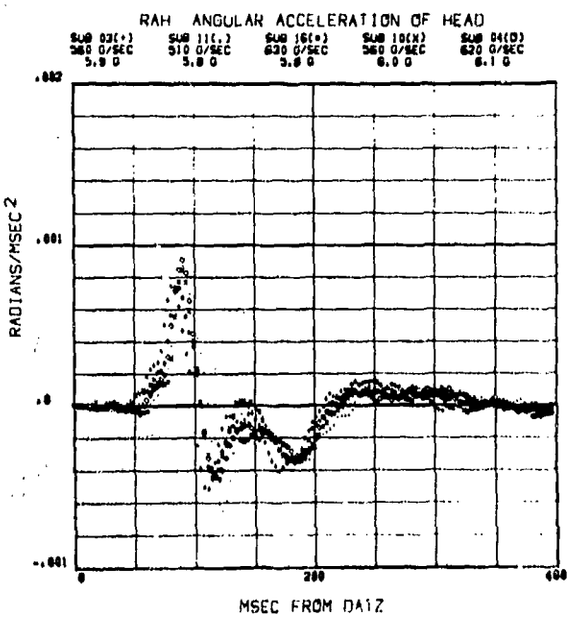

380

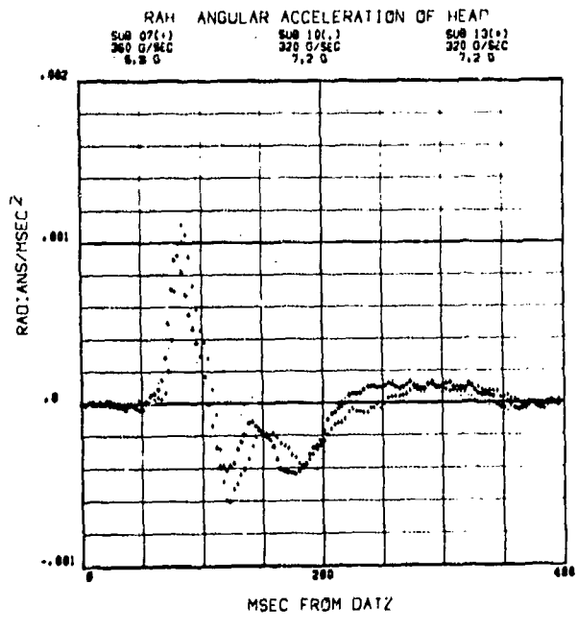

381

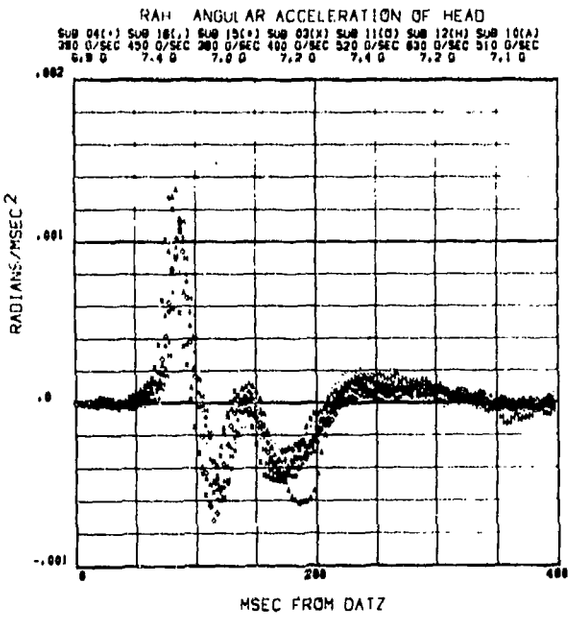

382

RAH ANGULAR ACCELERATION OF THE HEAD

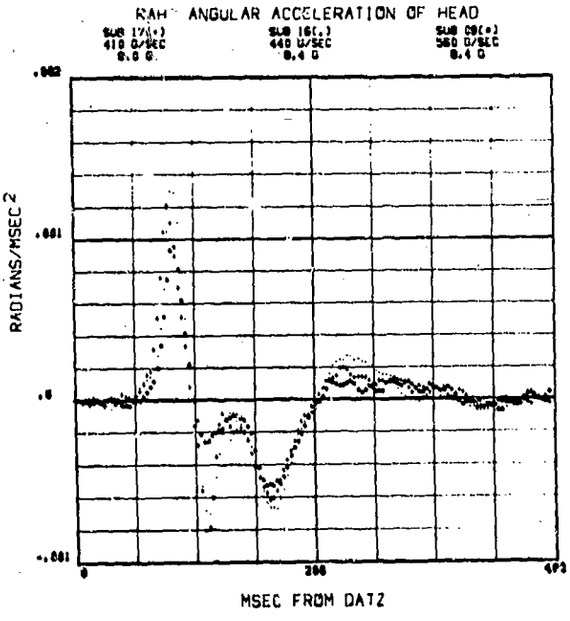

383

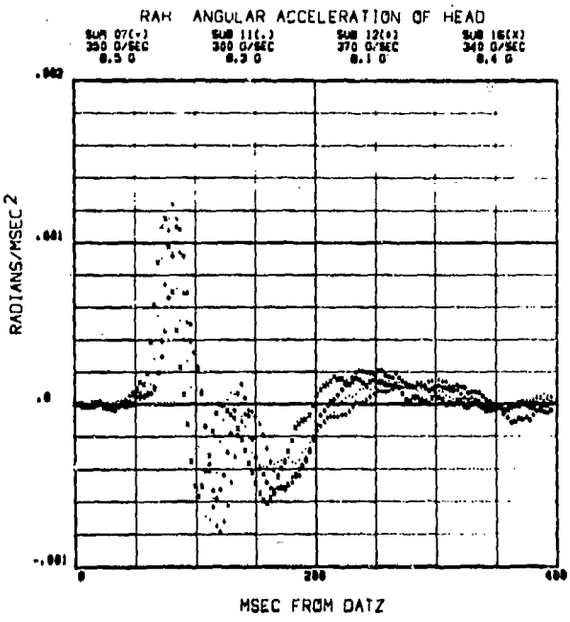

384

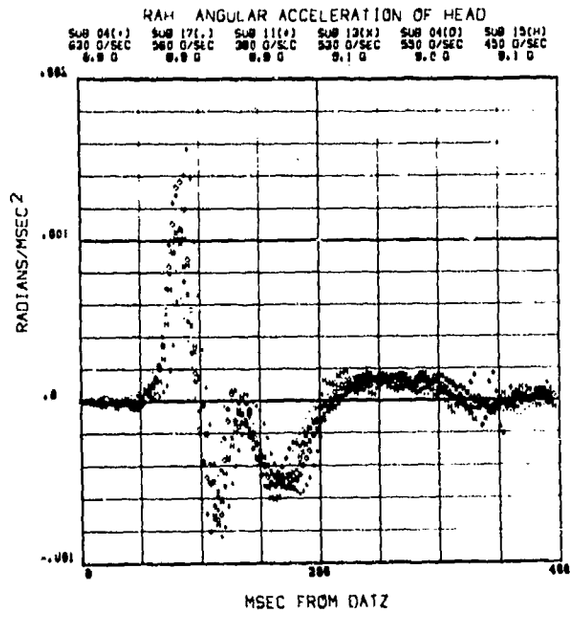

385

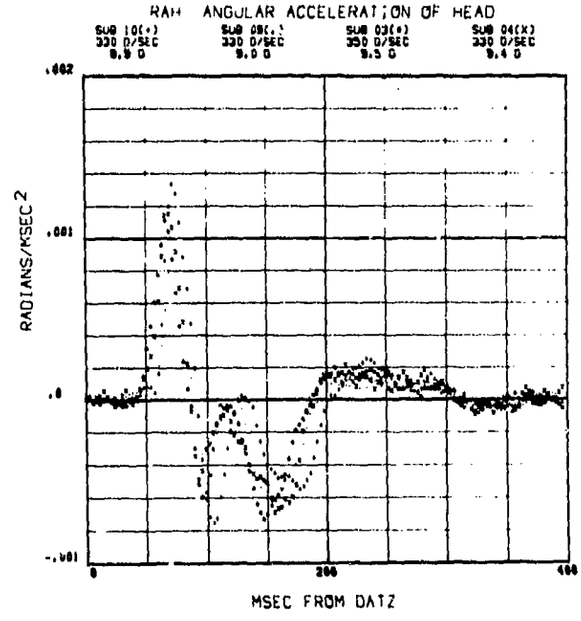

386

RAH ANGULAR ACCELERATION OF THE HEAD

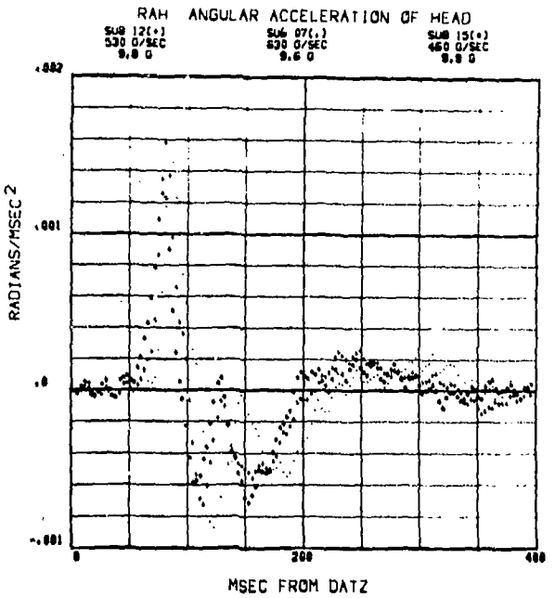

387

RVH ANGULAR VELOCITY OF HEAD

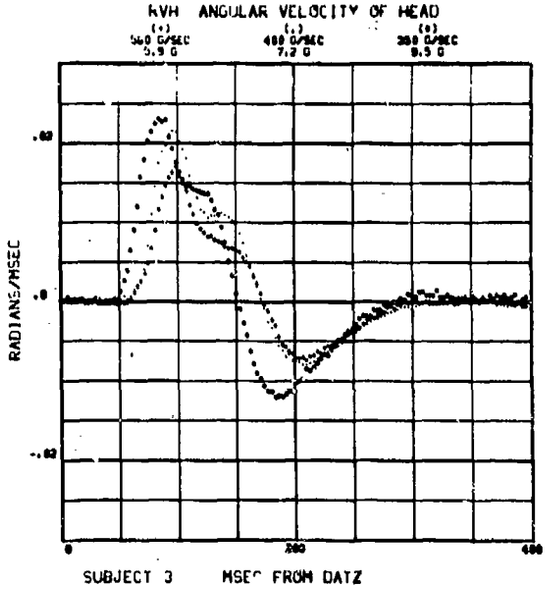

388

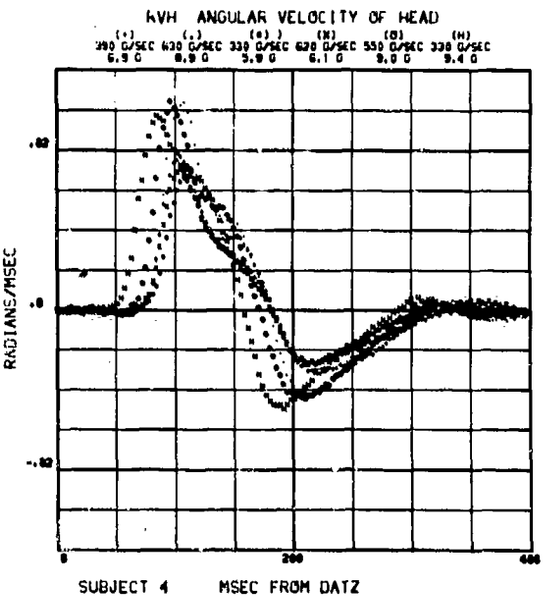

389

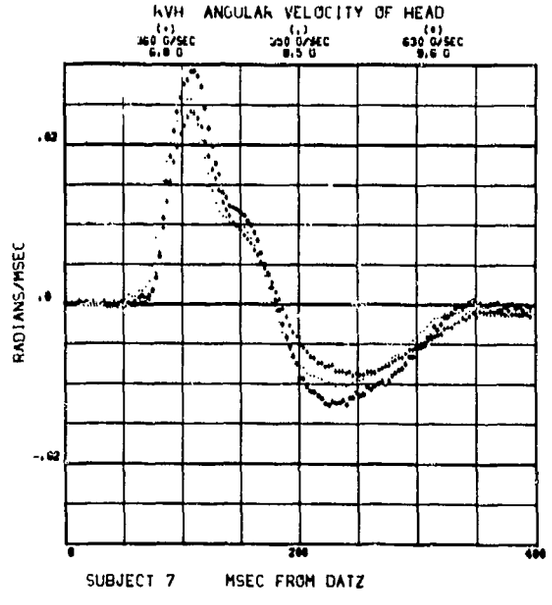

390

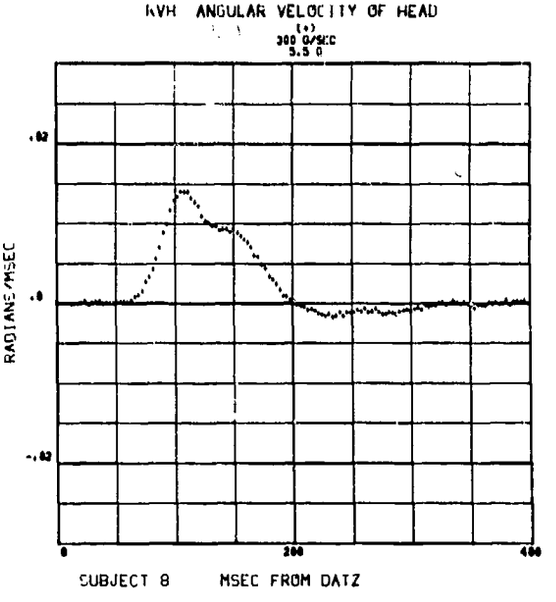

391

RVH ANGULAR VELOCITY OF THE HEAD

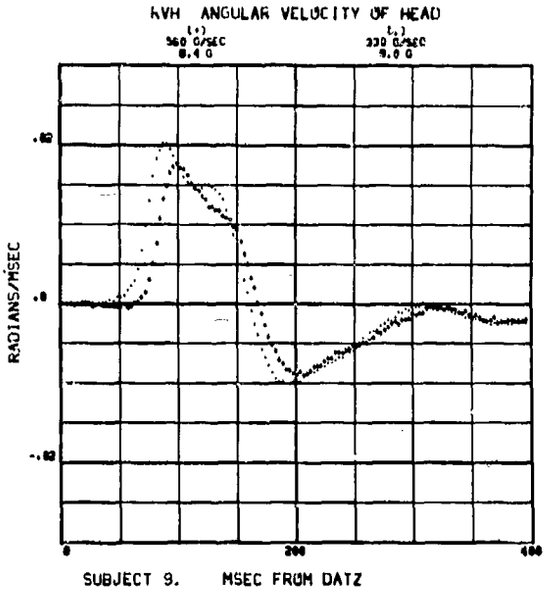

392

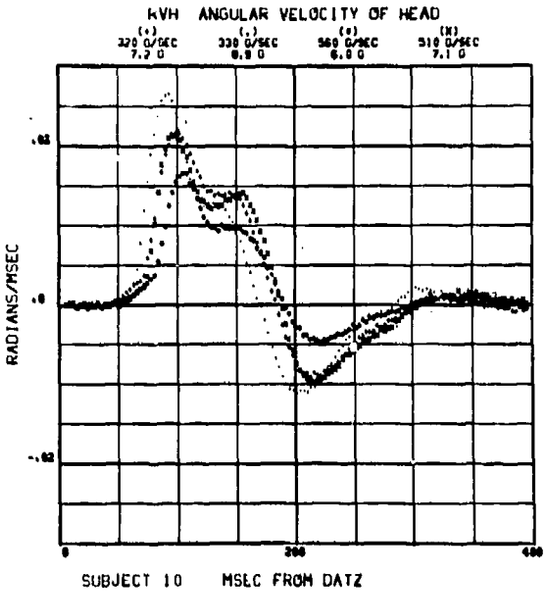

393

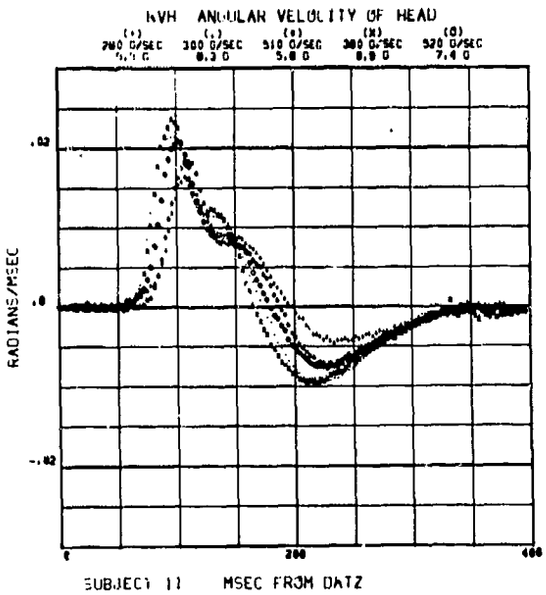

394

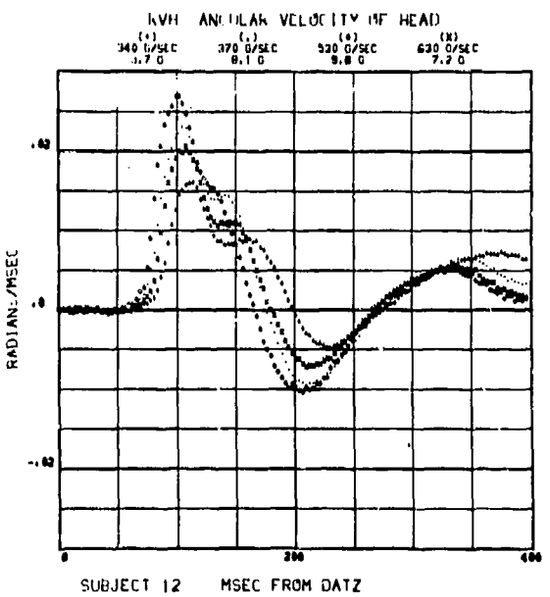

395

RVH ANGULAR VELOCITY OF THE HEAD

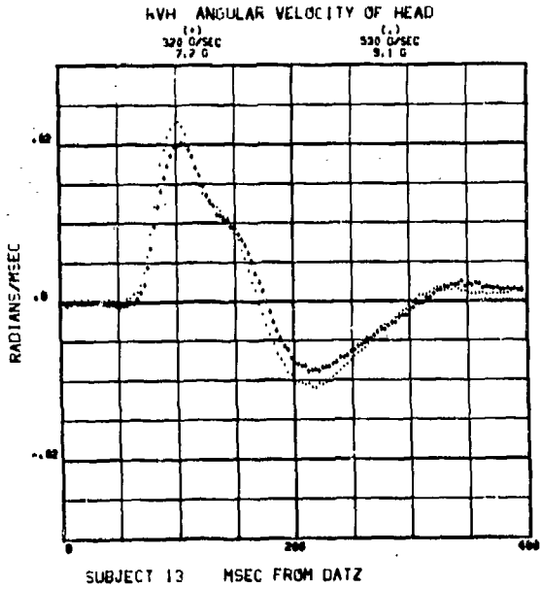

396

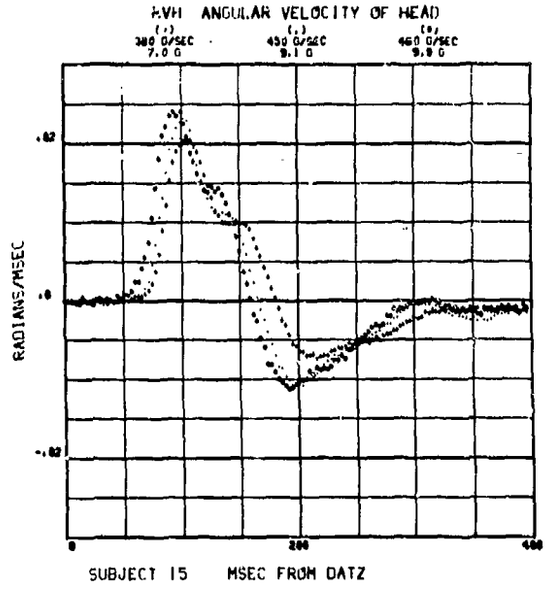

397

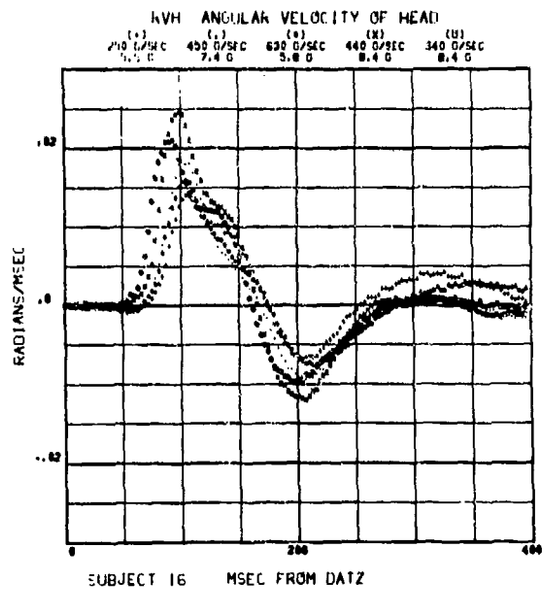

398

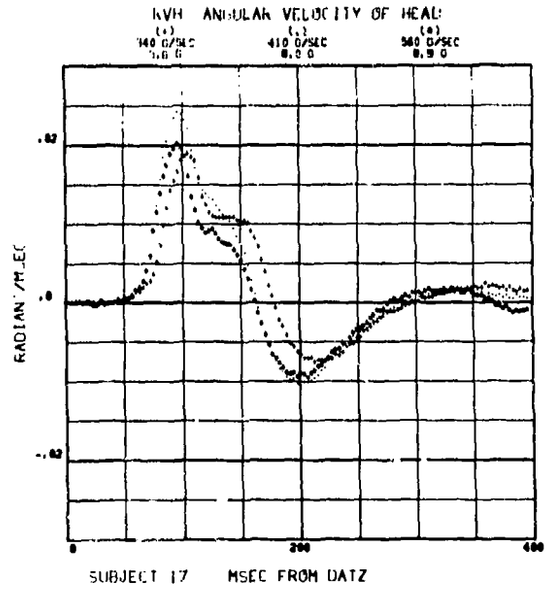

399

RVH ANGULAR VELOCITY OF THE HEAD

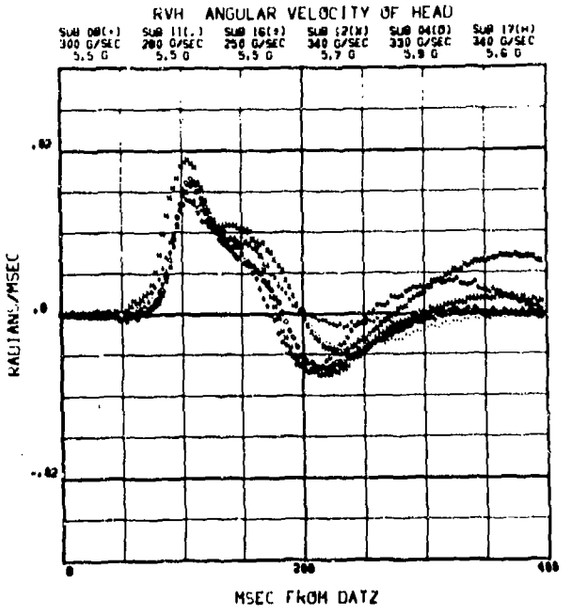

400

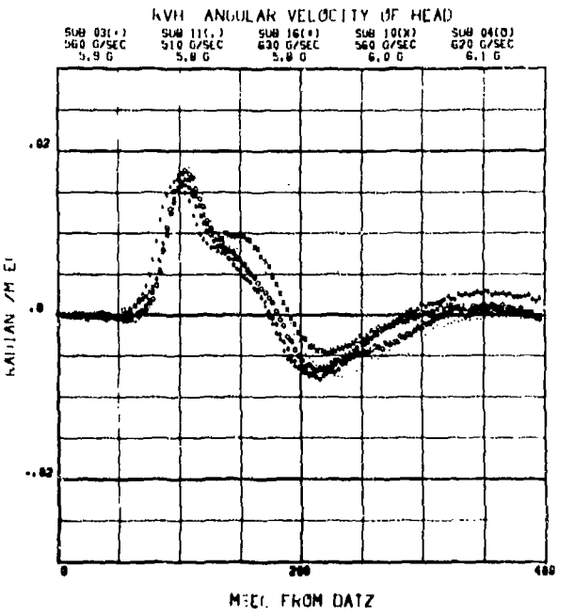

401

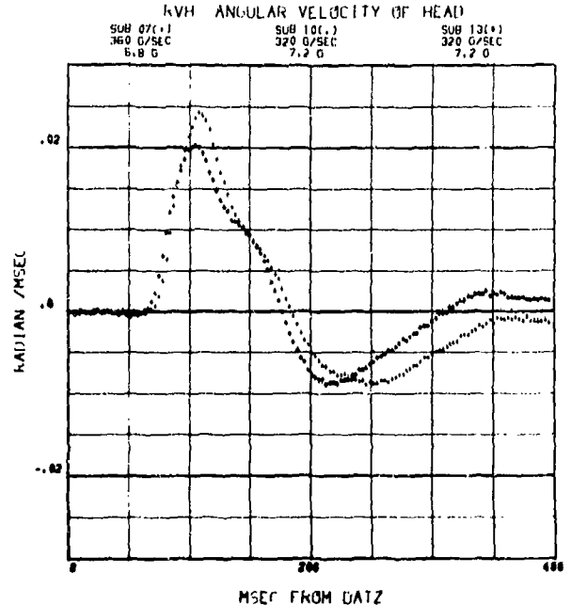

402

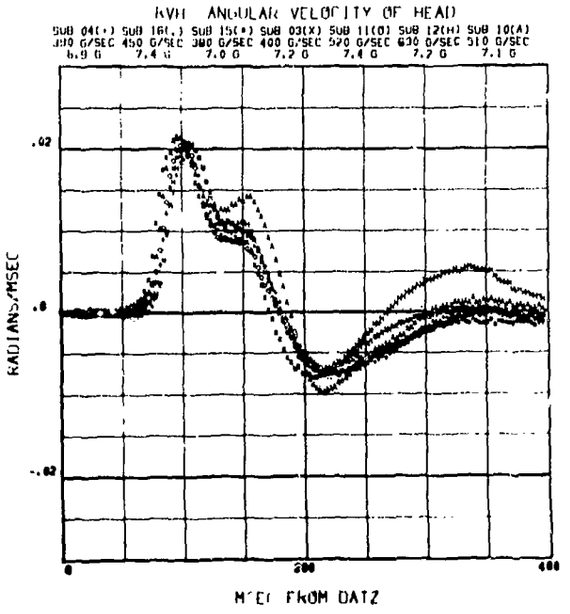

403

RVH ANGULAR VELOCITY OF THE HEAD

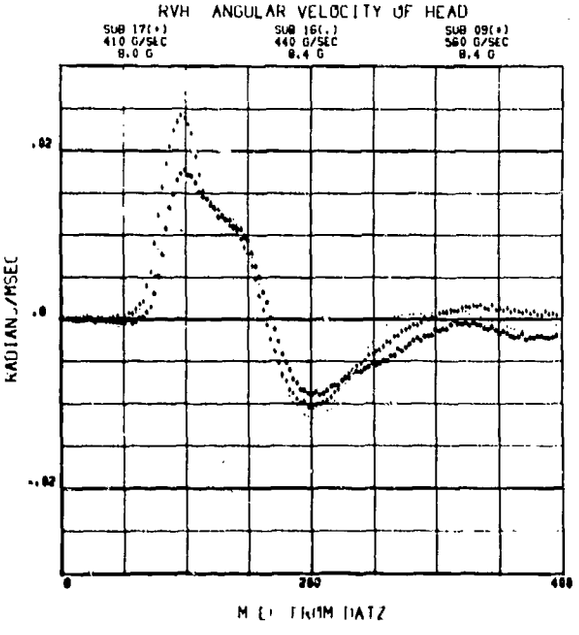

404

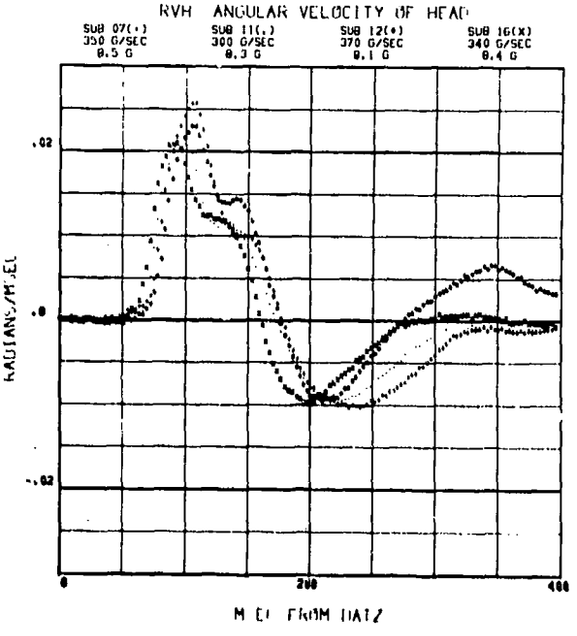

405

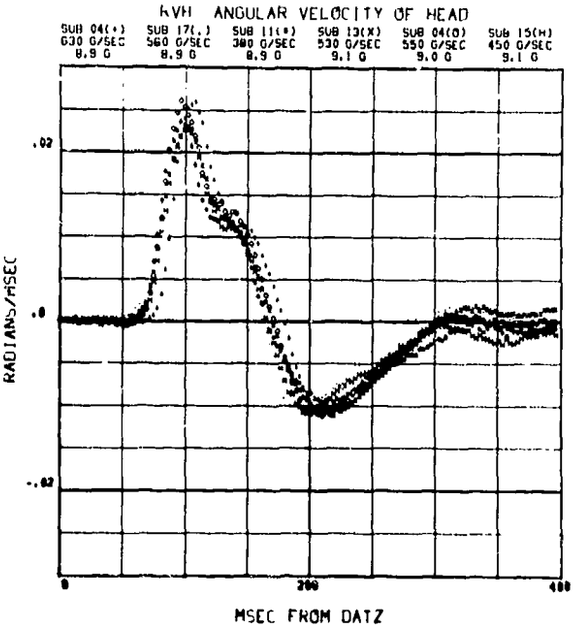

406

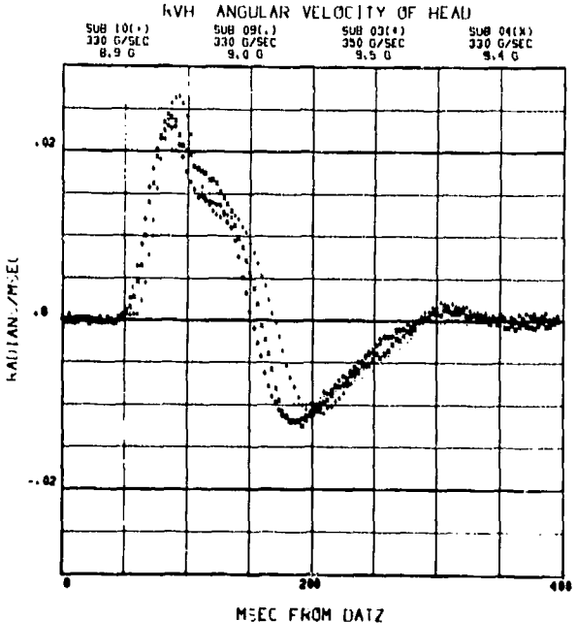

407

RVH ANGULAR VELOCITY OF THE HEAD

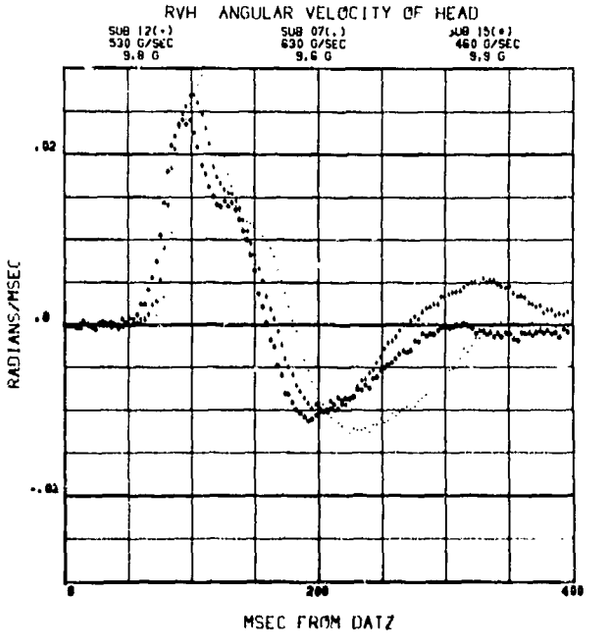

408

RHN ANGULAR VELOCITY OF THE HEAD RELATIVE TO T_1

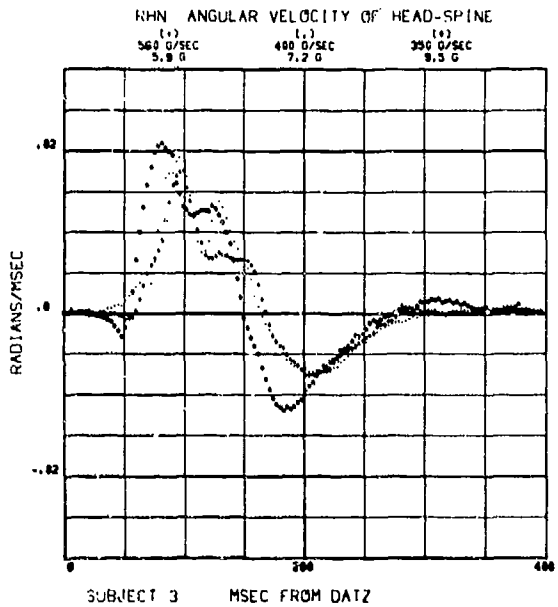

409

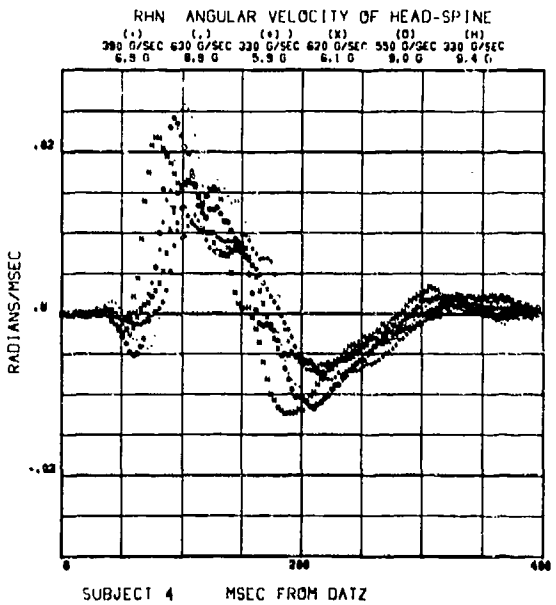

410

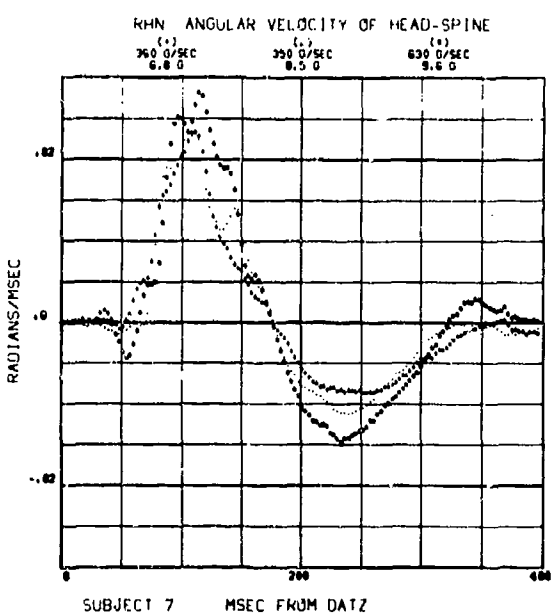

411

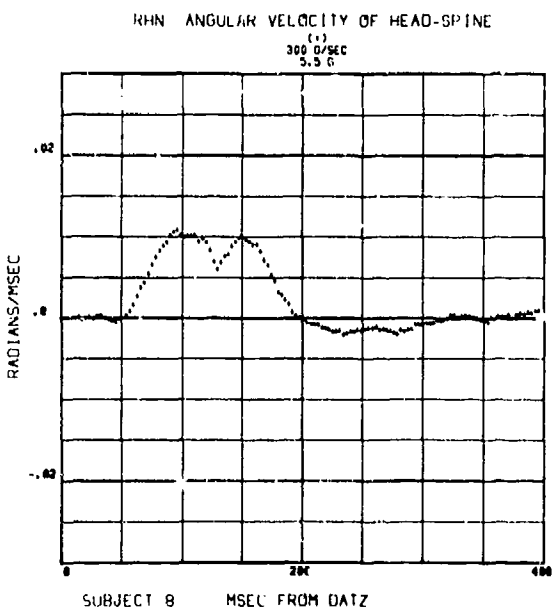

412

2. A check was made to eliminate any data having a camera timer reading prior to DPTZ (see program DSCALE). This insures the same beginning point for sensor and photographic data.

3. A check was made for missing or out of order data cards. Missing or out of order data cards aborted the run.

4. The horizontal and vertical scaling constants were applied respectively to each of the X and Z coordinates.

5. An output digital tape was written containing the X and Z scaled coordinates and the corresponding times. These tapes as well as all the photo data cards were and are maintained as a primary reference.

No interpolation was done for photographic data. When a photographic target was temporarily obscured by subject's anatomy or for any other reason, the readings for all frames affected were deleted. This can be observed in the plots of PDH vs RDH. Plots 639, 641, 644, 670, 671 and 672 are examples.

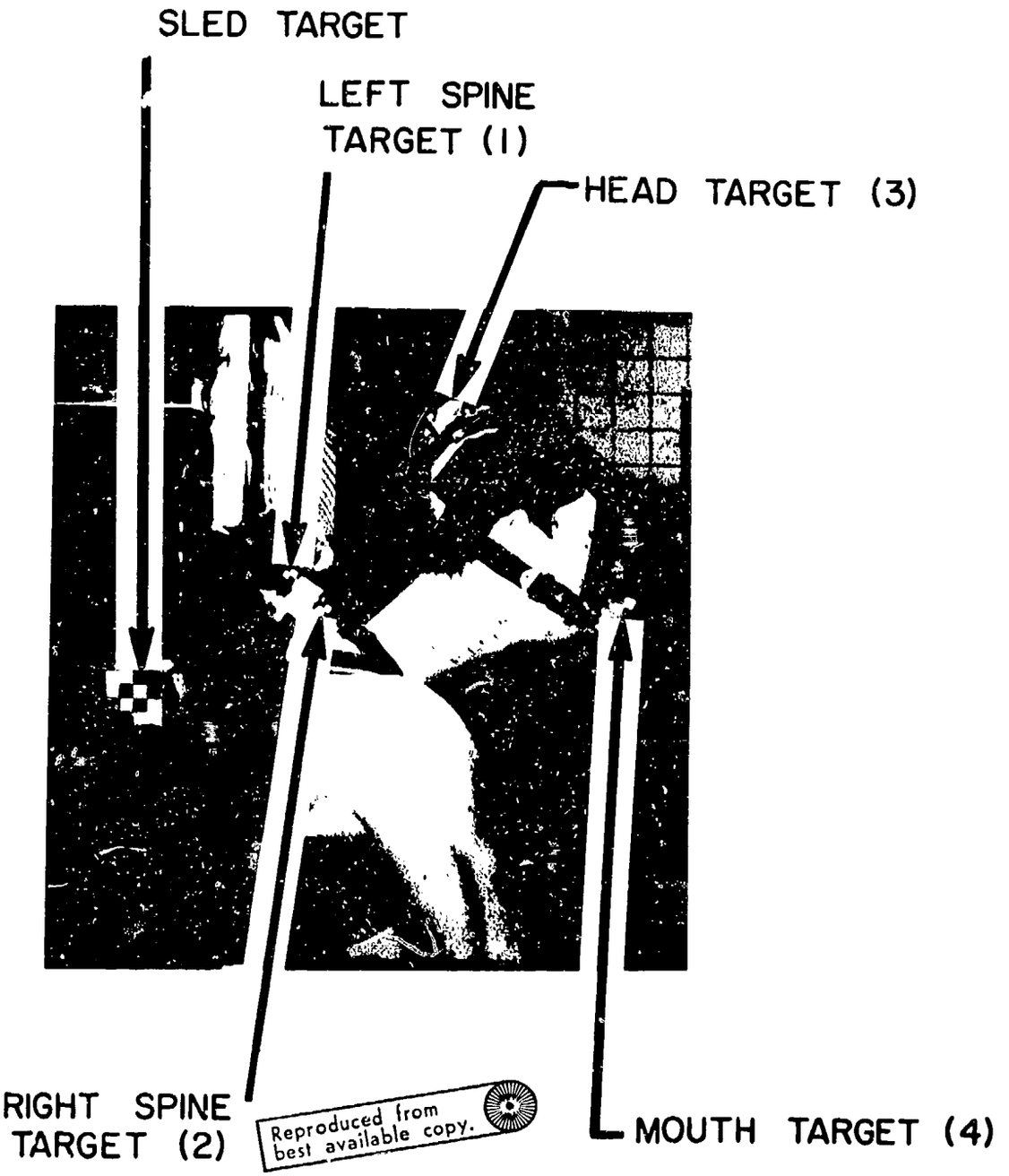

PHOTOGRAPHIC TARGETS WITH NUMERIC DESIGNATION

FIGURE DP-9

TABLE 1

REDUCED PHOTOGRAPHIC DATA CARD FORMAT

COLUMN	CONTENTS	SOURCE
1-4	Julian Date	ID Board
5-6	Time of Run	ID Board
7-9	Run Number	ID Board
10-12	Nominal Peak Sled Acceleration	ID Board
13	Camera Lateral - 1 Posterior - 2	Film
14-16	Subject Identification	ID Board
17-22	Time of Frame	Camera Timer on Film
23	Data Point Identification	By Definition
24-27	X Coordinate	Telereadex
28-31	Z Coordinate	Telereadex
77-80	Sequential Card Number	Telereadex

TABLE 2

PHOTOGRAPHIC DATA POINT IDENTIFICATION

CALIBRATION

Origin (0,0)	Center of target on chair back
Pt 0	Center of upper left target on calibration device
Pt 5	Center of upper right target on calibration device
Pt 6	Center of lower right target on calibration device

DATA

Origin (0,0)	Same as calibration
Pt 1	Center of left T_1 mount target
Pt 2	Center of right T_1 mount target
Pt 3	Center of head mount target
Pt 4	Center of mouth mount target

X-RAY ANTHROPOMETRY DATA PROCESSING AND INITIAL CONDITIONS

Coordinate measurements were performed at Eglin AFB on the same Benson-Lehner Telereadex machines which were utilized for the photographic data reduction. (See Photographic Data Processing) The X and Z grid of the Telereadex device established the coordinate reference about the arbitrary zero point or origin. The card format for digitized x-ray data was identical to the digitized photographic data with the addition of the x-ray number in card columns 69 through 74, as shown in Table 1. Table 3 provides x-ray data point identification for the skull and Table 4 similarly for the spine.

There is one difference in calibration between x-ray and photographic data that arises from the fact that a lead calibration rule was used for the x-ray instead of an L-shaped calibration device. Slight differences between the X and Z of the reader machine could be a source of error if the rule were read only once. Therefore, the two points of the rule were read twice; once with the rule image aligned substantially along the Z axis of the Telereadex and once with the rule substantially along the X axis.

In some cases the x-ray was not a "true" lateral or there may have been subject asymmetry. A best estimate of the Frankfort plane line was derived from reading the two external auditory meatus point marker locations and the two infraorbital notch point marker locations. The average of these readings was the best estimate of a line in the Frankfort plane. In those cases where the points overlapped, the readings were made twice to maintain consistency.

All x-rays and x-ray cards were and are maintained in files as a primary reference.

TABLE 3

X-RAY DATA POINT IDENTIFICATION

SKULL X-RAY

Point Identifier Number	Description
01	Z reading of one calibration point (skull data)
02	Z reading of second calibration point (skull data)
03	X reading of one calibration point (skull data)
04	X reading of second calibration point (skull data)
05	External auditory meatus superior edge center marker
06	External auditory meatus superior edge center marker
07	Infraorbital notch marker
08	Infraorbital notch marker
09	Head mount superior anterior screw hole point
10	Head mount superior middle screw hole point
11	Head mount superior posterior screw hole point
12	Head mount inferior anterior screw hole point
13	Head mount inferior middle screw hole point
14	Head mount inferior posterior screw hole point
15	Mouth mount superior anterior screw hole point
16	Mouth mount superior middle screw hole point
17	Mouth mount superior posterior screw hole point
18	Mouth mount inferior anterior screw hole point
19	Mouth mount inferior middle screw hole point
20	Mouth mount inferior posterior screw hole point

TABLE 4

CERVICAL SPINE X-RAY

Point Identifier Number	Description
51	Z reading of one calibration point (spine data)
52	Z reading of second calibration point (spine data)
53	X reading of one calibration point (spine data)
54	X reading of second calibration point (spine data)
55	Superior anterior corner of the body T_1
56	Superior posterior corner of the posterior spinous process of T_1
57	Inferior posterior corner of the posterior spinous process of T_1
61	T_1 mount, superior anterior screw hole point
62	T_1 mount, superior middle screw hole point
63	T_1 mount, superior posterior screw hole point
64	T_1 mount, inferior anterior screw hole point
65	T_1 mount, inferior middle screw hole point
66	T_1 mount, inferior posterior screw hole point

ANXRAY - The X-ray Anthropometry Program

ANXRAY is a FORTRAN program which executes the computations necessary to locate and orient the six accelerometers used in the two dimensional experiments within their respective anatomical coordinate systems.

Input to ANXRAY consists of computer cards containing digitized x-ray data. ANXRAY used this input in the following procedure:

1. The digitized data cards are read and X, Z coordinates are obtained for each point.

2. Points 01 through 04 are used to obtain scaling information for points 05 through 20. (See XRAY Point Identification Table)

$$CX = \left[\frac{(Z3 - Z4)^2 - (Z1 - Z2)^2}{(Z3 - Z4)^2 (X1 - X2)^2 - (X3 - X4)^2 (Z1 - Z2)^2}\right]^{\frac{1}{2}} \cdot (15.24) \qquad (1)$$

$$CZ = \left[\frac{(X3 - X4)^2 - (X1 - X2)^2}{(X3 - X4)^2 (Z1 - Z2)^2 - (X1 - X2)^2 (Z3 - Z4)^2}\right]^{\frac{1}{2}} \cdot (15.24) \qquad (2)$$

where 15.24 cm = 6 in and XK, ZK are the coordinates of point K.

3. The values of the remaining 16 points are scaled by these conversion factors:

$$XK = (XK) \cdot (CX) \qquad (3)$$

$$ZK = (ZK) \cdot (CZ) \qquad (4)$$

4. The position and orientation of the head anatomical coordinate system relative to an arbitrary reference frame established by the Telereadex reduction system are determined.

$$AH = (X5 + X6)/2 \qquad (5)$$

$$BH = (Z5 + Z6)/2 \qquad (6)$$

$$\emptyset H = \text{ARCTAN} \left[\frac{Z5 + Z6 - Z7 - Z8}{X5 + X6 - X7 - X8}\right] \qquad (7)$$

Careful consideration was given to appropriate quadrant assignment for the related angle which was obtained by the FORTRAN ARCTAN routine in all equations of all programs employing it.

5. Points 09 through 14 are used to compute the position and orientation of the head mount relative to the arbitrary reference frame.

$$AD = (X9 + X10 + X11 + X12 + X13 + X14)/6 \qquad (8)$$

$$BD = (Z9 + Z10 + Z11 + Z12 + Z13 + Z14)/6 \qquad (9)$$

For the orientation of the head mount, the coordinates for the superior screw holes are first averaged with the coordinates of the corresponding inferior screw holes:

$$XX1 = (X9 + X12)/2 \quad (10)$$

$$ZZ1 = (Z9 + Z12)/2 \quad (11)$$

$$XX2 = (X10 + X13)/2 \quad (12)$$

$$ZZ2 = (Z10 + Z13)/2 \quad (13)$$

$$XX3 = (X11 + X14)/2 \quad (14)$$

$$ZZ3 = (Z11 + Z14)/2 \quad (15)$$

This yields the coordinates for three points on the midline of the mount. A least squares technique is then used to calculate the slope of the best fit line using these points:

$$\emptyset D = \text{ARCTAN}\left[\frac{(\sum XX)(\sum ZZ) - 3(\sum XXZZ)}{(\sum XX)^2 - 3(\sum XX^2)}\right] \quad (16)$$

6. Points 15 through 20 are used in a similar manner to calculate the position and orientation of the mouth mount relative to the arbitrary reference frame: AM, BM and ØM.

7. The position and orientation of the head mount in the head anatomical coordinate system are then calculated:

$$XHD = (AD - AH)\,\text{COS}(\emptyset H) - (BD - BH)\,\text{SIN}(\emptyset H) \quad (17)$$

$$ZHD = (AD - AH)\,\text{SIN}(\emptyset H) + (BD - BH)\,\text{COS}(\emptyset H) \quad (18)$$

$$\emptyset HD = \emptyset D - \emptyset H \quad (19)$$

8. Similarly, the position and orientation of the mouth mount in the head anatomical coordinate system become:

$$XHM = (AM - AH)\,\text{COS}(\emptyset H) - (BM - BH)\,\text{SIN}(\emptyset H) \quad (20)$$

$$ZHM = (AM - AH)\,\text{SIN}(\emptyset H) + (BM - BH)\,\text{COS}(\emptyset H) \quad (21)$$

$$\emptyset HM = \emptyset M - \emptyset H \quad (22)$$

9. It is now possible to utilize a constant taken from the transducer mount drawings and the previously calculated location and orientation of the head and mouth mounts to calculate the position and orientation of the individual accelerometers in the head anatomical coordinate system.

$$L1 = 1.676654 \text{ cm}$$

$$XAFM = XHM + \tfrac{1}{2}\,L1\,\text{COS}(\emptyset HM) \quad (23)$$

$$ZAFM = ZHM - \tfrac{1}{2}\,L1\,\text{SIN}(\emptyset HM) \quad (24)$$

$$OAFM = \emptyset HM \quad (25)$$

$$XASM = XHM - \tfrac{1}{2}\ L1\ COS\ (\emptyset HM) \quad (26)$$

$$ZASM = ZHM + \tfrac{1}{2}\ L1\ SIN\ (\emptyset HM) \quad (27)$$

$$OASM = \emptyset HM \quad (28)$$

$$XAFD = XHD + \tfrac{1}{2}\ L1\ COS\ (\emptyset HD) \quad (29)$$

$$ZAFD = ZHD - \tfrac{1}{2}\ L1\ SIN\ (\emptyset HD) \quad (30)$$

$$OAFD = \emptyset HD \quad (31)$$

$$XASD = XHD - \tfrac{1}{2}\ L1\ COS\ (\emptyset HD) \quad (32)$$

$$ZASD = ZHD + \tfrac{1}{2}\ L1\ SIN\ (\emptyset HD) \quad (33)$$

$$OASD = \emptyset HD \quad (34)$$

10. The head span is calculated:

$$HSP = [\ (AM - AD)^2 + (BM - BD)^2\ ]^{\frac{1}{2}} \quad (35)$$

11. The skull x-ray processing is completed with the calculation of the head span line orientation relative to the +Z axis of the head anatomical coordinate system. From $\emptyset H$, the orientation of the head anatomical coordinate system +X axis relative to the x-ray +X axis, the orientation of the head anatomical +Z axis is calculated:

$$\emptyset HZ = \emptyset H \pm \pi/2 \quad (36)$$

where the sign is dependent on the sign of $\emptyset H$. Then, the orientation of the head span line relative to the x-ray +X axis is:

$$AHS = ARCTAN\ [(BM - BD)/(AM - AD)] \quad (37)$$

Finally, the desired orientation is:

$$AHS = AHS - \emptyset HZ \quad (38)$$

12. For spine x-ray anthropometry, points 51 through 54 are used to obtain scaling information for points 55 through 57 and 61 through 66. The procedure is exactly the same as that used to obtain scaling information for the skull x-ray .

13. The coordinates of points 55 through 57 and points 61 through 66 are scaled by these conversion factors. The procedure is the same as for the skull x-ray .

14. The position and orientation of the T_1 anatomical coordinate system relative to the arbitrary reference frame are calculated:

$$AN = X55 \quad (39)$$

$$BN = Z55 \quad (40)$$

$$\text{ØN} = \pi + \text{ARCTAN}\left[\frac{\text{BN} - [(\text{Z56} + \text{Z57})/2]}{\text{AN} - [(\text{X56} + \text{X57})/2]}\right] \quad (41)$$

15. Points 61 through 66 are used to compute the position and orientation (AT, BT and ØT) of the T_1 mount relative to the arbitrary reference frame in the same manner described for the head mount.

16. The position and orientation of the T_1 mount relative to the T_1 anatomical coordinate system are computed:

$$\text{XNT} = (\text{AT} - \text{AN})\ \text{COS}\,(\text{ØN}) - (\text{BT} - \text{BN})\ \text{SIN}\,(\text{ØN}) \quad (42)$$

$$\text{ZNT} = (\text{AT} - \text{AN})\ \text{SIN}\,(\text{ØN}) + (\text{BT} - \text{BN})\ \text{COS}\,(\text{ØN}) \quad (43)$$

$$\text{ØNT} = \text{ØT} - \text{ØN} \quad (44)$$

17. Finally, the position and orientation of the T_1 accelerometers are:

$$\text{XAFN} = \text{XNT} + \tfrac{1}{2}\ \text{L1}\ \text{COS}\,(\text{ØNT}) \quad (45)$$

$$\text{ZAFN} = \text{ZNT} - \tfrac{1}{2}\ \text{L1}\ \text{SIN}\,(\text{ØNT}) \quad (46)$$

$$\text{OAFN} = \text{ØNT} \quad (47)$$

$$\text{XASN} = \text{XNT} - \tfrac{1}{2}\ \text{L1}\ \text{COS}\,(\text{ØNT}) \quad (48)$$

$$\text{ZASN} = \text{ZNT} + \tfrac{1}{2}\ \text{L1}\ \text{SIN}\,(\text{ØNT}) \quad (49)$$

$$\text{OASN} = \text{ØNT} \quad (50)$$

The output from ANXRAY consists of punch cards containing the values computed. These cards were input to the ICONDS program; ICONDS added the ANXRAY computed values to the ICONDS output file.

ANXRAY Validation

ANXRAY validation was accomplished as follows:

1. An examination was made of the horizontal and vertical scaling constants. Any substantial difference would indicate improper calibration of the photographic data system.

2. An examination was made of the head span (XHSP) computed from the skull x-ray. This variable was one of the first and best indications of incorrect data reduction and could readily be compared with HSP from Program TROUTP.

3. The scaled coordinates of each point were plotted to provide a quick indication of data reduction.

4. The scaled coordinates were then backscaled to the scale of the x-ray and plotted. These plots were overlaid on their corresponding original x-rays. In all cases, the comparison was very good.

5. Finally, a straight edge was used to approximate the anatomical coordinate systems on the scaled coordinates plots. A protractor and ruler were then used to measure directly the positions and orientations which were computed in ANXRAY. There was no essential difference noted between the measured values and the computed values. It is not considered either feasible or necessary to further validate these data.

ICONDS - The Initial Conditions Program

ICONDS is a FORTRAN program which calculates the horizontal and vertical scaling constants for reduced photographic data and establishes the initial positions of the subject with respect to the Telereadex reference coordinate system; and the initial orientations of the subject head and neck with respect to the laboratory reference coordinate system.

ICONDS utilizes three sources of input data:

1. Average of pre-acceleration transducer data for each of the head, mouth and T_1 mounted accelerometers.

2. Punch cards containing the reduced photographic target coordinates for ten frames of calibration and ten frames of pre-acceleration photographic data. For the calibration, targets were located on an inverted L-shaped device of known size with arms perpendicular and parallel to gravity as shown in Figures DP-10 and DP-6. For the data, two targets were located on the T_1 mount and one each on the head mount, the mouth mount and the sled as shown in Figure DP-9.

3. X-ray anthropometric data consisting of the coordinates and orientation of the head and mouth accelerometers relative to the head anatomical coordinate system; and the coordinates and orientation of the T_1 accelerometers relative to the T_1 anatomical coordinate system. (See Program ANXRAY).

The first step in the execution of ICONDS is the calculation of average coordinates from the 10 frames of calibration for the upper left target, point 0; for the upper right target, point 5; and for the lower right target, point 6, as shown in Figure DP-10. Similarly, average coordinates from the 10 frames of data are calculated for the left T_1 target, point 1; the right T_1 target, point 2; the head target, point 3; and the mouth target, point 4, as shown in Figure DP-9.

The average coordinates from the calibration frames are used to convert the remaining reduced data from Telereadex units to centimeters and to correct for possible angular difference between the laboratory reference coordinate system and Telereadex reference coordinate system. As a first step in the conversion process, ICONDS calculates two angles. ALPHAX and ALPHAZ as shown in Figure DP-10:

$$\text{ALPHAX} = \text{ARCTAN}\,[(Z5 - Z0)/(X5 - X0)] \quad (1)$$

$$\text{ALPHAZ} = \text{ARCTAN}\,[(X6 - X5)/(Z5 - Z6)] \quad (2)$$

The small magnitude of these two angles permit averaging to obtain

$$\text{ALPHA} = (\text{ALPHAX} + \text{ALPHAZ})/2 \quad (3)$$

This angle ALPHA is defined as the angular difference between the Telereadex reference coordinate system and the laboratory reference coordinate system. An angle Beta in the Telereadex reference coordinate system would be (BETA - ALPHA) in the laboratory reference coordinate system. Due to possible variation in the horizontal and vertical measurement of the photographic reduction system, two

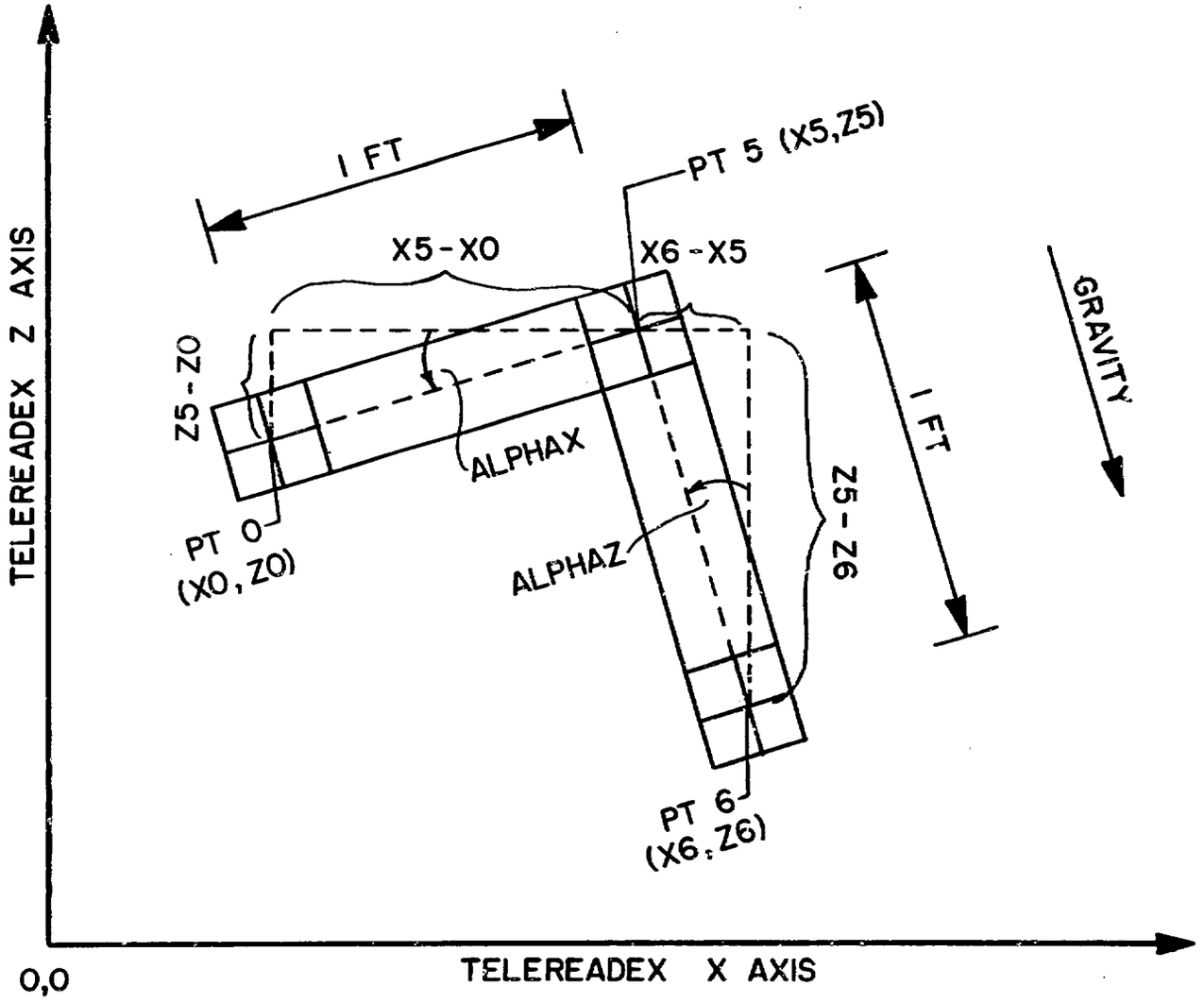

FIGURE DP-10 Illustration of the Angular Quantities used to Relate Telereadex Reference Coordinate System Z Axis to Laboratory Reference Coordinate System Z Axis (Gravity). ALPHAX and ALPHAZ are exaggerated for illustration.

conversion factors are calculated. Since the distances from point 0 to point 5 and from point 5 to point 6 are both one foot,

$$1 \text{ foot} = (X5 - X0)\ \cos(\text{ALPHA}) \text{ horizontal Telereadex units} \quad (4)$$

$$1 \text{ foot} = (Z5 - Z6)\ \cos(\text{ALPHA}) \text{ vertical Telereadex units} \quad (5)$$

The average coordinates of the targets shown in Figure DP-9 are divided by these constants to convert them to feet and then multiplied by 30.48 to convert them to centimeters.

Specific discussion of parameter derivation in ICONDS will be limited to those parameters which are utilized in the calculation of the output variables presented.

ADH is the angle formed by the line connecting the center of the head target and the center of the mouth target with the +X axis of the laboratory reference coordinate system, as shown in Figure DP-11.

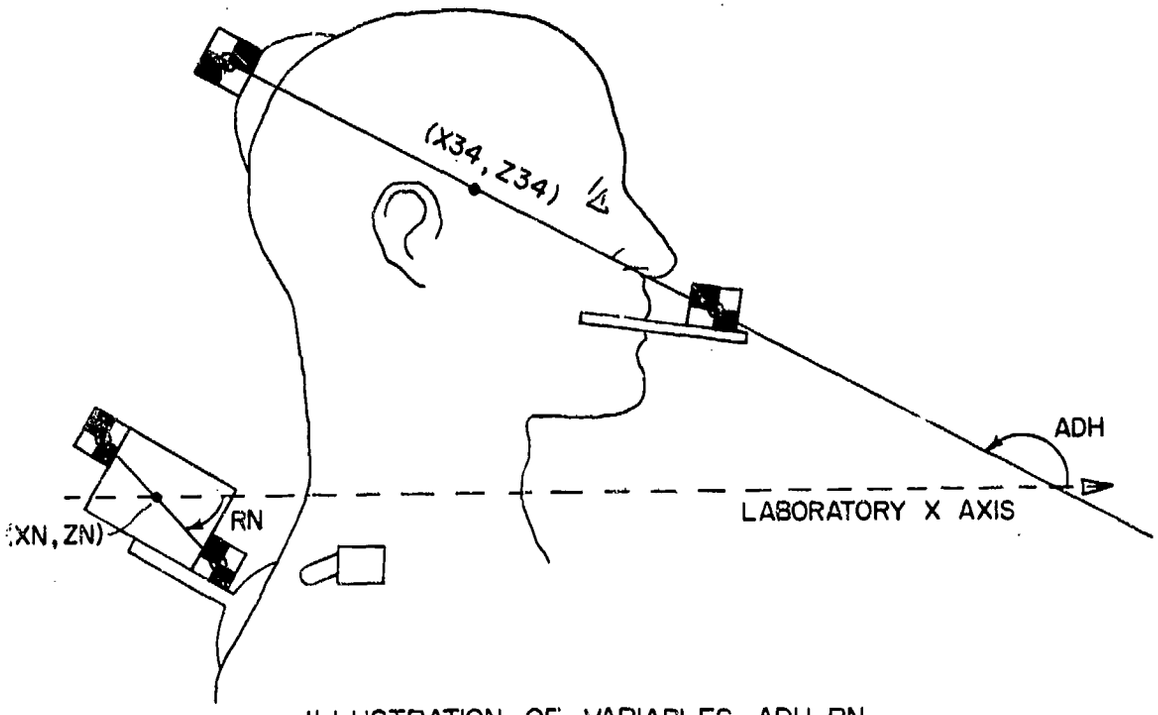

ILLUSTRATION OF VARIABLES ADH, RN,
AND POINTS X34, Z34, XN, ZN

FIGURE DP-11

$$\text{ADH} = \text{ARCTAN}\,[(Z3 - Z4)/(X3 - X4)] - \text{ALPHA} \quad (6)$$

X34, Z34 are the coordinates of the midpoint of the line joining the head and mouth targets with respect to the Telereadex reference coordinate system.

$$X34 = (X3 + X4)/2 \quad (7)$$

$$Z34 = (Z3 + Z4)/2 \quad (8)$$

XN, ZN are the coordinates of the midpoint of the line joining the two T_1 targets with respect to the Telereadex reference coordinate system.

$$XN = (X1 + X2)/2 \quad (9)$$

$$ZN = (Z1 + Z2)/2 \quad (10)$$

It should be noted that X34, Z34 and XN, ZN are corrected to the laboratory reference coordinate system prior to their being utilized as initial conditions. (See Program TROUTP)

RN is the angle formed by the line connecting the two T_1 targets with the +X axis of the laboratory reference coordinate system.

$$RN = \text{ARCTAN}\,[(Z2 - Z1)/(X2 - X1)] - \text{ALPHA} \quad (11)$$

ICONDS is a multi-run program processing any number of runs without reloading the program. In order to expedite the processing of ICONDS, the input cards are read from a card image digital tape which contains the ICONDS input data for all of the runs. The output from ICONDS was a digital tape containing 60 initial condition parameters which were either derived by ICONDS or provided by ANXRAY.

ICONDS Validation

ICONDS validation involved three different objectives:

1. Validation of the horizontal and vertical scaling constants developed by ICONDS for scaling photographic data.

2. Validation of the initial conditions which were computed from pre-acceleration photographic data.

3. Validation of the x-ray anthropometric data.

The best test for evaluating the horizontal and vertical scaling constants is the examiniation of scaled photographic data plots, particularly when those plots compare the scaled photographic data with independently scaled sensor data. An examination of the PDH (derived from the head angular position as computed from photographic data) vs RDH (derived from the scaled rate gyro) comparison plots 633 through 673 illustrates the precision and accuracy of photographic and sensor scaling.

The initial conditions which were computed from pre-acceleration photographic data include the scaled initial coordinates of the photographic targets and initial condition values which were verified in the validation of scaling constants. The values computed from these coordinates involve very basic equations (midpoint of a line joining two targets, slope of a line connecting two targets). These computations were carefully checked for accuracy.

Finally, the x-ray anthropometric values were computed in the program ANXRAY (See Program ANXRAY) and were validated therein. These values were input to ICONDS, and ICONDS only added them to its output.

The ICONDS output tape was and is maintained as a primary reference.

Figure DP-12 illustrates the flow of photographic and x-ray data to a UNIVAC 1108 output tape.

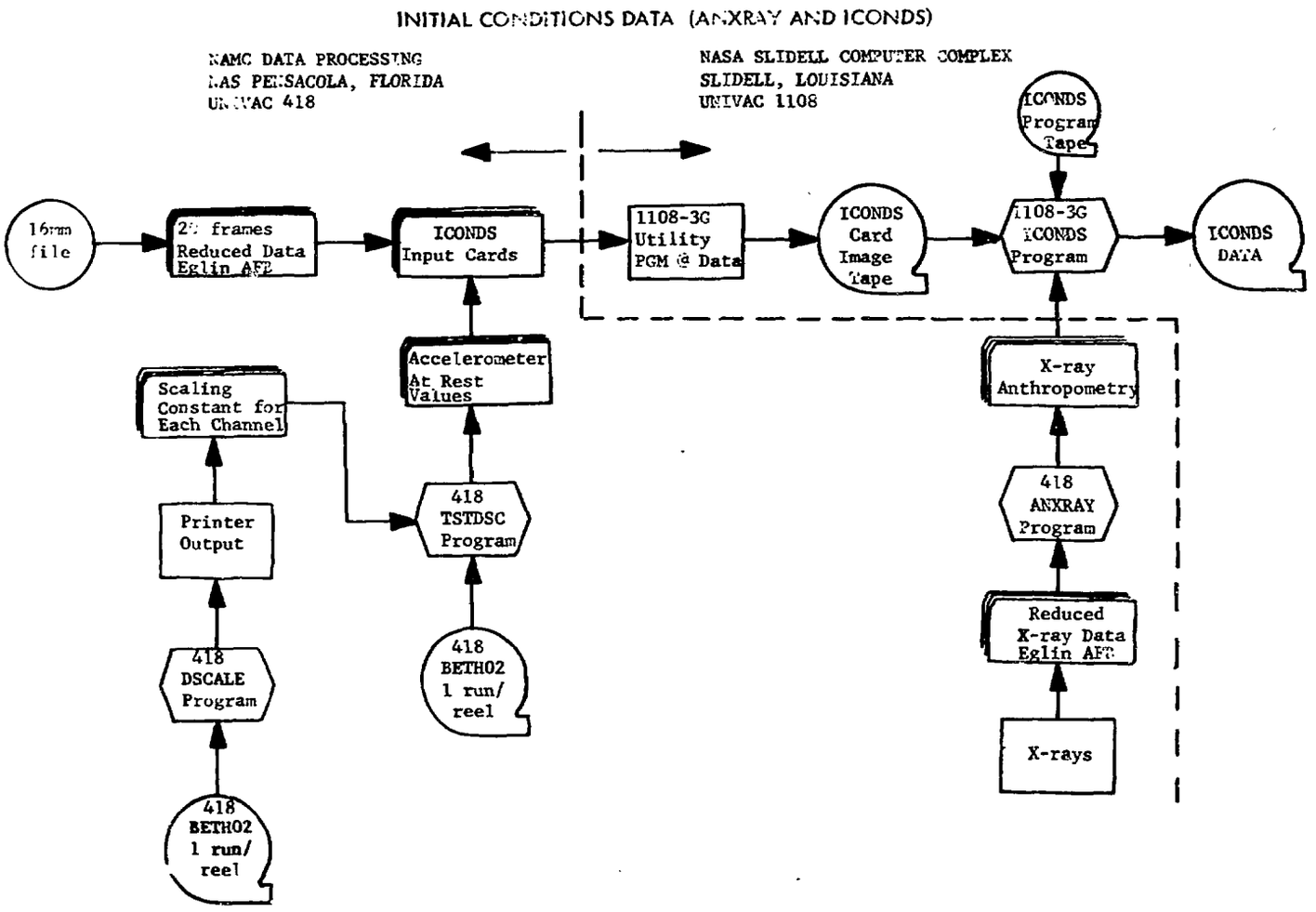
INITIAL CONDITIONS DATA (ANXRAY AND ICONDS)
NAMC DATA PROCESSING
LAS PENSACOLA, FLORIDA
UNIVAC 418
NASA SLIDELL COMPUTER COMPLEX
SLIDELL, LOUISIANA
UNIVAC 1108
16mm file
2? frames Reduced Data Eglin AFB
ICONDS Input Cards
1108-3G Utility PGM & Data
ICONDS Card Image Tape
ICONDS Program Tape
1108-3G ICONDS Program
ICONDS DATA
Accelerometer At Rest Values
Scaling Constant for Each Channel
418 TSTDSC Program
Printer Output
418 DSCALE Program
418 BETH02 1 run/ reel
418 BETH02 1 run/ reel
X-ray Anthropometry
418 ANXRAY Program
Reduced X-ray Data Eglin AFB
X-rays

FIGURE DP-12

The scaled data, photographic and sensor, were then subjected to output variables and transformation programs. Initial conditions and x-ray anthropometry were required by these programs.

SENSOR OUTPUT VARIABLES AND SUBSEQUENT TRANSFORMATIONS

OUTVAR - The Output Variables Program

OUTVAR is a FORTRAN program which takes scaled accelerometer and rate gyro data from an experimental run and combines this with the appropriate initial conditions data to compute various kinematic descriptors of subject motion.

Input to OUTVAR is the digital output tape from the DSCALE program, the digital output tape from the ICONDS program and a set of data cards which include run numbers, run processing options, and output medium choices.

Typically, a set of scaled input data (produced by program DSCALE) consists of the variables AFM, ASM, AFD, ASD, AFN, ASN, RVH, RVN and AXC where each of these three-character "labels" refers to a time series of approximately 1000 sensor values spaced 0.5 msec apart.

Since some experimental runs may not possess this set in total, OUTVAR will not attempt to compute any quantity which is a function of a missing variable. This selectivity of processing is implemented by subjugating the program's control to a run option number which is one of several parameters used to govern the program execution. The four options available to OUTVAR have the following meanings:

Option 1 .... process the run as having all variables.

Option 2 ....AFN, ASN, RVN and AXC are the only variables available, that is, there are no transducers at the head or mouth.

Option 3....all variables are present except the head accelerometers.

Option 4....all variables are present except the mouth accelerometers.

For each experimental run the set of scaled accelerometer and rate gyro data has an associated set of "initial conditions" information (see program ICONDS). In performing its functions, OUTVAR requires selected portions of this data.

When all the control parameters, scaled run data, and initial conditions information are read in, OUTVAR begins processing a run. The following discussion will be limited to those variables computed by OUTVAR which are presented in the plots and/or variables required in the computation of presented variables. The OUTVAR list in the Variable Definitions section gives precise variable definitions and cross-reference to appropriate figures.

OUTVAR calculates the angular acceleration of the head, RAH, and the angular acceleration of the spine, RAN, by smoothing and differentiating the head and the spine angular velocities (RVH and RVN respectively) measured by the rate gyros. The smoothing consists of an eleven-point central moving average on RVH and RVN and is followed by a three-point central differentiation formula.

The eleven-point central moving average on the set X(1) through X(1002) applied as follows:

$$\overline{X}_i = \left[\sum_{j=1}^{2i-1} X_j \right] / (2i - 1) \quad \text{for} \quad i = 1 \text{ to } 5 \tag{1}$$

$$\overline{X}_i = \left[\sum_{j=i-5}^{i+5} X_j \right] / 11 \quad \text{for} \quad i = 6 \text{ to } 997 \tag{2}$$

$$\overline{X}_i = \left[\sum_{j=2i-1002}^{1002} X_j \right] / (2005 - 2i) \quad \text{for } i = 998 \text{ to } 1002 \tag{3}$$

The three-point central differentiation formula for the ith point is:

$$XDOT_i = \frac{\overline{X}_{i+1} - \overline{X}_{i-1}}{2h} = \frac{\overline{X}_i - \overline{X}_{i-1}}{2h} + \frac{\overline{X}_{i-1} - \overline{X}_i}{2h} \tag{4}$$

where h is the interval step size (0.5 msec).

Inserting the values of RVH and RVN in place of the X values in the algorithms above results in RAH and RAN respectively, as represented by equation (4).

RAH as used in the co-location corrections was obtained by this method. The RAH which is presented in the plots was obtained by filtering RVH with a second-order numerical filter with a damping ration (ζ) of 0.6 and a natural frequency ($\omega_n/2\pi$) of 50 Hertz. The filtered RVH was then differentiated in accordance with equation (4).

RPN and RPH, angular displacements of the spine and head, are computed by integrating RVN and RVH. In both instances the trapezoidal rule is employed and the ICONDS angles ADH and RN are used as initial conditions.

The trapezoidal rule algorithm on the set X(1) through X(1002) is applied as follows

$$Y_1 = P_o \text{ (where } P_o \text{ is the initial position)}$$

$$Y_2 = Y_1 + (X_1 + X_2) \cdot (h/2) \tag{5}$$

.
.
.

$$Y_i = Y_{i-1} + (X_{i-1} + X_i) \cdot (h/2) \tag{6}$$

.
.
.

$$Y_{1002} = Y_{1001} + (X_{1001} + X_{1002}) \cdot (h/2) \tag{7}$$

where h is the integration step size (0.5 msec).

OUTVAR corrects the head, mouth and spine acceleration for non-colocation of the anterior and superior accelerometers within each mount system. Theoretically, it is desired that the anterior and superior accelerations be a measure of orthogonal acceleration components at one specific point on each mount; however, due to the physical impossibility of mounting two accelerometers at the same point they are mounted so that they measure orthogonal accelerations at two distinct points which are equidistant from and colinear with the throretically desired point (Figure DP-13).

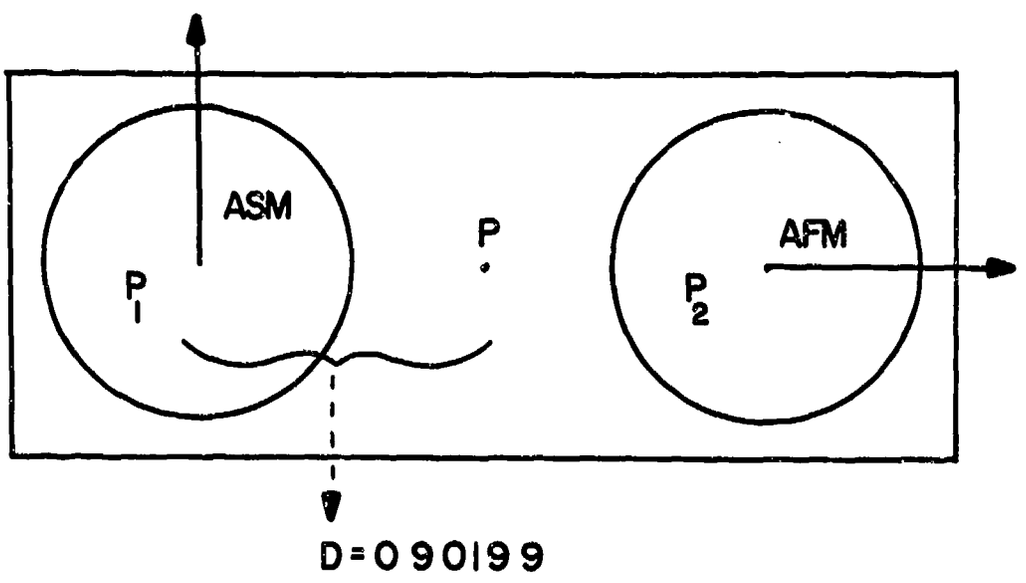

FIGURE DP-13 Geometry of Accelerometer Pair Within the Mouth Mount

By utilizing the angular acceleration and angular velocity of both the head and spine, a pair of corrected accelerations are computed for each mount which represent the desired orthogonal accelerations at the midpoint of the line joining the centers of the accelerometers.

Given the configuration of accelerometers as shown in Figure DP-13, where the anterior acceleration is recorded for point P_2 and the superior for point P_1, the anterior and superior accelerations at point P are:

$$AFM_p = AFM_{p_2} + D.\omega^2 \quad (8)$$

$$ASM_p = ASM_{p_1} + D.\alpha \quad (9)$$

where ω = the angular velocity of the head, RVH, α = the angular acceleration of the head, RAH, and D is the distance from the midpoint of the accelerometer to the midpoint of the line connecting the centers of the two accelerometers. Similar corrections are made for the head and spine mounts; except that in the case of the spine corrections, ω is RVN and α is RAN. These "corrected" accelerations are assigned the same three-character names as were the input accelerations and subsequent program computational requirements referencing the individual mount accelerations are furnished with the corrected accelerations.

By two successive applications of the trapezoidal algorithm to the sled acceleration data AXC, with initial velocity and position zero, we derive the sled velocity XVC and position XDC relative to the laboratory reference coordinate system.

As output, OUTVAR is able to deliver some seventy variables representing angular and linear acceleration, velocity and displacement of head and spine instrumentation coordinate systems.

OUTVAR is a multi-run program enabling these procedures to be executed for thirty runs without reloading the program.

OUTVAR Validation

To validate the computing software of OUTVAR for algorithm, programming and computational errors, simulated data were generated.

The input data required by OUTVAR consists of DSCALE and ICONDS data, both on digital tape.

DSCALE data designed to simulate a fully instrumented run should consist of six subject acceleration data streams (AFM, ASM, AFD, ASD, AFN, ASN), two subject angular velocity data streams (RVH and RVN) and one sled acceleration data stream (AXC).

ICONDS simulation data must consist of 60 quantities describing the simulated initial conditions and including simulated x-ray anthropometric data.

A model will be described which was the basis for generating the required simulated test data.

Consider an apparatus of five rods (L_1 , L_2 , L_3 , L_4 , L_5) connected as shown in Figure DP-14. In the list of definitions which follow, all fixed numerical quantities are chosen to bear a close resemblance to typical experimental values and to keep calculations as simple as possible.

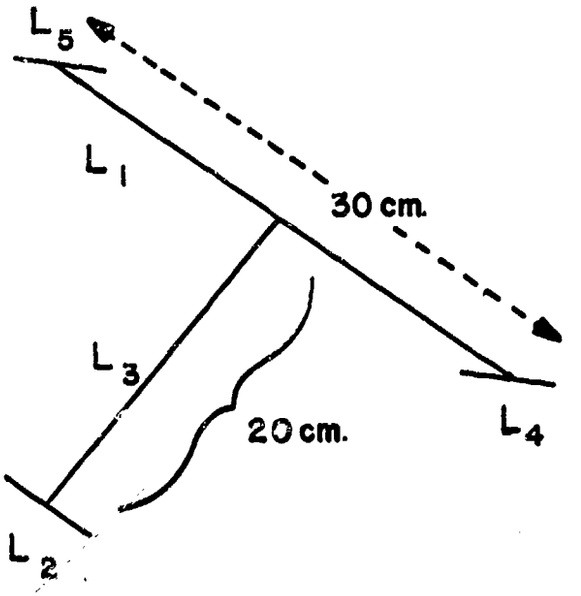

FIGURE DP-14 Illustration of Simulation Model

1. L_1 will act as the line joining the center of the head mount to the center of the mouth mount. Let its length be 30 centimeters, a number resembling typical headspans.

2. L_2 will represent the line which joins the two corner-mounted phototargets of the spine mount.

3. L_3 will be the line joining the center of L_2 to the center of L_1 . Its value shall be 20 centimeters, a value close to those computed from initial conditions data.

4. L_4 and L_5 will represent the lines joining the centers of the anterior and superior accelerometers at the mouth and head mounts respectively. They will cross L_1 at their centers and in both cases it will be assumed that the sensitive axes of the anterior and superior accelerometers are respectively colinear with and perpendicular to these lines. The length of L_4 is equal to the length of L_5 which is equal to .90199 cm, the value used in program OUTVAR.

It would also be possible to add a sixth rod L_6 whose center would coincide with the juction of L_2 and L_3 and which would have the same length as L_4 and L_5 and would represent the line joining the centers of the spinal accelerometers. Since

this rod would not move relative to L_2 it is only necessary to keep its relative position in mind as seen in Figure DP-15.

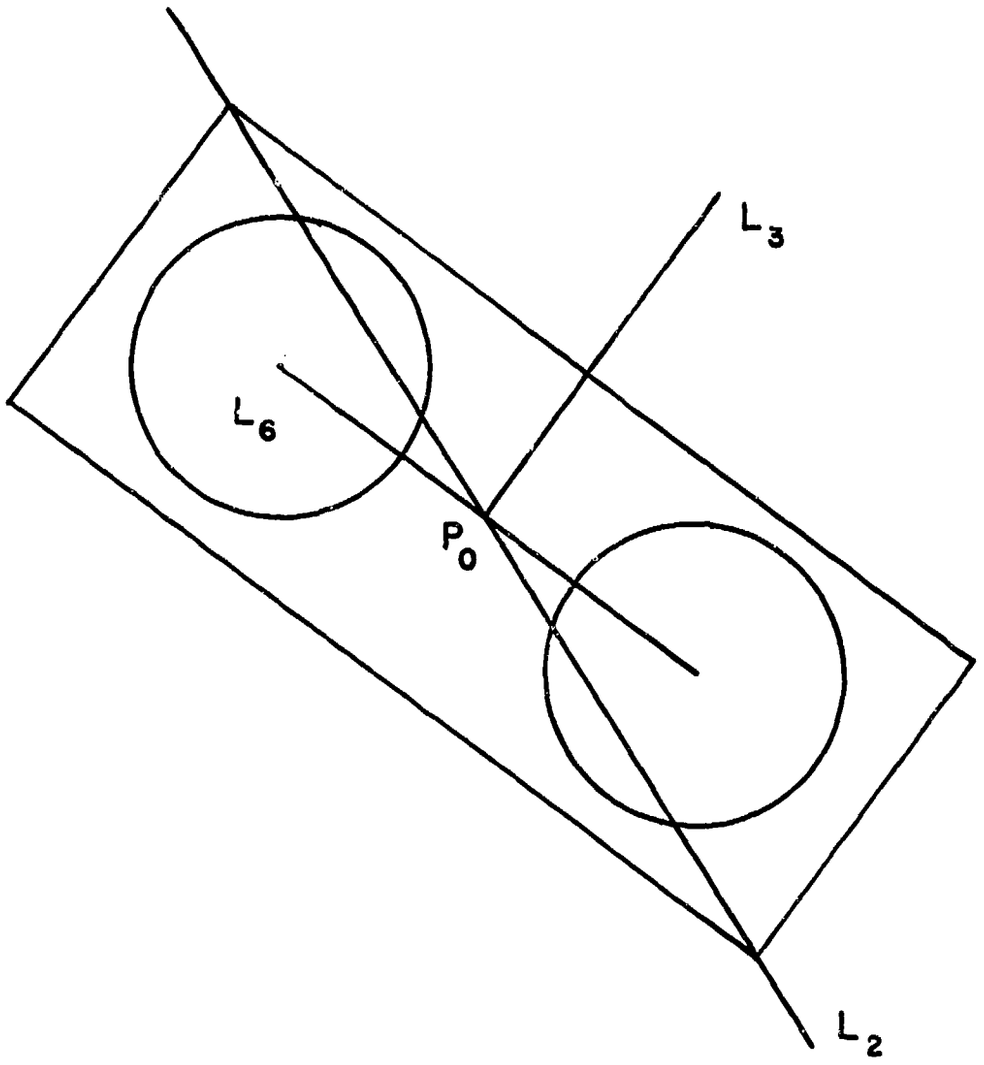

FIGURE DP-15 Illustration of Spine Mount Simulation Data

Programs OUTVAR and TROUT do not see the complex linkages uniting experimental components so that separate simplified driving functions may be applied to produce linear acceleration and angular acceleration.

Let the input sled acceleration be given by,

$$a(t) = (-250\,g/sec) \cdot (t) \qquad \text{for } 0 \le t \le 40 \text{ msec} \qquad (10)$$

$$a(t) = (250\,g/sec) \cdot (t) - 20g \qquad \text{for } 40 \text{ msec} \le t \le 80 \text{ msec} \qquad (11)$$

$$a(t) = 0 \qquad \text{for } 80 \text{ msec} \le t \le 500 \text{ msec} \qquad (12)$$

That is, the sled acceleration waveform will be an isosceles triangle with a base of 80 milliseconds and height of -10g's, representing a nominal 10g run at onset of 250g's per second.

It will be assumed that this sled acceleration is passed unchanged to the generator apparatus and is applied in such a way that only translation of the apparatus is effected and that there is no rotation due to its action.

A controlled rotational effect will be superimposed on the apparatus as follows: At the end of the experiment, 500 msec after its start, the orientation of the apparatus is to be -70 degrees relative to the laboratory reference coordinate system X axis, having sustained a rotation of -50 degrees about the spine point P_0 (Figure DP-15) while not having sustained any internal relative rotations. The average angular velocity of both L_1 and L_2 is therefore -100 degrees/sec. In order that a non-zero angular acceleration be involved, let the spine and head rods L_2 and L_1 sustain an angular velocity given by

$$\omega(t) = (800 \text{ degrees/sec}^2) \cdot (t) \qquad 0 \le t \le 250 \text{ msec} \qquad (13)$$

$$\omega(t) = (-800 \text{ degrees/sec}^2) \cdot (t) + 400 \text{ degrees/sec} \qquad 250 \text{ msec} \le t \le 500 \text{ msec} \qquad (14)$$

This results in the required average angular velocity of -100 degrees/sec. Figures DP-16 and DP-17 depict both the linear and angular driving functions.

A program was written to derive the appropriate data streams for both DSCALE and ICONDS simulated data when the data generator apparatus is driven by these functions with the initial conditions.

Once the simulated ICONDS and DSCALE data had been generated and recorded on digital tape in the proper formats, program OUTVAR was run using these tapes as input. Correction for non-colocation was specified. The critical test for OUTVAR's accuracy is in the output variables XDH and ZDH, the X and Z coordinates of the displacement of the center of the head relative to the laboratory reference coordinate system. If these values are correct then OUTVAR is performing properly.

The predicted values for these quantities after 500 msec into the "model" experiment are

$$X = -161.638 \text{ cm}$$

$$Z = 6.840 \text{ cm}$$

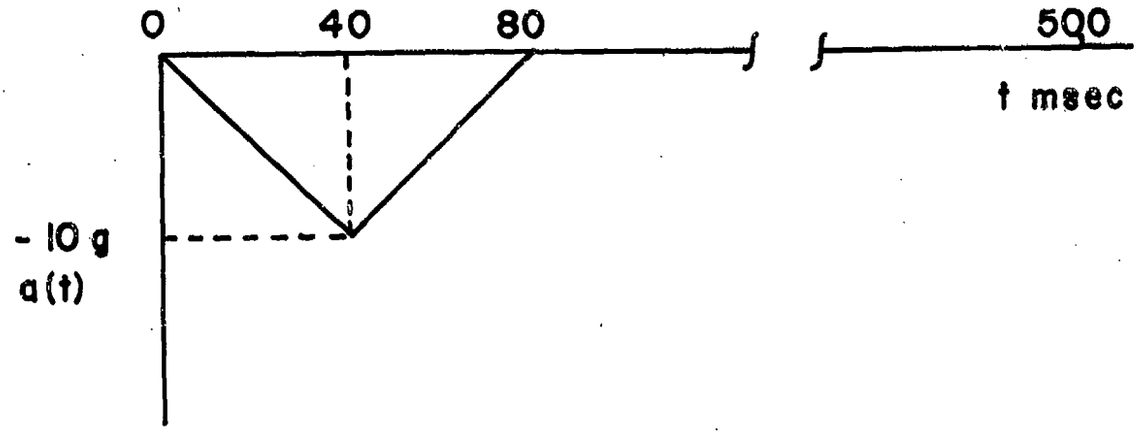

FIGURE DP-16 Illustration of Simulated Sled Acceleration
(Linear Driving Function)

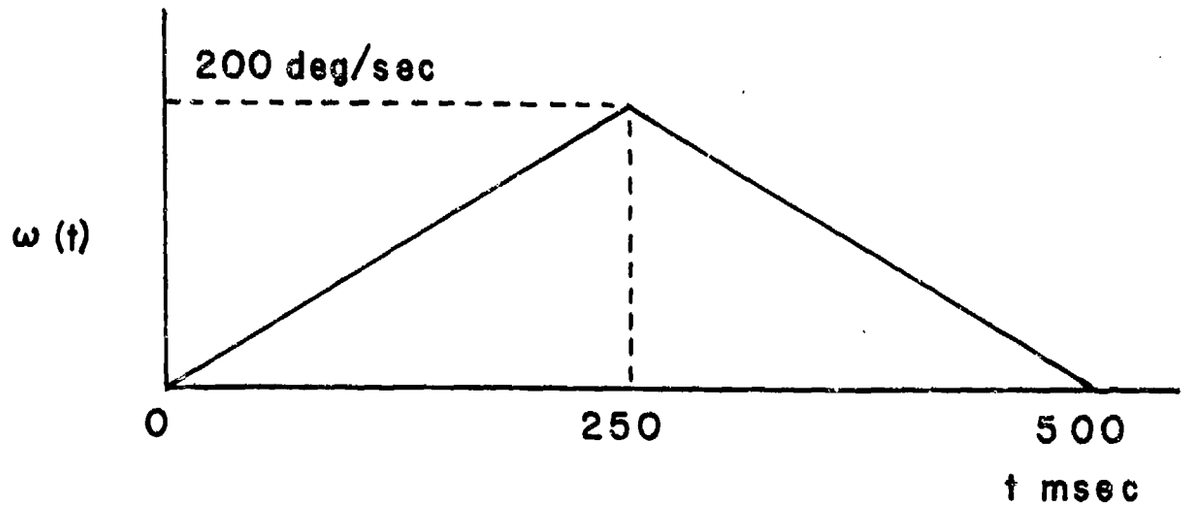

FIGURE DP-17 - Illustration of Simulated Angular Velocity
(Angular Driving Function)

The values computed by OUTVAR are

$$X = -161.616 \text{ cm}$$

$$Z = 6.813 \text{ cm}$$

which gives rise to an absolute difference of

$$|\Delta X| = 0.022 \text{ cm}$$

$$|\Delta Z| = 0.027 \text{ cm}$$

The source of these small errors is most likely:

1. The colocation correction of simulated accelerations is computed using angular accelerations derived from the simulated accelerations prior to colocation correction. This will lead to small computational errors.

2. Small errors are contributed by round off.

Evaluation of the simulated OUTVAR output data demonstrated that the difference in computed values and predicted values could be considered insignificant.

The output from OUTVAR was a digital tape containing approximately 70 variables for up to 30 runs. These tapes were and are maintained as a primary reference.

When the OUTVAR processing was completed, x-ray anthropometric data and center of gravity data were used to transform data to anatomical coordinate systems and to the head C.G.

TROUT - The Sensor Data Transformation Program

TROUT is a FORTRAN program which accepts input data from OUTVAR, DSCALE and ICONDS, and converts accelerations to head anatomical coordinates utilizing ANXRAY data to locate anatomical reference points. It will also, on request, transform the data to the head principal coordinate system.

Input to TROUT consists of:

1. Co-located acceleration variables AFM, ASM, AFD, ASD, AFN, ASN; measured angular velocities of the head and neck RVH and RVN; and derived angular accelerations RAN and RAH from OUTVAR and DSCALE.

2. Anthropometric data such as OAFM, OAFD, XAFM, ZAFM, XASM, ZASM, XAFD, ZAFD, XASD, ZASD, AHS. (See program ANXRAY)

3. Other data such as ANGCG, the angle between the head principal coordinate system +X axis and the head anatomical coordinate system +X axis; XCGR, ZCGR, which are the X and Z displacements of the head principal coordinate system origin relative to the head anatomical coordinate system.

The major calculating algorithm in TROUT is a subroutine which transforms accelerations measured at, and relative to, a coordinate system at one point in a rigid body to accelerations which would be measured at and relative to a different coordinate system at a second point in the rigid body. This transformation utilizes a standardized form of the formula for rigid-body kinematic acceleration plus a rotation of the new acceleration vector into the new coordinate system.

Specific variable deriviation will be limited to those variables presented in the plots and/or those variables required in the computation of variables presented in the plots: 1FM, 1SM, 4FM, 4SM, 1FD, 1SD, 4FD, 4SD, 4XM, 4ZM. See TROUT list in Variable Definitions section for precise definitions and cross-reference to appropriate figures.

Program TROUT first calculates the magnitude P and direction θ of the vector from the first coordinate system origin, where the acceleration vector is known to the point in the rigid body at which it is to be calculated.

Then using the known acceleration vector along with the angular acceleration (RAH) and velocity (RVH), program TROUT calculates the acceleration vector at the second point. This is the new acceleration vector but it is expressed in terms of the old coordinate system. The final step is to perform a rotation of coordinates by the appropriate angle so that the new acceleration vector is expressed in terms of the new coordinate system.

Using the input quantities as required the following quantities are calculated:

$$X_1 = (XAFM + XASM)/2 \tag{1}$$

$$Z_1 = (ZAFM + ZASM)/2 \tag{2}$$

$$P_1 = (X_1^2 + Z_1^2) \tag{3}$$

$$\theta_1 = OAFM + ARCTAN\,(Z_1 / X_1) \tag{4}$$

where P_1 and θ_1 represent the magnitude and direction of the vector from the center of the mouth mount to the head anatomical coordinate system.

Then, the acceleration vector at the head anatomical coordinate system origin (1FM, 1SM) is calculated from the mouth acceleration data (AFM, ASM) as follows:

$$\begin{pmatrix} 1FM \\ 1SM \end{pmatrix} = \begin{pmatrix} \cos\phi & -\sin\phi \\ \sin\phi & \cos\phi \end{pmatrix} \cdot \left[\begin{pmatrix} AFM \\ ASM \end{pmatrix} + P_1 \begin{pmatrix} \cos\theta_1 & -\sin\theta_1 \\ \sin\theta_1 & \cos\theta_1 \end{pmatrix} \right] \cdot \begin{pmatrix} -(RVH)^2 \\ RAH \end{pmatrix} \tag{5}$$

where $\phi = -OAFM$.

To proceed from the head anatomical coordinate system to the head principal coordinate system, the vector (XCGR, ZCGR) is rotated to the head principal coordinate system:

$$\begin{pmatrix} X_2 \\ Z_2 \end{pmatrix} = \begin{pmatrix} \cos\phi & -\sin\phi \\ \sin\phi & \cos\phi \end{pmatrix} \cdot \begin{pmatrix} XCGR \\ ZCGR \end{pmatrix} \tag{6}$$

where ϕ = ANGCG and (X_2, Z_2) is the vector after rotation.

$$P_2 = (X_2^2 + Z_2^2)^{\frac{1}{2}} \tag{7}$$

$$\theta_2 = -ANGCG + ARCTAN\,(Z_2/X_2) \tag{8}$$

where P_2 and θ_2 represent the magnitude and direction of the vector from the head anatomical coordinate system origin to the head principal coordinate system origin.

Then the acceleration vector at the head center of gravity is

$$\begin{pmatrix} 4FM \\ 4SM \end{pmatrix} = \begin{pmatrix} \cos\phi & -\sin\phi \\ \sin\phi & \cos\phi \end{pmatrix} \cdot \left[\begin{pmatrix} 1FM \\ 1SM \end{pmatrix} + P_2 \begin{pmatrix} \cos\theta_2 & -\sin\theta_2 \\ \sin\theta_2 & \cos\theta_2 \end{pmatrix} \cdot \begin{pmatrix} -(RVH)^2 \\ RAH \end{pmatrix} \right] \quad (9)$$

where ϕ = ANGCG.

The above procedure is repeated using the head acceleration data (AFD, ASD) to generate (1FD, 1SD) and(4FD, 4SD). The new quantities relating to the head mount are:

$$X_3 = (XAFD + XASD)/2 \quad (10)$$

$$Z_3 = (ZAFD + ZASD)2 \quad (11)$$

$$P_3 = (X_3^2 + Z_3^2)^{1/2} \quad (12)$$

$$\theta_3 = OAFD + \arctan(Z_3/X_3) \quad (13)$$

where P_3 and Θ_3 represent the magnitude and direction of the vector from the center of the head mount to the head anatomical coordinate system.

$$\begin{pmatrix} 1FD \\ 1SD \end{pmatrix} = \begin{pmatrix} \cos\phi & -\sin\phi \\ \sin\phi & \cos\phi \end{pmatrix} \cdot \left[\begin{pmatrix} AFD \\ ASD \end{pmatrix} + P_3 \begin{pmatrix} \cos\theta_3 & -\sin\theta_3 \\ \sin\theta_3 & \cos\theta_3 \end{pmatrix} \cdot \begin{pmatrix} -(RVH)^2 \\ RAH \end{pmatrix} \right] \quad (14)$$

where ϕ = -OAFD

and

$$\begin{pmatrix} 4FD \\ 4SD \end{pmatrix} = \begin{pmatrix} \cos\phi & -\sin\phi \\ \sin\phi & \cos\phi \end{pmatrix} \left[\begin{pmatrix} 1FD \\ 1SD \end{pmatrix} + P_2 \begin{pmatrix} \cos\theta_2 & -\sin\theta_2 \\ \sin\theta_2 & \cos\theta_2 \end{pmatrix} \cdot \begin{pmatrix} -(RVH)^2 \\ RAH \end{pmatrix} \right] \quad (15)$$

where ϕ = ANGCG

Finally, a simple rotation from the head principal coordinate system to the laboratory reference coordinate systems gives

$$\begin{pmatrix} 4XM \\ 4ZM \end{pmatrix} = \begin{pmatrix} \cos\phi & -\sin\phi \\ \sin\phi & \cos\phi \end{pmatrix} \cdot \begin{pmatrix} 4FM \\ 4SM \end{pmatrix} \quad (16)$$

where ϕ = RPH + AHS - ANGCG - $\pi/2$

Trout Validation

The input data required by TROUT consists of DSCALE, ICONDS, AND OUTVAR data, all on digital tape.

To test the computing software of TROUT for algorithm,programming, and computational errors, the simulated DSCALE and ICONDS data used to validate OUTVAR and the resulting simulated OUTVAR output data (See description of program OUTVAR) were used as input to TROUT. In addition, the simulated head principal coordinate system was defined to have its origin at X = 2cm, Z = 2cm relative to the head anatomical coordinate system origin and +X axis oriented 20 degrees clockwise from the +X axis of the head anatomical coordinate system.

Once TROUT had been run on the model data, verification followed with checkout of two specific areas:

1. The accelerations computed for the head anatomical and head principal coordinate systems had to be the same whether computed from mouth mount or head mount data. Both sources did indeed produce the same results for each of the coordinate systems in question.

2. The fact that results match for both sources does not mean the accelerations are correct. Furthermore, it says nothing of the T_1 anatomical coordinate system. By checking the final positions of each coordinate system against predicted values the entire program becomes verified. That is, if all coordinate systems have accurate positions then the accelerations and velocities leading to these positions are assumed accurate.

Table 5 gives the x and z coordinates of position of each coordinate system origin relative to the laboratory reference coordinate system.

TABLE 5

TROUT Positions at 1/2 sec (centimeters)

Name	Variable	Predicted Value	Computed Value	Δ
T1 Anatomical	3XN	-160.93	-160.95	.02
Coordinate System	3ZN	4.93	4.96	.03
Head Anatomical	3XM	-160.93	-160.91	.02
Coordinate System	3ZM	4.93	4.97	.04
Head Principal	6XM	-158.11	-158.08	.03
Coordinate System	6ZM	4.69	4.71	.02

Any significant errors in 4XM and 4ZM which are acceleration variables would manifest themselves as part of the errors in 6XM and 6ZM which are final position variables. It can be seen by examination of the final column that there is essentially no error introduced into the data by the TROUT program.

TROUT is a multi-run program processing up to 30 runs at a time. The output from TROUT is a digital tape containing up to 36 variables for each of the runs processed. These tapes were and are preserved as a primary reference.

Figure DP-18 gives a summary illustration of the data flow from DSCALE to TROUT.

SENSOR OUTPUT VARIABLES AND TRANSFORMATION DATA (OUTVAR AND TROUT)

NASA SLIDELL COMPUTER COMPLEX
SLIDELL, LOUISIANA
UNIVAC 1108-3C

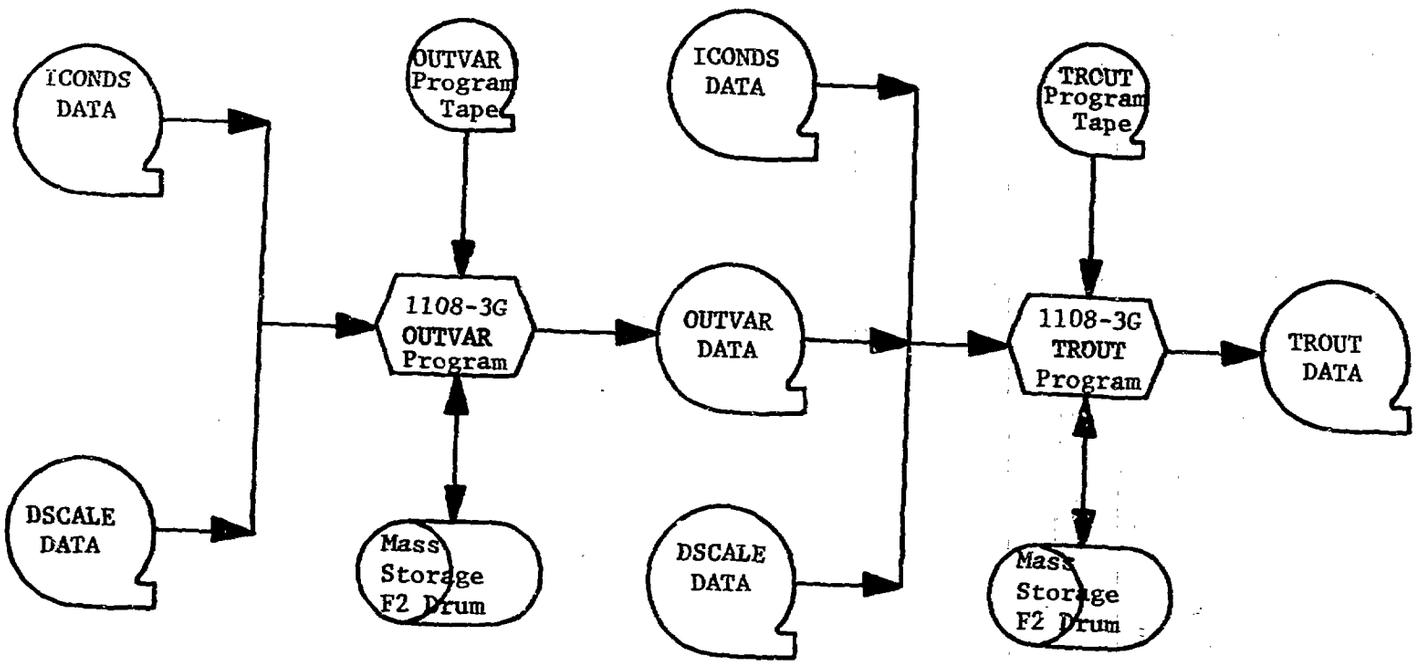

FIGURE DP - 18

PHOTOGRAPHIC OUTPUT VARIABLES AND TRANSFORMATIONS

TROUTP - The Photographic Data Transformation Program

TROUTP is a FORTRAN program which computes the motion of the head anatomical coordinate system, the T_1 anatomical coordinate system and the head principal coordinate system from photographic data. Each system's motion is described in terms of the X and Z position of its origin relative to the sled reference coordinate system.

Furthermore, the position vectors to the head anatomical coordinate system and the head principal coordinate system from the origin of the T_1 anatomical coordinate system are computed. These position vectors are in terms of magnitude and orientation relative to the +X axis of the laboratory reference coordinate system.

Input to TROUTP consists of the following:

1. The scaled X and Z coordinates of photographic targets 1 through 4 and their corresponding time in msecs (TMS) from approximately 250 frames of film. These coordinates are relative to the Telereadex reference coordinate system. (See Photographic Data Processing)

2. The output from the ICONDS program which includes the ANXRAY anthropometric data.

3. The components of displacement of the origin of the head principal coordinate system relative to the head anatomical coordinate system.

Specific discussion of the variables computed in TROUTP will be limited to those variables presented in the plots and/or those variables required in the computation of variables presented. See the TROUTP list of the Variable Definitions Section for precise definitions and cross-reference to appropriate figures.

The first function of TROUTP is to express the input photographic data relative to the sled reference coordinate system. TROUTP rotates the input coordinates through the angle ALPHA (ICONDS input) which is defined to be the magnitude of the angular displacement of the Telereadex reference coordinate system relative to the laboratory reference coordinate system. The rotated values are thus relative to the sled reference coordinate system since their origin is the sled photographic target and their orientation is that of the laboratory reference coordinate system.

Once the photographic data has been expressed in the sled reference coordinate system, the displacement of the head target center relative to the mouth target center is computed:

$$HSP = [(X3 - X4)^2 + (Z3 - Z4)^2]^{\frac{1}{2}} \quad (1)$$

Angles RN and ADH are then computed:

$$RN = \text{ARCTAN}\,[(Z2 - Z1)/(X2 - X1)] \quad (2)$$

$$ADH = \text{ARCTAN}\,[(Z3 - Z4)/(X3 - X4)] \quad (3)$$

RN is the angle formed by the line connecting the two T_1 targets with the X axis of the laboratory reference coordinate system. (Figure DP-11). ADH is the angle formed by the line connecting the head target and the mouth target with the X axis of the laboratory reference coordinate system . (Figure DP-11)

RN is used to develop the angle NRN which is the angular displacement of the +X axis of the T_1 anatomical coordinate system relative to the +X axis of the laboratory reference coordinate system.

$$NRN = RN - (-0.2 - OAFN) \tag{4}$$

where OAFN (ANXRAY input) is the angular displacement of the +X axis of the transducer T_1 instrumentation coordinate system relative to the +X axis of the T_1 anatomical coordinate system; and, from the geometry of the spine mount, the line connecting the two T_1 targets has an angular displacement of 0.2 radians relative to the +X axis of the transducer T_1 instrumentation coordinate system.

ADH is used to develop the angle PDH which is the angular displacement of the +X axis of the head anatomical coordinate system relative to the +X axis of the laboratory reference coordinate system.

$$PDH = ADH - (\pi/2 - AHS) \tag{5}$$

where AHS (ANXRAY input) is the angular displacement of the -X axis of the photographic head instrumentation coordinate system relative to the +Z axis of the head anatomical coordinate system.

Having computed the orientations of the anatomical coordinate systems relative to the laboratory reference coordinate system, TROUTP computes the components of displacement (XNA, ZNA) of the origin of the T_1 anatomical coordinate system relative to the origin of the sled reference coordinate system. From the rotated X and Z coordinates of the two T_1 targets, the coordinates of the center of the spine mount relative to the sled reference coordinate system are computed:

$$XN = (X1 + X2)/2 \tag{6}$$

$$ZN = (Z1 + Z2)/2 \tag{7}$$

Similarly, from XAFN, ZAFN, XASN, ZASN (ANXRAY input), the coordinates of the center of the spine mount (XNC, ZNC) relative to the T_1 anatomical coordinate system are computed:

$$XNC = (XAFN + XASN)/2 \tag{8}$$

$$ZNC = (ZAFN + ZASN)/2 \tag{9}$$

Therefore, the coordinates XNA, ZNA are

$$\begin{vmatrix} XNA \\ ZNA \end{vmatrix} = \begin{vmatrix} XN \\ ZN \end{vmatrix} - \begin{vmatrix} \cos\phi & -\sin\phi \\ \sin\phi & \cos\phi \end{vmatrix} \cdot \begin{vmatrix} XNC \\ ZNC \end{vmatrix} \quad (10)$$

where ϕ = NRN.

The next function of TROUTP is to compute the components of displacement of the origin of the head principal coordinate system (XCL, ZCL) relative to the origin of the sled reference coordinate system. From the rotated X and Z coordinates of the head target and of the mouth target, the coordinates of the mid-point of the line connecting the head and mouth targets relative to the sled reference coordinate system are computed:

$$X34 = (X3 + X4)/2 \quad (11)$$

$$Z34 = (Z3 + Z4)/2 \quad (12)$$

(See Figure DP-13) Similarly, from XAFM, XASM, XAFD, XASD, ZAFM, ZASM, ZAFD and ZASD (ANXRAY input), the coordinates of the midpoint of the head-mouth line (XC, ZC) relative to the head anatomical coordinate system are computed:

$$XC = (XAFM + XASM + XAFD + XASD)/4 \quad (13)$$

$$ZC = (ZAFM + ZASM + ZAFD + ZASD)/4 \quad (14)$$

The coordinates of the origin of the head anatomical coordinate system (XHA, ZHA) relative to the sled reference coordinate system may be derived as follows:

$$\begin{vmatrix} XHA \\ ZHA \end{vmatrix} = \begin{vmatrix} X34 \\ Z34 \end{vmatrix} - \begin{vmatrix} \cos\phi & -\sin\phi \\ \sin\phi & \cos\phi \end{vmatrix} \cdot \begin{vmatrix} XC \\ ZC \end{vmatrix} \quad (15)$$

where ϕ = PDH.

Finally, if XCG, ZCG represent the coordinates of the origin of the head principal coordinate system relative to the head anatomical coordinate system (Input to TROUTP),

$$\begin{vmatrix} XCL \\ ZCL \end{vmatrix} = \begin{vmatrix} XHA \\ ZHA \end{vmatrix} + \begin{vmatrix} \cos\phi & -\sin\phi \\ \sin\phi & \cos\phi \end{vmatrix} \cdot \begin{vmatrix} XCG \\ ZCG \end{vmatrix} \quad (16)$$

where ϕ = PDH

From XNA, ZNA and XCL, ZCL, TROUTP computes the magnitude of displacement of the head principal coordinate system origin relative to the T_1 anatomical coordinate system origin.

$$MCT = [(XCL - XNA)^2 + (ZCL - ZNA)^2]^{\frac{1}{2}} \quad (17)$$

The polar angle (ACT) of MCT is also computed:

$$ACT = ARCTAN\ [(ZCL - ZNA)/(XCL - XNA)] \quad (18)$$

It should be noted that a special version of TROUTP, TROUTH, calculates the same variables using the same algorithms, but is designed to accept as input, scaled photographic data obtained from the filming of the subject's normal head nod rather than the usual photographic data from the acceleration experiments.

TROUTP Validation

Validation of TROUTP was based on simulated data generated by a model essentially similar to the model used to generate data for OUTVAR validation. (See program OUTVAR for detailed description of the model) There were, however, certain differences necessary to accommodate photographic input data and the structure of the program TROUTP.

The first difference was that no linear acceleration was used. The model testing OUTVAR and TROUT used a linear acceleration $a(t)$ as well as a rotation $\omega(t)$ as driving functions. $a(t)$ was necessary since sensor data consisted of acceleration signals, one component of which was a linear acceleration which ultimately would contribute to position relative to a fixed lab frame. Photographic data is referenced to a moving frame (the origin of the sled reference coordinate system) and hence does not involve linear translation. Therefore, only $\omega(t)$ was chosen as a driving function, the same $\omega(t)$ that was used before.

$$\omega(t) = (-800 \text{ degrees/sec}^2)t \qquad \text{for } 0 \leq t \leq 250 \text{ msec} \quad (19)$$

$$\omega(t) = (800 \text{ degrees/sec}^2)t - 400 \text{ degrees/sec} \qquad \text{for } 250 \text{ msec} \leq t \leq 500 \text{ msec} \quad (20)$$

The second difference involved the internal geometry of the model. The T_1 anatomical system was chosen to be at coordinates (2cm, 2cm) relative to a coordinate system formed by the juction of L_3 and L_2 and having axes along these lines. The orientation of the T_1 anatomical coordinate system would coincide with the laboratory reference system as an initial condition. The head anatomical coordinate system as used in testing TROUT stayed the same (i.e. 2cm to the right of the junction of L_1 and L_2 on L_1) with the orientation of the laboratory reference coordinate system as an initial condition. The head principal coordinate system was chosen to be at (2cm, 2cm) relative to the head anatomical coordinate system. Figure DP-19 represents all of these positions at $t = 0$.

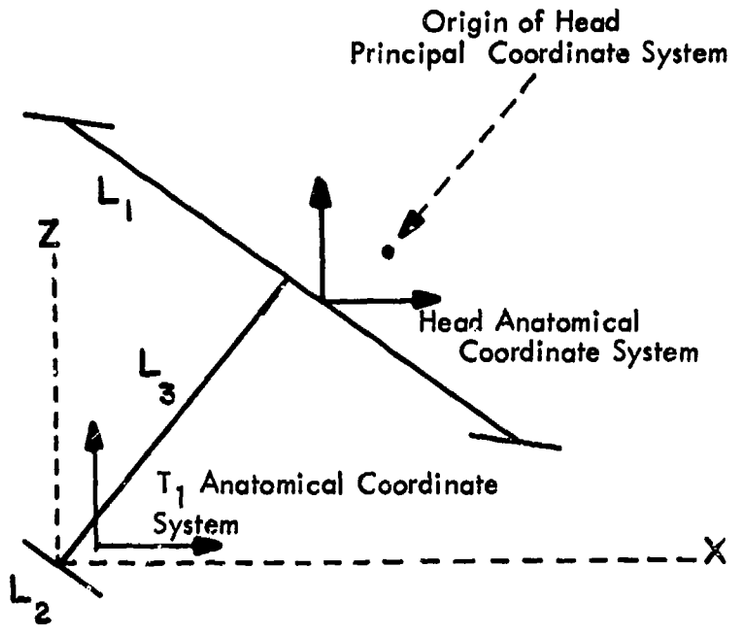

TROUTP Simulation Model

FIGURE DP-19

The positions of the various coordinate systems at t = 500 msec were to be compared with predicted values from the model. Due to a fault in a printing routine it was necessary to perform the check at the 250th data point (correspond to 498 milliseconds into the run) instead of the 251st point. The following is a table of computed values against predicted values, for TROUTP variables referenced in this presentation. It can easily be seen that all errors are on the order of 10^{-5} centimeters and probably represent errors due to the truncation in the predicted values. These are considered insignificant.

TABLE 5

COMPARISON OF COMPUTED vs PREDICTED VALUES
(at t = 498 msec)

Variable Name	Computed Value	Predicted Value	$\lvert\Delta\rvert$
PDH	-.87263 rad	-.87263 rad	-
XHA	19.47774 cm	19.47775 cm	1×10^{-5}
ZHA	4.96160 cm	4.96156	4×10^{-5}
NRN	-.87264 rad	-.87264 rad	-
XNA	2.56346 cm	2.56346 cm	-
ZNA	-1.19527 cm	-1.19526 cm	1×10^{-5}
XCL	22.29541 cm	22.29540 cm	1×10^{-5}
ZCL	4.71518 cm	4.71518 cm	-
MCT	20.59814 cm	20.59813 cm	1×10^{-5}
ACT	.29103 rad	.29103 rad	-

Since the algorithms and processing are the same, validation of TROUTP as discussed in the previous section is considered to constitute adequate validation of TROUTH.

TROUTP is a multi-run program able to process up to 30 runs at a time. The output from TROUTP is a digital tape containing the variables calculated for the runs processed. These tapes were and are preseerved as a primary reference.

Figure DP-20 illustrates the total photographic data flow.

PHOTOGRAPHIC OUTPUT VARIABLES AND TRANSFORMATION DATA (TROUTP)

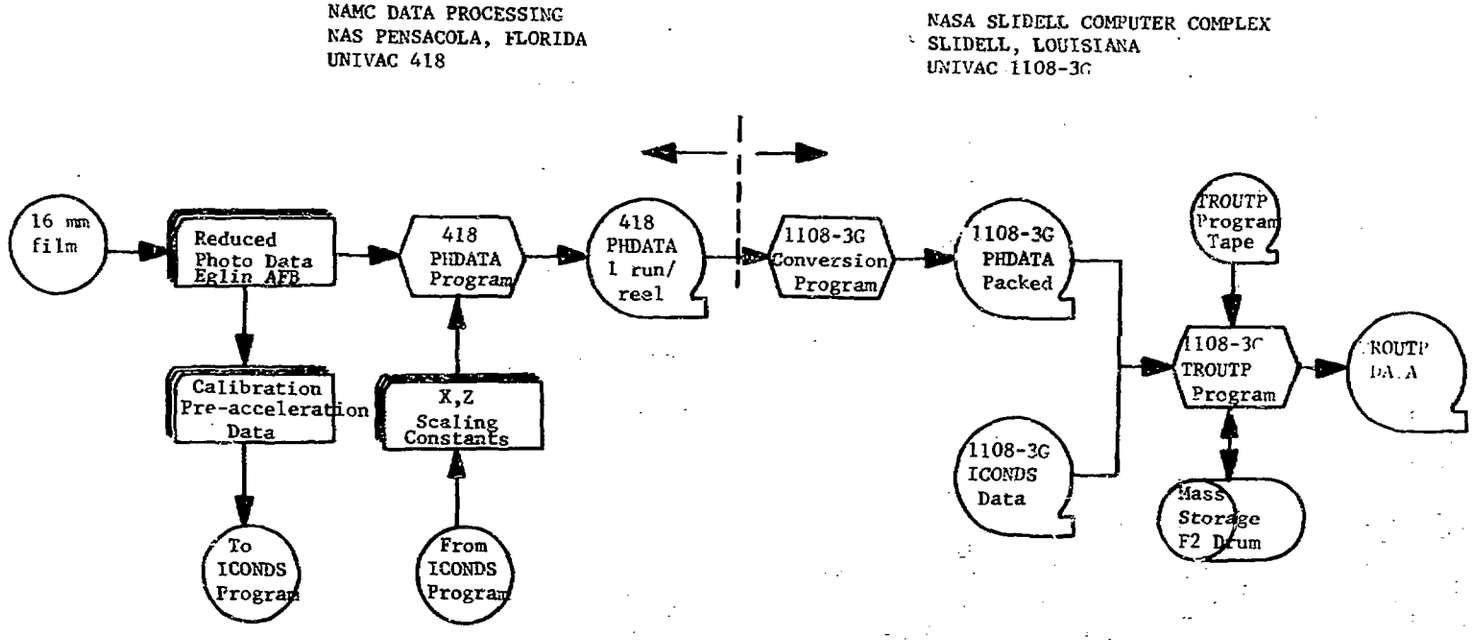

FIGURE DP-20

POST-EXPERIMENT CONDITIONING OF CERTAIN DATA PRESENTED IN THIS REPORT

Gilbert Willems M.S.E.E. and William Anderson M.A.Phys.

INTRODUCTION

The majority of the data collected during the human impact experiments conducted at Wayne State University was of sufficient quality to be useable in post-experiment analysis without further conditioning. However, the quality of a small subset of this data was found to be enhanced considerably by judicious application of certain conditioning techniques, such as filtering and time correlation; these techniques and the justification for their use are detailed in the remainder of this section.

APPLICATION OF FILTERING TECHNIQUES

Filtering was introduced into some of the data to perform one of two functions: reduction of excessive noise or as a pre-smoother prior to performing differentiation. Of the recorded sensor data, only the sled acceleration traces were sufficiently noisy to require filtering. This excessive noise has been attributed to the fact that an undamped, high bandwidth accelerometer was hard mounted to the sled; consequently, not only was its own natural frequency excited, but sled resonances were also sensed, yielding traces sufficiently noisy to hamper data analysis.

Several variables, particularly photometrically derived displacements were differentiated. The original variables while not sufficiently noisy as to require filtering, did contain some high frequency jitter, which would tend to be accentuated by differentiation. This latter phenomenon can readily be understood heuristically if note is made of the fact that the derivative of a function at any given point is a measure of the slope of the function at that point. Therefore, since high frequencies are associated with steep slopes, the noise exaggeration effect of differentiation occurs. To minimize this effect, all variables subjected to differentiation were first appropriately filtered.

Selection of a filtering criterion is dependent on two important requirements:

1. The filter bandwidth must be sufficient to "pass" all significant signal components.

2. Distortion in time due to phase shift must be avoided.

Appropriate filter cutoff frequencies were selected by first performing a spectral analysis via standard Fast Fourier Transform (FFT) techniques, in order to establish the spectral location of the significant signal components. Time axis distortion was avoided by properly accounting for time delays due to filter phase shift, and correcting the time axis.

The filters chosen for this effort are representable by one of the following two second order transfer functions:

$$\frac{\text{output}}{\text{input}} = \frac{\frac{s^2}{\omega_1^2} + \frac{2\zeta_1}{\omega_1} s + 1}{\frac{s^2}{\omega_2^2} + \frac{2\zeta_2}{\omega_2} s + 1} \quad (1) \quad \text{or} \quad \frac{\text{output}}{\text{input}} = \frac{1}{\frac{s^2}{\omega_2^2} + \frac{2\zeta_2}{\omega_2} s + 1} \quad (2)$$

In these transfer functions ω_1 and ω_2 are the numerator and denominator break frequencies respectively (in radians/sec), and ζ_1 and ζ_2 are the damping ratios; s is the Laplace operator. The second characterization allows a 40 db/decade rolloff beyond the passband. The inclusion of the numerator term on the first transfer function allows the insertion of an additional "notch" anywhere along the frequency axis. Partically, however, the insertion of the notch is feasible only if inserted significantly beyond the denominator breakpoint, since the rolloff is changed to a constant attenuation beyond the notch.

The derivation of a digital algorithm to represent the indicated transfer functions is readily obtained from the state space representation of the cited filters, both of which are represented in block diagram form in Figure 1. In this figure the integrator outputs are defined as state variables x_1 and x_2. If a low pass mechanization is desired, x_1 is used as the output; if in addition, a notch is desired, E_{out} is the output. From the figure, the vector-matrix filter equations are readily obtained:

$$\begin{bmatrix} \dot{x}_1 \\ \dot{x}_2 \end{bmatrix} = \begin{bmatrix} 0 & 1 \\ \omega_2^2 & -2\zeta_2 \omega_2 \end{bmatrix} \begin{bmatrix} x_1 \\ x_2 \end{bmatrix} + \begin{bmatrix} 0 \\ \omega_2^2 \end{bmatrix} E_{in} \quad (3)$$

E_{out} is obtainable as a linear combination of x_1 and x_2:

$$E_{out} = \frac{\omega_2^2}{\omega_1^2} E_{in} + \frac{(1 - \omega_2^2)}{\omega_1^2} x_1 + \frac{(2\zeta_1 \omega_1 - 2\zeta_2 \omega_2)}{\omega_1^2} x_2 \quad (4)$$

The above vector-matirx differential equation is of the general form

$$\dot{x} = Ax + Bu \quad (5)$$

whose solution is given by:

$$x(t) = e^{At} x(o) + e^{At} \int_o^t e^{-A\tau} Bu(\tau) d\tau \quad (6)$$

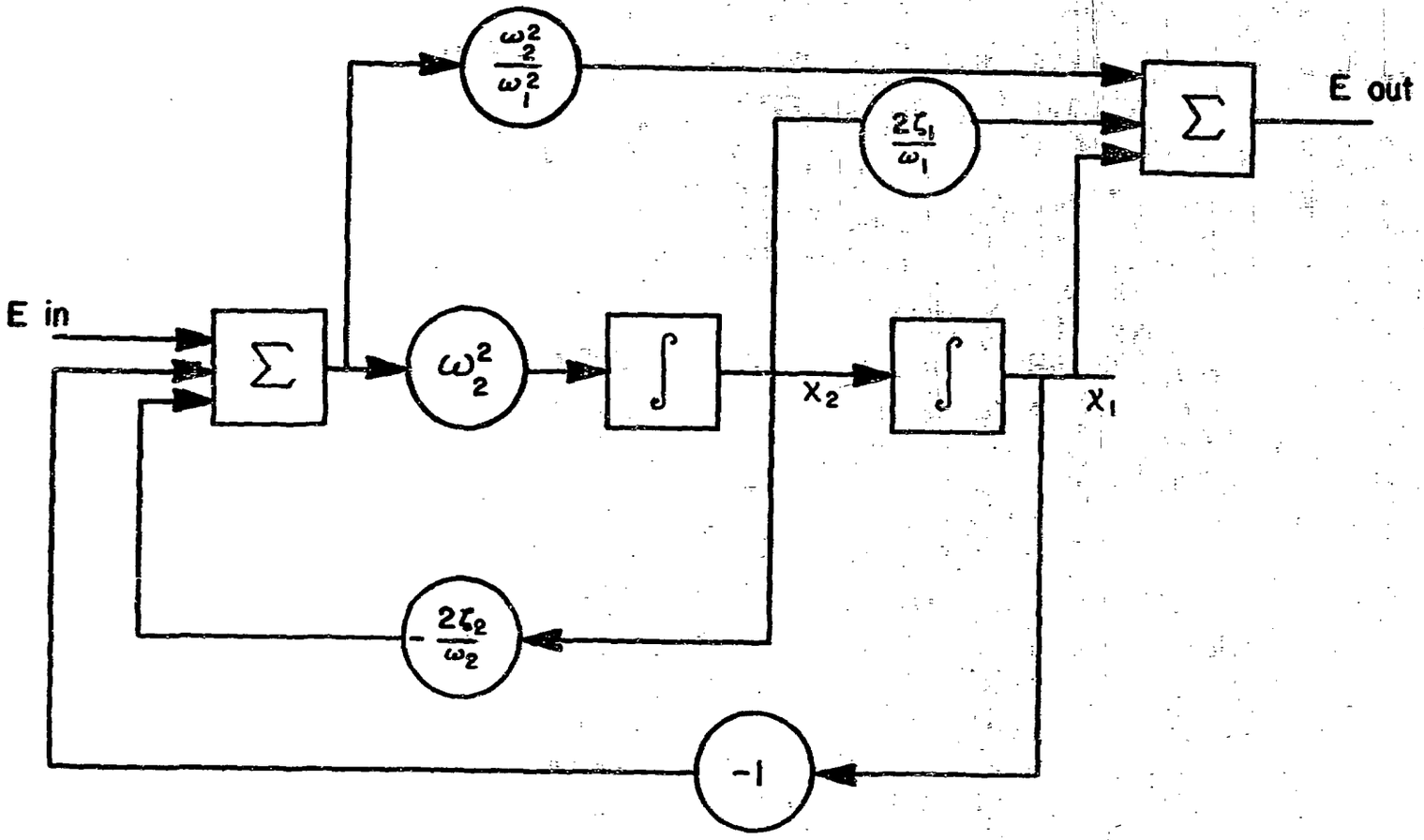

GENERALIZED FILTER BLOCK DIAGRAM

FIGURE 1

Since the data of interest is discrete (due to the digitization process) the solution for the discrete form of subject set of differential equation is needed. A recursive relation exists that allows the computation of the system state at time (k + 1)T based on knowledge of the state at time kT; k is a running index and T is the sampling interval. The recursive relation is given by a formula. (Reference 1)

$$x(k+1)T = G(T)\,x(kT) = H(T)\,u(kT) \tag{7}$$

where $G(T) = e^{At}$; $H(T) = \int_0^T e^{A\tau}\, d\tau\ B$ (8)

The solution of the subject difference equation reduces essentially to computing e^{At} and its integral over T, a tedious, but straightforward task which is rendered simpler by the following substitutions:

$$\zeta_2\,\omega_2 = \alpha \quad ; \quad \omega = \omega_2\sqrt{1-\zeta_2^2} \tag{9}$$

The resulting solution then becomes:

$$\begin{bmatrix} x_1(k+1) \\ x_2(k+1) \end{bmatrix} = \begin{bmatrix} A_{11} & A_{12} \\ A_{21} & A_{22} \end{bmatrix} \begin{bmatrix} x_1(k) \\ x_2(k) \end{bmatrix} + \begin{bmatrix} \omega_2^2 F_{12} \\ \omega_2^2 F_{22} \end{bmatrix} E_{1n}(k) \tag{10}$$

where:

$$A_{11} = e^{-\alpha T}\left(\cos\omega T + \frac{\alpha}{\omega}\sin\omega T\right) \tag{11}$$

$$A_{12} = \frac{1}{\omega}\left(e^{-\alpha T}\sin\omega T\right) \tag{12}$$

$$A_{21} = -\frac{(\alpha^2+\omega^2)}{\omega}\left[e^{-\alpha T}\sin\omega T\right] \tag{13}$$

$$A_{22} = e^{-\alpha T}\left[\cos\omega T - \alpha/\omega\sin\omega T\right] \tag{14}$$

$$F_{12} = \frac{-e^{-\alpha T}}{\omega(\alpha^2+\omega^2)}\left(\alpha\sin\omega T + \omega\cos\omega T\right) + \frac{1}{\alpha^2+\omega^2} \tag{15}$$

$$F_{22} = A_{12} \tag{16}$$

From the original equation, $E_{out}(k)$ is inferred to be (17)

$$E_{out}(k) = \frac{\omega_2^2}{\omega_1^2} E_{in}(k) + \left(1 - \frac{\omega_2^2}{\omega_1^2}\right) x_1(k) + \frac{(2\zeta_1 \omega_1 - 2\zeta_2 \omega_2)}{\omega_1^2} x_2(k)$$

Therefore, the digital algorithm consists of mechanizing the three equations for $x_1(k+1)$, $x_2(k+1)$ and $E_0(k)$. Required inputs are the sequence to be filtered $E_{in}(k)$, and the initial states $x_1(0)$ and $x_2(0)$. $x_1(0)$ represents the value of $E_{in}(k)$ at $t = 0$, whereas, $x_2(0)$ is the initial slope of $E_{in}(k)$. The latter is often not known, in which case it can be estimated or set to zero; this may sometimes cause a transient for a few sampling intervals, a common filter initialization problem. In actual filtered data $x_2(0)$ was zero and transients have not presented a problem.

As previously noted, amplitude distortion is avoided by selecting a filter breakpoint that lies beyond the significant signal frequencies as determined via spectral analysis. Phase shift, however, poses a different problem since there is <u>always some</u> phase shift for all non-zero frequencies. Filter phase shift causes a time delay in the data, defined by:

$$\text{Time delay} \Big|_{\text{given frequency}} = T_d \text{ (secs)} = \frac{\phi}{F} \qquad (18)$$

where ϕ = phase shift in degrees

F = frequency in degrees/sec

It is obvious from the above equations that if we can somehow obtain a <u>linear</u> phase-frequency relationship, then T_d is a constant since it would be defined by the slope of the straight line represented by the T_d equation given above. Filters with such a linear phase characteristic in the signal region are called "constant group delay filters" since each frequency component is delayed the same amount T_d. The <u>only</u> distortion caused by such filters is a pure time shift (delay) by the amount T_d; therefore, the data are easily corrected by applying an equivalent leading shift to the time axis.

The phase shift for any second order transfer characteristic is given by:

$$\phi \text{ (degrees)} = \tan^{-1}\left(\frac{2\zeta_i \omega \omega_i}{\omega_i^2 - \omega^2}\right) \qquad (19)$$

Where ζ_i and ω_i are the damping ratio and natural frequency of the ith second order transfer characteristic and ω is the particular frequency for which we apply ϕ. For a numerator term, ϕ is positive, and negative for a denominator term.

Phase linearity is a function of the specific filter parameters selected. Appropriate parameters can be selected heuristically without undue difficulty with the aid of normalized frequency response plots for the general filter forms. (2) All filters used for data presented in this report were selected with above considerations in mind. For example, the sled accelerometer data were filtered twice; first by a 100 Hz filter with a notch at 500 Hz, then by a 40 Hz low pass section notched at 100 Hz. The composite frequency response is shown in Figure 2, where it is seen that flat response has been preserved well beyond 20 Hz, the established upper limit of signal frequencies. The phase shift in this range is shown in Figure 3, which establishes that good phase linearity has been obtained.

The actual filter parameters for each filtered variable included in this report are shown in Table 1. In each case the time delay was automatically computed during the filtering process and the appropriate corrective time shift introduced in the respective time axis. Sample "before and after" traces for sled acceleration are shown in Figures 4 and 5.

RUN CLASSIFICATION CRITERIA

Due to the variability of accelerator performance, a continuum of sled acceleration and rates of onset were obtained at Wayne State University, rather than the few preset discrete levels. For this reason, some grouping logic was required so that manageable subsets of data could be obtained. The approach used was to establish several "nominal" levels of each variable as follows:

"g" level - 2, 2.5, 3, 4, 5, 6, 7, 8, 9, 10

rate of onset (g's/sec) - 100, 150, 200, 250, 300, 350, 400, 500, 600, 700, 800, 900

This procedure required assignment of a specific sled acceleration and rate of onset level to each run, which presented an additional problem due to the nature of the sled acceleration data. The filtered accelerometer traces such as shown in Figure 5 are a considerable improvement over the original data. With few exceptions, the onset side is of sufficient quality for accurate determination of rate of onset. However, there are enough variations (low frequency oscillations) around the peak to make an accurate assessment of the time of occurrence of the peak acceleration difficult. Therefore, a new algorithm was created to yield the "best" (in a least squares sense) ideal triangular waveform approximation to the filtered sled acceleration traces. This algorithm consisted of the following:

1. Determine the peak acceleration based on the filtered data.

2. Compute the 20% and 80% points.

3. Using all data between these points, compute the best straight line fit in a least squares sense. This was done independently for the positive and negative slopes of the traces.

4. The intersection of these lines was used to define the peck acceleration and the time of occurrence of the peak. The positive slope of the fitted line defined

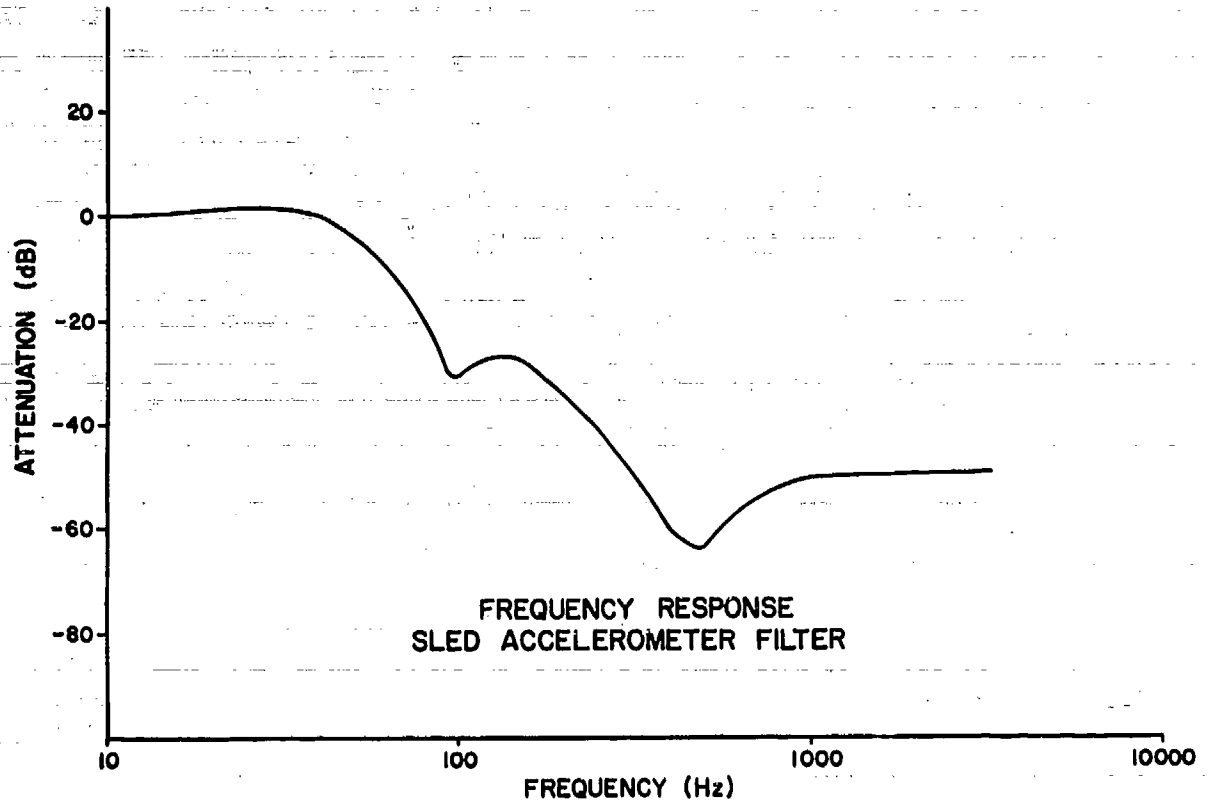

FIGURE 2

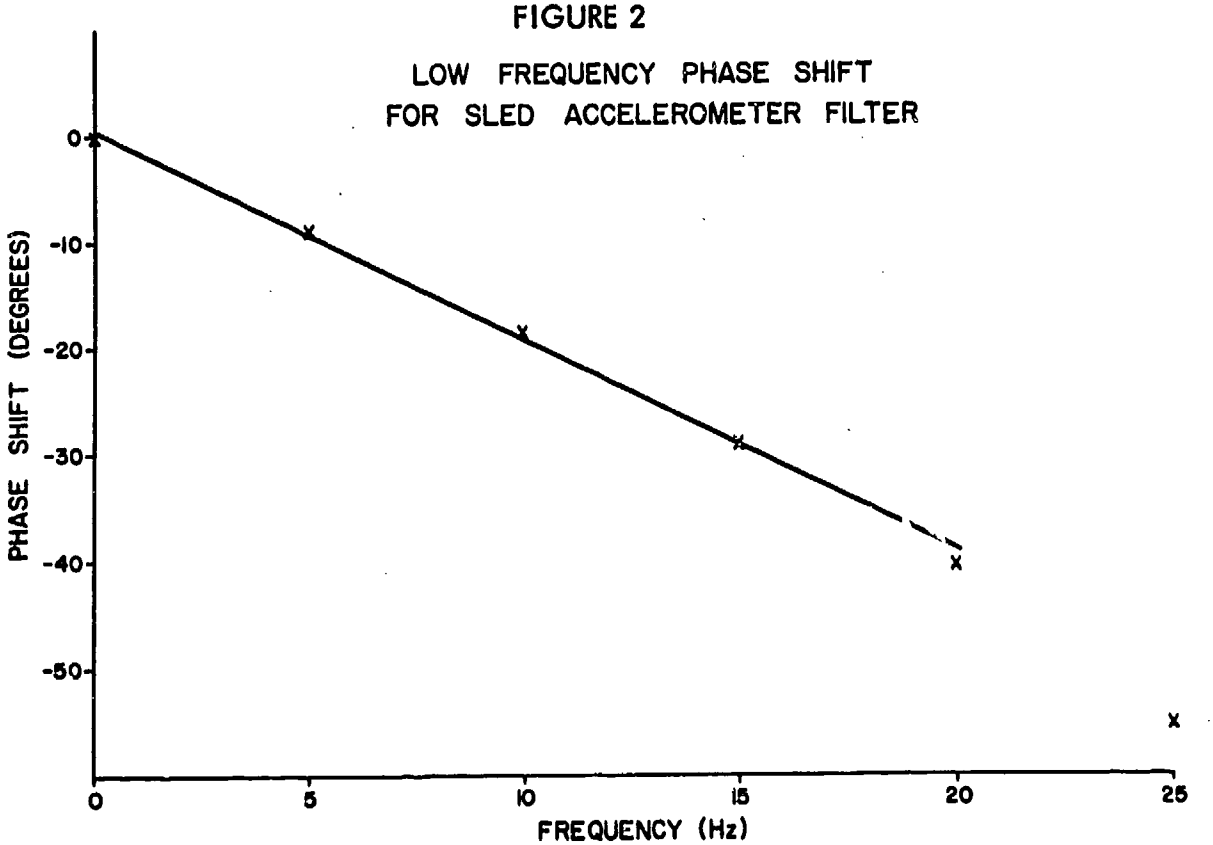

FIGURE 3

TABLE 1 FILTER PARAMETERS

* Variable Name	ω_1	ω_2	ζ_1	ζ_2	Remarks
AXC	3141.6 / 628.3	628.3 / 251.3	.1 / .1	.6 / .6	1st pass / 2nd pass
RVH	None	314.16	None	.6	Notch not used
XCL	None	188.5	None	.6	Notch not used
ZCL	None	188.5	None	.6	Notch not used
XNA	None	188.5	None	.6	Notch not used
ZNA	None	188.5	None	.6	Notch not used

* See variable definition list in Theoretical Mechanics Chapter

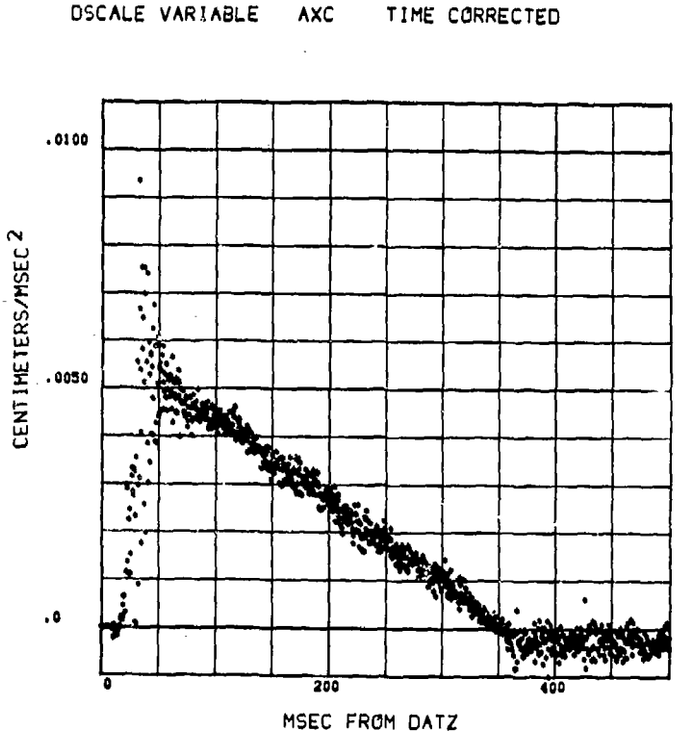

FIGURE 4

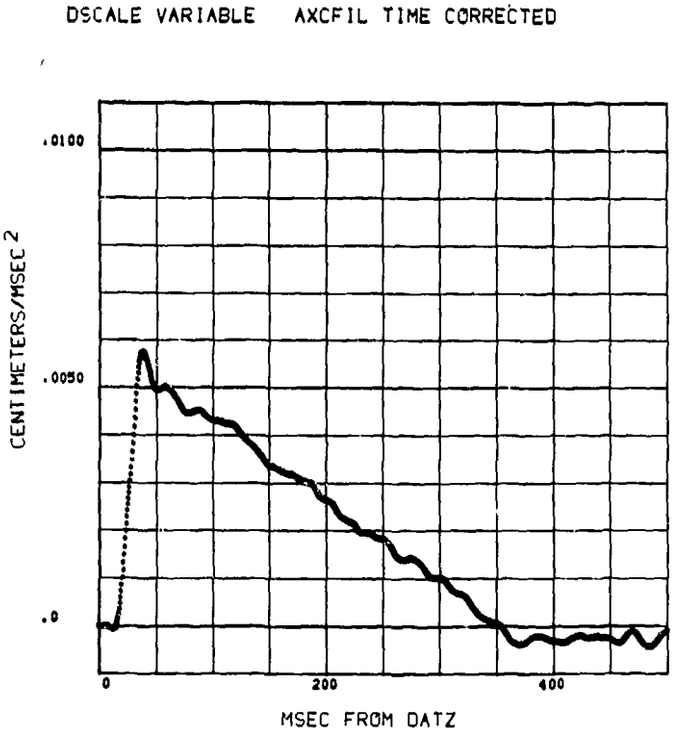

FIGURE 5

the rate of onset. This technique was evaluated by comparing it with previously used ones and found to be significantly superior to previous data in that excellent time correlation among similar runs was obtained.

The data obtained were fitted into one of the previously mentioned categories if it was within + 10% of same. If not, it was left unclassified. In those instances where the + 10% criteria overlapped into two possible nominal categories, the data were fitted to the group to which it was nearest quantitatively. For purposes of this report, the above criteria were broadened somewhat, in order to include a representative number of experiments in each desired category. For example, runs nominally assigned to the 250 g and 350 g levels were grouped with the 300 g runs, and assigned to the latter level.

Selection of sled acceleration parameters for the data presented in this report was based on the above criteria, since these have yielded groupings with very small dispersions in terms of peak acceleration, rate of onset, and time to peak for similar run groupings.

TIME CORRELATION BETWEEN PHOTO AND SENSOR DATA

Two different systems were used to collect data during the WSU impact acceleration experiments: (1) the photo system; and (2) the sensor system. Within either system all the recorded data were found to be well aligned with respect to time. Between systems, however, many runs have exhibited a considerable misalignment, a phenomenon attributable to the fact that a central, synchronized timing system such as IRIG was not employed.

It was necessary, therefore, to find an accurate estimate for the timing misalignment between systems, which was performed as follows: The values for angular displacement of the head derived from the photo data (ADH) are generally in good agreement with the values derived from the rate gyro (RPH), except for a time shift. To determine the shift, the photo values were compared with the rate gyro values for all time shifts + 50 msec from nominal in 0.5 msec increments. The criterion used for evaluating the comparison was the cross correlation coefficient, calculated as

$$P_{xy}(\tau) = \frac{\Sigma x_i y_i - \frac{\Sigma x_i \Sigma y_i}{n}}{\left[\left(\Sigma x_i^2 - \frac{\Sigma x_i^2}{n}\right)\left(\Sigma y_i^2 - \frac{\Sigma y_i^2}{n}\right)\right]^{\frac{1}{2}}} \qquad (20)$$

Where

$P_{xy}(\tau)$ = cross correlation coefficient as a function of time shift.

x_i = i^{th} photo data point.

y_i = sensor data point correspondeing to the $_i$th photo data point after photo data has been shifted.

n = total number of photo data points.

τ = time shift of photo data ranging from - 50 msec to + 50 msec, in 0.5 msec increments.

As P xy (τ) increases to 1 the relationship between x and y values becomes more closely approximated by an equation of the form

$$x_i = ay_i + b \tag{21}$$

As P xy (τ) decreases from 1 the linear relationship becomes less able to account for differences between the x and y values.

Thus, the best agreement between the two data series occurs at the time shift τ at which P xy (τ) is maximum.

A computer program was written to calculate P xy (τ) for the different τ values for each run, and to list the run number, the best estimate of the time shift for the photo data, and the corresponding cross correlation value.

Results for the data presented in this report are summarized in Table 2.

REFERENCES

(1) Ogata, K. State Space Analysis of Control Systems, pp 337-340, Prentice-Hall, 1967.

(2) Del Toro & Parker, Principles of Control Systems Engineering, pp 185-190, McGraw Hill, N.Y., 1950.

TABLE 2

RESULTS OF THE TIME CORRELATION ANALYSIS BETWEEN PHOTO AND SENSOR DATA FOR HEAD ANGULAR DISPLACEMENT

SUBJECT NO.	PEAK G	ROO	PHOTO TAU (Correction to Time Axis)	CROSS CORRELATION
007	6.8	360	6.000	1.000
004	6.9	390	5.500	1.000
008	5.5	300	1.500	.999
011	5.5	280	6.500	1.000
016	5.5	250	4.000	1.000
010	7.2	320	4.000	1.000
012	5.7	340	5.500	1.000
016	7.4	450	5.000	1.000
004	8.9	630	4.000	.999
007	8.5	350	3.500	1.000
004	5.9	330	8.000	.999
017	5.6	340	2.500	1.000
011	8.3	300	-3.500	1.000
010	8.9	330	-3.500	.999
012	8.1	370	3.000	.999
003	5.9	560	11.000	1.000
017	8.0	410	1.500	.999
011	5.8	510	9.000	1.000
015	7.0	380	2.500	1.000
013	7.2	320	3.500	1.000
017	8.9	560	2.000	1.000
016	5.8	630	9.000	1.000
011	8.9	380	-2.500	1.000
003	7.2	400	1.000	1.000
016	8.4	440	.000	.999
010	6.0	560	8.500	1.000
004	6.1	620	12.000	1.000
009	8.4	560	3.000	1.000

TABLE 2 (Continued)

SUBJECT NO.	PEAK G	ROO	PHOTO TAU (Correction to Time Axis)	CROSS CORRELATION
012	9.8	530	8.000	1.000
011	7.4	520	26.000	1.000
009	9.0	330	14.500	.999
016	8.4	340	14.000	.998
012	7.2	630	12.500	.995
010	7.1	510	11.500	.999
003	9.5	350	2.000	1.000
013	9.1	530	15.500	.995
004	9.0	550	25.000	.978
007	9.6	630	33.000	.993
004	9.4	330	7.000	.998
015	9.1	450	5.000	.998
015	9.9	460	9.500	.999

RESULTS CHAPTER

RUN GROUPINGS

All runs in this report were conducted at Wayne State University between 30 January and 23 April 1969.

For this report, forty-one runs were selected on the basis that: (a) no transducer or camera failures had occurred during the run; (b) all data were available from both photographic and transducer instrumentation systems; (c) the runs were fully instrumented with a sled peak acceleration category of 6 G or higher; (d) all data processing had been completed in time to include the runs in this report. There are numerous additional runs which were excluded by not appearing in all 4 categories.

The runs were grouped by volunteer sitting height percentile and by subject and sled peak acceleration category as noted in Table 1, and by volunteer as shown in Table 2.

To show repeatability, two nearly identical runs each on three subjects are presented. One subject had two pairs of nearly identical runs. The subjects and their runs are presented in Table 3.

The overall results are presented in 755 black and white computer-drawn plots, numbered consecutively from 1 through 755 and individually labeled. They are listed in the plot table of contents and presented in a separate plot section. The variable symbols are defined in detail in the Theoretical Kinematics section of the report. Careful attention was given to clarity of presentation to facilitate comparison of the curves on each plot. In several cases this required plotting fewer data words than available on the data tapes to prevent overlap of the curve symbols. The appearance of the data is unchanged as seen by comparing identical variable curves in which both every word was plotted; and every sixth word was plotted. The plotting density is as follows:

Plot	Plot Density
1 - 36 78 - 86 128 - 136 367 - 429	Every sixth data word (N=6)

Plot	Plot Density
178 - 366 430 - 516 521, 568, 592 612 - 632	Every other data word (N=2)
37 -77 87 - 127 137 - 177 493 - 520 522 - 567 569 - 591 593 - 611 633 - 755	Every data word (N=1)

The time interval between plot points for variables derived from sensor data is N x 0.5 msec, where N is indicated above. For variables derived from photographic data the relation is N x 2.0 msec.

Variable Discussion

Plots 1 through 27 present the performance of the accelerator, grouped by sled peak acceleration and rate of onset of acceleration. The sled acceleration as presented has been filtered as explained in the section on signal conditioning. Because of the demonstrated repeatability, the grouping by sled peak acceleration and rate of onset of acceleration is an excellent way of establishing categories for presentation of the variables measured from the experimental subjects.

Plots 28 through 177 present the Cartesian components and magnitudes of the linear acceleration computed at the head C.G. Each variable is presented grouped first by sled peak acceleration category and then with the same curves as individual plots. The Cartesian components 4XM, 4ZM are quite detailed and complex. The peaks and time of peak repeatability is illustrated on the plots grouped by sled acceleration category. The resultant magnitude, 4XZ, of the components 4XM and 4ZM has two characteristic peaks. The first peak is sharp occurring at about 75 milliseconds after DATZ for all runs. The repeatability within sled acceleration grouping is illustrated. The maximum resultant of about 27 G's occurred in plot 176, subject 11, 8.9G, 380 g/sec.

The linear velocity data measured on the subject is presented on plots 178 through 303. Each variable is plotted grouped by subject and then grouped by sled peak acceleration. The Cartesian components and magnitude of the head C. G. linear velocity relative to the sled are represented by XCV, ZCV, and XZV. The magnitude XZV demonstrates two successive peaks which are repeatable in peak and time for DATZ at a given run level. The peaks systematically increase in value with increasing sled peak acceleration level. The maximum velocity of about 480 centimeters per second occurred on plot 240 on subjects 07, 9.6G, 630 G/sec and 12, 9.8G, 530 G/sec.

The analogous linear velocities of the head relative to T_1 are XNV, ZNV, and NNV. These variables illustrate the velocity of the head C. G. with the velocity of the first thoracic vertebra subtracted. The only change is a relatively small reduction of the velocity peaks.

The linear displacement of the head C. G. relative to the anterior superior corner of the first thoracic vertebra is shown in plots 304 through 366 as Cartesian components XCN, ZCN and magnitude MCT. The X component XCN shows apparent increase in amplitude with sled acceleration. The Z component ZCN decreases, and then becomes negative or, stated differently, goes below a line perpendicular to gravity and passing through the T_1 origin, with increasing sled acceleration. This result was anticipated due to the increasing anterior bending of the head and neck with higher acceleration. The magnitude MCT shows little change. The small change present is a decrease in value up to 3 to 3.5 centimeters. For these three variables the response is apparently very repeatable and characteristic.

The plots of MCT as a function of time should be considered in conjunction with the headnod and dynamic event plots of MCX, MCZ arranged by subject, plots 493 through 516. Both the headnod (HEDNOD DATA) and the dynamic event (PHOTOGRAPHIC DATA) plots illustrate segments approximating the arc of a circle. There are no apparent major differences between the arcs from headnod and the dynamic event. Time increases with each data point from the upper left to the lower right on the plots. The plots are presented to illustrate the geometry of the impact induced motion (PHOTOGRAPHIC DATA) as compared with the geometry of a voluntary headnod (HEDNOD DATA). Also, these can be used with a protractor to determine MCT for any angular increment desired, with the zero point of the protractor placed on the origin of the plot coordinate system.

The angular acceleration of the head, RAH is shown in plots 367 through 387. There is a characteristic triphasic response lasting from 50 to 225 milliseconds after DATZ. The response is repeatable from subject to subject within sled acceleration

level. The first peak increases with increasing sled peak acceleration. The maximum angular acceleration of approximately 91,000 degrees per second squared was reached on subject 12, 9.8G, 530 G/sec, plot 387.

The angular velocity of the head (RVH) is presented in plots 388 through 408. The response illustrates the same degree of repeatability as RAH. Also an increasing response with increasing sled acceleration is evident. The shape of the curve and time of peaks are consistent with its differentiated value RAH. The maximum value of about 1,700 degrees per second is slightly less than 30 radians per second on plot 408, subject 07, 9.6G, 630G/sec. A higher peak from a run not included in this group was previously reported (1).

The angular velocity of the head relative to T_1 (RHN) is illustrated in plots 409 through 420. RHN is angular velocity of head (RVH) minus the angular velocity of T_1 (RVN). The effect of this subtraction is minimal. Therefore, RHN has a shape and amplitude similar to RVH. The most consistent result is that RHN is slightly smaller in peak amplitude than RVH. This was anticipated since regardless of the tightness of torso restraint, T_1 will have some small anterior displacement and rotation yielding an angular velocity.

Angular displacement of the head, PDH, is demonstrated in plots 430 through 450. All curves of PDH show a characteristic and repeatable pattern. The maximum change in PDH from initial value to peak value was 91 degrees occurring on plot 450, subject 07, 9.6G, 630G/sec. Also, the maximum angular displacement is increased with increasing peak acceleration of the sled.

The angular displacement of T_1 (NRN) is shown in plots 451 through 471. These plots show a much smaller angular displacement of T_1 as compared with the angular displacement of the head. Presumably this is a function of the restraint system, among other factors.

The angular displacement of the head relative to T_1 (PHN) is calculated by subtracting NRN from PDH, plots 472 through 492. PHN has only minor changes from PDH. Essentially, the peak of PHN is less than PDH due to the small angular displacement of T_1.

The plots from 1 through 516 contain substantially all the results of the report.

Repeatability Discussion

Repeatability is demonstrated by plots 517 through 611. The runs thus selected were paired according to the following criteria:

a) identical subject

b) essentially identical sled peak acceleration

c) similar rate of onset of sled acceleration

Four pairs of runs were thus identified. It should be noted that the initial conditions within a selected pair of runs were not precisely controlled. However, they were carefully measured and are represented for all variables by the first value on the plots. This is an important consideration since differences in initial conditions from run to run on the same subject may be a source of variation in the ensuing response.

The repeatability plots include those of the acceleration transformed to the head C.G. from the mouth and head accelerometer pairs. This is the 4FM vs. 4FD comparison, and the 4SM vs. 4SD comparison. It is therefore possible, with the two plots from the paired runs to compare the repeatability of several functions.

In addition, all variables which are presented in plots 1 through 492 except for XVC and XDC are presented for the 4 pairs selected. A completely repeatable response would be illustrated by identical traces of the paired observations on each plot. Review of each plot shows only minor differences between paired observations. The largest of these differences can be seen to be associated with variations of the initial conditions evident from the first values on the plots. In most cases each variable is repeatable to approximately the same degree as the sled acceleration trace. In these plots every digital data word is plotted.

Quality Control Discussion

Quality control is illustrated by the group of plots from 612 to 755. HSP is the headspan distance from the mouth target to the head target and is illustrated in plots 612 through 632. It should be a constant throughout the experimental run. Also the value should be identical for a given subject for all runs. Plots 612 to 623 grouped by subject show that the maximum difference in the initial value of HSP is only 5 millimeters. For most subjects the difference is even less. This small distance approaches the effective resolution of the photographic system. Review of HSP grouped by sled peak acceleration category, plots 624 to 632, show the amount of variation developing during the dynamic event. This variation remains quite small for most subjects for most runs. In the worst case, maximum change was 5% of the HSP value. As such it confirms the following presumptions:

a) the response of the head was two dimensional in the mid-sagittal plane.

b) the head and attached mounts acted as a rigid body.

c) the effects of error introduced by the photographic data system, including scaling, were satisfactorily controlled.

d) the mounts were placed on the head in the same place from run to run on the same subject.

Review of the headspan plots also discloses those precise data points where photographic data acquisition was incomplete. This is indicated by gaps in the individual traces. It should be noted that these gaps are carried throughout all variables derived from photographic data. No interpolation has been used except as required for differentiation routines as defined in the signal conditioning section, Table 1. Even in those cases the gaps are maintained in the finally presented differentiated variable. The reason for the gaps is that the targets were not acquired by the camera, usually because some portion of the mount straps or the anatomy occluded the target.

A comparison of angular displacement of the head, PDH, derived from photographic data; and angular displacement of the head, RDH, derived from the rate gyroscope output by integration, is presented in plots 633 to 673. By definition they should be identical. Some minor differences can be seen by reviewing the plots. This comparison validates:

a) the ability of the sensor data system to supply accurate angular displacement information.

b) the scaling and accuracy of both sensor and photographic data.

c) the validity of the measured response due to the fact that the measurement systems are independent.

d) the two dimensional nature of the response.

e) the minimal error due to parallax in the photographic data system.

Plots 674 through 755 are presented as evidence of validation of the coordinate system transformation procedure applied to the measured data. The variables in these plots are components of the acceleration at the center of gravity of the head derived from the mouth mount acceleration and the head mount acceleration which are independently measured. By definition the measurements should be identical. The plots illustrate the correspondence and limited variation between the two independent measurements. The lack of variance tends to verify:

a) coplanar placement of the accelerometers, in the plane of induced motion.

b) accurate analog recording of the data.

c) accurate analog to digital conversion of the data.

d) accurate scaling of the data.

e) accurate execution of the programs which transform the data.

f) stability of the mounts on the head and at the mouth.

g) motion of the head, and attached mounts and transducers as a rigid body.

h) accuracy of the x-ray anthropometry methodology.

In summary the results are a selected sample of 41 runs illustrating major variables and features of the data. The 29 variables presented represent only a sample of those available. The runs presented represent about 25% of those eventually available.

The best representation of the results is the plotted data. Much more information is inherent in these plots and the digital data bank from which they were derived than could be described in a single monograph.

Spectral Characteristics of the Sampled Data by William Anderson

The Fourier coefficients of the measured photo time series were calculated. In all cases the amplitudes of the Fourier components for frequencies greater than 30 HZ were at noise levels. This substantiates the assumption that a photo sampling rate of 500 frames/sec is adequate, and also indicates that a 30 HZ low-pass filter would be suitable for removing noise from the signal.

The Fourier coefficients of the measured rate gyro time series were also calculated. The rate gyro signals normally had Fourier components at noise levels for frequencies larger than 40 HZ. Consequently, a 50 HZ low-pass filter was used to remove noise from the signals. The spectral analysis of the data series also demonstrated that the frequency response of the rate gyros (64 Hz, $\pm$4 Hz) was adequate.

The Fourier coefficients of the measured accelerometer time series were calculated. The frequencies at which the amplitudes dropped into the noise regions were dependent on the peak sled acceleration and the amount of mount slippage, if any, that was present.

For some data it was suspected that the frequency response of the accelerometer was attenuating the signal. The accelerometer calibrations yielded a range of natural frequencies from 112 Hz to 165 Hz, and a range of damping ratios from 0.5 to 0.8. However, when the data was compensated for the accelerometer attenuation no significant change was observed. Thus, it may be concluded that the frequency characteristics of the measured accelerometer data have been preserved.

It should be mentioned here that, except for sled acceleration, the only filtering done was to smooth data enough to calculate time derivatives.

Volunteer Results Discussion

The two hundred and thirty-six human exposures among the total volunteer group of 17 subjects were conducted without injury. Complete records of the examinations at time of qualification, at time of departure from the program and at time of follow-up one or more years after cessation of the experiments disclosed no pathological changes. Examination before and after each run are on record and revealed only minor surface abrasion of a few areas of skin covered by the restraint system. In every case the subject continued his usual duty and off-duty activities after the post-run examination.

REFERENCE

(1) Ewing, C. L.; Thomas, D. J.; Patrick, L. M.; Beeler, G. W.; and Smith, M. J.: Living human dynamic response to $-G_x$ impact acceleration. II - Accelerations measured on the head and neck. Proceedings of the Thirteenth Stapp Car Crash Conference. New York: Society of Automotive Engineers, Inc., 1969, pp. 400 - 415.

RUN DISTRIBUTION BY VOLUNTEER SITTING HEIGHT AND SLED ACCELERATION CATEGORY

Percentile Group	Subject No.	Category Acc.	Category Onset	Actual Acc.	Actual Onset
12th - 30th	017	6	300	5.6	340
	013	7	300	7.2	320
	015	7	500	7.0	380
	009	8	500	8.4	560
	017	8	500	8.0	410
	009	9	300	9.0	330
	013	9	500	9.1	530
	015	9	500	9.1	450
	017	9	500	8.9	560
	015	10	500	9.9	460
47th - 60th	016	6	300	5.5	250
	004	6	300	5.9	330
	016	6	500	5.8	630
	003	6	500	5.9	560
	004	6	500	6.1	620
	016	7	500	7.4	450
	003	7	500	7.2	400
	004	7	500	6.9	390
	016	8	300	8.4	340
	016	8	500	8.4	440
	003	9	300	9.5	350
	004	9	300	9.4	330
	004	9	500	8.9	630
	004	9	500	9.0	550
87th - 96th	011	6	300	5.5	280
	012	6	300	5.7	340
	008	6	300	5.5	300
	011	6	500	5.8	510
	010	6	500	6.0	560
	007	7	300	6.8	360
	010	7	300	7.2	320
	011	7	500	7.4	520
	012	7	500	7.2	630
	010	7	500	7.1	510
	011	8	300	8.3	300
	012	8	300	8.1	370
	007	8	300	8.5	350
	011	9	300	8.9	380
	010	9	300	8.9	330

RUN DISTRIBUTION BY VOLUNTEER SITTING HEIGHT AND SLED ACCELERATION CATEGORY

Percentile Group	Subject No.	Category		Actual	
		Acc.	Onset	Acc.	Onset
87th - 96th	012	10	500	9.8	530
	007	10	500	9.6	630

TABLE R-1

RUN DISTRIBUTION BY SUBJECT AND SLED PEAK ACCELERATION

12th to 30th Percentile

Subject No.	Percentile	Actual Acc.	Actual Onset
013	12%	7.2	320
		9.1	530
009	18%	8.4	560
		9.0	330
015	29%	7.0	380
		9.1	450
		9.9	460
017	30%	5.6	340
		8.0	410
		8.9	560

47th to 60th Percentile

016	47%	5.5	250
		7.4	450
		5.8	630
		8.4	440
		8.4	340
003	53%	5.9	560
		7.2	400
		9.5	350
004	60%	6.9	390
		8.9	630
		5.9	330
		6.1	620
		9.0	550
		9.4	330

87th to 96th Percentile

011	87%	5.5	280
		8.3	300
		5.8	510
		8.9	380
		7.4	520
012	88%	5.7	340
		8.1	370
		9.8	530
		7.2	630

RUN DISTRIBUTION BY SUBJECT AND SLED PEAK ACCELERATION

87th to 96th Percentile

Subject No.	Percentile	Actual Acc.	Actual Onset
008	95%	5.5	300
007	96%	6.8	360
		8.5	350
		9.6	630
010	96%	7.2	320
		8.9	330
		6.0	560
		7.1	510

TABLE R-2

REPEATABILITY PLOTS

Subject	Actual Acceleration	Actual Rate of Onset
004	8.9 & 9.0	630 & 550
004	5.9 & 6.1	330 & 620
010	7.2 & 7.1	320 & 510
016	8.4 & 8.4	440 & 340

TABLE R-3

CONCLUSIONS

The considerable theoretical, experimental, data processing, and analytical effort described has resulted in development of a detailed and validated set of data describing the complete two dimensional kinematic response of the human head relative to the first thoracic vertebra and selected reference coordinate systems. The described responses are for 41 $-G_x$ impact acceleration experiments on 12 human subjects with torso and pelvic restraint.

From careful examination of the results, it would appear that:

a) the response of the unrestrained human head and neck to $-G_x$ impact acceleration is two dimensional in the mid-sagittal plane.

b) the response is characteristic, and repeatable.

c) simultaneous photographic and sensor measurement of the response is possible, thus permitting cross validation.

d) adequate presentation of the response requires detailed plotting of the variables as a function of time. Tabular presentation of variable peak magnitudes is not an adequate way of presenting the complexities of human dynamic response.

e) the utilization of the theoretical mechanics of rigid body motion is a valid experimental design basis for measuring the response of human head and neck to impact acceleration.

From the methods of measurement it is further concluded that:

a) the use of x-ray anthropometry permits X, Y and Z coordinate description of the position of the center of gravity of the head within a head anatomical coordinate system.

b) the use of x-ray anthropometry and the center of gravity determination makes it possible to express the data at the center of gravity of the head rather than at the anatomical mounts. This permits description of the response in a way which is independent of: anatomical variations from subject to subject; possibly from species to species; location of instrumentation mounting.

c) the sampling rates of the photographic data system and the frequency response of the sensor data system were sufficiently broad band to measure completely the response, in the reported experiments.

d) the automatic data acquisition, reduction, and analysis of the measurements makes it possible to conduct the large number of experiments of this type necessary to achieve statistical significance. The computer-drawn plots of the data illustrate the success of the effort. However, the variables presented in the report are only a partial sampling of what is presently available. Exhaustive and effective use of the data requires large scale digital computer interaction with the data base on a continuing basis. The specific interaction should be determined by the specific problem posed.

Certain other conclusions can be drawn regarding the utilization of the data, which can be used for: (a) the evaluation of any proposed two dimensional analog of the human head or neck up to 9.9G peak vehicle acceleration, in the $-G_x$ direction, and up to 800G/sec rate of onset of acceleration; (b) comparison of the response of non-human primates to the human response, which establishes a means for calibrating non-human impact acceleration experiments; (c) an exact measure of the inertial input to the various physiological system of primates, therefore serving as a basis to which to relate physiological responses to impact acceleration.

Finally, the measurement of the kinematics, numerical documentation of the anatomy by x-ray, and measurement of the center of gravity of the head in the head anatomy make it feasible to develop a valid dynamic model of the human head and neck.

PLOT SECTION

TABLE OF CONTENTS

PLOT SECTION

TABLE OF CONTENTS

PLOT SECTION

TABLE OF CONTENTS

PLOT SECTION

TABLE OF CONTENTS

AXC SLED ACCELERATION

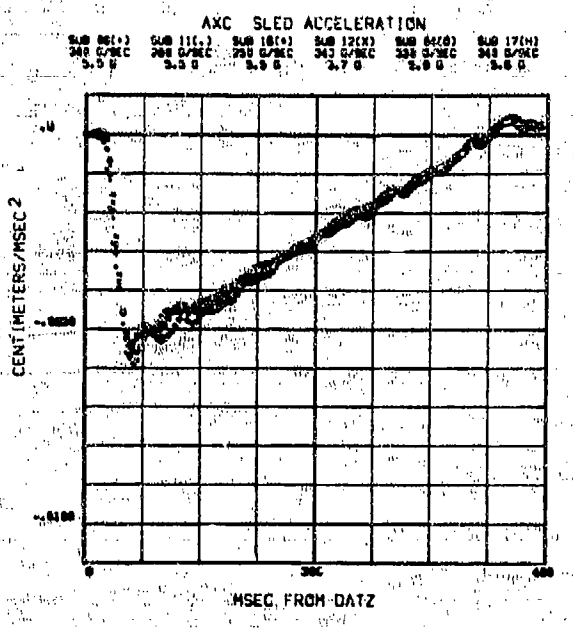

1

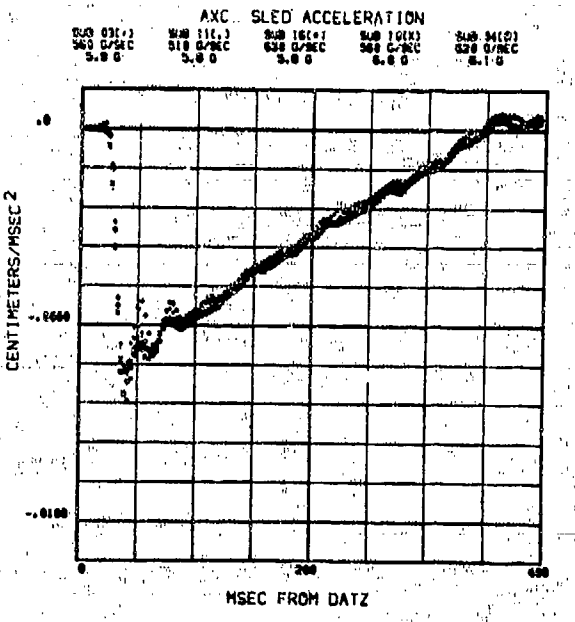

2

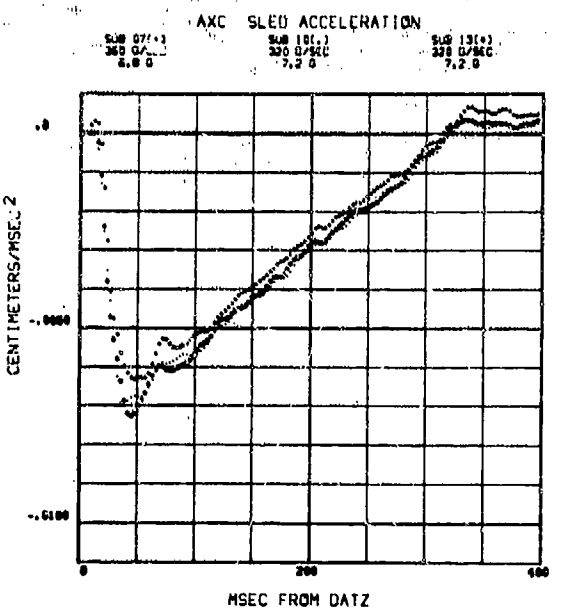

3

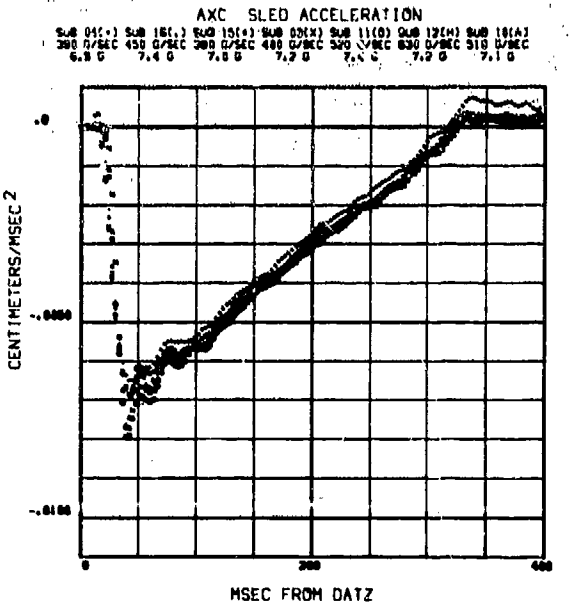

4

AXC SLED ACCELERATION

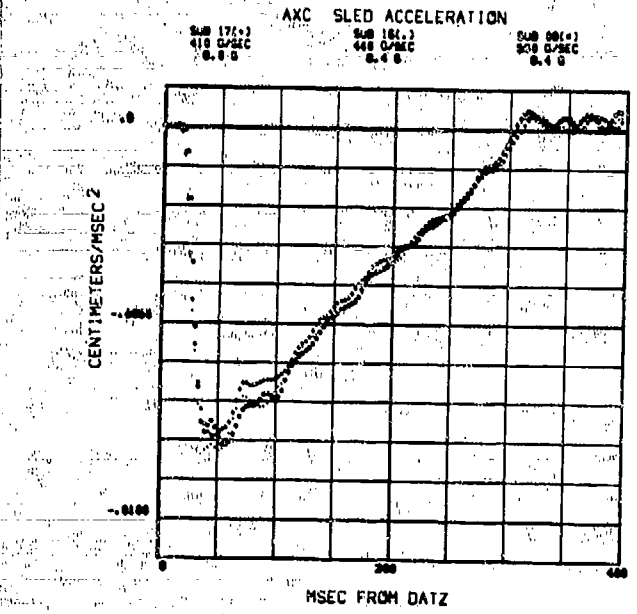

5

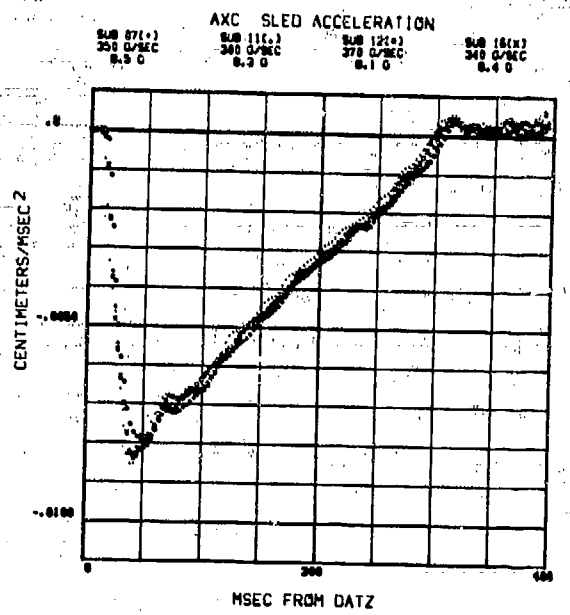

6

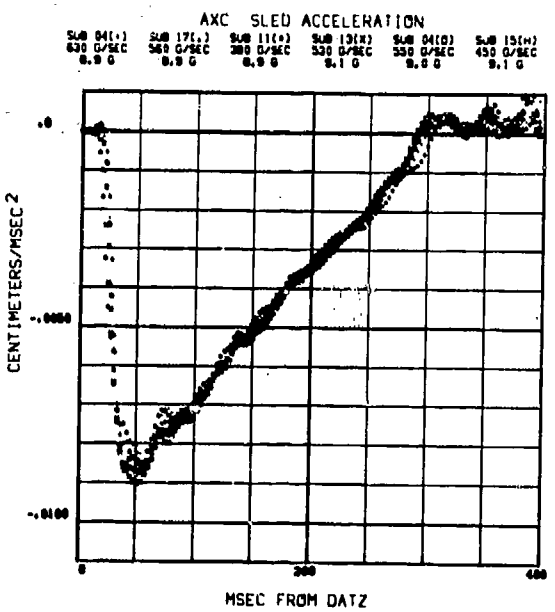

7

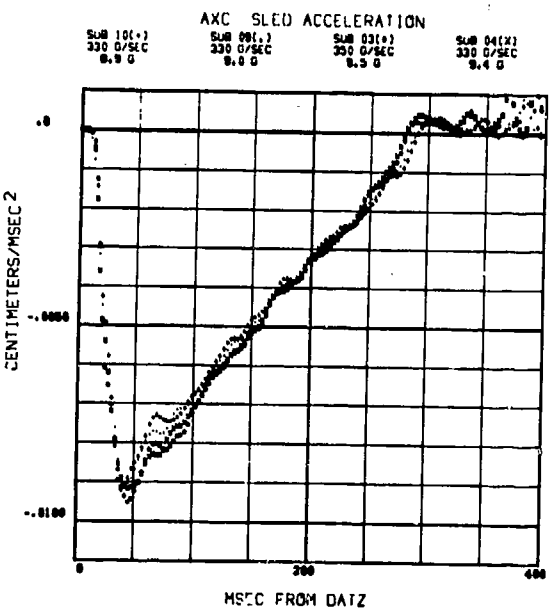

8

AXC SLED ACCELERATION

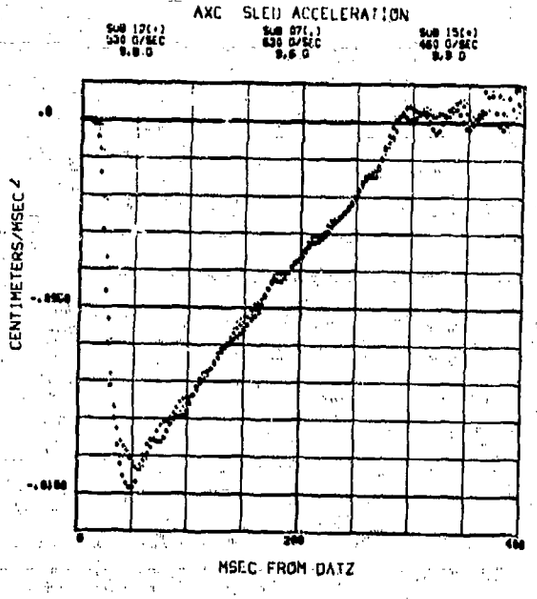

9

XVC SLED VELOCITY

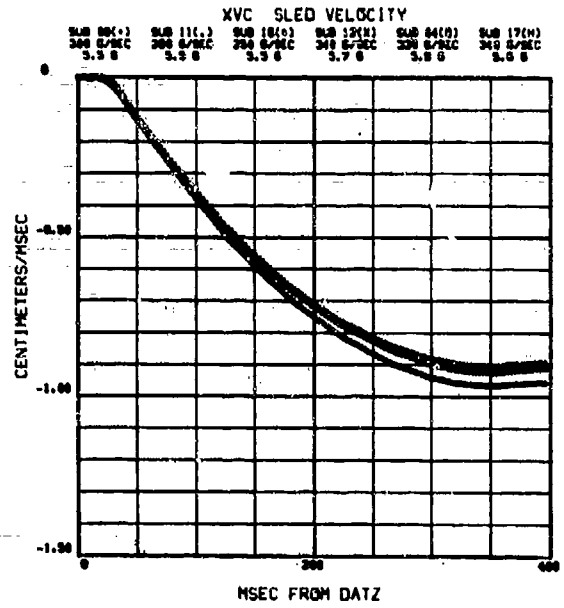

10

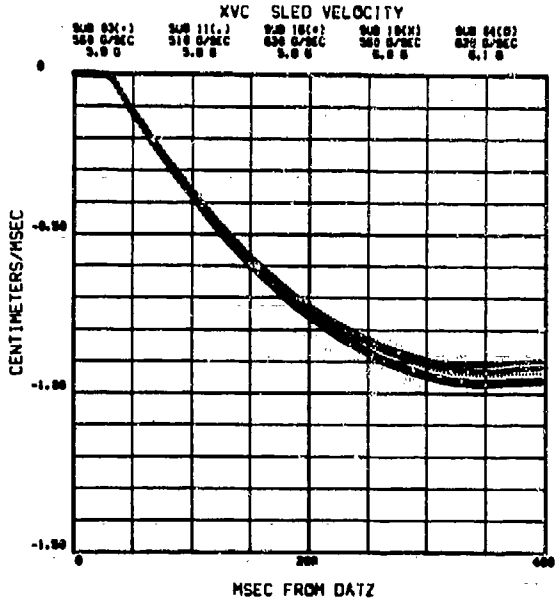

11

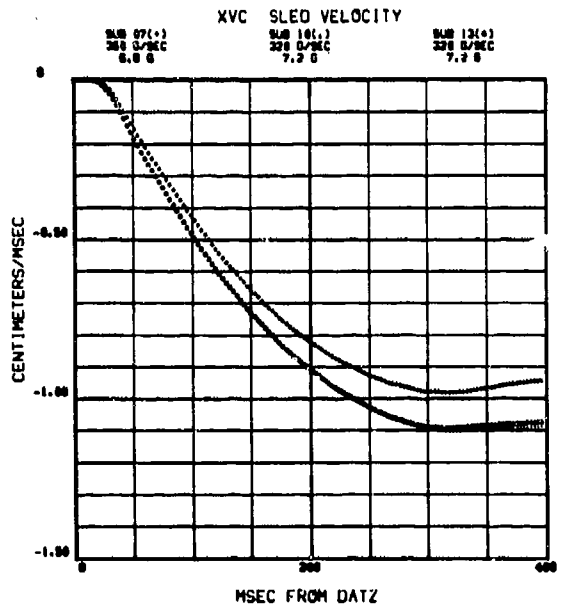

12

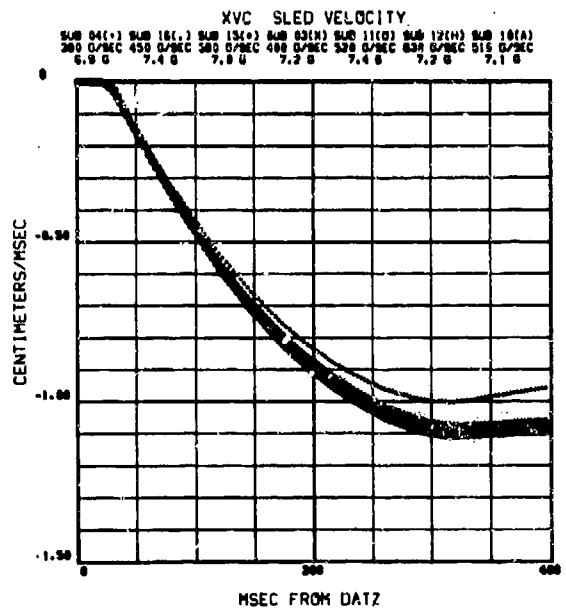

13

XVC SLED VELOCITY

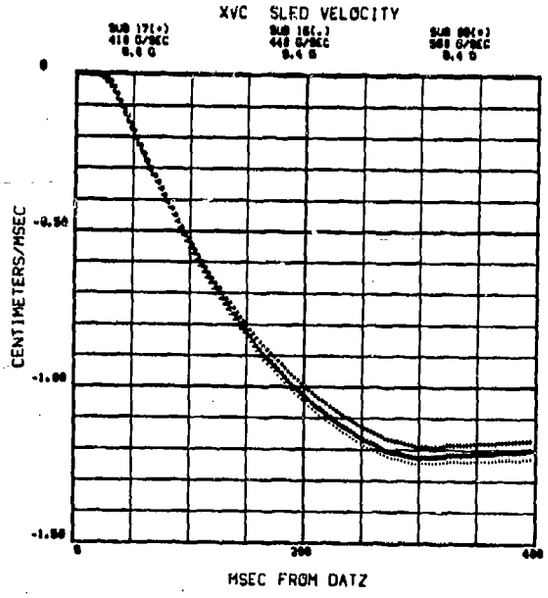

14

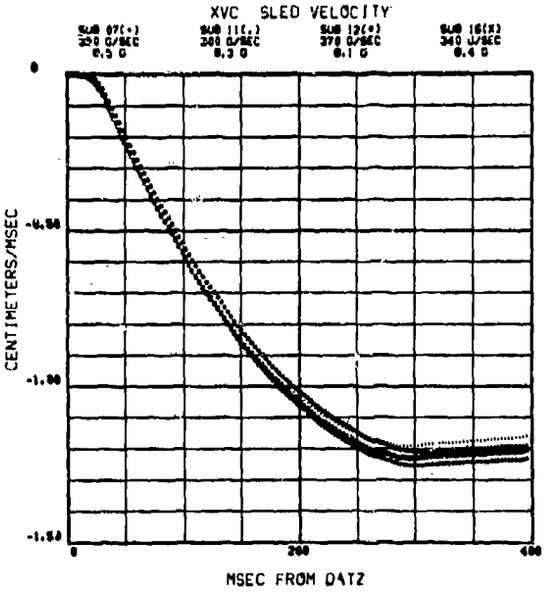

15

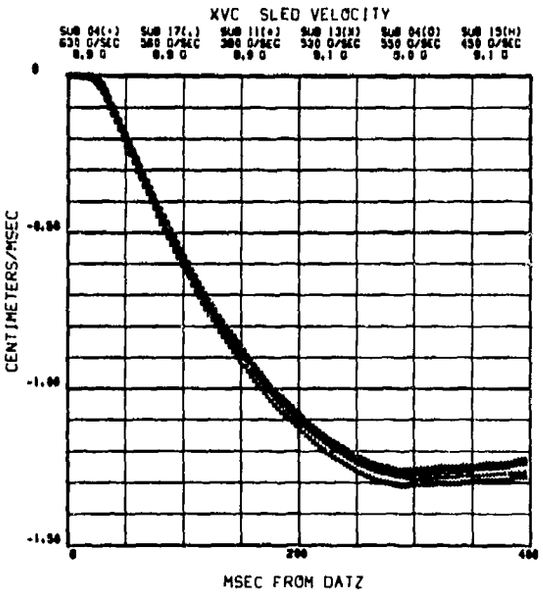

16

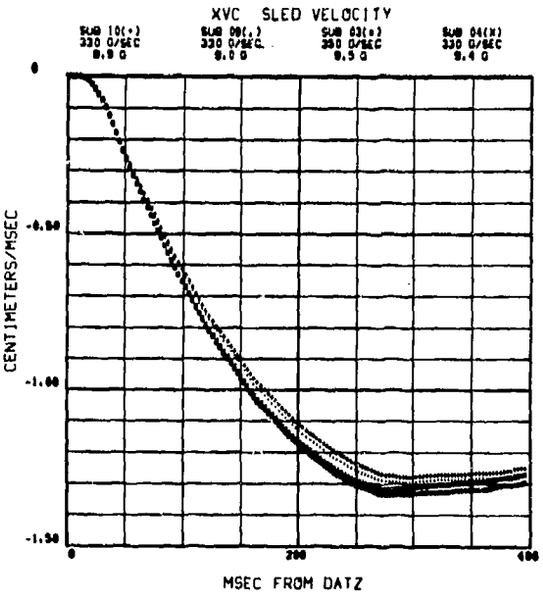

17

XVC SLED VELOCITY

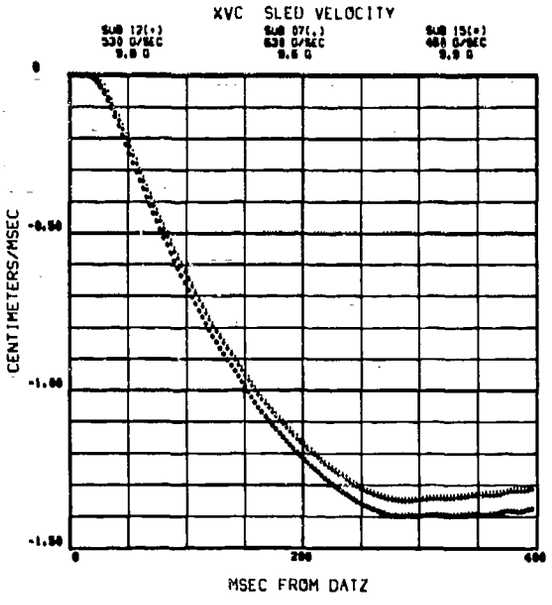

XDC SLED DISPLACEMENT

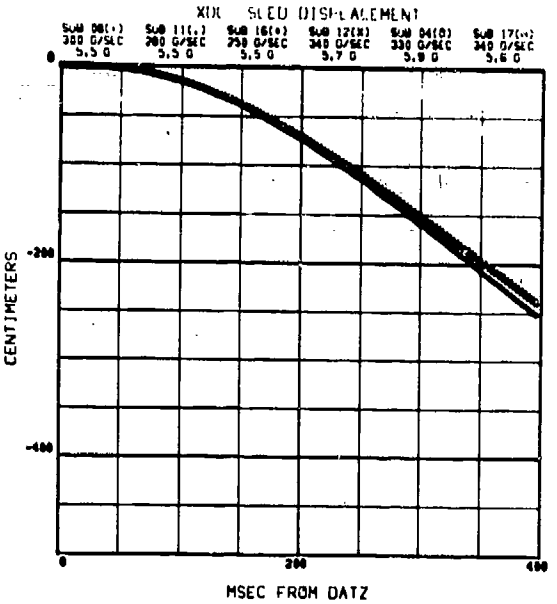

19

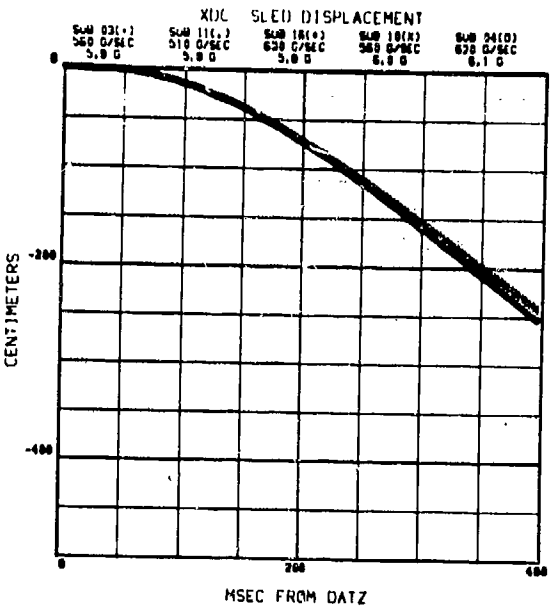

20

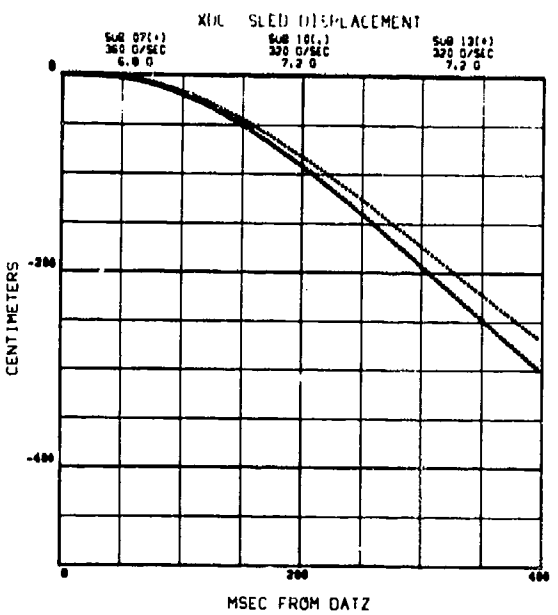

21

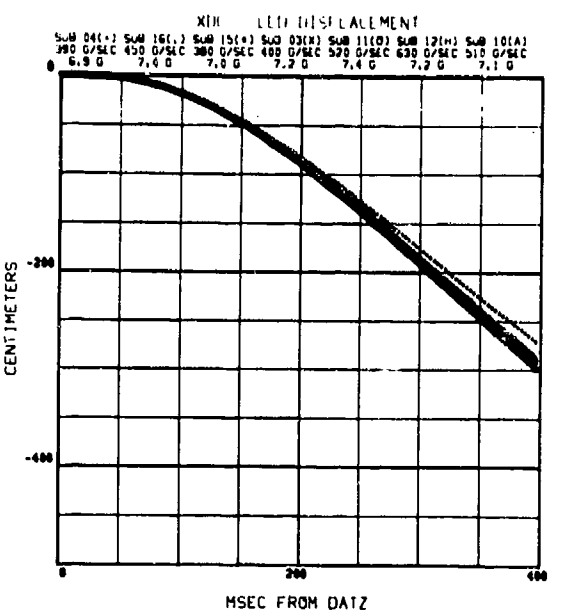

22

XDC SLED DISPLACEMENT

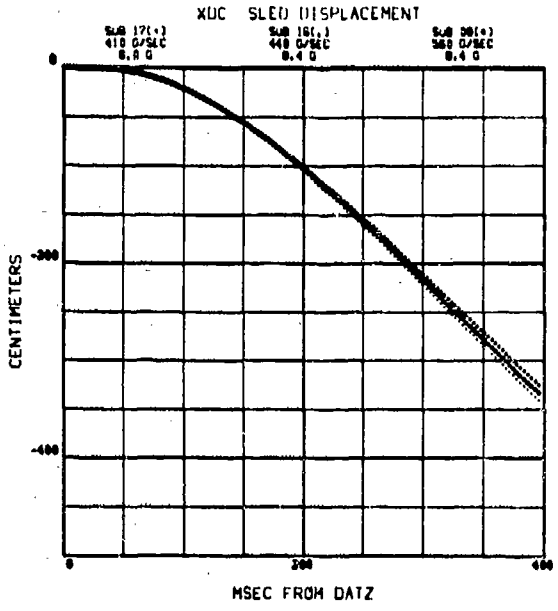

23

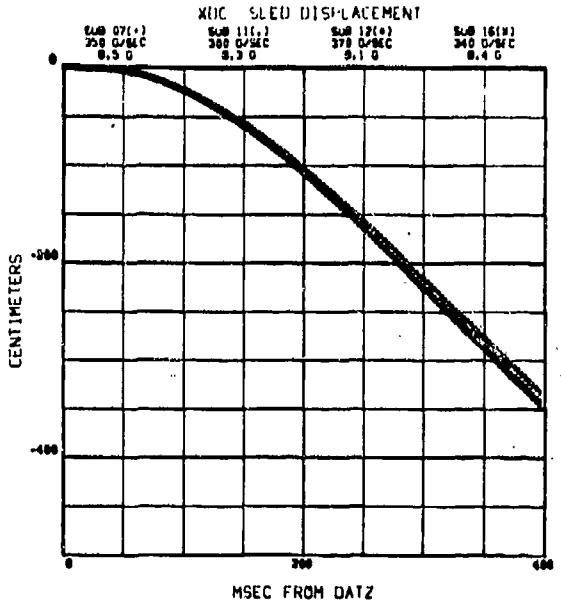

24

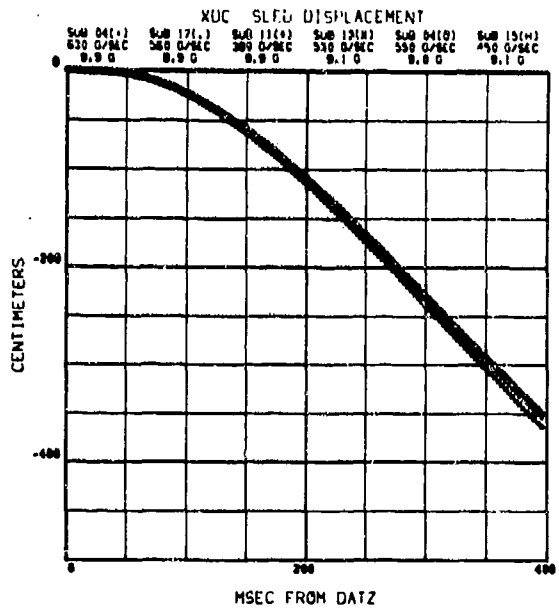

25

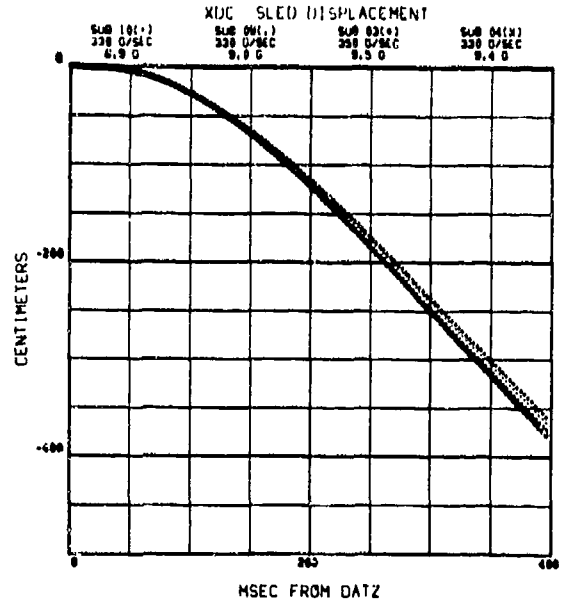

26

XDC SLED DISPLACMENT

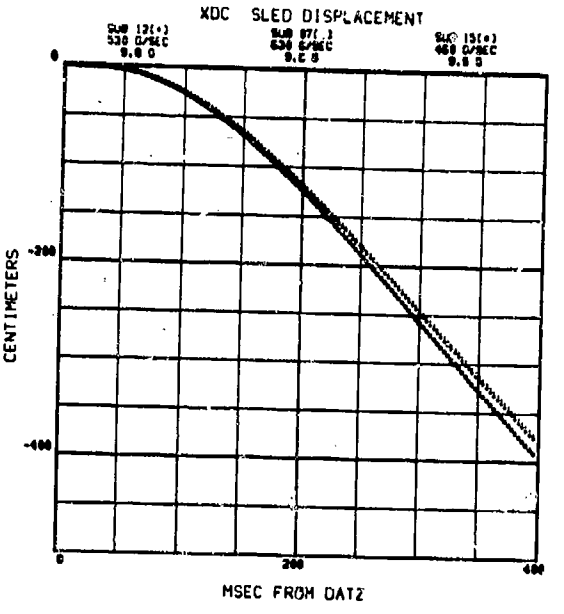

4XM ACCELERATION OF HEAD C.G. IN X DIRECTION

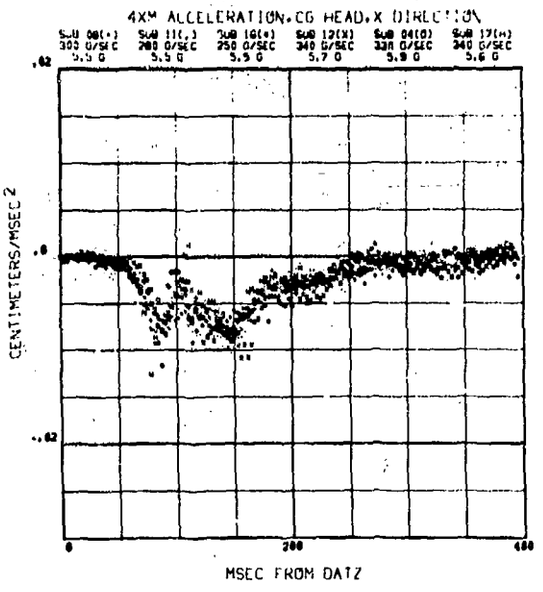

28

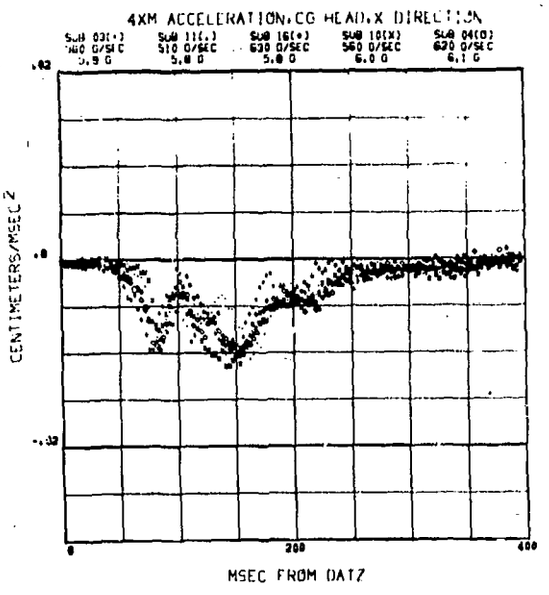

29

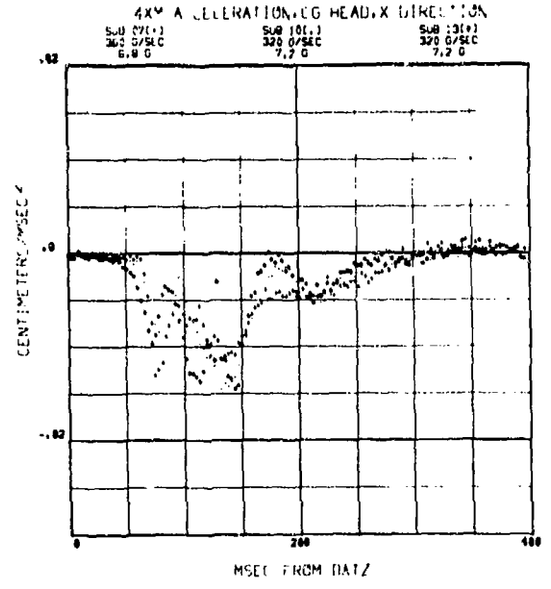

30

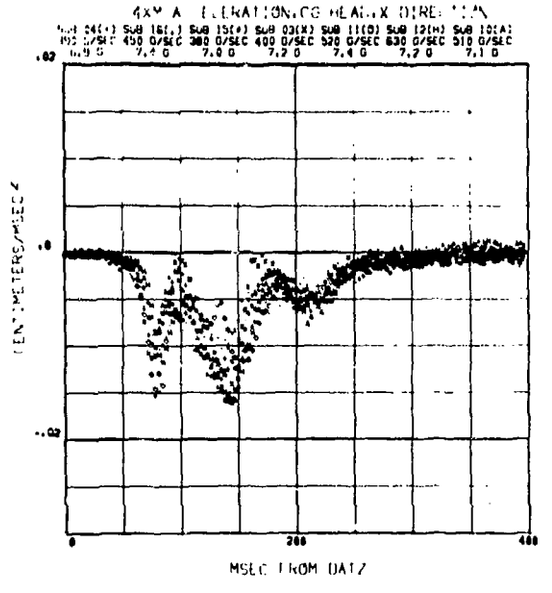

31

4XM ACCELERATION OF HEAD C.G. IN X DIRECTION

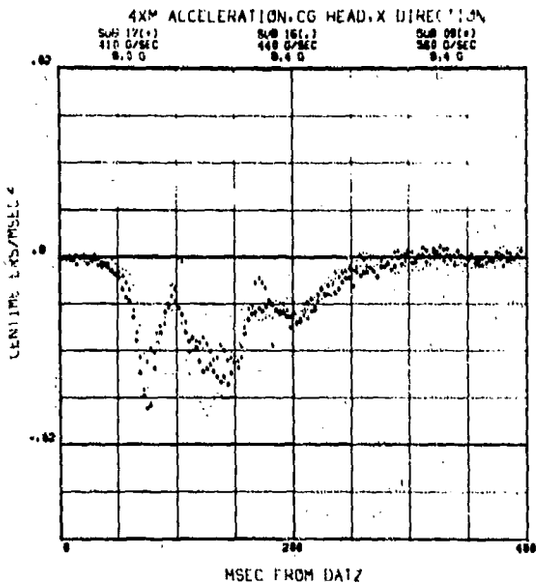

32

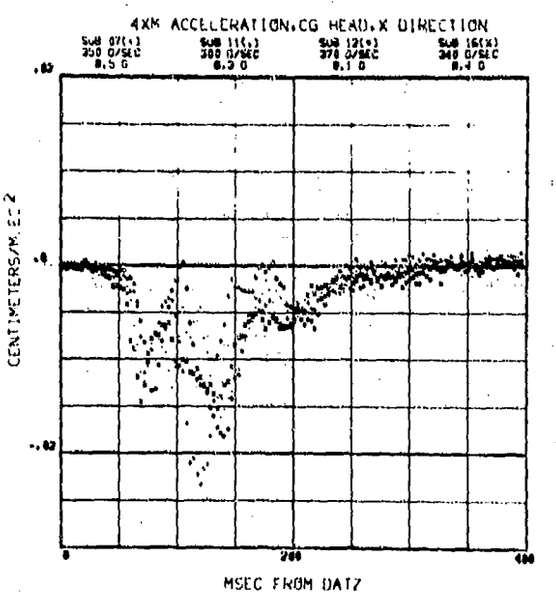

33

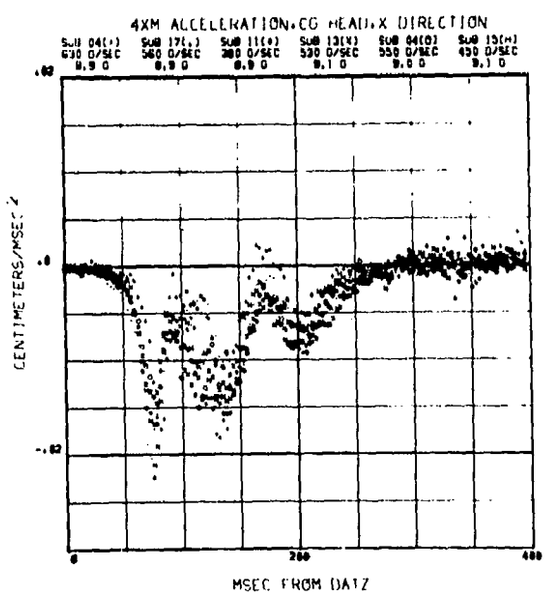

34

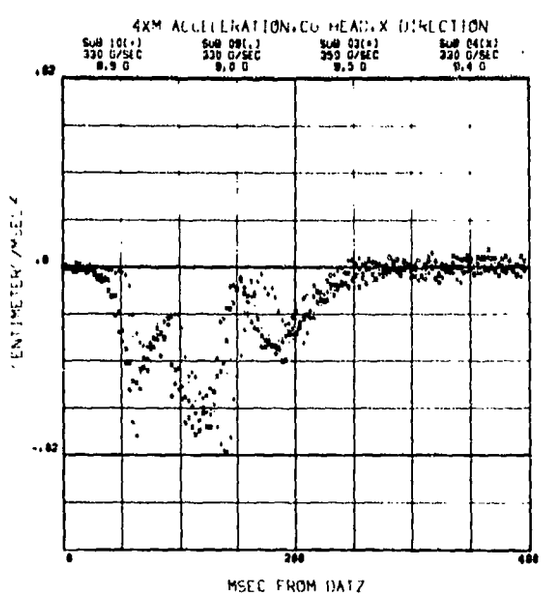

35

4XM ACCELERATION OF HEAD C.G. IN X DIRECTION

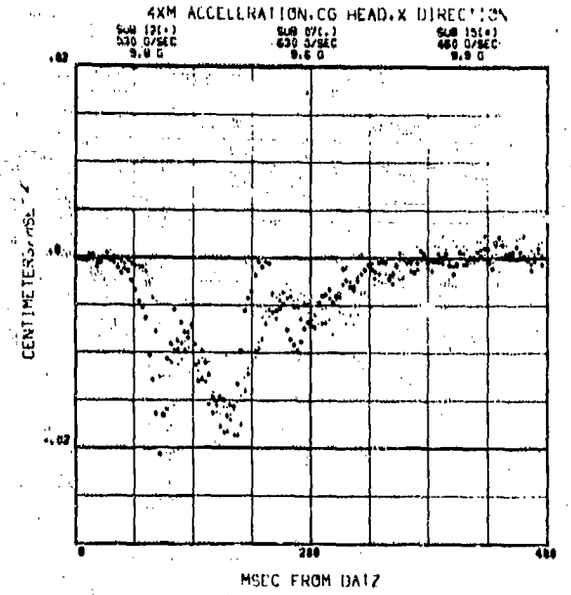

36

4XM ACCELERATION OF HEAD C.G. IN X DIRECTION

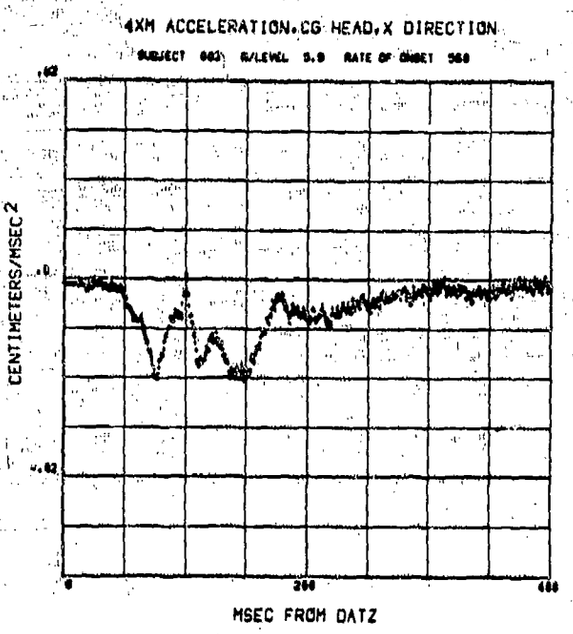

37

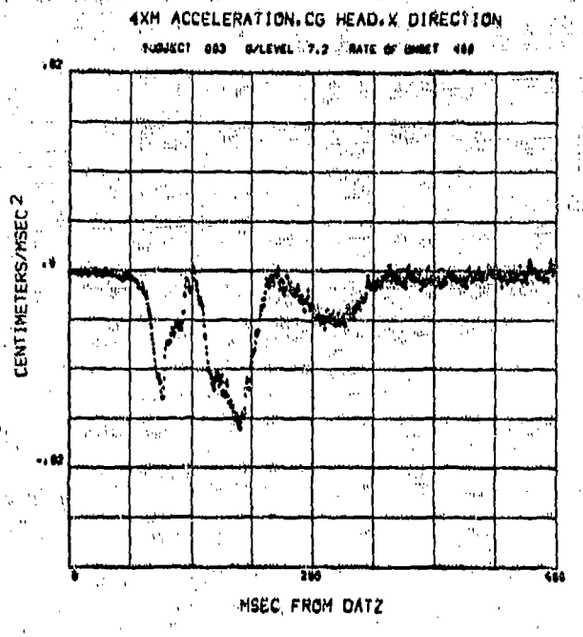

38

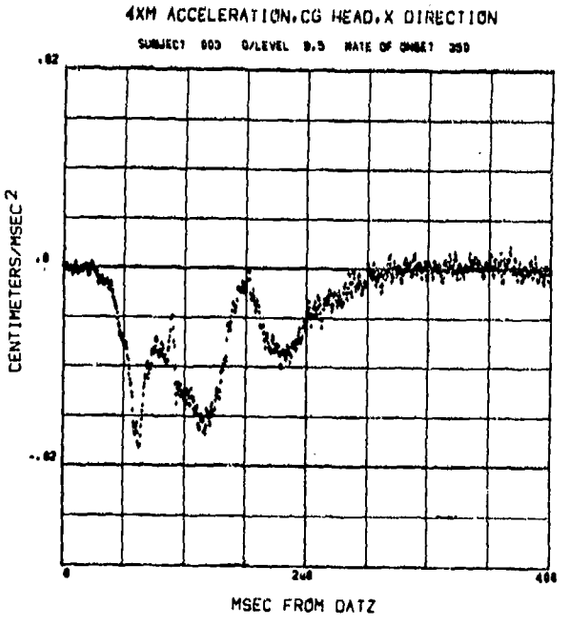

39

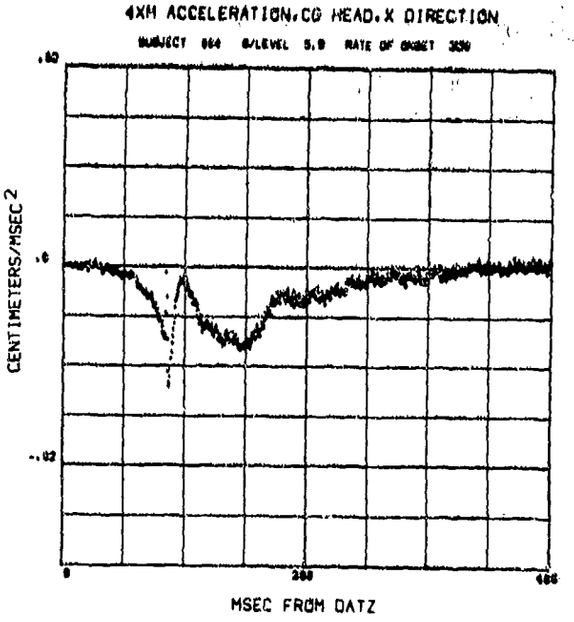

40

4XM ACCELERATION OF HEAD C.G. IN X DIRECTION

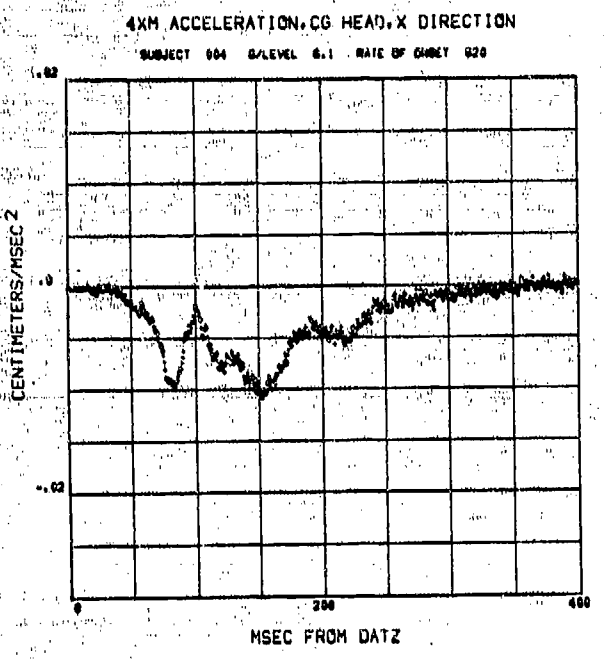

41

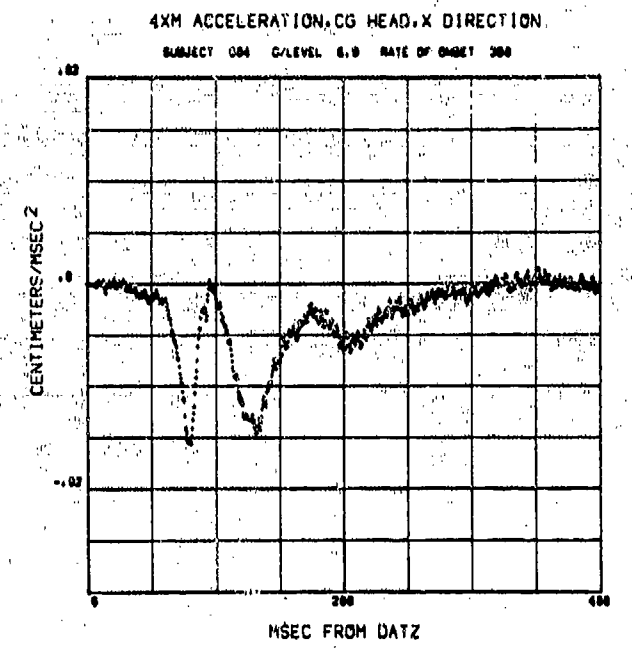

42

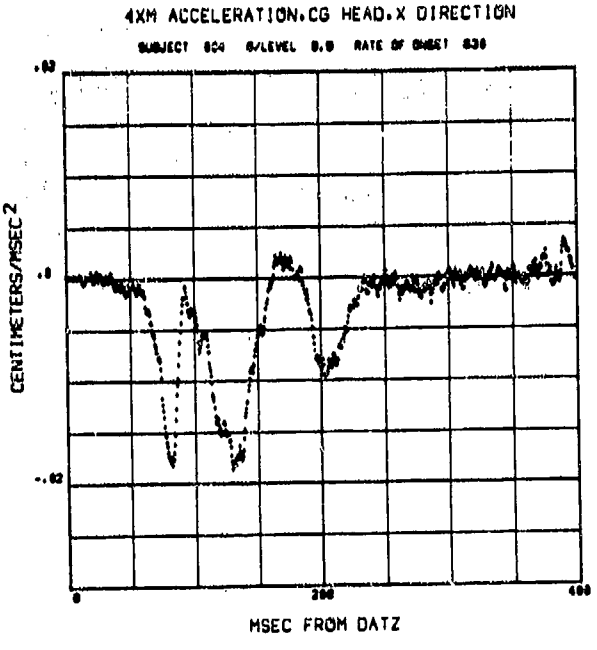

43

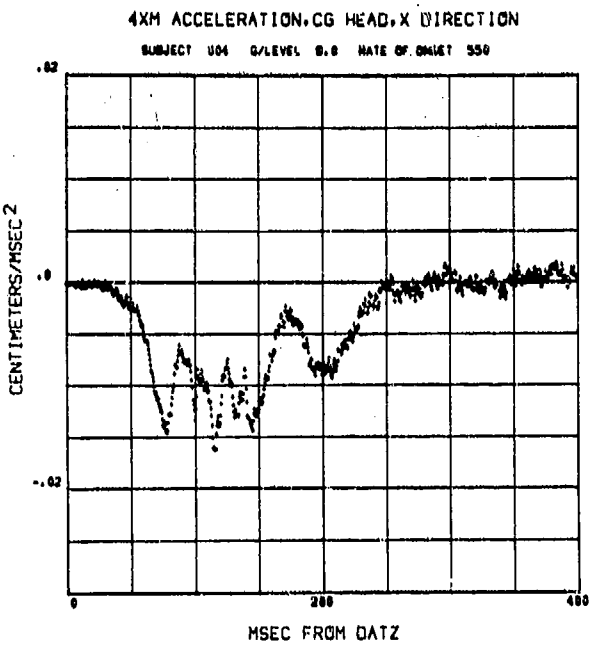

44

4XM ACCELERATION OF HEAD C.G. IN X DIRECTION

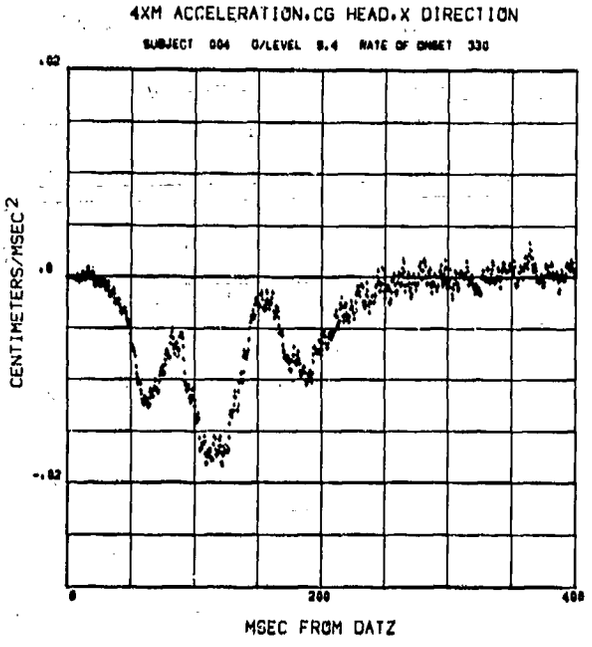

45

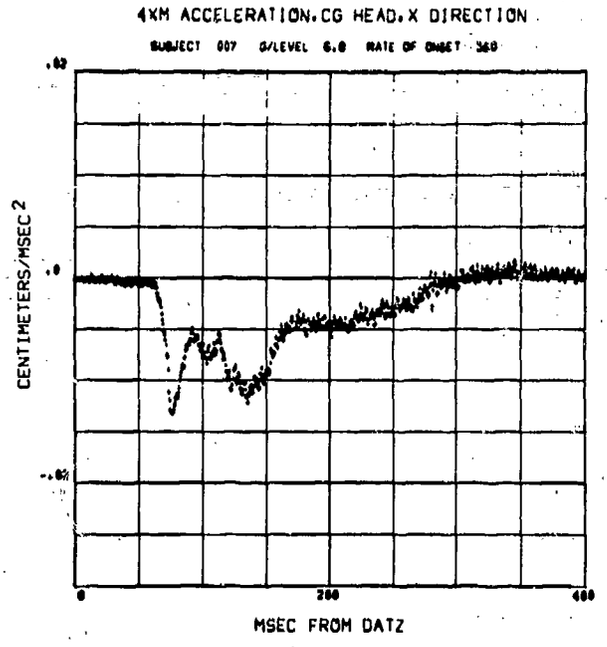

46

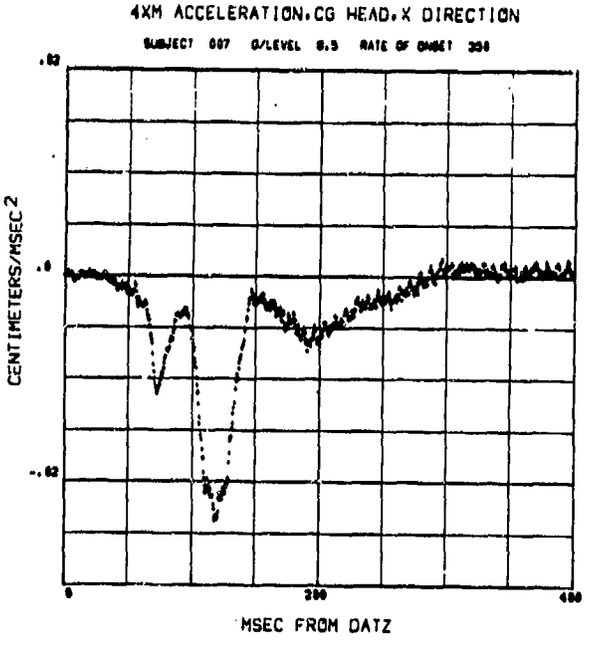

47

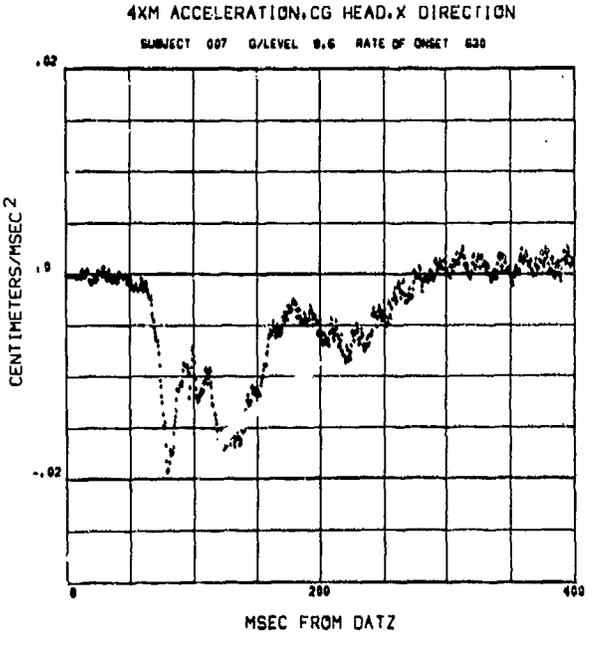

48

4XM ACCELERATION OF HEAD C.G. IN X DIRECTION

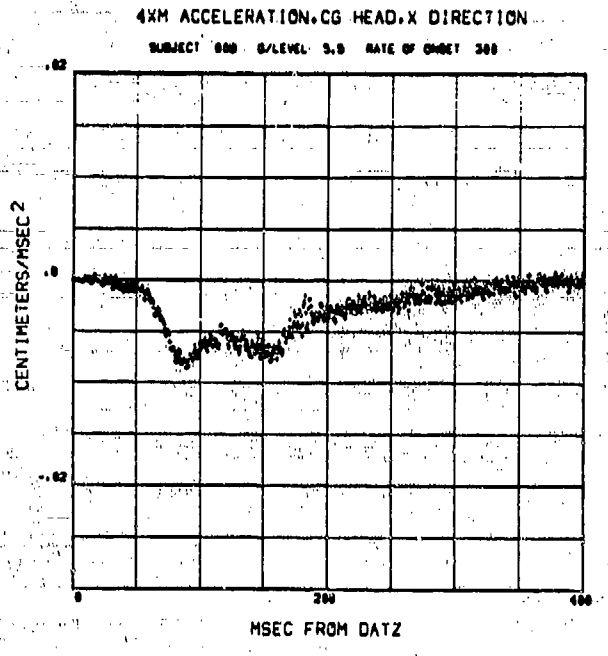

49

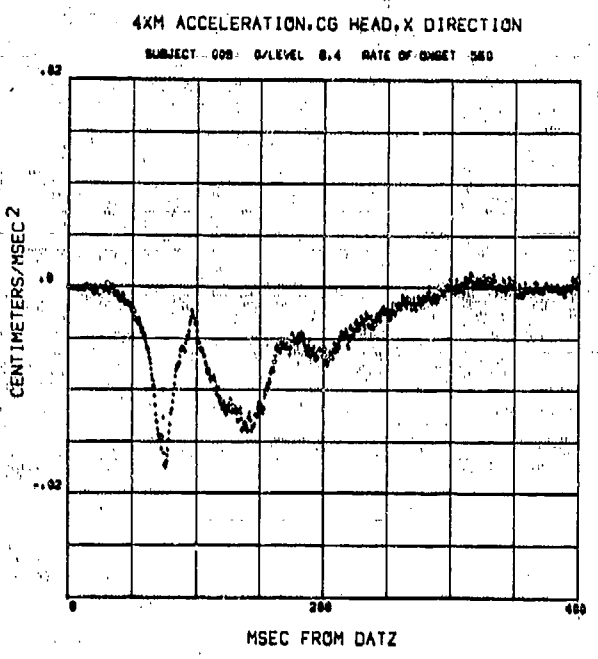

50

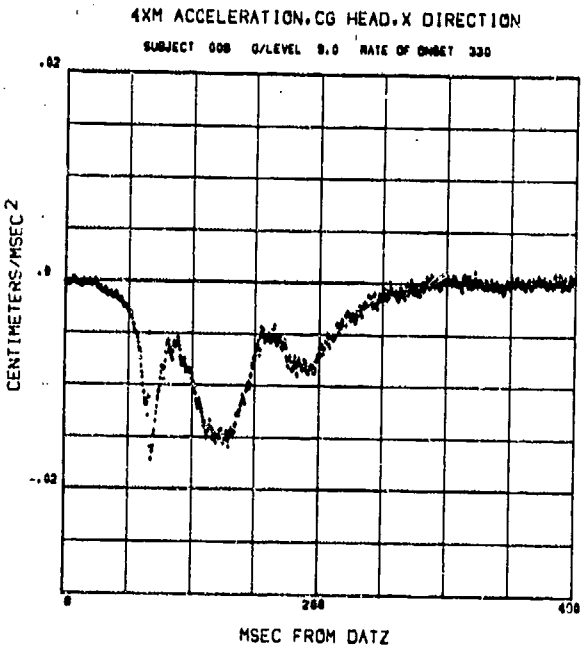

51

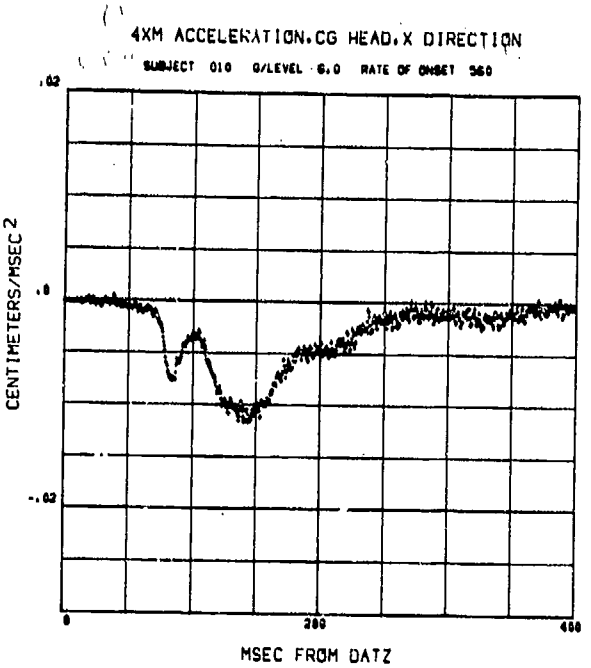

52

4XM ACCELERATION OF HEAD C.G. IN X DIRECTION

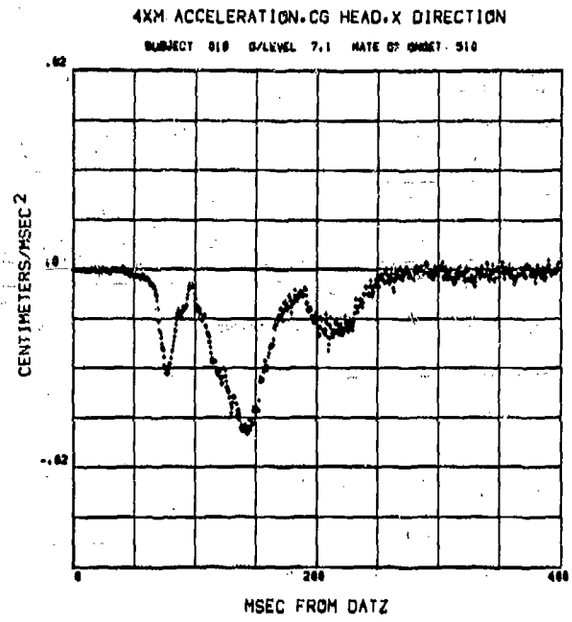

53

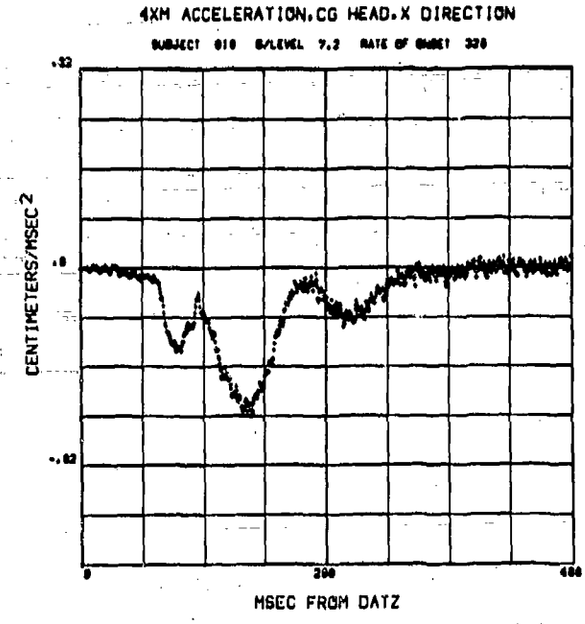

54

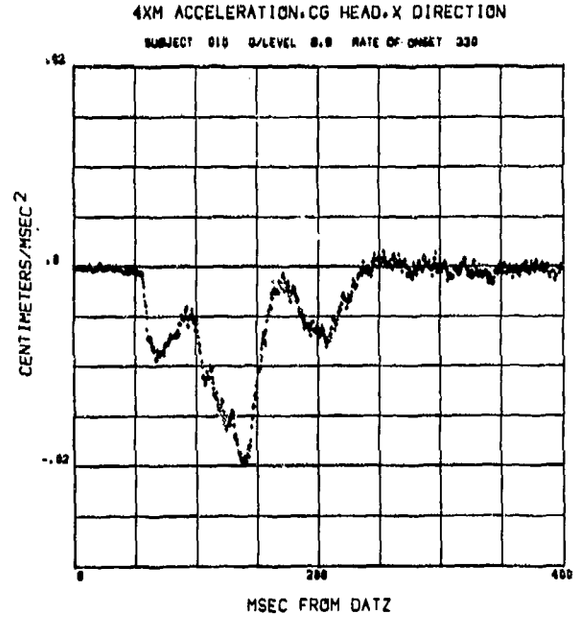

55

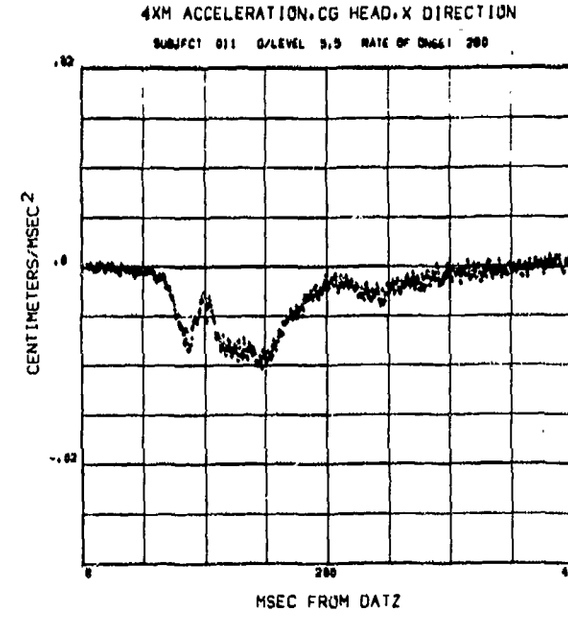

56

4XM ACCELERATION OF HEAD C.G. IN X DIRECTION

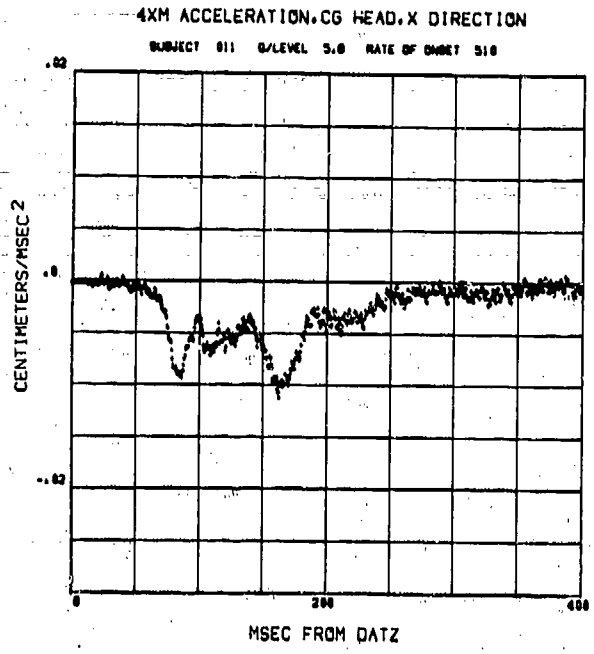

57

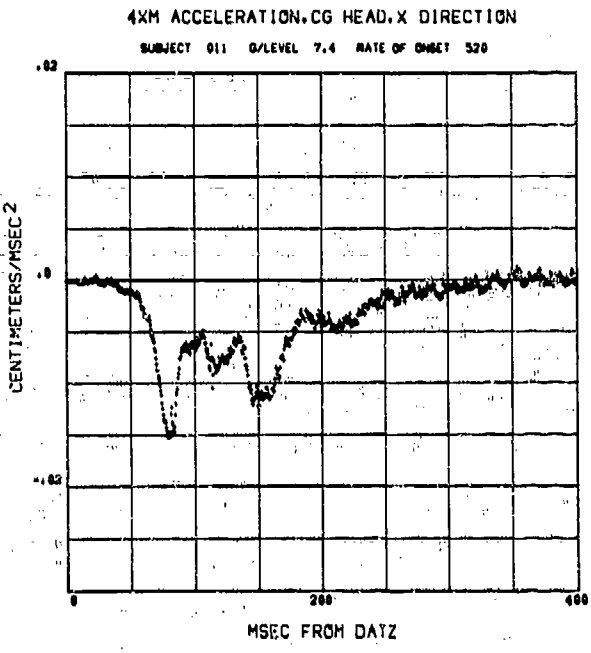

58

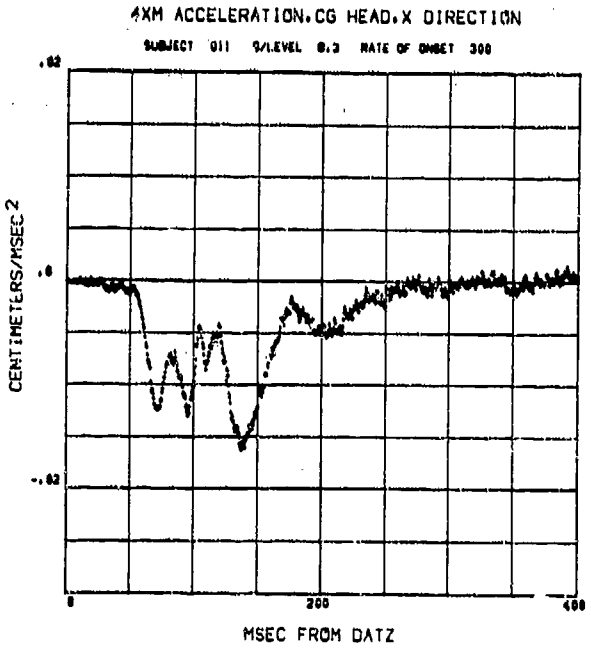

59

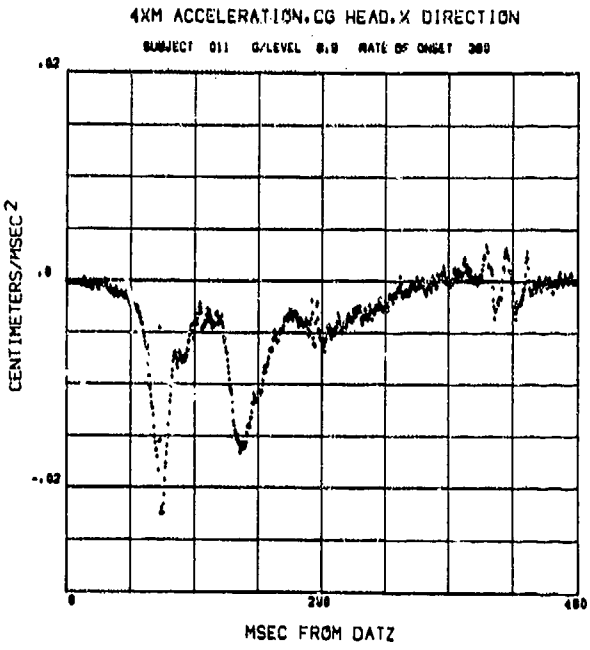

60

4XM ACCELERATION OF HEAD C.G. IN X DIRECTION

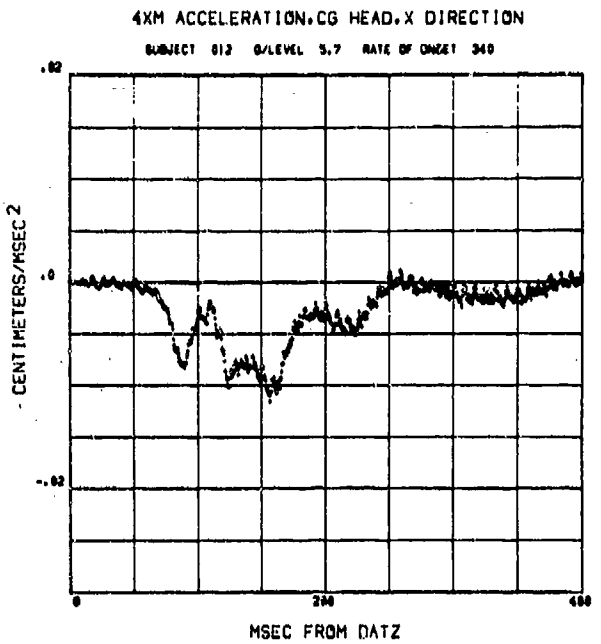

61

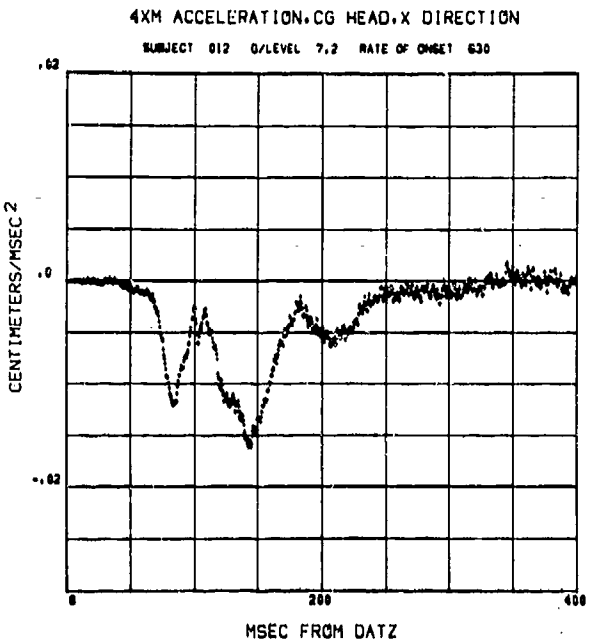

62

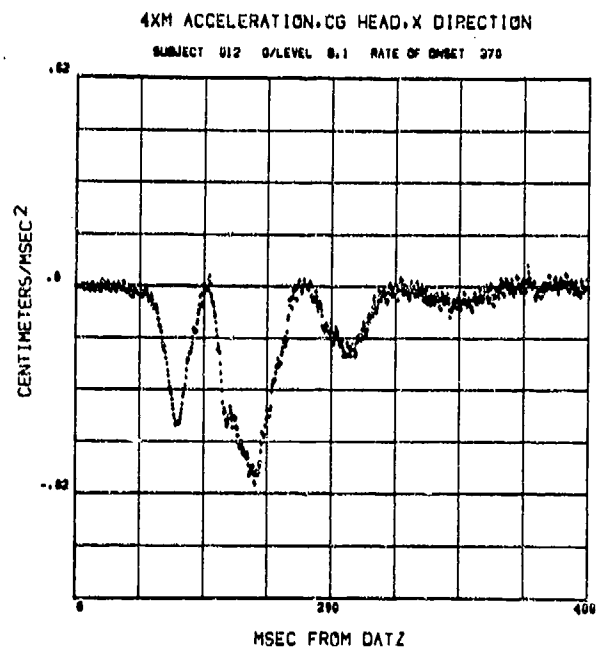

63

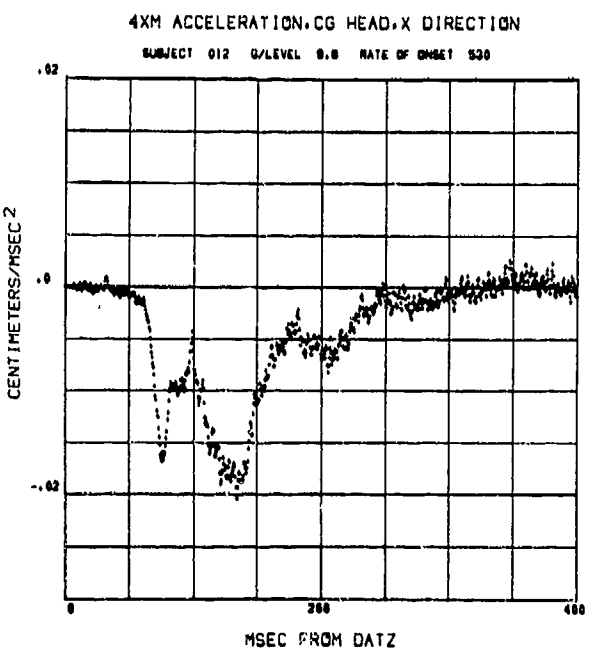

64

4XM ACCELERATION OF HEAD C.G. IN X DIRECTION

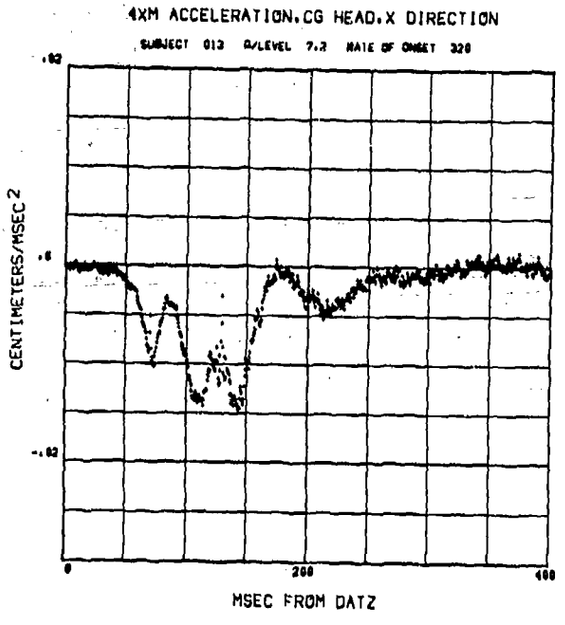

65

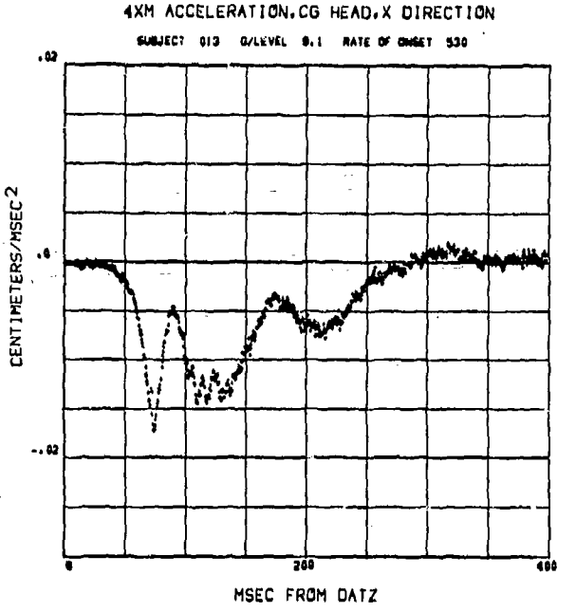

66

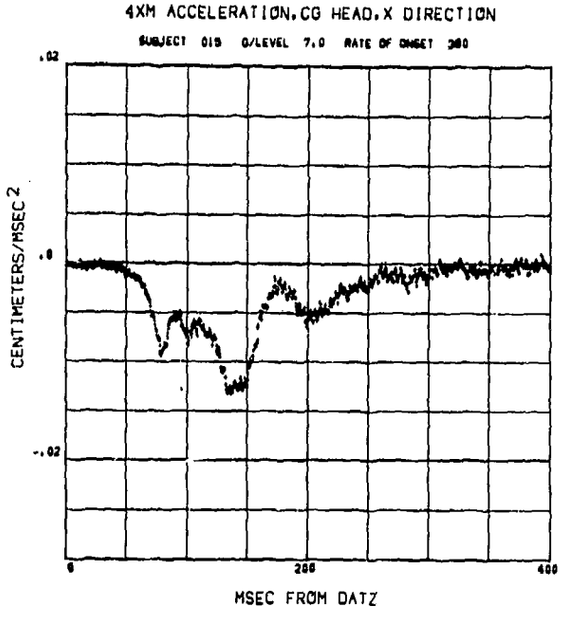

67

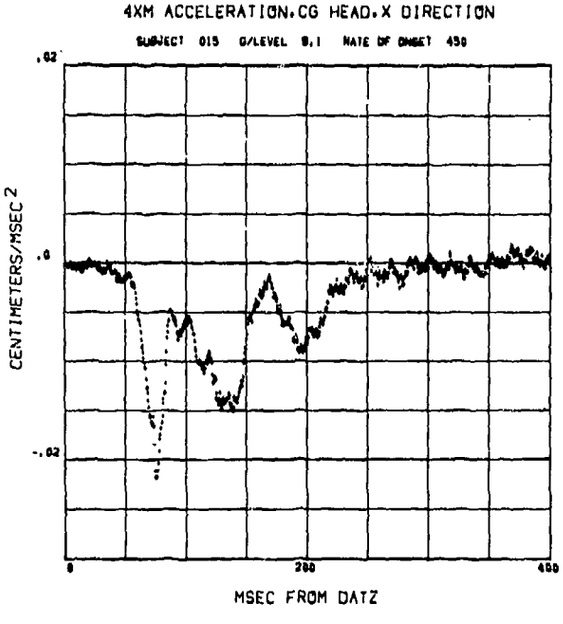

68

4XM ACCELERATION OF HEAD C.G. IN X DIRECTION

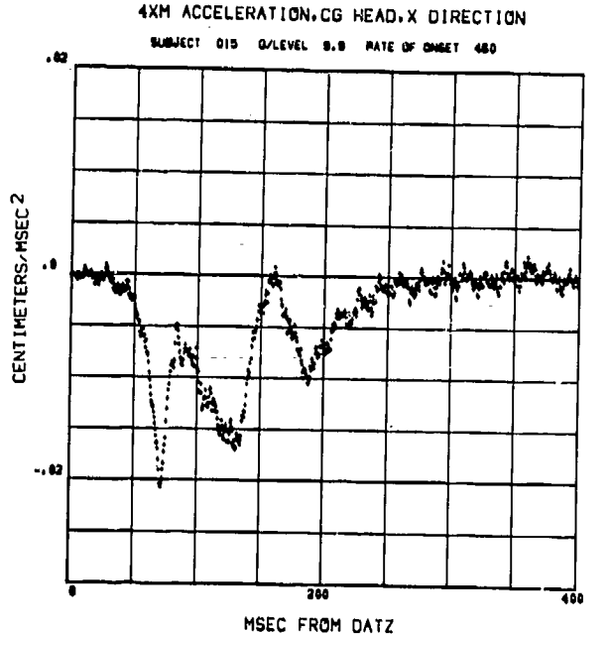

69

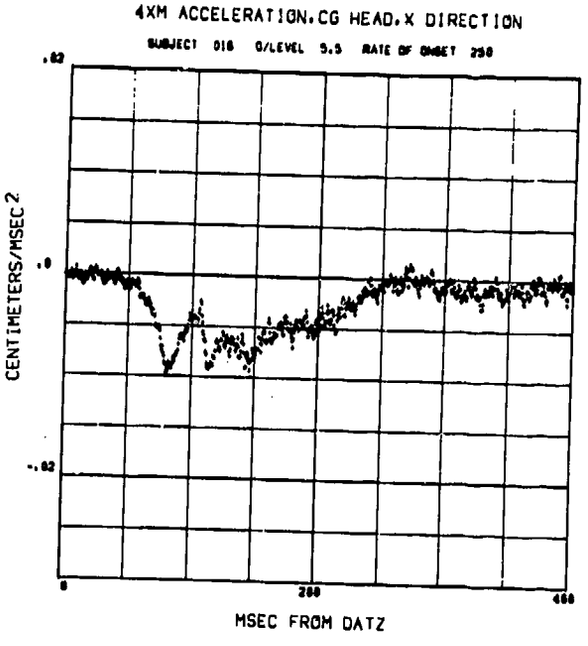

70

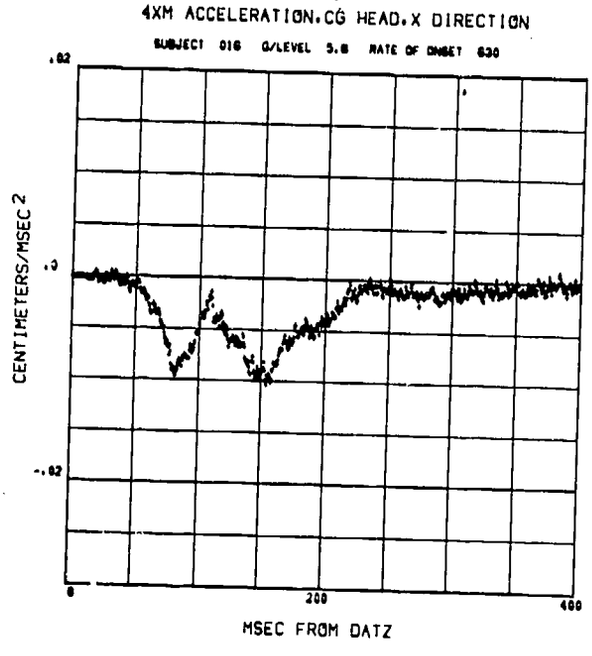

71

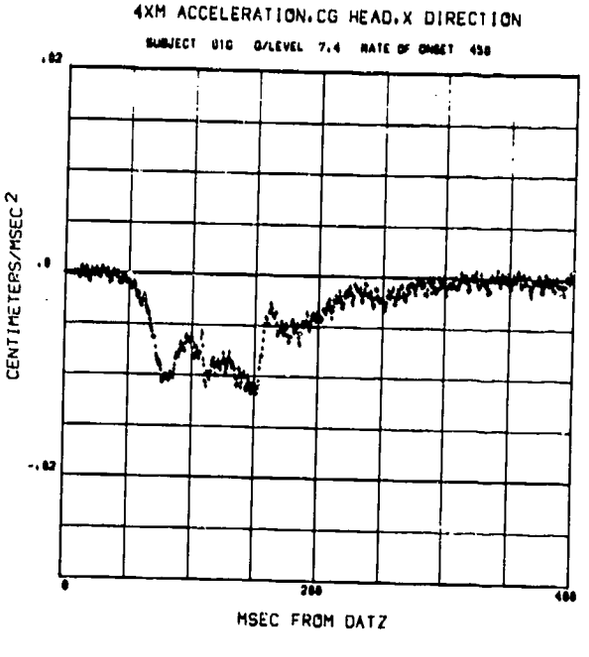

72

4XM ACCELERATION OF HEAD C.G. IN X DIRECTION

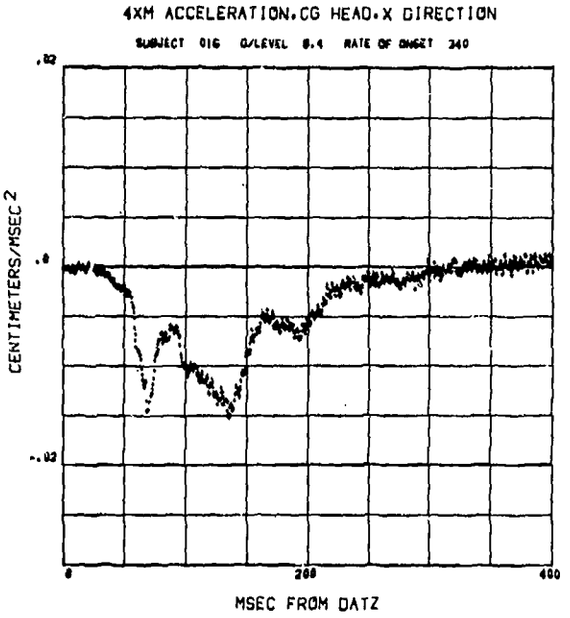

73

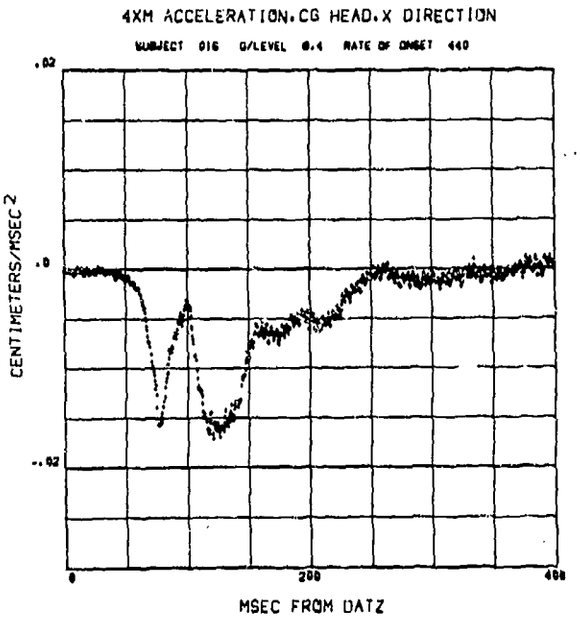

74

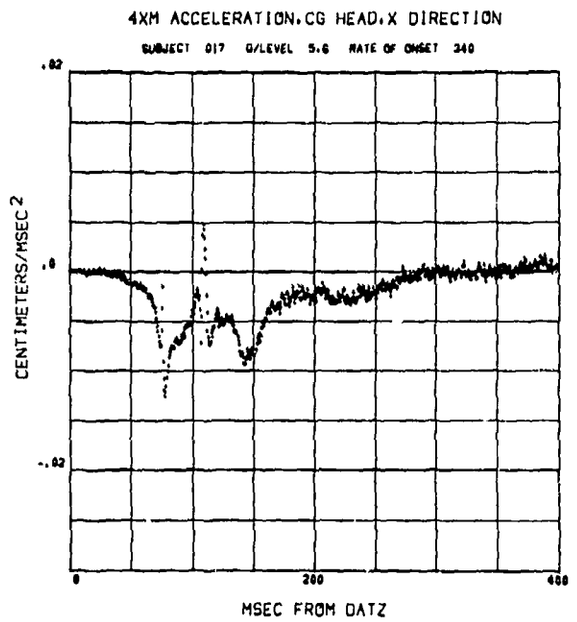

75

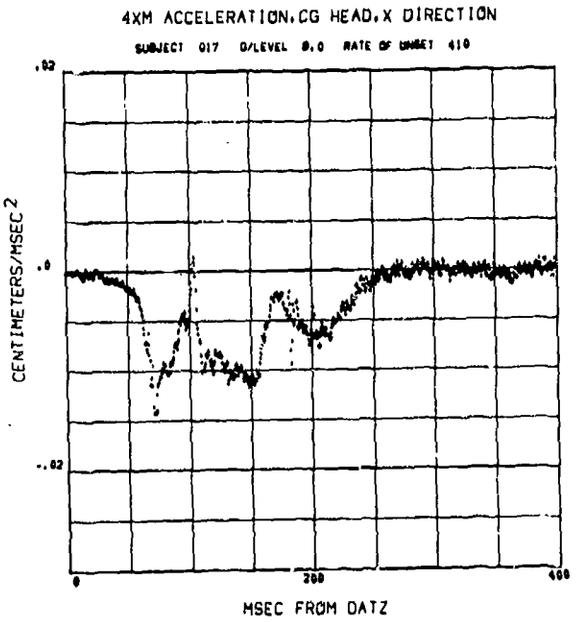

76

RHN ANGULAR VELOCITY OF THE HEAD RELATIVE TO T_1

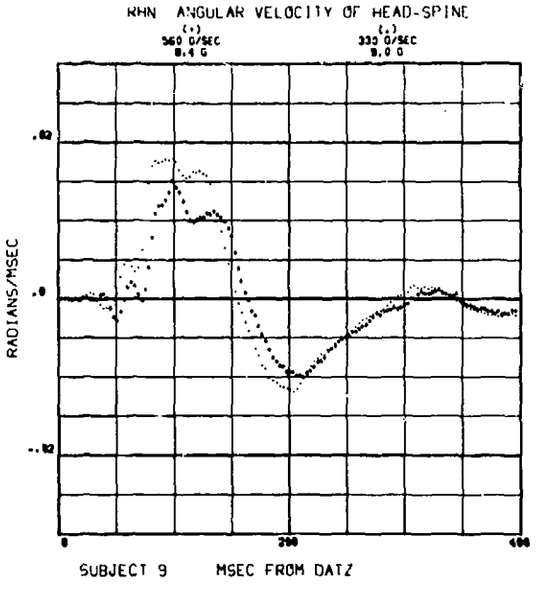

413

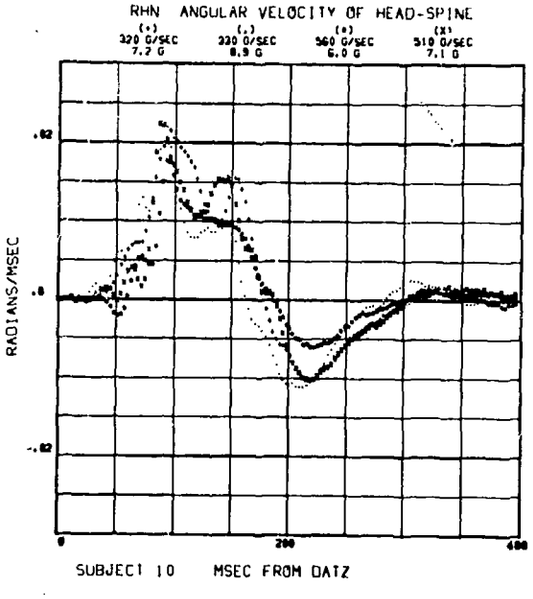

414

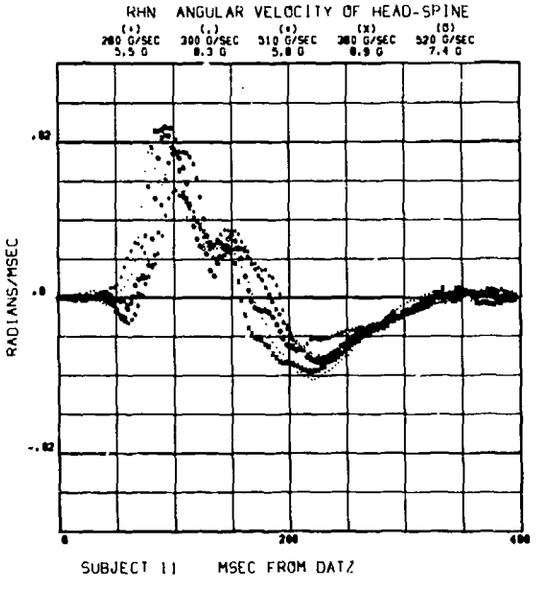

415

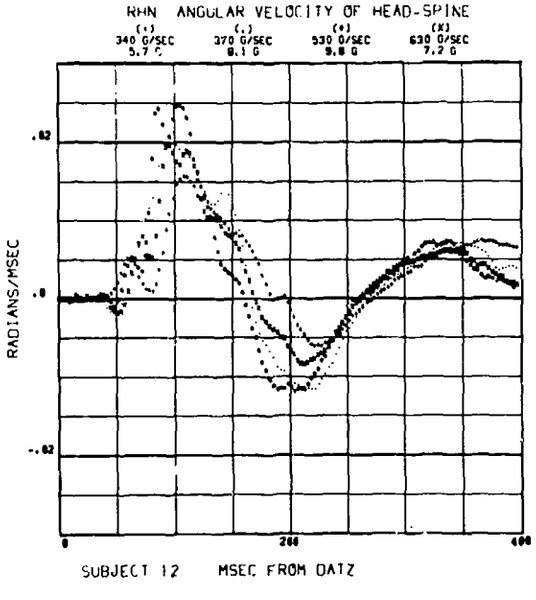

416

RHN ANGULAR VELOCITY OF THE HEAD RELATIVE TO T_1

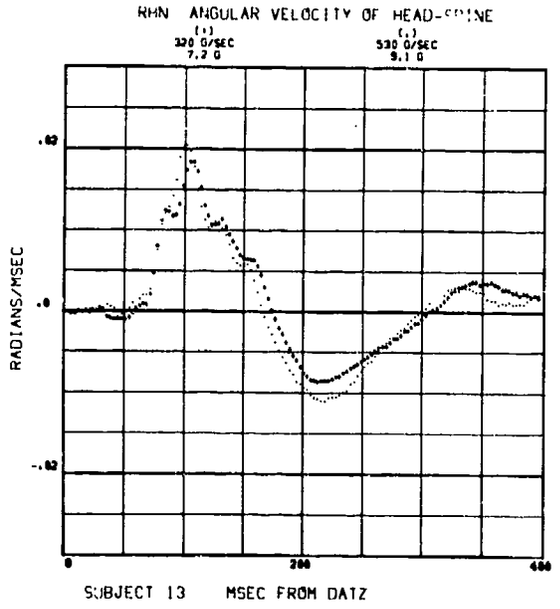

417

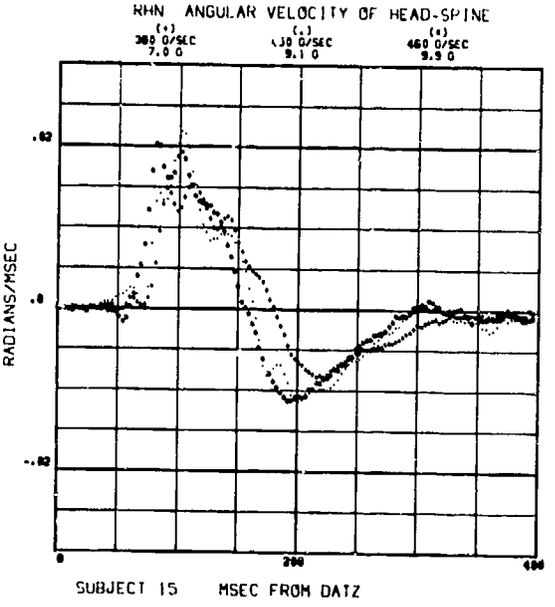

418

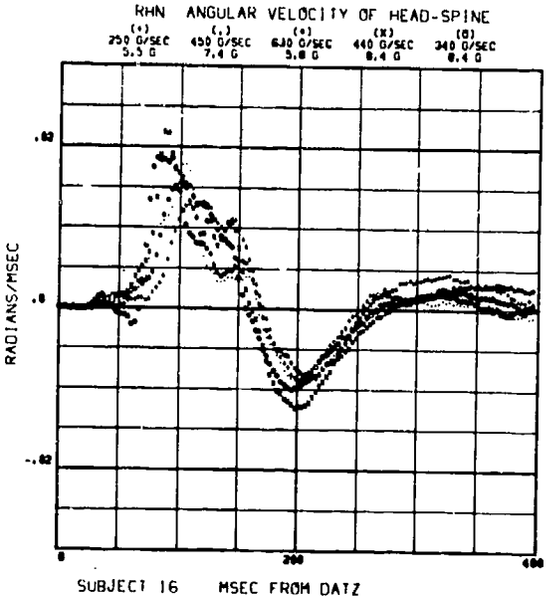

419

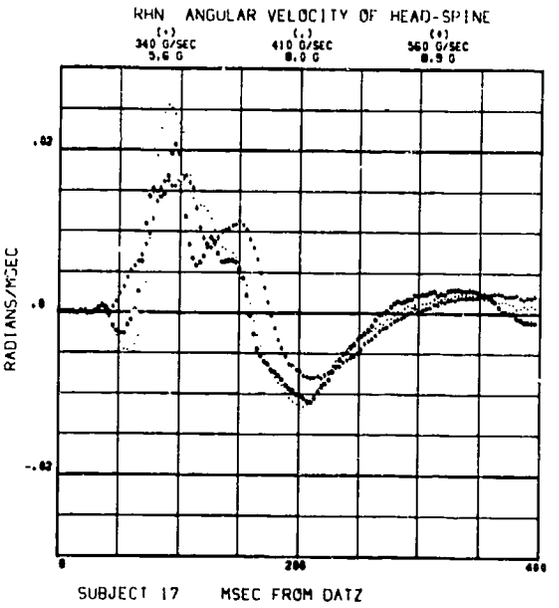

420

RHN ANGULAR VELOCITY OF THE HEAD RELATIVE TO T_1

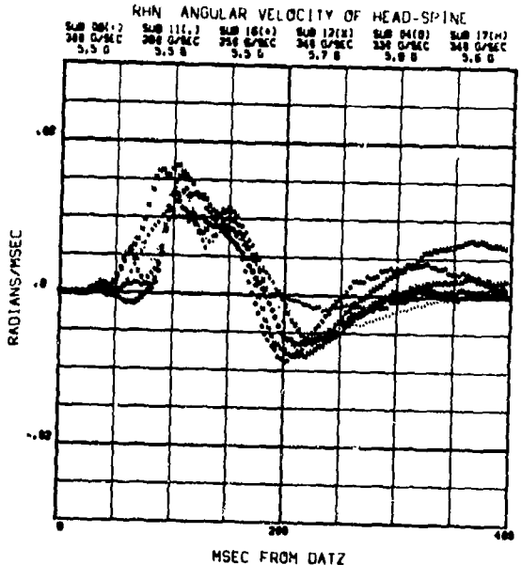

421

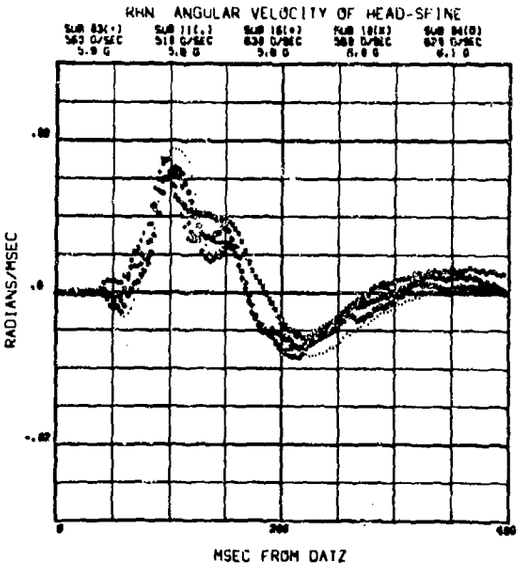

422

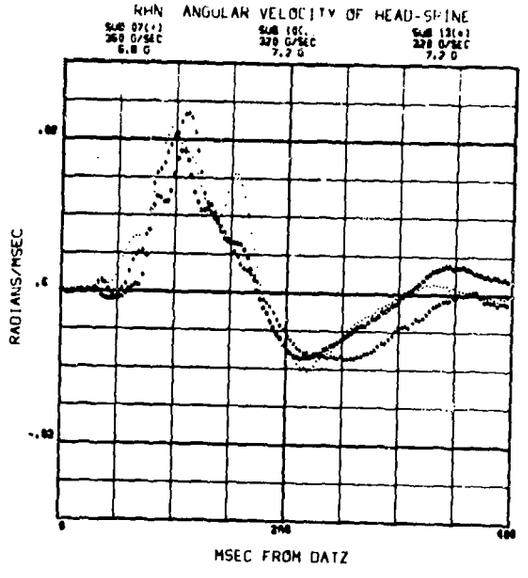

423

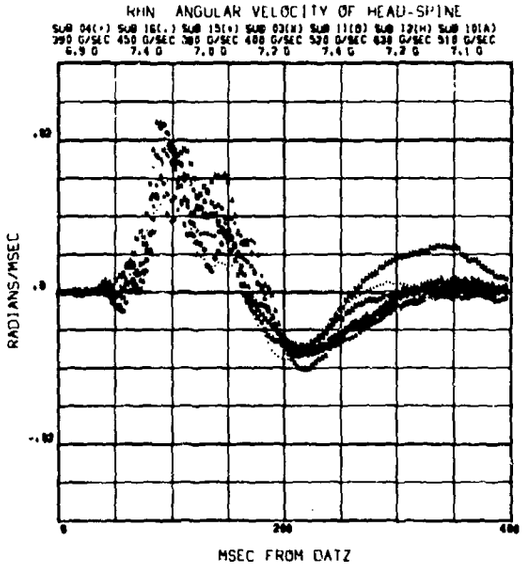

424

RHN ANGULAR VELOCITY OF THE HEAD RELATIVE TO T_1

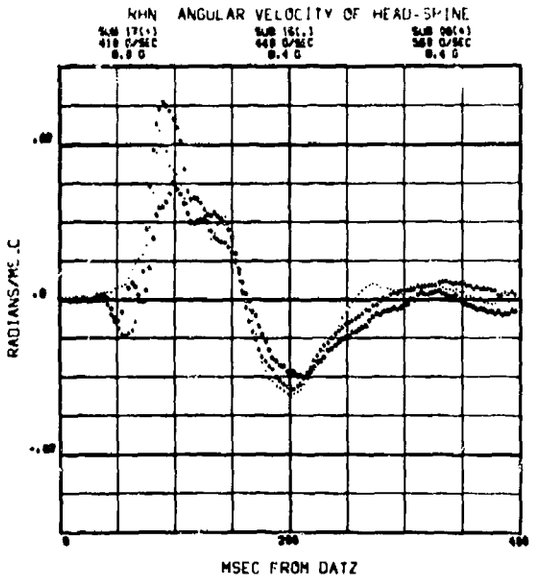

425

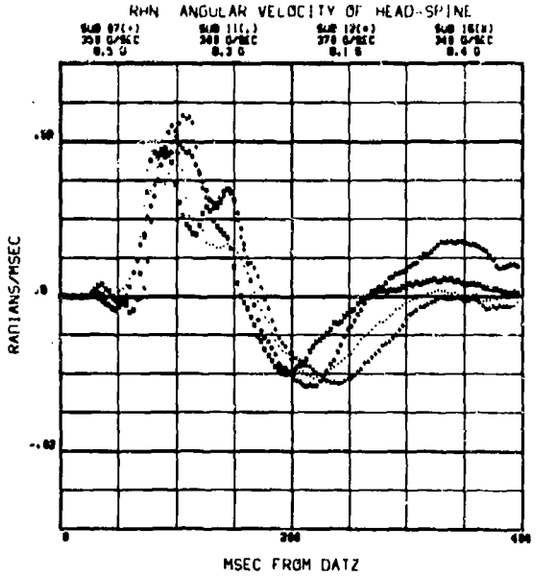

426

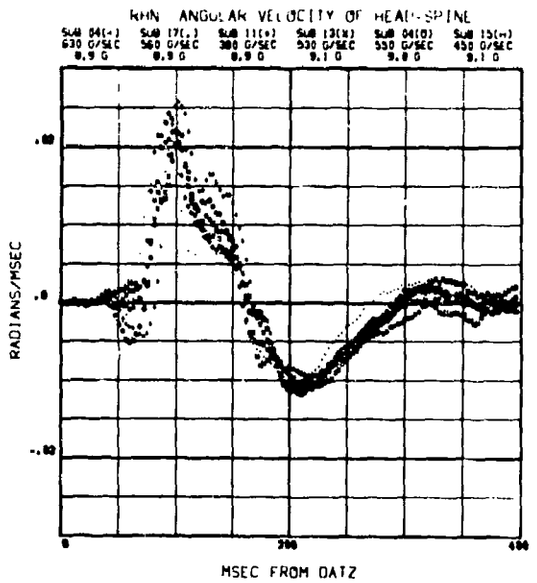

427

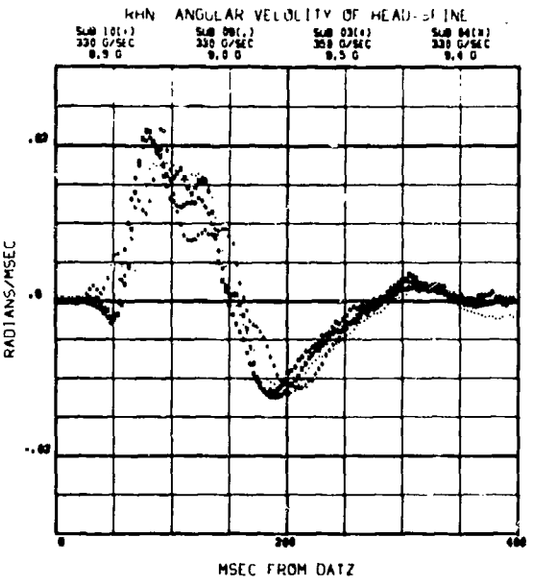

428

RHN ANGULAR VELOCITY OF THE HEAD RELATIVE TO T_1

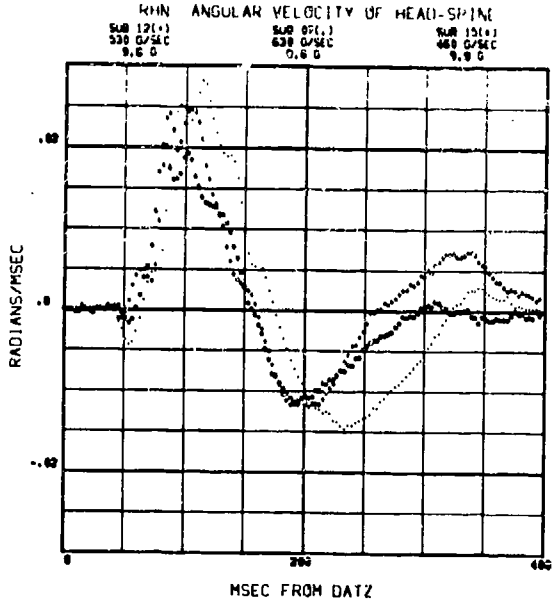

429

PDH ANGULAR DISPLACEMENT OF THE HEAD

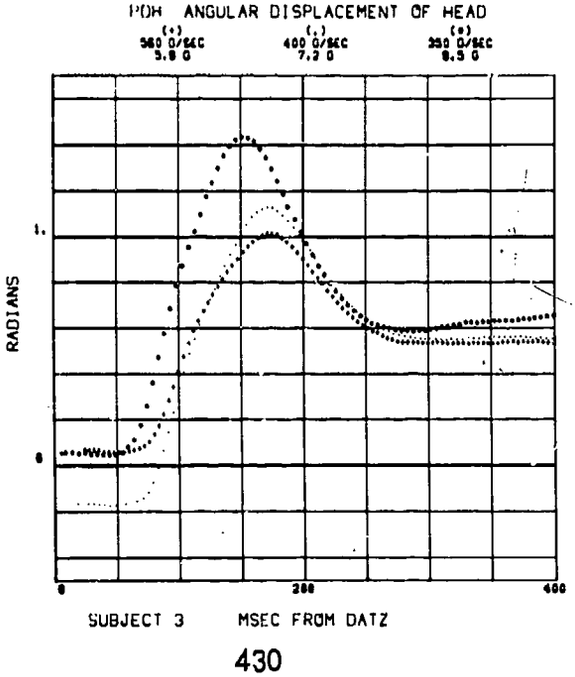

430

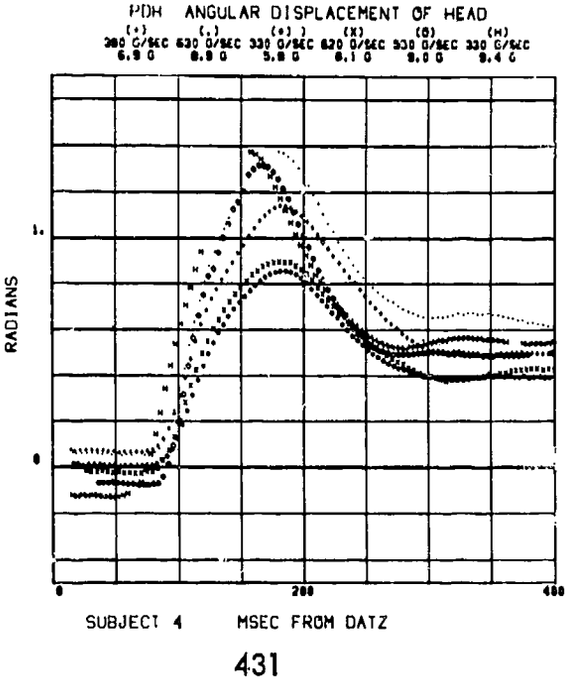

431

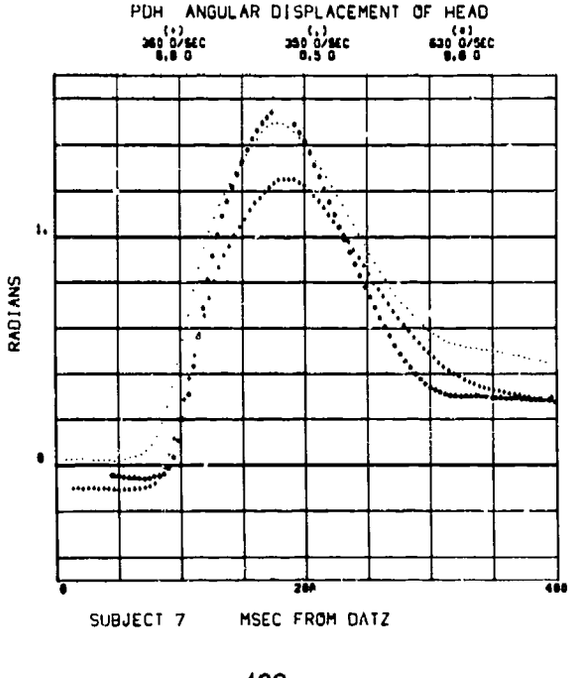

432

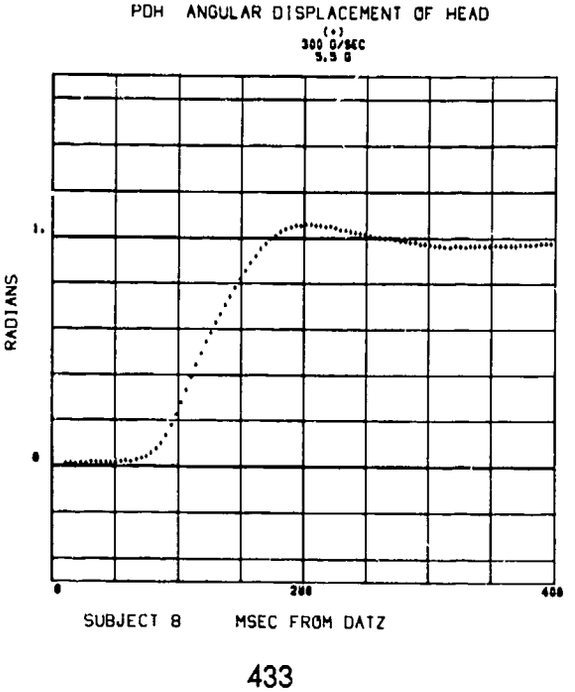

433

PDH ANGULAR DISPLACEMENT OF THE HEAD

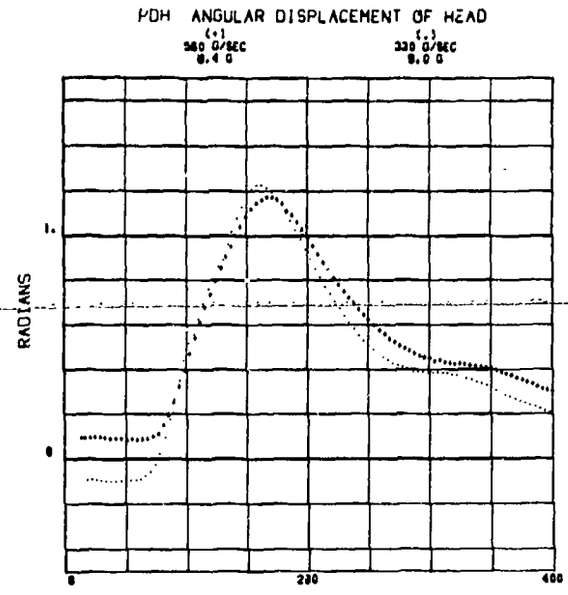

434

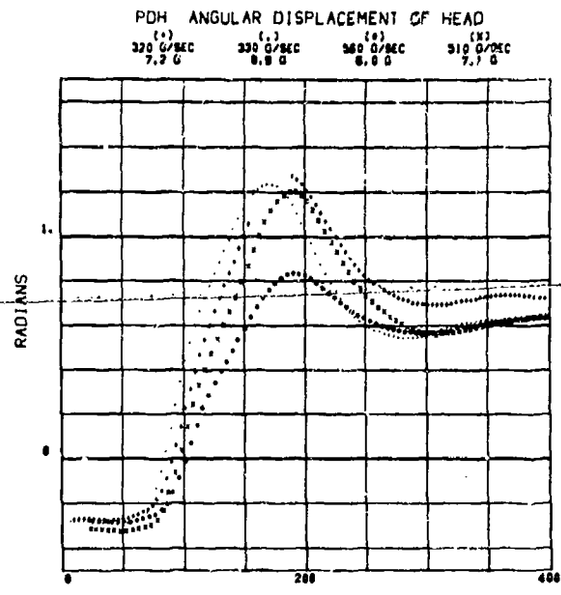

435

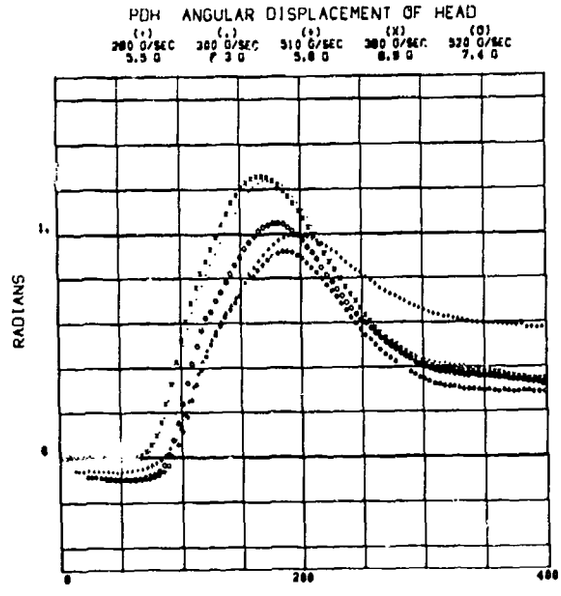

436

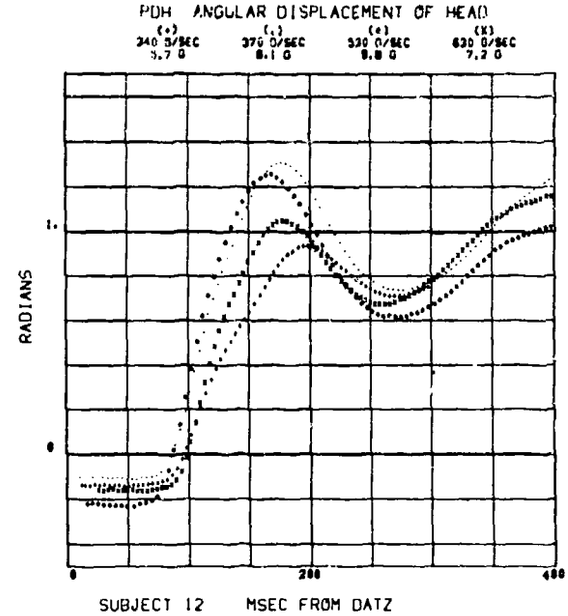

437

PDH ANGULAR DISPLACEMENT OF THE HEAD

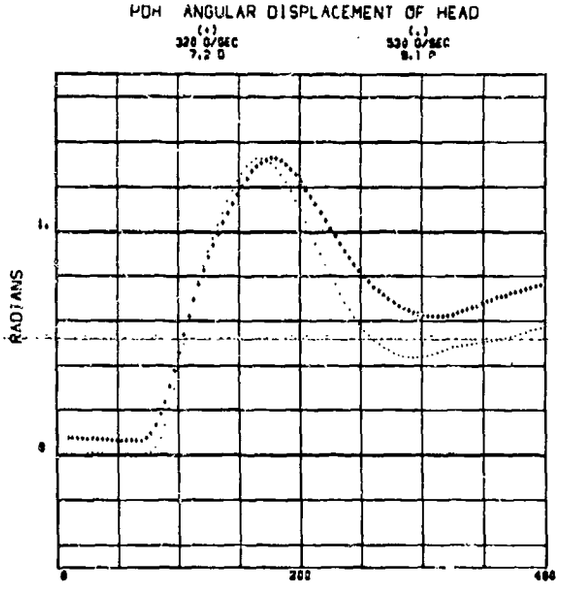

438

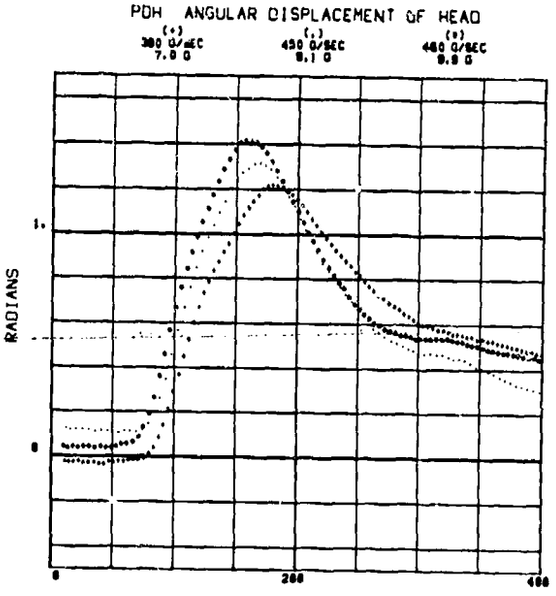

439

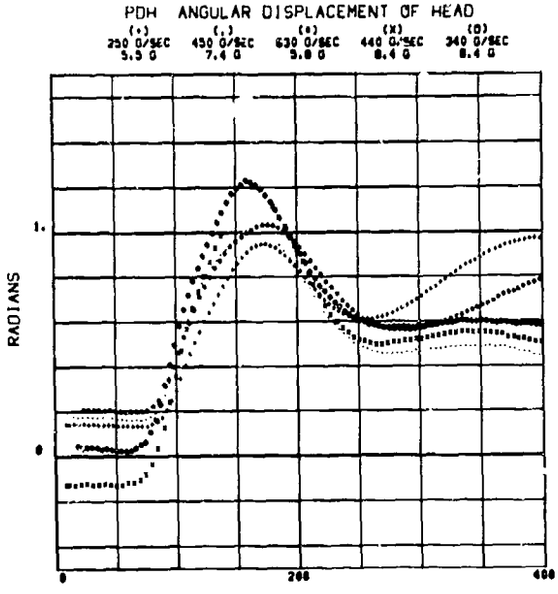

440

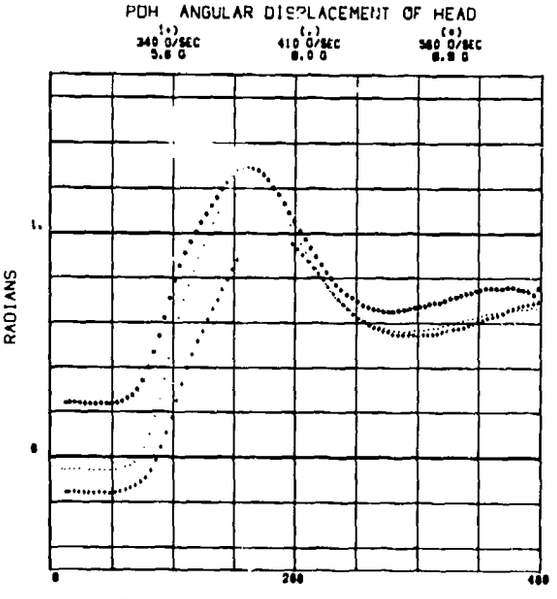

441

PDH ANGULAR DISPLACEMENT OF THE HEAD

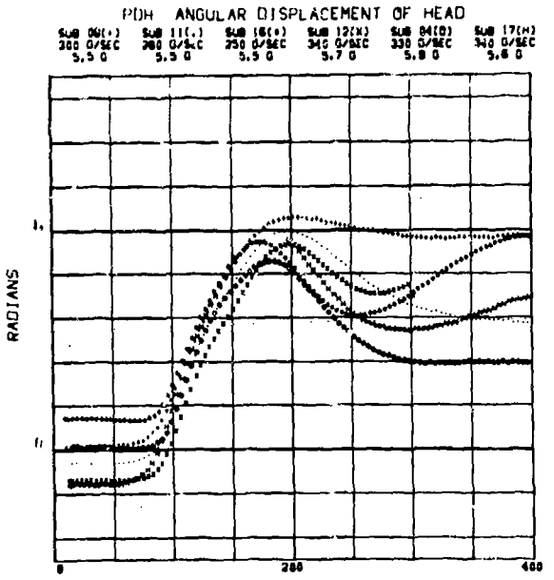

442

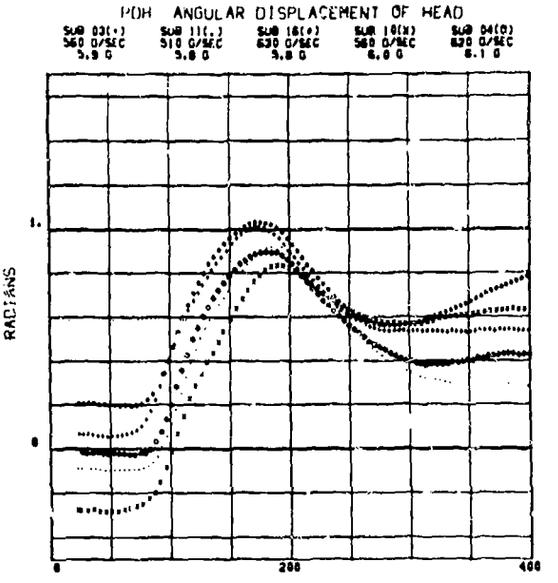

443

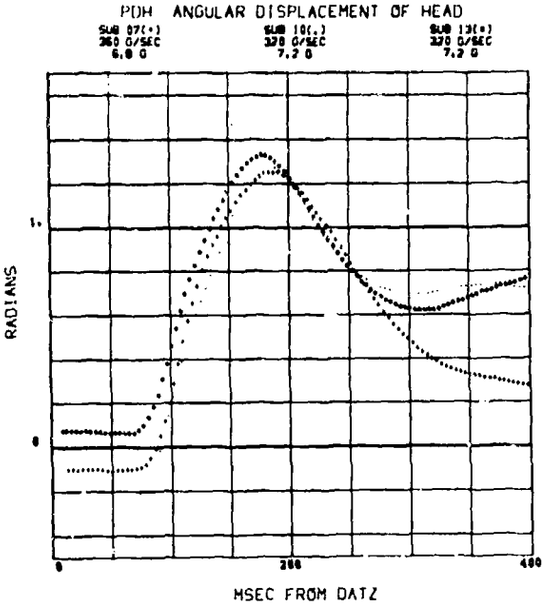

444

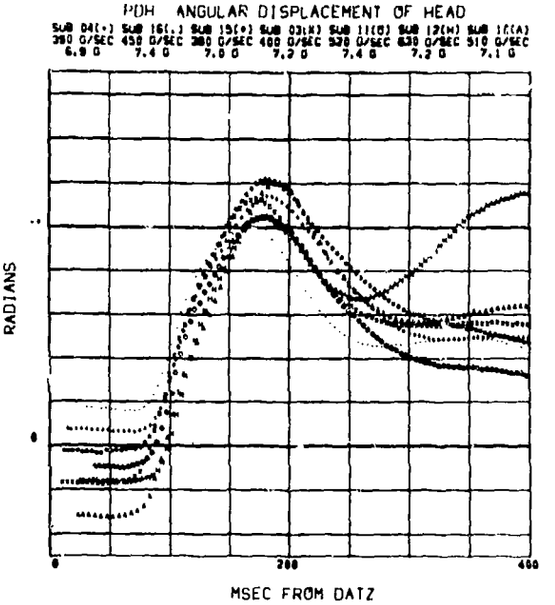

445

PDH ANGULAR DISPLACEMENT OF THE HEAD

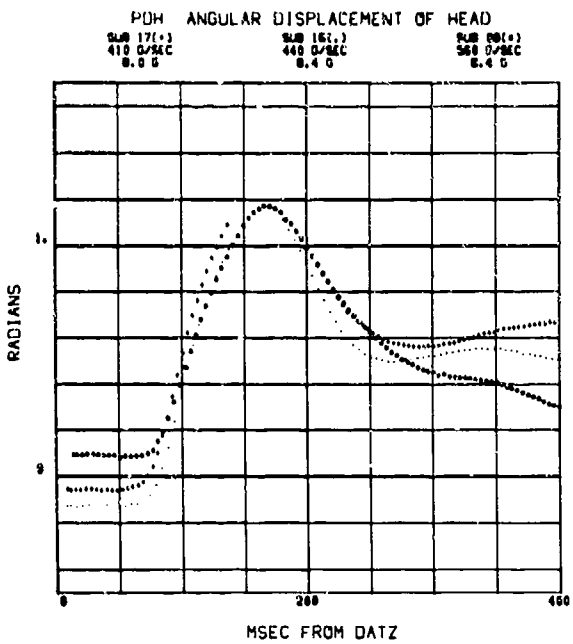

446

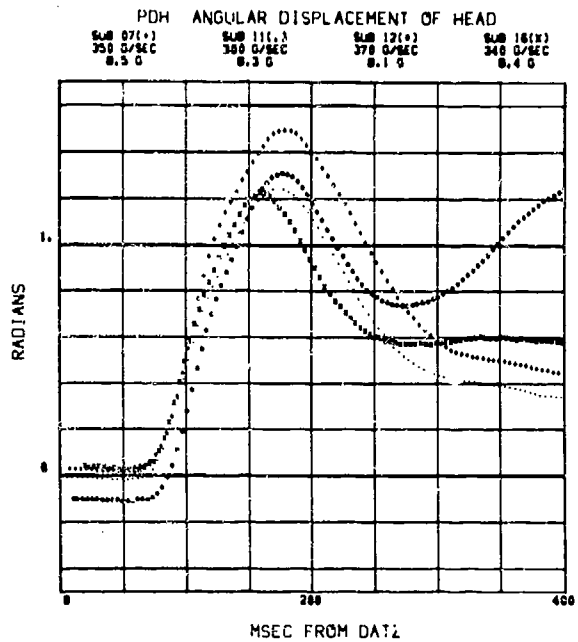

447

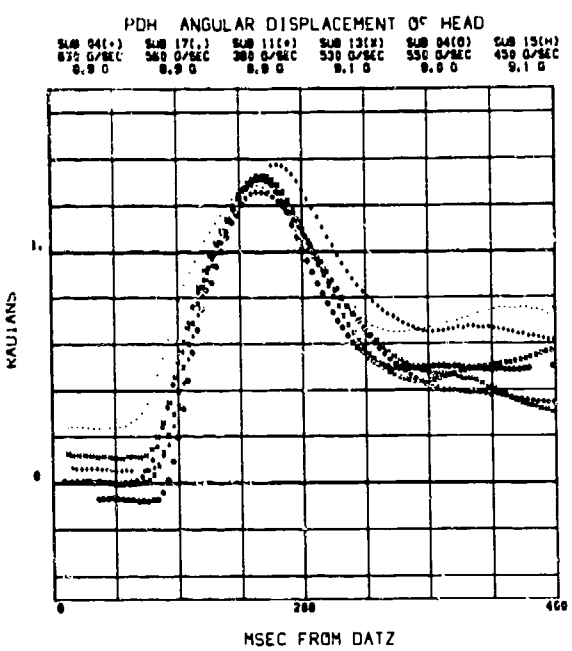

448

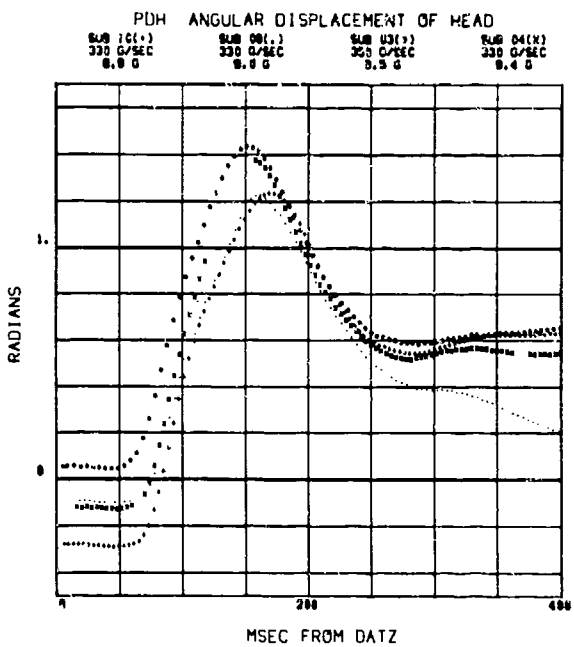

449

PDH ANGULAR DISPLACEMENT OF THE HEAD

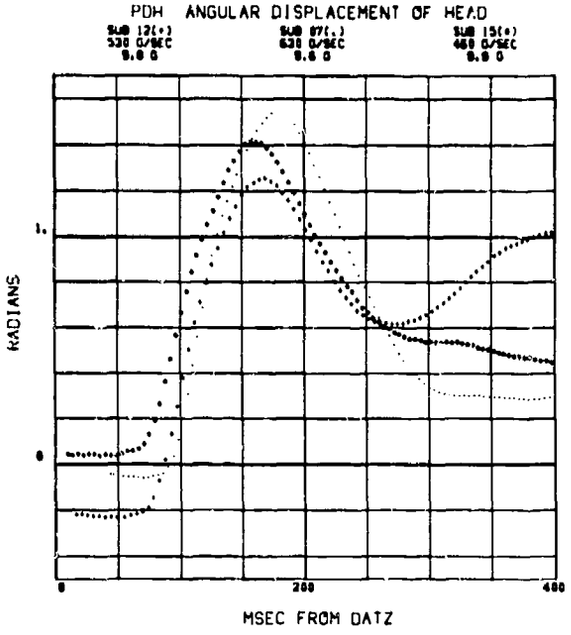

450

NRN ANGULAR DISPLACEMENT OF T_1

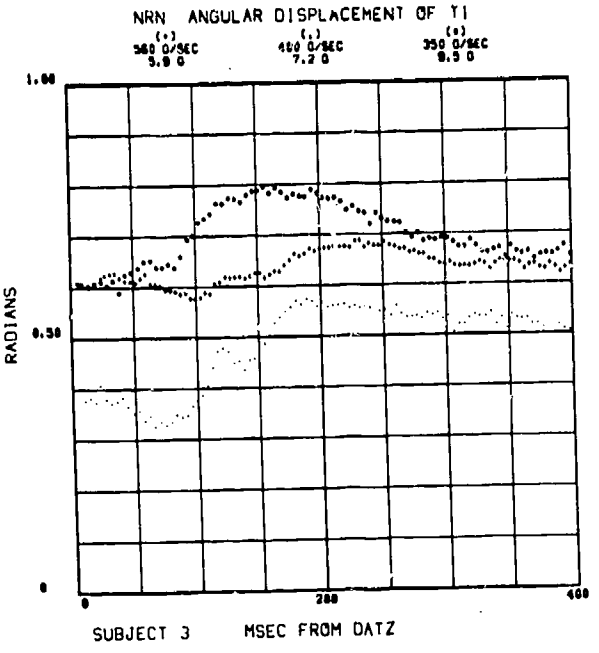

451

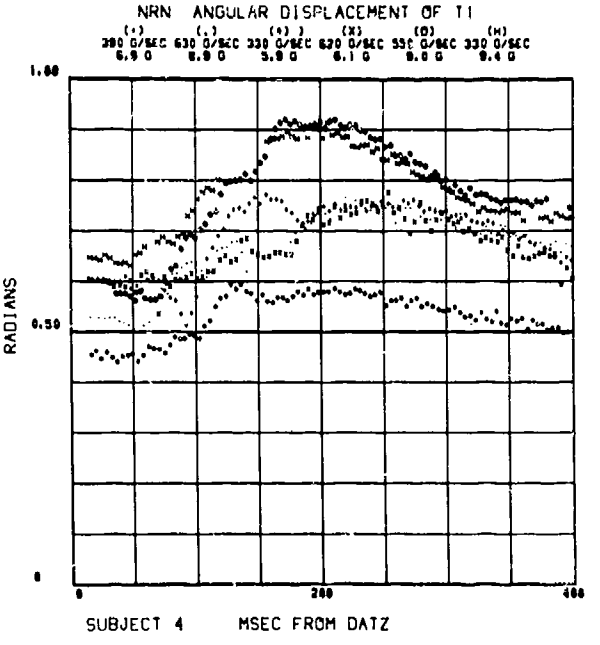

452

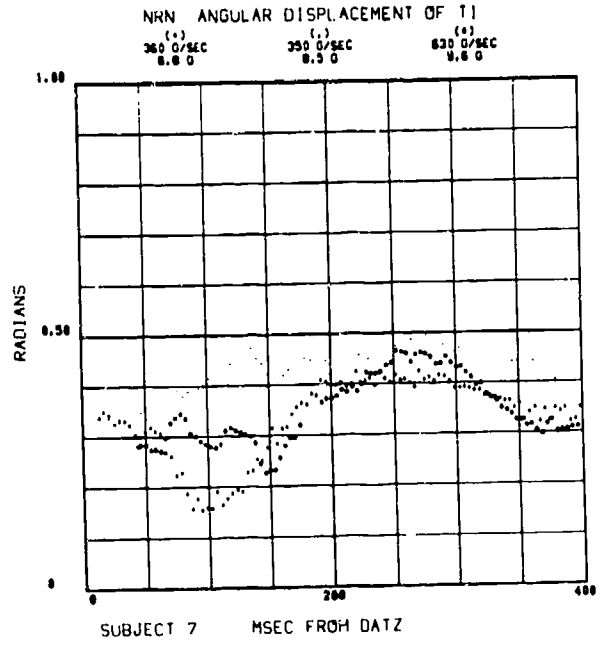

453

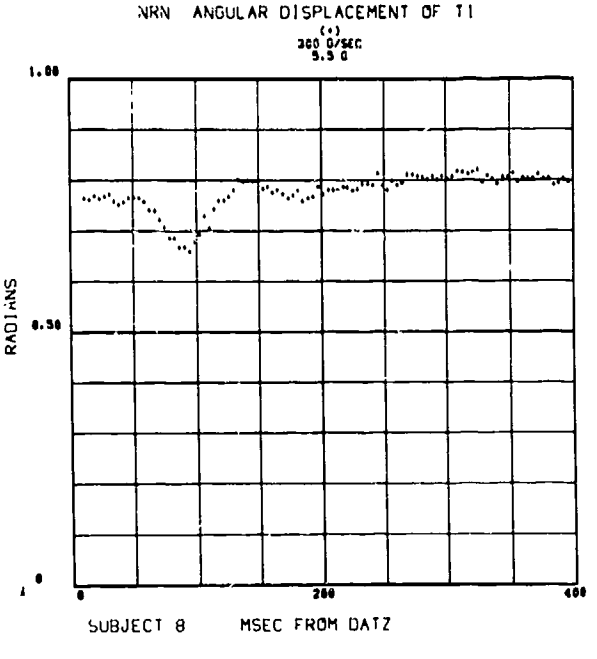

454

NRN ANGULAR DISPLACEMENT OF T_1

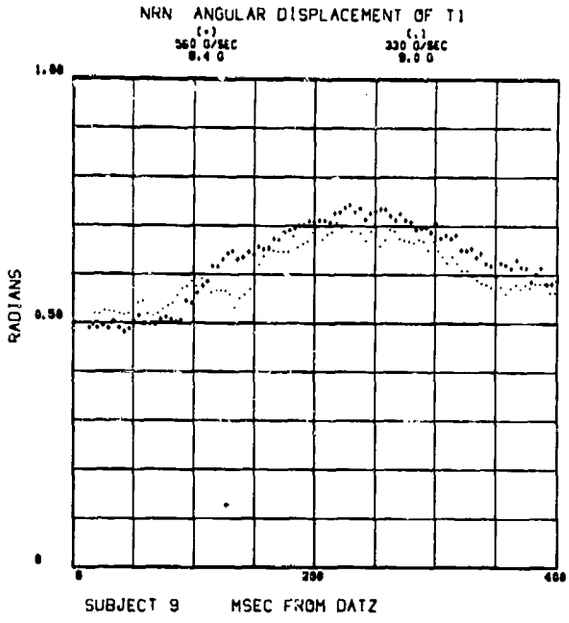

455

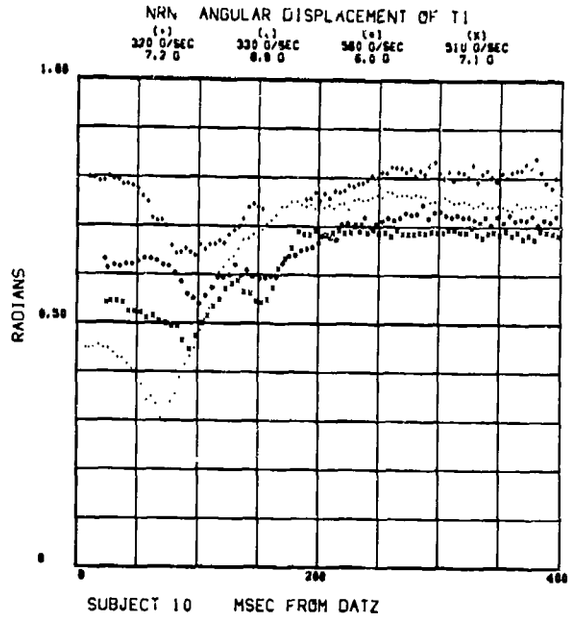

456

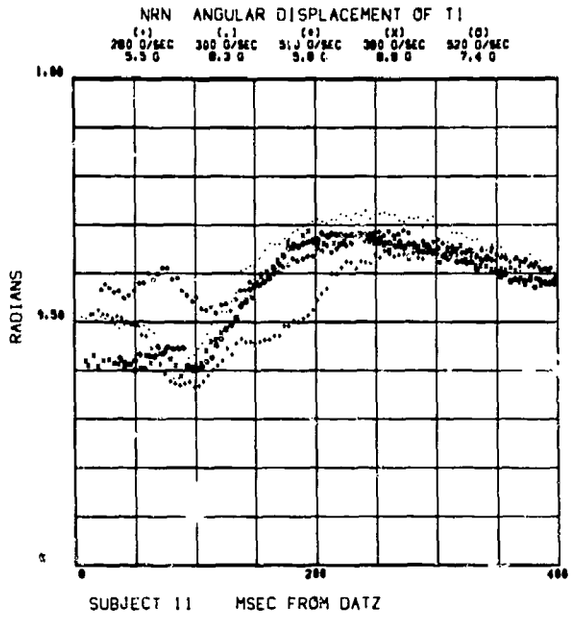

457

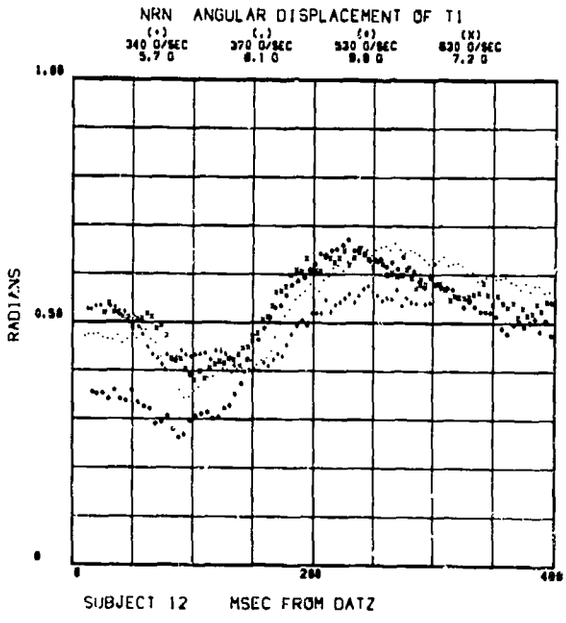

458

NRN ANGULAR DISPLACEMENT OF T_1

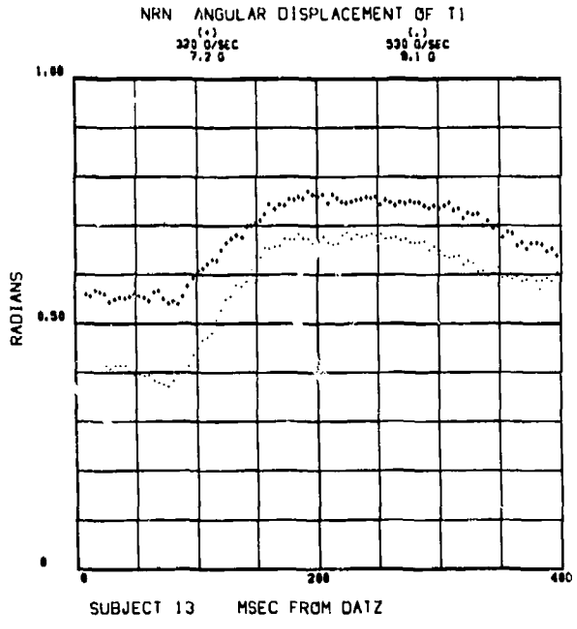

459

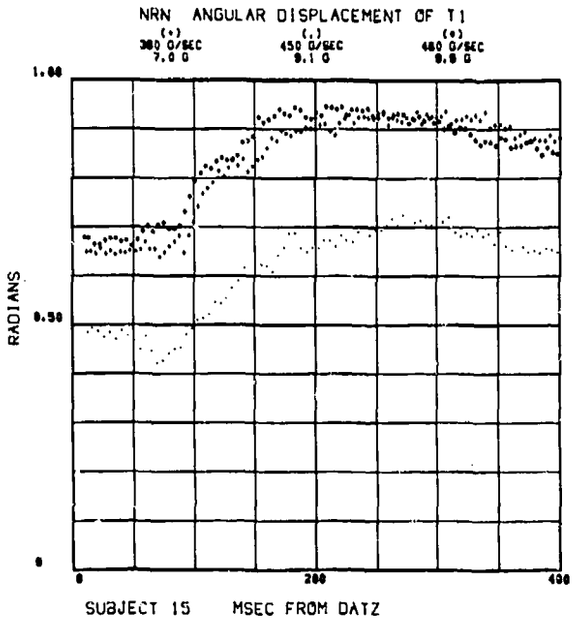

460

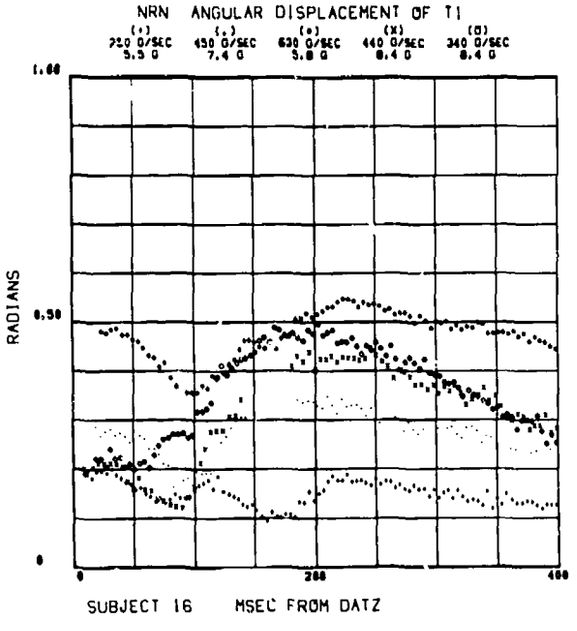

461

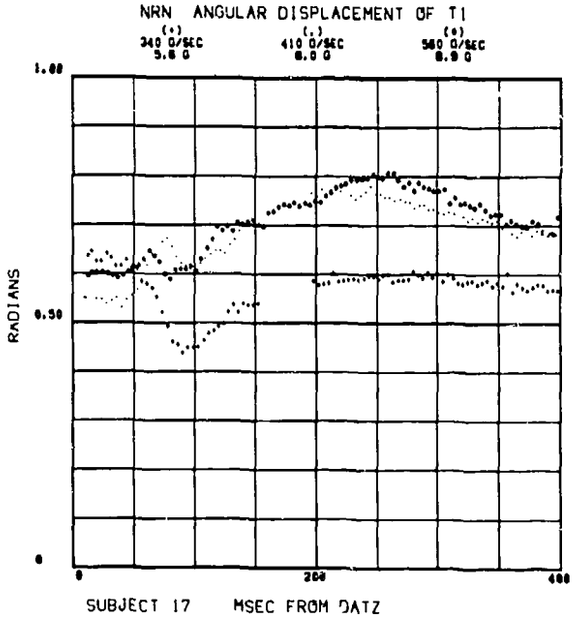

462

NRN ANGULAR DISPLACEMENT OF T_1

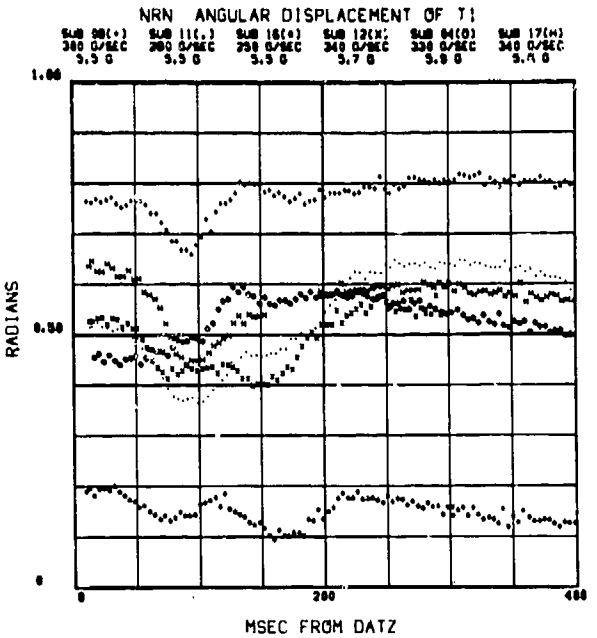

463

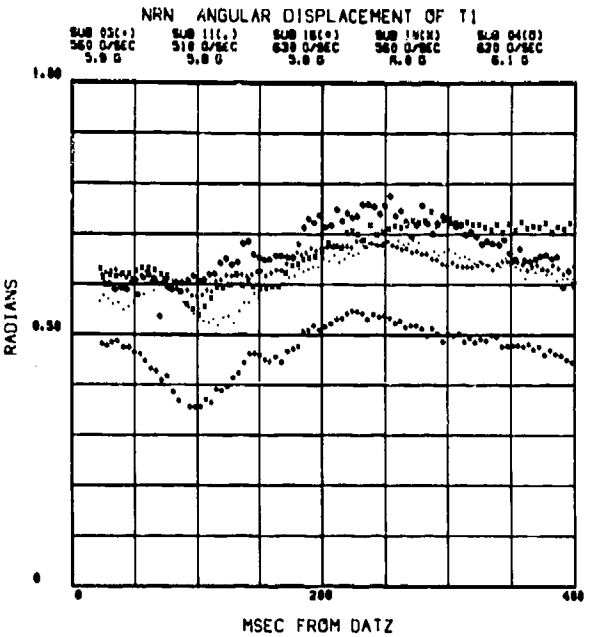

464

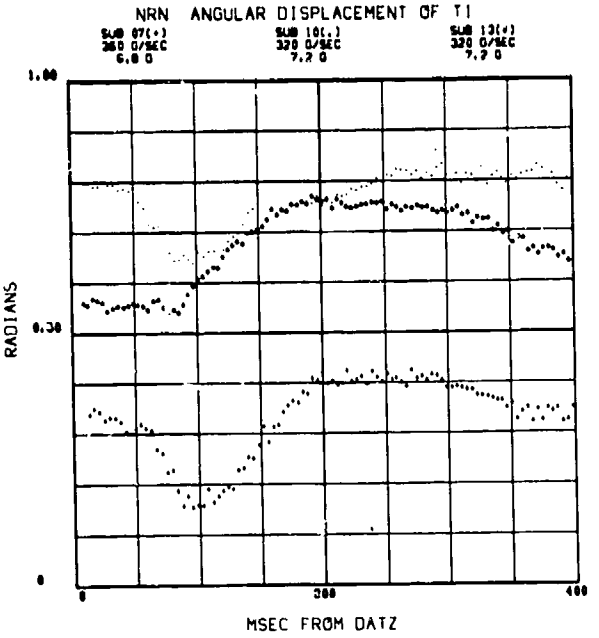

465

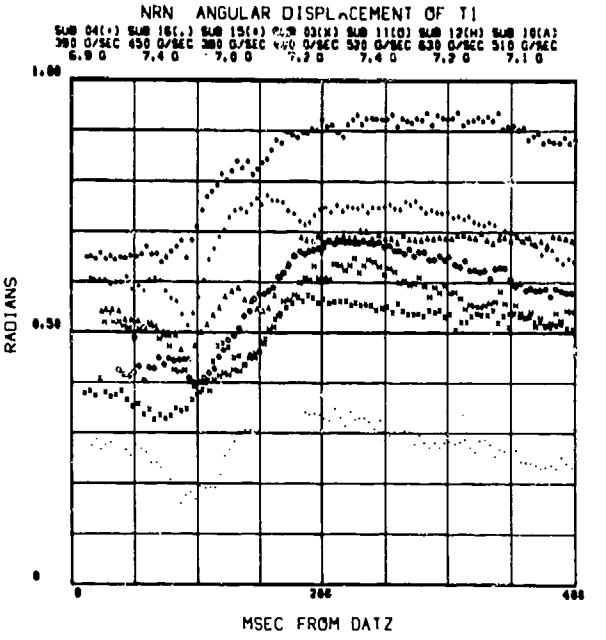

466

NRN ANGULAR DISPLACEMENT OF T_1

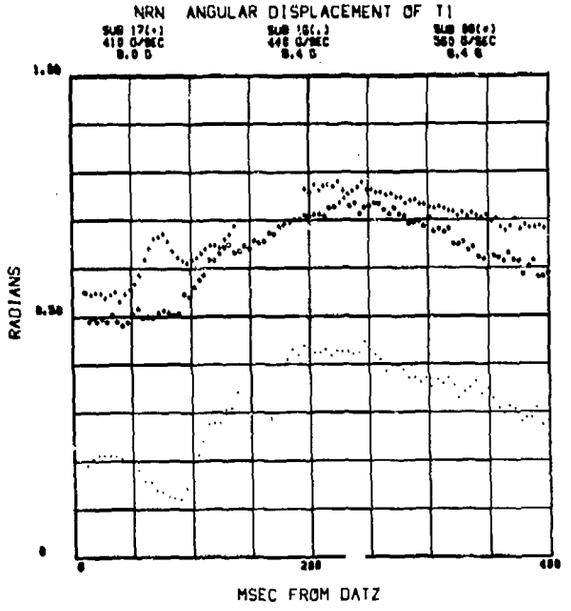

467

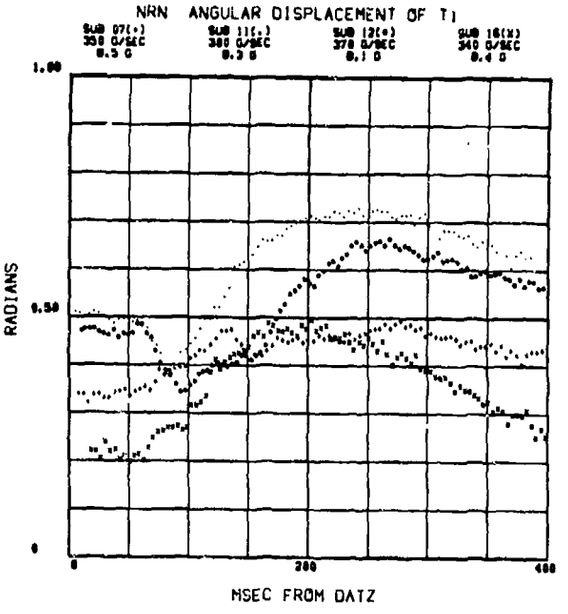

468

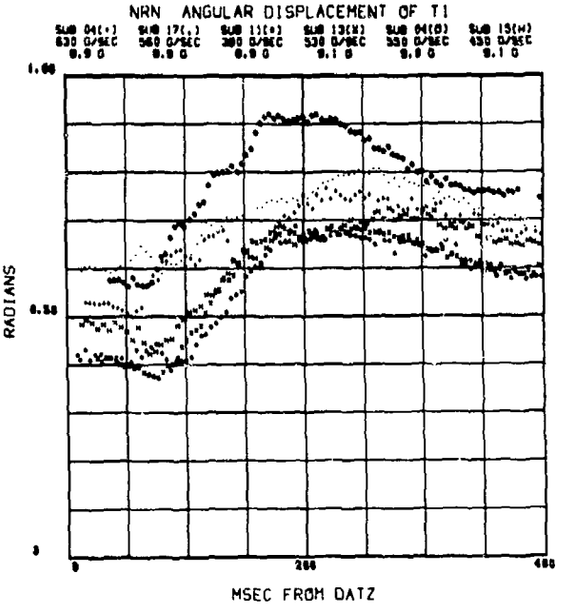

469

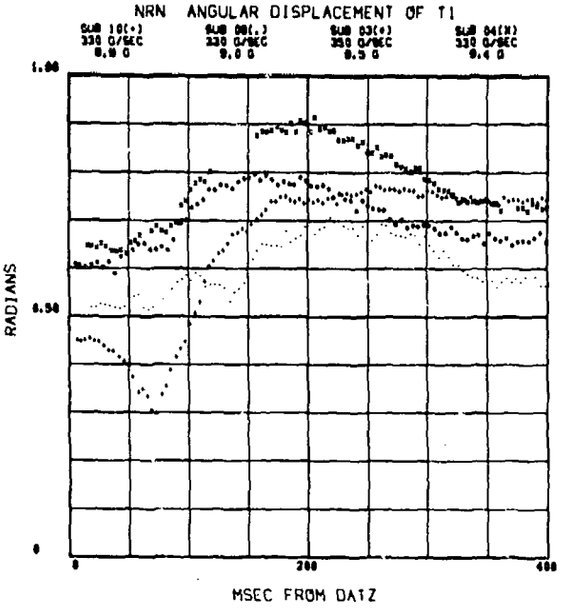

470

NRN ANGULAR DISPLACEMENT OF T_1

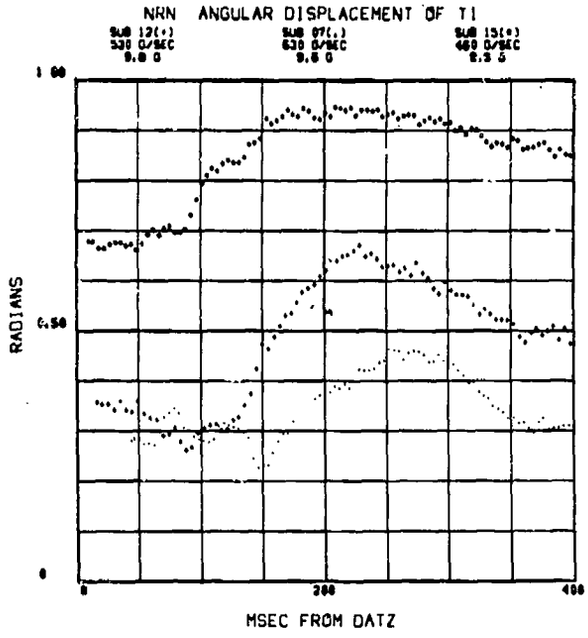

471

PHN ANGULAR DISPLACEMENT OF THE HEAD RELATIVE TO T_1

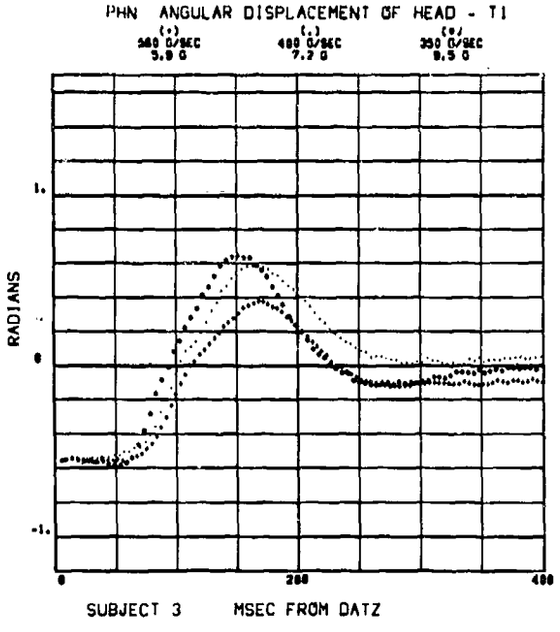

472

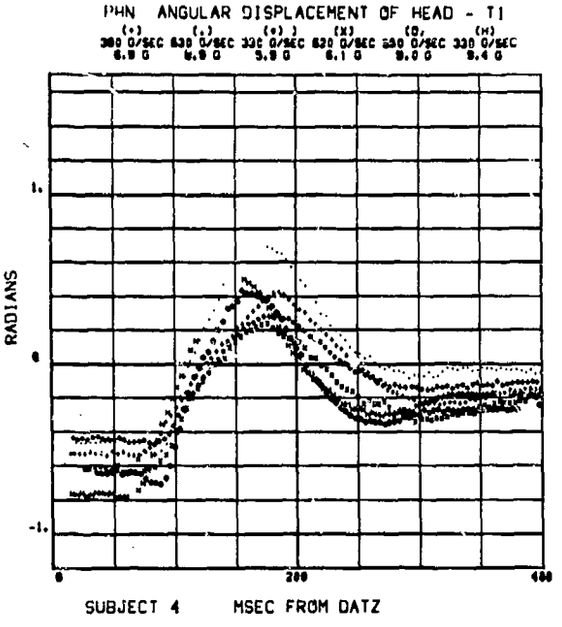

473

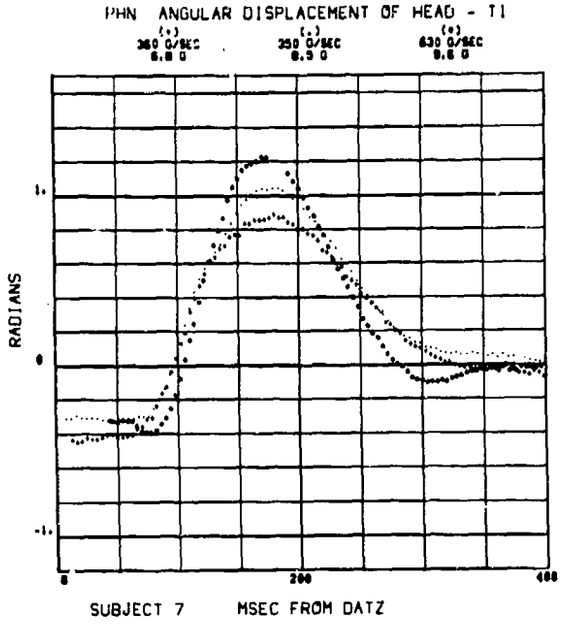

474

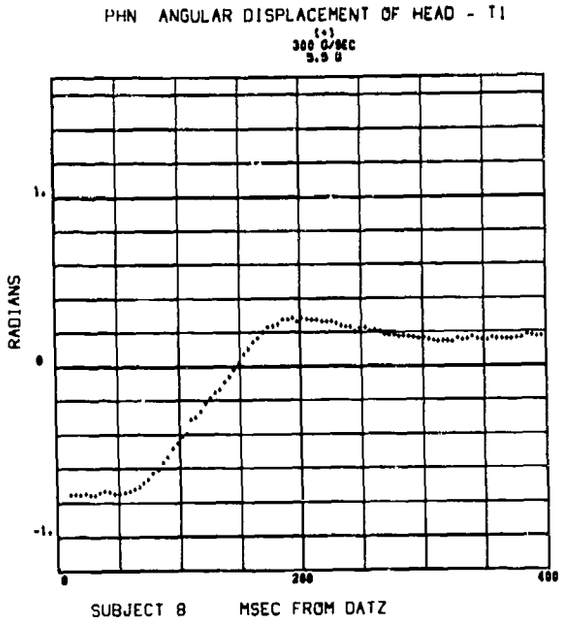

475

PHN ANGULAR DISPLACEMENT OF THE HEAD RELATIVE TO T_1

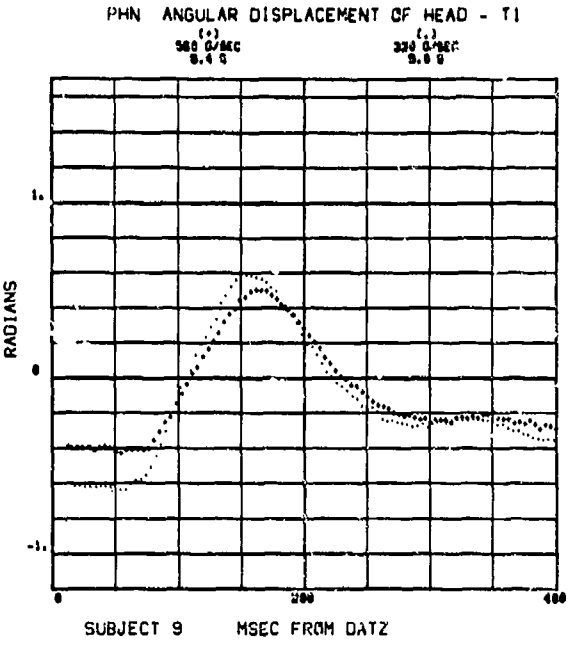

476

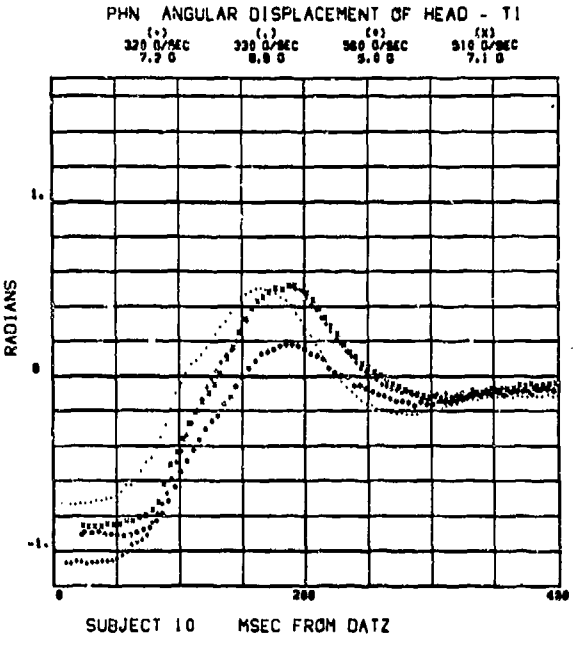

477

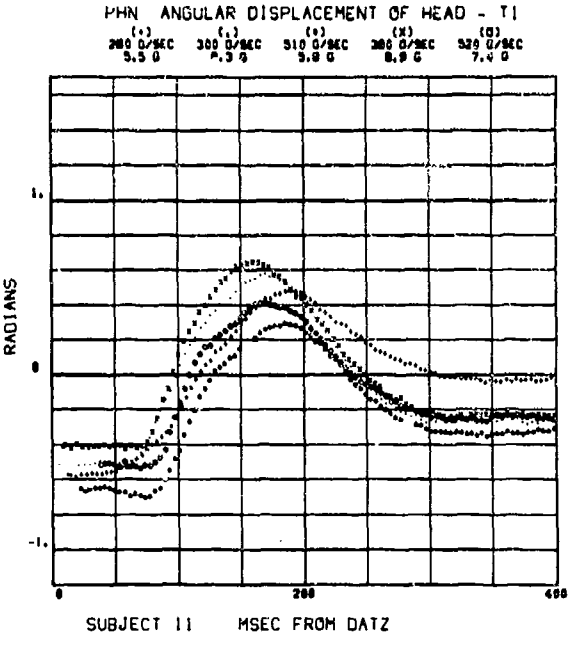

478

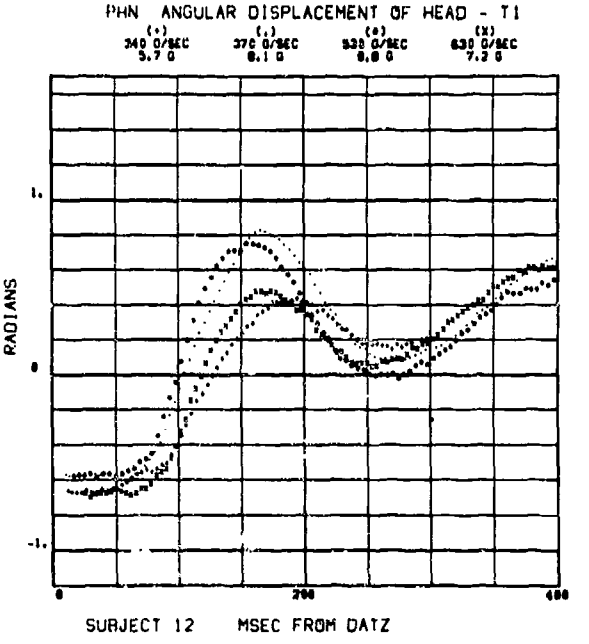

479

PHN ANGULAR DISPLACEMENT OF THE HEAD RELATIVE TO T_1

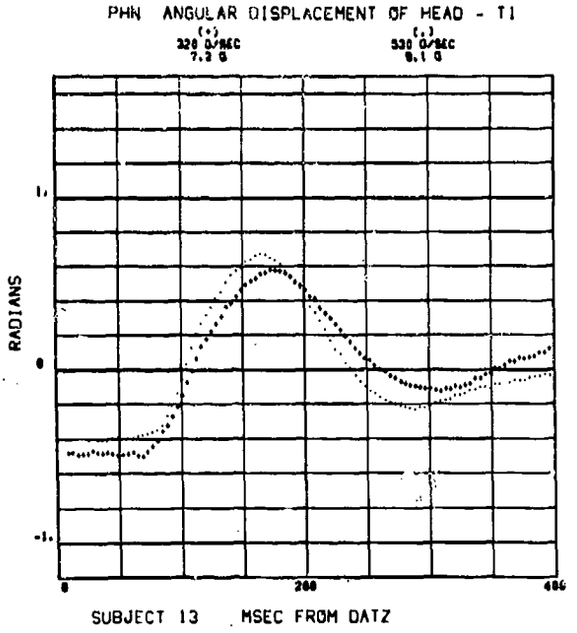

480

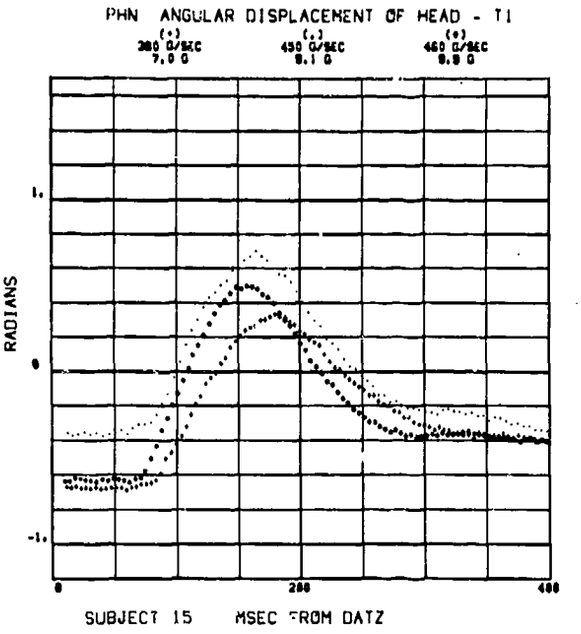

481

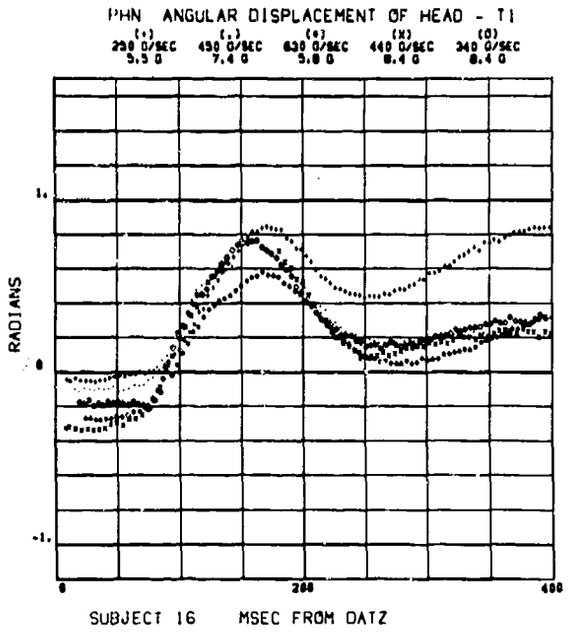

482

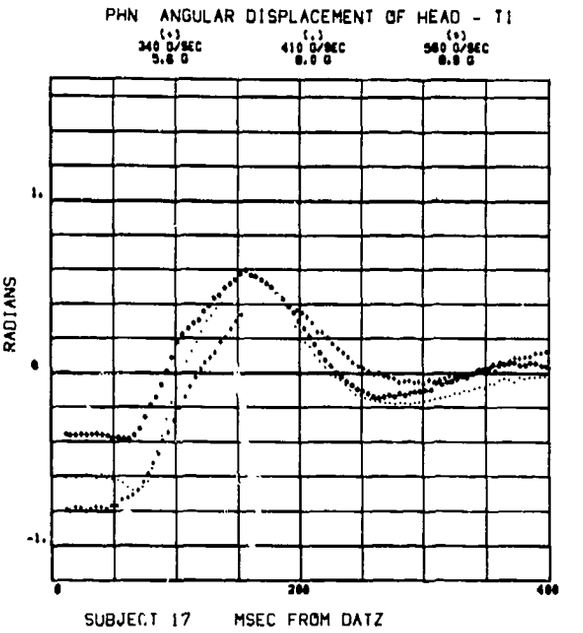

483

PHN ANGULAR DISPLACEMENT OF THE HEAD RELATIVE TO T_1

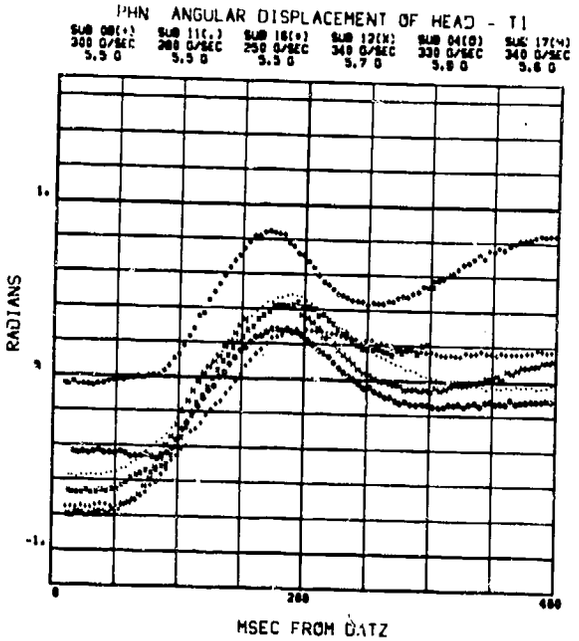

484

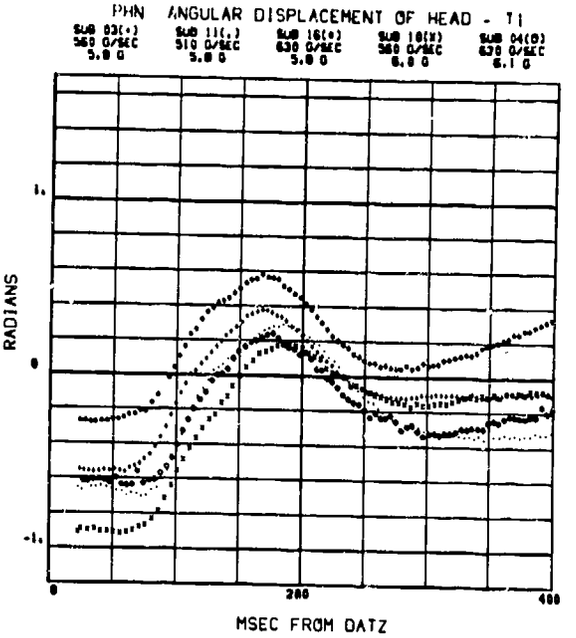

485

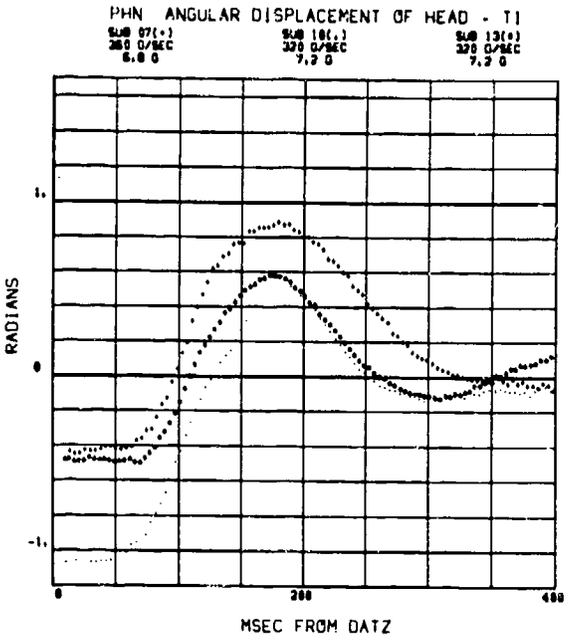

486

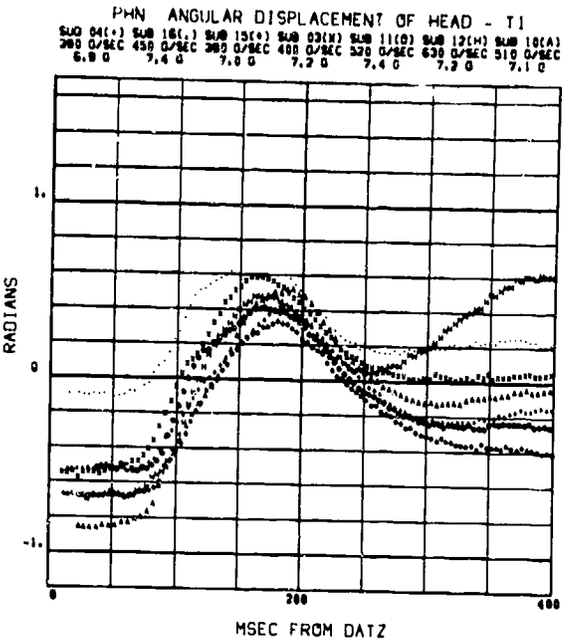

487

PHN ANGULAR DISPLACEMENT OF THE HEAD RELATIVE TO T_1

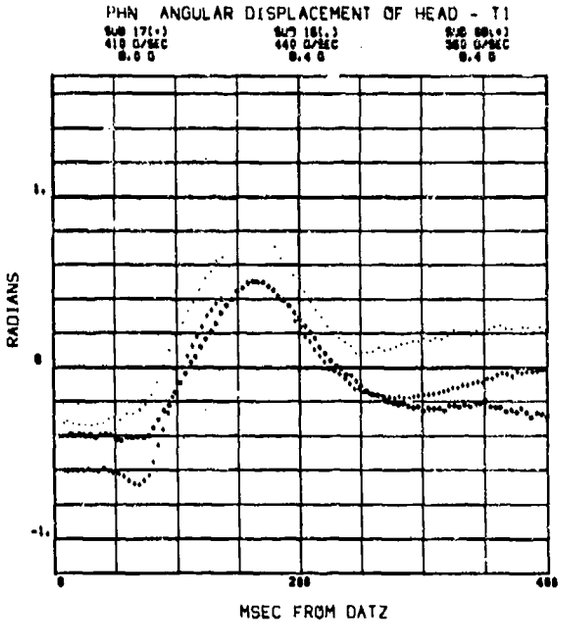

488

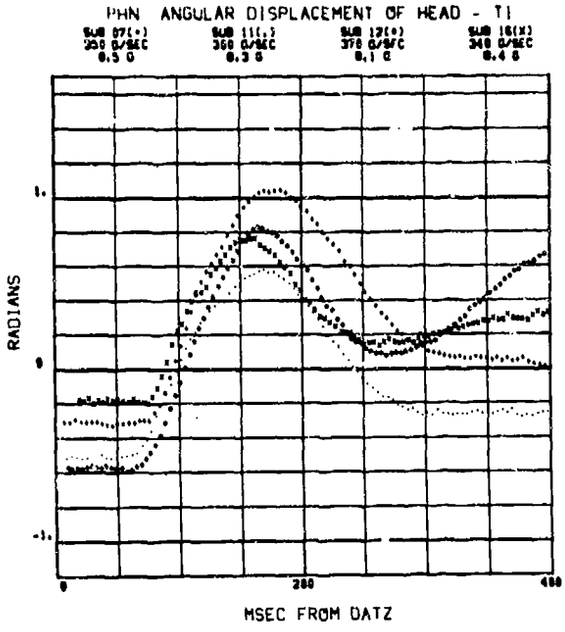

489

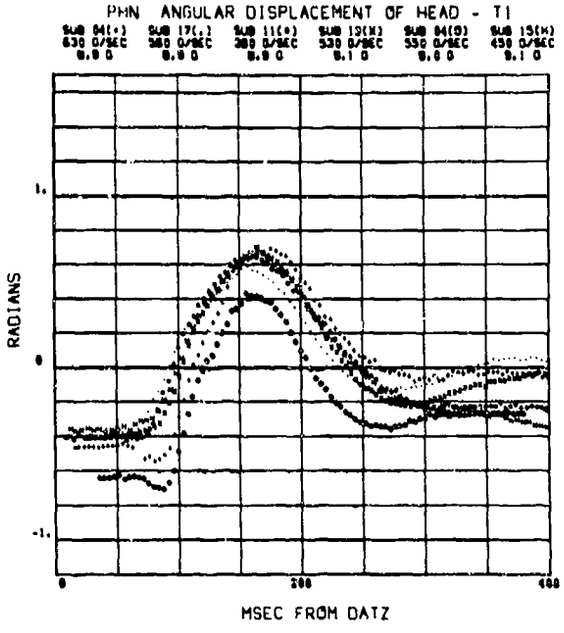

490

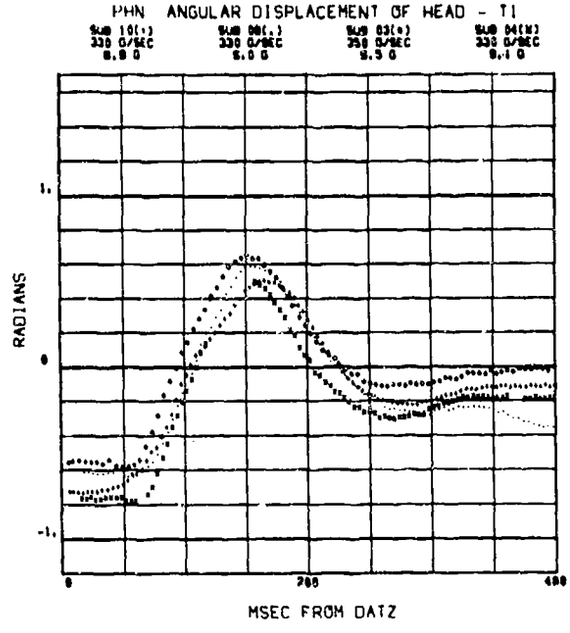

491

PHN ANGULAR DISPLACEMENT OF THE HEAD RELATIVE TO T_1

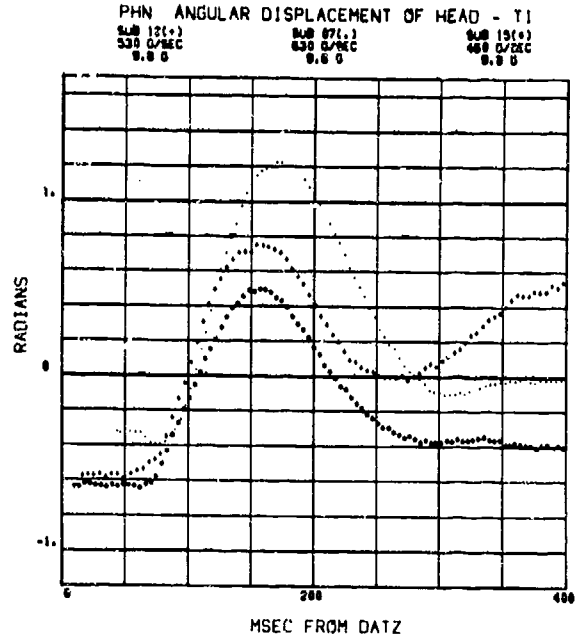

492

MCX, MCZ COMPONENTS OF HEAD C.G. DISPLACEMENT DURING NORMAL HEADNOD AND DURING THE DYNAMIC EVENT

493

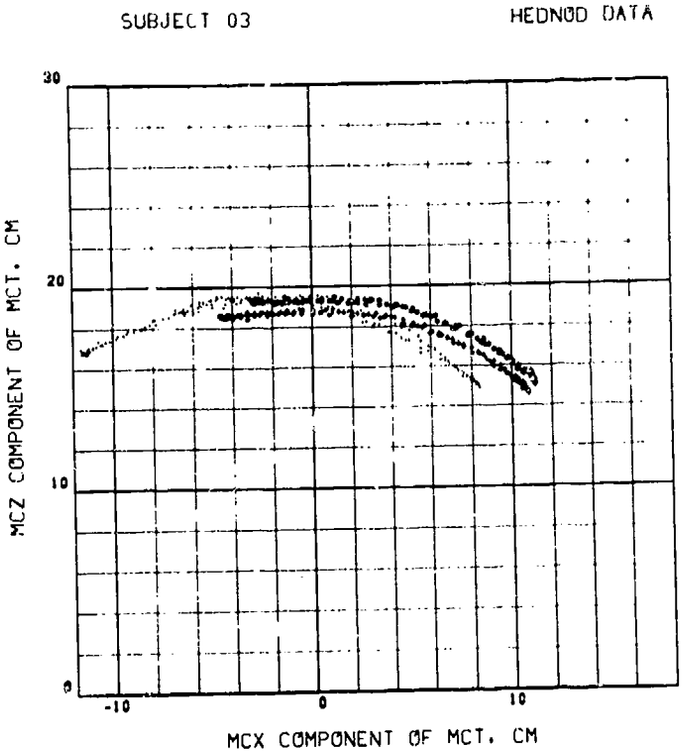

494

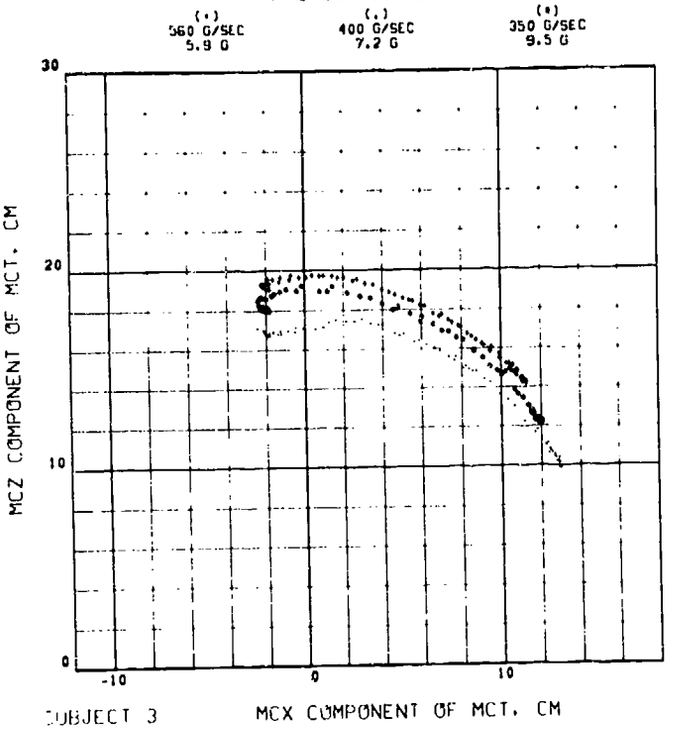

MCX, MCZ COMPONENTS OF HEAD C.G. DISPLACEMENT DURING NORMAL HEADNOD AND DURING THE DYNAMIC EVENT

495

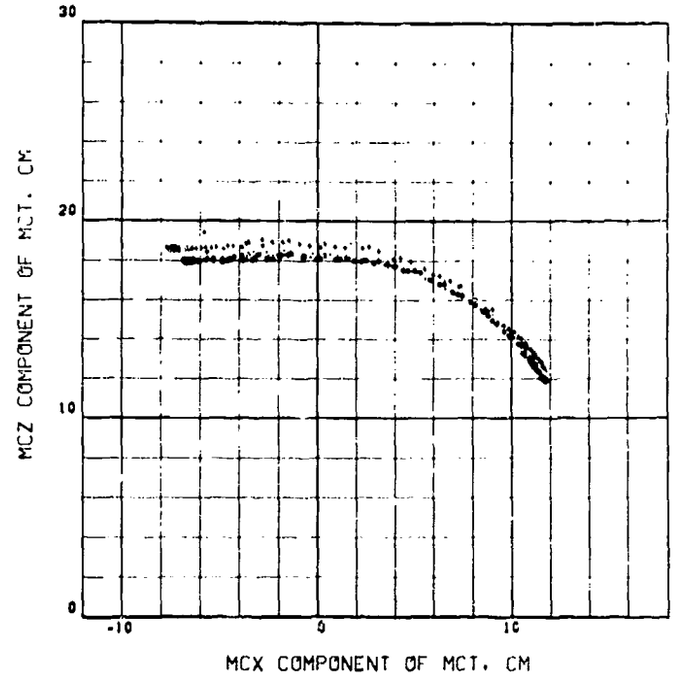

496

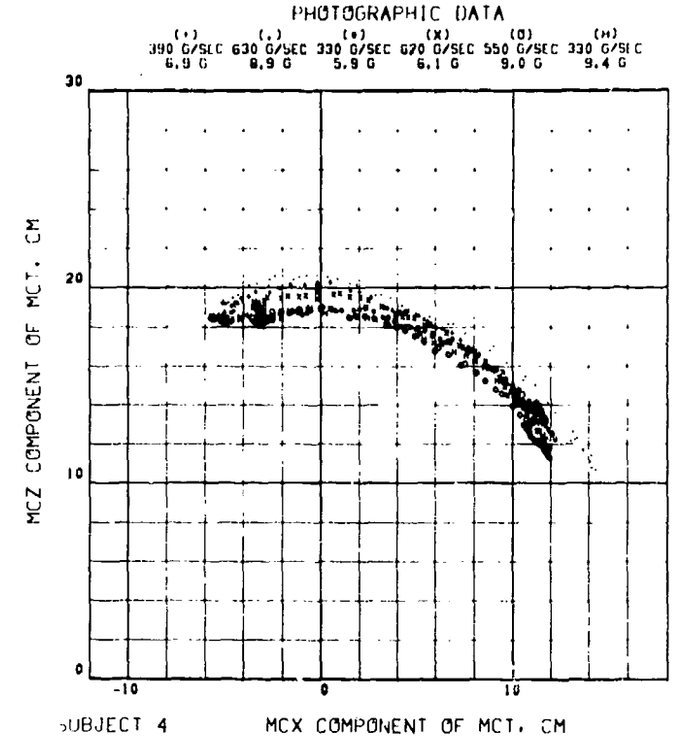

MCX, MCZ COMPONENTS OF HEAD C.G. DISPLACEMENT DURING NORMAL HEADNOD AND DURING THE DYNAMIC EVENT

SUBJECT 07 HEDNOD DATA

497

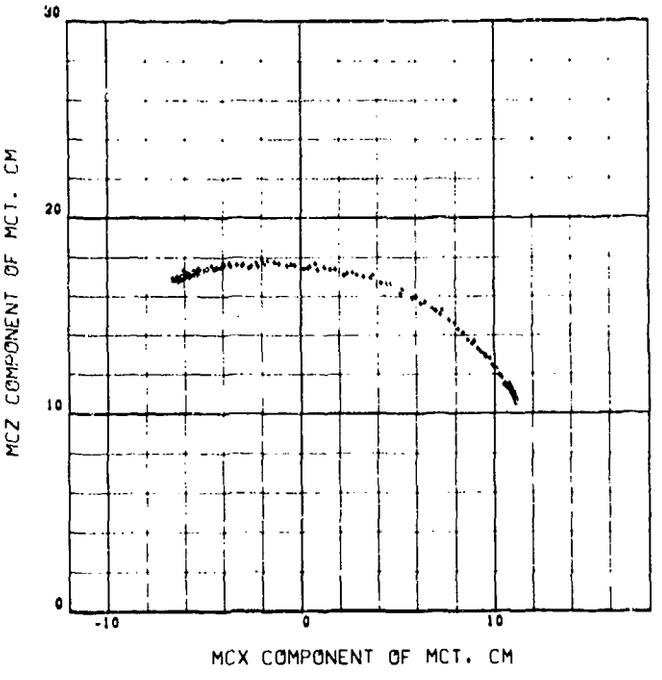

PHOTOGRAPHIC DATA

498

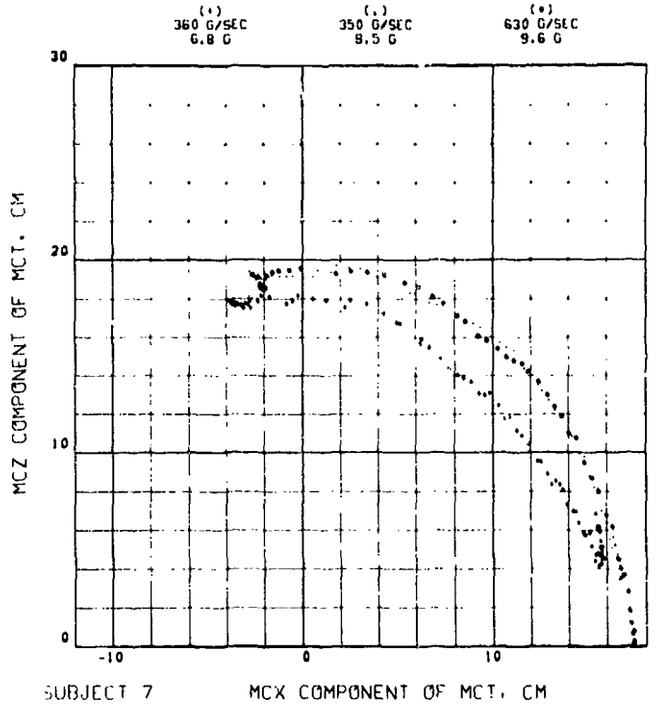

SUBJECT 7 MCX COMPONENT OF MCT. CM

MCX, MCZ COMPONENTS OF HEAD C.G. DISPLACEMENT DURING NORMAL HEADNOD AND DURING THE DYNAMIC EVENT

SUBJECT 08 HEDNOD DATA

499

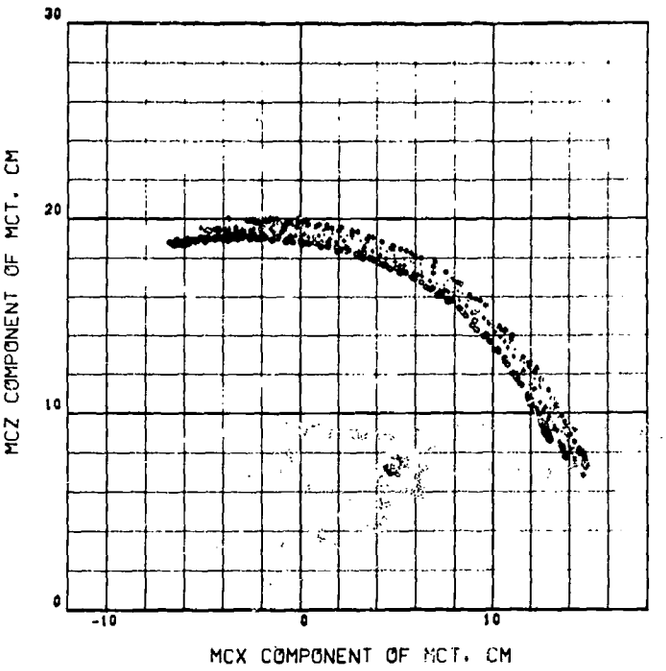

PHOTOGRAPHIC DATA

(+)
300 G/SEC
5.5 G

500

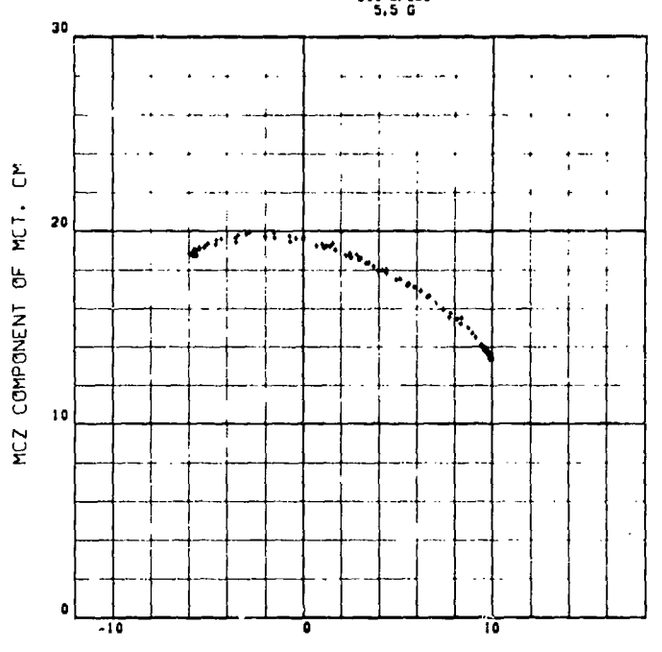

SUBJECT 8 MCX COMPONENT OF MCT. CM

MCX, MCZ COMPONENTS OF HEAD C.G. DISPLACEMENT DURING NORMAL HEADNOD AND DURING THE DYNAMIC EVENT

SUBJECT 09 HEDNOD DATA

501

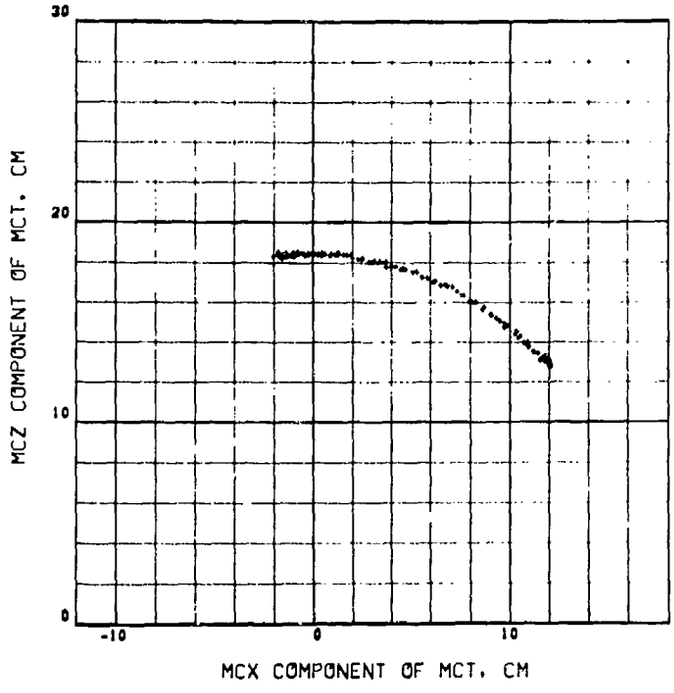

PHOTOGRAPHIC DATA

502

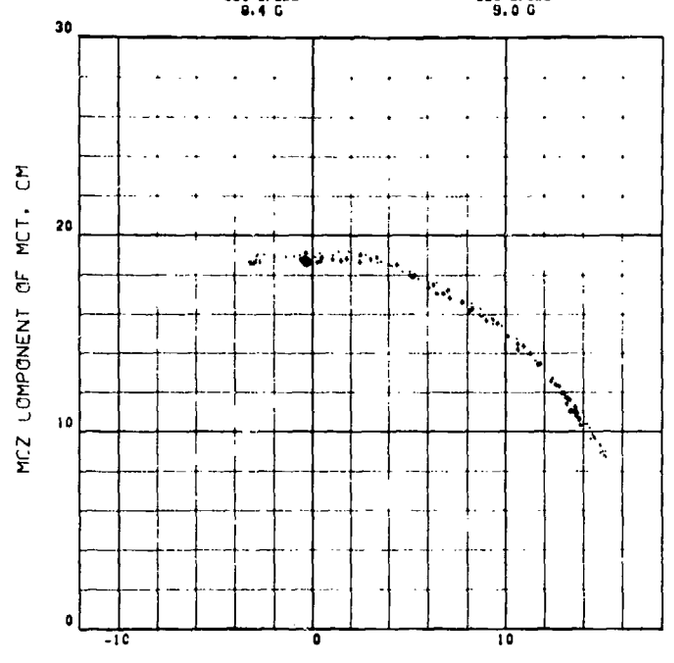

SUBJECT 9 MCX COMPONENT OF MCT, CM

MCX, MCZ COMPONENTS OF HEAD C.G. DISPLACEMENT DURING NORMAL HEADNOD AND DURING THE DYNAMIC EVENT

503

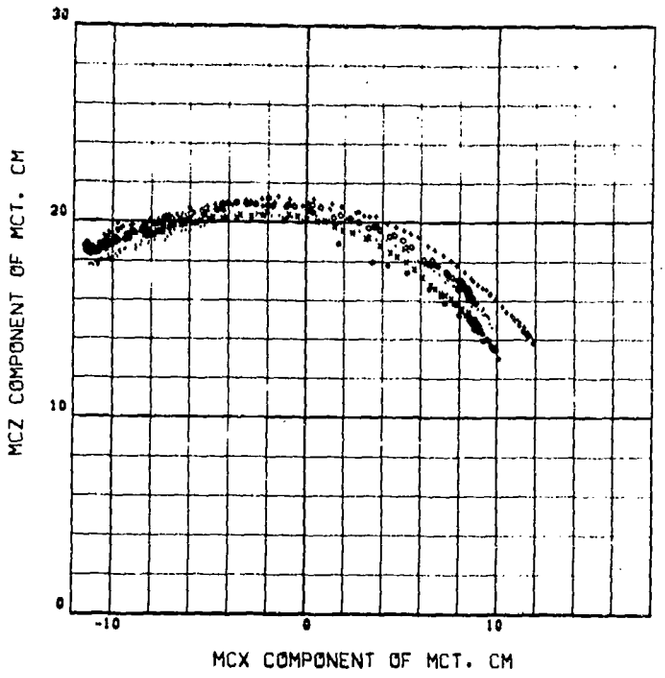

504

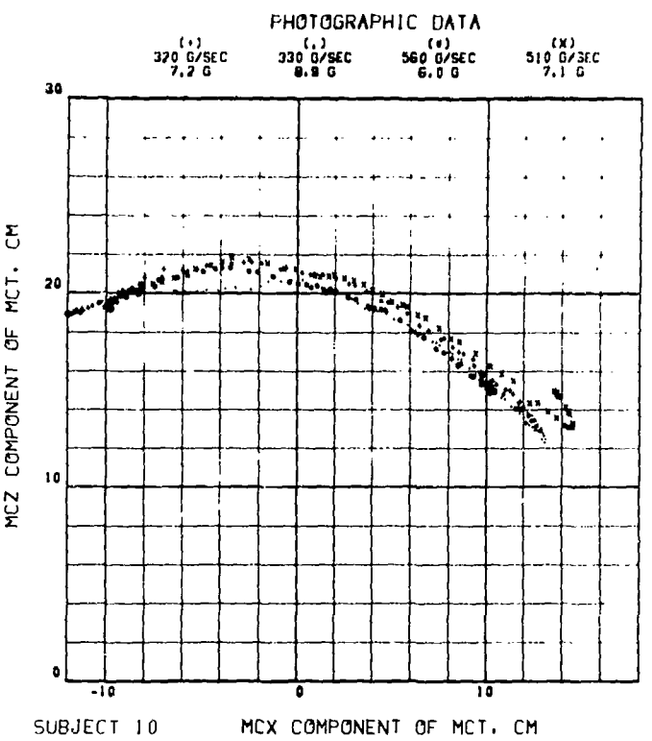

MCX, MCZ COMPONENTS OF HEAD C.G. DISPLACEMENT DURING NORMAL HEADNOD AND DURING THE DYNAMIC EVENT

505

SUBJECT 11 HEDNOD DATA

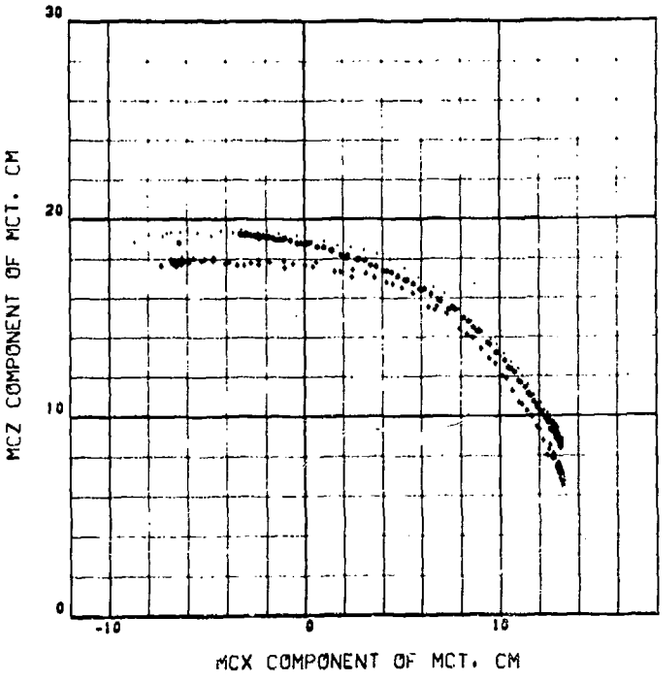

506

PHOTOGRAPHIC DATA

(+) 280 G/SEC 5.5 G
(.) 300 G/SEC 8.9 G
(*) 510 G/SEC 5.8 G
(X) 380 G/SEC 8.9 G
(O) 520 G/SEC 7.4 G

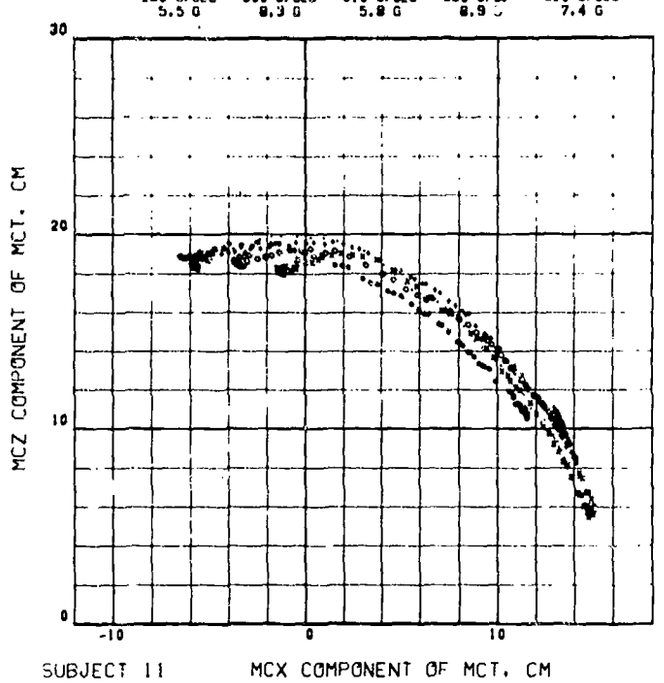

SUBJECT 11 MCX COMPONENT OF MCT. CM

MCX, MCZ COMPONENTS OF HEAD C.G. DISPLACEMENT DURING NORMAL HEADNOD AND DURING THE DYNAMIC EVENT

SUBJECT 12 HEDNØD DATA

507

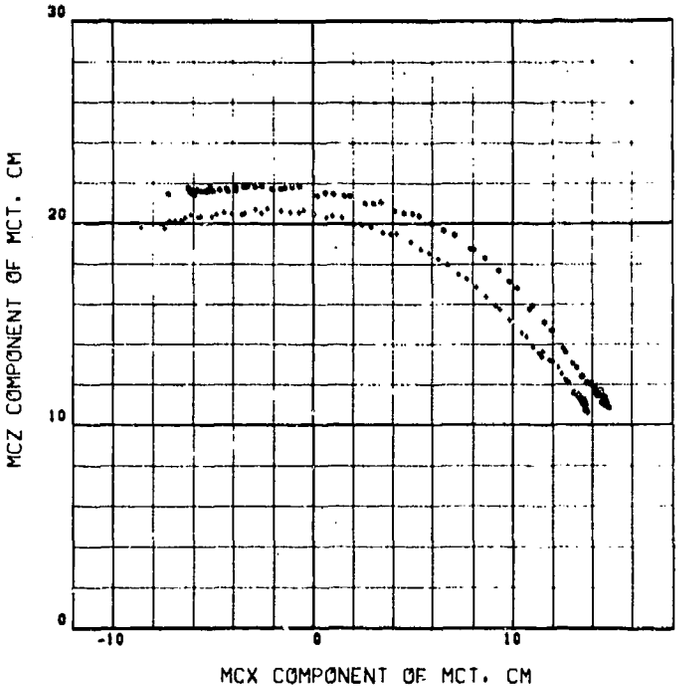

PHOTØGRAPHIC DATA

508

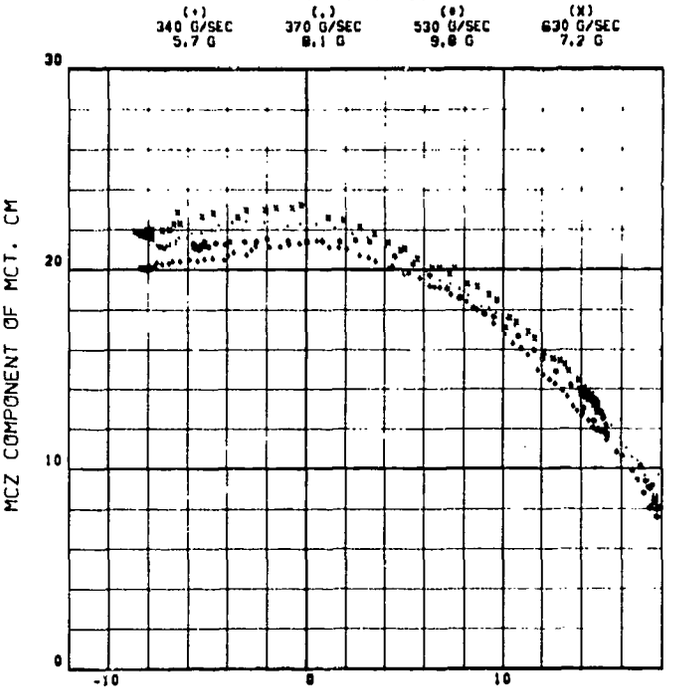

SUBJECT 12 MCX COMPONENT ØF MCT. CM

MCX, MCZ COMPONENTS OF HEAD C.G. DISPLACEMENT DURING NORMAL HEADNOD AND DURING THE DYNAMIC EVENT

SUBJECT 13 HEDNOD DATA

509

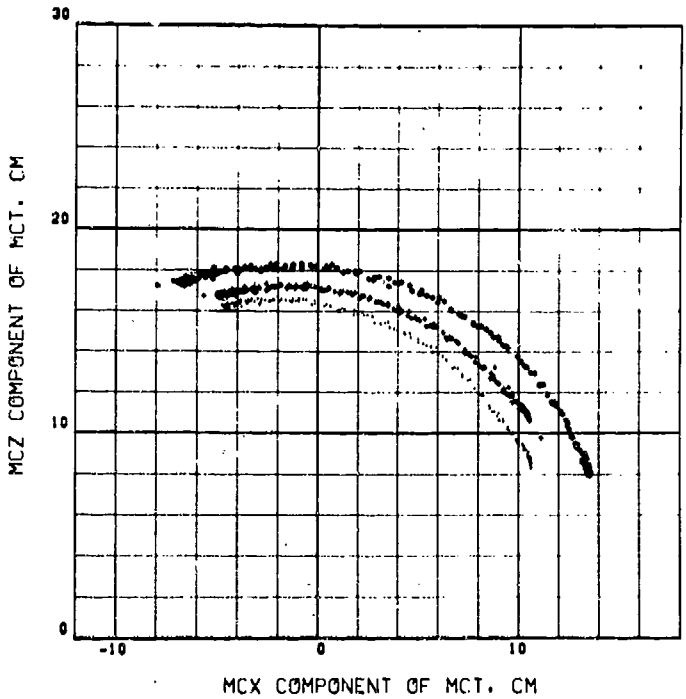

PHOTOGRAPHIC DATA

510

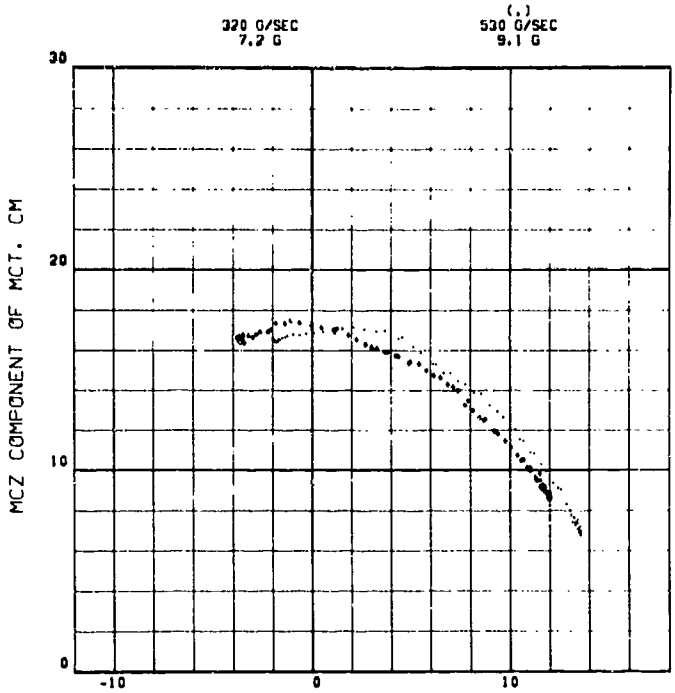

SUBJECT 13 MCX COMPONENT OF MCT. CM

MCX, MCZ COMPONENTS OF HEAD C.G. DISPLACEMENT DURING NORMAL HEADNOD AND DURING THE DYNAMIC EVENT

SUBJECT 15 HEDNOD DATA

511

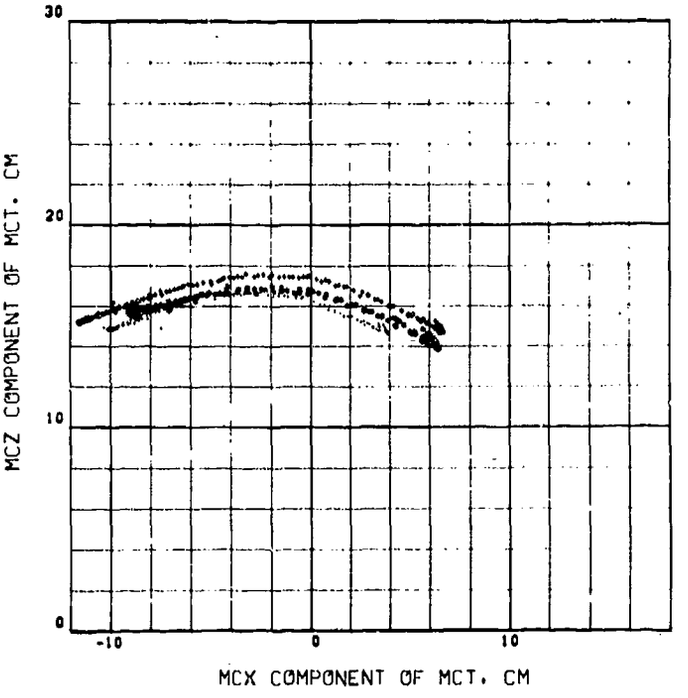

PHOTOGRAPHIC DATA

512

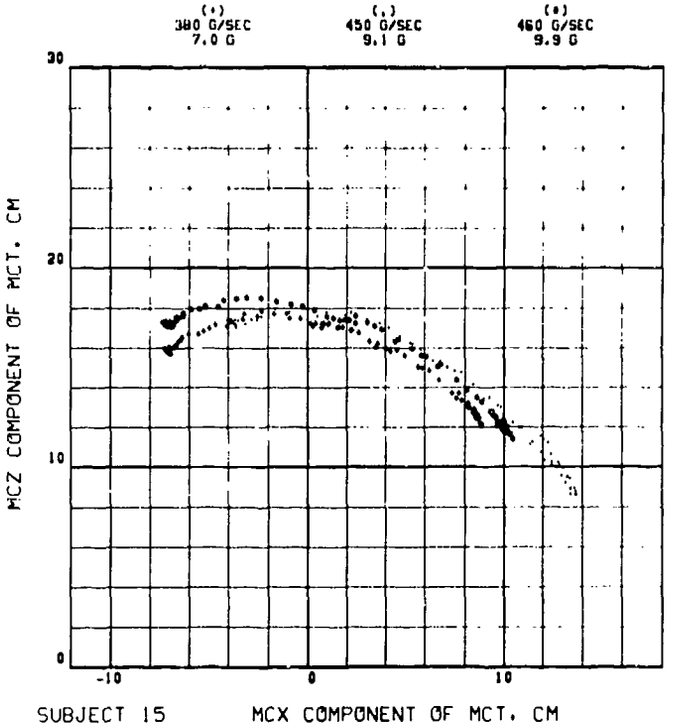

SUBJECT 15 MCX COMPONENT OF MCT. CM

MCX, MCZ COMPONENTS OF HEAD C.G. DISPLACEMENT DURING NORMAL HEADNOD AND DURING THE DYNAMIC EVENT

SUBJECT 16 HEDNOD DATA

513

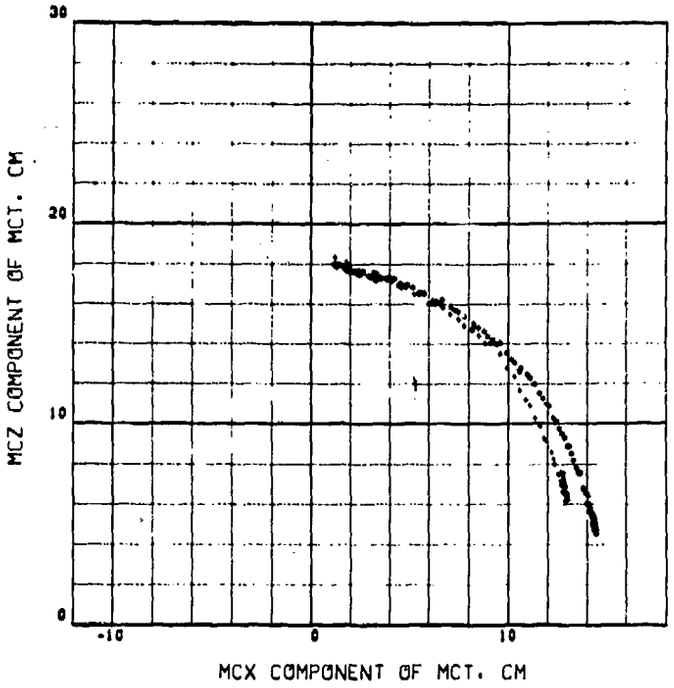

PHOTOGRAPHIC DATA

514

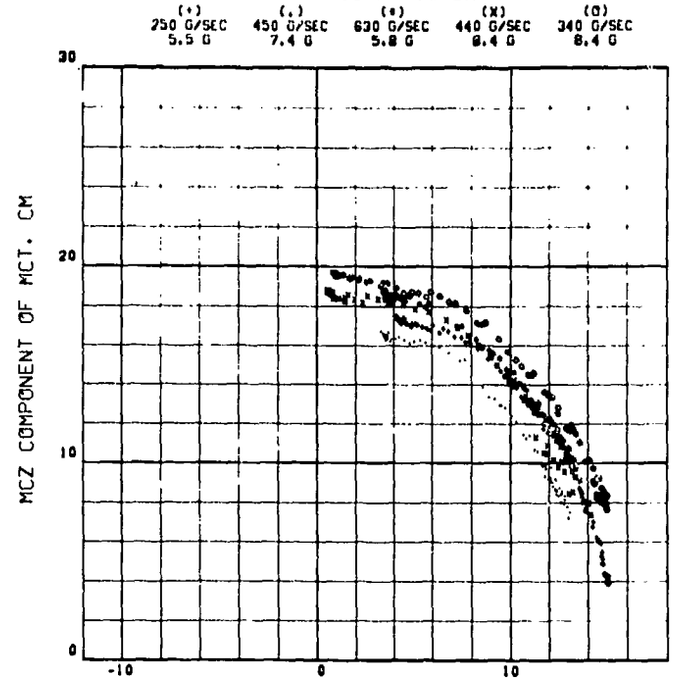

SUBJECT 16 MCX COMPONENT OF MCT. CM

MCX, MCZ COMPONENTS OF HEAD C.G. DISPLACEMENT DURING NORMAL HEADNOD AND DURING THE DYNAMIC EVENT

SUBJECT 17 HEDNOD DATA

515

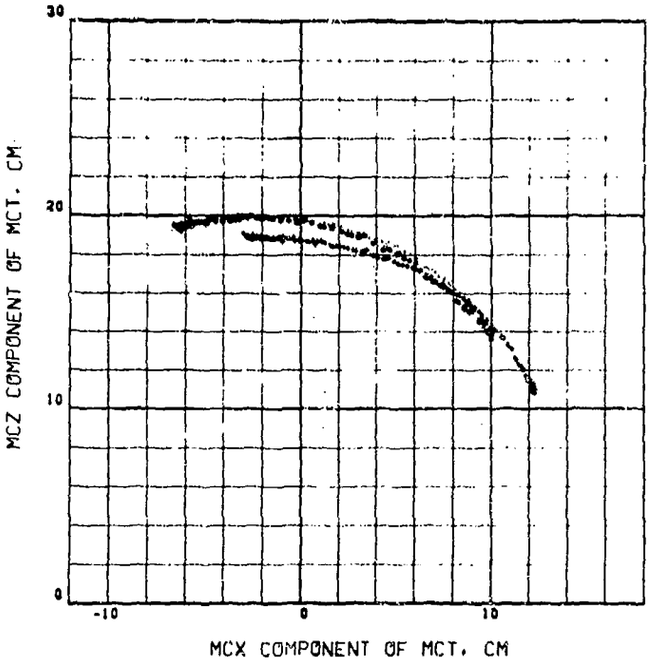

PHOTOGRAPHIC DATA

516

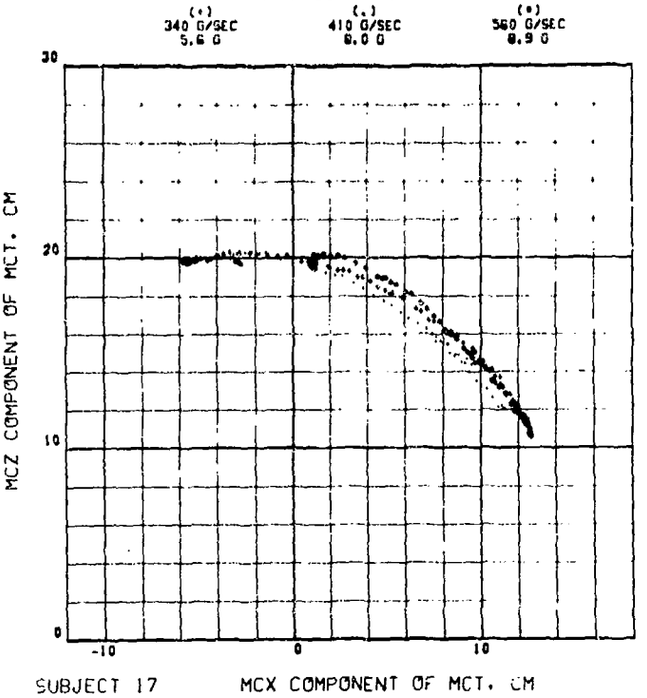

SUBJECT 17 MCX COMPONENT OF MCT. CM

REPEATABILITY, PAIRED RUNS ALL VARIABLES, SUBJECT 004

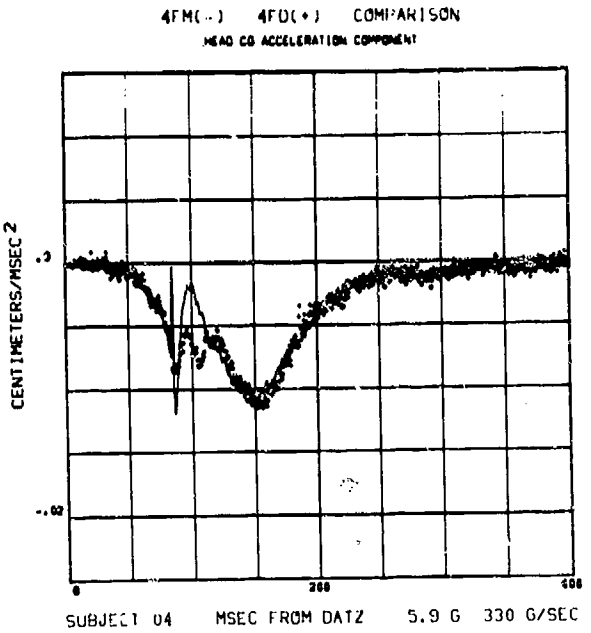

517

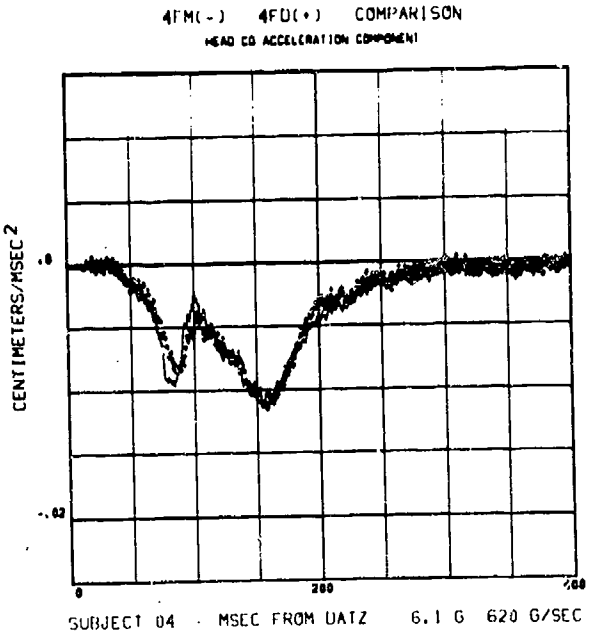

518

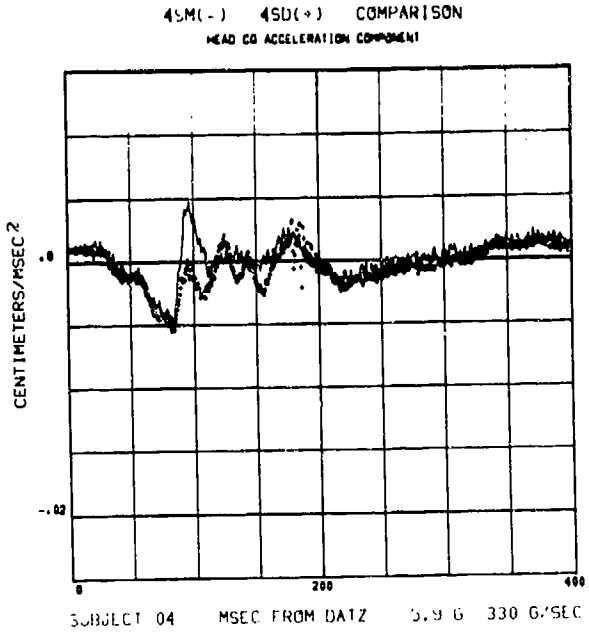

519

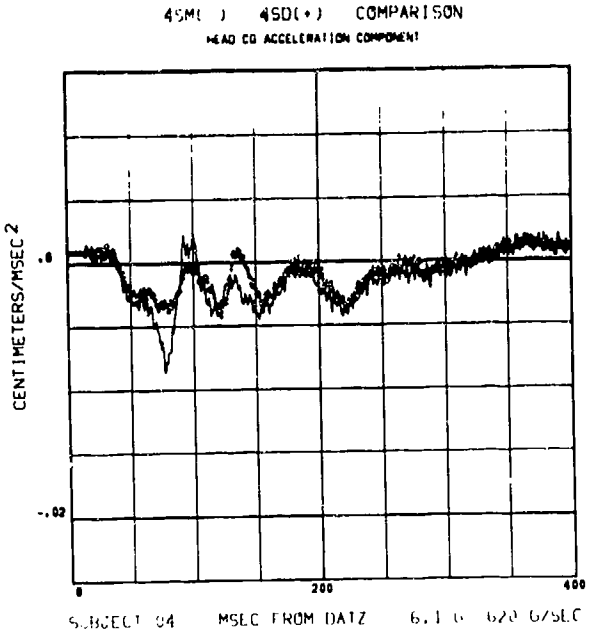

520

REPEATABILITY, PAIRED RUNS ALL VARIABLES, SUBJECT 004

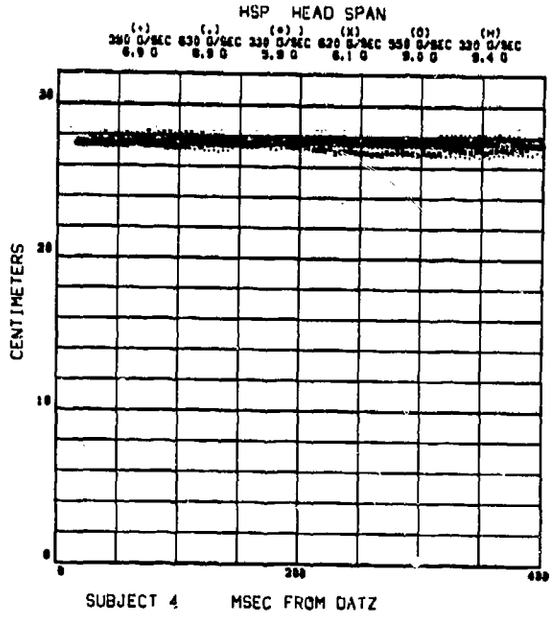

521

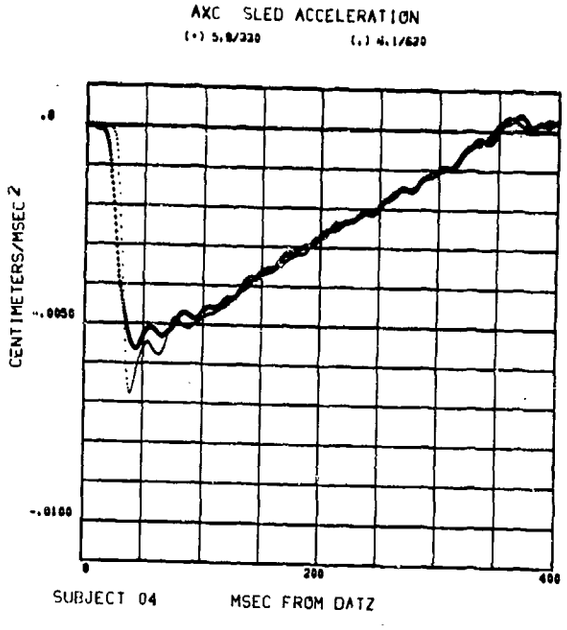

522

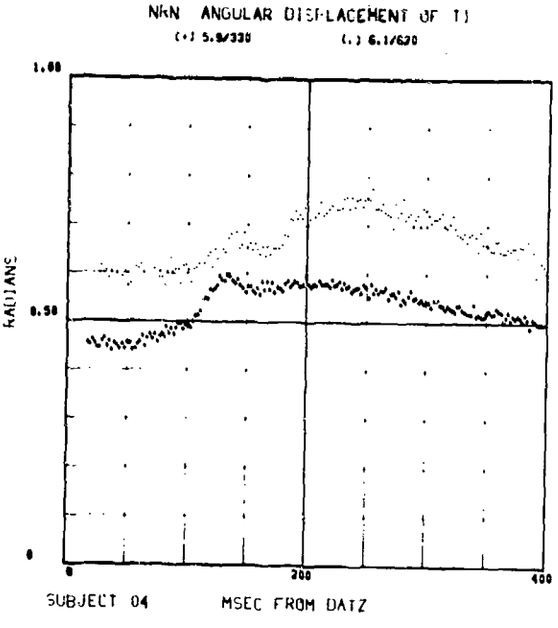

523

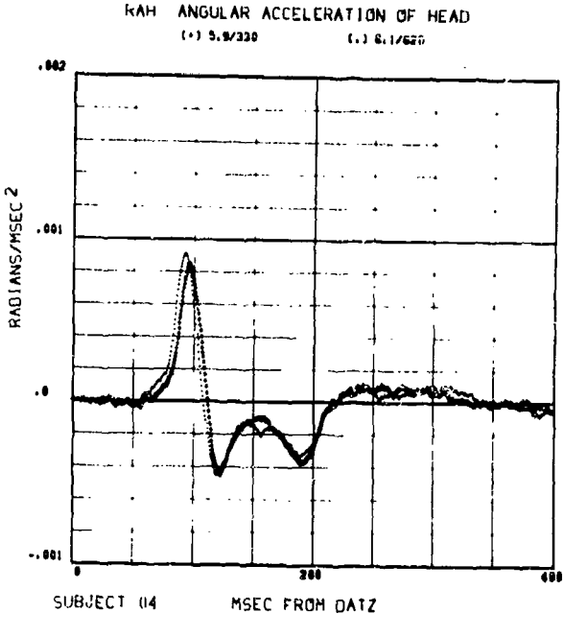

524

REPEATABILITY, PAIRED RUNS ALL VARIABLES, SUBJECT 004

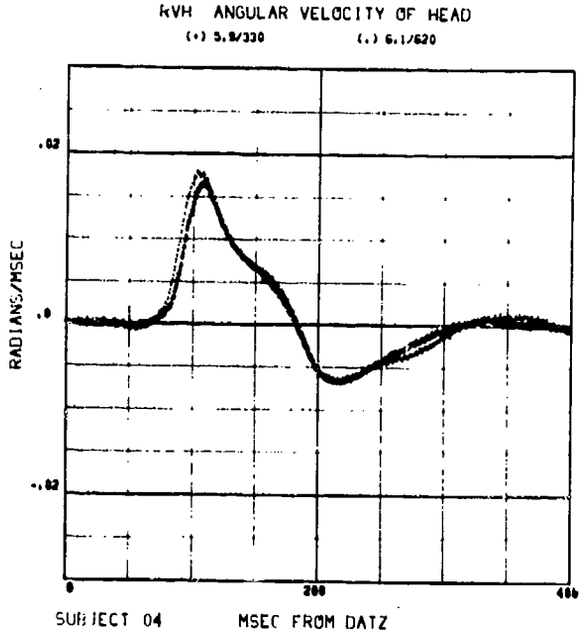

525

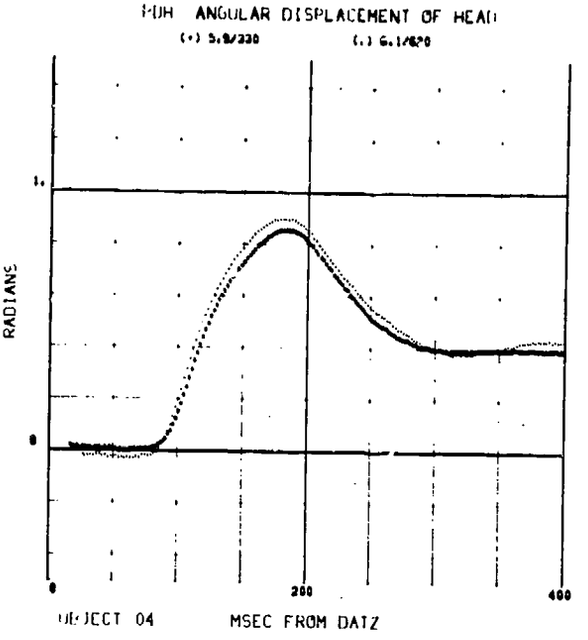

526

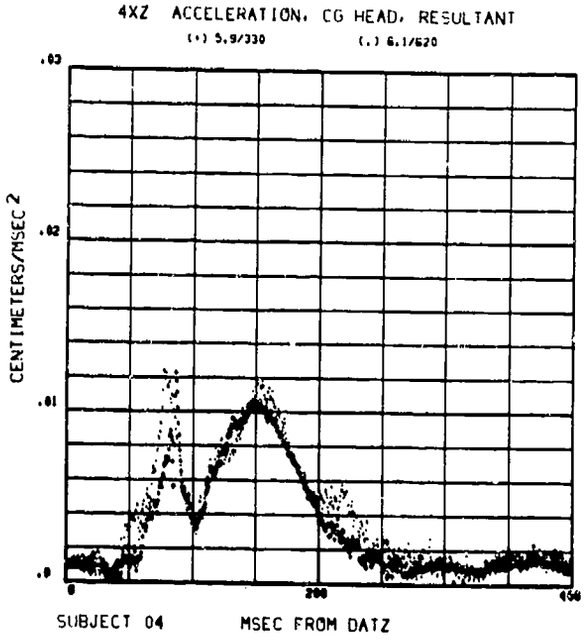

527

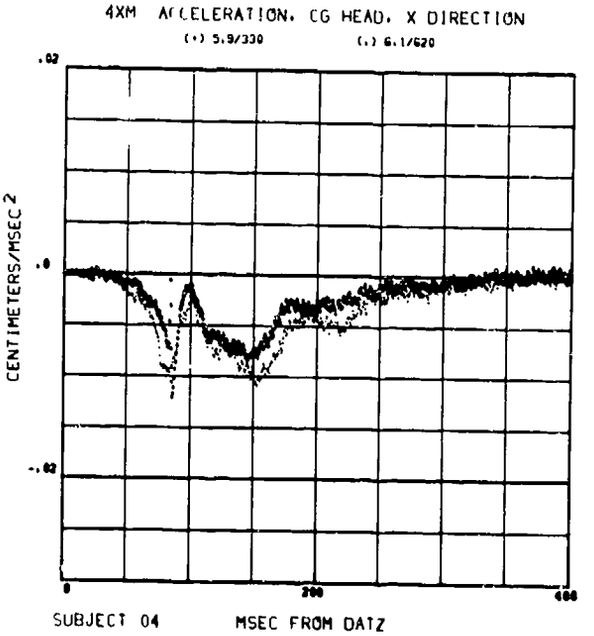

528

REPEATABILITY, PAIRED RUNS ALL VARIABLES, SUBJECT 004

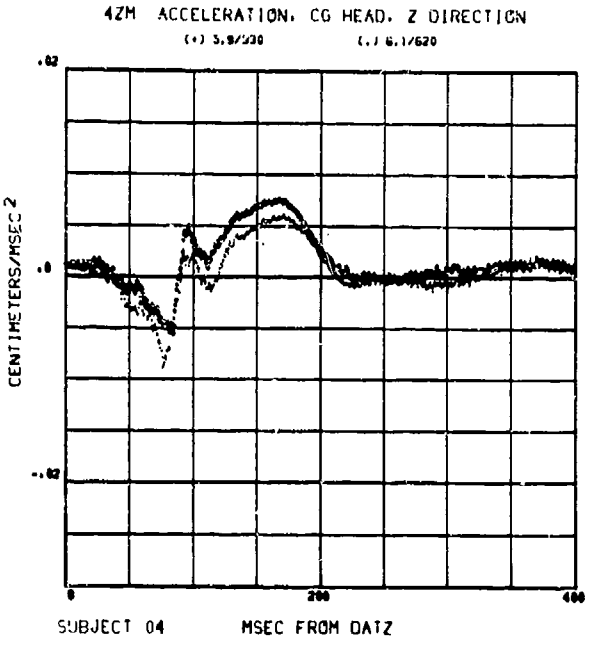

529

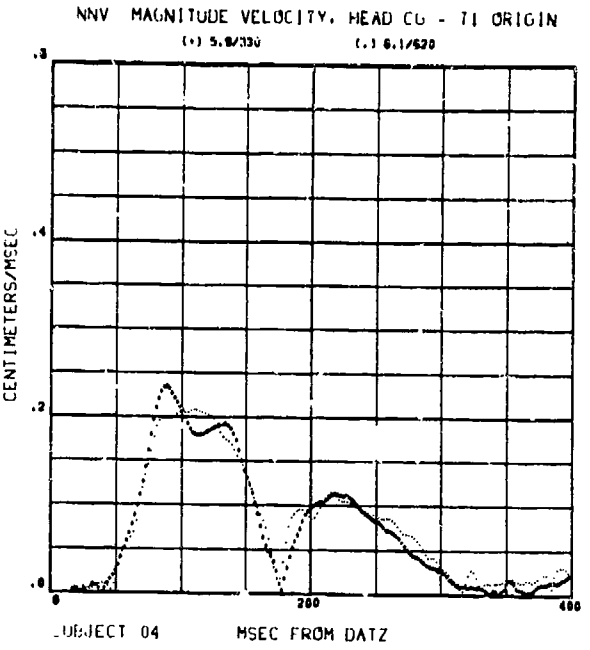

530

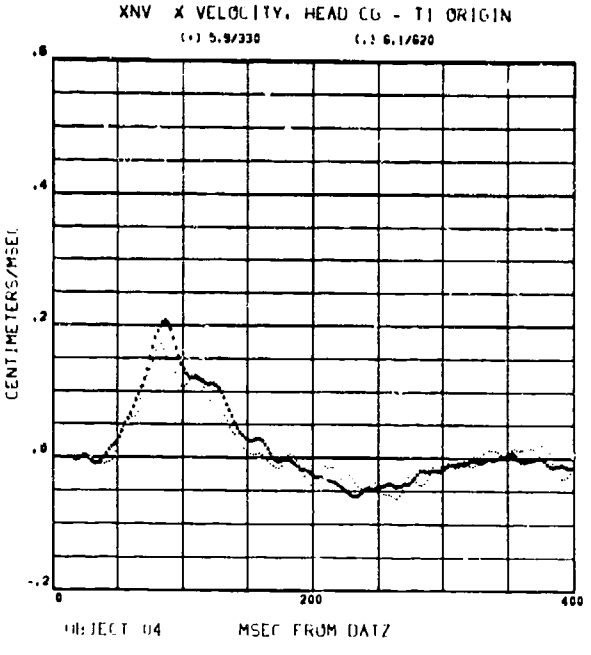

531

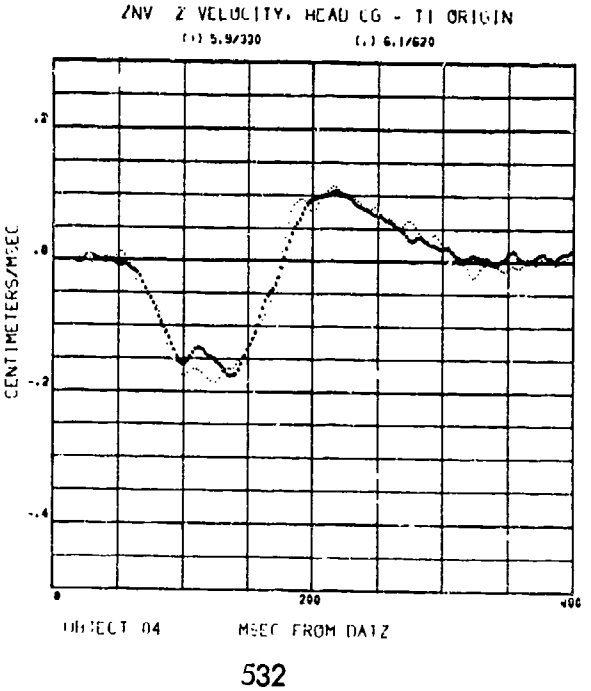

532

REPEATABILITY, PAIRED RUNS ALL VARIABLES, SUBJECT 004

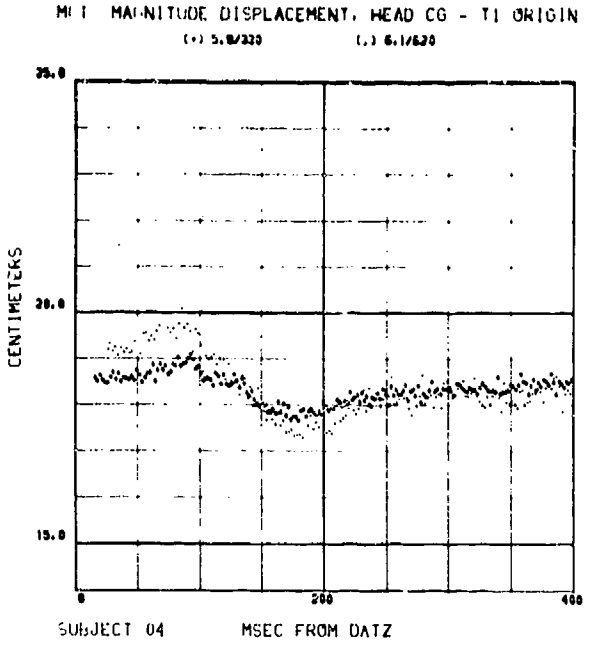

533

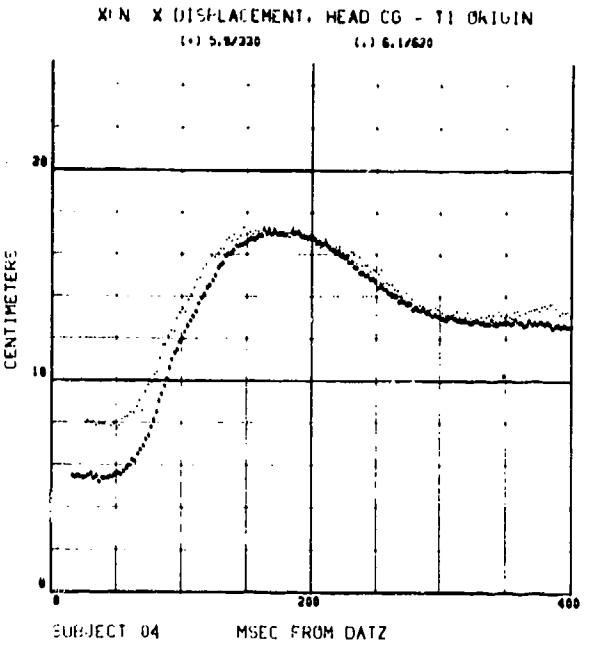

534

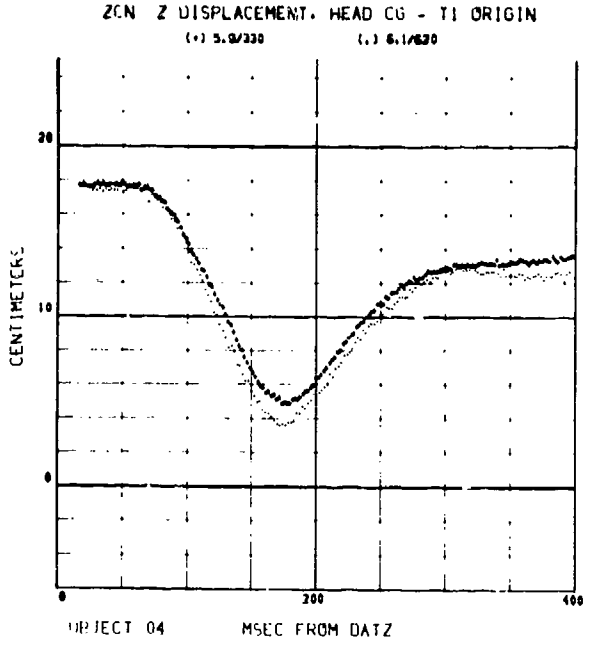

535

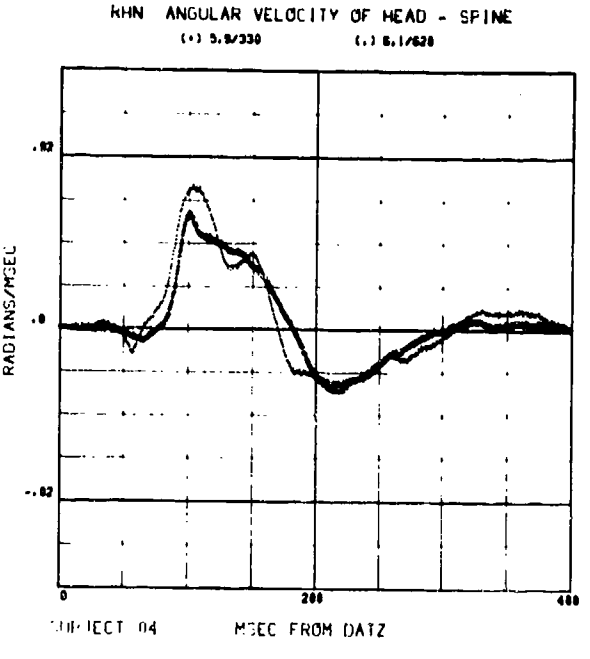

536

REPEATABILITY, PAIRED RUNS ALL VARIABLES, SUBJECT 004

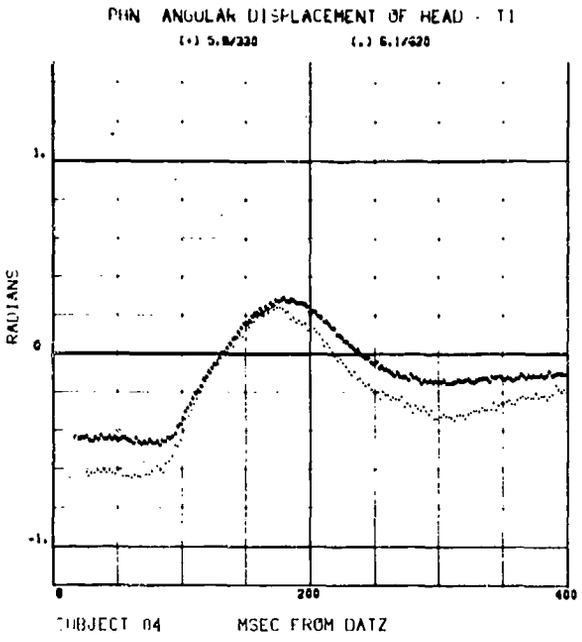

537

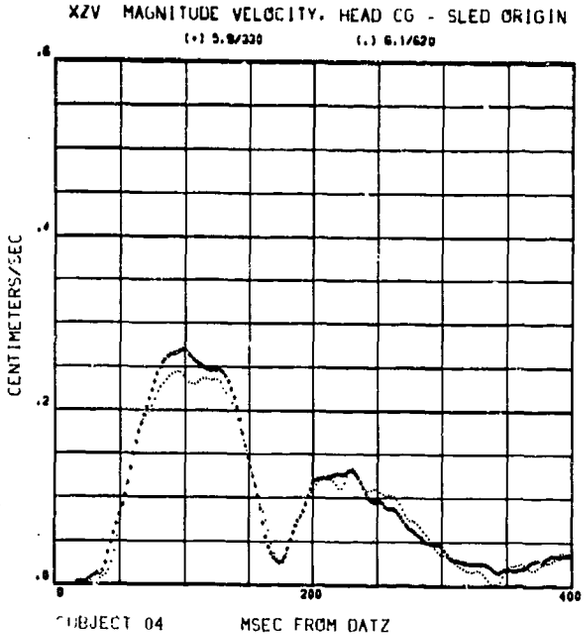

538

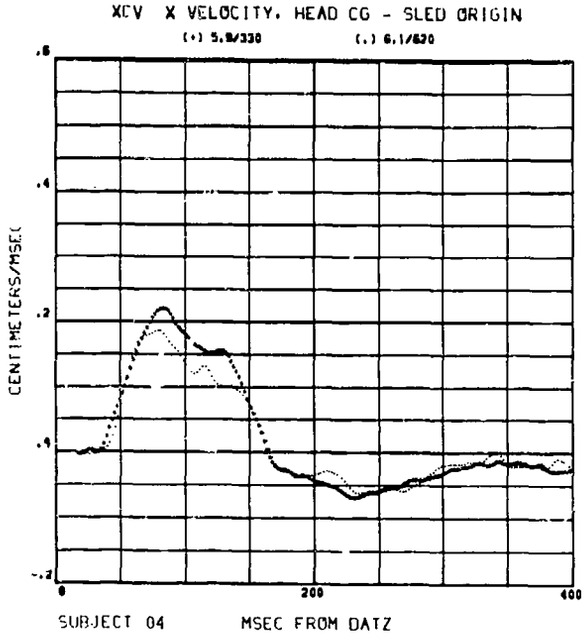

539

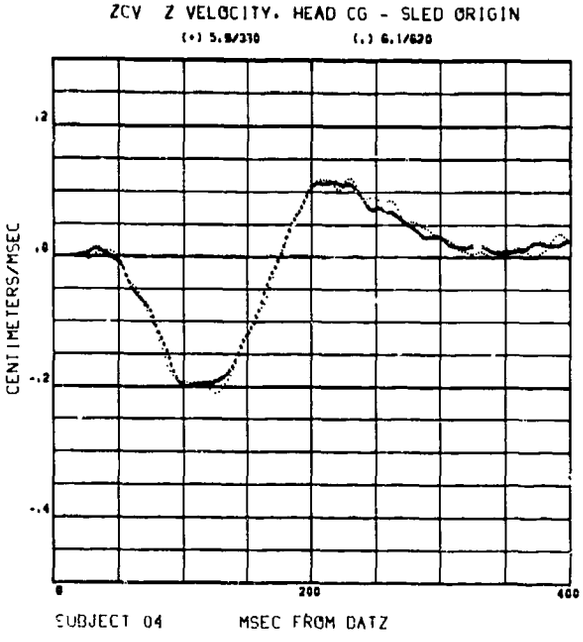

540

REPEATABILITY, PAIRED RUNS ALL VARIABLES, SUBJECT 004

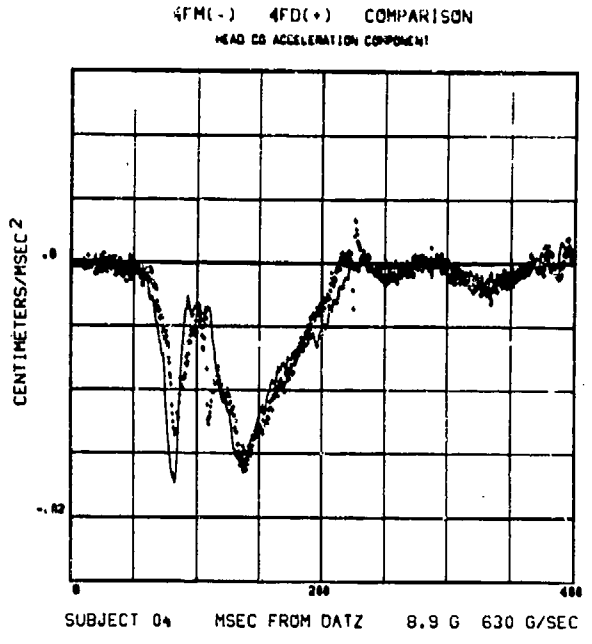

541

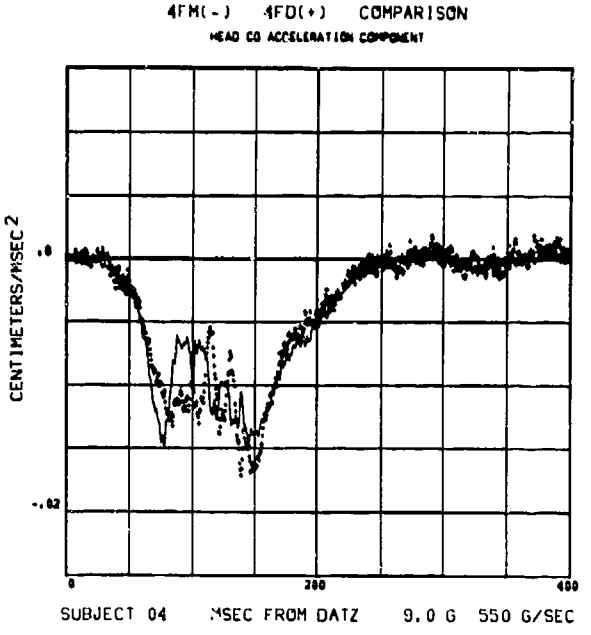

542

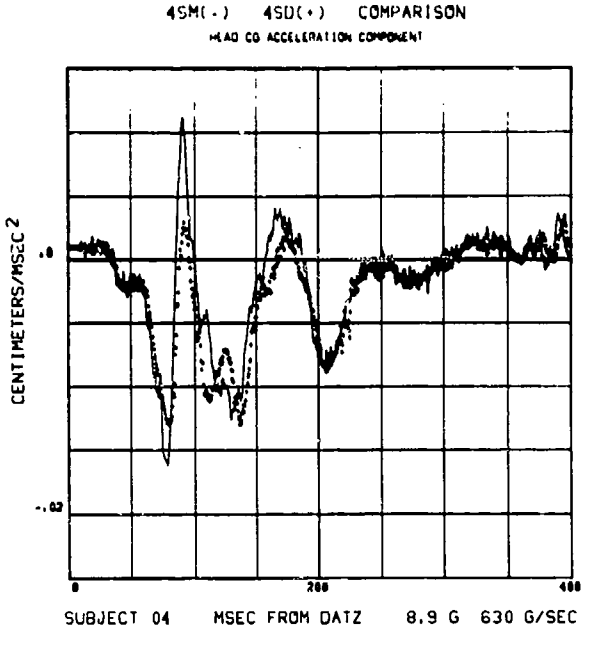

543

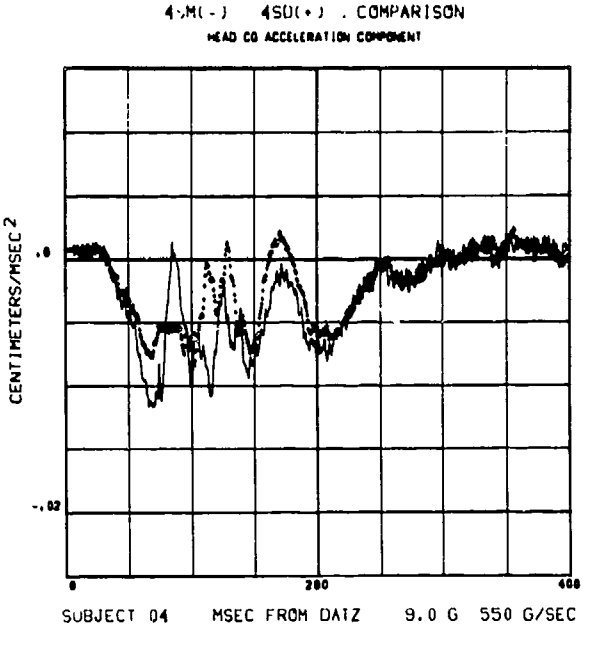

544

REPEATABILITY, PAIRED RUNS ALL VARIABLES, SUBJECT 004

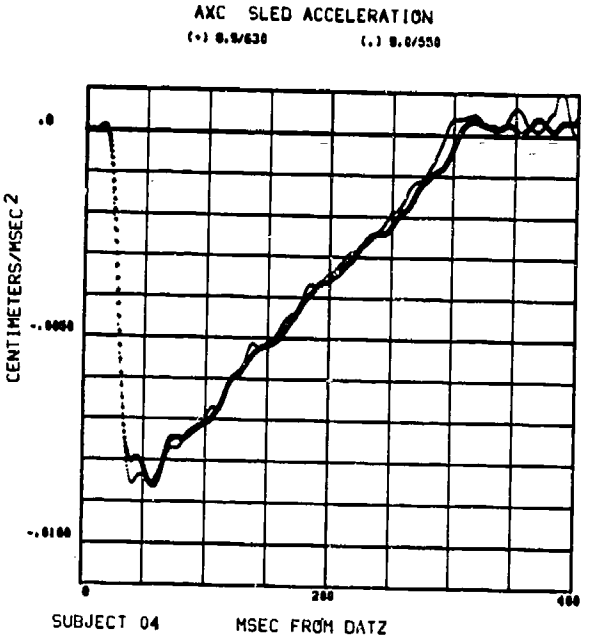

545

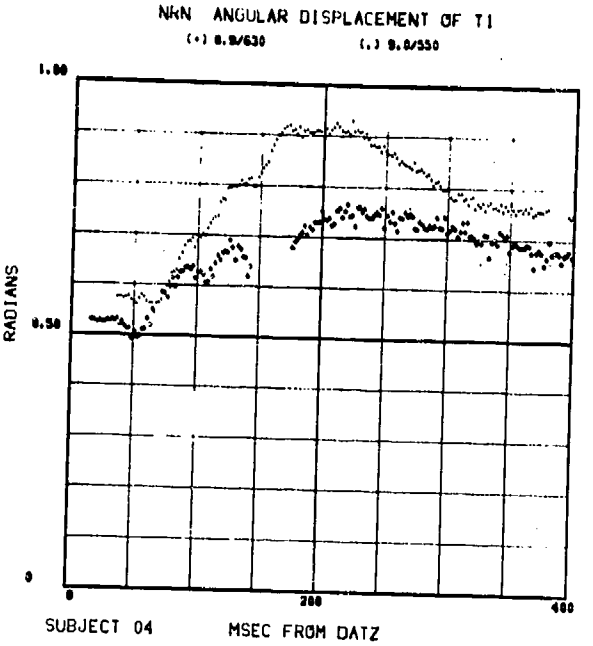

546

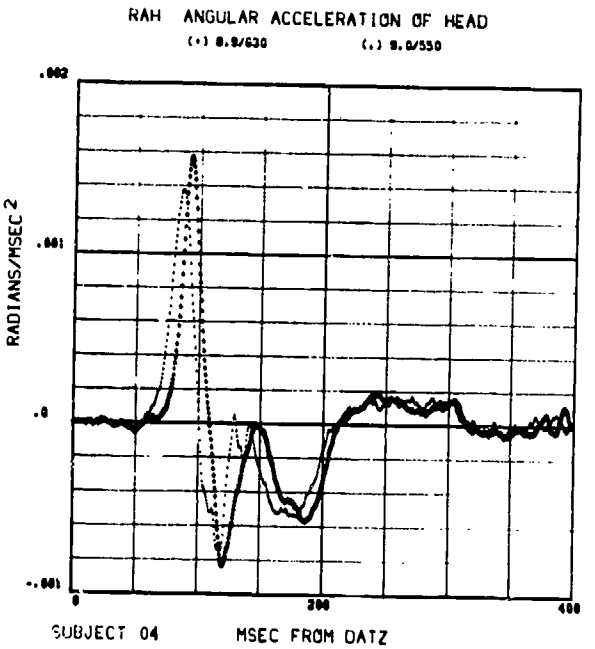

547

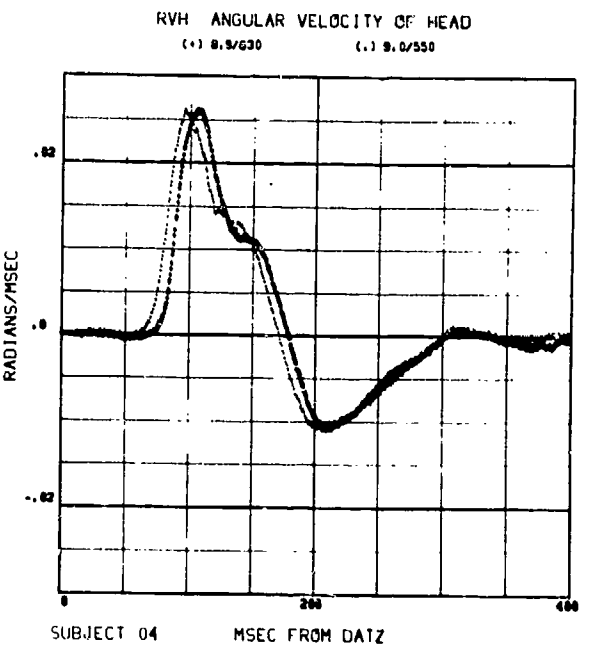

548

REPEATABILITY, PAIRED RUNS ALL VARIABLES, SUBJECT 004

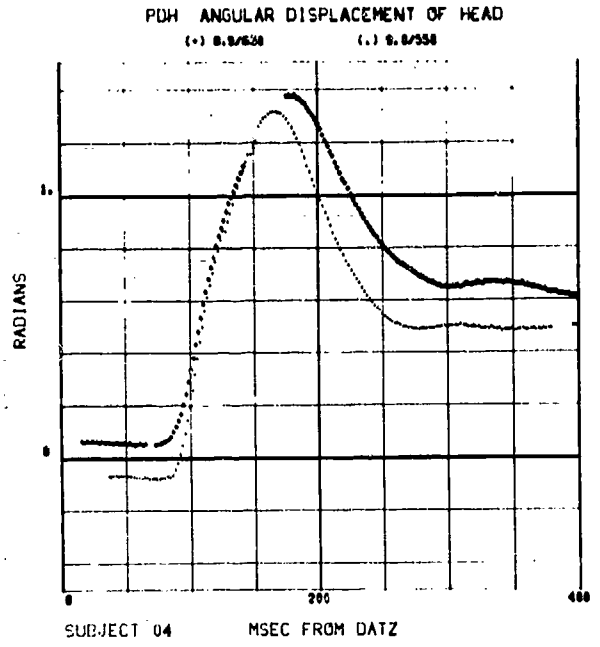

549

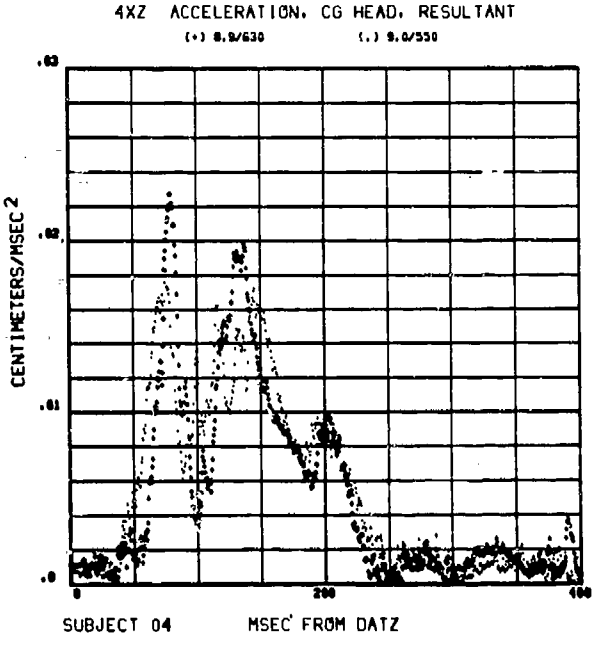

550

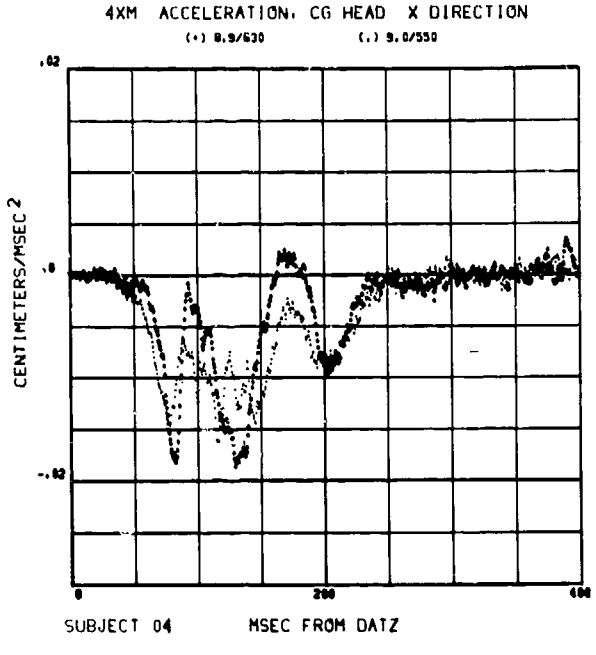

551

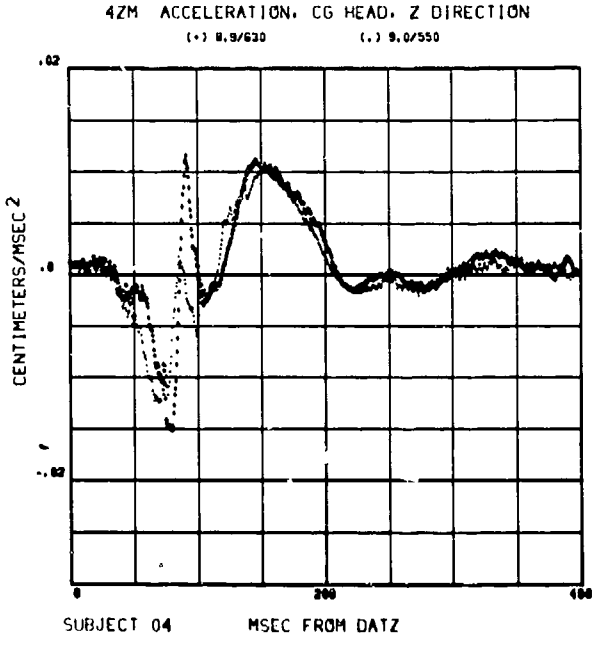

552

REPEATABILITY, PAIRED RUNS ALL VARIABLES, SUBJECT 004

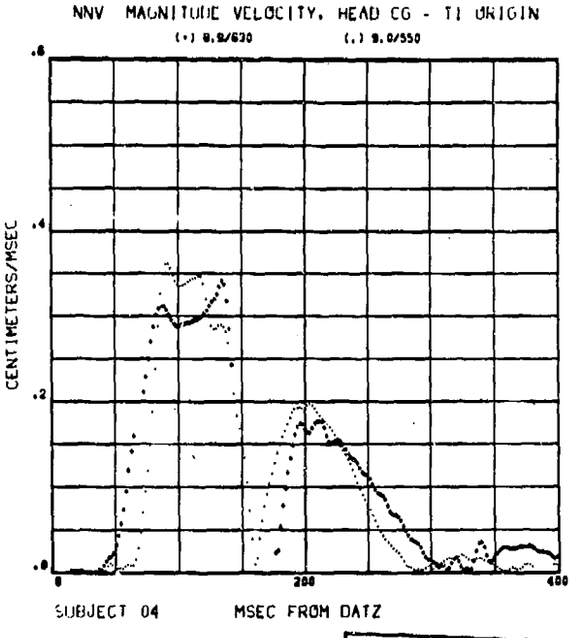

553

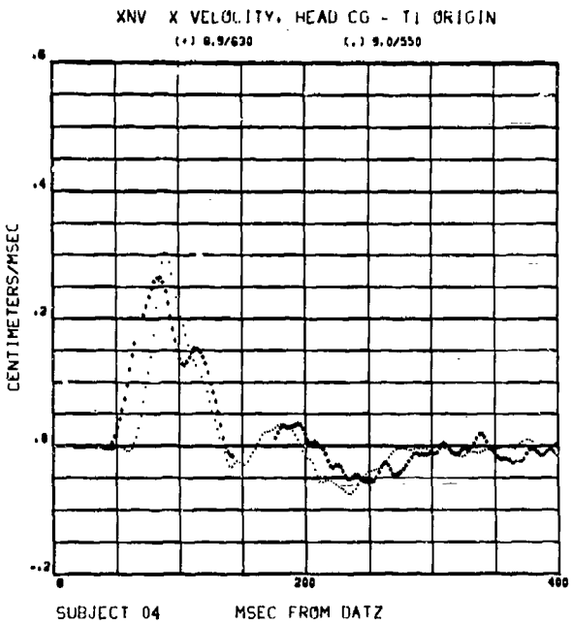

554

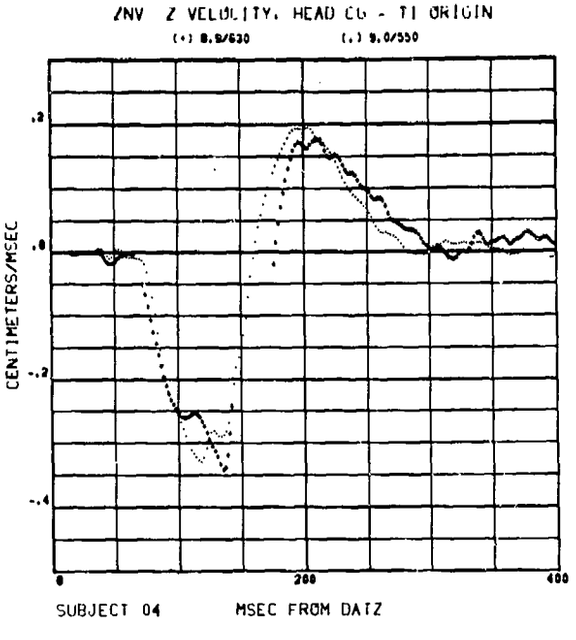

555

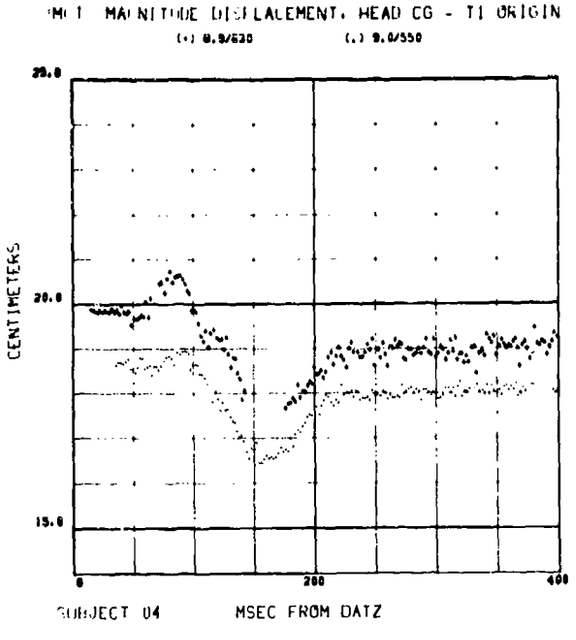

556

REPEATABILITY, PAIRED RUNS ALL VARIABLES, SUBJECT 004

XCN X DISPLACEMENT, HEAD CG - T1 ORIGIN

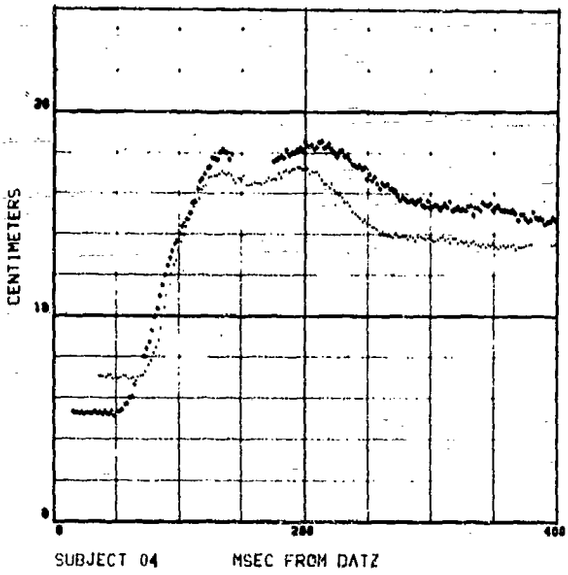

557

ZCN Z DISPLACEMENT, HEAD CG - T1 ORIGIN

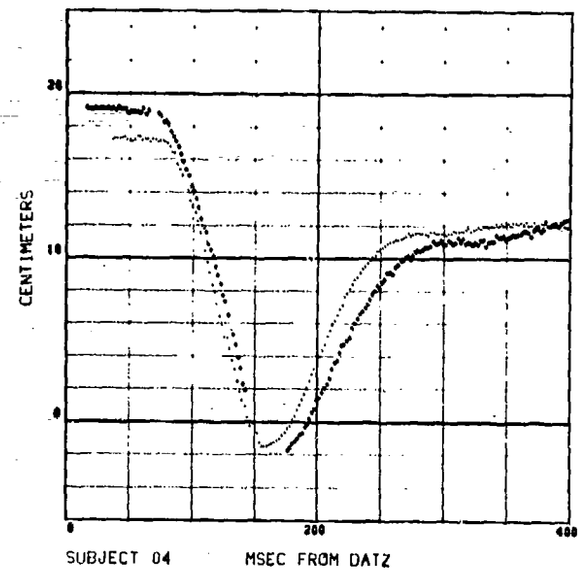

558

WHN ANGULAR VELOCITY OF HEAD - SPINE

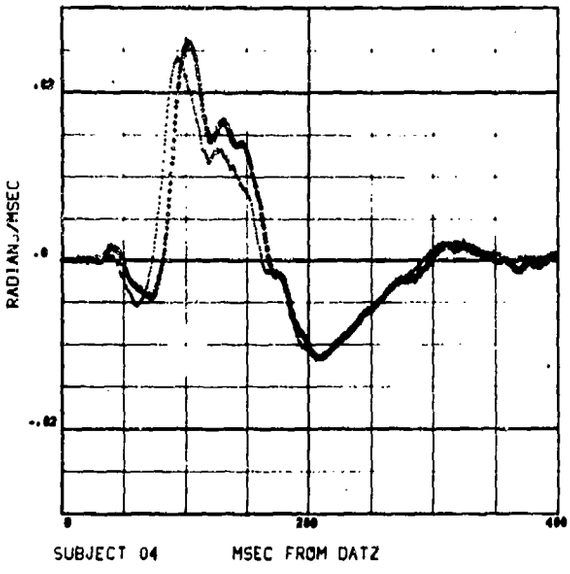

559

PHN ANGULAR DISPLACEMENT OF HEAD - T1

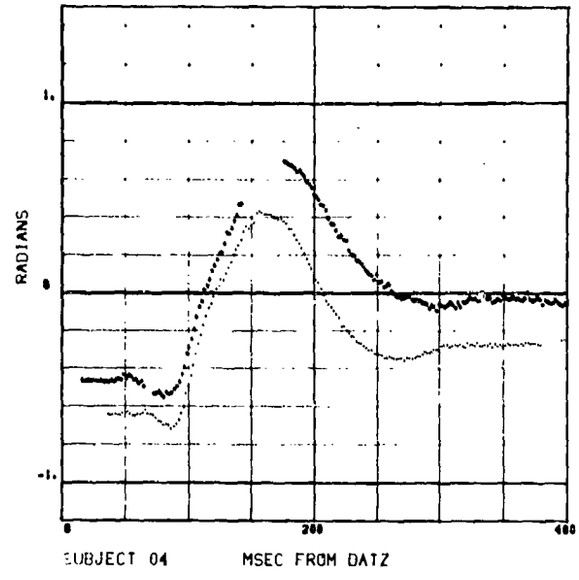

560

REPEATABILITY, PAIRED RUNS ALL VARIABLES, SUBJECT 004

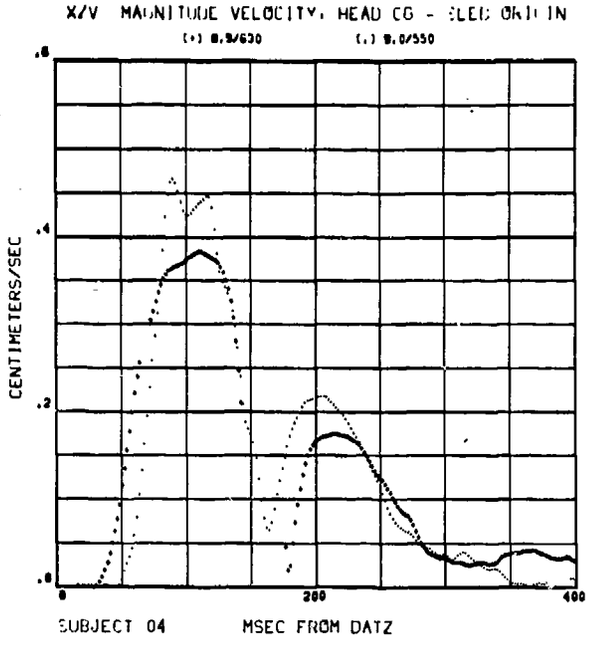

561

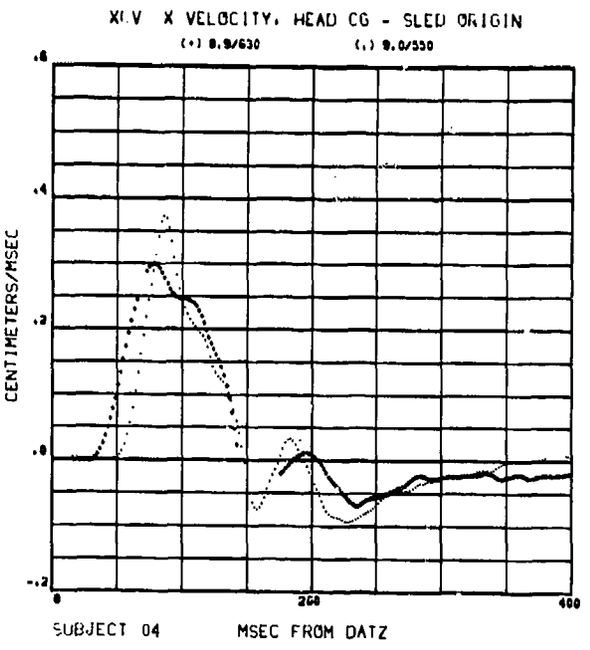

562

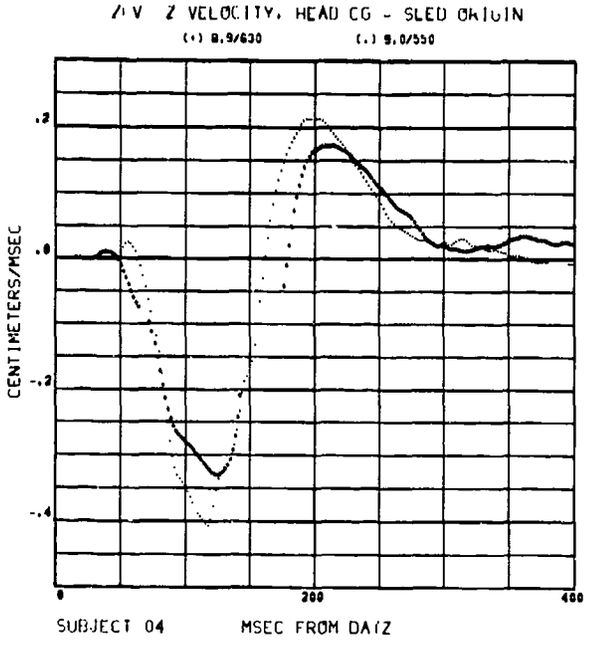

563

REPEATABILITY, PAIRED RUNS ALL VARIABLES, SUBJECT 010

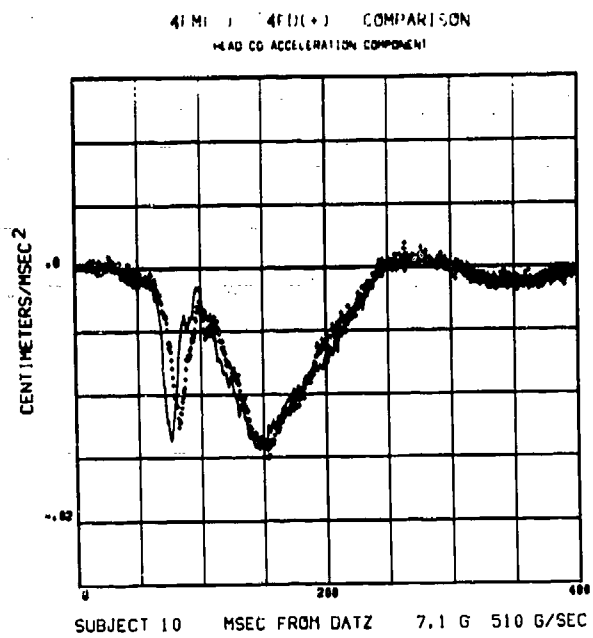

564

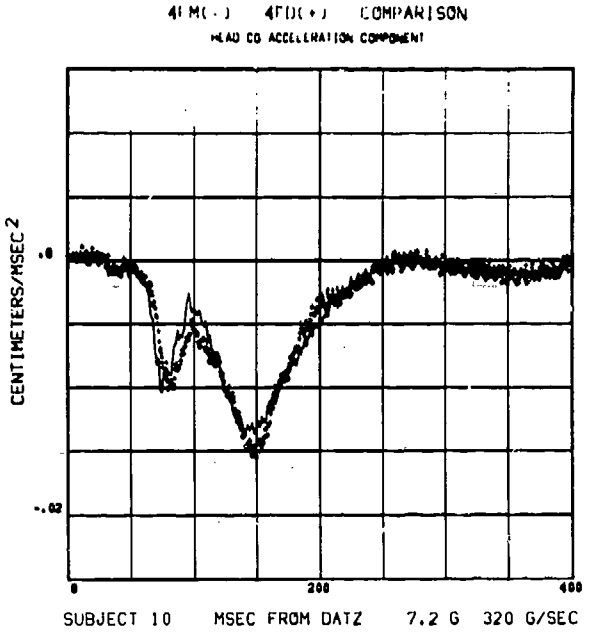

565

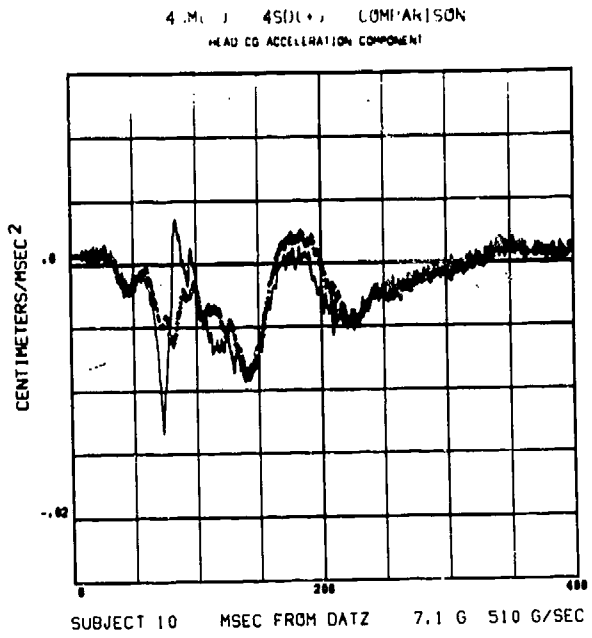

566

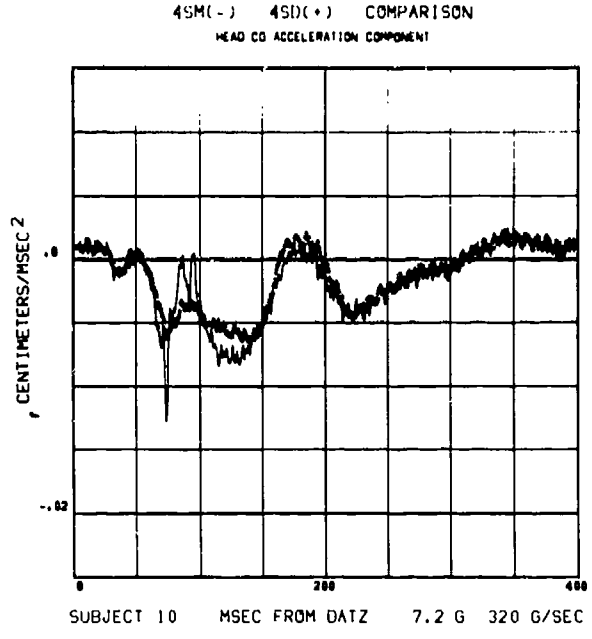

567

REPEATABILITY, PAIRED RUNS ALL VARIABLES, SUBJECT 010

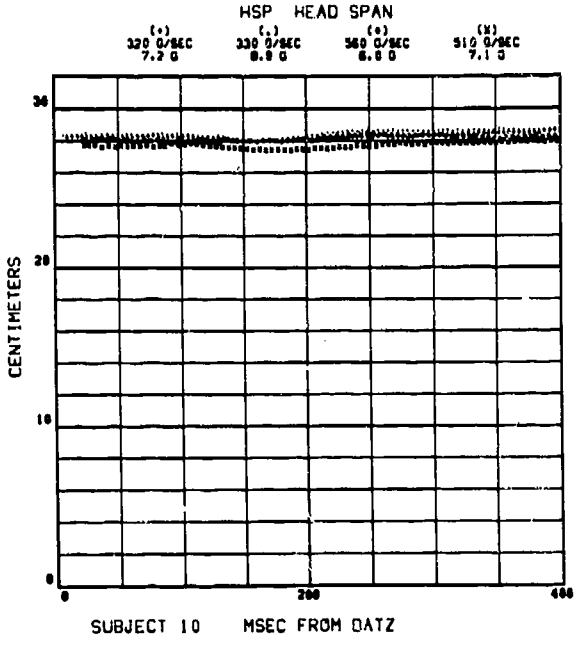

568

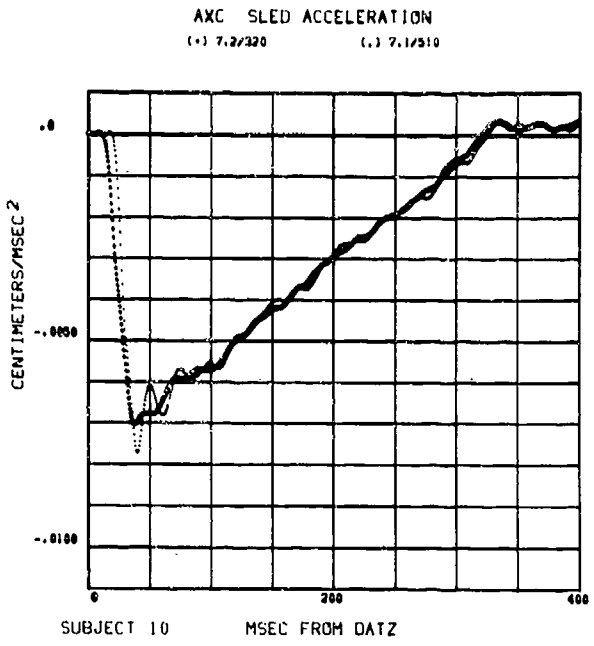

569

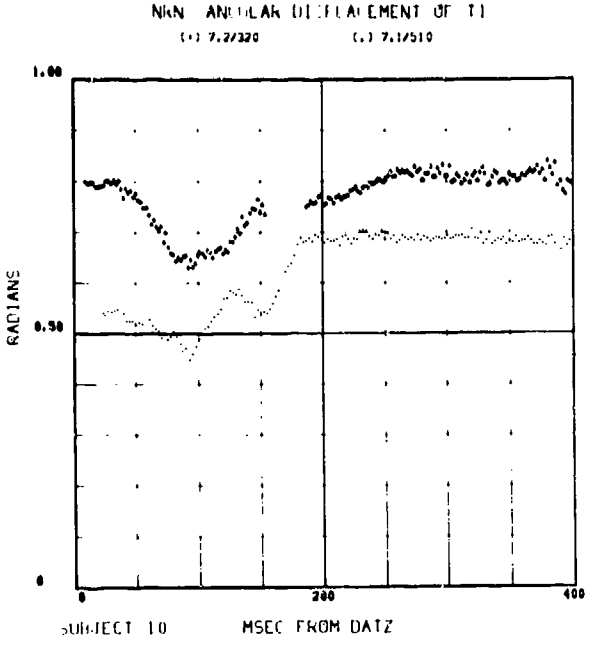

570

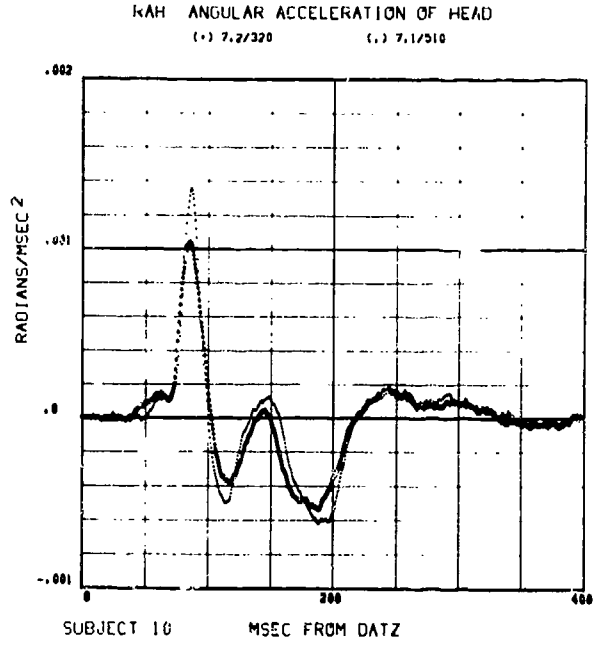

571

REPEATABILITY, PAIRED RUNS ALL VARIABLES, SUBJECT 010

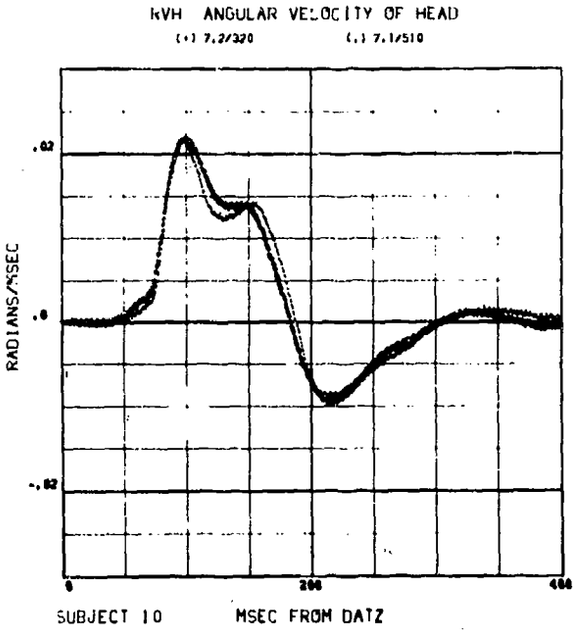

572

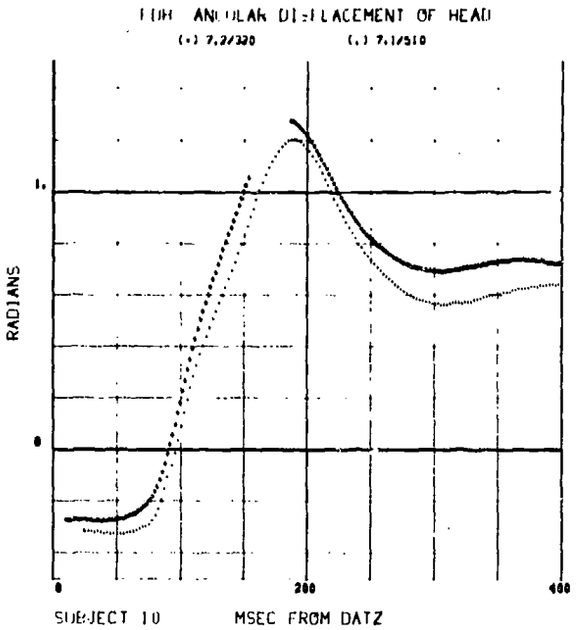

573

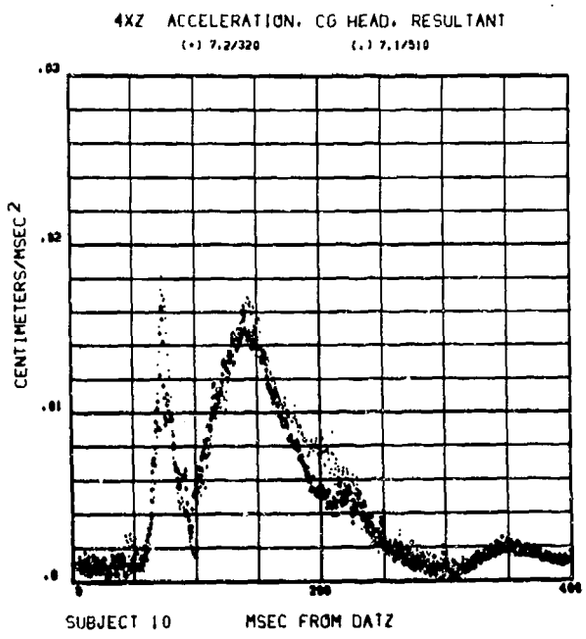

574

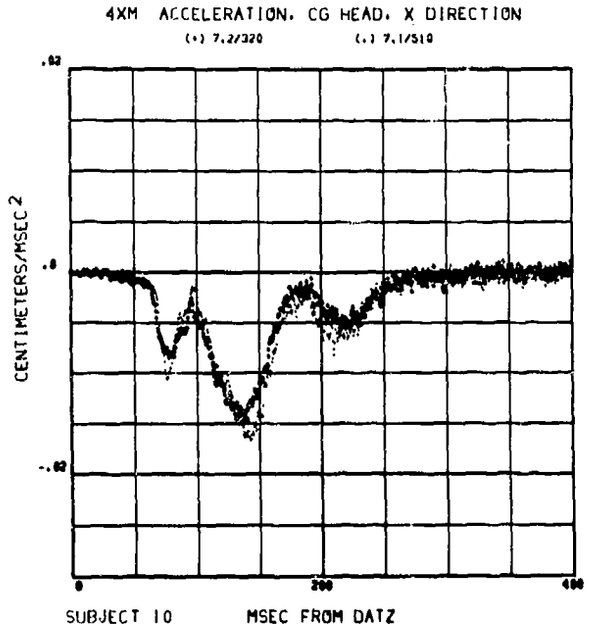

575

REPEATABILITY, PAIRED RUNS ALL VARIABLES, SUBJECT 010

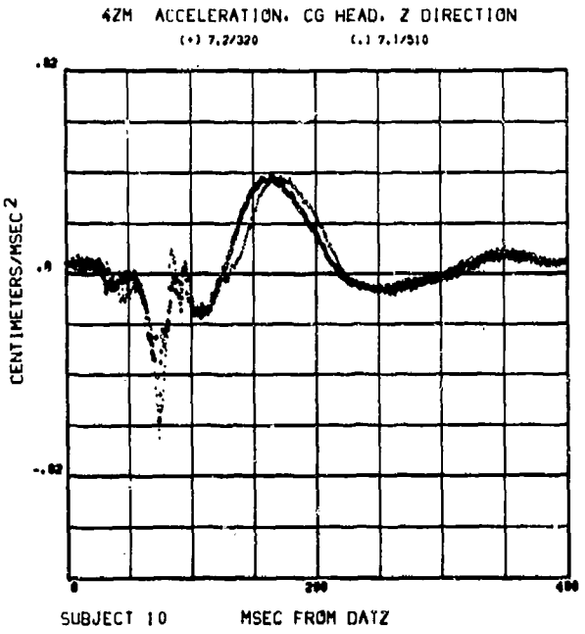

576

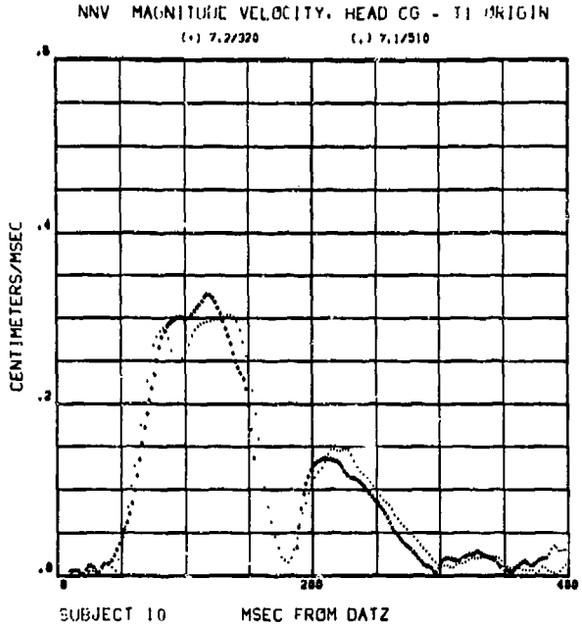

577

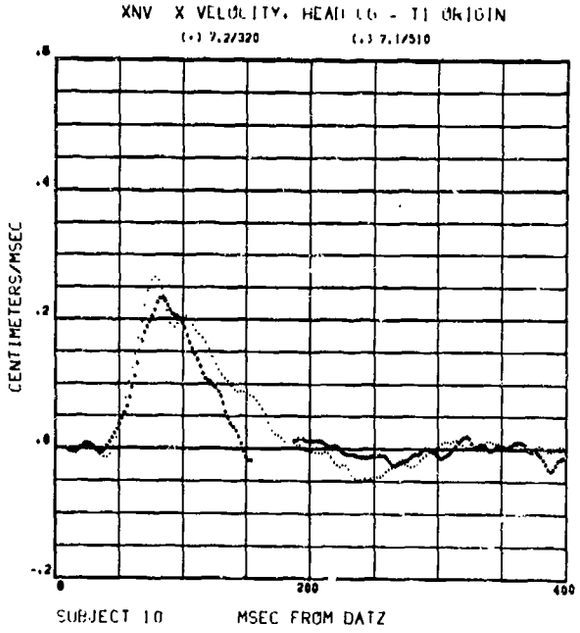

578

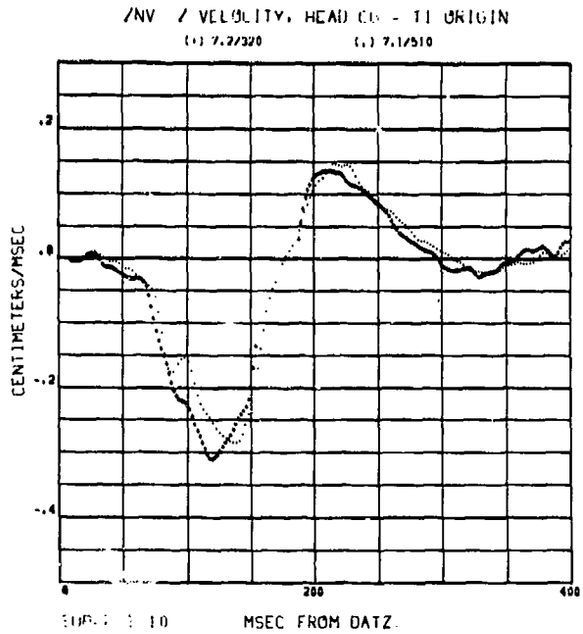

579

REPEATABILITY, PAIRED RUNS ALL VARIABLES, SUBJECT 010

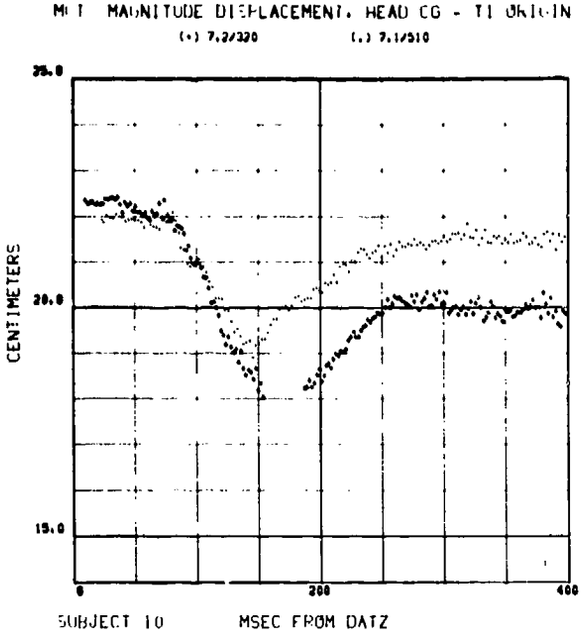

580

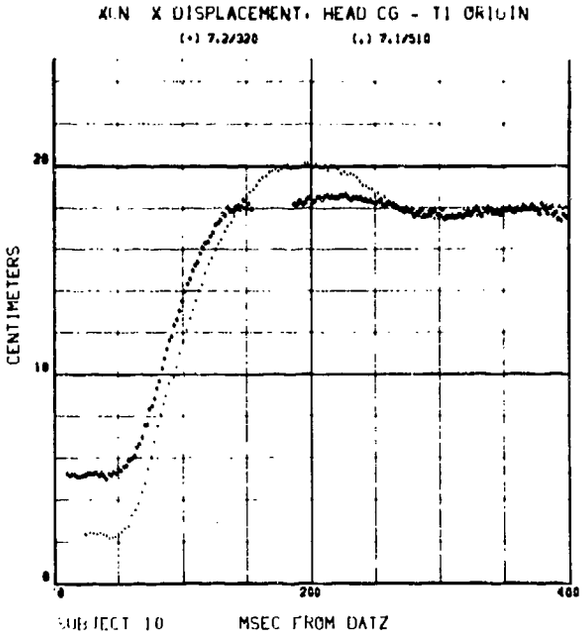

581

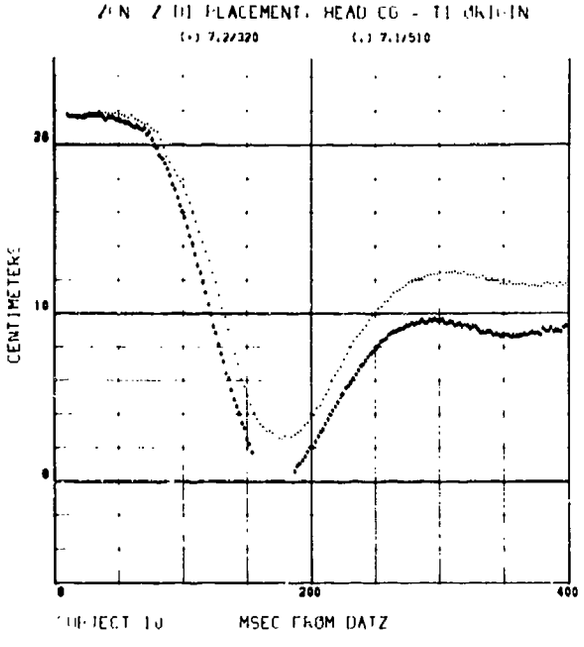

582

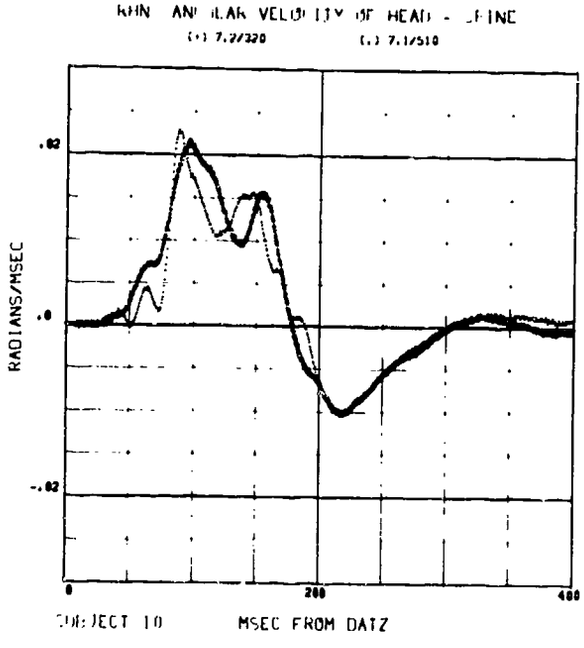

583

REPEATABILITY, PAIRED RUNS ALL VARIABLES, SUBJECT 010

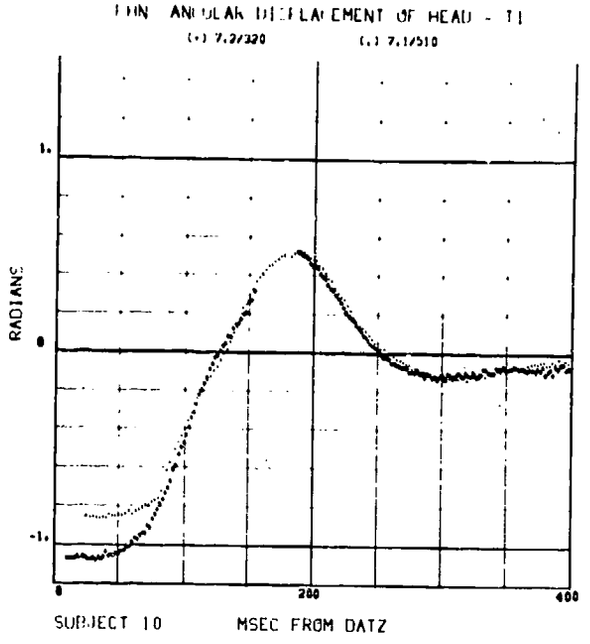

584

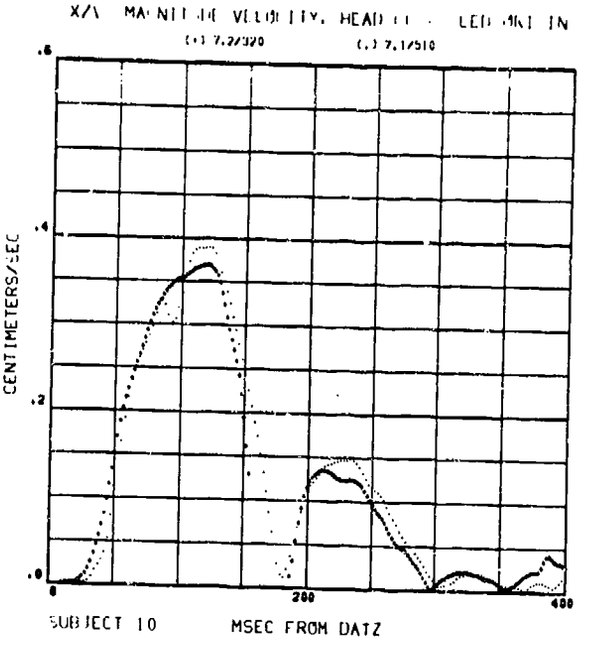

585

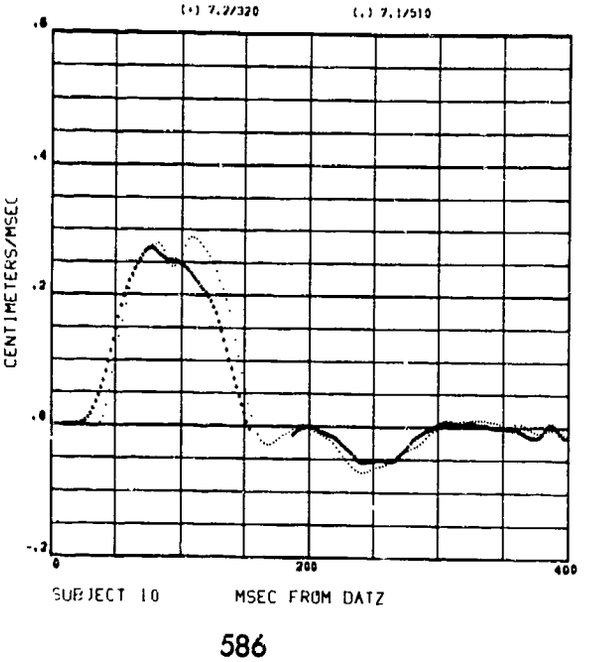

586

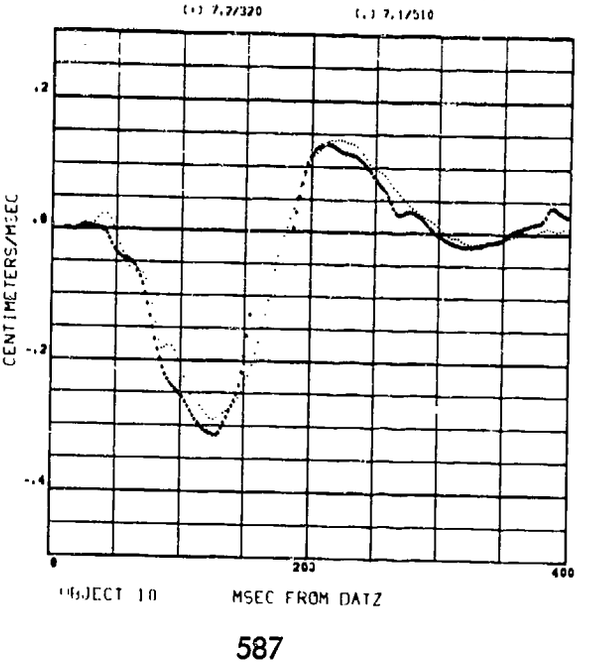

587

REPEATABILITY, PAIRED RUNS ALL VARIABLES, SUBJECT 016

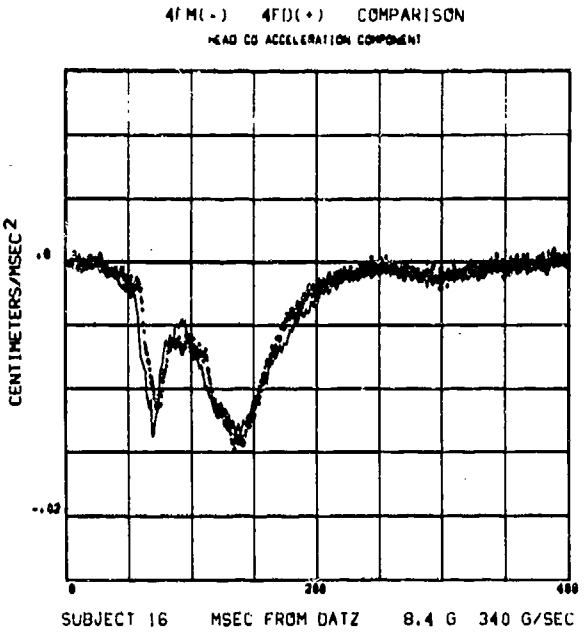

588

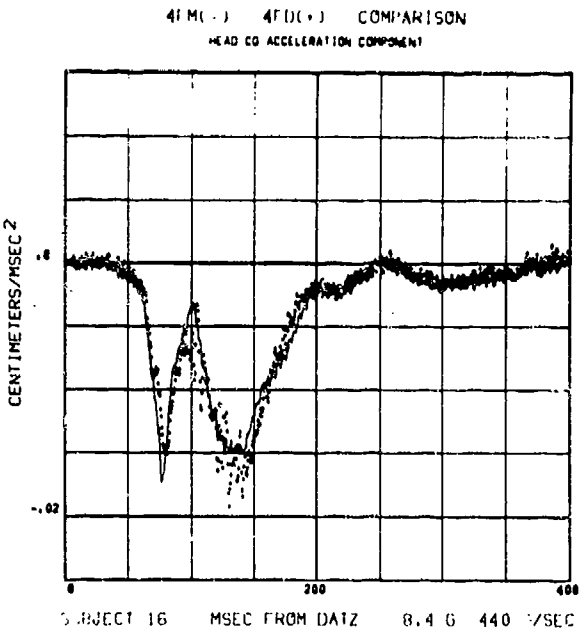

589

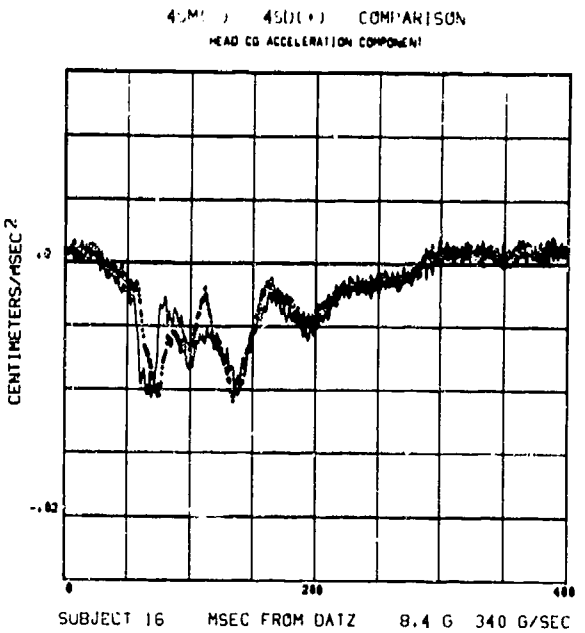

590

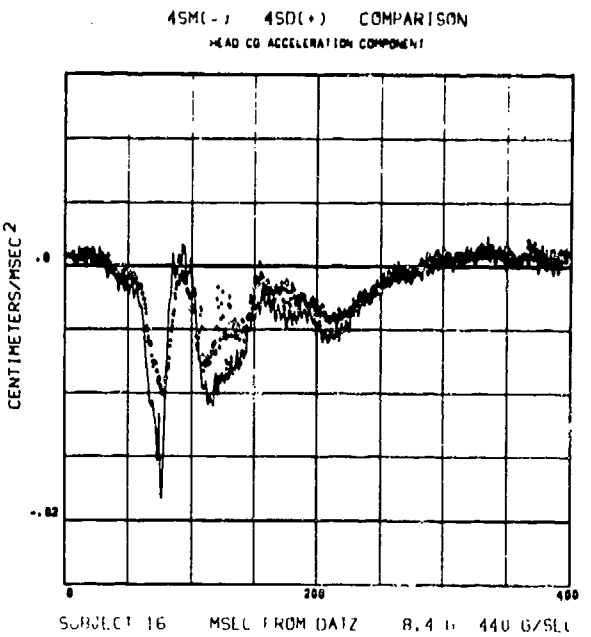

591

REPEATABILITY, PAIRED RUNS ALL VARIABLES, SUBJECT 016

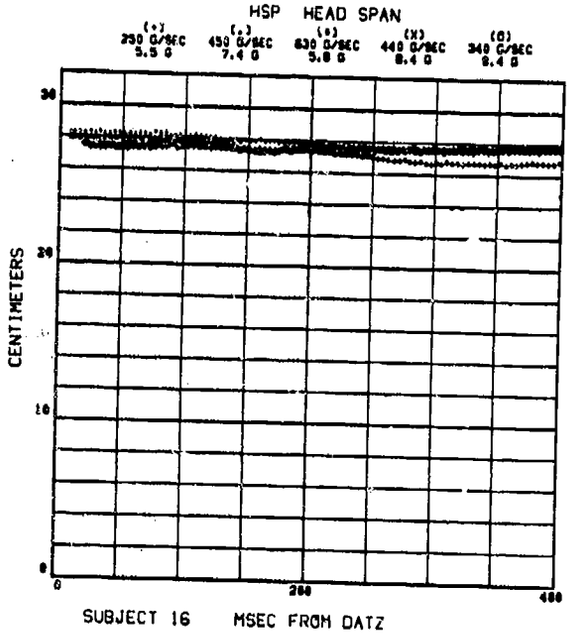

592

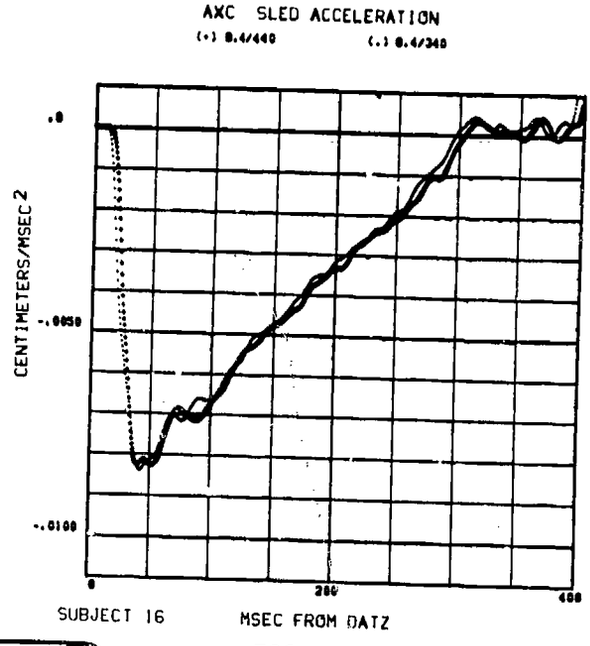

593

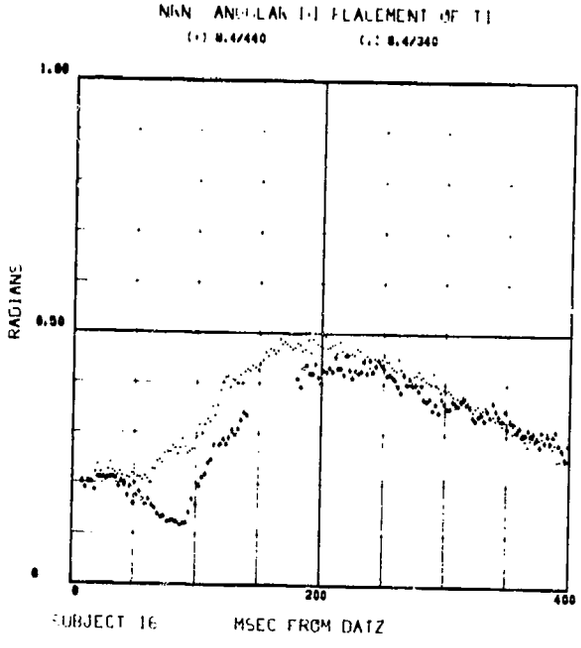

594

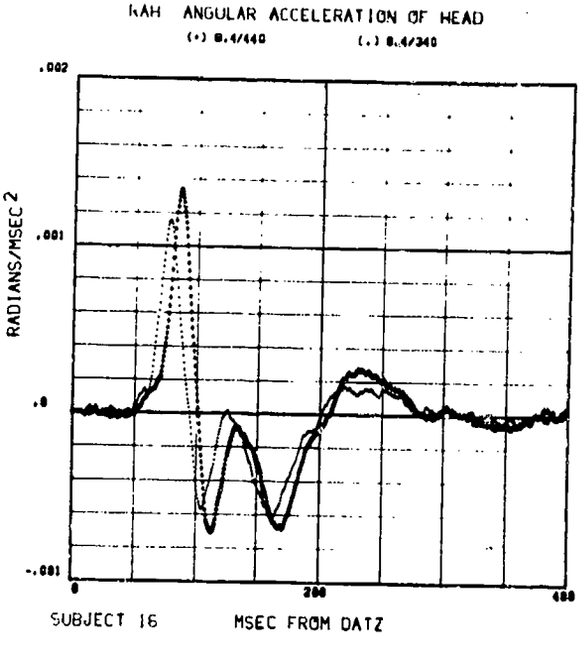

595

REPEATABILITY, PAIRED RUNS ALL VARIABLES, SUBJECT 016

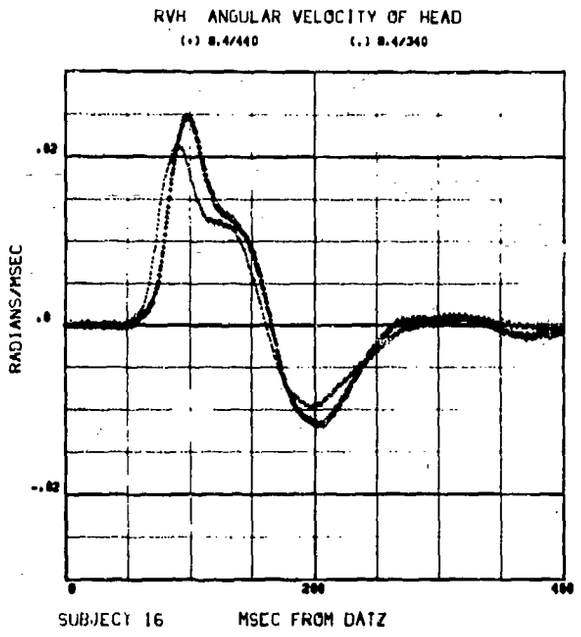

596

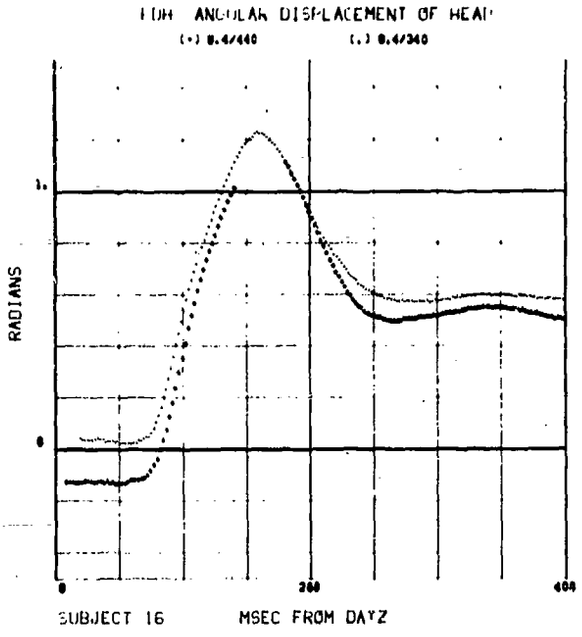

597

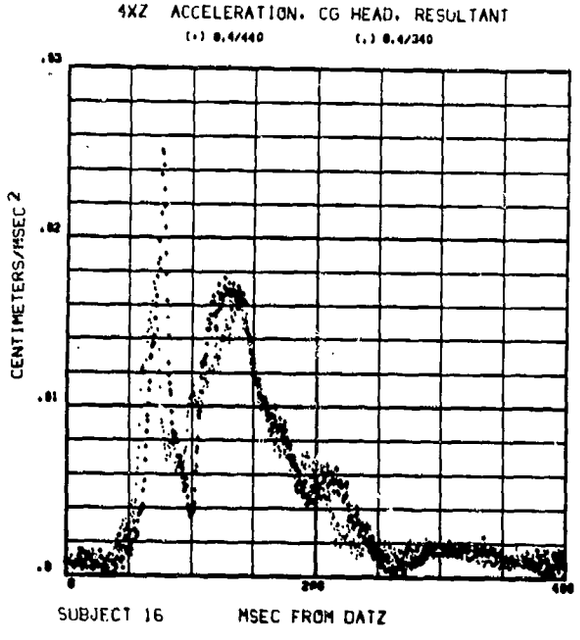

598

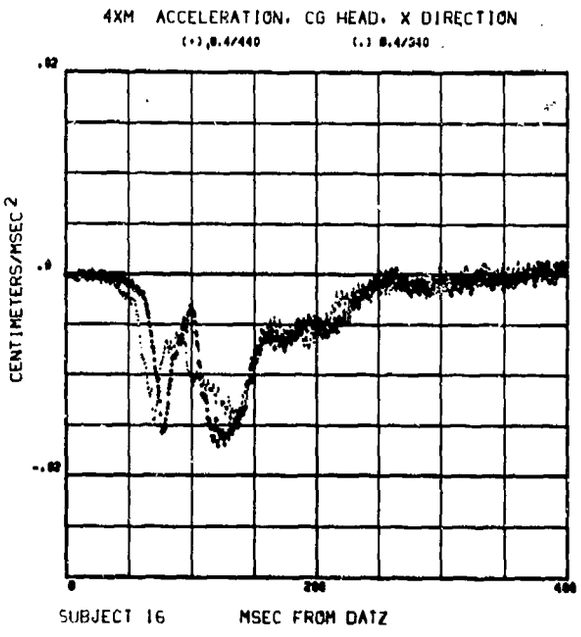

599

REPEATABILITY, PAIRED RUNS ALL VARIABLES, SUBJECT 016

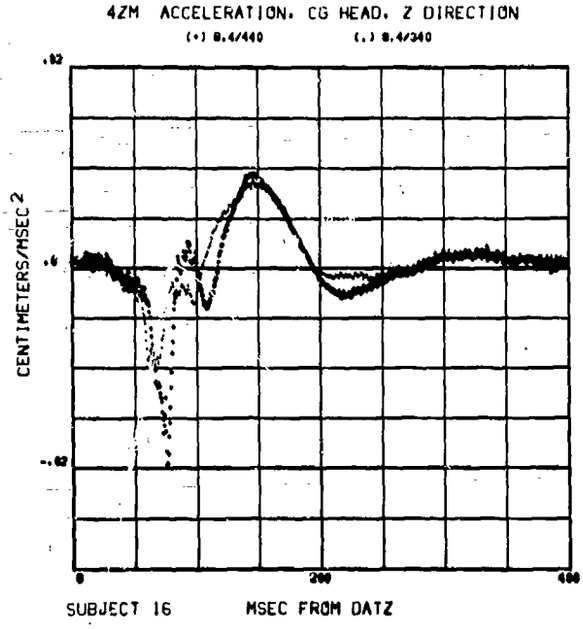

600

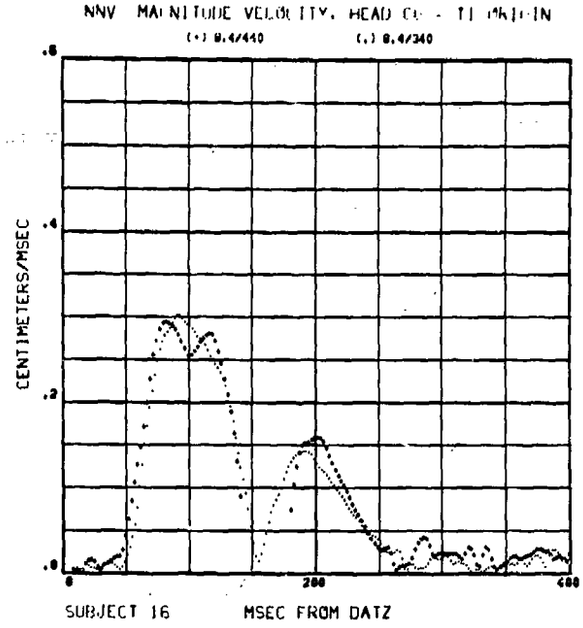

601

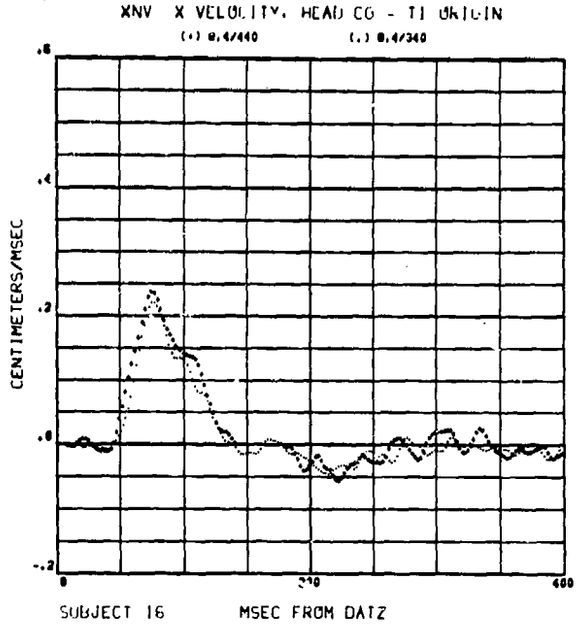

602

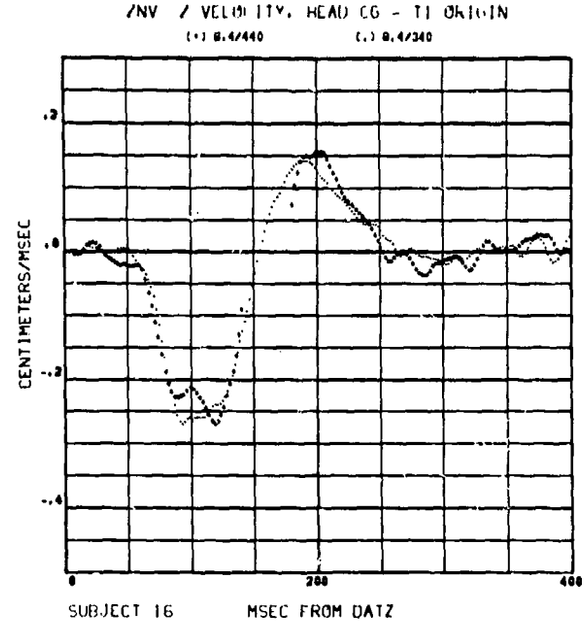

603

REPEATABILITY, PAIRED RUNS ALL VARIABLES, SUBJECT 016

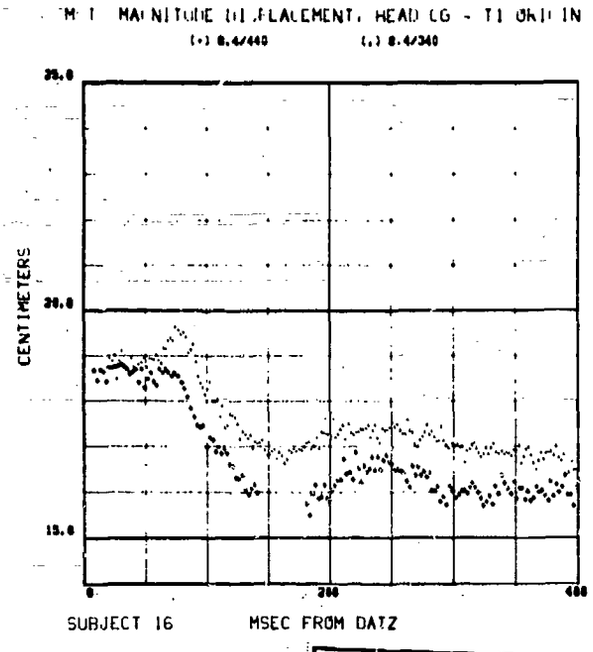

604

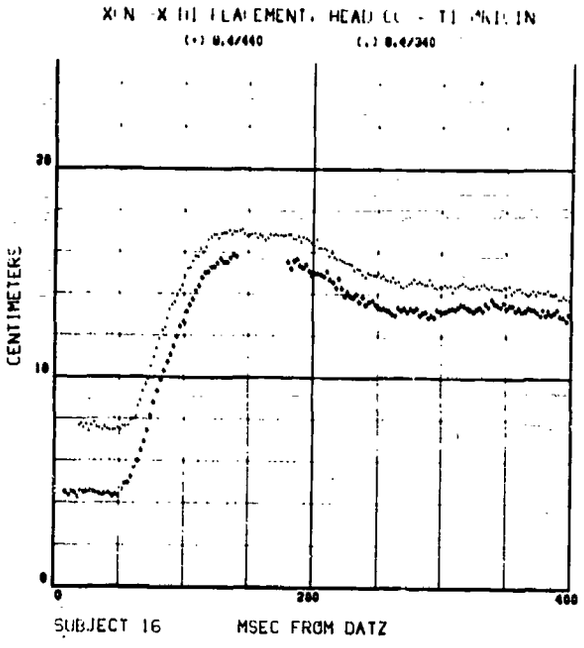

605

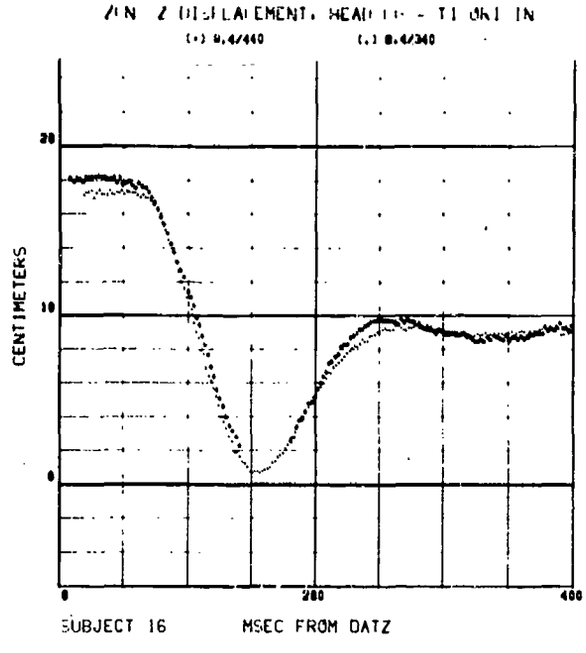

606

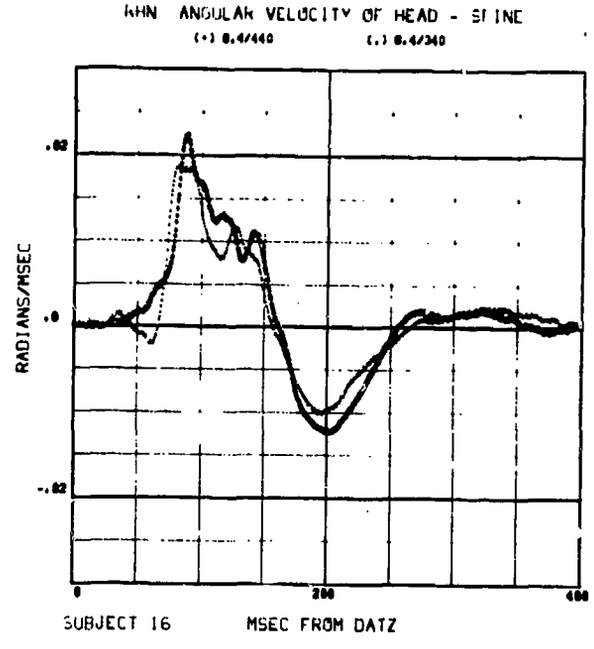

607

REPEATABILITY, PAIRED RUNS ALL VARIABLES, SUBJECT 016

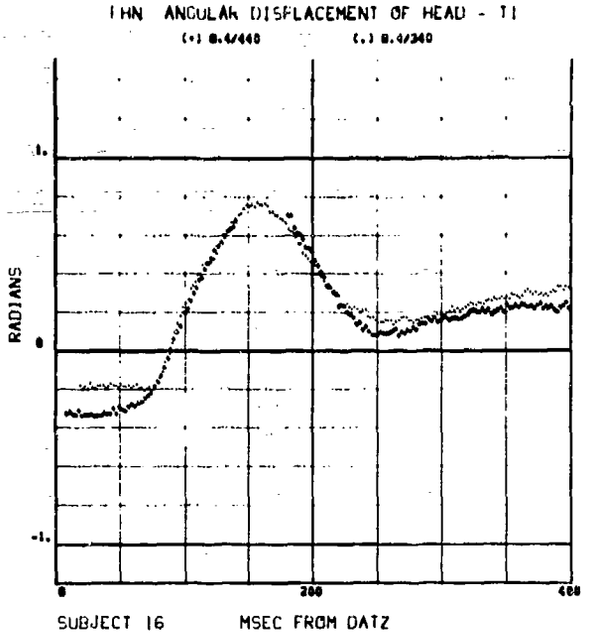

608

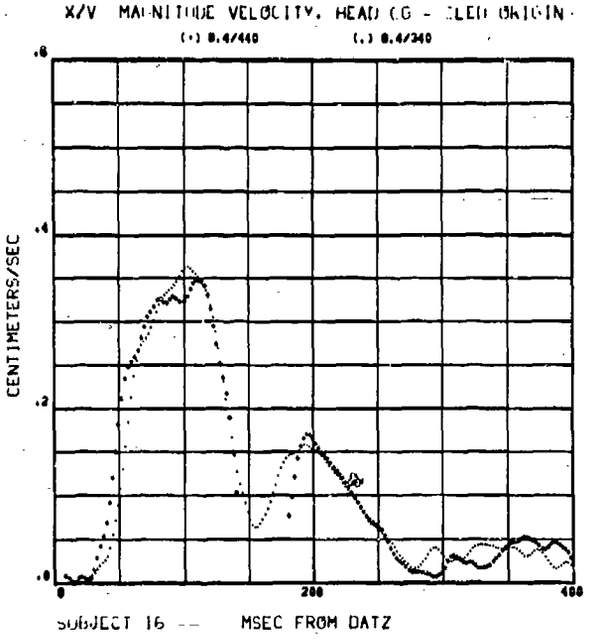

609

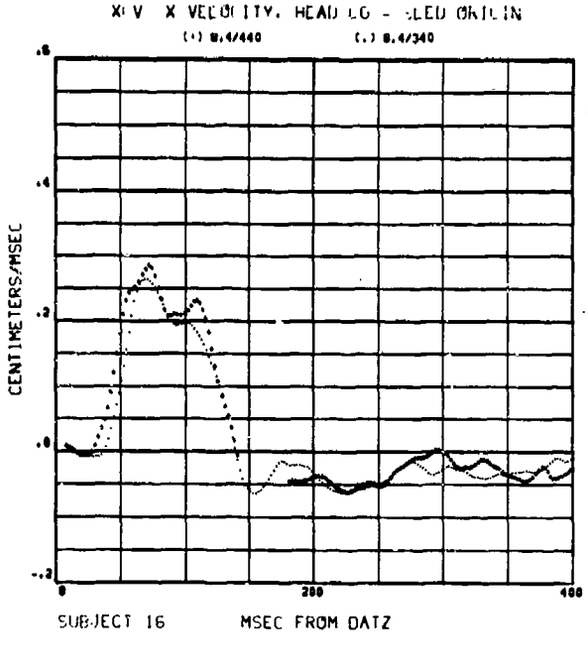

610

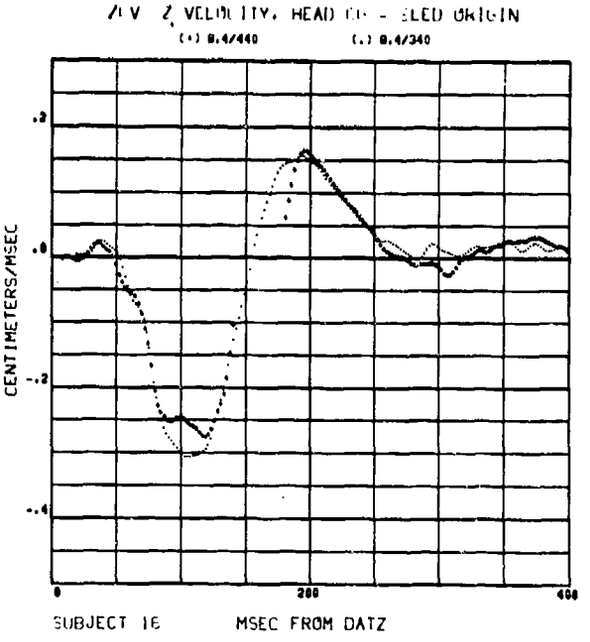

611

HSP HEADSPAN

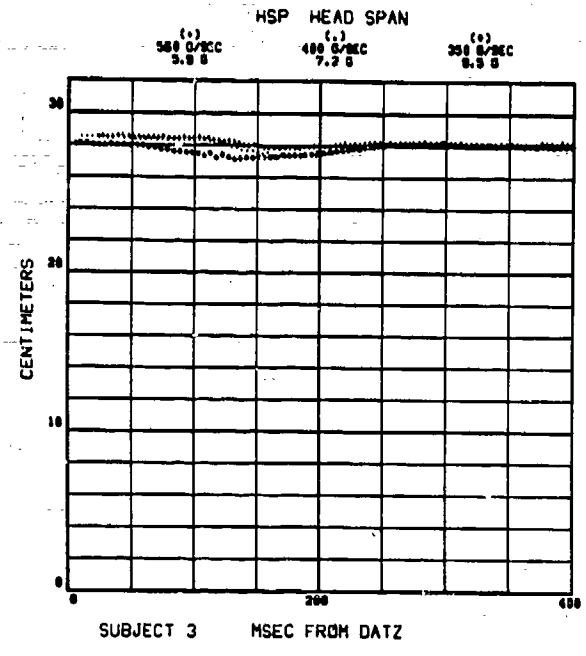

612

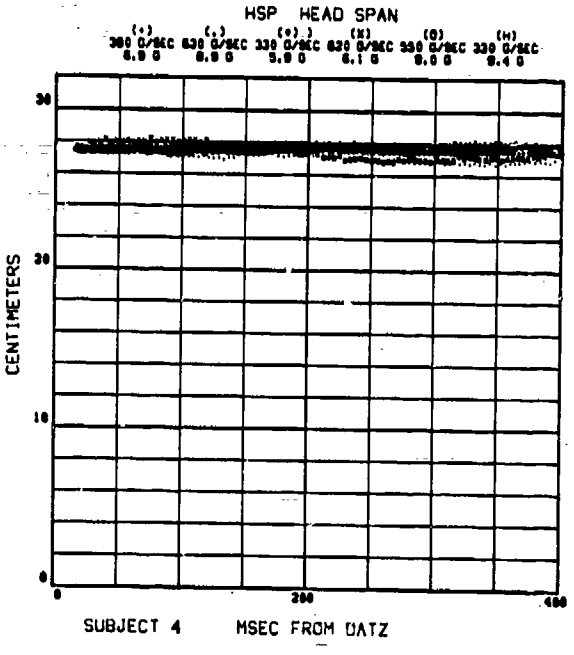

613

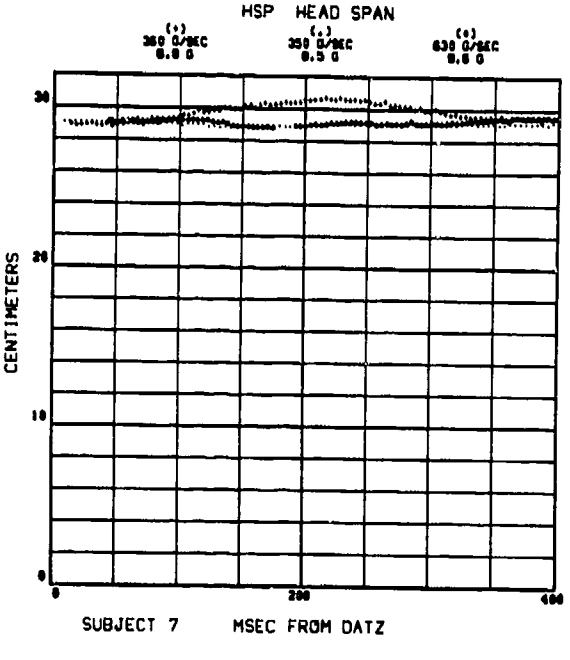

614

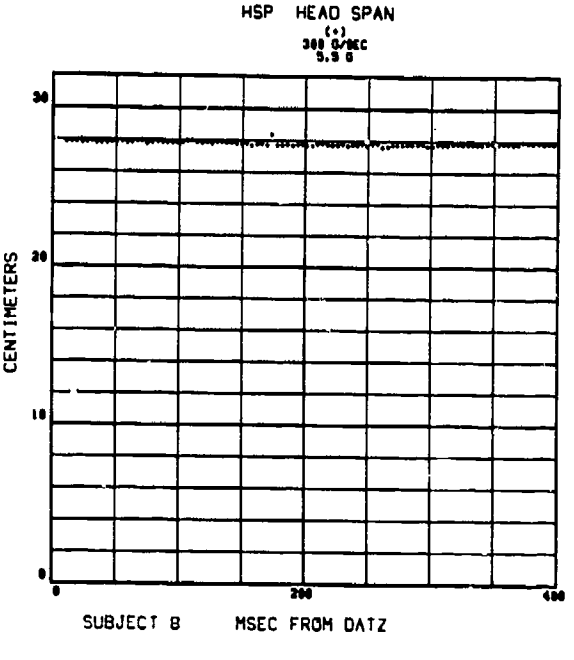

615

HSP HEADSPAN

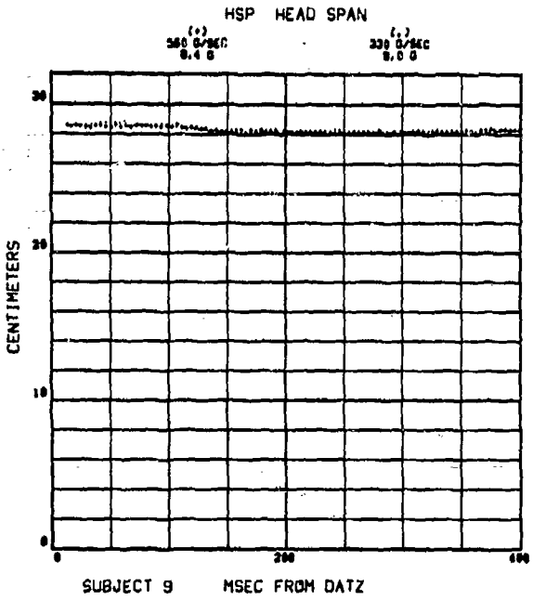

616

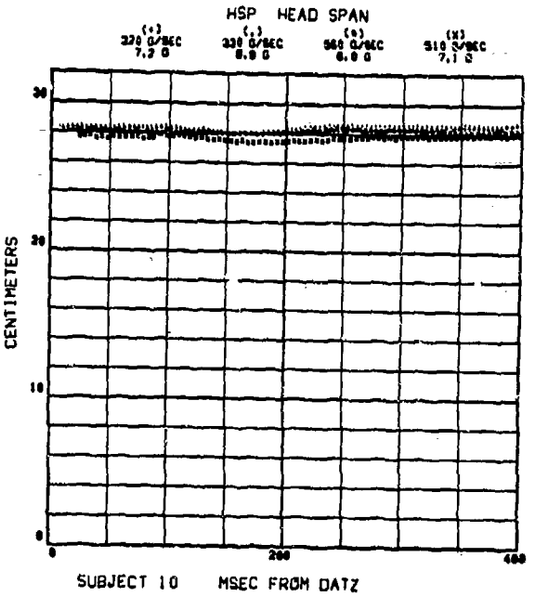

617

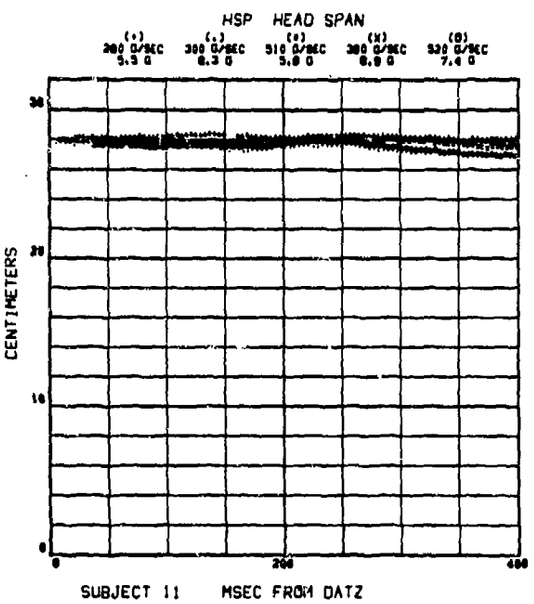

618

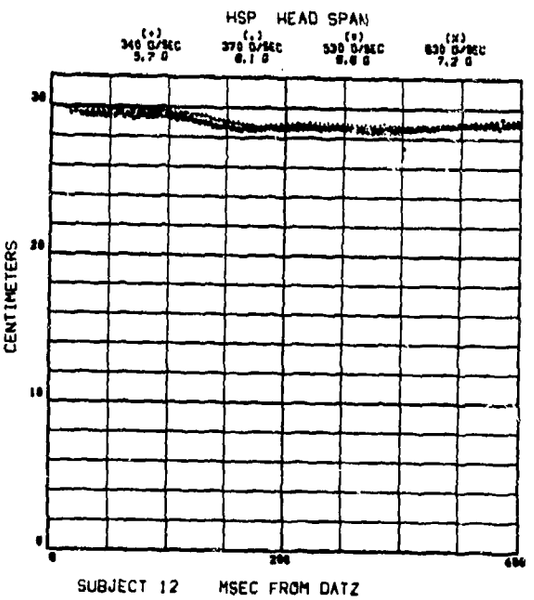

619

HSP HEADSPAN

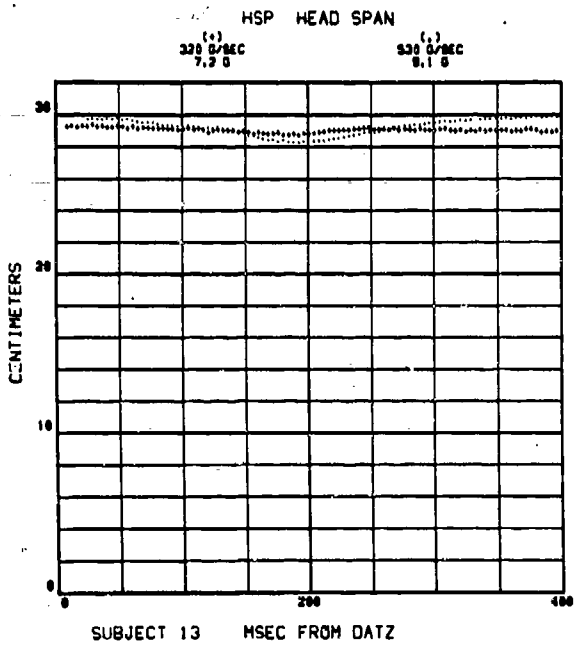

620

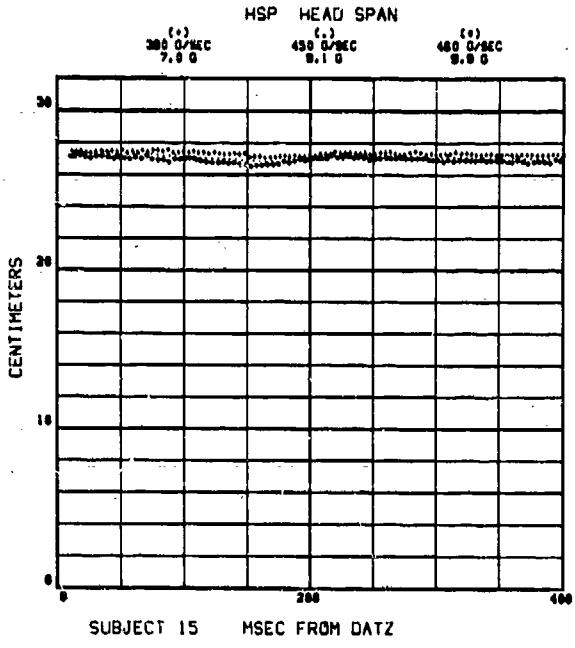

621

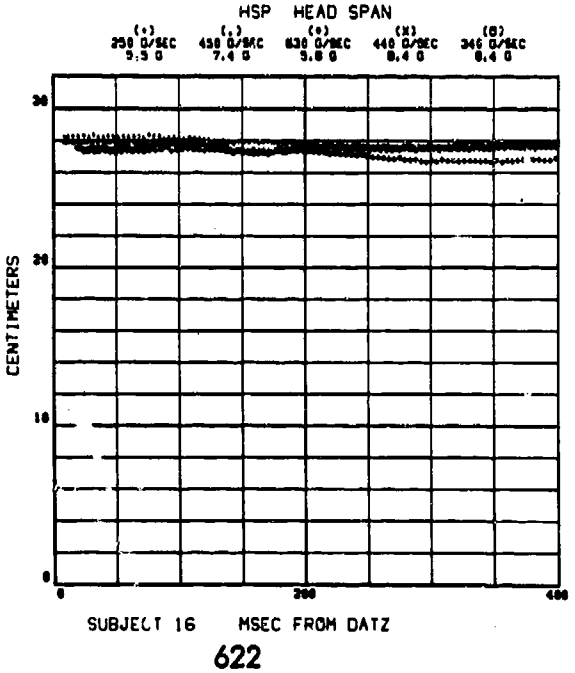

622

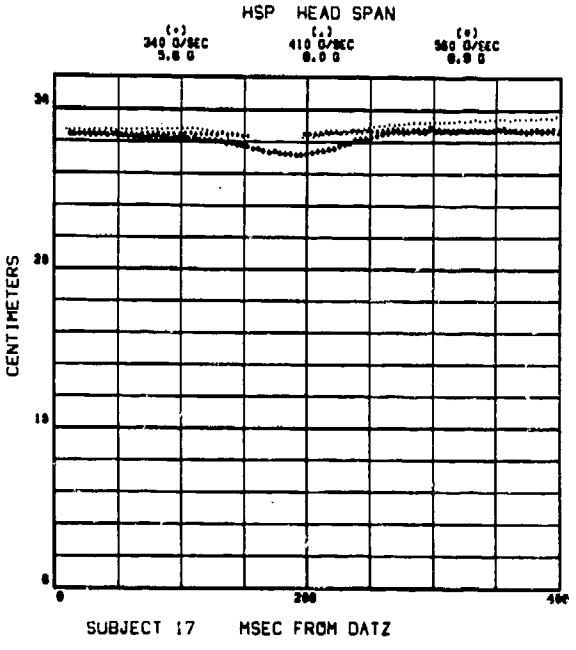

623

HSP HEADSPAN

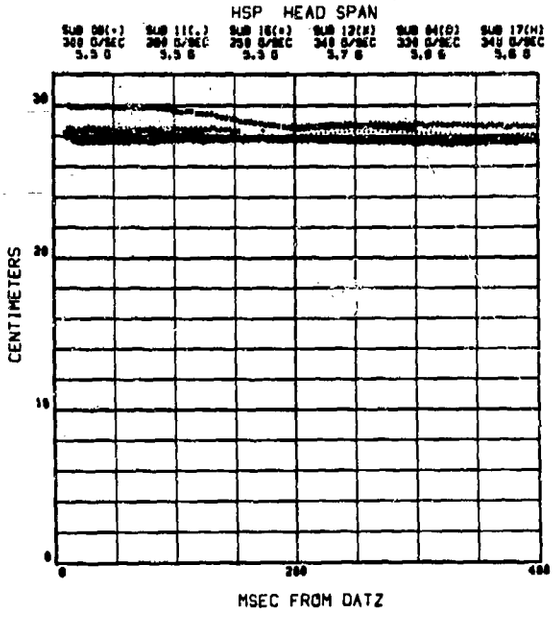

624

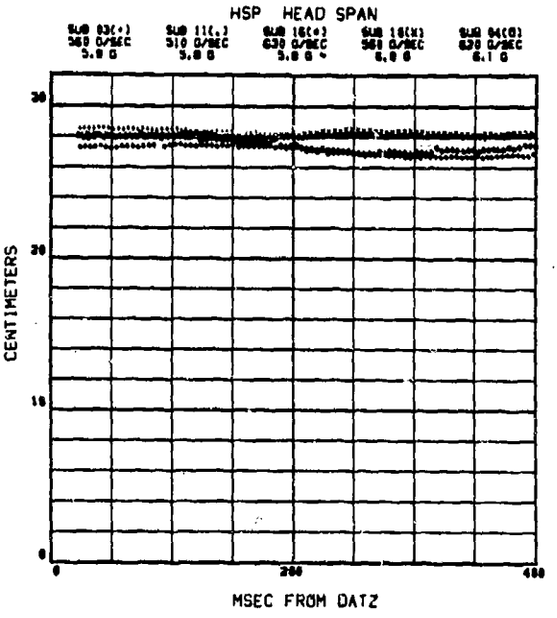

625

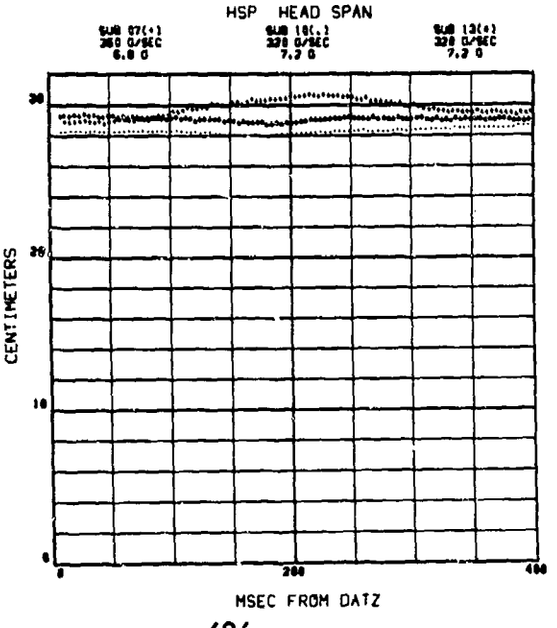

626

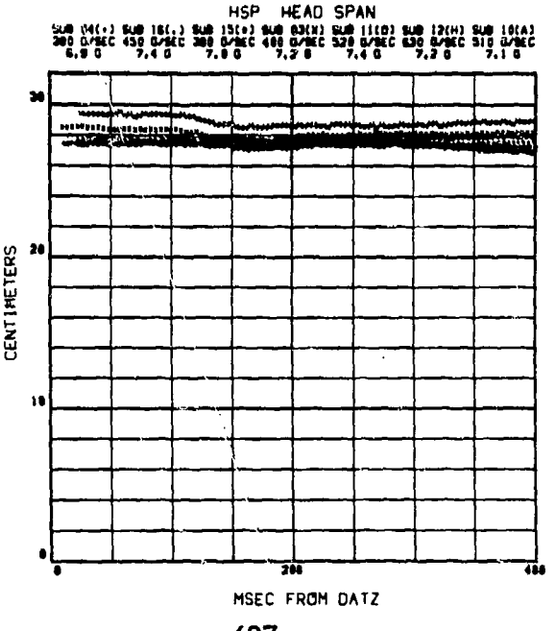

627

HSP HEADSPAN

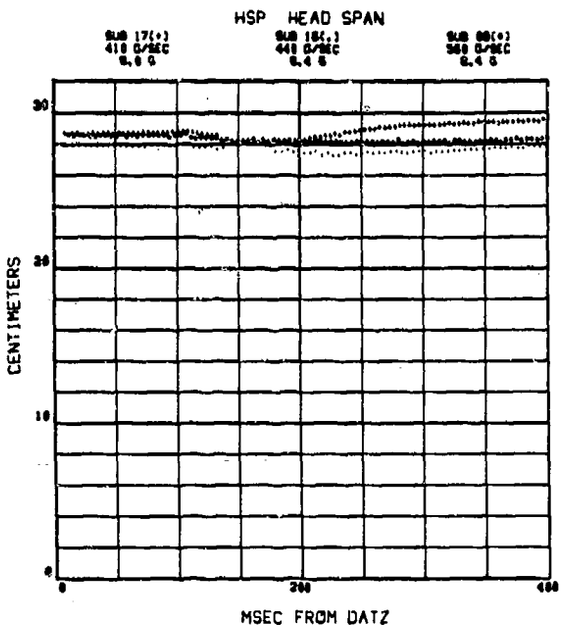

628

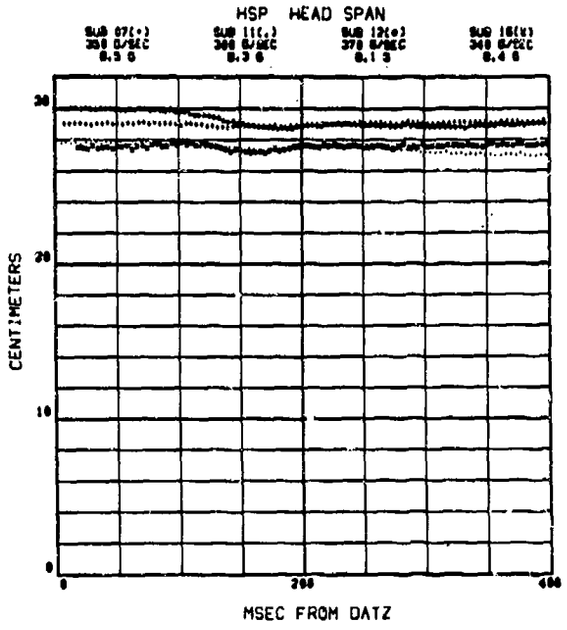

629

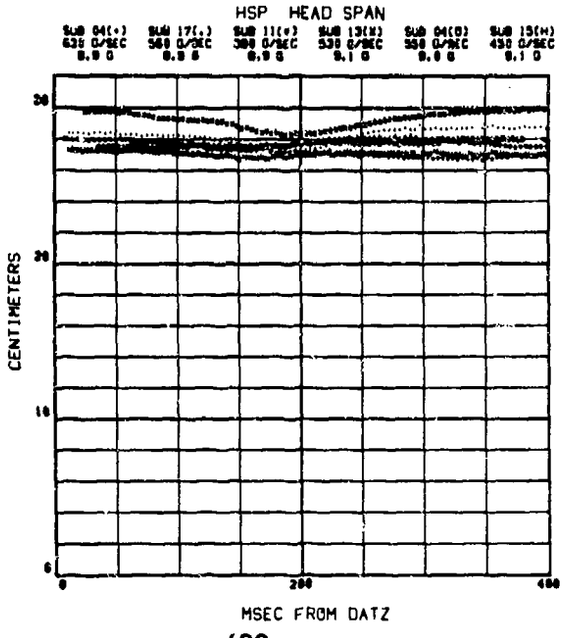

630

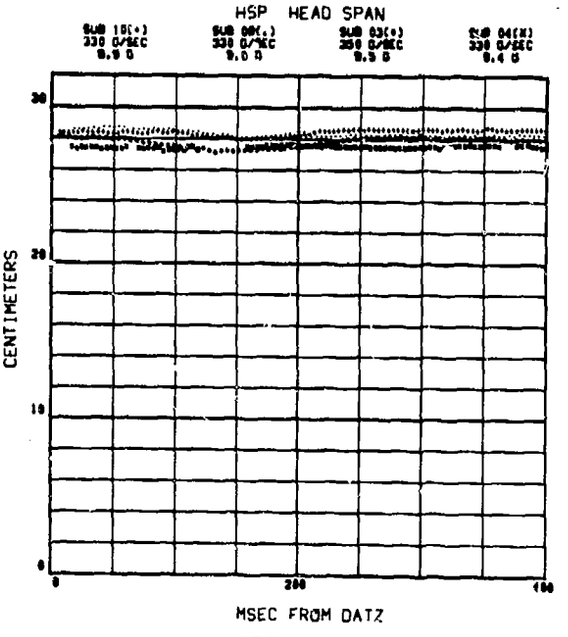

631

HSP HEADSPAN

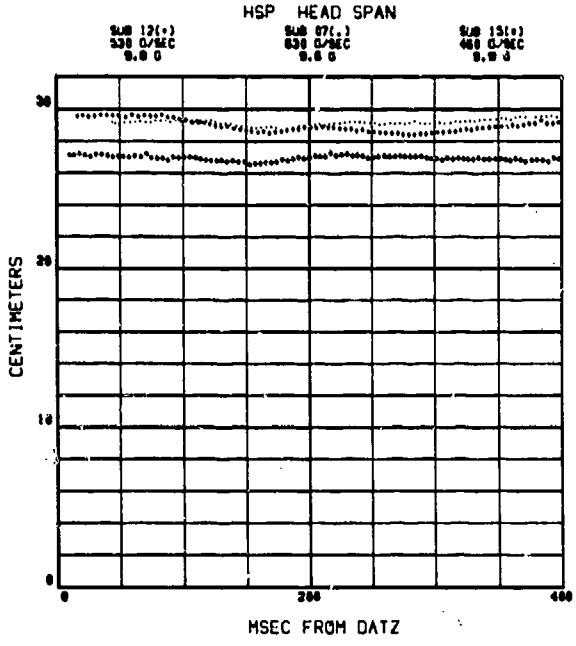

632

PDH, RDH, COMPARISON OF ANGULAR DISPLACEMENT OF HEAD

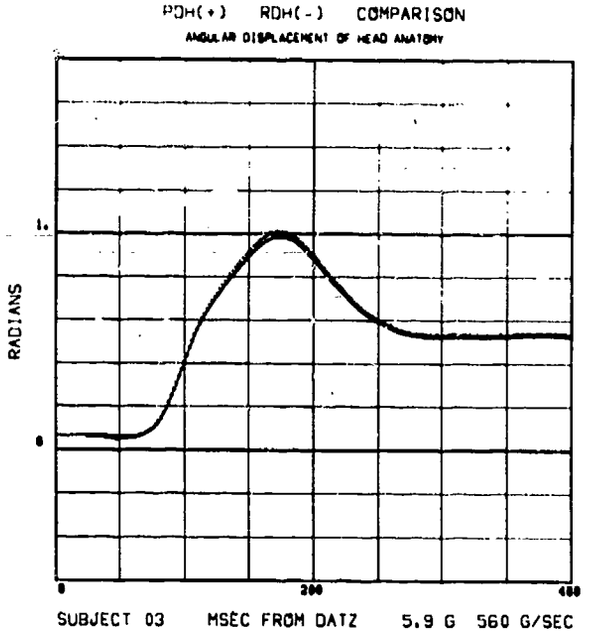

633

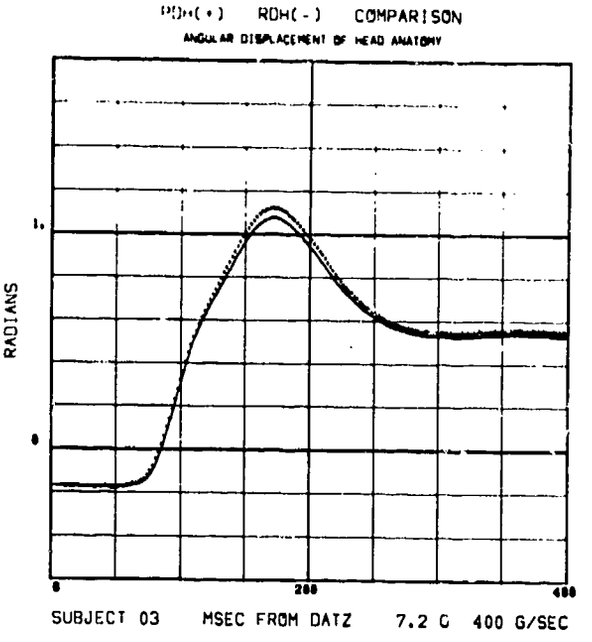

634

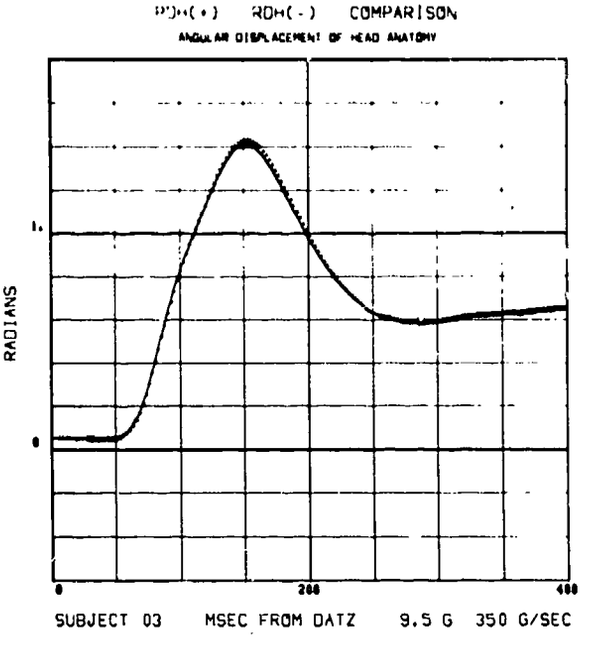

635

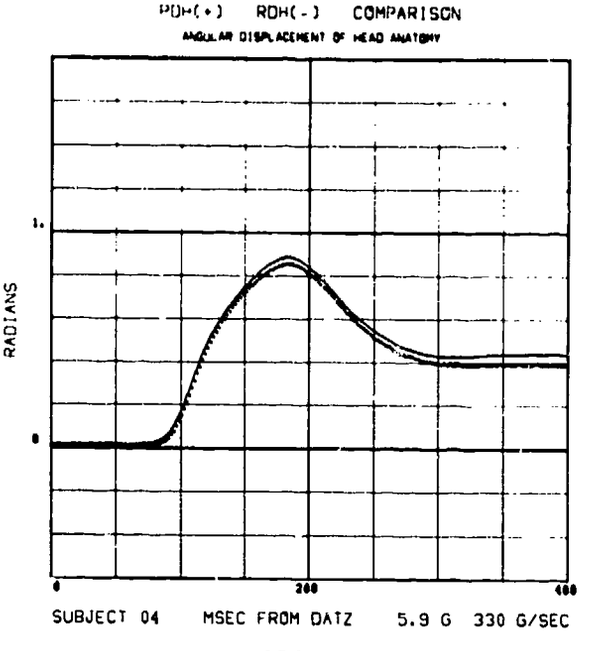

636

PDH, RDH, COMPARISON OF ANGULAR DISPLACEMENT OF HEAD

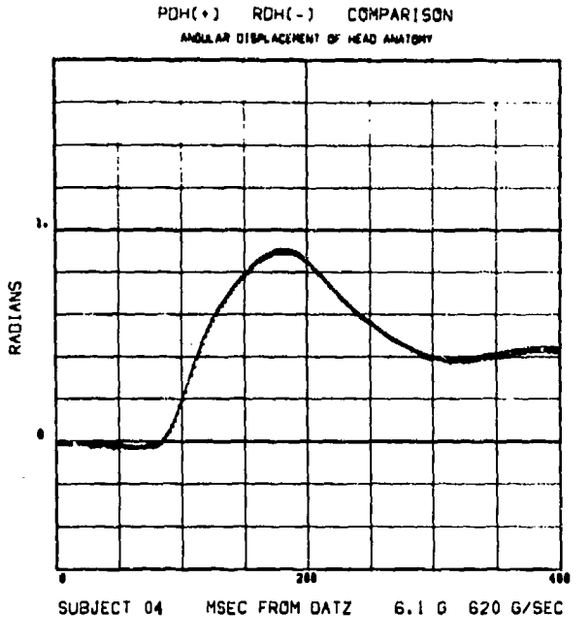

637

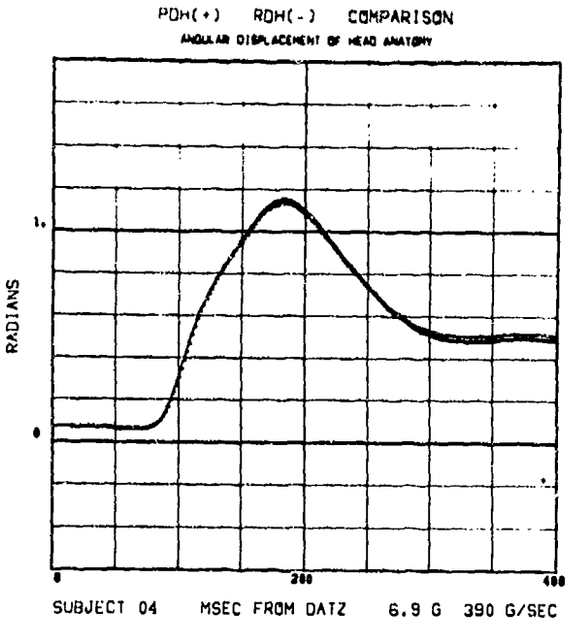

638

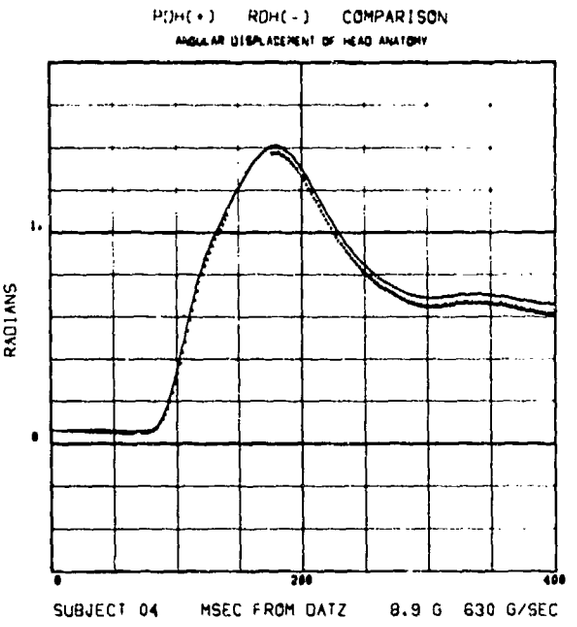

639

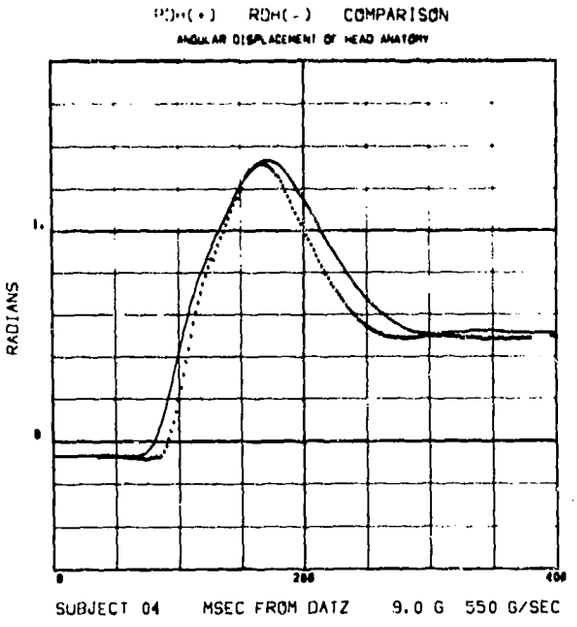

640

PDH, RDH, COMPARISON OF ANGULAR DISPLACEMENT OF HEAD

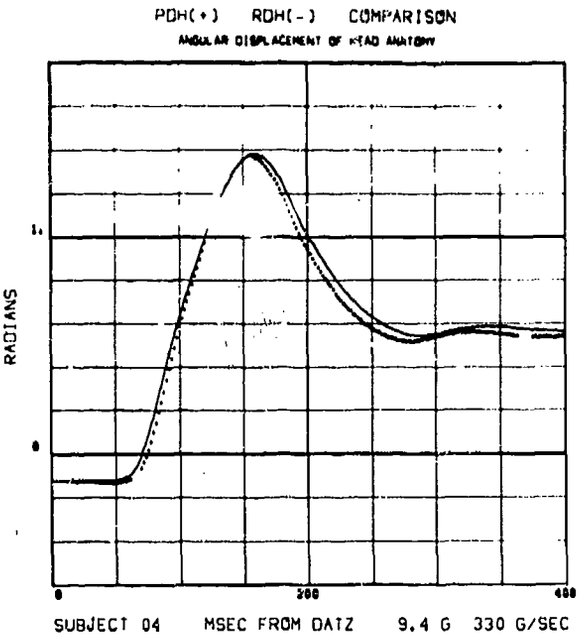

641

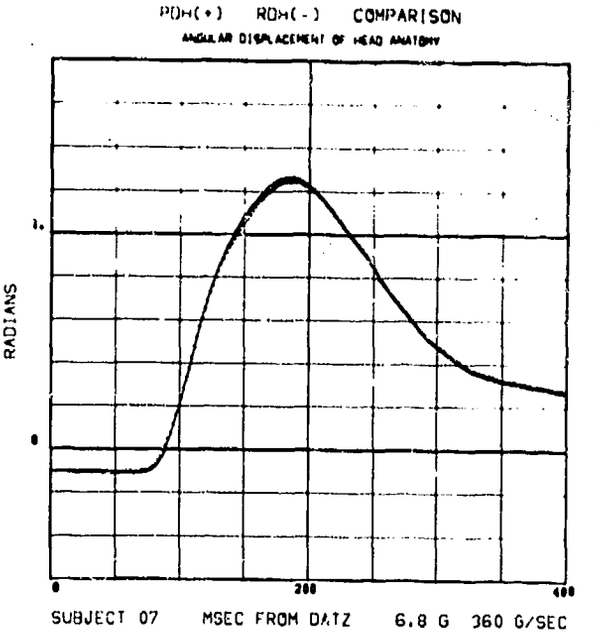

642

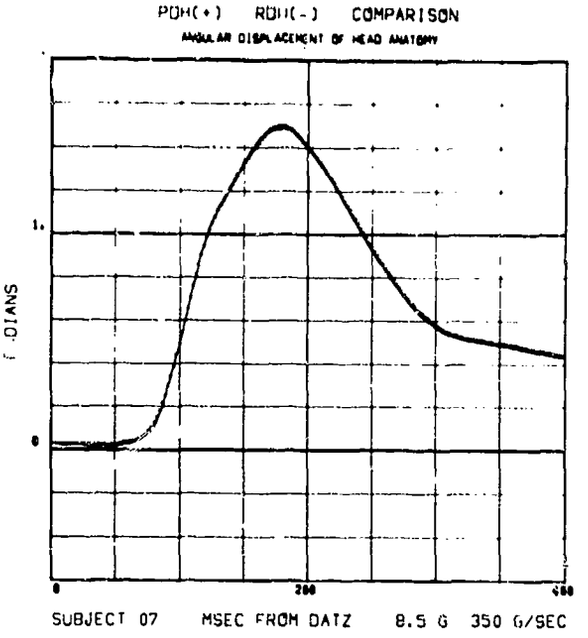

643

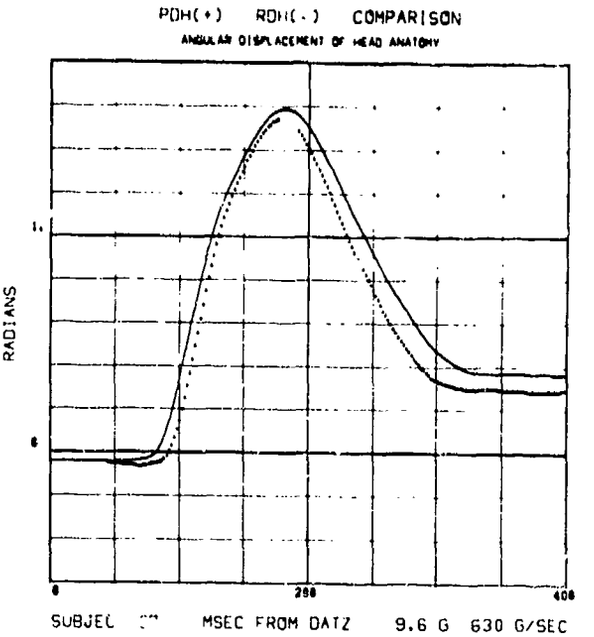

644

PDH, RDH, COMPARISON OF ANGULAR DISPLACEMENT OF HEAD

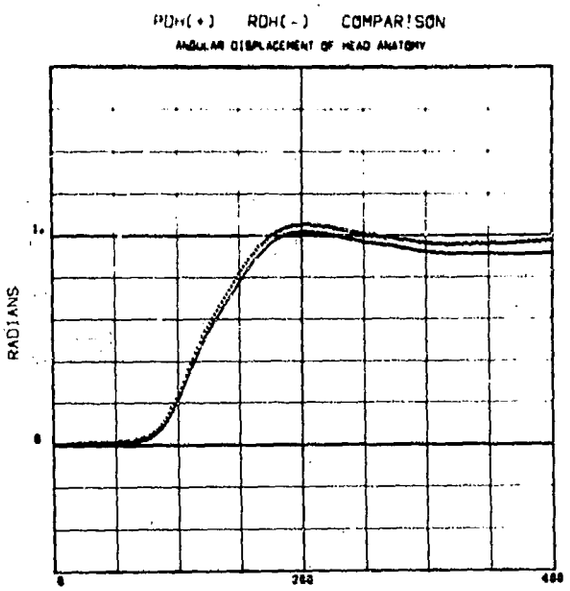

SUBJECT 08 MSEC FROM DATZ 5.5 G 300 G/SEC

645

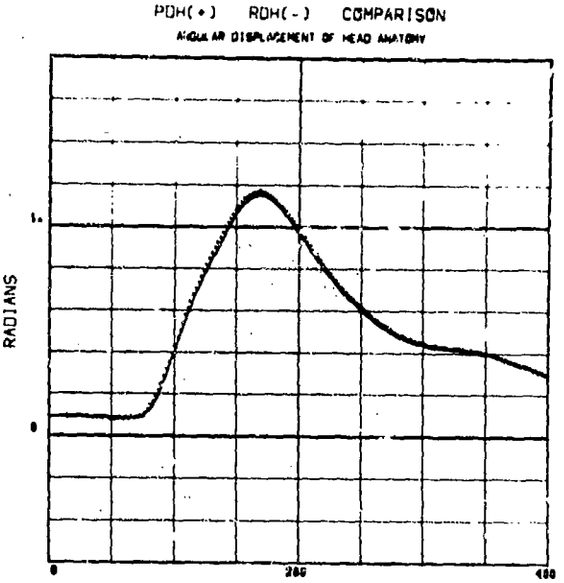

SUBJECT 09 MSEC FROM DATZ 8.4 G 560 G/SEC

646

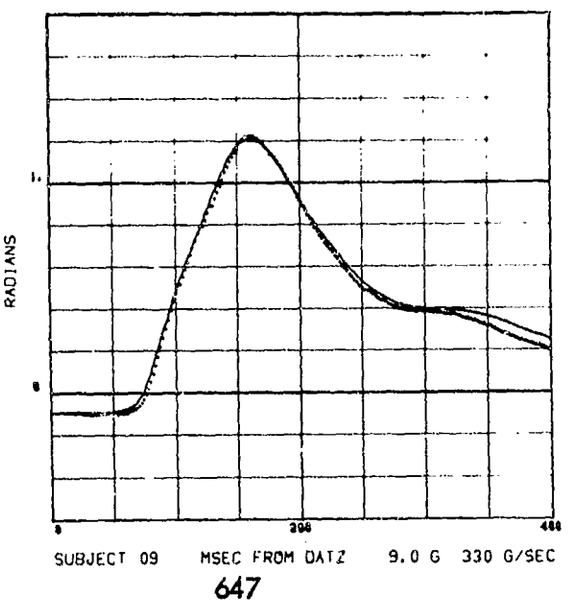

SUBJECT 09 MSEC FROM DATZ 9.0 G 330 G/SEC

647

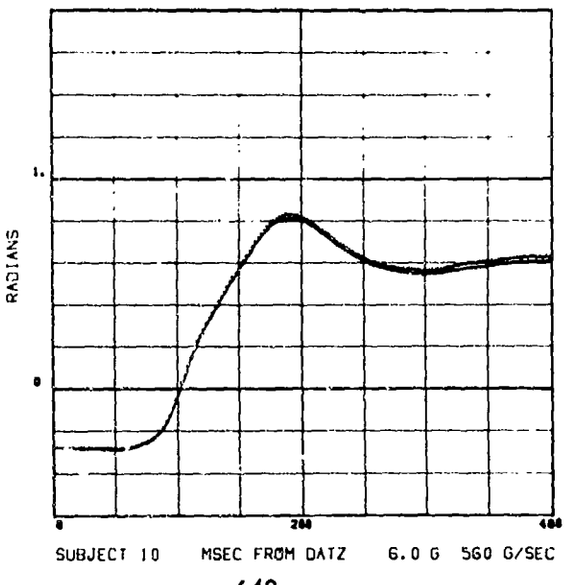

SUBJECT 10 MSEC FROM DATZ 6.0 G 560 G/SEC

648

PDH, RDH, COMPARISON OF ANGULAR DISPLACEMENT OF HEAD

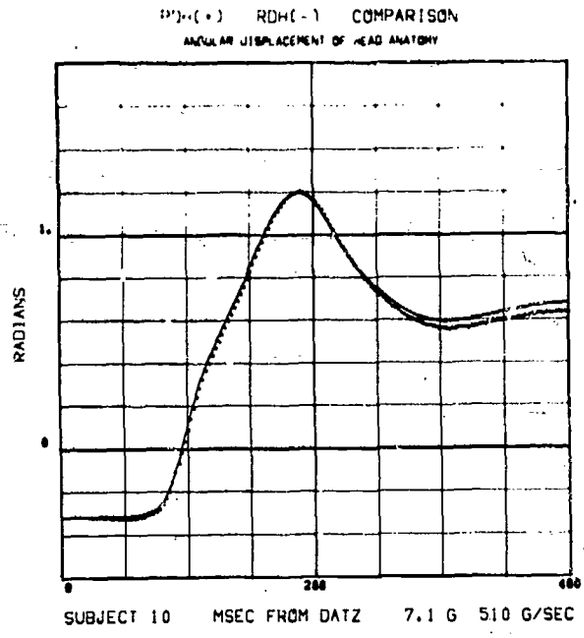

649

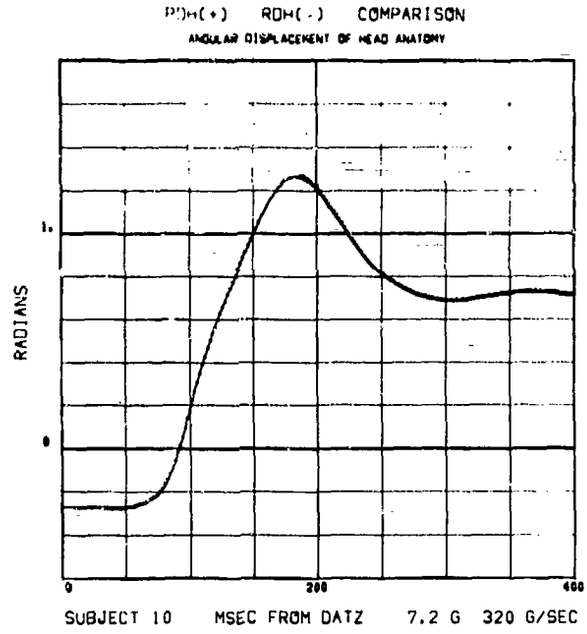

650

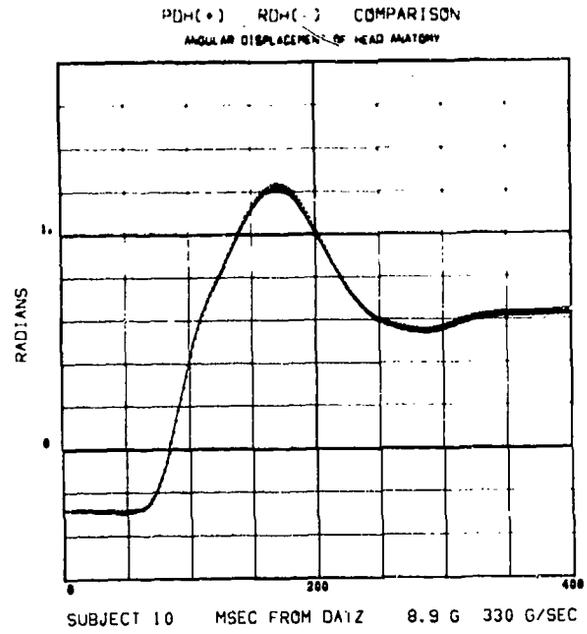

651

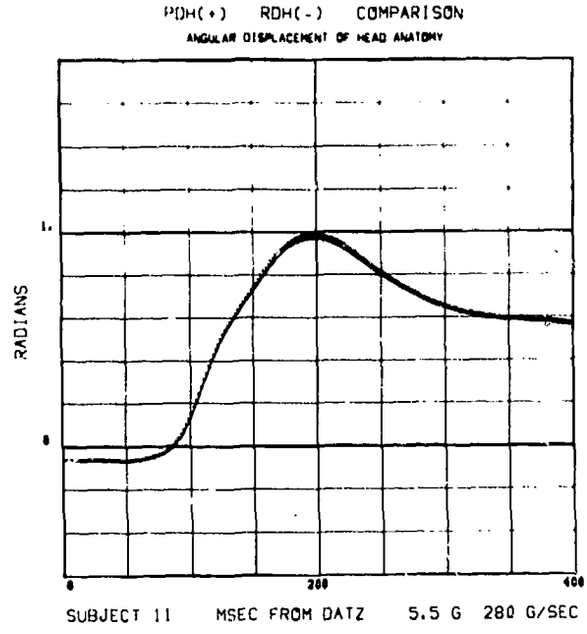

652

PDH, RDH, COMPARISON OF ANGULAR DISPLACEMENT OF HEAD

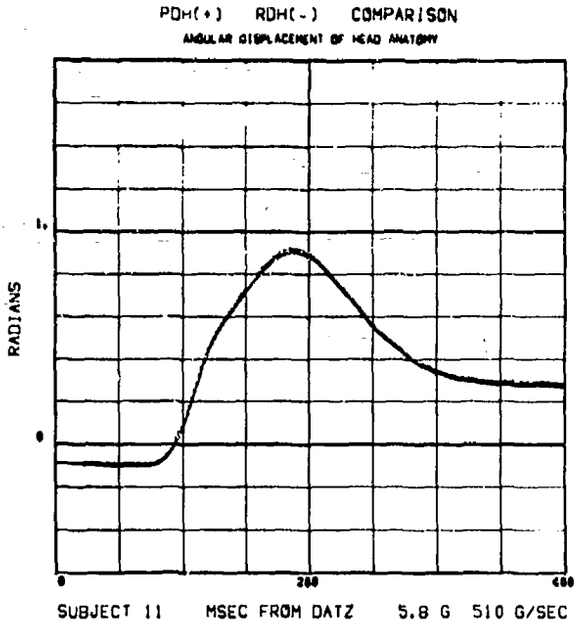

653

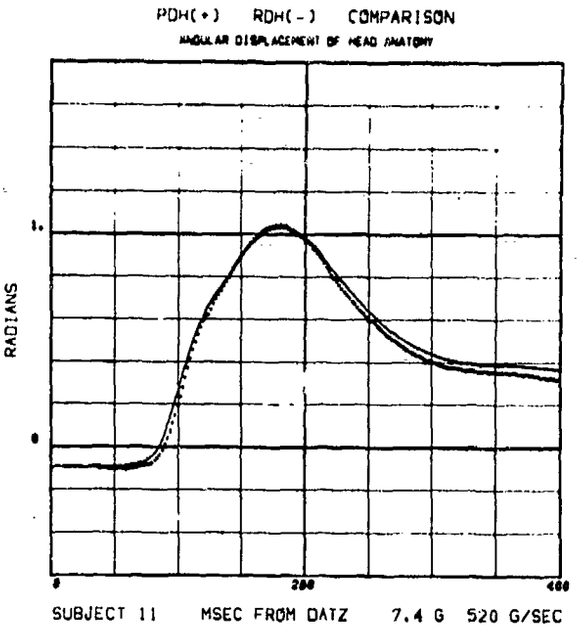

654

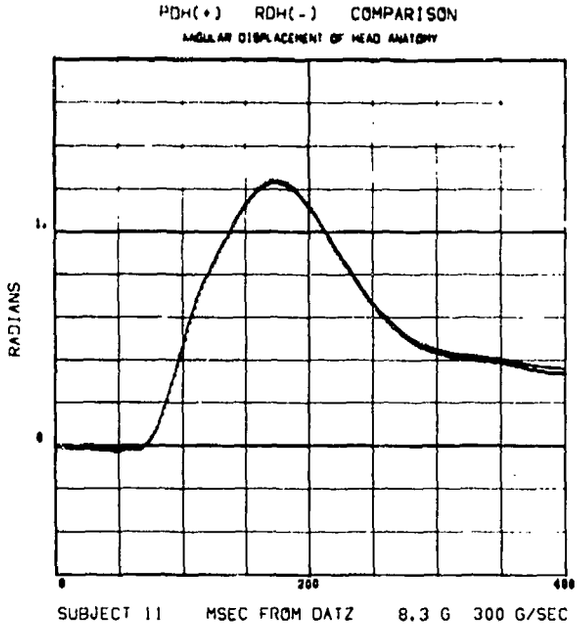

655

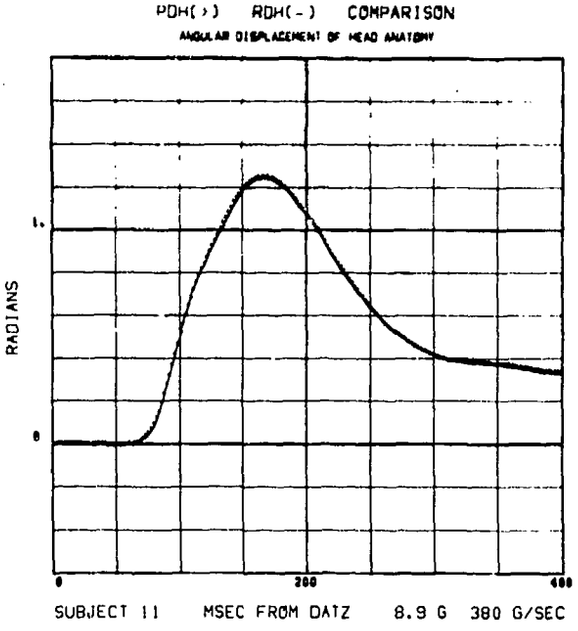

656

PDH, RDH, COMPARISON OF ANGULAR DISPLACEMENT OF HEAD

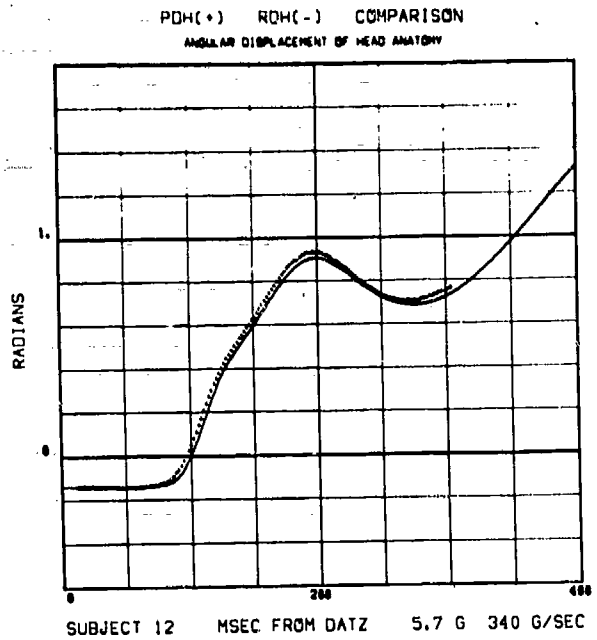

657

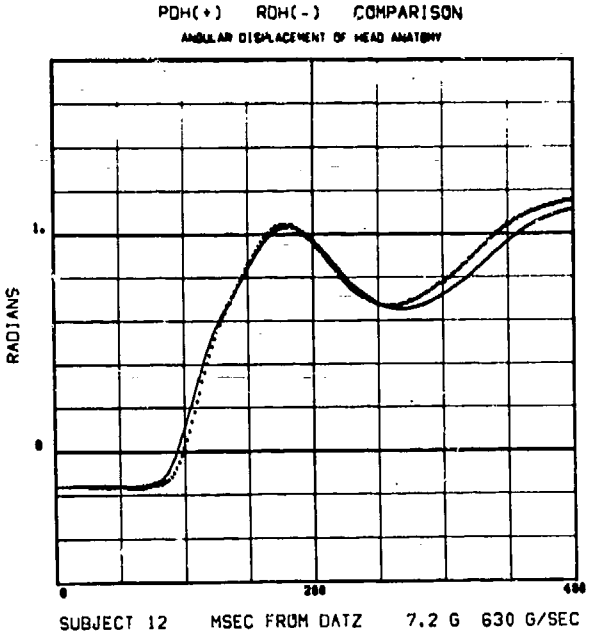

658

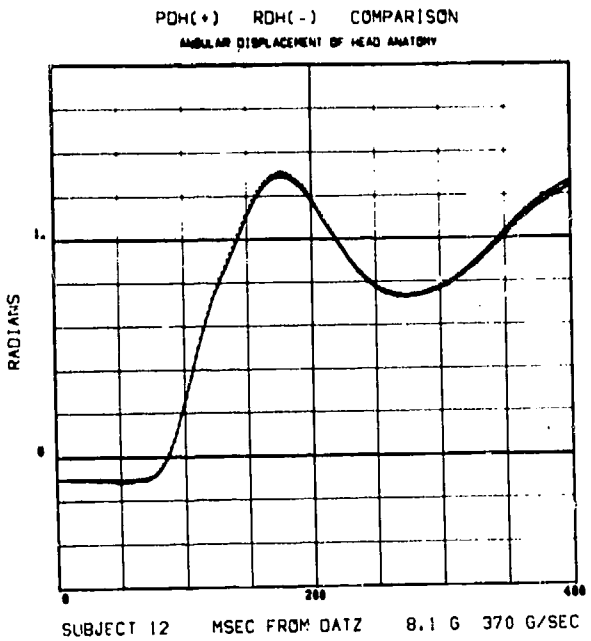

659

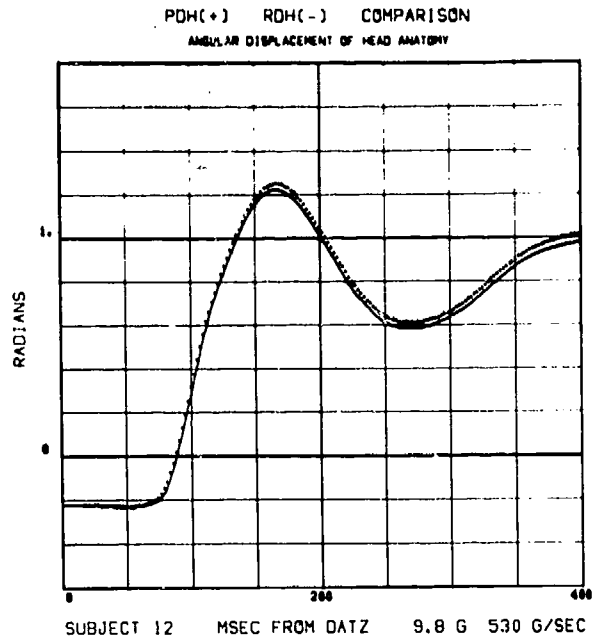

660

PDH, RDH, COMPARISON OF ANGULAR DISPLACEMENT OF HEAD

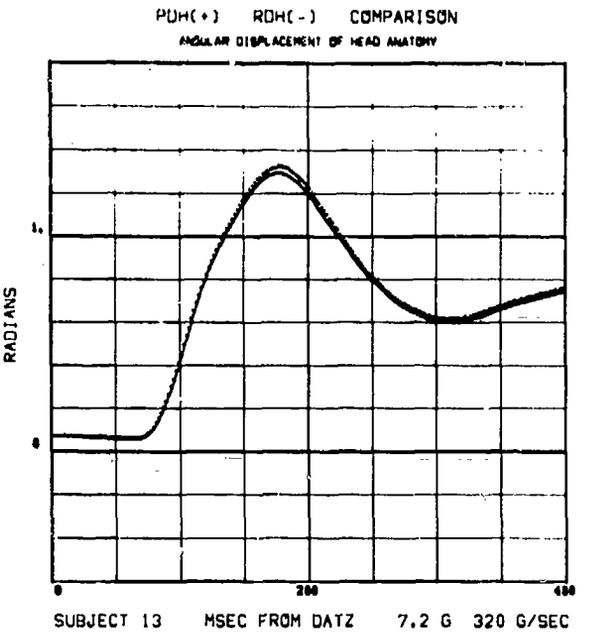

661

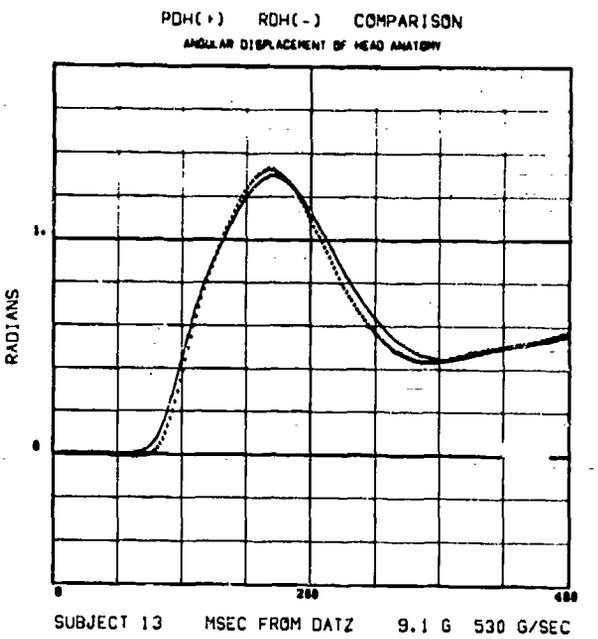

662

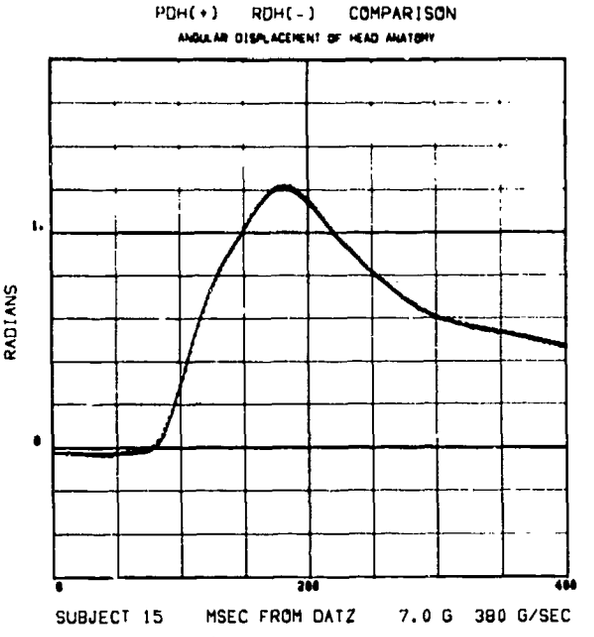

663

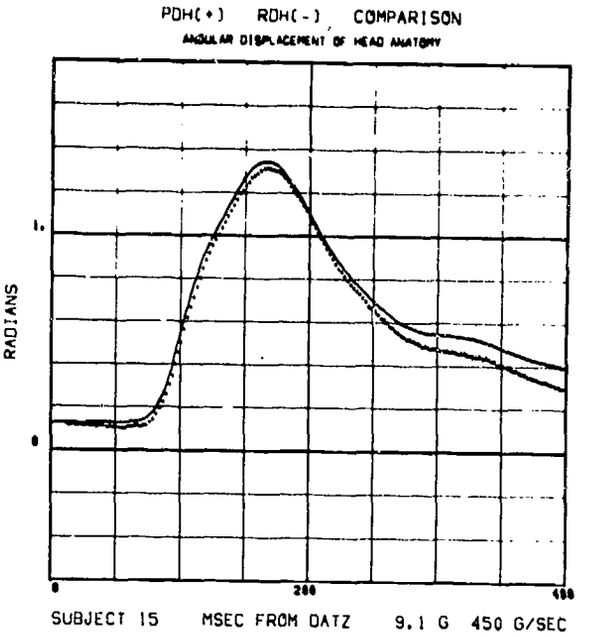

664

PDH, RDH, COMPARISON OF ANGULAR DISPLACEMENT OF HEAD

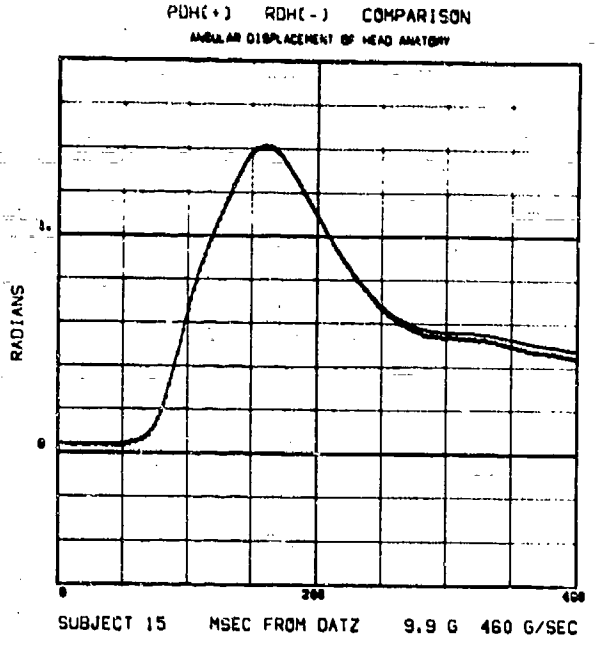

665

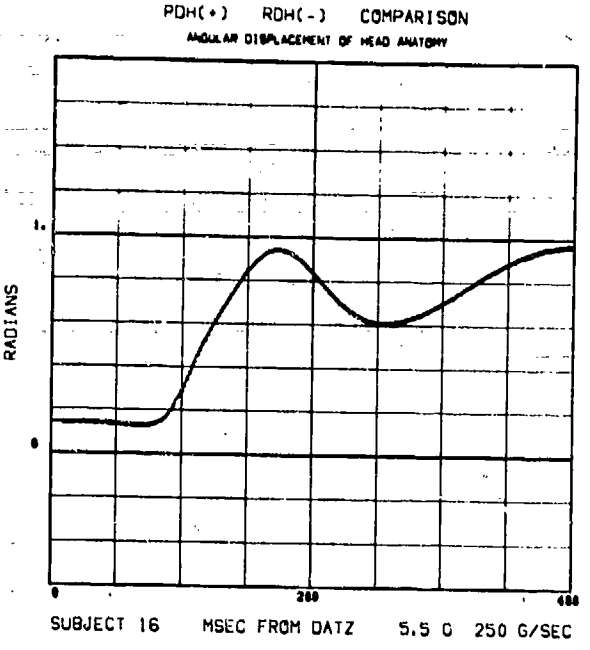

666

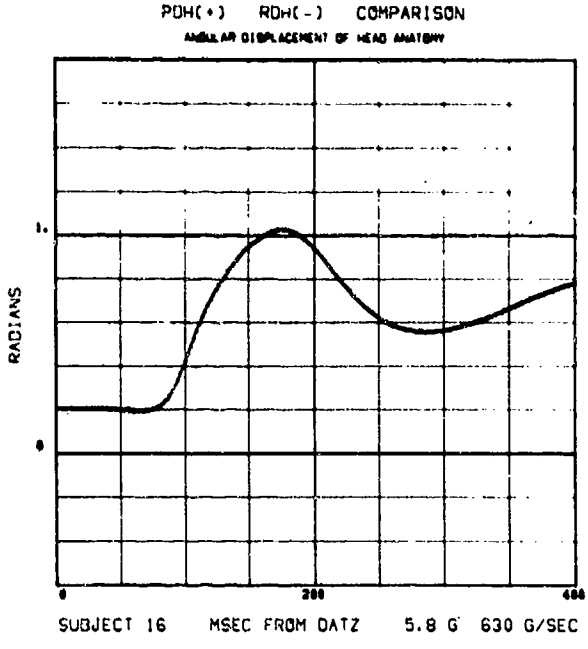

667

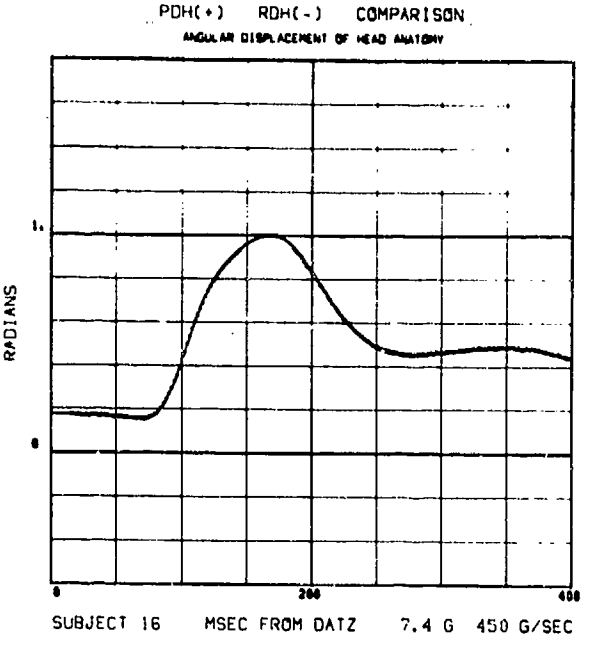

668

PDH, RDH, COMPARISON OF ANGULAR DISPLACEMENT OF HEAD

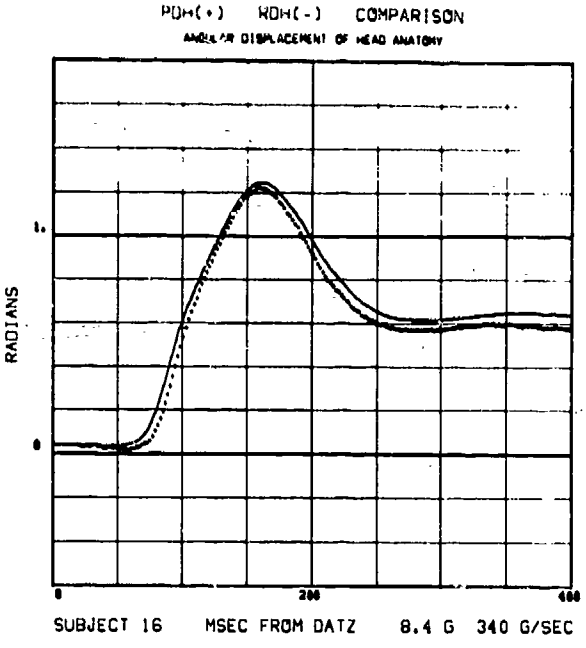

669

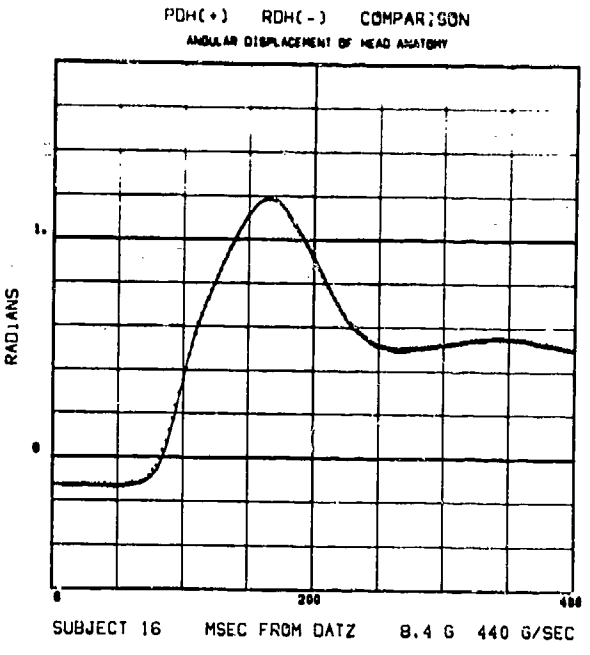

670

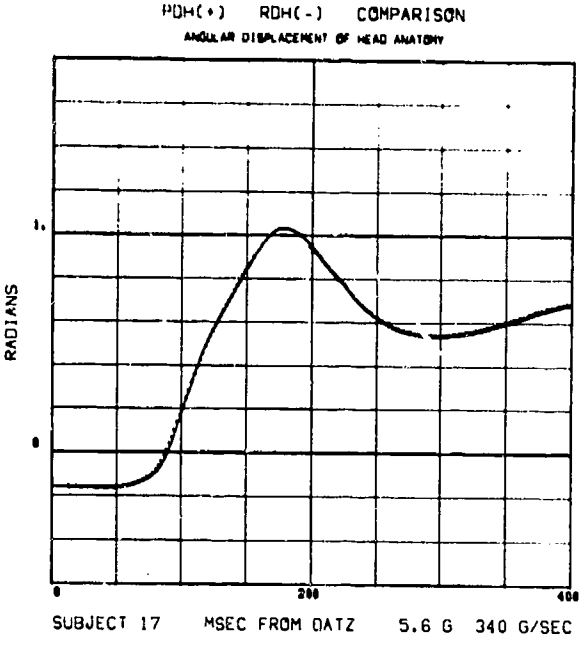

671

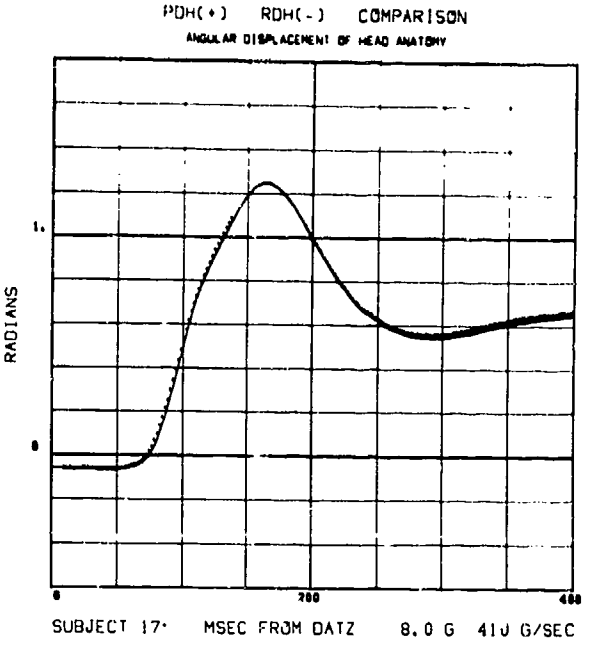

672

PDH, RDH, COMPARISON OF ANGULAR DISPLACEMENT OF HEAD

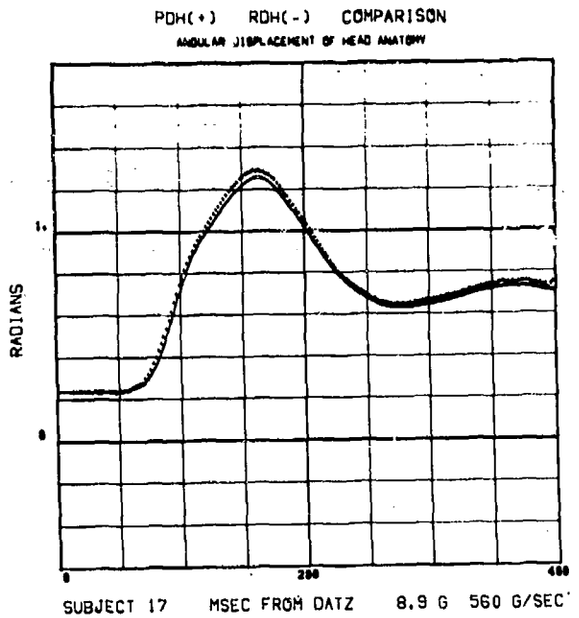

673

4FM, 4FD, COMPARISON OF HEAD C.G. ACCELERATION COMPONENTS

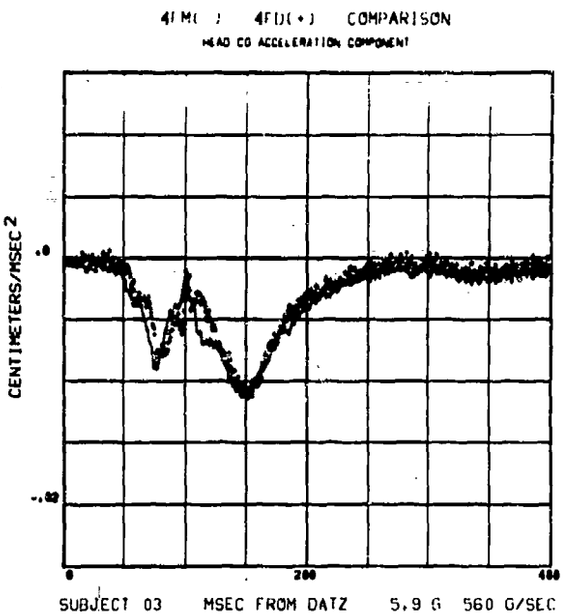

674

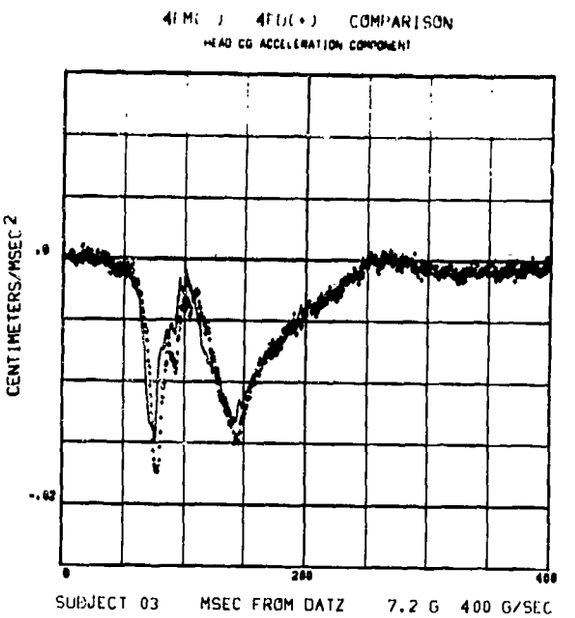

675

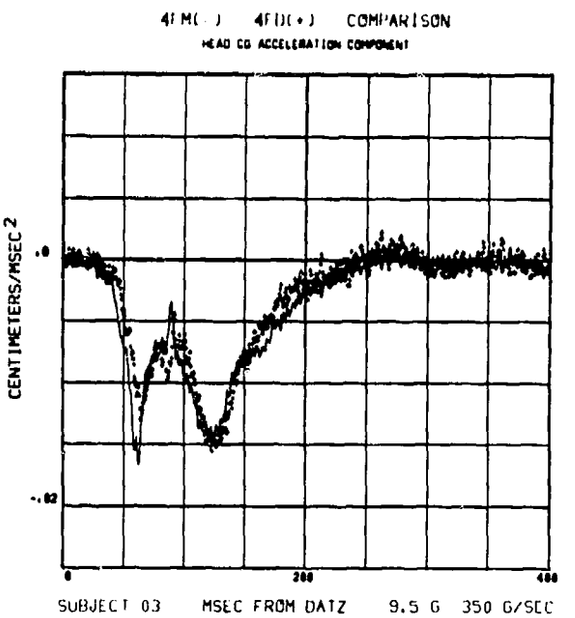

676

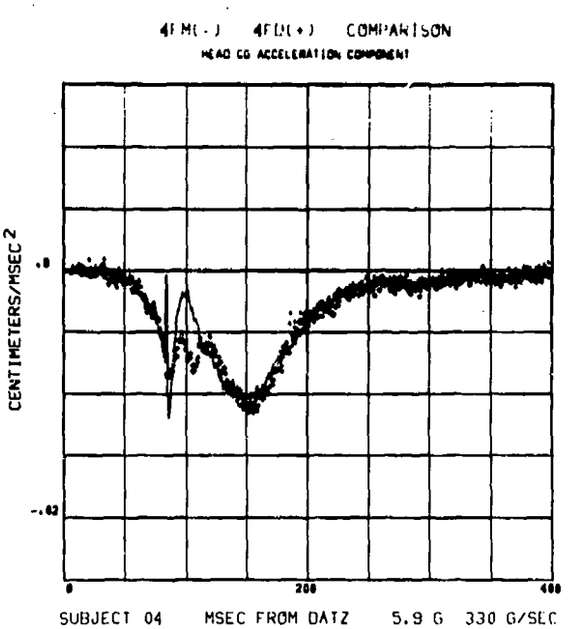

677

4FM, 4FD, COMPARISON OF HEAD C.G. ACCELERATION COMPONENTS

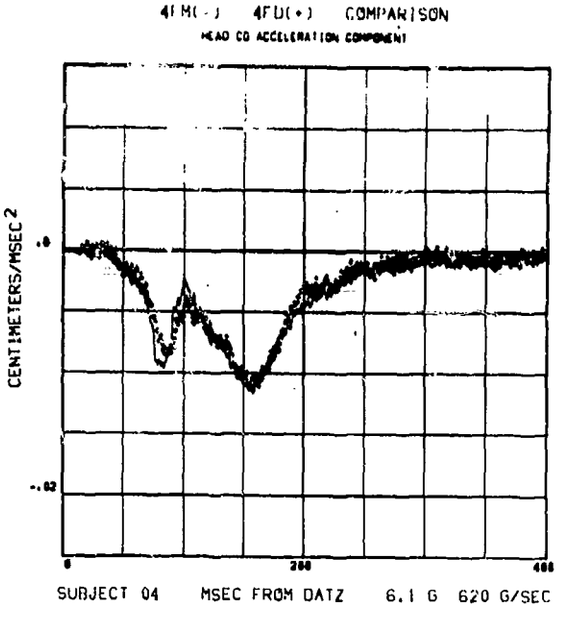

678

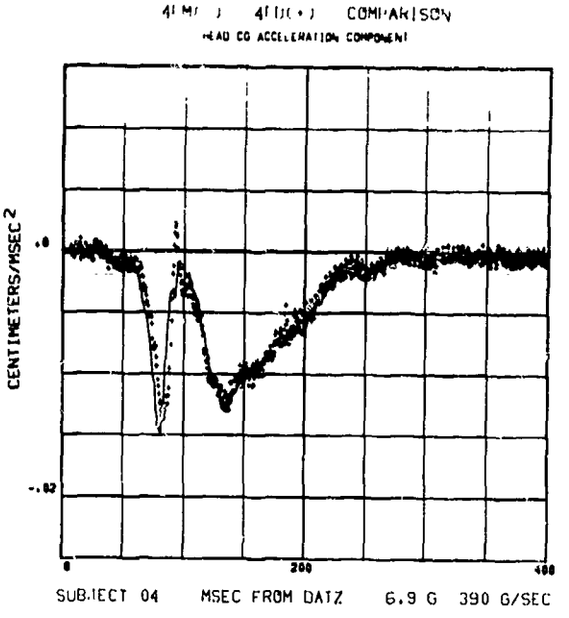

679

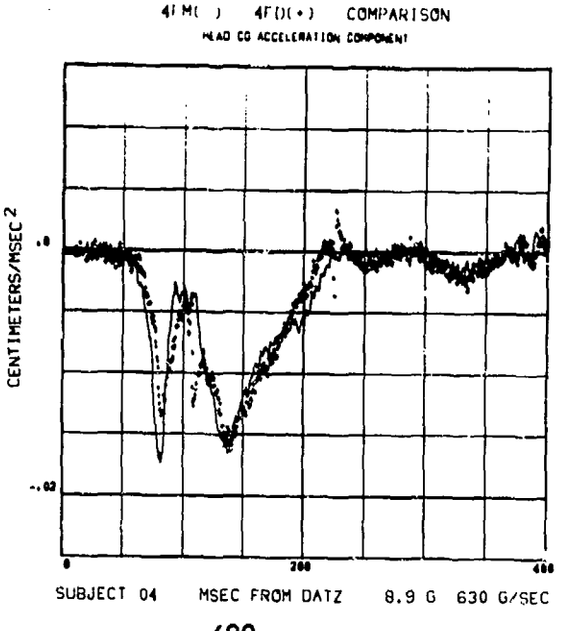

680

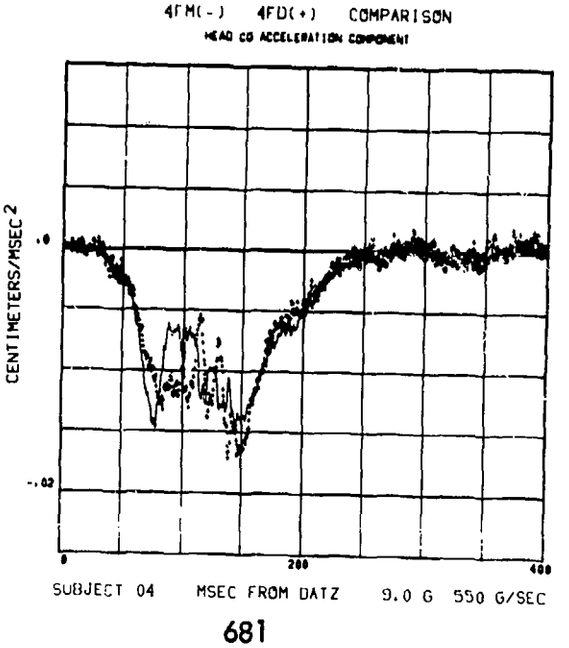

681

4FM, 4FD, COMPARISON OF HEAD C.G. ACCELERATION COMPONENTS

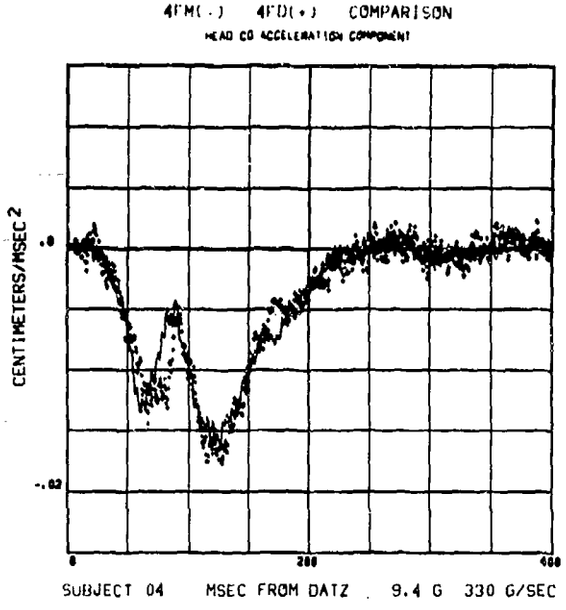

682

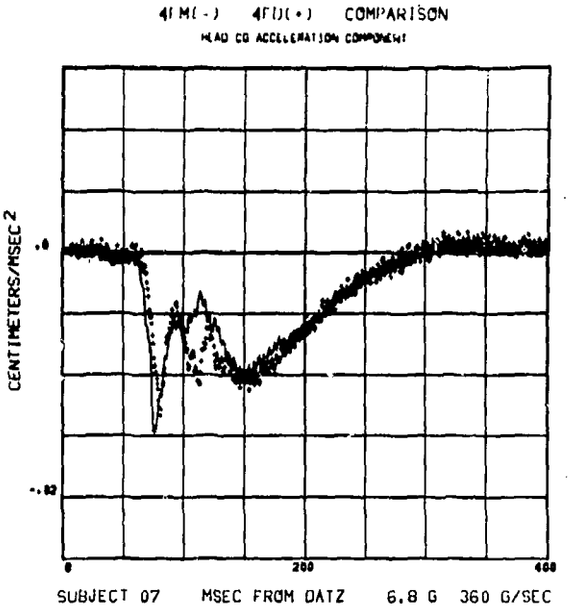

683

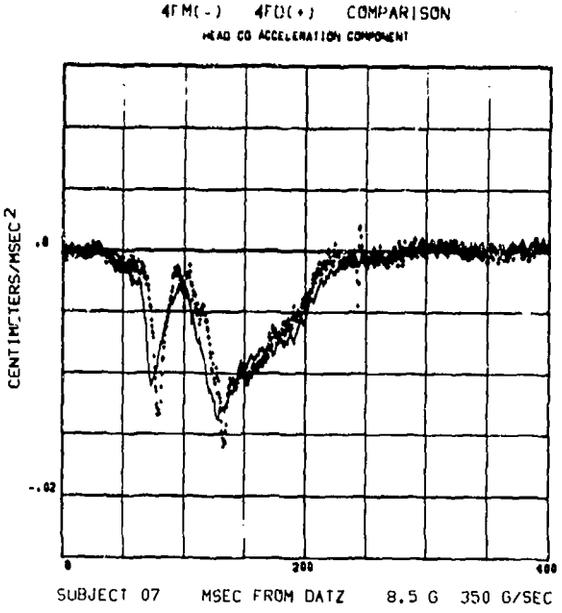

684

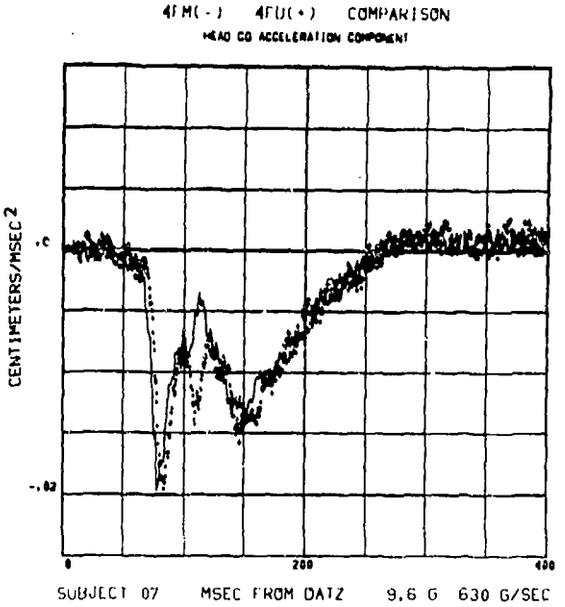

685

4FM, 4FD, COMPARISON OF HEAD C.G. ACCELERATION COMPONENTS

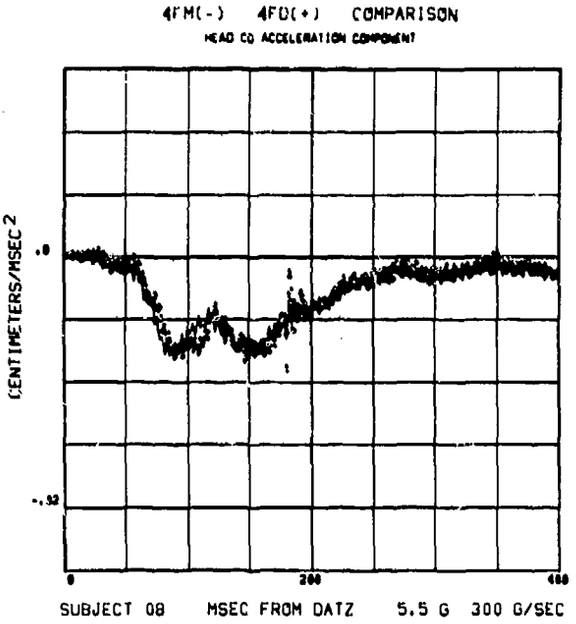

686

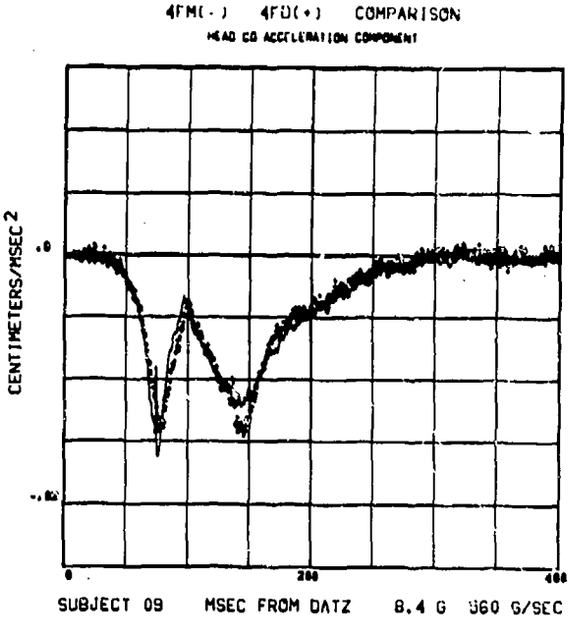

687

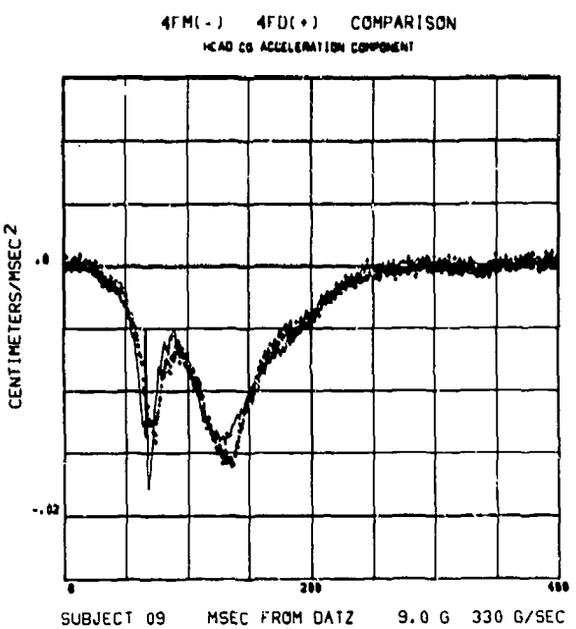

688

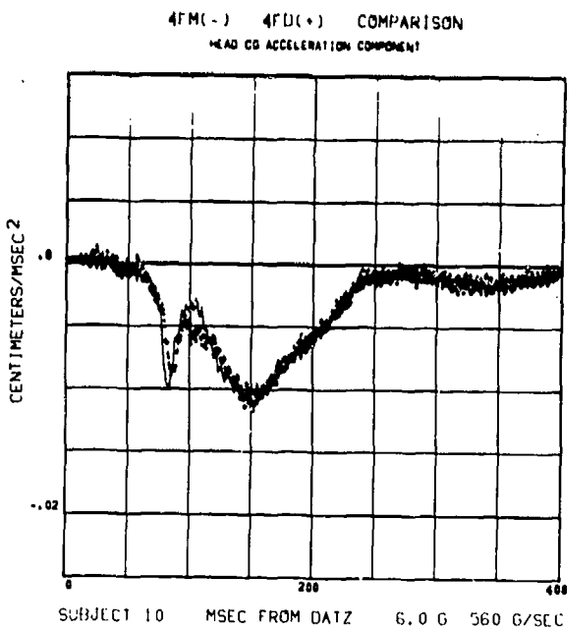

689

4FM, 4FD, COMPARISON OF HEAD C.G. ACCELERATION COMPONENTS

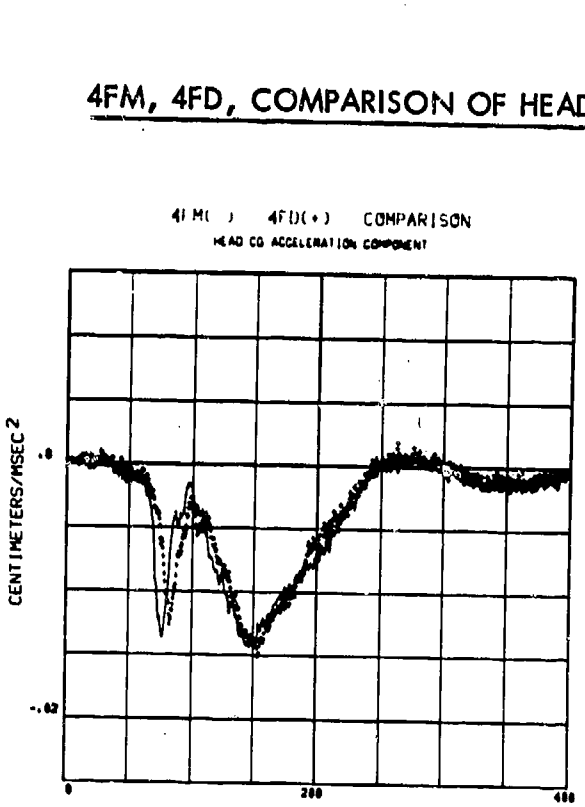

690

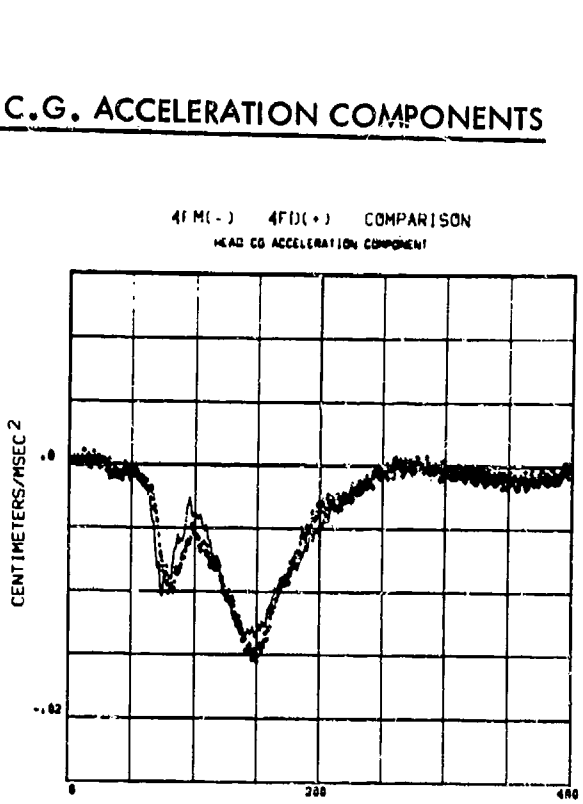

691

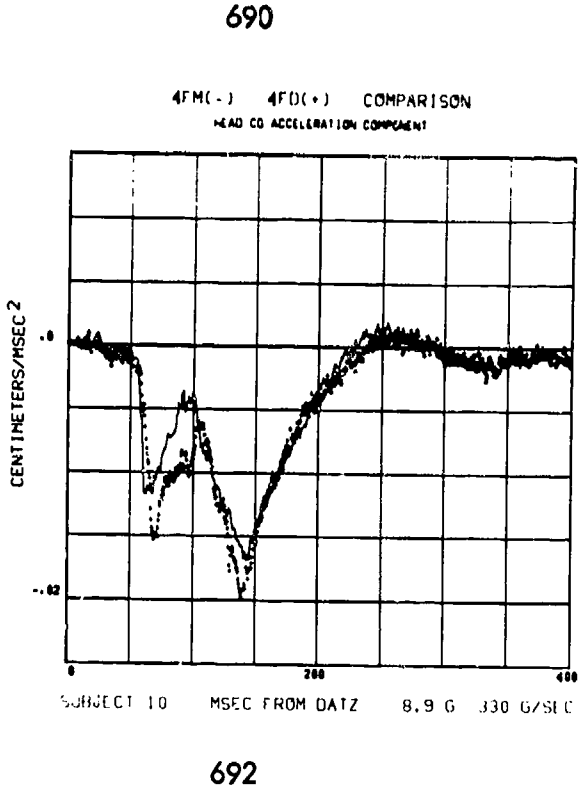

692

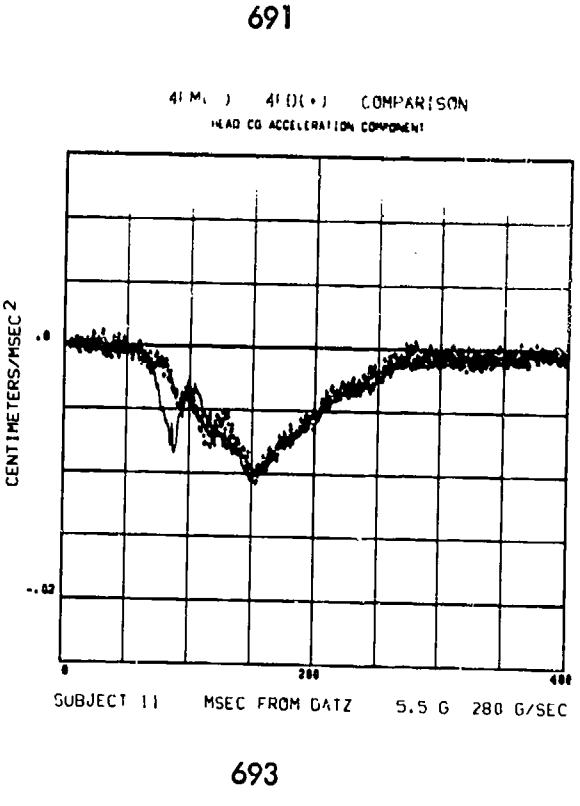

693

4FM, 4FD, COMPARISON OF HEAD C.G. ACCELERATION COMPONENTS

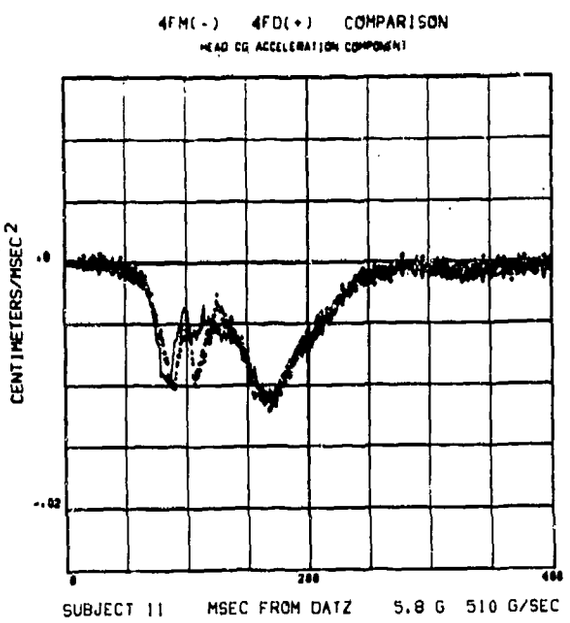

694

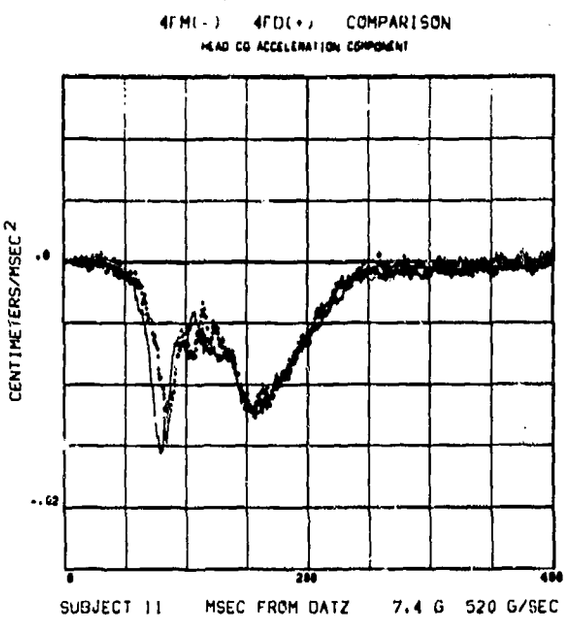

695

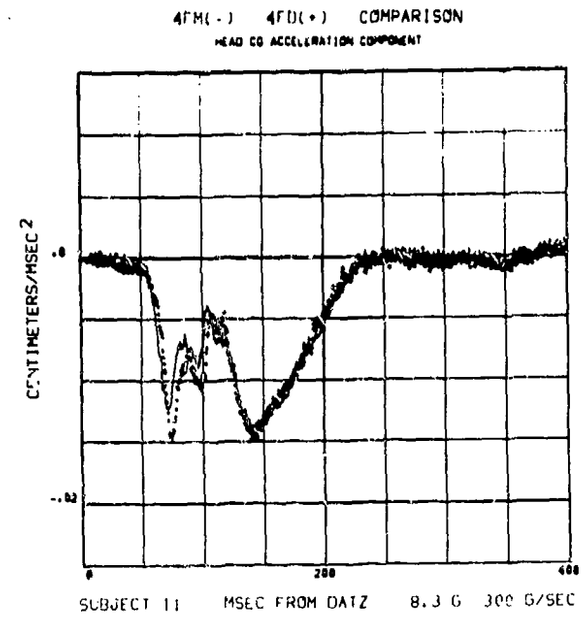

696

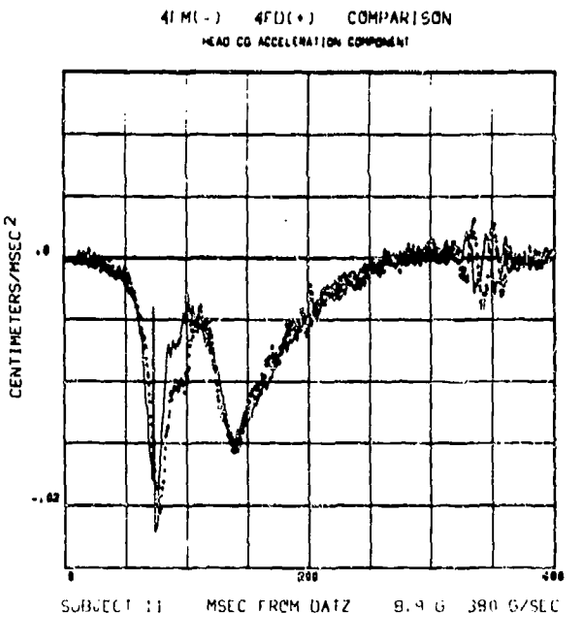

697

4FM, 4FD, COMPARISON OF HEAD C.G. ACCELERATION COMPONENTS

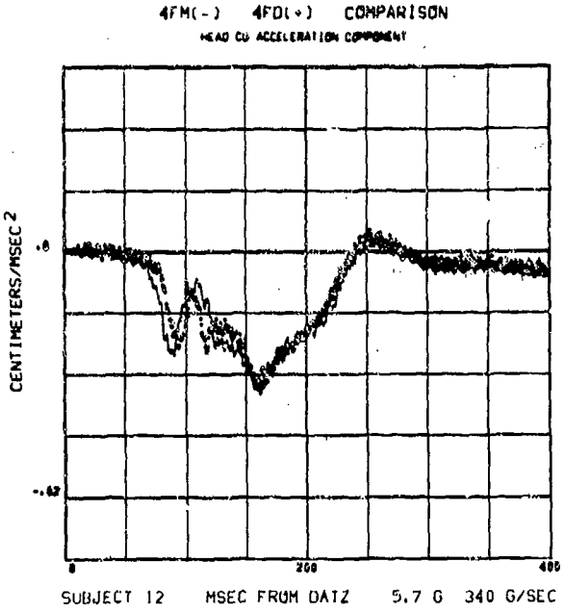

698

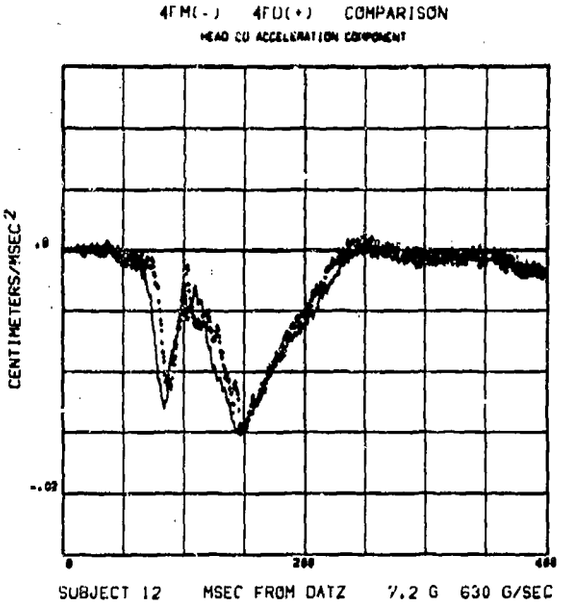

699

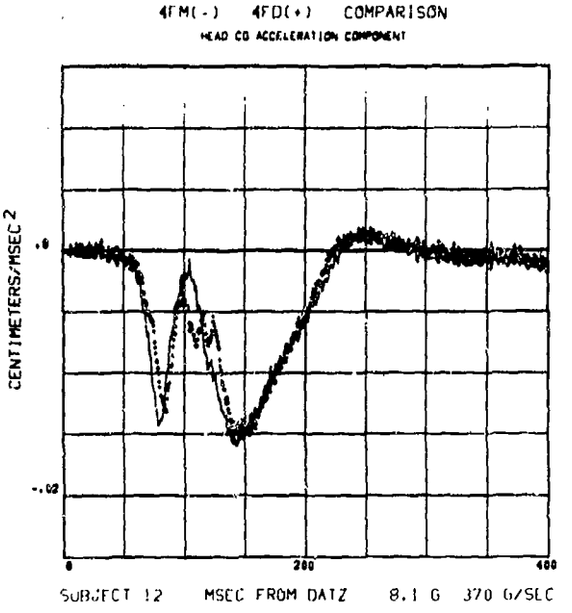

700

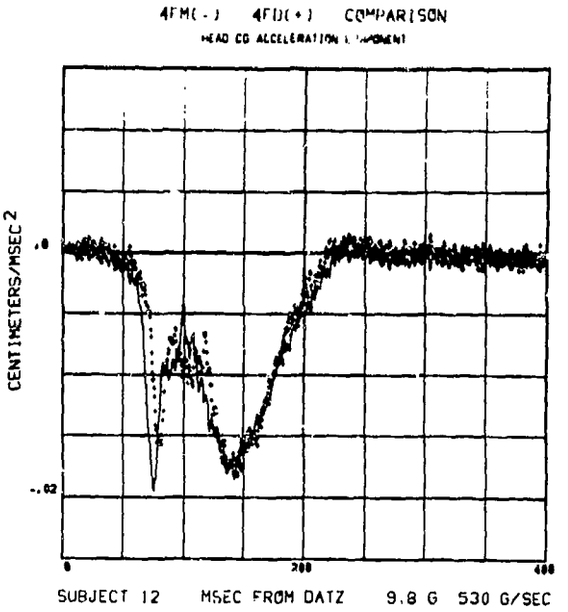

701

4FM, 4FD, COMPARISON OF HEAD C.G. ACCELERATION COMPONENTS

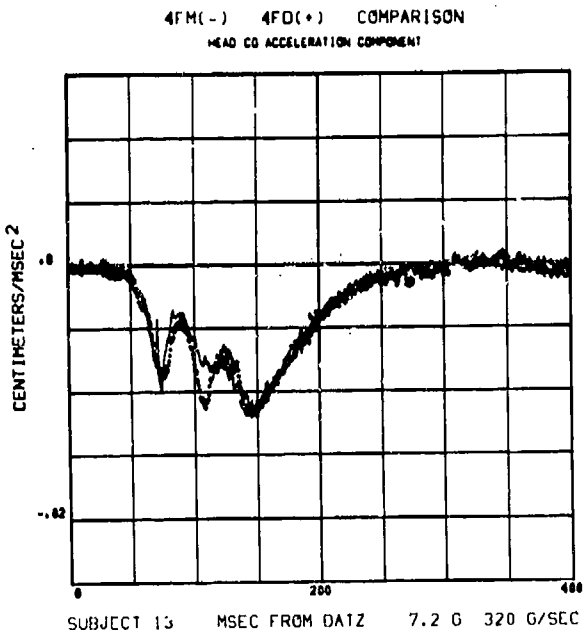

702

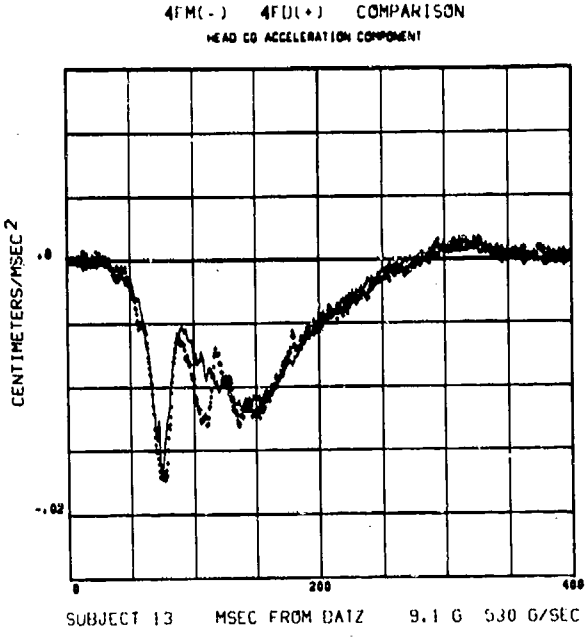

703

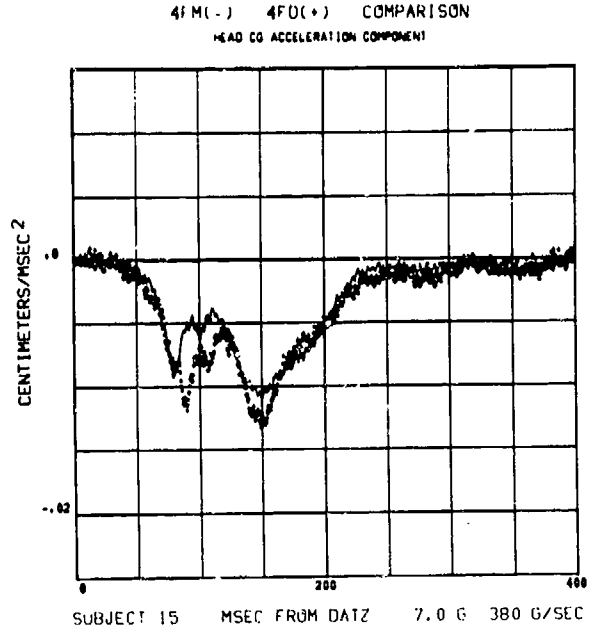

704

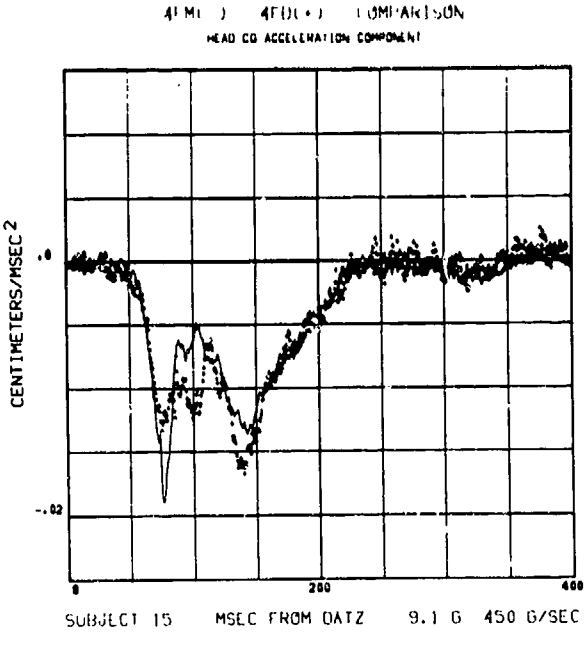

705

4FM, 4FD, COMPARISON OF HEAD C.G. ACCELERATION COMPONENTS

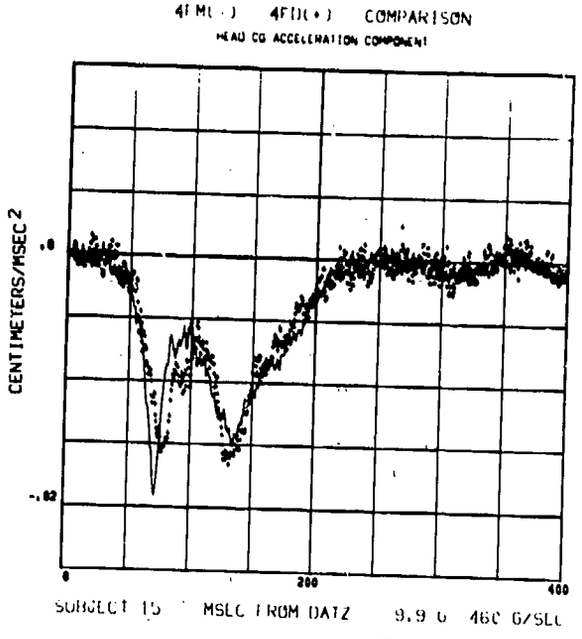

706

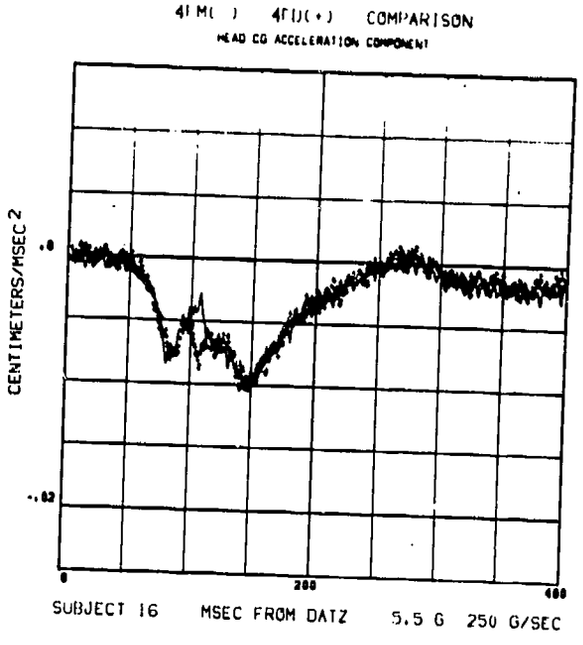

707

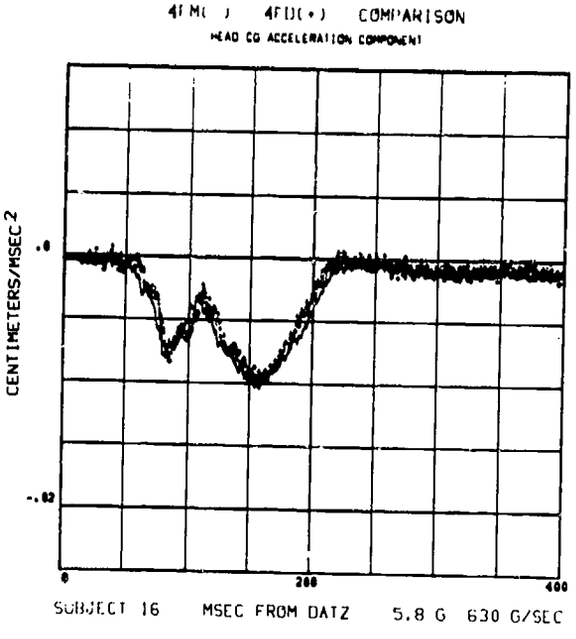

708

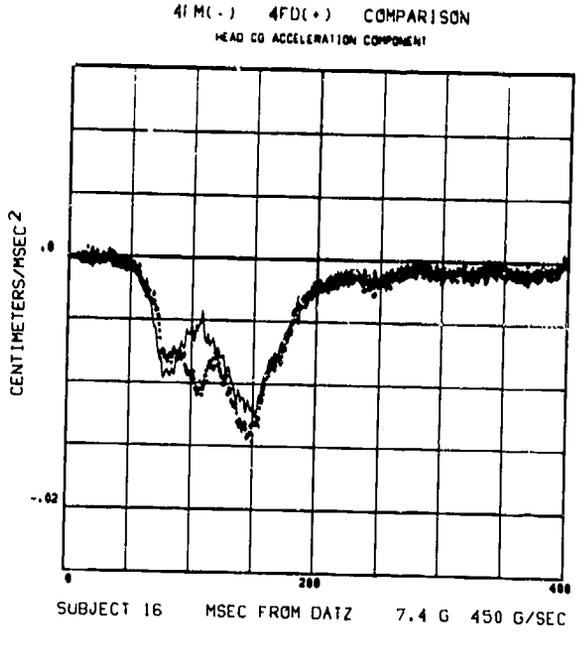

709

4FM, 4FD, COMPARISON OF HEAD C.G. ACCELERATION COMPONENTS

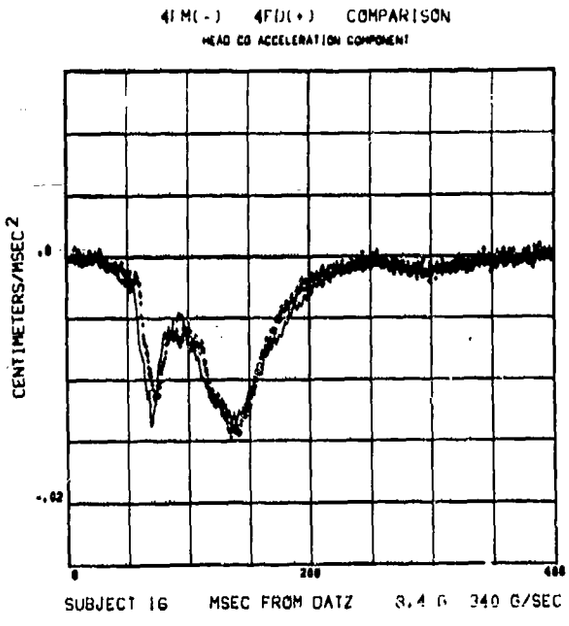

710

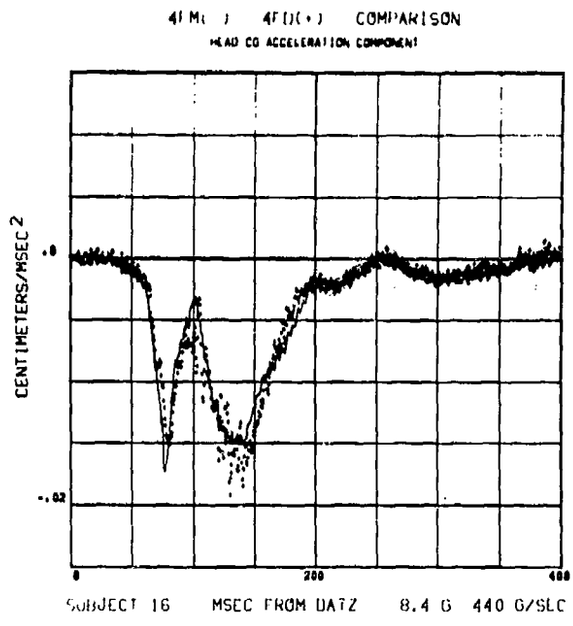

711

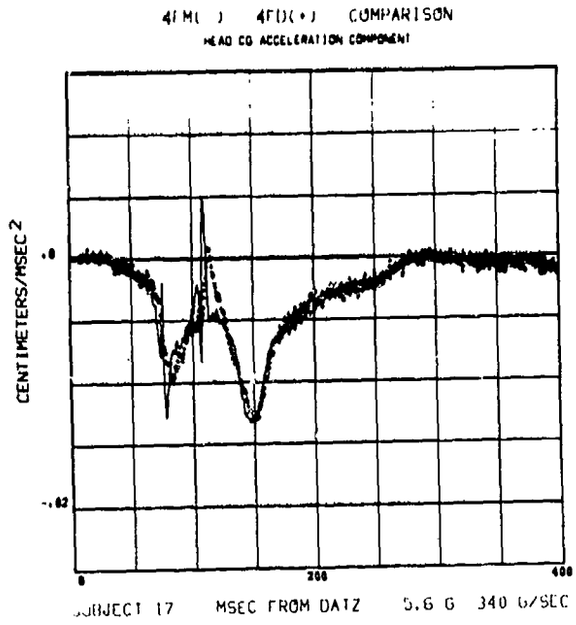

712

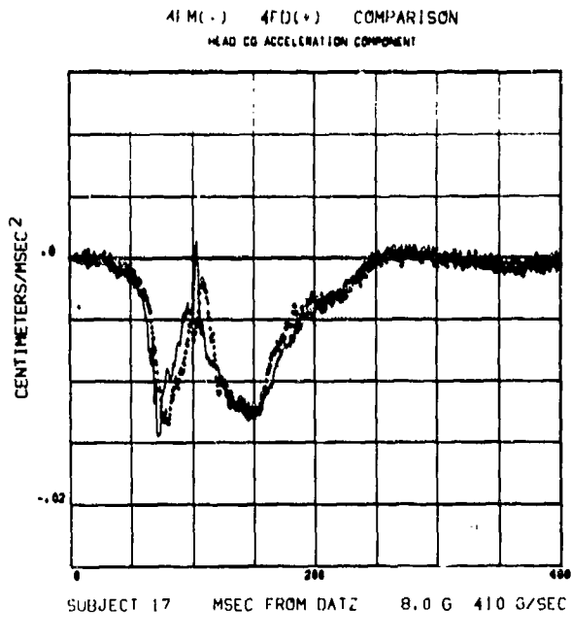

713

4FM, 4FD, COMPARISON OF HEAD C.G. ACCELERATION COMPONENTS

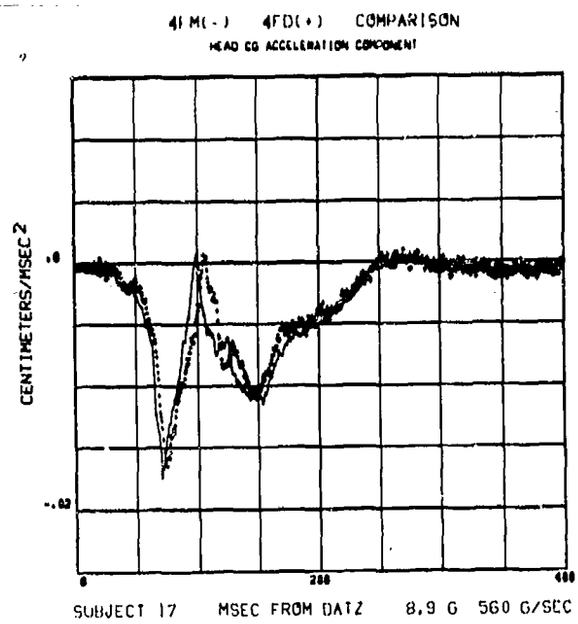

714

4SM, 4SD, COMPARISON OF HEAD C.G. ACCELERATION COMPONENTS

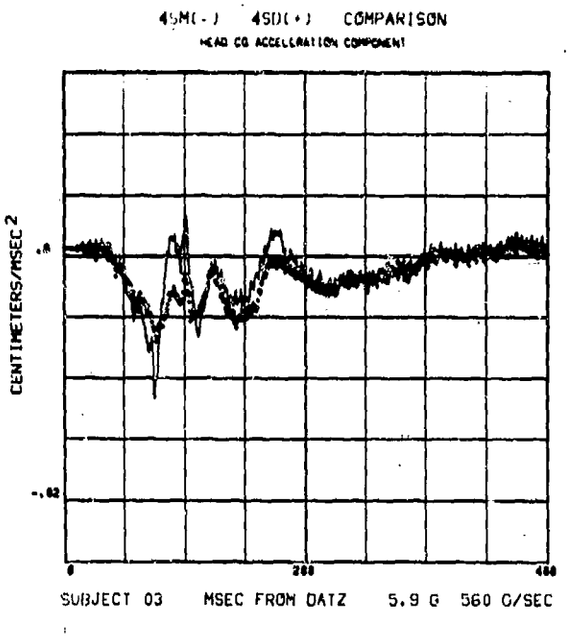

715

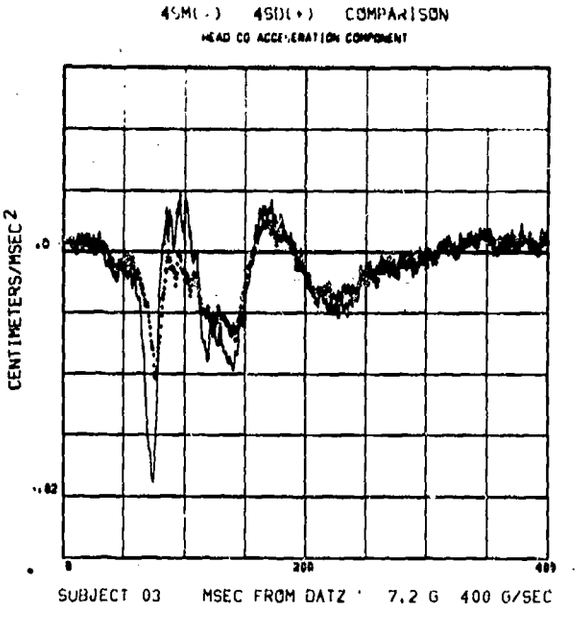

716

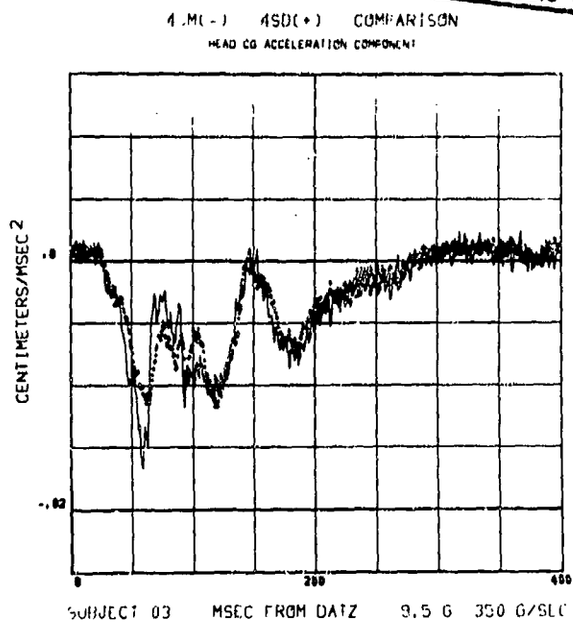

717

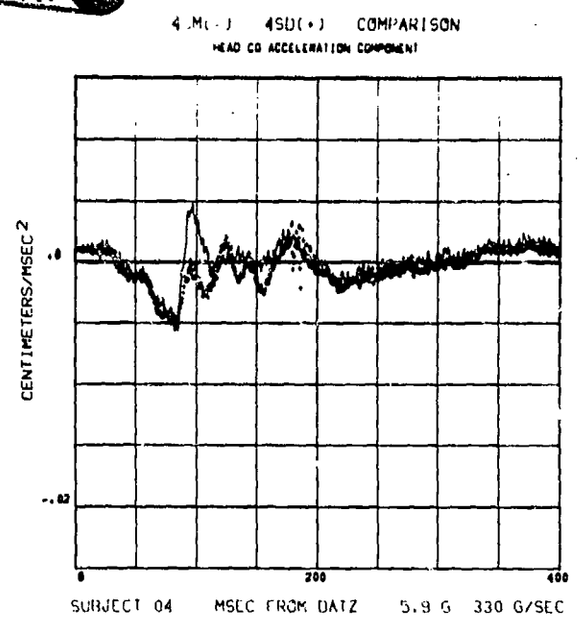

718

4SM, 4SD, COMPARISON OF HEAD C.G. ACCELERATION COMPONENTS

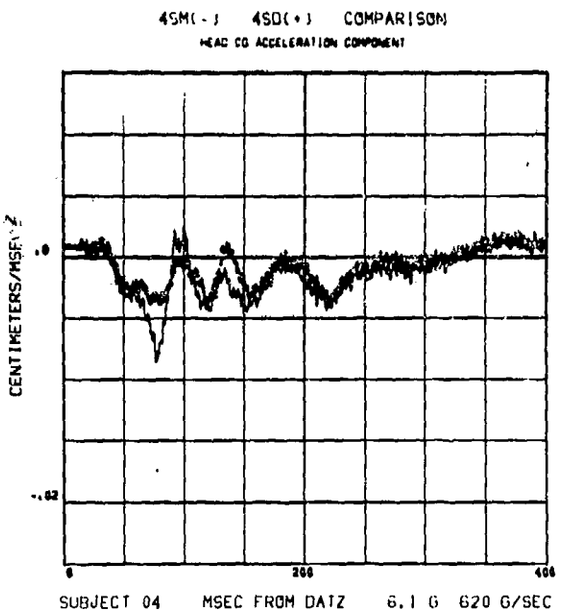

719

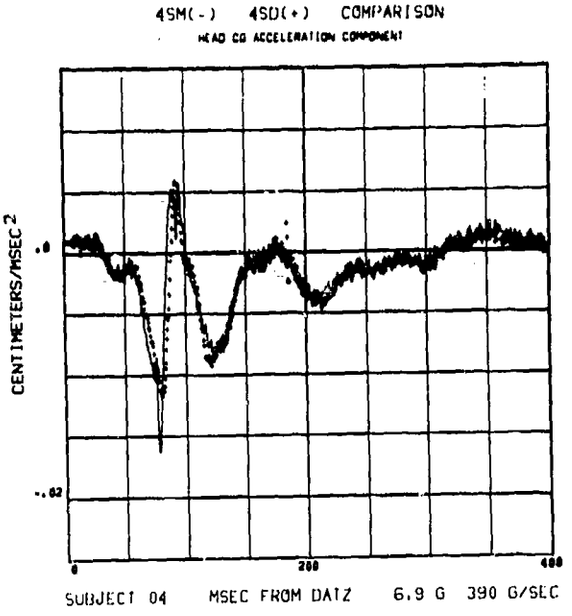

720

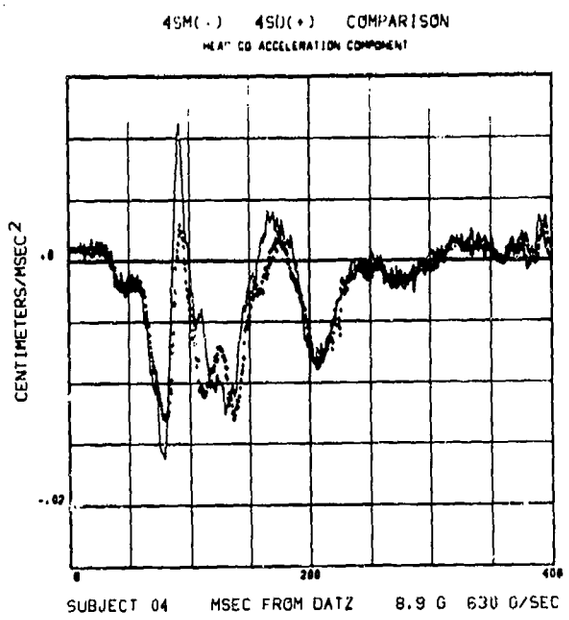

721

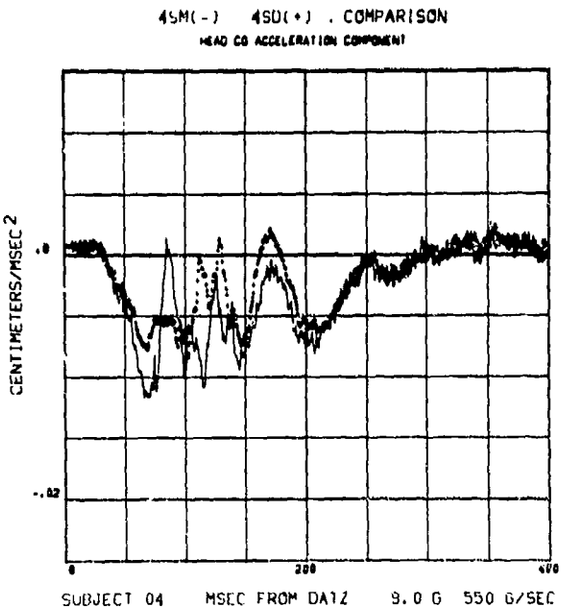

722

4SM, 4SD, COMPARISON OF HEAD C.G. ACCELERATION COMPONENTS

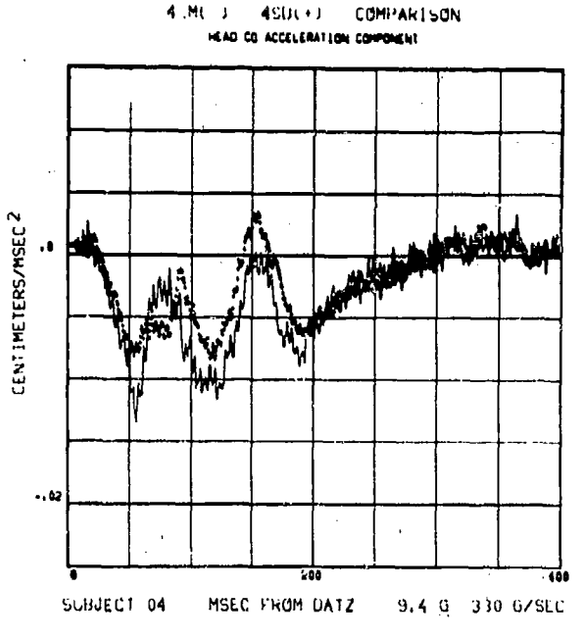

723

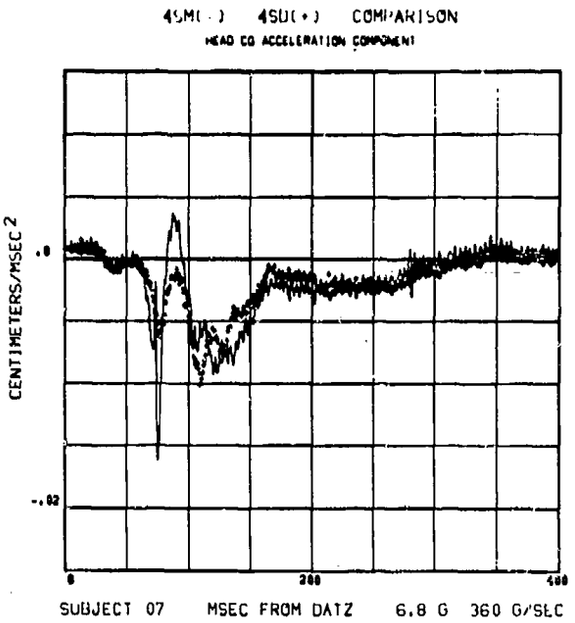

724

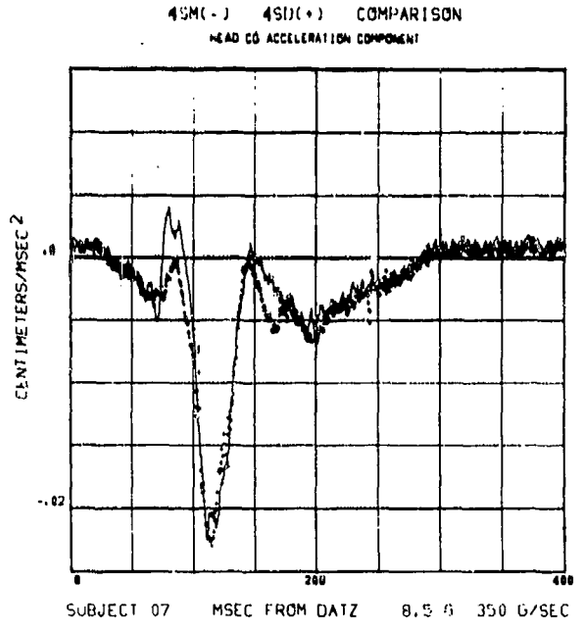

725

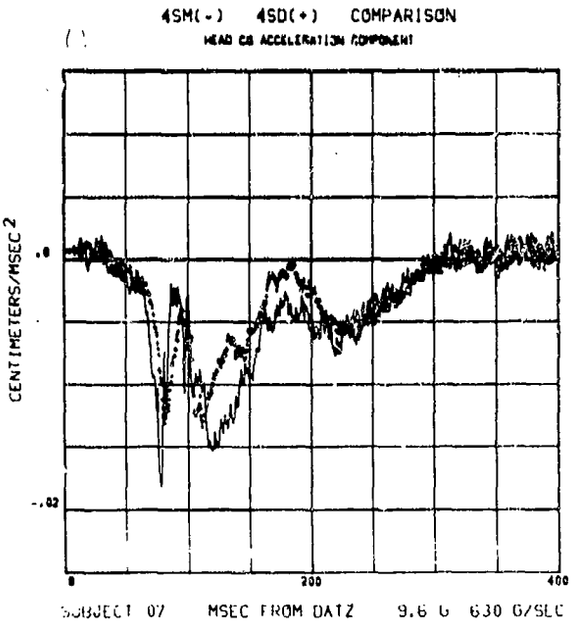

726

4SM, 4SD, COMPARISON OF HEAD C.G. ACCELERATION COMPONENTS

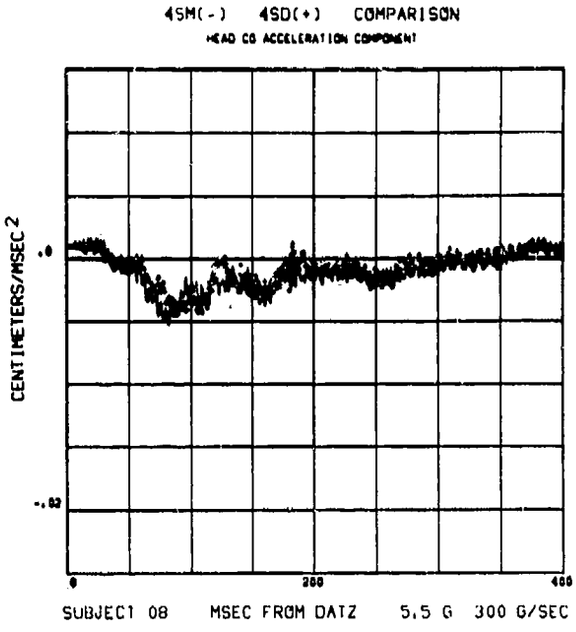

727

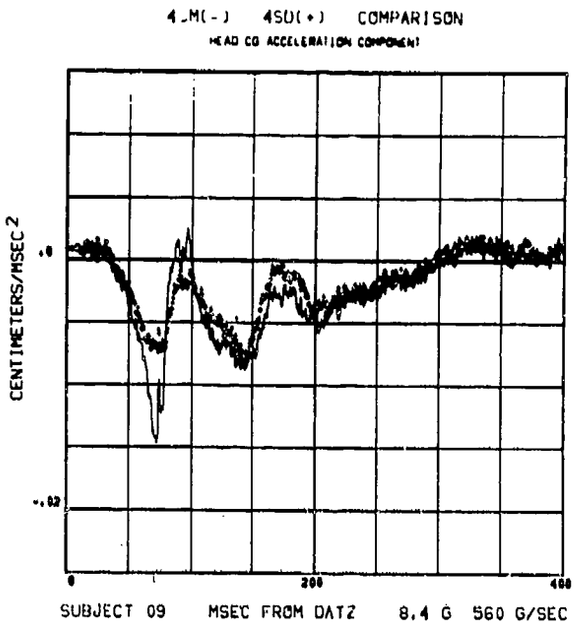

728

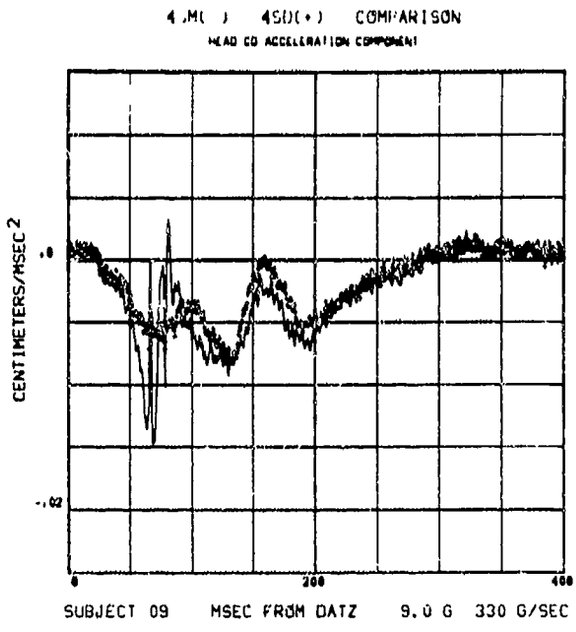

729

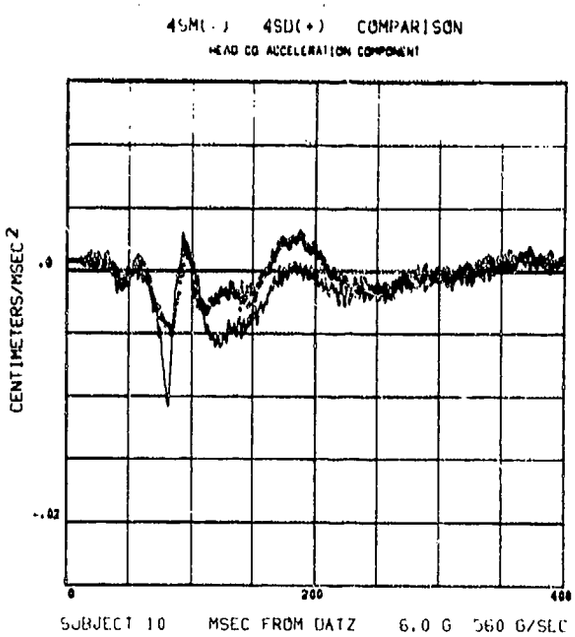

730

4SM, 4SD, COMPARISON OF HEAD C.G. ACCELERATION COMPONENTS

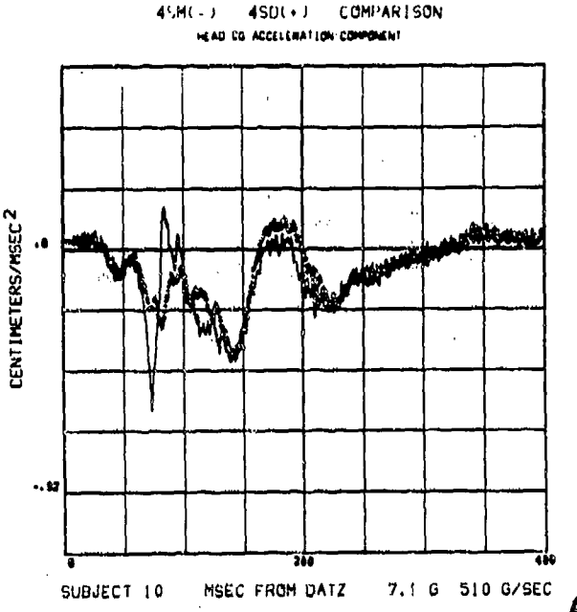

731

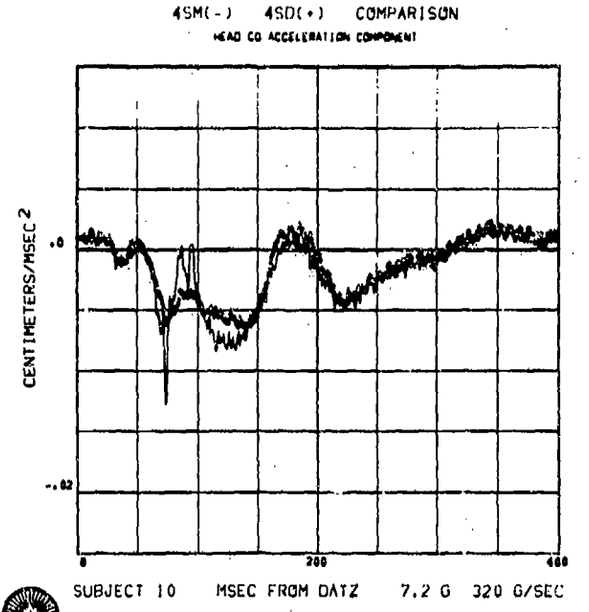

732

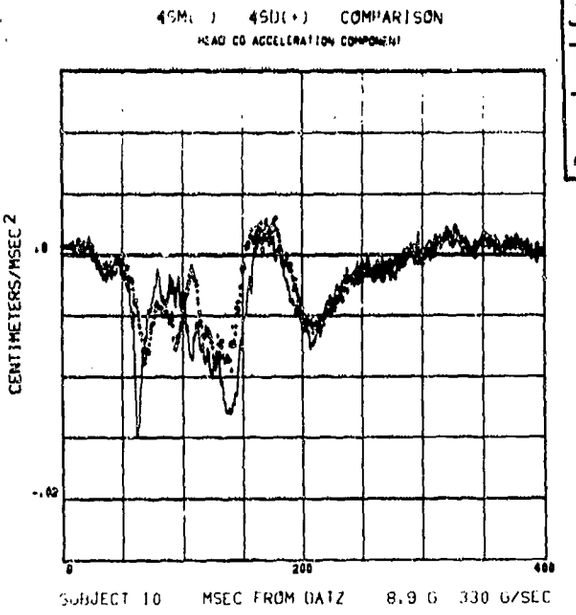

733

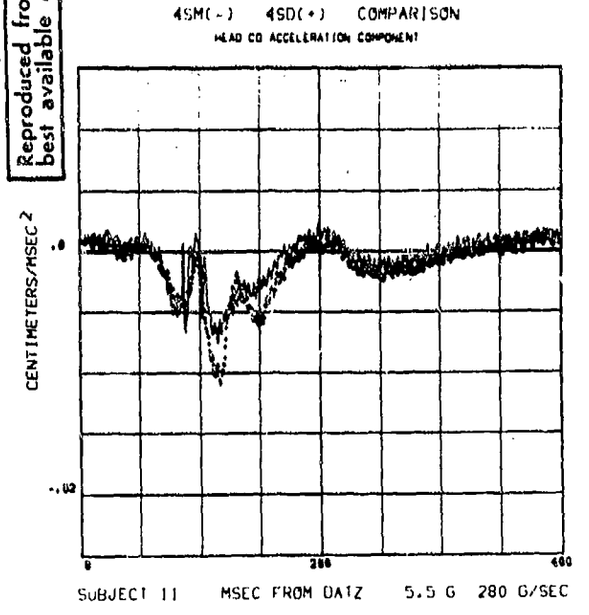

734

4SM, 4SD, COMPARISON OF HEAD C.G. ACCELERATION COMPONENTS

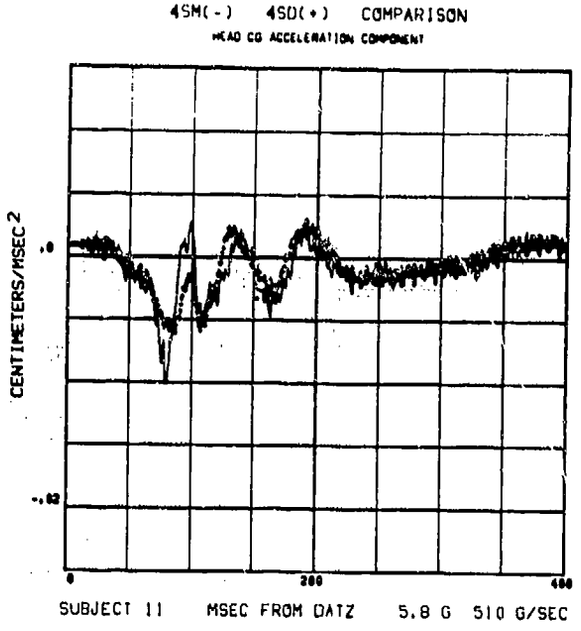

735

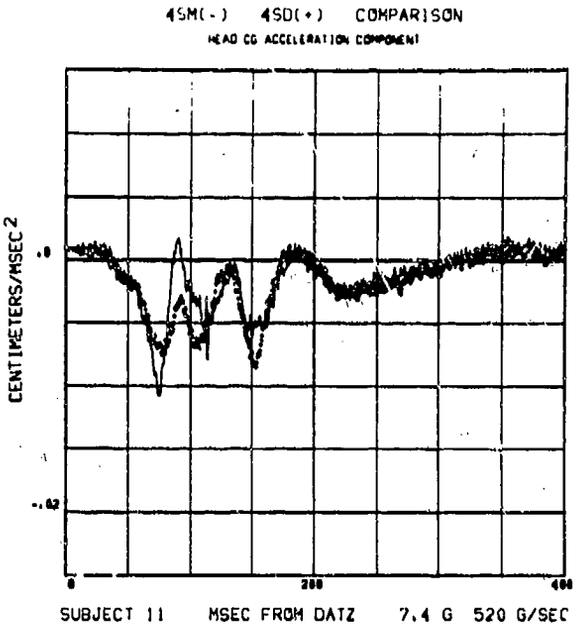

736

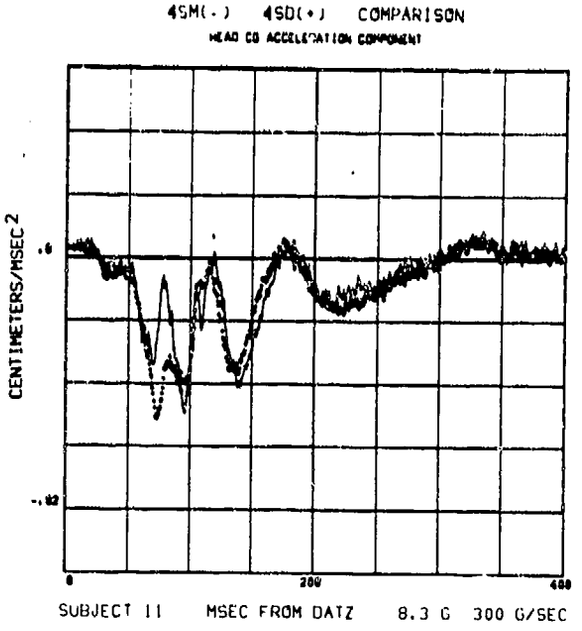

737

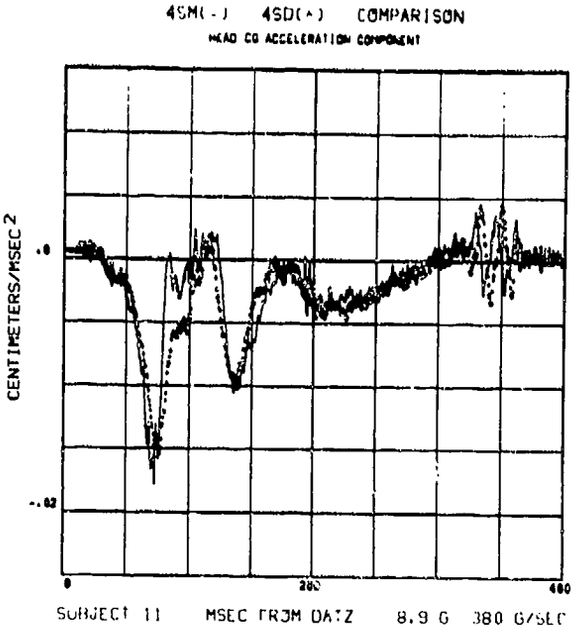

738

4SM, 4SD, COMPARISON OF HEAD C.G. ACCELERATION COMPONENTS

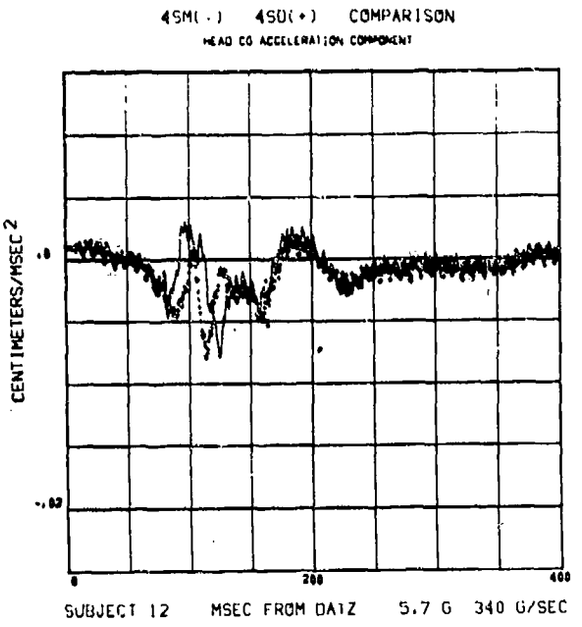

739

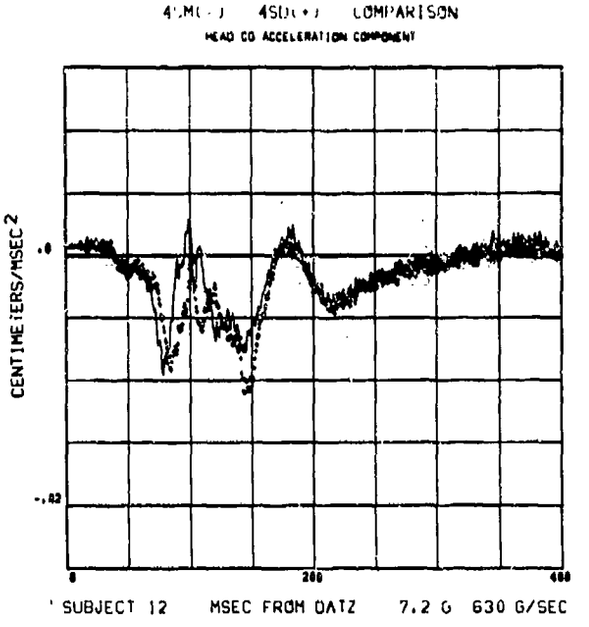

740

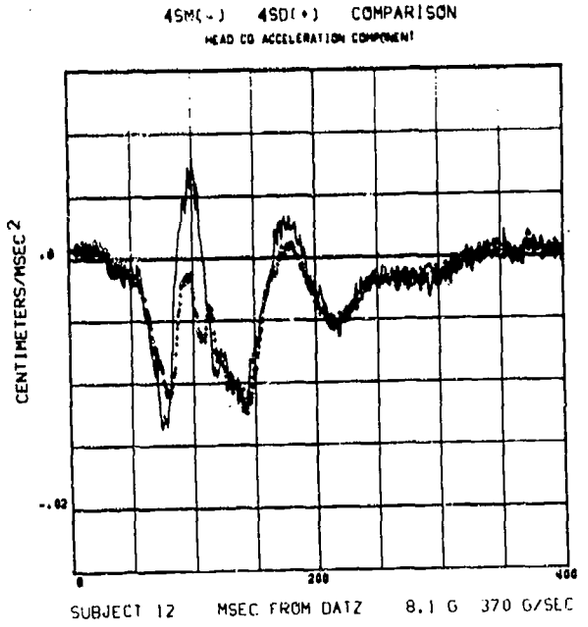

741

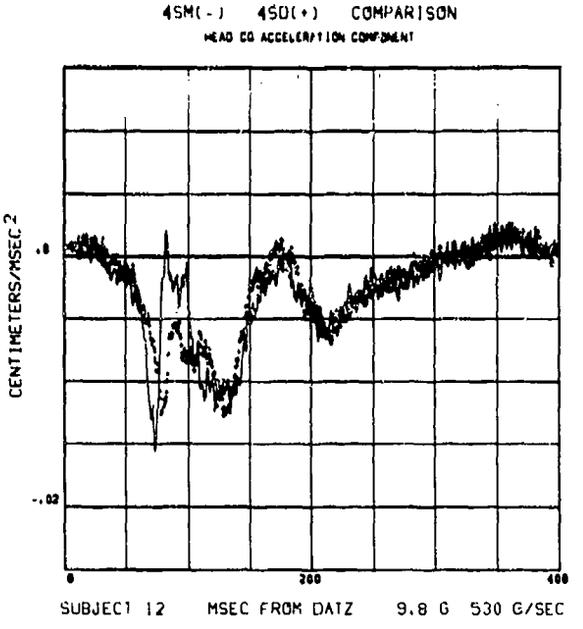

742

4SM, 4SD, COMPARISON OF HEAD C.G. ACCELERATION COMPONENTS

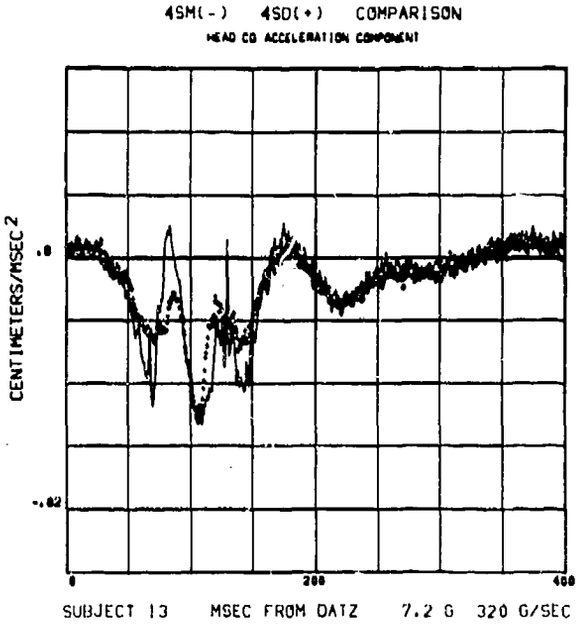

743

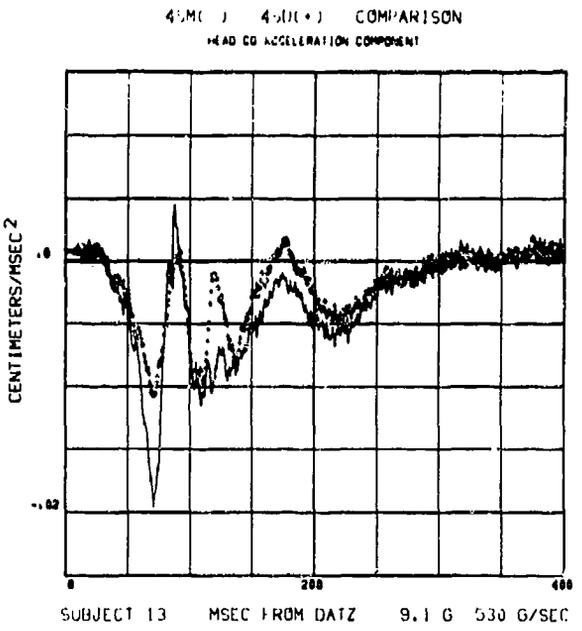

744

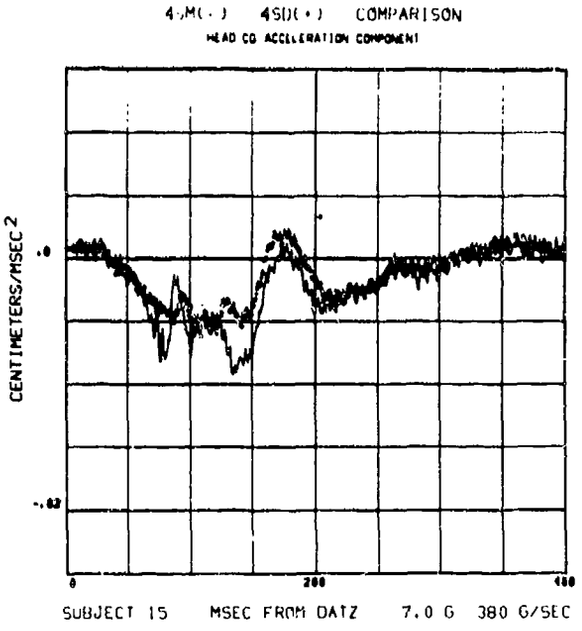

745

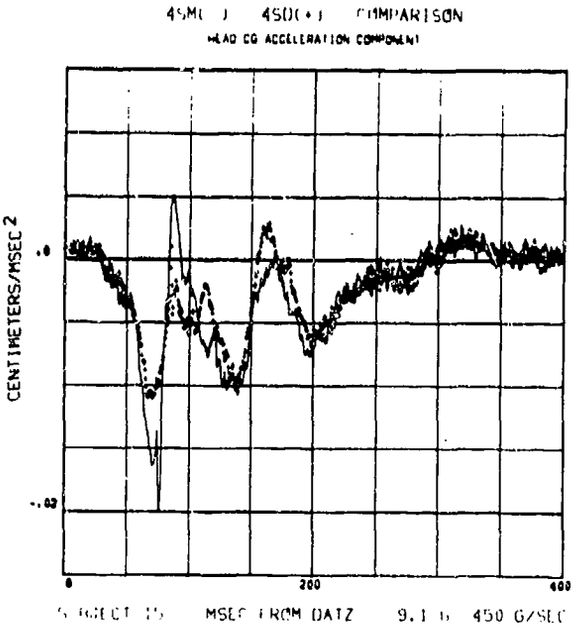

746

4SM, 4SD, COMPARISON OF HEAD C.G. ACCELERATION COMPONENTS

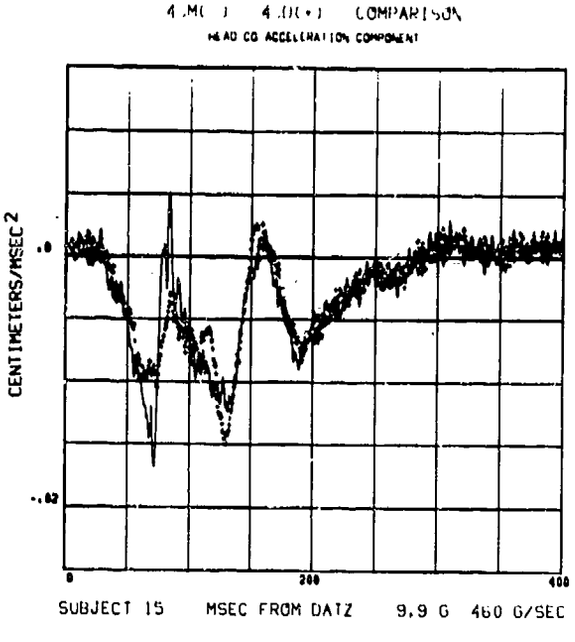

747

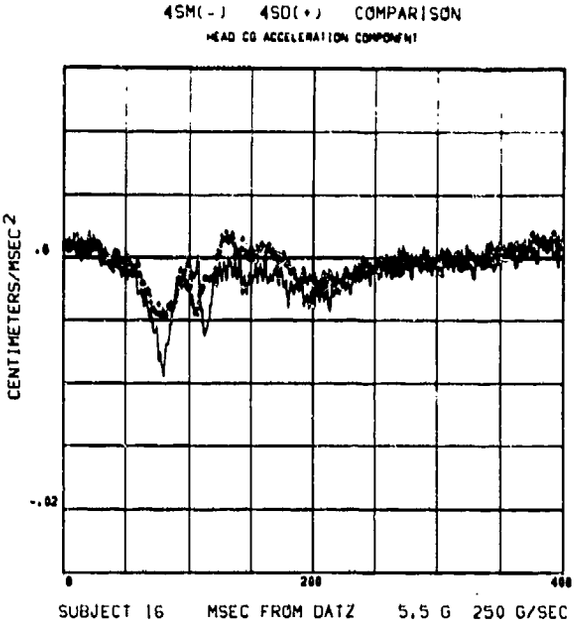

748

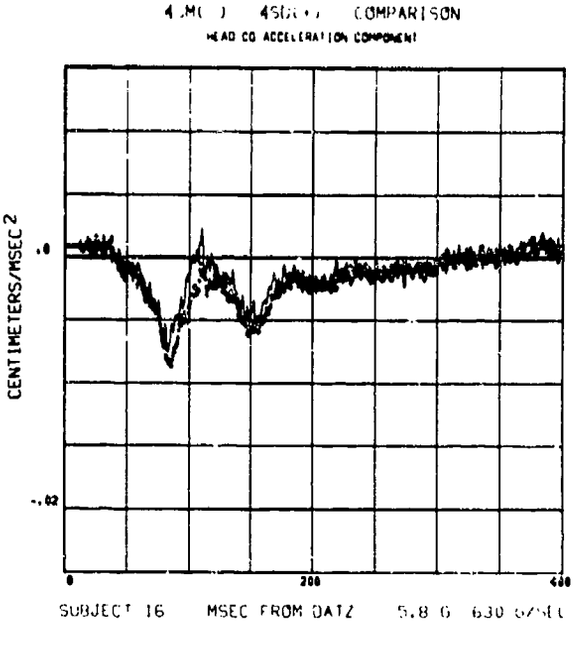

749

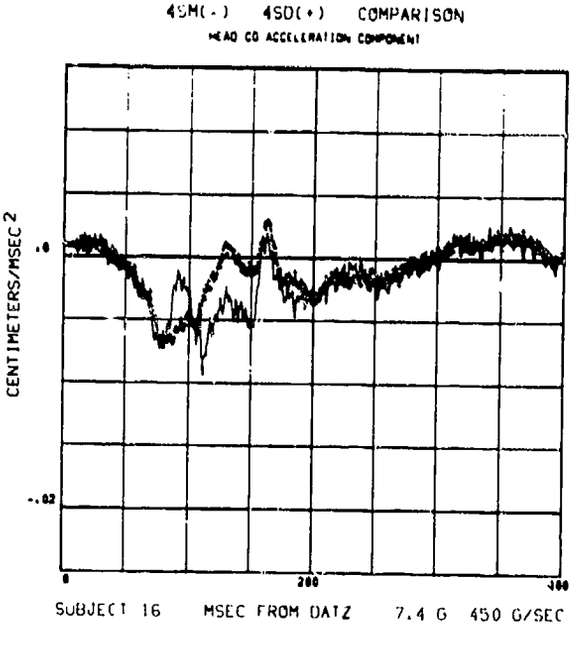

750

4SM, 4SD, COMPARISON OF HEAD C.G. ACCELERATION COMPONENTS

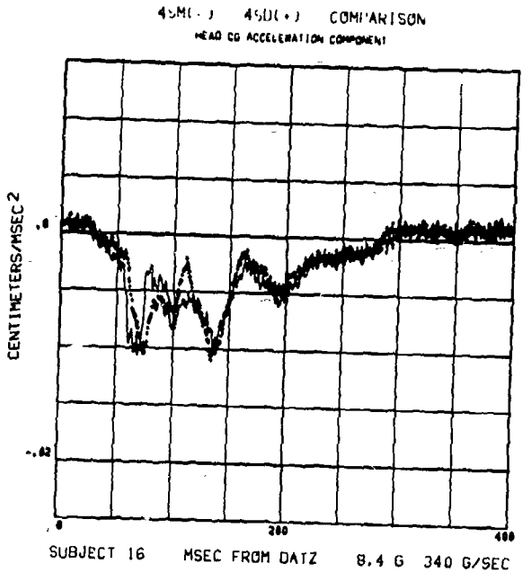

751

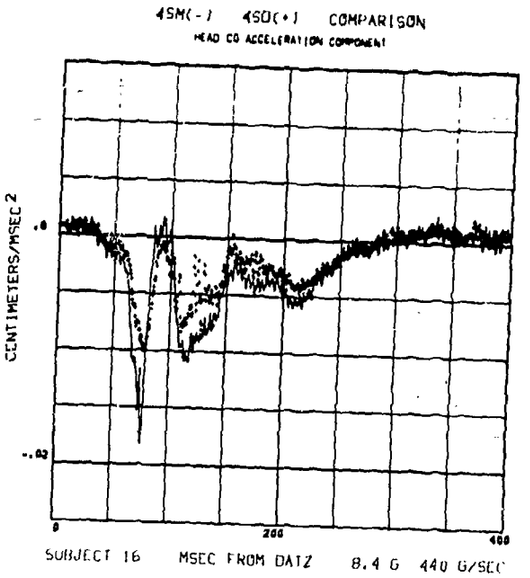

752

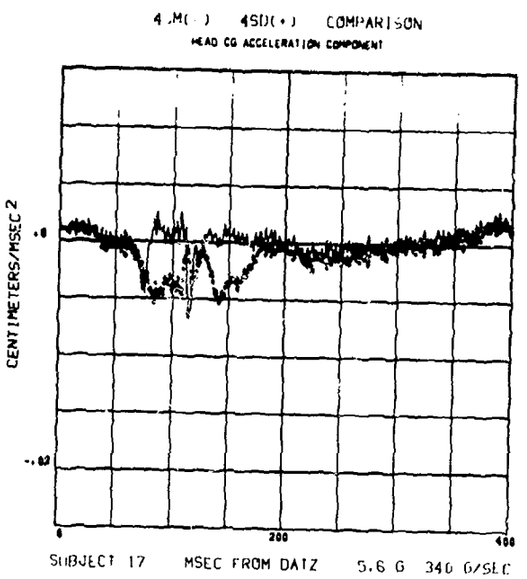

753

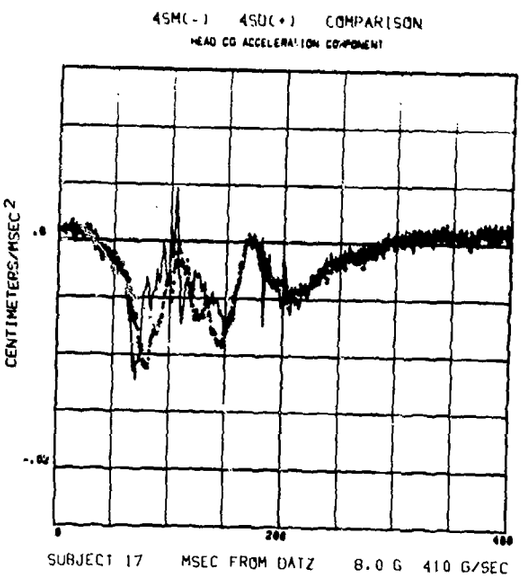

754

4SM, 4SD, COMPARISON OF HEAD C.G. ACCELERATION COMPONENTS

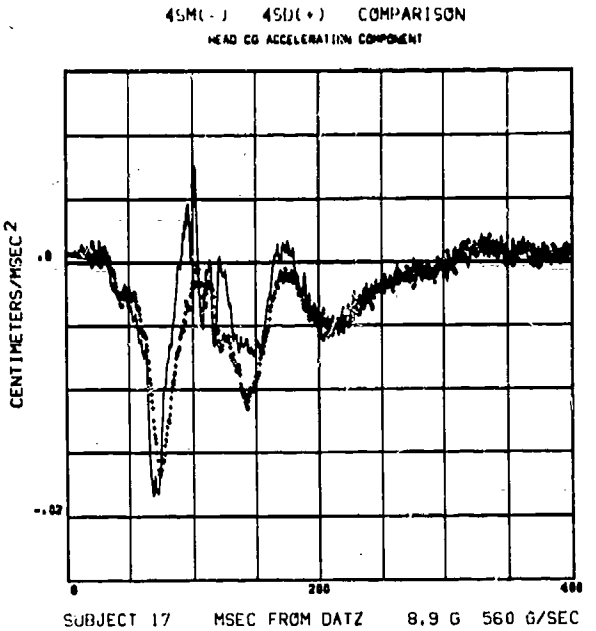

755